



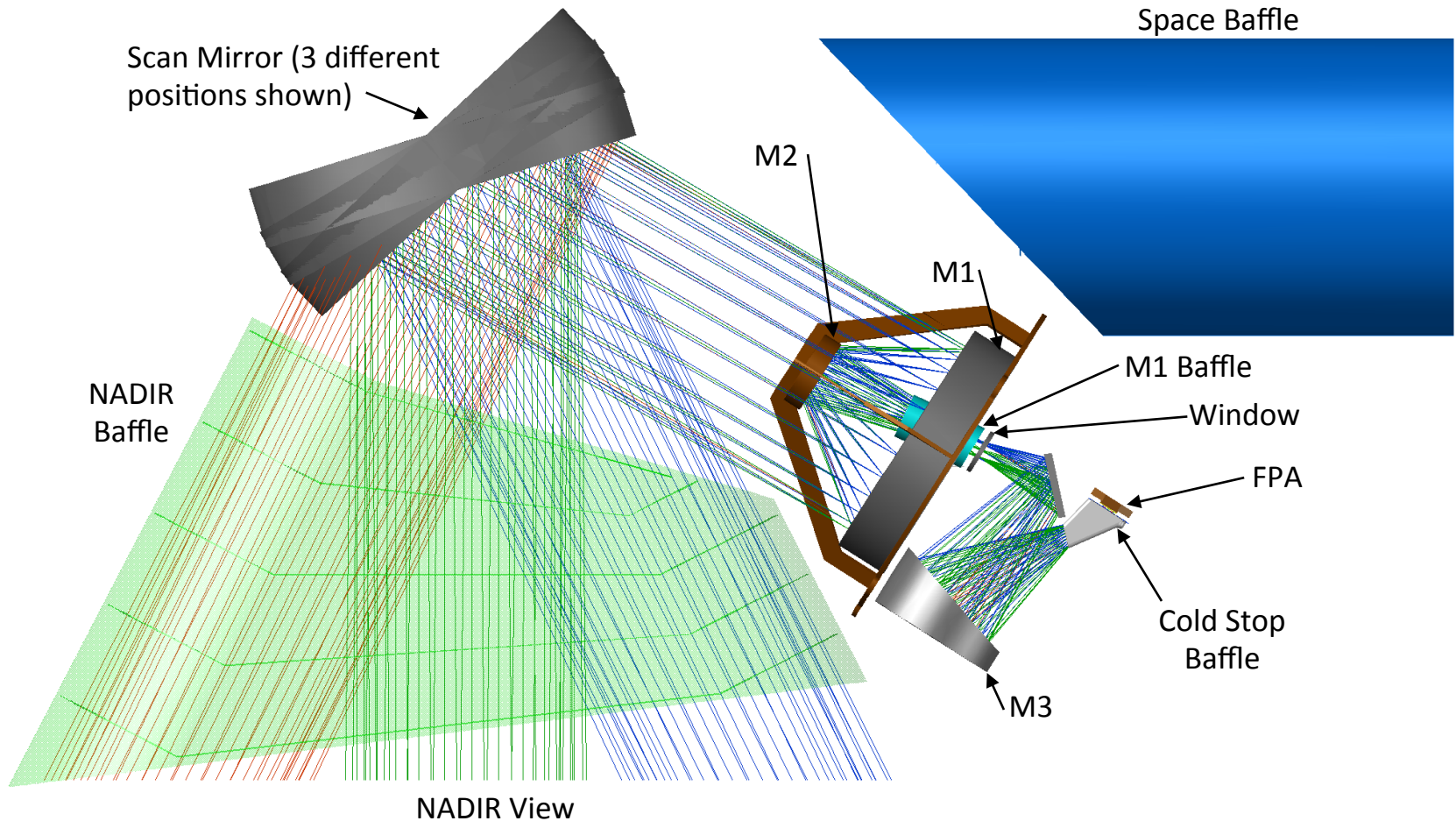
Prototype HypIRI-TIR (PHyTIR) Test Results

William R. Johnson and PHyTIR Team

Jet Propulsion Laboratory, California Institute of Technology, 4800 Oak Grove
Drive, Pasadena, CA, USA 91109-8099

Optical Prescription

- Optical Prescription: Three-Mirror Anastigmat Telescope with Scan Mirror





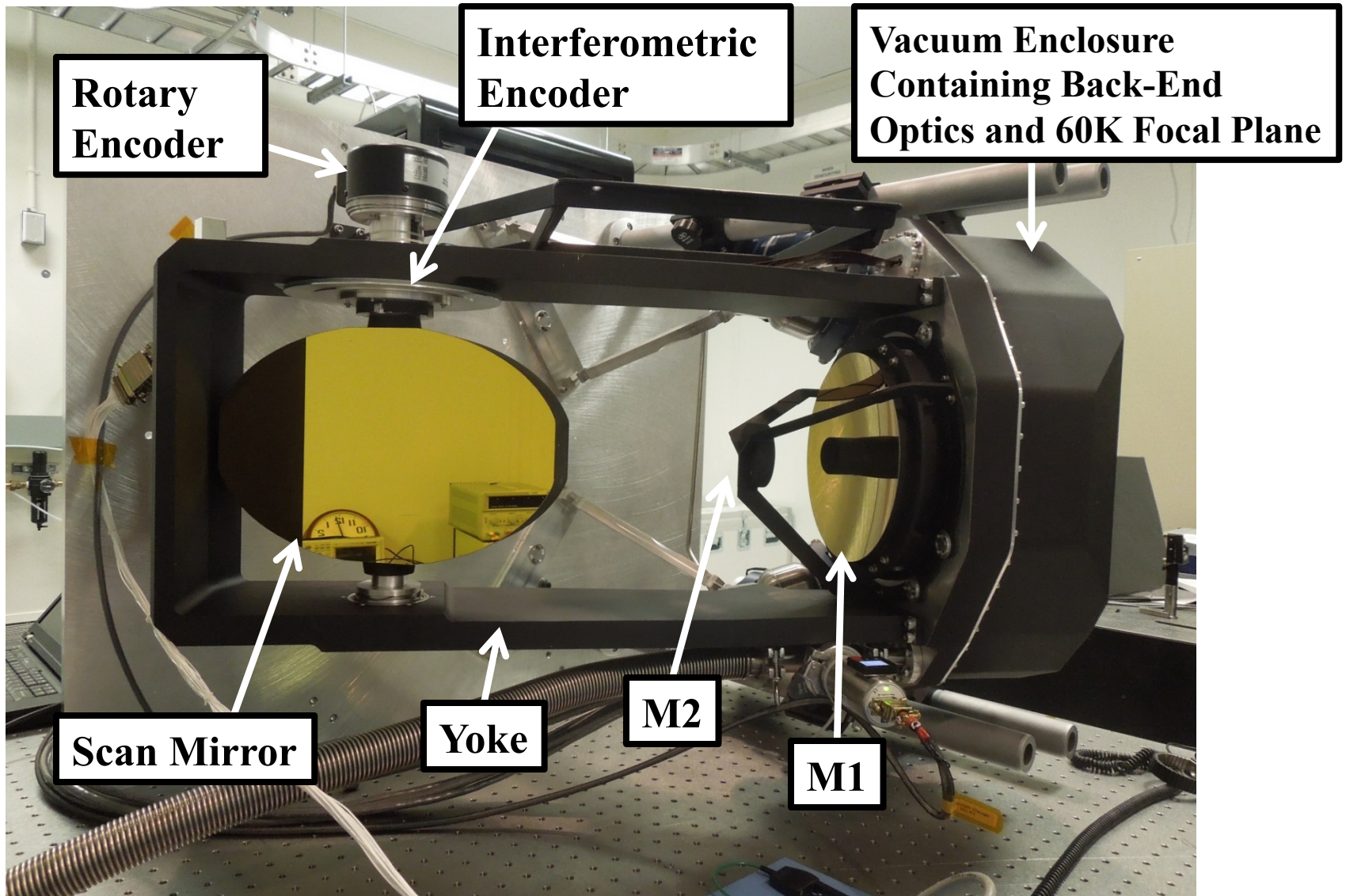
Optical Prescription

PHyTIR Optical Design Parameters	
Effective Focal Length*	415.3mm
Speed	F/2
Aperture Size	207.7mm
Pixel pitch	40 μ m
IFOV	96.308 μ rad (single pixel)
FOV	1.4126 $^{\circ}$ (along track scanning)
Dwell time	32 μ s
Spectral coverage	3.5 μ m to 12.5 μ m
Optical MTF _{Nyquist}	50% polychromatic, all fields (no spider)
Scan mirror rotation rate	14.15rpm (double sided scan mirror)
Altitude*	623km
FOV*	51 $^{\circ}$ (cross track scanning)
Cross track pixels*	9287
Swath*	596km
Swath overlap*	10% along track pixels

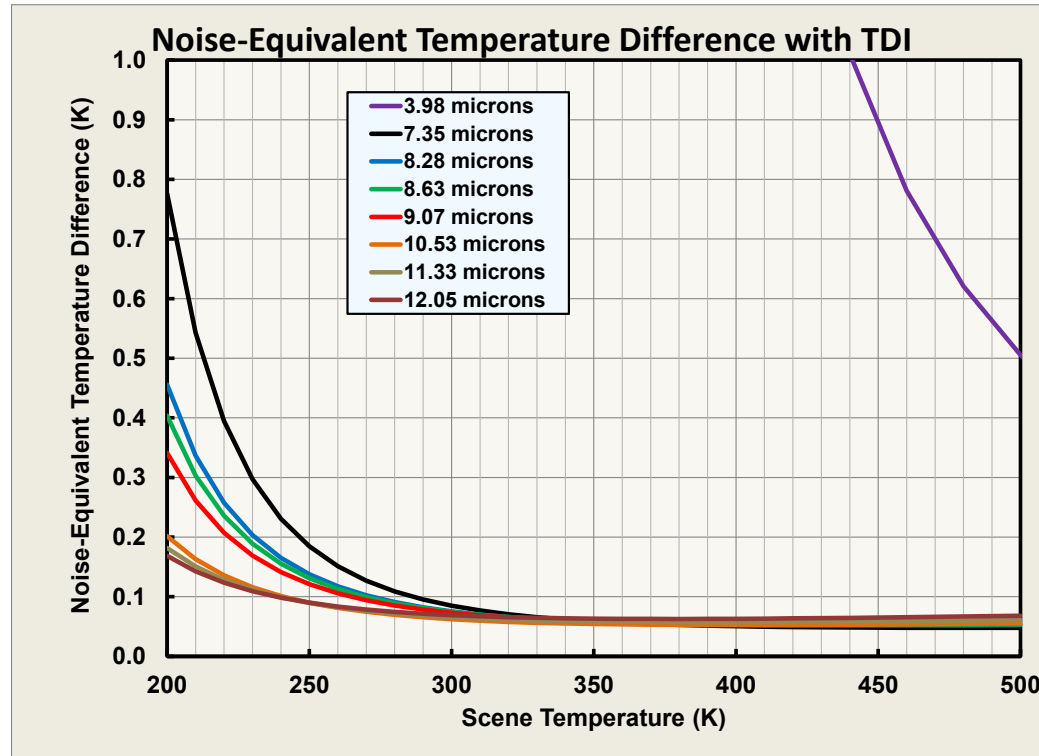
* HyspIRI-TIR specific

- PHyTIR optics consists of 6 reflecting surfaces, 4 transmitting surfaces. (5 mirrors, 2 windows)
- Optics and baffles will operate in an ambient environment (approximately 295K).
- Focal plane assembly (including cold stop) will operate at 60K.
- All reflective optics are aluminum with optical surfaces overcoated with protected gold (> 98% reflectance). Transmissive window will use BBAR coated ZnSe ($\tau > 95\%$). Non-optical, baffles and contact surfaces will be coated with appropriate thermal coatings.
- Cold stop to be polished aluminum facing focal plane and black facing optics.

PHyTIR Prototype



Baseline Calculated Performance



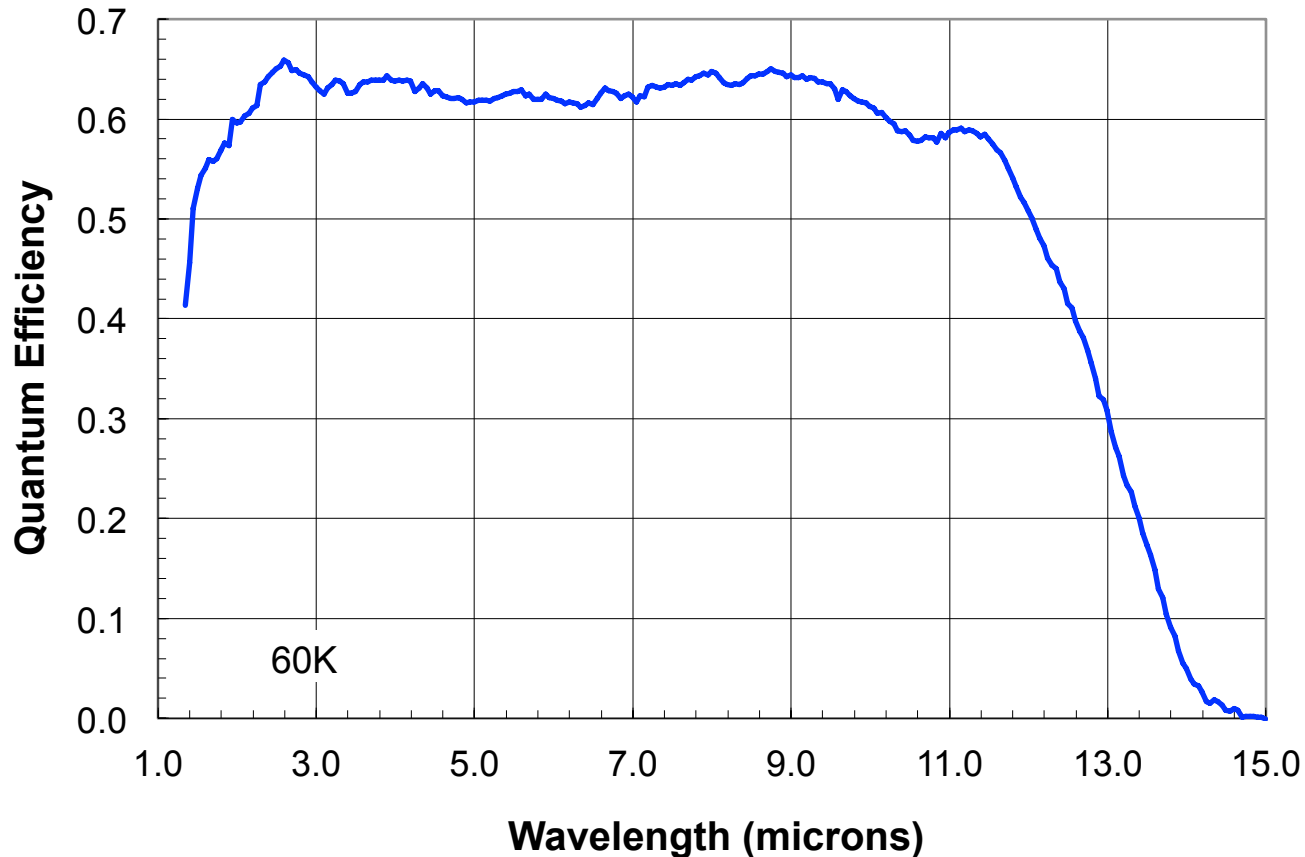
HypIRI-TIR Focal Plane Model Assumption Summary

	Wavelength (μm)	Bandwidth (μm)	Well Size (Me ⁻)	QE	Read noise (e ⁻)	Dark Current (e ⁻)	Optics Transmission (%)
Band 1	3.98	0.015	6.79	0.7	876	235	0.5
Band 2	7.35	0.32	6.29	0.7	876	235	0.63
Band 3	8.28	0.34	6.55	0.7	876	235	0.63
Band 4	8.63	0.35	6.63	0.7	876	235	0.63
Band 5	9.07	0.36	6.65	0.7	876	235	0.63
Band 6	10.53	0.54	8.8	0.7	876	235	0.63
Band 7	11.33	0.54	8.3	0.7	876	235	0.63
Band 8	12.05	0.52	7.5	0.7	876	235	0.63



PHyTIR test results

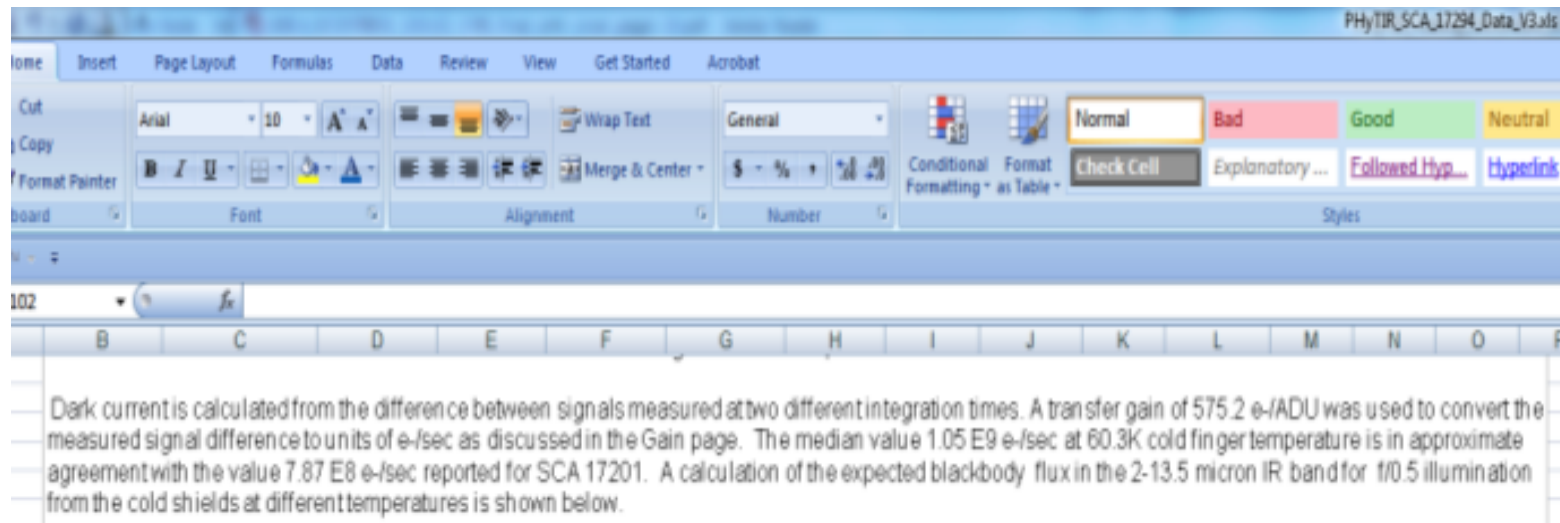
Measured Quantum Efficiency



This plot shows QE measured on a Process Evaluation Chip (PEC) detector fabricated on the same MBE layer as the SCA detector array.



Measured Focal Plane Dark Current



The dark current was measured to be $\sim 183e^-$ which exceeds the performance of the current baseline estimate of $235e^-$



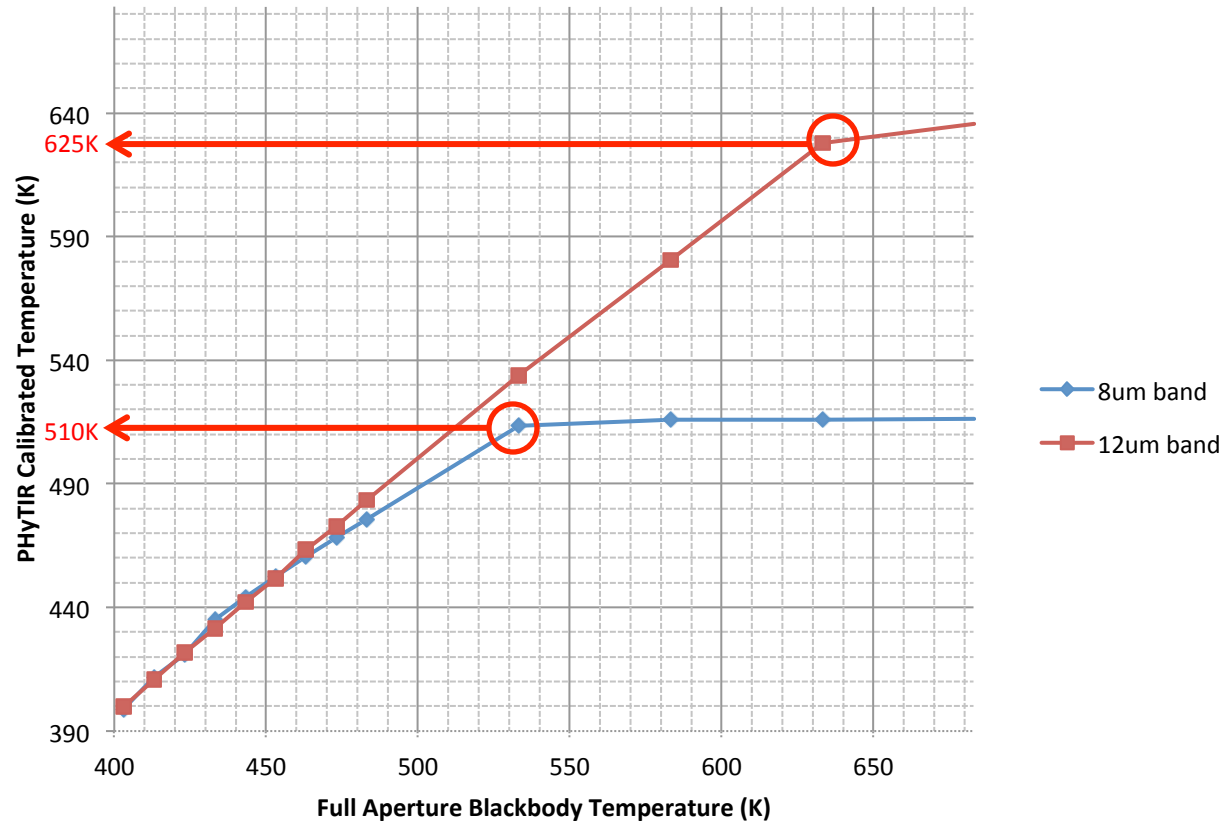
Measured Focal Plane Well Size

HyspIRI-TIR focal plane array well depth measurement									
Parameter	Band 1	Band 2	Band 3	Band 4	Band 5	Band 6	Band 7	Band 8	units
System Transfer Gain	574.2	550.5	550.5	573.5	574.0	733.3	705.5	656.6	e/adu
Rail to Rail Signal Swing	10825	10825	10825	10825	10825	10825	10825	10825	ADU
Rail to Rail Well Depth	6.22E+06	5.96E+06	5.96E+06	6.21E+06	6.21E+06	7.94E+06	7.64E+06	7.11E+06	e

The well depth was measured by taking the signal difference between a saturated and a starved frame multiplied by the gain is the well depth in electrons. The values are within the range expected for the HyspIRI-TIR array. Both Band 6 and 7 have the significant increase expected.

System measurement: Saturation temperature

PHyTIR Saturation Test

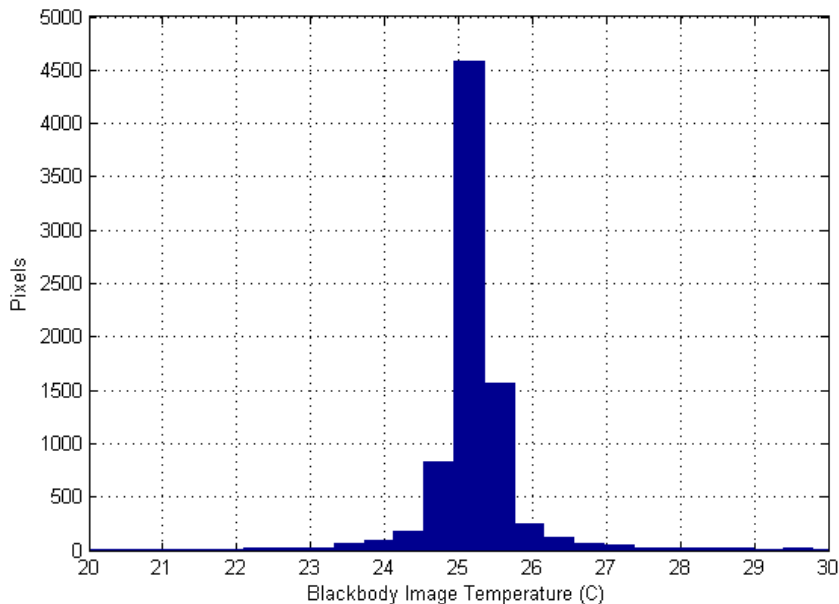


Demonstrates that long-wavelength bands (8 and 12 μm in PHyTIR) do not saturate below 480 K, as required.

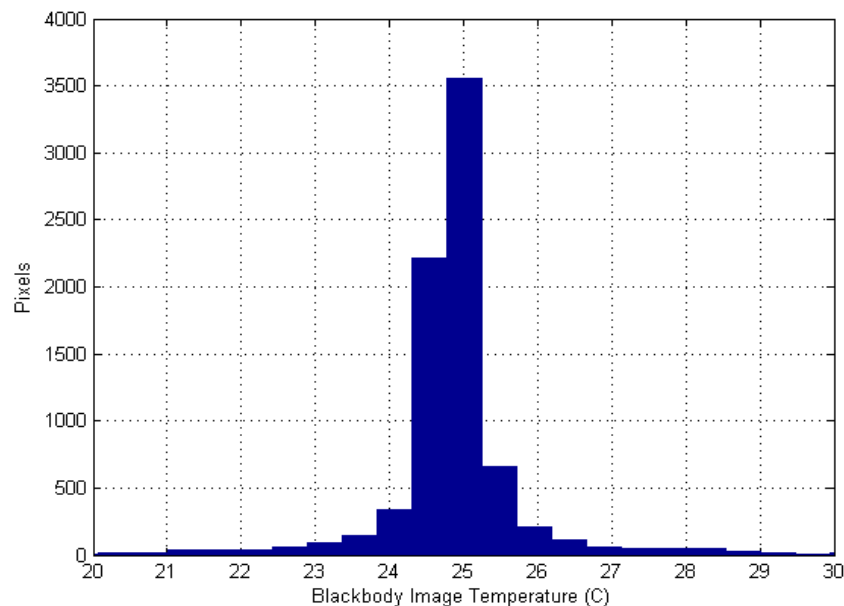
System measurement : Noise equivalent delta temperature (NE Δ T)



8 μ m
(32 cols x 256 rows)



12 μ m
(32cols x 256 rows)



Pixel temperatures retrieved in each band with 25 C blackbody, 10 minutes after calibration at required readout speed. PHyTIR would normally be calibrated every 2 seconds. Demonstrates yield (99.8 % response) within columns needed to define a spectral band and that PHyTIR meets S:N specification.

System measurement : Noise equivalent delta temperature (NE Δ T)



test temp range: 8C to 48C , temporal SNR determined using single pixel over 256 integrations.								
FPA 60k, SHELL < 200K								Comments
	12 μ m band				8 μ m band			
Gain	ADU	NE Δ T			ADU	NE Δ T		$\Delta\tau_{\text{noise}}$
125	32.2484	2108.632	mk		57.5	1182.609	mk	1.7
250	151.719	500.9261	mk		274.6875	276.678	mk	1.9
375	279.0458	301.0259	mk		501.7813	167.4036	mk	2.1
500	402.8105	223.4301	mk		724.1875	124.2772	mk	2.25
625	532.6	180.2478	mk		958	100.2088	mk	2.4
750	663.5425	156.7345	mk		1.20E+03	86.71725	mk	2.6
875	791.7059	136.4143	mk		1.38E+03	78.27221	mk	2.7
1000	915.2353	120.1877	mk		1.50E+03	73.11399	mk	2.75

Detail for previous slide. Demonstrates that gains are available that meet required signal to noise at single pixel level. Required is < 200 mK.



The Earth Observer. May - June 2013. Volume 25, Issue 3.

Editor's Corner

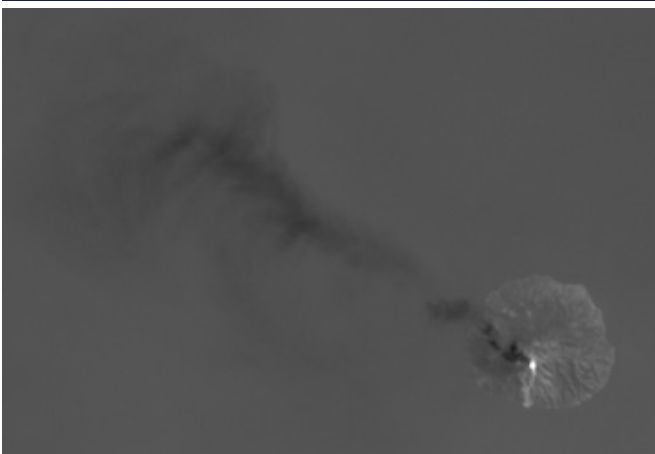
Steve Platnick

EOS Senior Project Scientist

Every Earth-observing mission that has ever flown began as an inspiring vision of what might be possible, followed by a long and challenging journey as the vision confronted reality—both technical and financial. As those who have been involved in developing missions and instruments can attest, it is a journey of many years. Of course some visions never make it to space, but the ones that do are typically based on demonstrated and mature technology.

In 1998, as the first missions of the Earth Observing System (EOS) began to launch, NASA established the Earth Science Technology Office (ESTO) as a testbed to develop technology that could be used for future missions and instruments. ESTO uses an end-to-end approach for demonstrating advanced and cost-effective technologies that help NASA fulfill its science objectives. To date, more than 37% of ESTO-funded technologies have been infused into Earth-observing spaceborne and airborne missions. Please turn to page 22 to read more about recent ESTO projects.

continued on page 2



These images of Paluweh volcano, in the Flores Sea, Indonesia, were obtained on April 29, 2013 by the Landsat Data Continuity Mission's (LDCM) Operational Land Imager (OLI) [*top*] and Thermal Infrared Sensor (TIRS) [*bottom*]. The image pair illustrates the value of having both OLI and TIRS on LDCM. Indeed, "the whole is greater than the sum of its parts." The OLI captures a high-resolution visible image of the plume showing the white cloud of ash drifting northwest over the darker forests and water. Adding the TIRS image allows us to "see" into the infrared and reveals a bright white "hot spot" over the volcano, surrounded by cooler ash clouds, and highlighting TIRS ability to detect very small changes in temperature over small distances—down to about 0.10 °C (0.18 °F). **Credit:** Robert Simmon, NASA's Earth Observatory, using data from the U.S. Geological Survey and NASA.

the earth observer

eos.nasa.gov

In This Issue

Editor's Corner Front Cover

Feature Articles

Transitioning NASA Earth-observing Satellite Data to the Operational Weather Community	4
NASA Intensifies Hurricane Studies with CYGNSS	12
ESTO: Benefitting Earth Science through Technology	22

Meeting/Workshop Summaries

2012 CLARREO Science Definition Team Meeting Summary	30
SMAP Calibration/Validation Workshop	32
HysPpRI Science and Application Workshop Summary	38

In The News

First Light for ISERV Pathfinder, Space Station's Newest 'Eye' on Earth	40
2013 Wintertime Arctic Sea Ice Maximum Fifth Lowest on Record	42

Regular Features

NASA Earth Science in the News	44
NASA Science Mission Directorate – Science Education and Public Outreach Update	46
Science Calendars	47

Reminder: To view newsletter images in color, visit: eospsa.nasa.gov/earth-observer-archive.

As an example, the Soil Moisture Active–Passive (SMAP¹) mission—the first planned “Decadal Survey²” mission—reaped benefits from ESTO’s *observing system simulation experiments* (OSSEs) conducted under the Advanced Information Systems Technology Program.

¹ SMAP is scheduled to launch in late 2014.

² The National Research Council’s 2007 Earth Science Decadal Survey—*Earth Science and Applications from Space: National Imperatives for the Next Decade and Beyond* (www.nap.edu/catalog.php?record_id=13405).

The OSSEs are leading to refinements in land surface models to reduce uncertainties in retrievals of key hydrologic parameters and make the best use of SMAP data. Be sure to read the update on SMAP’s calibration/validation activities on page 32.

Of course, the journey doesn’t end when the instruments are deployed in the field or in orbit—in fact, it’s just beginning. NASA has made great strides in getting its unique measurement and product datasets into the hands of scientists, decision makers, policy makers, and the like. Doing so requires a committed partnership between data providers and end users. This is exactly the goal of NASA’s Short-term Prediction Research and Transition (SPoRT) program. Established in 2002 to demonstrate the weather forecasting application of realtime EOS measurements, the SPoRT project has grown into an end-to-end research-to-operations activity focused on the use of advanced modeling and data assimilation techniques, nowcasting tools, and unique high-resolution multispectral data from satellites to improve short-term weather forecasts on regional and local scales. Beginning on page 4, we present the different NASA products and research capabilities that are being transitioned to end users.

We also continue our coverage of NASA’s ongoing and upcoming missions and instruments. The Operation IceBridge mission has been an opportunity to test existing technologies on NASA aircraft, evaluate new satellite instrument concepts, and update observations of land and sea ice. There have been several campaigns conducted over the past few years, with the most recent having just concluded. The IceBridge team began measuring sea ice, mapping sub-ice bedrock, and gathering data on Greenland’s glaciers in mid-March. Twenty-six science flights were flown out of Thule Air Base and Kangerlussuaq in Greenland, along with a short deployment in Fairbanks, AK. The data collected during ICEBridge expands upon the record that began with the Ice, Clouds, and Land Elevation Satellite (ICESat) in 2003, “bridging” the gap in satellite observations between ICESat (which ended in 2010) and the planned ICESat-2 mission (scheduled for launch in 2016).

In our last issue, we reported on the successful launch of the Landsat Data Continuity Mission (LDCM) on February 11. Three months later LDCM took its place in the Morning Constellation. The spacecraft performed its fourth and final ascent burn on April 12 and is now situated so that it obtains eight-day phasing with Landsat 7, and passes the Afternoon Constellation at a safe distance behind Aura. Its two instruments³ appear to be in good working order and are already obtaining spectacular images—such as the image pair

³ The LDCM instruments include the Operational Land Imager (OLI) and Thermal Infrared Sensor (TIRS).

shown on page 1. On May 30, NASA officially passes control of LDCM over to the U.S. Geological Survey, and it is at that point that the satellite becomes known as Landsat 8.

Meanwhile, Landsat 5 personnel began the satellite's *Phase 2* exit activities with a deorbit burn successfully performed on April 17. The team plans to execute burns every week until the fuel runs out.

Previously, we reported on the Tropospheric Emissions: Monitoring of Pollution (TEMPO⁴) EV-I mission. On page 12 of this issue we have a report on the Cyclone Global Navigation Satellite System (CYGNSS) mission, selected through the EV-2 solicitation. Scheduled to launch in 2016, CYGNSS will employ an innovative design that will feature eight nanosatellites, launched from the same spacecraft, flying in close proximity to one another. This *constellation* of observatories will allow unprecedented temporal and spatial coverage of

⁴ TEMPO was chosen as an Earth Venture Instrument (EVI-1) mission. A report on TEMPO appears in the March–April 2013 issue [Volume 25, Issue 2, pp.10-15].

the core environment of developing tropical cyclones than current scatterometers can obtain. While improved hurricane forecasting is not CYGNSS mission's primary objective, it is hoped that hurricane prediction—in particular, hurricane intensity forecasts—will improve as a result of the data that the mission returns.

Finally, I am pleased to announce the redesign of the Earth Observing System Project Science Office (EOSPSO) website at eosps0.gsfc.nasa.gov. The user interface has changed significantly which allows for more straightforward navigation through the site. To view this newsletter issue in color, or to access issues that date back to March–April 1999, click on *The Earth Observer Newsletter* menu option and click on the desired issue listed on the index page. An extended explanation of new features—*Announcing a New Look for the EOS Project Science Office Website*—appears on page 41 of this issue. We hope you enjoy the new site! ■



This image shows Saunders Island and Wolstenholme Fjord with Kap Atholl in the background observed during an IceBridge survey flight over Greenland. Sea ice coverage in the fjord ranges from thicker, white ice seen in the background, to thinner, *grease ice* and *leads* showing open ocean water in the foreground. **Credit:** NASA/Michael Studinger

Transitioning NASA Earth-observing Satellite Data to the Operational Weather Community

Gary Jedlovec, NASA's Marshall Space Flight Center, SPoRT Project Scientist, gary.jedlovec@nasa.gov

Established in 2002 to demonstrate the potential for using real-time EOS measurements in weather forecasting, the Short-term Prediction Research and Transition (SPoRT) project has grown into an end-to-end, research-to-operations activity focused on using advanced modeling and data assimilation techniques, nowcasting tools, and unique high-resolution multispectral data from satellites to improve short-term weather forecasts on regional and local scales.

Introduction

Beginning in 1999 with the launch of the Terra satellite, NASA embarked on the development of a comprehensive Earth Observing System (EOS) satellite fleet to measure the impact of human activities on Earth's geological, biological, and atmospheric processes. Scientists analyzing the vast amounts of data from the large suite of instruments flown by NASA over the last 15 years have made important revelations about the climate of the Earth and the complex nonlinear processes that govern its change. Equally important are the measurements these sensors take of smaller-scale and faster-changing atmospheric features, which govern faster-changing Earth system processes, such as weather.

Getting these unique measurements into the hands of decision makers in a timely fashion, however, presents a challenge that requires a committed partnership between data providers and end users. Without such cooperation new data, tools, and enhanced forecast techniques that are provided to the operational users, effectively fall to the bottom of a "valley of death," and never get successfully implemented or used. (The phrase "valley of death" is a metaphor for the barriers and obstacles separating research results and operational applications.) The National Research Council (NRC) 2000¹ and 2003² reports indicate that successful transitions require understanding the importance and risks of transition, developing appropriate transition plans, providing adequate resources for the transitions, and implementing continuous communication and feedback between the research and operational communities.

Established in 2002 to demonstrate the potential for using these real-time EOS measurements in weather forecasting, the Short-term Prediction Research and Transition (SPoRT³) project has grown into an end-to-end, research-to-operations activity focused on using advanced modeling and data assimilation techniques, nowcasting tools, and unique high-resolution multispectral data from satellites to improve short-term weather forecasts on regional and local scales. While initially funded by NASA's Research and Analysis Program, SPoRT also supports the objectives of the Applied Science Program by demonstrating innovative uses and practical benefits of NASA-generated Earth science data, scientific knowledge, and research technology. SPoRT has developed and follows a conceptual transition of *research-to-operations* (R2O) model, which involves close collaboration with the end user and provides a "footbridge" over the valley of death. The transition of research data to the operational community better prepares forecasters for the use of new weather data, since NASA's instruments are often precursors to instruments flown by the National Oceanic and Atmospheric Administration (NOAA) on later operational weather satellites. This article describes this transition-to-operations model and the activities that contribute to its success.

Background

The concept of using NASA's EOS observations to improve weather forecasting dates back to the early 1990s; in particular it has been a priority for the Advanced Infrared Sounder Science Team from its inception. The deliberations most relevant to the development of SPoRT began in 2001, when Earth Science Division program managers from NASA Headquarters and NASA's Marshall Space Flight Center (MSFC) began discussing the possibility. Several key activities around that time facilitated the

¹ National Research Council, 2000: *From research to operations: Weather satellites and numerical weather prediction—Crossing the valley of death*. National Academy Press, Washington, DC, ISBN: 0-309-56291-0, 96 pp.

² National Research Council, 2003: *Satellite observations of the Earth's environment: Accelerating the transition of research to operations*. National Academy Press, Washington, DC, ISBN: 0-309-52462-8, 182 pp.

³ The SPoRT website is weather.msfc.nasa.gov/sport.

concept of a regional center to transition EOS data to the operational weather community. NASA had recently launched several of its new EOS satellites to make global observations of the Earth-atmosphere-ocean system to better understand the Earth's climate and how it might be changing. Additionally, numerous low-cost direct-broadcast ground receiving stations were being installed across the country to make real-time data from new EOS instruments—such as the Moderate Resolution Imaging Spectroradiometer (MODIS) onboard Terra and Aqua, and the Atmospheric Infrared Sounder (AIRS) and Advanced Microwave Scanning Radiometer for EOS (AMSR-E) onboard Aqua—available to the user community. At that time, NASA was also establishing a collaborative partnership with the Department of Defense and NOAA to create the Joint Center for Satellite Data Assimilation (JCSDA) to focus on assimilating NASA satellite data into global weather models to improve medium-range (two-to-seven-day) weather forecasts. The SPoRT mission to focus on improving short-term weather forecasts on regional and local scales nicely complemented that of the JCSDA.

At the same time, NOAA's National Weather Service (NWS) was planning to relocate and open a new weather forecast office in Huntsville, AL, to be collocated with NASA scientists from MSFC's Earth Science Office, and the atmospheric research and educational components of the University of Alabama. The potential synergy between the three organizations working together to advance weather diagnostics, nowcasting, and forecasting techniques as a result of the EOS program was electrifying! MSFC scientists developed a proposal to use EOS observations from the direct-broadcast data streams across the country to do just that. NASA funded the initial and subsequent follow-on proposal to facilitate the use of EOS data in NWS forecast offices to improve short-term weather prediction.

The SPoRT program has undergone significant development since its inception in 2001. The program is currently in the third phase of a multiphase project. Initial development focused on working closely with NWS staff to understand how they do business, identifying forecast problems and matching them to unique NASA observational and modeling capabilities, and establishing a successful paradigm for the transition of research capabilities to the operational weather environment. Early successes with transitioning MODIS data (February 2003) and local ground-based total-lightning data (April 2003) into AWIPS⁴, and demonstrating the impact NASA satellite data could have on regional modeling activities provided encouragement for the second phase of the project. During the second phase, SPoRT expanded its interactions with end users and their forecast problems, and assessed the impact NASA observations had on Weather Service operations across the country. SPoRT is now in a third phase, where it has partnered with NOAA's proving grounds and test beds to demonstrate the utility of future NOAA operational sensors. SPoRT also provides the tools and technology to transition additional data and research capabilities to a broader segment of the community—including the private sector.

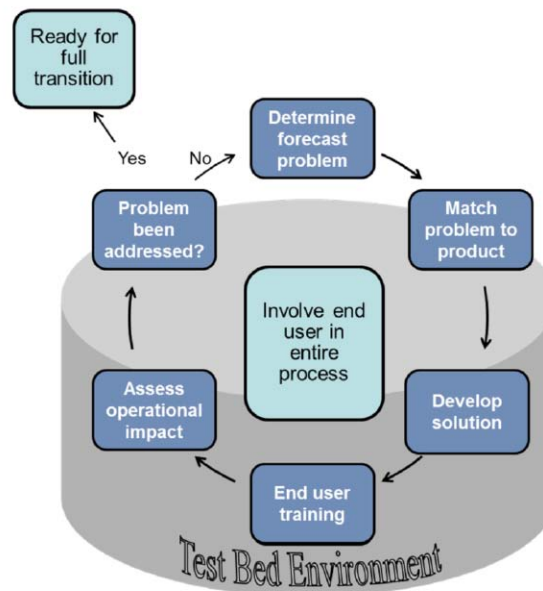
The SPoRT Paradigm: An Approach to Transitioning Research Capabilities to Weather Forecast Operations

The transition of NASA research and experimental data to the operational weather community for evaluation and use requires a committed partnership between data providers and end users. SPoRT bridges the gap between these two groups to make unique data and products developed by the research community available to the operational weather community. SPoRT derives a variety of products from a suite of EOS instruments and works with other data providers in the transition of other unique products to various end users. This paradigm is visually depicted in **Figure 1** (next page). Initial interaction with potential end users involves a site visit to the end-user facilities to learn about operational constraints and forecast issues. The knowledge gained from such a visit allows SPoRT staff members to match a particular research data or capability to a forecast problem. Potential approaches or solutions are typically discussed with end users to establish priorities and a baseline for collaboration.

⁴ AWIPS stands for Advanced Weather Interactive Processing System, an advanced processing, display, and telecommunications system used by the NWS.

The transition of NASA research and experimental data to the operational weather community for evaluation and use requires a committed partnership between data providers and end users. SPoRT bridges the gap between these two groups to make unique data and products developed by the research community available to the operational weather community.

Figure 1. The SPoRT paradigm for successful transition of research data to the operational weather community.



The successful use of transitioned products requires that end users be aware of the capabilities, strengths, and weaknesses of the solution being transitioned to their environment. SPoRT develops and conducts several different types of training, all of them conveying the application of the new data or technique, strengths, weaknesses, and limitations, and also includes end-user application examples, taken directly from the users' decision support systems.

This close interaction from the start reassures the end user that SPoRT is focused on helping them do their job. Potential solutions are demonstrated and refined in a *test bed environment* that simulates operational constraints. The test bed environment, which can be at SPoRT, an end-user facility, or even a third-party location, includes the use of end-user decision support systems (for the NWS these are typically AWIPS, NAWIPS⁵, or AWIPS II) along with the pertinent real-time data streams. To make the transition successful, it is important that the new capabilities be integrated into the end-user decision-support system so that they can be easily used with other end-user data and capabilities. Solutions that seem viable (i.e., meet end user requirements for functionality, timeliness, display, etc.) are further demonstrated and ultimately evaluated in a broader collaborative arrangement that usually includes several collaborative offices or a quasi-operational test bed with similar interests or needs.

The successful use of transitioned products requires that end users be aware of the capabilities, strengths, and weaknesses of the solution being transitioned to their environment. SPoRT develops and conducts several different types of training, all of them conveying the application of the new data or technique, strengths, weaknesses, and limitations—and also includes end-user application examples, taken directly from the users' decision support systems. This training takes the form of short self-guided modules, user-focused quick guides, distance training with the product developer, and even face-to-face science sharing sessions. Examples of these training modules can be found on the SPoRT website (weather.msfc.nasa.gov/sport) under *Transitions > Training*. End users often participate in developing these training aids.

It is important to understand the degree of impact the solution, new product, tool, or forecast capability may have in the operational environment. This assessment is usually done directly in the operational environment (with several end users) or at different locations. Short surveys are used to ascertain the impact of the new product on operational decision-making in the end-user environment. The surveys must not be a burden on the end user, but must allow for both quantitative and qualitative input on the utility of the product. The surveys used by SPoRT can be found on the SPoRT website under *Transitions > Surveys*. The activities of the transition process and the outcome of numerous end-user responses to the product surveys form an *assessment study*. These results are used to guide either broader product transition or a re-evaluation of the transition process.

⁵ NAWIPS stands for the National Center for Environmental Prediction's Pre Advanced Weather Interactive Processing System. NAWIPS is being integrated into the second-generation AWIPS (AWIPS II) systems.

Partners and End Users

There are many individuals and groups who contribute to and benefit from the success of the SPoRT project. The primary *SPoRT stakeholders* (i.e., those who invest in and gain from the success of the project) are the NASA Research and Analysis and Applied Science Programs, the NOAA program offices, the NWS Office of Science and Technology (OST), and forecasters at the NWS Weather Forecast Offices (WFOs). Managers in these organizations provide funding and give guidance and direction to ongoing and future SPoRT research and transitional activities. The NWS and the collaborating WFOs are major stakeholders in the activity, since they provide direct in-kind support through their allocation of forecasters, Science and Operations Officers (SOOs), and Information Technology Officers (ITOs) in the transition of SPoRT products into AWIPS, and the education, training, and assessment assistance they provide. *SPoRT beneficiaries* are those who benefit from the success of the project. The NASA and NOAA entities are *direct beneficiaries* of the success of the SPoRT program. In addition to the WFOs—who interact with and receive products and capabilities from SPoRT—other beneficiaries include collaborating private sector partners who also receive value-added products to improve their weather forecasts. State and county emergency managers and the general public are *indirect beneficiaries* of SPoRT's success through improved forecasts provided by the WFOs.

Figure 2 shows the locations of SPoRT's *collaborative partners*—both supporting and end users. *Supporting partners* help SPoRT conduct the research and transitional activities by providing technical expertise, computational resources, data, and/or other enabling capabilities. *SPoRT end users* include forecasters at the various collaborating NWS WFOs, and other operational weather entities such as some of NOAA's National Centers for Environmental Prediction (NCEPs). The forecasters and environmental managers at these facilities have particular needs that can uniquely be met through the use of NASA's research capabilities. SPoRT currently works collaboratively with twenty-three WFOs and several NCEPs including the Weather Prediction Center, Ocean Prediction Center, and the National Hurricane Center. While the majority of the SPoRT end users are forecasters at these various WFOs and NCEPs across the U.S., the adaptation and use of SPoRT products in NOAA test beds, in proving ground activities, and for weather disaster applications show the relevance of SPoRT's activities to a broader segment of the applied weather community.

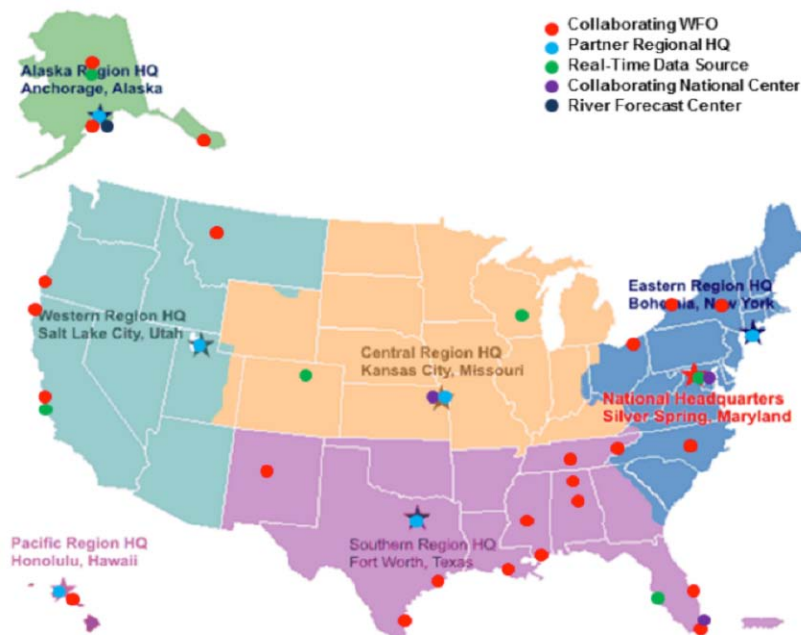


Figure 2. Map showing locations of SPoRT collaborative partners—including both supporting partners and end users.

The primary SPoRT stakeholders (i.e., those who invest in and gain from the success of the project) are the NASA Research and Analysis and Applied Science Programs, the NOAA program offices, the NWS Office of Science and Technology (OST), and forecasters at the NWS Weather Forecast Offices (WFOs). Managers in these organizations provide funding and give guidance and direction to ongoing and future SPoRT research and transitional activities.

SPoRT provides a suite of products from various NASA sensors that enhance the feature detection capabilities beyond that which is typically achieved using operational satellite data alone.

NASA Products and Research Capabilities Transitioned to End Users

SPoRT provides a suite of products from various NASA sensors to its end users for their decision-making processes. A list of these data and products and the forecast challenges that they support, are presented in **Table 1**. Basic MODIS imagery from NASA's Terra and Aqua satellites portrays atmospheric water vapor, cloud, and surface features—providing an increase in spatial resolution by a factor of sixteen over existing Geostationary Operational Environmental Satellite (GOES) imagery. Forecasters use the MODIS imagery to better understand the current environment (i.e., weather conditions), leading to improved situational awareness that helps support short-term forecasts and weather-related decisions. A suite of products derived from the basic imagery provides additional feature detection capability not readily available with operational satellite data. For example, the numerical difference in the shortwave and longwave infrared window channels on MODIS provides a useful means of discriminating between low clouds and fog, particularly at night when conventional visible imagery is unavailable. Derived products—such as sea surface temperature and various vegetation indices—provide qualitative information on variations in surface conditions affecting the development of clouds and other local weather processes.

The large data volume associated with the high-resolution MODIS imagery is often a challenge for operational decision support systems used by many end users. The data volume provided to end users is often reduced by using data fusion techniques. As an example, the production of red-green-blue (RGB) channel combinations provides

Table 1. SPoRT product suite provided to end users.

INSTRUMENT/PRODUCT	FORECAST PROBLEM
MODIS (onboard Terra and Aqua)	
Imagery (visible, 3.9, 6.7, 11 μm)	Improve situational awareness
Suite of RGB products (true and false color snow, air mass, night- and daytime microphysics, dust)	Cloud structure, obstructions to visibility, extent of snow cover
Fog/low cloud (3.9 - 11 μm)	Improve situational awareness
Land and sea surface temperature (LST, SST)	Surface forcing for clouds and convection
SST and ice mask (Great Lakes and Arctic Ocean)	Coastal processes, lake effect precipitation
NDVI/GVF	Model initiation/improved forecasts
AMSR-E (onboard Aqua)/AMSR2 (onboard GCOM-W1)	
Rain rate, cloud water	Coastal weather, data in void regions
Sea surface temperature (SST)	Coastal weather
Total-Lightning Data (ground-based)	
Source/flash density	Severe weather, lightning safety
Multi-sensor composites	
SST (MODIS, GOES, AMSR)	Short-term weather forecast improvement
GOES-MODIS hybrid imagery (visible, 3.9, 6.7, 11 μm)	Improved situational awareness
Hybrid RGB suite	Improved situational awareness
Suomi NPP Products	
VIIRS imagery (visible, 3.9, 11 μm)	Improved situational awareness
Suite of VIIRS RGB products (true, air mass (w/Crosstrack Infrared Scanner), night- and daytime microphysics, dust)	Cloud structure, obstructions to visibility, storm dynamics
VIIRS DNB (low light) – radiance, reflectance, RGB	Improved situational awareness

INSTRUMENT/PRODUCT	FORECAST PROBLEM
Passive Microwave	
Tropical Rainfall Measuring Mission (TRMM) Microwave Imager [TMI] 37 GHz (V/H), 85 GHz (V/H), composite	Precipitation monitoring, storm dynamics
Miscellaneous	
Land Information System (LIS) – soil moisture	Convective initiation, drought monitoring, flooding
Ozone Monitoring Instrument (OMI, onboard Aura)	
NOAA’s National Environmental Satellite, Data, and Information Service (NESDIS) sulfur dioxide (SO ₂)	Volcanic ash monitoring
AIRS (onboard Aqua)	
Carbon monoxide (CO), ozone (O ₃) imagery	Fires, air quality, storm dynamics

the information content of many channels in one product. SPoRT has developed and transitioned a suite of RGB composite imagery products to end users for: monitoring the change in surface visibility due to low clouds, fog, or smoke (true color); differentiating snow on the ground from low clouds (false color snow product); and identifying air mass properties and tropopause fold regions (air mass), cloud properties (day and night microphysics), and airborne dust (dust product). **Figure 3** presents an example of the RGB air mass product in AWIPS at a collaborative WFO. Note that by ingesting the data into the end-users’ decision support systems, forecasters can integrate the data with other products and use existing tools to highlight characteristics of the research data for others to use.

Although the polar orbits of the Terra and Aqua satellites limit data availability to between two and four times daily at mid-latitudes, these image data and derived products are regularly used to improve situational awareness at most of the SPoRT collaborative weather offices. To address forecasters’ complaints that it is difficult to animate the polar orbiting imagery because of the infrequent orbital passes and varying spatial coverage, SPoRT developed a geostationary–polar hybrid product from GOES and Polar-orbiting Environmental Satellites (POES), consisting of a continuous loop of operational GOES imagery complemented by MODIS imagery at the available overpass times. This hybrid image product preserves spatial resolution of the polar-orbiting data and the animation capability of the geostationary observing platform.

Several products from the AMSR-E instrument were made available to coastal forecast offices to monitor precipitation associated with approaching storms and tropical weather systems outside the range of land-based radar systems (until instrument failure in 2011). AMSR2 data from the Japanese Global Change Observation Mission–Water (GCOM-W1) satellite will soon be transitioned to replace the AMSR-E data stream.

Early in the collaborative process SPoRT also transitioned some unique total-lightning measurements from several NASA ground-based lightning networks. A number of WFOs have used lightning source and flash density products derived from

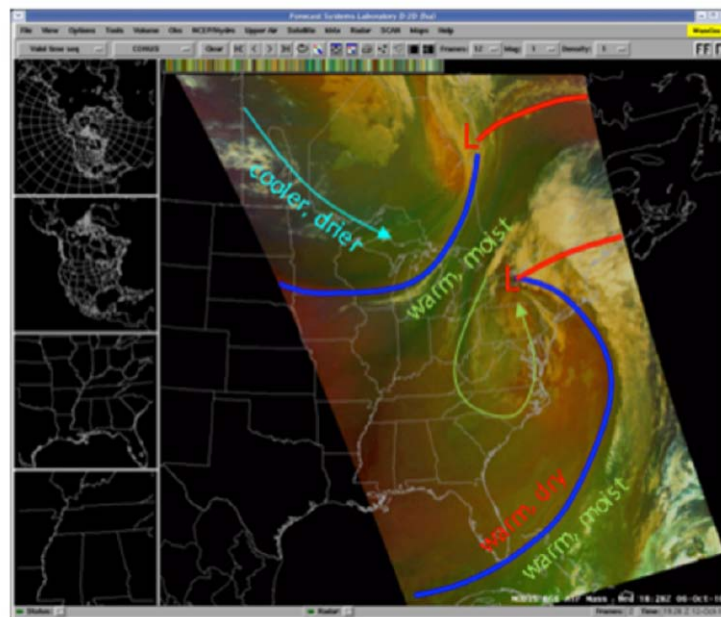


Figure 3. MODIS air mass product displayed in AWIPS.

A number of WFOs have used lightning source and flash density products derived from total-lightning network data, along with Doppler radar, to improve the lead time for predicting severe-weather-producing tornadoes and damaging hail, as well as for lightning safety.

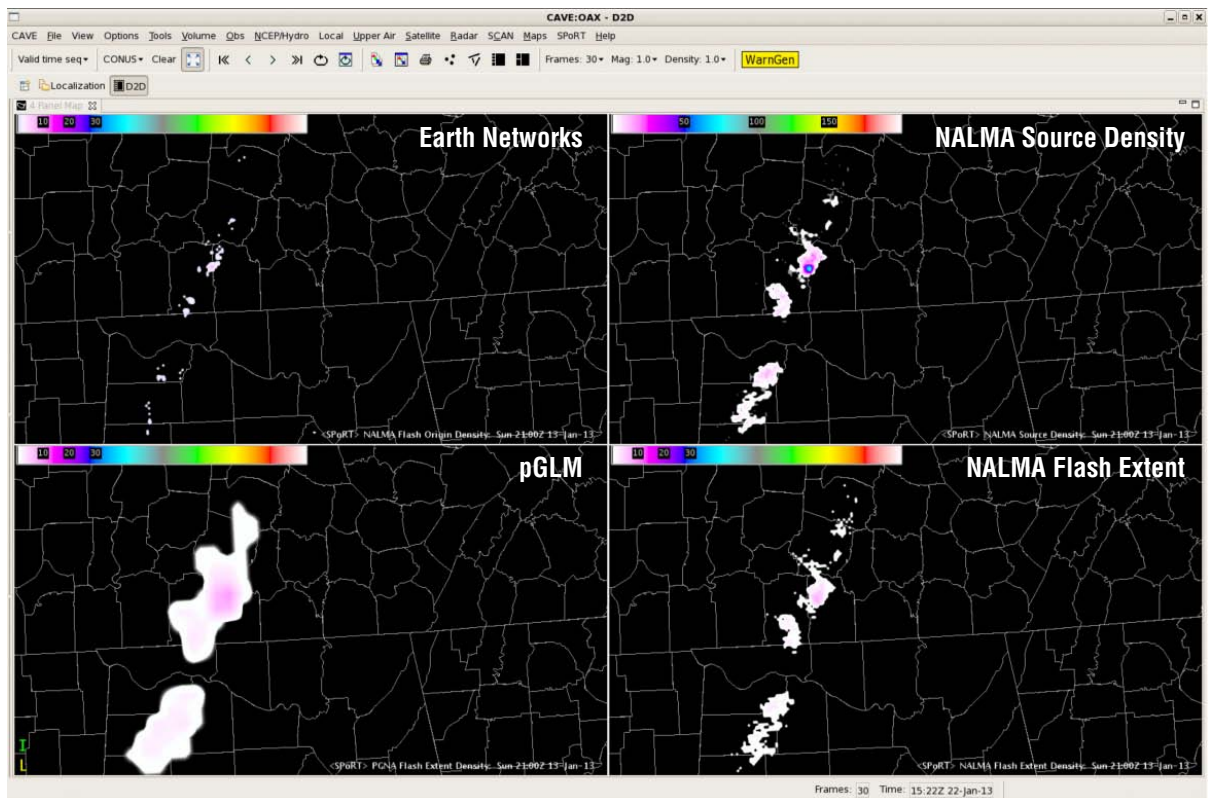
total-lightning network data, along with Doppler radar, to improve the lead time for predicting severe-weather-producing tornadoes and damaging hail, as well as for lightning safety. An example of total-lightning data products from the North Alabama Lightning Mapping Array (NALMA), the Earth Networks Total Lightning Network⁶, and the pseudo Geostationary Lightning Mapper (pGLM)—that previews future observing capabilities from the GOES-R satellite—as displayed in AWIPS II at the Huntsville WFO is presented in **Figure 4**. Transitioning these unique lightning products gives forecasters an edge in providing severe-weather guidance and lightning-safety information to the general public. The current distribution of total-lightning products includes data from seven different networks that have been transitioned to twelve WFOs and several NCEPs.

In addition to products derived directly from quasi-instantaneous swaths of data from a single sensor, SPoRT produces several multisatellite/multitime products such as the MODIS Normalized Difference Vegetation Index (NDVI) and Greenness Vegetation Fraction (GVF) products and the passive microwave/infrared cloud-free composite sea surface temperature product to improve local situational awareness and to assimilate into weather models run by individual WFOs for local model applications.

The success of SPoRT's transition to operations activities is measured in a number of ways including the number of peer-reviewed publications, transitional successes, community recognition, and end-user satisfaction. While the transition of a variety of new products and research capabilities to the end-user community is an important metric, the impact of the product and the satisfaction of the end user with the NASA research capabilities are equally important for both products transitioned and tools developed and provided to carry out successful transitions. Feedback on the success of these transitions is obtained through user surveys and documented in assessment studies and reports. Community recognition of SPoRT as an important partner to help facilitate other transitions is equally important. Recognition of SPoRT as “the place to go” for help in transitioning unique NASA weather products to the operational weather community demonstrates the success of the program.

Figure 4. Total lightning products displayed in AWIPS II.

⁶ For more information, visit: www.earthnetworks.com/OurNetworks/LightningNetwork.aspx.



Opportunities for the community to partner with SPoRT are available through regular Research Opportunities in Space and Earth Science (ROSES) proposal solicitations. Newly developed transitional activities undertaken by other agencies—but using the SPoRT paradigm, capabilities, or information—are an additional measure of project success. Peer-reviewed publications on new research and transitional capabilities and techniques used to develop them are another key metric to document the success of the project. The publication rate may depend on the changing emphasis of the project; from time-to-time, more emphasis is put on transition rather than research. Publication of transitional results and assessments are also appropriate, although they may not always appear in peer-reviewed forums.

While transitioning EOS satellite data and products demonstrates the utility of the NASA data for weather forecasting and other societal applications, the research data also serve as precursor or proxy datasets to future NOAA operational instruments such as those of the Joint Polar Satellite System (JPSS) and the GOES-R satellite programs. Through the transition and use of data that simulate observing capabilities of instruments on these future observing systems (like the pGLM), SPoRT is helping prepare and train forecasters for the use of these next-generation capabilities. SPoRT has been participating in NOAA's JPSS and GOES-R Proving Ground activities for the last several years by working with its collaborative development partners (at the NOAA Cooperative Institute for Mesoscale Satellite Studies and the Cooperative Institute for Research in the Atmosphere) to transition these unique capabilities to operational end users. Eight of SPoRT's collaborative WFOs and all five of the collaborating NCEPs receive and evaluate the utility of proxy products in their forecast operations. Of particular interest is the use of data from the NASA/NOAA Visible Infrared Imaging Radiometer Suite (VIIRS) on the Suomi National Polar-orbiting Partnership (NPP) satellite, not only to simulate the spatial and spectral capabilities of the future GOES-R Advanced Baseline Imager (ABI), but also to directly improve situational awareness and short-term weather forecast capabilities for a variety of end users. SPoRT provides high-resolution imagery from VIIRS [including a suite of RGB products, and radiance and reflectance products from the new low-light sensor [or day-night band (DNB)]] to its end users. The DNB senses reflected moonlight from clouds, smoke, and surface features and visible emission from fires and city lights, and improves the nighttime detection of atmospheric features when only coarse-resolution infrared data are available.

Summary and Future Opportunities

Through these efforts, SPoRT strives to be a focal point and facilitator for the transfer of unique Earth science technologies to the operational weather community, with an emphasis on short-term forecasting. To achieve this vision, the SPoRT project will continue to address new data and technologies and develop and test solutions to critical forecast problems, and integrate solutions into end-user decision-support tools.

Future SPoRT activities will focus both on diagnostic analysis of new NASA Decadal Survey data, such as those from the upcoming Soil Moisture Active Passive (SMAP) mission, as well as data from the Global Precipitation Measurement (GPM) missions and the assimilation of these data into regional weather forecast models using land data assimilation capabilities within the NASA Land Information System. SPoRT plans to transition additional total-lightning network data and to generate additional value-added lightning products for use by the operational weather community. New RGB products and accompanying training are also planned for the near future. Given its commitment to be at the forefront, SPoRT will transition all current and future products into the new NWS decision-support system (AWIPS II) as it is implemented across the country. ■

While transitioning EOS satellite data and products demonstrates the utility of the NASA data for weather forecasting and other societal applications, the research data also serve as precursor or proxy datasets to future NOAA operational instruments such as those of the Joint Polar Satellite System (JPSS) and the GOES-R satellite programs.

NASA Intensifies Hurricane Studies with CYGNSS

Christopher Ruf, University of Michigan, Space Physics Research Laboratory, cruf@umich.edu

Allison Lyons, University of Michigan, adlyons@umich.edu

Alan Ward, NASA's Goddard Space Flight Center/Wyle, alan.b.ward@nasa.gov

Historically, it has been difficult to obtain space-based measurements of ocean surface vector winds in regions with heavy precipitation.

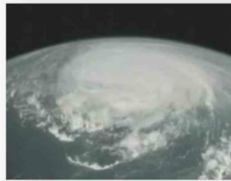
Rationale for CYGNSS

*Hurricane track forecasts have improved in accuracy by about 50% since 1990, largely as a result of improved mesoscale and synoptic modeling and data assimilation. On the other hand, in that same period there has been essentially no improvement in the accuracy of intensity forecasts—an observation that is widely recognized not only by national research institutions¹, but also by the popular press—see **Figure 1**.*

A hurricane intensity forecast is critically dependent on accurate wind measurements in the core of the developing tropical cyclone. Current hurricane intensity forecasts are limited by two factors: inaccuracy of current ocean surface wind measurements and inadequate sampling of the rapidly evolving core environment. Historically, it has been difficult to obtain space-based measurements of ocean surface vector winds² in regions with heavy precipitation. While supplementing satellite observations with aircraft-based observations has helped improve accuracy in some instances, wind-speed estimates in the inner core of a hurricane continue to be a challenge.

Irene forecasts on track; not up to speed on wind

(A.P. wire service, August 29, 2011)



going. But what it would do when it got there was another matter. Predicting a storm's strength still baffles meteorologists. Every giant step in figuring out the path highlights how little progress they've made on another crucial question: How strong?

by Seth Borenstein & Christine Amario: ...the forecast after Irene hit the Bahamas had it staying as a Category 3 and possibly increasing to a Category 4. But it weakened and hit as a Category 1...“We're not completely sure how the interplay of various factors is causing the strength of a storm to change,” [National Hurricane Center Director Bill] Read said. One theory is that a storm's strength is dependent on the storm's inner core. Irene never had a classic, fully formed eye wall even going through the Bahamas as a Category 3. “Why it did that, we don't know,” Read said. “That's a gap in the science.”

Figure 1: Excerpt from article on the Associated Press Wire Service, August 29, 2011.

Tropical cyclones form from *mesoscale convective systems* (MCSs³). In the tropics, MCSs account for more than half of the total rainfall, and their development is critically dependent on complex interactions between ocean surface properties, moist-atmosphere thermodynamics, radiation, and convective dynamics. Unfortunately, most current space-based active and passive microwave instruments are in polar low-Earth orbits

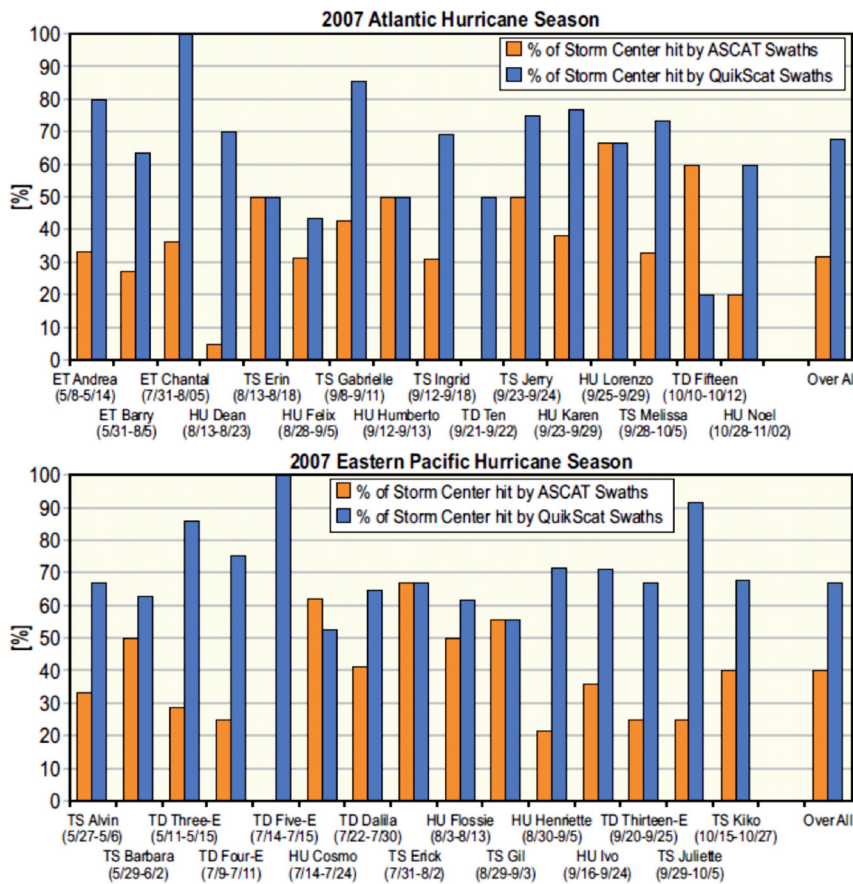
(LEOs) that maximize global coverage but leave significant “data gaps” over the tropics. Further, a single, broad-swath, high-resolution scatterometer system cannot resolve synoptic-scale spatial detail everywhere on the globe, and in particular not over the tropics. The revisit times of current on-orbit instruments range between 12 hours and several days, and are similarly not sufficient to capture the rapidly changing environment at the core of a tropical cyclone.

As a striking example, **Figure 2** (next page) shows the percentage of times that the core of every tropical depression, storm, and cyclone from the 2007 Atlantic and Pacific storm seasons was successfully imaged by the Quick Scatterometer (QuikSCAT) or Advanced Scatterometer (ASCAT). Sometimes, the core is missed when an organized system passes through an imager's coverage gap; other times, it is because the storm's motion is appropriately offset from the motion of the imager's swath. The figure highlights the fact that, in many cases, tropical cyclones are observed

¹ *Hurricane Warning: The Critical Need for a National Hurricane Research Initiative*, National Science Foundation, NSB-06-115, 2007; Hurricane Forecast Improvement Project, NOAA, 2008

² These include NASA's Quick Scatterometer (QuikSCAT), which flew on the SeaWinds mission, the Advanced Scatterometer (ASCAT) on the European Organization for the Exploitation of Meteorological Satellites' (EUMETSAT) METOP series of satellites, and the Oceansat-2.

³ Tropical cyclones, mesoscale convective complexes, squall lines, lake effect snow, and polar lows are all weather phenomena that form from MCSs.



ET = Extratropical HU = Hurricane TD = Tropical Depression TS = Tropical Storm

less than half the time. One particularly egregious case is Hurricane Dean, for which ASCAT was able to observe it during less than 5% of its life cycle.

The goal of NASA’s Cyclone Global Navigation Satellite System (CYGNSS) is to resolve these two principal deficiencies with current tropical cyclone intensity forecasts. Selected as a Venture Class mission⁴, CYGNSS—with a tentative launch date of 2016—uses an innovative design that employs eight small satellites carried into orbit on a single launch vehicle. The eight satellites will comprise a *constellation* that will allow the observatories to fly in close proximity to each other to measure the ocean surface wind field with unprecedented temporal resolution and spatial coverage, under all precipitating conditions, and over the full dynamic range of wind speeds experienced in a tropical cyclone. (The constellation concept is described in greater detail below.) It will do so by combining the all-weather performance of Global Positioning System (GPS)-based *bistatic scatterometry* with the sampling properties of a dense microsatellite (microsat) constellation—see *CYGNSS Heritage: Using GPS Reflectometry for Geophysical Measurements* on page 17. In orbit, the observatories will receive both direct and reflected signals from GPS satellites. The direct signals pinpoint CYGNSS observatory positions, while the reflected signals respond to ocean surface roughness, from which wind speed is retrieved. **Figure 3** illustrates the improvements that

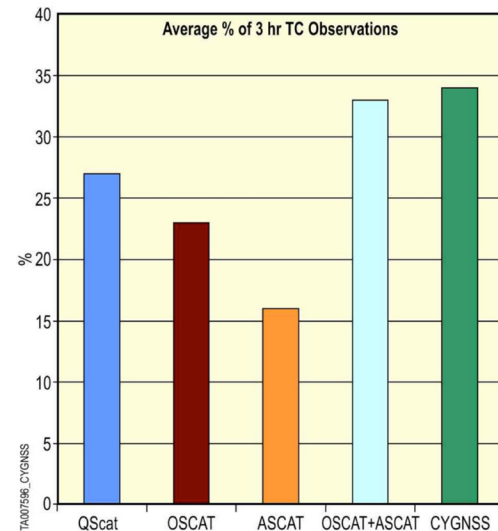
The system will allow us to probe the inner core of hurricanes for the first time from space to better understand their rapid intensification.

—**Christopher Ruf** [University of Michigan—CYGNSS Principal Investigator]

⁴ Venture Class missions are intended to be principal-investigator-led, rapidly developed, cost-constrained missions/instruments for NASA’s Earth Science Division. The September–October 2010 issue of *The Earth Observer* [Volume 22, Issue 5, pp. 13-18] described the program. CYGNSS was selected in June 2012 from among several proposals submitted for the EV-2 Announcement of Opportunity.

Figure 2. These graphs show the percentage of times the center of named tropical cyclones were observed by either the QuikSCAT (blue) or ASCAT (orange) polar-orbiting scatterometers during the 2007 Atlantic [*top graph*] and Pacific [*bottom graph*] hurricane season. Poor performance results from the coverage gaps and infrequent revisit times are characteristic of polar-orbiting wide-swath imagers.

Figure 3. This graph shows the percentage of three-hour intervals during the 2005 Atlantic hurricane season in which each of three ocean wind scatterometers [QuikSCAT (QScat), OSCAT, and ASCAT] would have sampled the inner core region of every tropical cyclone that occurred that year. Also included is the percentage sampled by the combined OSCAT+ASCAT constellation (since these two scatterometers are currently operational) and the percentage that would have been sampled by CYGNSS, had it been in orbit at the time. CYGNSS will have a substantially higher sampling capability of tropical storm inner core regions than any one scatterometer—and will be comparable to the combined capabilities of ASCAT and OSCAT.



CYGNSS relies on an innovative design that will deploy eight observatories flying together in a constellation—an approach that has a heritage in Earth science observations.

CYGNSS observations are expected to achieve over those from current scatterometers, using the 2005 Atlantic hurricane season as an example.

CYGNSS Measurement Concept: Constellation Flying Provides More Coverage

CYGNSS relies on an innovative design that will deploy eight observatories flying together in a constellation—an approach that has a heritage in Earth science observations. For example, the A-Train⁵ constellation consists of several satellite missions flying within precise distances of one another. NASA and its partners have also deployed multiple satellites from a single launch vehicle. The Gravity Recovery and Climate Experiment (GRACE⁶) satellites, for example, were launched by the same vehicle and fly in precision formation—a key feature of the mission concept. Similarly, the CloudSat and the Cloud–Aerosol Lidar and Infrared Pathfinder Satellite Observations (CALIPSO) satellite missions were comanifested. However, as one might expect, launching eight satellites from a single launch vehicle presents new engineering challenges that must be carefully planned and executed.

As described earlier, sampling by a single observatory results in both poor spatial coverage and temporal resolution of tropical cyclone evolution. The constellation approach overcomes these limitations—see *Coverage Comparison: CYGNSS Constellation versus ASCAT* on the next page. The constellation will sample the ocean more frequently than a single satellite would, resulting in a more highly resolved view of the ocean’s surface. Each observatory simultaneously tracks scattered signals from up to four independent transmitters in the operational GPS network. The number of observatories and orbital inclination are chosen to optimize the tropical cyclone sampling properties. The result is a dense cross-hatch of sample points on the ground that cover the critical latitude band between $\pm 35^\circ$ with an average revisit time of 4.0 hours. The spatial coverage possible with CYGNSS is illustrated in **Figure 4** on the next page.

The CYGNSS Observatories: Eight Self-contained Digital Doppler Mappers

The CYGNSS observatory design accommodates the solar power arrays, the GNSS antennas required by the Delay Doppler Mapping Imager (DDMI), and other launch

⁵ “A-Train” is the popular nickname for the Afternoon Constellation of satellites that includes NASA’s Aqua, Aura, CloudSat, and the Cloud-Aerosol Lidar and Infrared Pathfinder Satellite Observations (CALIPSO) missions, as well as the Japan Aerospace Exploration Agency’s (JAXA) Global Change Observation Mission-Water (GCOM-W1). The second Orbiting Carbon Observatory (OCO-2) is expected to join them in 2014. For more information, visit: atrain.nasa.gov.

⁶ A description of the GRACE mission and its accomplishments during its first ten years in orbit appears in the March–April 2012 issue of *The Earth Observer* [Volume 24, Issue 2, pp. 4–13].

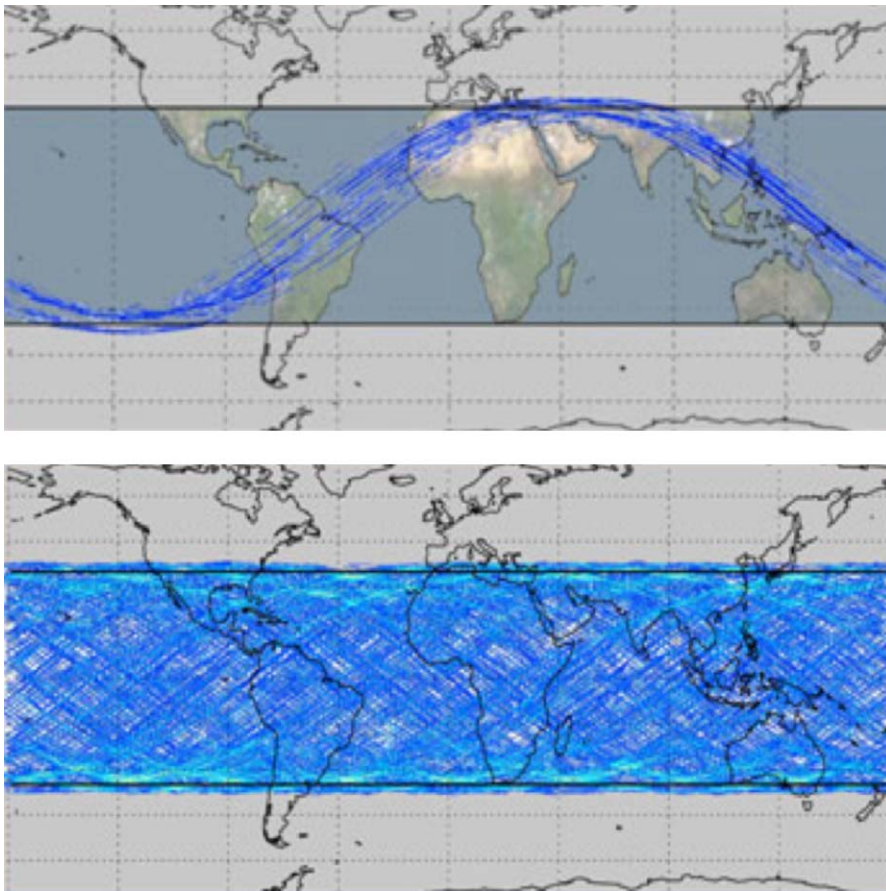
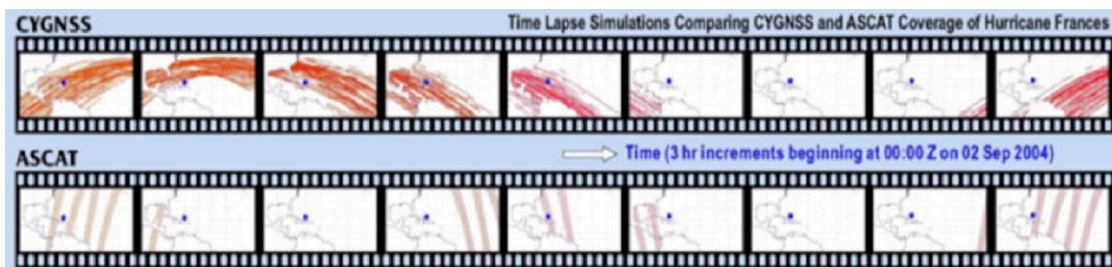


Figure 4: Each low-Earth-orbiting CYGNSS observatory will orbit at an inclination of 35° and be capable of measuring 4 simultaneous reflections, resulting in 32 wind measurements per second across the globe. The orbit inclination was selected to maximize the dwell time over latitudes at which hurricanes are most likely to occur. The result will be high-temporal-resolution wind-field imagery of tropical cyclone genesis, intensification, and decay. Shown here are planned CYGNSS ground tracks for 90 minutes [*top*] and a full 24-hour period [*bottom*].

constraints—see **Figure 5** on the next page. The design also incorporates functional and selective redundancy for critical systems. Observatory attitude is three-axis stabilized using horizon sensors, a magnetometer, pitch momentum wheels, and torque rods. Observatory mass and power are estimated to be ~18 kg (~40 lbs) and ~49 W, respectively.

Coverage Comparison: CYGNSS Constellation versus ASCAT

This figure depicts a time-lapse simulation comparing the spatial and temporal sampling properties of CYGNSS [*top row*] and ASCAT [*bottom row*], assuming they had both been in orbit on September 2, 2004, when Hurricane Frances made U.S. landfall. Data from satellite coverage models for both ASCAT and CYGNSS were projected onto archival storm track records for Frances to create the maps. Each frame represents all samples taken within a three-hour interval. The inner core of Frances is shown as a large blue dot in each frame. ASCAT, with its relatively narrow swath width, does not sample the inner core very frequently, whereas the much wider and more dispersed effective swath of the CYGNSS constellation would have allowed for much more-frequent sampling. The average revisit time for inner-core sampling for CYGNSS is predicted to be 4.0 hours, with a median revisit time of 1.5 hours.



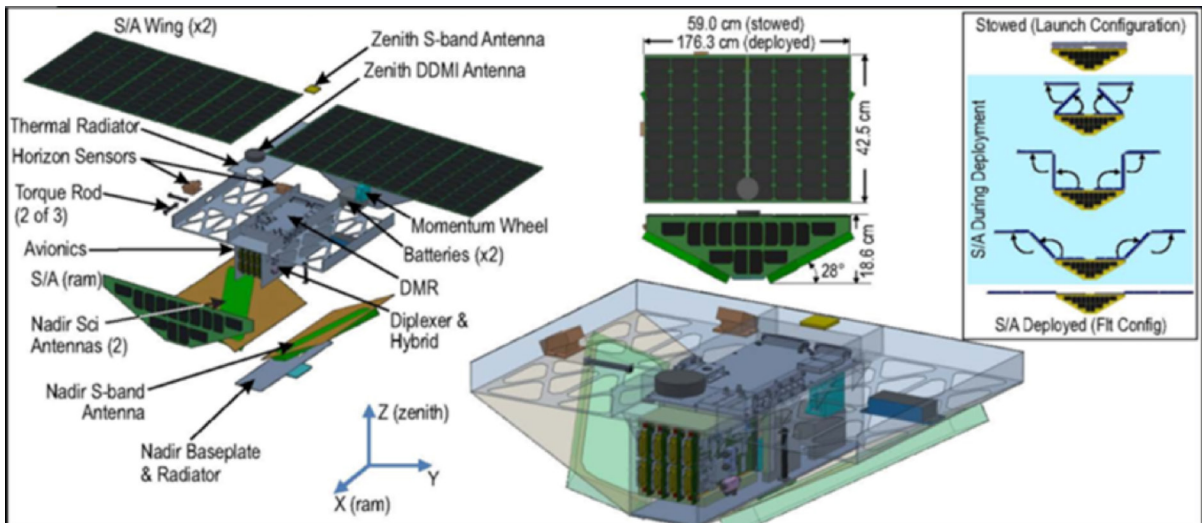


Figure 5. This figure shows a CYGNSS observatory. The exploded view shows individual subsystems, including the science payload's Delay Doppler Mapping Imager (DDMI) antennas and receiver electronics [DMR]. Solar array deployment, performed after ejection from the launch deployment module, is also illustrated.

The onboard systems have been designed to minimize the need for ground-based, time-tagged command sequences for each observatory for routine operations. This helps to enable a simplified and automated sequence of science observations and engineering calibration procedures that can operate unattended during normal Science Mode.

Each observatory is deployed from the launch vehicle with solar arrays stowed, and can remain in this configuration indefinitely. After deployment from the launch vehicle, each observatory transitions automatically through three initial states before reaching *Standby Mode*, where it will remain until all eight satellites are ready for use. Upon completion of commissioning activities, the observatories will transition into the *Science Mode* of operation. At this point, aside from the brief engineering verification test modes described below, the DDMI is set to Science Mode for the duration of the mission⁷. In Science Mode, subsampled Delay Doppler Maps (DDMs) are generated onboard and downlinked with a 100% duty cycle.

In developing the design concepts for the CYGNSS observatories, the systems engineering team sought to ensure the safety of the observatories without ground intervention. The onboard systems have been designed to minimize the need for ground-based, time-tagged command sequences for each observatory for routine operations. This helps to enable a simplified and automated sequence of science observations and engineering calibration procedures that can operate unattended during normal Science Mode. With the DDMI in its Science Mode, the observatory is set to maintain all nominal operations without additional commands. The primary “routine” activity performed on a regular basis is communication with the ground network to downlink the accumulated science and engineering data.

Launch/Commissioning Activities

CYGNSS is currently scheduled for launch in 2016; details (e.g., location and launch vehicle) are still to be determined. After launch, the mission begins with *engineering commissioning* of the observatories and science instruments. Additional *science commissioning* activities for the observatories will begin once the solar arrays are deployed on every observatory in the constellation and will continue for a period of two-to-four weeks.

Engineering Commissioning

Since each observatory functions independently, *engineering commissioning* activities for satellites and instruments may progress in an interleaved manner: Within a single communications pass, activities will be performed on a single observatory; however, it is not necessary to complete all commissioning tasks on one observatory before progressing to the next observatory in the constellation. Similarly, it is also unnecessary to ensure that each observatory is at the same “step” in a commissioning sequence. This independence allows a flexible scheduling approach to be used in setting up commissioning passes and does not delay commissioning activities for all observatories if a single satellite requires extra time while an off-nominal issue is being addressed.

⁷ The only other interruption to Science Mode will be brief returns to *Calibration/Validation Mode* performed biannually—see **Data Products** section for details.

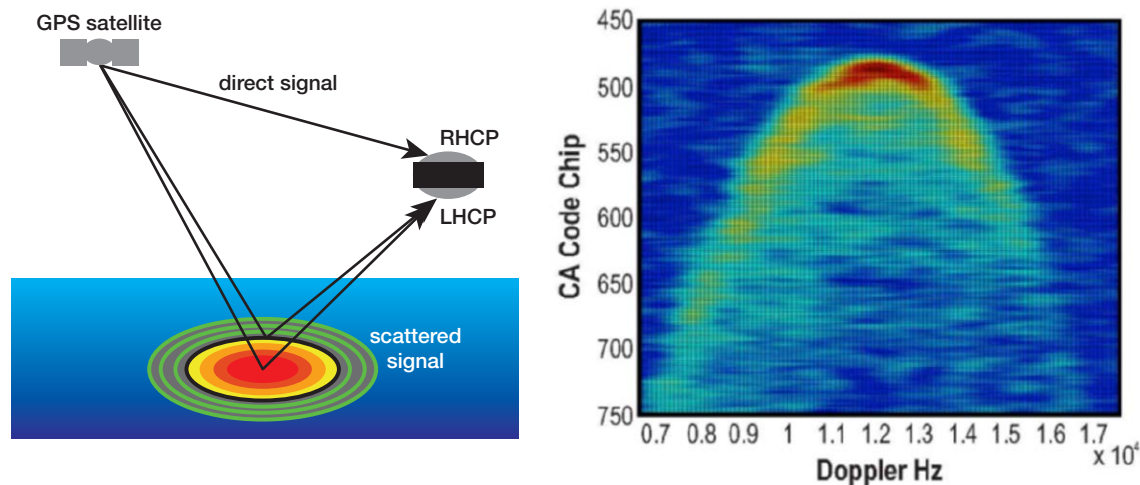
CYGNSS Heritage: Using GPS Reflectometry for Geophysical Measurements

For some years, GPS receivers have been used to provide position, velocity, and time measurements to satellite platforms in low Earth orbit. In a similar way, they are also used for ground-based navigation. Beyond navigation however, GPS signals have been increasingly used for remote sensing. Signals at *L-band*¹—with a bandwidth between 2 and 20 MHz—are broadcast globally from an altitude of ~20,000 km (~12,427 mi) and are used to measure, amongst other things, tectonic plate motion and ionospheric and tropospheric parameters. Furthermore, signals from other Global Navigation Satellite Systems (GNSS²) are becoming available: There will soon be more than 120 such signal sources in space.

The United Kingdom Disaster Monitoring Constellation (UK-DMC-1³) space-based demonstration mission showed that a microsatellite-compatible passive instrument potentially could make valuable geophysical measurements using *GPS reflectometry*. The left side of the figure below diagrams how the process works. The direct GPS signal is transmitted from the orbiting GPS satellite and received by a right-hand circular polarization (RHCP) receive antenna on the *zenith* (i.e., top) side of the spacecraft that provides a coherent reference for the coded GPS transmit signal. The quasispecular, forward-scattered signal that returns from the ocean surface is received by a *nadir*- (i.e., downward-) looking left-hand circular polarization (LHCP) antenna on the nadir side of the spacecraft. The scattered signal contains detailed information about its roughness statistics, from which local wind speed can be derived.

The image on the right below shows *scattering cross section* as measured by UK-DMC-1 and demonstrates its ability to resolve the spatial distribution of ocean surface roughness. This type of scattering image is referred to as a *Delay Doppler Map* (DDM).

There are two different ways to estimate ocean surface roughness and near-surface wind speed from a DDM. The *maximum scattering cross-section* (the darkest shades in the graph) can be related to roughness and wind speed.



[Left.] GPS signal propagation and scattering geometries for *ocean surface bistatic quasispecular scatterometry*. The position of the spacecraft is determined from the direct GPS signal; the surface winds are determined by the indirect signal (scattered off the ocean surface). Combining the position and scattering information allows for the creation of Delay Doppler Maps (DDM), from which ocean surface vector wind speeds can be inferred. [Right.] An example DDM showing the spatial distribution of the ocean surface scattering measured by the UK-DMC-1. Scattering cross section is plotted as a function of Doppler Shift (x-axis) and propagation time of flight (y-axis), which is measured in units of Coarse Acquisition GPS Code or “Chips.” See text for further details.

¹ The L-band portion of the electromagnetic spectrum covers the range from 1 to 2 GHz, and is commonly used for satellite communications.

² The current Global Navigation Satellite System (GNSS) currently includes two fully operational networks: the U.S. Global Positioning Satellite (GPS) system and the Russian Globalnaya Navigatsionnaya Sputnikovaya Sistema (GLONASS). By 2020 the European Union [Galileo] and China [COMPASS] should have fully functional GNSS systems. Other nations are also working on their own systems, that may eventually become part of the network.

³ The Disaster Monitoring Constellation (DMC) was deployed in 2003. It was constructed by a U.K.-based company called Surrey Satellite Technology Ltd. (SSTL) and the University of Surrey (Guildford, U.K.), and is comprised of several remote sensing satellites operated for the Algerian, Nigerian, British, and Chinese governments by DMC International Imaging.

This, however, requires *absolute calibration* of the DDM, which is not always available. Wind speed can also be estimated from a *relatively calibrated* DDM, using the *shape of the scattering arc* (the lighter shades in the graph). The arc represents the departure of the actual *bistatic scattering* from the theoretical *purely specular case*—i.e., scattering from a perfectly flat ocean surface—which appears in the DDM as a single-point scatterer. The latter approach imposes more-relaxed requirements on instrument calibration and stability than does the former. However, it derives its wind speed estimate from a wider region of the ocean surface, and thus has lower spatial resolution.

After UK-DMC-1, development of wind-speed retrieval algorithms from DDMs became an active area of research and resulted in the design of a new instrument called the Space GNSS Receiver – Remote Sensing Instrument (SGR-ReSI⁴). Like its predecessor, the instrument can make valuable scattering measurements using GPS, but it has greater onboard data storage capacity and can process the raw data into DDMs in real time. It also has been designed with flexibility so it can be programmed while in orbit for different purposes—e.g., tracking new GNSS signals when needed, or applying spectral analysis to received signals.

In effect, the SGR-ReSI fulfils in one module what has historically been handled by three separate units on earlier spacecraft. Specifically,

- it performs all the core functions of a space GNSS receiver, with front-ends supporting up to eight single or four dual-frequency antenna ports;
- it is able to store a quantity of raw sampled data from multiple front ends, or processed data in its one-gigabyte solid-state data recorder; and
- it has a dedicated reprogrammable field-programmable gate array (FPGA) coprocessor (a Xilinx *Virtex 4*).

Each CYGNSS observatory will be equipped with a Digital Doppler Mapping Instrument (DDMI), based on the SGR-ReSI design. The DDMI will generate DDMs continuously at a low data rate, which will provide a source for ocean roughness measurements across the ocean. In special situations, such as when passing over an active tropical cyclone, the instrument can be operated in *Raw Data Mode*, where 60 seconds of raw sampled data is accumulated. This allows researchers to fully analyze and re-analyze the acquired data using different processing schemes to ensure that the nominal DDM mode of operation is not losing important geophysical data.

⁴ SSTL and the University of Surrey teamed with the National Oceanographic Centre in Southampton, U.K., University of Bath, and Polar Imaging Ltd. to develop SGR-ReSI.

A large wind field intercomparison database will be assembled from a variety of sources including buoys, other satellite-based instruments, and global meteorological and oceanographic model assimilations.

Science Commissioning

Science commissioning takes place after engineering commissioning activities are completed. At this time, the observatory will be operated in its nominal Science Mode, and preliminary Level-2 (L2) wind speed data products⁸ will be produced. A large wind field intercomparison database will be assembled from a variety of sources including buoys, other satellite-based instruments, and global meteorological and oceanographic model assimilations. During science commissioning the ground-processing algorithms used to produce L2 data will be refined. The data assimilation tools, which ingest L2 data into numerical weather prediction forecast models, are also tested.

Ground System Overview

The CYGNSS ground system—shown in **Figure 6**, next page—consists of: a Mission Operations Center (MOC), located at the Southwest Research Institute's (SwRI) Planetary Science Directorate in Boulder, CO; a Science Operations Center (SOC), located at the University of Michigan's Space Physics Research Laboratory in Ann Arbor, MI; and a Ground Data Network, operated by Universal Space Network (USN) and

⁸ A list of planned CYGNSS data products appears at aoss-research.engin.umich.edu/missions/cygnss/data-products.php. Data are expected to be publicly available about a year after launch.

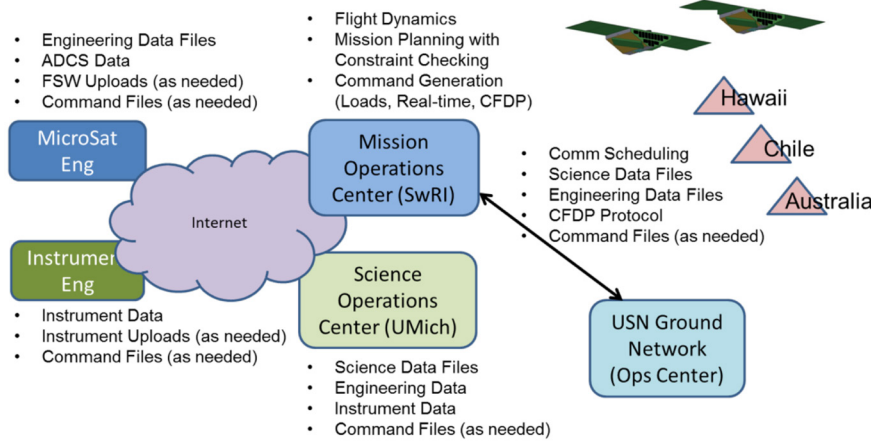


Figure 6. Diagram showing an overview of the components of the CYGNSS ground system.

consisting of existing *Prioranet*⁹ ground stations in South Point, HI, in Santiago, Chile, and in Western Australia, some 400 km (~248.5 mi) south of Perth, and at the MOC facility. Additional interfaces between the MOC and the microsat engineering team and the DDMI instrument engineering teams are also supported. The MOC coordinates operational requests from all facilities and develops long-term operations plans. Each of these components is described in more detail below.

Mission Operations Center (MOC)

During the mission the CYGNSS MOC is responsible for mission planning, flight dynamics, and command and control tasks for each of the observatories in the constellation. These primary MOC tasks include:

- Coordinating activity requests;
- scheduling ground network passes;
- maintaining the Consultative Committee for Space Data Systems (CCSDS) File Delivery Protocol (CFDP) ground processing engine;
- collecting and distributing engineering and science data;
- tracking and adjusting the orbit location of each observatory in the constellation;
- trending microsat data;
- creating real-time command procedures or command loads required to perform maintenance and calibration activities; and
- maintaining configuration of onboard and ground parameters for each observatory.

Science Operations Center (SOC)

The CYGNSS SOC will be responsible for the following items related to calibration/validation activities, routine science data acquisition and special requests, and data processing and storage:

- Supporting DDMI testing and validation both prelaunch and on-orbit;
- providing science operations planning tools;
- generating instrument command requests for the MOC;
- processing Levels 0 through 3 science data; and

The CYGNSS ground system consists of: a Mission Operations Center (MOC), located at the Southwest Research Institute’s (SwRI) Planetary Science Directorate in Boulder, CO; a Science Operations Center (SOC), located at the University of Michigan’s Space Physics Research Laboratory in Ann Arbor, MI; and a Ground Data Network, operated by Universal Space Network (USN) and consisting of existing Prioranet ground stations in South Point, HI, in Santiago, Chile, in Western Australia, some 400 km (~248.5 mi) south of Perth, and at the MOC facility.

⁹ *Prioranet* was specifically designed for comprehensive communications and ground support to Earth-orbiting satellite. For more information, visit: www.scspace.com/ground-network-prioranet-1.

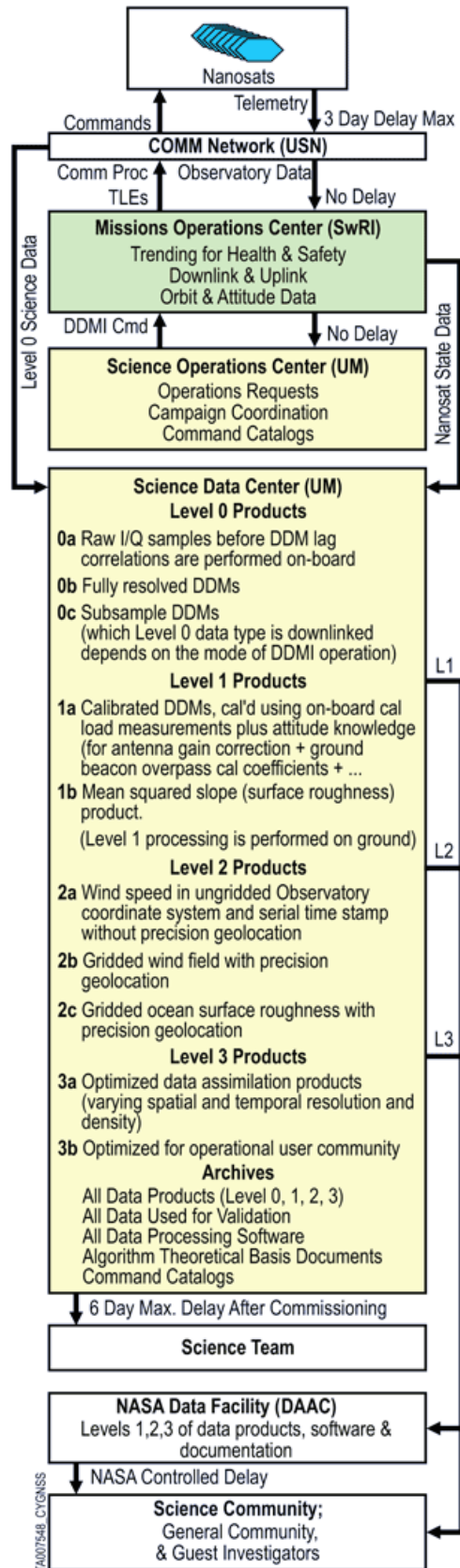


Figure 7. CYGNSS Data Flowchart. This figure illustrates how the data flows from the CYGNSS observatories to the various elements of the ground system for processing, to the DAAC for archiving, to the science team for analysis, and ultimately to the broader user community for application. The planned CYGNSS data products are also listed.

- archiving Level 0-3 data products, DDMI commands, code, algorithms, and ancillary data at a NASA Distributed Active Archive Center.

Ground Data Network

CYGNSS selected USN to handle ground communications because of their extensive previous experience with missions similar to CYGNSS. Collocation of a back-up CYGNSS MOC server at the USN Network Management Center (NMC) can also be supported.

Each of the observatories in the CYGNSS constellation will be visible to the three ground stations within the USN for periods that average between 470 and 500 seconds of visibility per pass. Each observatory will pass over each of the three ground stations six-to-seven times each day, thus providing a large pool of scheduling opportunities for communications passes. MOC personnel will schedule passes as necessary to support commissioning and operational activities. High-priority passes will be scheduled to support the solar array deployment for each observatory.

For all subsequent stages, the MOC schedules nominal passes for the USN stations for each observatory in the constellation per the USN scheduling process. Each observatory can accommodate gaps in contacts with storage capacity for greater than 10 days' worth of data with no interruption of science activities.

Data Products

The data returned from CYGNSS are expected to expand our knowledge of the rapidly changing environment in the core of a developing tropical cyclone—see **Figure 7** for details on data flow and a list of planned CYGNSS data products. The SOC is responsible for data product development and dissemination. After science commissioning is complete and the mission enters its nominal science operations stage, the L2 data will be made available for public release. The CYGNSS science team members will use the fully calibrated L2 data for their own research and make it available to the external user science community and eventually to operational users. Calibration/validation assessment of L2 data quality continues for the life of the mission using an updated version of the same wind field intercomparison database used during science commissioning. Twice a year, nominally at the beginning and end of the Atlantic hurricane season, engineering performance will be verified by a brief (approximately two-week) repeat of the instrument calibration activities performed during engineering commissioning.

Application of CYGNSS to Hurricane Forecasting

As stated above, the primary goals of CYGNSS are to measure ocean surface wind speeds in all weather conditions—including those inside the eyewall—and measuring wind speed with sufficient frequency to resolve genesis and rapid intensification in the inner core of a tropical cyclone. In addition to success with these two primary objectives, there

is likely to be a secondary benefit with direct societal relevance: The CYGNSS team will produce and provide ocean surface wind speed data products to the operational hurricane forecast community and help them assess the value of these products for use in their retrospective studies of potential new data sources. In time, this information will be incorporated into models used to predict the evolution of hurricanes.

While improved hurricane forecasting is not the CYGNSS mission's primary objective, it is hoped that hurricane prediction—in particular, hurricane intensity forecasts—will improve as a result of the data that the CYGNSS mission returns.

Acknowledgment

Parts of this article have been extracted from some proceedings papers of a recent technical conference focusing on CYGNSS. The citations for those papers can be found at aoss-research.engin.umich.edu/missions/cygnss/reference-material.php.

For More Information

Some of the text and graphics that appear in this article have been extracted from these sources and adapted for use in *The Earth Observer*:

General information about the CYGNSS mission (e.g., science, technology, data products)

CYGNSS-Michigan.org.

List of references on topics mentioned herein (e.g., GNSS, ocean surface scattering, aircraft observations, spaceborne observations)

aoss-research.engin.umich.edu/missions/cygnss/reference-material.php. ■

*While improved hurricane forecasting is **not** the CYGNSS mission's primary objective, it is hoped that hurricane prediction—in particular, hurricane intensity forecasts—will improve as a result of the data that the CYGNSS mission returns.*

Aqua AIRS Version 6 Level 3 Data Release

The Atmospheric Infrared Sounder (AIRS) Project and NASA's Goddard Earth Sciences Data and Information Services Center (GES DISC) are pleased to announce the availability of *Aqua AIRS Version 6 Level 3* data. The AIRS Version 6 processing code has a number of improvements in addition to the Level 2 improvements from which it is built.

Significant changes include:

- Level 3 support products, which contain profile data at 100 vertical levels;
- a "TqJoint" grid, which contains gridded data for a common set of temperature and water vapor observations; and
- water vapor and trace gas products that are now reported both as layer and level quantities.

For additional information and to access to these data, visit:

disc.sci.gsfc.nasa.gov/datareleases/aqua-airs-version-6-level-3.

ESTO: Benefitting Earth Science through Technology

Andrea Martin, Earth Science Technology Office, andrea.s.martin@nasa.gov

Through flexible, science-driven, competitive solicitations, ESTO-funded technologies have supported many Earth observing measurements. Today, the portfolio of ESTO projects consists of nearly 700 active and completed tasks.

Satellites, airborne missions, and complex computer models all require advanced technologies to collect and process Earth observing data to increase our understanding of system phenomena. Demand for more, newer, and higher-quality Earth observations requires smaller, lighter, more-advanced remote-sensing tools as well as advanced data and computing systems. To meet these demands, NASA's Earth Science Division created the Earth Science Technology Office (ESTO). Along with the other ESD programs¹, ESTO is helping to ensure that quality Earth science data are being collected and used for a more-complete understanding of the planet.

ESTO was established in 1998 to manage the development of technologically advanced, reliable, and cost-effective components, instruments, and information systems that would help NASA meet its science objectives. Through flexible, science-driven, competitive solicitations, ESTO-funded technologies have supported Earth observing measurements, as well as some space science activities and commercial applications. Today, the portfolio of ESTO projects consists of nearly 700 active and completed tasks. These projects represent work at over 100 different government institutions, universities, and private corporations. More than 37% of "graduated" ESTO technologies have been infused into Earth-observing spaceborne and airborne missions, operational modeling systems and information networks, commercial uses, and other NASA purposes outside of the Earth sciences. An additional 43% of projects have a path identified for possible infusion.



ESTO employs an end-to-end approach to technology development. The investment strategies are planned carefully by working closely with the science and technology community to identify upcoming technology needs that could help fill mission and science requirements. The needs are met through competitive peer-reviewed solicitations to fund varying projects with differing methods to best address community requirements. ESTO often funds several projects that work toward advancing a similar technology or meeting a specific mission's requirements. Funding competing technologies ensures that future Earth science objectives can and will be met. ESTO assesses the maturity of funded technologies and leverages investments by working closely with other NASA programs and partnering with federal agencies, academia, and industry. Therefore, the end products—based on needs of the community and selected competitively and completed collaboratively—have a high likelihood of being infused into future missions and measurements.

The ESTO projects are managed through two main program areas: *Observation Technology* and *Information Technology*. A pilot program area, In-Space Validation of Earth Science Technologies (InVEST), was recently added to validate observation and/or information technologies from space. The Observation Technology Program is responsible for the Instrument Incubator Program (IIP), which supports projects that develop technologies that lead to Earth-observing instruments, sensors, and systems; and the Advanced Component Technologies (ACT) program, which supports projects that develop components and instrument subsystems. The Information Technology Program manages the Advanced Information Systems Technology (AIST) projects that process, archive, access, and visualize Earth-science data for the benefit of the Earth-science community. Each of these components will be discussed in more detail here.

Observation Technology Program

Instrument Incubator Program

The IIP fosters the development and assessment of innovative ground-based, aircraft-based, and engineering demonstrations of new remote sensing instrumentation.

¹ Other ESD programs include Flight, Research and Analysis, and Applied Sciences.

Projects managed by IIP develop smaller, lighter instruments, which often take less time to build and cost less than the development of traditional instrumentation. By funding new instruments very early in their life cycle and then demonstrating their performance, IIP projects that are slated for space-based applications typically encounter less development risk, lower cost, and reduced schedule overruns when the instrumentation for satellites is developed.

Most of the current IIP investments are directly tied to the needs of NASA's Decadal Survey missions². For example, the upcoming Hyperspectral Infrared Imager (HyspIRI) mission will require a spaceborne thermal infrared (TIR) imager as one of its two major instruments³. To demonstrate a possible TIR technology prior to mission implementation, ESTO funded Principal Investigator (PI) **Simon Hook** [NASA/ Jet Propulsion Laboratory (JPL)] to develop and test the airborne Hyperspectral Thermal Emission Spectrometer (HyTES). Airborne HyTES data can be used to help HyspIRI scientists and engineers determine the optimal band locations for the TIR instrument on the spaceborne platform and can be used by the science community to gather high-resolution surface temperature and emissivity measurements. These data can be used for a variety of studies, including observing thermal and gas anomalies from volcanoes. Measurements over different land-surface types and emissions such as sulfur dioxide, methane, and ammonia could also be used to help determine whether HyTES could be useful for in-depth gas studies.

In addition, HyTES offers both high spatial and spectral resolution—a feature not found on current NASA hyperspectral thermal imagers. This compact instrument collects data in the spectral range of 7.5–12 μm . The success of the first test flights indicates that HyTES could be a valuable resource for both refining the measurement requirements for HyspIRI's TIR instrument and for the science community to use in various ecosystem and natural-disaster applications. Since the initial flights⁴ HyTES team members have been working on various improvements to the instrument. HyTES will fly again in coming months to acquire new data over selected sites to assess these improvements and evaluate the data's suitability for science studies.

Advanced Component Technologies

The ACT program funds and manages subsystem-level technologies that can include altimeters, control systems, or laser systems used for lidar. The ACT also develops new ways to perform measurements and to process data products to expand research and application capabilities. Some technologies developed under ACT are directly infused into mission designs by flight projects, while others graduate to different programs, like IIP, for further development and testing.

The ACT program investments can offer answers to big questions with difficult solutions. For example, the proposed Active Sensing of CO₂ Emissions over Nights, Days, and Seasons (ASCENDS) mission will need a high-power fiber-laser source to measure oxygen (O₂) from space. This measurement can be used to help determine the mixing ratio of carbon dioxide (CO₂) in the atmosphere. An ACT-managed project titled *Laser Remote Sensing of O₂ for Determination of CO₂ Mixing Ratio and Sensing of Climate Species*, led by PI **Jeremy Dobler** [ITT Exelis Geospatial Systems], is one ESTO project that has been tasked with developing the instrumentation and algorithms that could make O₂ measurements from space possible, leading to a more-complete picture of Earth's changing climate. Measurements like this will be key to the success of the planned ASCENDS mission.



This spectral cube represents HyTES-collected data over Cuprite, NV—a mining district commonly used for hyperspectral imaging testing and calibration/validation flights—on July 20, 2012. The data were collected as part of HyTES' first flights. The three bands [150 (10.08 μm), 100 (9.17 μm), and 58 (8.41 μm)] are displayed as red, green, and blue respectively as an image cube.
Image credit: Simon Hook

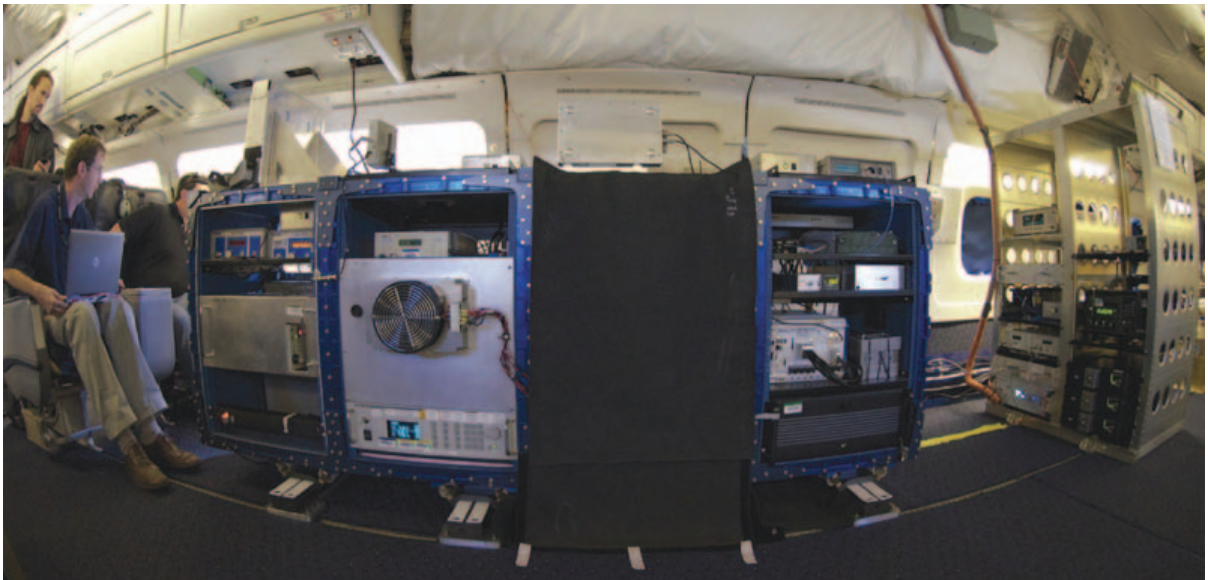
² Following completion of the first Decadal Survey in 2007, the National Research Council prioritized 15 satellite missions to enable NASA to provide the public with ongoing information about global climate and climate change. To learn more about the program, visit: nasascience.nasa.gov/earth-science/decadal-surveys.

³ To learn more about progress of plans for HyspIRI, see page 38 of this issue.

⁴ HyTES had its first flight in the summer of 2012.

The mechanisms inherent to optical fibers set an upper limit on the achievable amplified power, so meeting the power and efficiency needed for ASCENDS' lidar is an extremely difficult task. This, however, is precisely the kind of technology development challenge that the ACT program can address.

Dobler's team is developing an *integrated path differential-absorption* (IPDA) lidar instrument to meet ASCENDS' requirements for measuring O₂. As part of the IPDA development effort, the team has developed the first high-power, narrow-spectral-linewidth fiber-laser source at a wavelength of 1262 nm—which corresponds to an O₂ absorption feature that can be used for spectroscopic lidar measurements. This achievement was made onboard a NASA DC-8 in 2011; however, the power of the amplifier was lower than the 5 W necessary to take these same measurements from space. Mechanisms inherent to optical fibers set an upper limit on the achievable amplified power, so meeting the power and efficiency needed for ASCENDS' lidar is an extremely difficult task. This, however, is precisely the kind of technology development challenge that the ACT program can address. The program is funding efforts to help develop fibers through various techniques, including doping phosphosilicate fibers with additional elements such as fluorine. These specialty fibers are under development and testing as part of a second ACT project; therefore, Dobler's team should be able to overcome the fiber power limitations to meet the requirements necessary to take O₂ measurements from space in the 1260 nm spectral band. This is an example of how ACT's investments in exploring various solutions for required component technology are helping to ensure that upcoming missions will be able to meet their measurement requirements.



Fisheye lens photo of CO₂ and O₂ components integrated on the NASA DC-8 aircraft, from 2011. **Image credit:** Jeremy Dobler

Information Technology Program

Advanced Information Systems Technology

The AIST identifies, develops, and demonstrates advanced information system technologies to increase the accessibility and utility of Earth science data, and to enable new science measurements and information products to be used by the scientific and applications communities. Typical AIST projects include modeling tools, sensor webs, data processors, and visualization tools. Some AIST projects augment existing tools—such as NASA's Land Information System (LIS) model.

Land-use and water-resource managers often make decisions that rely on information calculated by specialized computer models like LIS. A key feature of this modeling software is the ability to assimilate NASA land-surface observations into land-surface models. The conventional data assimilation approach used by LIS and other NASA data assimilation systems assumes that model state predictions are unbiased relative to the observations. As a result, additional techniques are needed to remove such systematic errors prior to incorporating Earth observations. The ESTO's AIST program has funded a project that addresses this issue by designing and implementing optimization and uncertainty modeling tools to enhance LIS. **Christa Peters-Lidard** [NASA's

Goddard Space Flight Center—*PI* led the LIS-Optimization (LIS-OPT) and LIS-Uncertainty Estimation (LIS-UE) efforts, which added new infrastructure to LIS to augment existing data assimilation capabilities. The goal was to improve modeling using both parameter estimation and uncertainty estimation. The new LIS gives decision makers both improved environmental prediction and uncertainty information.

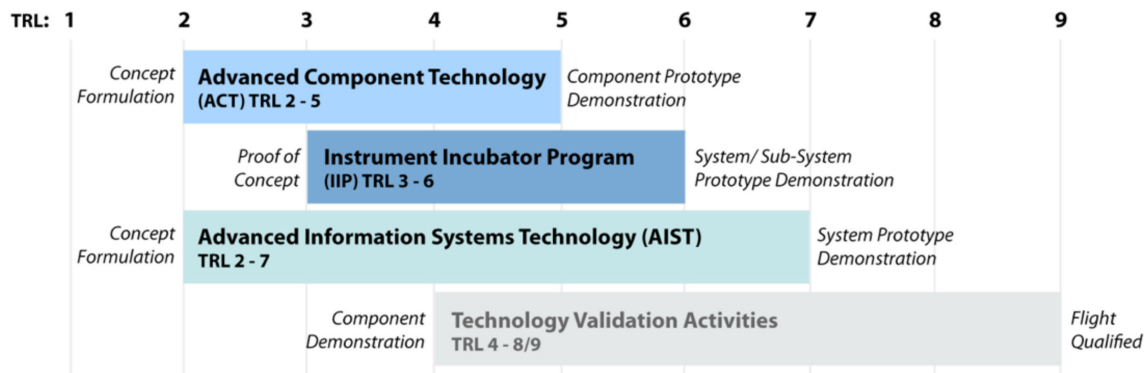
The project team conducted case studies and *observing system simulation experiments* (OSSEs) to compare the LIS outputs before and after the inclusion of LIS-OPT and LIS-UE. The first OSSE focused on using NASA observations to improve the values and uncertainty estimates of *soil hydraulic properties*—key land-surface model parameters. These improvements translated to improved land-surface model predictions and reduced uncertainty. Because one case study (Walnut Gulch, AZ) covered data from a limited time, this OSSE highlighted the observation that LIS-OPT used in conjunction with LIS-UE could be a useful strategy for mitigating bias prior to assimilating datasets from newly launched missions. This could mean that new mission data, like the soil moisture data that will be collected by the upcoming Soil Moisture Active Passive (SMAP) mission⁵, will be available for parameter refinement soon after they are collected—as opposed to waiting for a longer data record to accrue. This is just one example of an AIST project that is leading to major improvements in increasing the reliability of modeling NASA-generated Earth-observation data.

The new Land Information System (LIS) gives decision makers both improved environmental prediction and uncertainty information.

Technology Readiness Levels

The progress of ESTO projects is monitored through the use of Technology Readiness Levels (TRLs). This nine-point scale helps to categorize emerging technologies in terms of their readiness for infusion, with TRL 9 being “mission proven” though successful mission operations on either ground or in space. While the definitions of TRLs are slightly different for software than for the more-common hardware definitions, they remain successful at accurately articulating and reflecting the stages of the software development process.

On average, ESTO projects enter ESTO management at approximately TRL 3. At this level a proof of concept has been met. The ESTO projects “graduate” at a TRL 6, meaning that a model or prototype has been demonstrated in a relevant end-to-end environment. To see a full list of TRLs and a brief description of each level for both hardware and software, visit: esto.nasa.gov/technologists_trl.html.



This graph depicts where ESTO investments generally fall on the TRL scale by program area. **Image credit:** ESTO

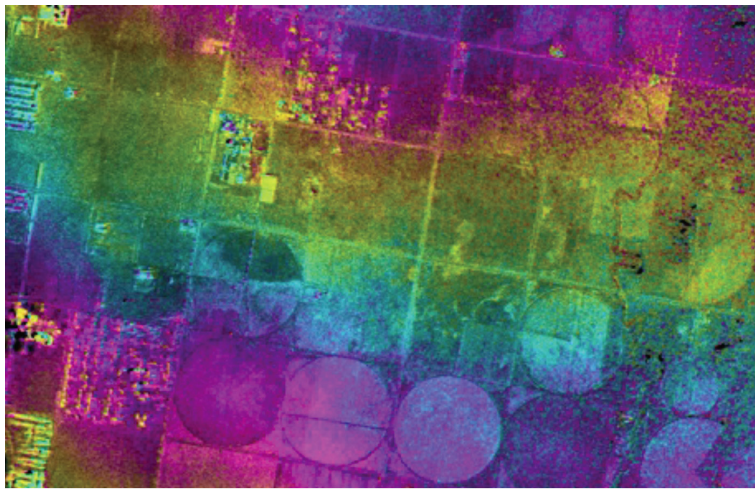
ESTO’s Partnership Program

The ESTO often works closely with partner groups within NASA’s ESD on technologies of shared interest. For instance, ESTO has teamed with the Research and Analysis (R&A) program to integrate existing instruments—often instruments that were first funded as part of an IIP solicitation—into platforms managed by NASA’s Airborne Science Program. The Airborne Instrument Technology Transition (AITT) program

⁵ Read more about the progress of SMAP calibration/validation efforts in preparation for its 2014 launch on page 32 of this issue.

for example—funded by R&A and managed in conjunction with ESTO—provides campaign-ready airborne instrumentation that can participate in field experiments, evaluates satellite instrument concepts, and provides calibration and validation of spaceborne instruments.

Consequently, AITT projects support many of NASA's Decadal Survey Earth-observing missions—one example being the second Ice, Cloud, and land Elevation Satellite (ICESat-2) that will collect valuable measurements on ice sheets and sea ice. The concern is that undersampling, especially in glacial areas, could lead to ice-volume estimation errors. Airborne instruments can help bridge these impeding data gaps. In 2009, as part of International Polar Year, a swath-mapping airborne sensor flew over Greenland, collecting data for high-resolution ice-surface topography maps to gain a clear picture of ice volume in that area. **Delwyn Moller** [Remote Sensing Solutions—*PI*], led an AITT-funded effort to take what was learned during that airborne campaign and develop an improved, permanently available, K_a -band Uninhabited Aerial Vehicle Synthetic Aperture Radar (UAVSAR)-configured interferometer. The instrument—named the Airborne Glacier and Land Ice Surface Topography Interferometer (GLISTIN-A)—has modified the International Polar Year interferometer that flew over



0 2 4 6 8 10 12 14

First-look at uncalibrated elevation data (in meters) obtained by GLISTIN-A over the Rosamond Lake area in Los Angeles County, CA, from an altitude of about 5.7 miles (~9.2 km). **Image credit:** Delwyn Moller

Greenland with a new K_a -band up-and-down-converter chain and a state-of-the-art solid-state power amplifier. These improvements will allow higher peak transmit power and the ability to *ping-pong*, a mode of operation that allows the antenna to alternately transmit and receive, which improves the vertical accuracy of data. The current configuration of GLISTIN-A is being transitioned for flight on the NASA Global Hawk (GLISTIN-H) where it will be able to provide quality data on ice topography in areas that are often deemed too remote for in-depth study. The information the interferometer collects will be able to complement the data collection

by ICESat-2 to provide the cryospheric science community with data collection over areas in the polar regions, like some glacial areas, that might not be routinely sampled by satellite missions.

New and Future Programs

Beyond the challenges being addressed through Earth science technology research and development, other obstacles must be overcome to successfully implement emerging technologies in science missions and campaigns. Once a technology achieves its technical targets in the laboratory, the next step is to show that it can work as designed under real-world operating conditions. *Validation*, performed for airborne and spaceborne platforms, is a critical step in mitigating the risk associated with new technologies that have not been thoroughly tested and verified; this can be a source of mission delays and cost overruns. To mitigate these risks, ESTO is actively facilitating and pursuing opportunities to flight qualify various emerging technologies—such as instrument components and information systems—in relevant environments, through partnerships (like the AITT program described above), both within and outside of NASA. To date, over 70 ESTO technologies have been demonstrated onboard airplanes, uninhabited aerial vehicles, and high-altitude balloons.

The space environment, particularly, imposes harsh conditions on the components and systems of satellite missions that cannot be fully simulated in the confines of Earth's atmosphere. Therefore, instruments and components for spaceborne applications cannot be adequately validated on the ground or as part of an airborne system.

With the advances in small, low-cost “standard” satellites that can gain easy access to space, it is possible to demonstrate and validate some hardware components and information systems. An example is *CubeSats*—10-cm (~4-in)-cube form factor platforms that are launched as secondary payloads on larger satellite missions. CubeSats are leading the way as a standard platform to cost-effectively launch and test new technologies. Costing as little as one-to-two million U.S. dollars, CubeSats are usually built and launched within 18 to 24 months from acceptance of the original concept proposal.

The ESTO recognizes the need for validation in the space environment and the possibilities CubeSats present, and has funded (for example) the development and launch of the Michigan Multipurpose Minisat (M^3), which carries the CubeSat Onboard Processing Validation Experiment (COVE) payload. COVE was developed to address the data-processing needs of future missions that are expected to collect higher-volume and higher-quality data. For example, the Multi-angle Spectropolarimetric Imager (MSPI), which is an IIP project (and a candidate for the Aerosol, Cloud, Ecosystems (ACE) mission concept) will produce 95 megabytes of data per second, per camera, for each of its nine cameras. However, there is currently no way to get that amount of raw data from space to the ground. One solution proposed by the COVE payload was to move the first stage of ground processing to onboard the satellite in a new radiation-hard-by-design *field-programmable gate array* (FPGA). This would reduce downlink requirements by two orders of magnitude. COVE, including the MSPI algorithm and the new FPGA, was launched on the M^3 CubeSat⁶ in 2011. Access to space was enabled via the NASA Human Exploration and Operations Mission Directorate, CubeSat Launch Initiative.

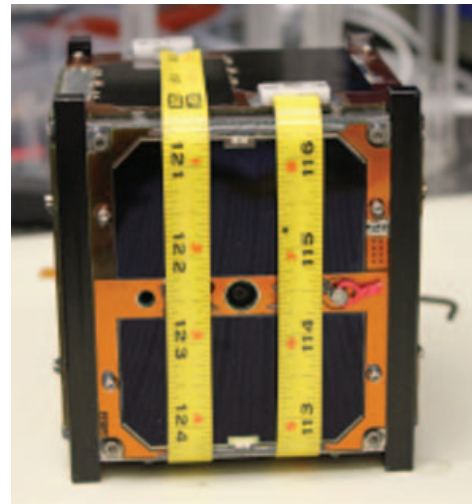
In addition to M^3 , ESTO is developing and implementing other CubeSat projects. For example, the GEOstationary Coastal and Air Pollution Events (GEO-CAPE) Read Out Integrated Circuit (ROIC) Flight Experiment [GRIFEX] project will verify the engineering and performance of an ACT-developed, all-digital, high-frame-rate readout integrated circuit for the GEO-CAPE mission concept. GRIFEX has been designed to meet the specific requirements of GEO-CAPE, but could also be used for other imaging instruments. The Intelligent Payload Flight Experiment (IPEX) will demonstrate the Intelligent Payload Module (IPM)—a candidate for the HypSIRI mission. The IPEX CubeSat will return low-latency data products via direct broadcast. IPM should reduce the HypSIRI raw data rate (in GBps) by a factor of at least twenty. IPEX and a second M^3 CubeSat will be launched in the fall of 2013 on a National Reconnaissance Office satellite mission as secondary payloads.

With the successful experiences of past and current CubeSat projects and the need to validate more technologies than the ones already funded, ESTO has initiated a new pilot program called In-Space Validation of Earth Science Technologies (InVEST). By developing a new program area, highly specialized validation projects can more appropriately be selected and managed. A request for information was released in 2011; the first InVEST solicitation was posted in the fall of 2012⁷ through the NASA Research Opportunities in Space and Earth Sciences (ROSES). By validating Earth science technologies in space long before integration on an Earth-observing mission, the risks involved in developing successful Earth science missions will be reduced. Once validated, existing Earth science related technology is more ready for rapid infusion.

⁶ M^3 was built by the University of Michigan's Student Space Systems Fabrication Laboratory. It was a secondary payload to the Suomi National Polar-orbiting Partnership spacecraft.

⁷ Awards for the 2012 InVEST solicitation were announced on April 30, 2013. The four awards can be viewed at esto.nasa.gov/files/solicitations/INVEST_12/ROSES2012_InVEST_awards.html.

M^3 CubeSat carrying COVE.
Image credit: Michigan's Student Space Systems

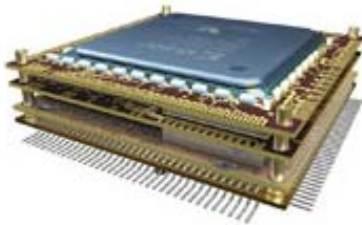
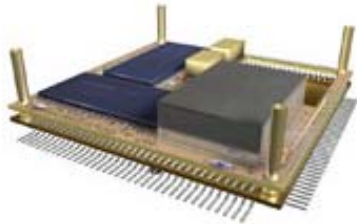


The IPEX CubeSat. Image credit: California Polytechnic State University

From top to bottom, the unique stacking technology for RTIMS: First layer of components added to the package; remaining layers assembled; pure epoxy resin molding; nickel and gold plating; and final tantalum shielding. **Image credit:** Jeff Herath [LaRC]

Infusion of ESTO Technologies

Over the course of 15 years of technology developments, advances, and validation, many ESTO technologies have been integrated into field campaigns, Earth-observing missions, planetary missions, or commercial applications. Many are fulfilling the roles for which they were intended and are making contributions to science and society. Some projects have even been infused into multiple platforms for various uses far outside their initial objective.



Field campaigns for example, are regular early adopters of ESTO technologies. Beginning in 2009 the NASA IceBridge campaign has collected data on the internal layering and bottom topography of ice sheets using the Pathfinder Advanced Radar Ice Sounder (PARIS)—a high-altitude sounding radar. During the summer of 2012 the Two-Column Aerosol Project, led by the U.S. Department of Energy, used the ESTO-funded High Spectral Resolution LIDAR (HSRL-2) to help quantify aerosol properties, radiation, and cloud characteristics.

The ESTO's AIST program funded the Radiation Tolerant Intelligent Memory Stack (RTIMS) project at NASA's Langley Research Center (LaRC) as part of a 2002 solicitation. The memory module was initially developed for Earth-observing missions at geostationary and low-Earth orbits for real-time data processing in harsh space environments. What made RTIMS useful for spaceborne applications also made it useful for data processing in the hard radiation environment found on Mars. RTIMS is now operating on the Chemistry and Camera (ChemCam) instrument on the Mars Rover Curiosity. As part of ChemCam, RTIMS controls the firing of the laser beam that pulverizes rock for analysis, data acquisition and buffering, and communication with the Rover Computer Element. RTIMS is small enough to easily fit in the palm of your hand, yet it safeguards ChemCam's observations with novel radiation-shielding and radiation-mitigation technologies. The memory module also employs a radiation event detection system and triple-redundant digital memory, plus in-flight reconfigurability. These features all enable RTIMS to overcome both hardware and software errors and to adapt to changing mission conditions.

Curiosity is not the only instantiation where RTIMS is proving itself useful. Astrium, a European aerospace company, is integrating RTIMS into a communications satellite, and is evaluating it for other projects. Another partner in the development of RTIMS, 3D Plus Inc., has also commercialized modules, which can be used for any application where radiation-tolerant memory and computing are needed.

Sometimes, ESTO projects aren't directly infused into a NASA mission, but can still contribute to the technology used for Earth observations. The recently selected Earth Venture Instrument—the Tropospheric Emissions: Monitoring of Pollution (TEMPO⁸)—was influenced by early technology investments made by ESTO. The TEMPO mission will provide a spectrometer that collects ultraviolet and visible data on major pollutants including ozone, nitrogen dioxide, sulfur dioxide, formaldehyde, and aerosols from 22,000 miles (~35,405 km) above Earth's equator. Two IIP projects have played—and will continue to play—a pivotal role in the development and operation of TEMPO. The Geostationary Spectrograph for Earth and Atmospheric Science Applications (GeoSpec) and Geostationary Trace Gas and Aerosol Sensor Optimization (GeoTASO) projects have been critical in bringing together the TEMPO instrument

⁸ Learn about TEMPO in the March–April issue of *The Earth Observer* [Volume 25, Issue 2, pp. 10-15].

and science team members as they worked to develop airborne prototype spectrometers and the algorithms required to measure air quality.

The work being completed on GeoTASO, an airborne spectrometer for trace gas and aerosol studies, is also contributing to development of the TEMPO sensor design. The algorithm sensitivities related to the GeoTASO sensor design will help match the TEMPO sensor design to its specific algorithm needs. In addition, GeoTASO's reconfigurable sensor will test algorithm performance over a range of parameters such as optimal spectral sampling. Polarization sensitivities will help dictate TEMPO's sensor parameter choices. Algorithm refinement for GeoTASO will also ensure that when TEMPO is launched, the retrieval algorithms will be readily and reliably applicable to the data collected. When TEMPO is fully operational, the airborne GeoTASO instrument will be available for use as a possible validation tool for the TEMPO mission.

Conclusion

While ESTO is a relatively young program in NASA's history, it has made great strides over the past 15 years in managing technology development that have enabled new science measurements, faster data processing, lighter payloads, and development of greatly improved models. By tying the needs of the science and user communities to the technologies developed, ESTO has been able to anticipate the needs of current and future NASA Earth-observing missions and objectives. The smaller, lighter, more-cost-effective, and improved technologies have had far-reaching impact—not just in terms of addressing the needs of the Earth Science Division Flight program, but also with regard to meeting the needs of planetary missions like Curiosity, and commercial applications for remote sensing.

In coming years, ESTO will continue to actively manage technology development for NASA's Earth science community, as the program also begins addressing the need for in-space validation. The well-tested technological advances to come will help to ensure a bright future for Earth and planetary missions, science measurements, and discovery in general.

To learn more about ESTO, visit: esto.nasa.gov. You can follow ESTO on Twitter: @NASAESTO. ■

In coming years, ESTO will continue to actively manage technology development for NASA's Earth science community as the program also begins addressing the need for in-space validation. The well-tested technological advances to come will help to ensure a bright future for Earth observing missions, science measurements, and discovery in general.

Share Your Field Experience on NASA's Earth Observatory

Do you have a NASA-related field campaign or other field work coming up this year? Would you like to publicize it on one of NASA's most popular Earth science websites? For the past four years the Earth Observatory has supported blogging for over 15 field campaigns ranging from ocean cruises in the North Atlantic and Galapagos, to airborne campaigns over California and the Arctic, to examinations of glaciers in Antarctica and the taiga in Siberia.

Publishing on the Earth Observatory puts your campaign in front of nearly 70,000 weekly email subscribers and thousands of other readers via RSS and social media. We provide the blogging system and promotion; you provide your experiences and photos. For example, **Lora Koenig** [NASA's Goddard Space Flight Center (GSFC)] has just returned from Greenland where she has been on the ice studying the aquifer. You can read about her experience at earthobservatory.nasa.gov/blogs/fromthefield/category/greenland-aquifer-expedition.

To learn more about the site, visit: *Notes from the Field* on the Earth Observatory at earthobservatory.nasa.gov/blogs/fromthefield.

Let the Earth Observatory help you communicate your science to the public. For more information or to ask questions, email **Kevin Ward** [GSFC—*Earth Observatory Manager*] at kevin.a.ward@nasa.gov.

2012 CLARREO Science Definition Team Meeting Summary

Rosemary Baize, NASA's Langley Research Center, rosemary.r.baize@nasa.gov

Bruce Wielicki, NASA's Langley Research Center, bruce.a.wielicki@nasa.gov

Amber Richards, NASA's Langley Research Center/Science Systems and Applications, Inc., amber.l.richards@nasa.gov

The fourth meeting of the Climate Absolute Radiance and Refractivity Observatory (CLARREO) Science Definition Team (SDT) was held at the University of Colorado Laboratory for Atmospheric and Space Physics (LASP) in Boulder, CO, October 16-18, 2012. CLARREO SDT members from LASP hosted the meeting and provided the team with a tour of their instrument calibration/test facilities and on-site Mission Operations and Science Operations Centers.

David Young [NASA's Langley Research Center (LaRC)—*Project Scientist*] welcomed attendees to the meeting and highlighted the team's recent publications—e.g., 31 journal papers published from pre-formulation studies (20 in 2012 alone); 9 journal papers submitted or in review; and 24 more in preparation. He emphasized the important role the science team is playing in creating and disseminating new scientific knowledge related to the CLARREO mission. Young also noted progress made by the SDT, working in coordination with engineers, to identify an alternative International Space Station (ISS) mission concept that optimizes science, cost, and risk. Finally, he reviewed options being discussed with NASA Headquarters (HQ) for continuing the work of the SDT past April 2013—the current expiration date. **Ken Jucks** [NASA HQ—*Program Scientist*] noted that the CLARREO science objectives remain a high priority for NASA's Earth science community, and thanked the team for their publications. Following Young and Jucks, members of the SDT provided updates on their CLARREO-specific activities since the last meeting in Hampton, VA in May 2012.

The technical portion of the meeting highlighted the accomplishments made by the SDT in advancing the CLARREO-related science goals over the past six months. Members of the SDT delivered talks on the infrared (IR), reflected solar (RS), and Global Navigation Satellite System—Radio Occultation (GNSS-RO) instruments, as well as special topics presentations¹ during the two-and-a-half-day meeting. Presentations focused primarily on investigations of the information content of CLARREO measurements; studies of the use of CLARREO data for reference intercalibration of other sensors; studies related to alternative, cost-effective mission architectures; and progress reports on continuing technology demonstrations

¹ These topics include a framework for multi-instrument intercalibration (MIIC) operations, CLARREO accommodations on the Japanese Experiment Module on the ISS, and the economic value of improved climate observations.

of achieving on-orbit absolute accuracy verification of the IR and RS spectrometers. The meeting agenda and many of the presentations can be viewed at clarreo.larc.nasa.gov by pulling down the *Workshops and Conferences* tab. A few of the highlights from the presentations are given below, listed by major topic area.

Alternative Implementation Options: Venture Class and International Space Station

The CLARREO team continues to explore multiple options for getting instruments to make key CLARREO observations into orbit. Several concepts were competitively pursued in 2011 and 2012 through the Venture Class Program. The Far-Infrared Explorer (FIREX) and Zeus IR spectrometers and the Earth Climate Hyperspectral Observatory (ECHO) RS spectrometer were all proposed under Earth Venture-2 (EV-2) solicitation. The Zeus and ECHO instrument concepts were also proposed under the Earth Venture Instrument (EVI-1) call. While none of these were ultimately selected, all three CLARREO-related instruments were rated as being technically mature [i.e., having a Technology Readiness Level (TRL) of 6 or greater²]. **Hank Revercomb** [University of Wisconsin-Madison (UW)] provided a debrief of the EV-2 review for the Zeus proposal and shared lessons learned for the future. The other option being considered is deploying CLARREO-related instruments on the ISS. **Barry Dunn** [LaRC] presented results from a study showing that the combined CLARREO IR and RS instruments could be readily accommodated on the Japanese Experiment Module Exposed Facility. The ISS implementation option has also shown the ability to obtain 73% of CLARREO baseline mission science value at approximately 40% of the Mission Concept Review defined cost.

Technology Demonstrations of CLARREO Climate Change Accuracy for IR and RS Spectra

Dave Johnson [LaRC] and **Kurt Thome** [NASA's Goddard Space Flight Center (GSFC)] provided updates on the CLARREO IR and RS Calibration Demonstration Systems (CDS), respectively. Construction of both instruments was successfully completed in 2012. In 2013 the CDS efforts will focus on verifying that CLARREO-level accuracies have been

² TRL is a measure that the Earth Science Technology Office (ESTO) uses to assess how *mature*—ready for use in space—a given technology is. To learn more, see *ESTO: Benefiting Earth Science through Technology* on page 22 of this issue.

achieved with full error budgets and having undergone National Institute of Standards and Technology (NIST) reviews. In addition, comparisons are planned with the UW IR spectrometer—giving CLARREO the type of independent verification that is the hallmark of accurate metrology. UW is also advancing vacuum and vibration qualification testing to achieve TRL 6 on both component and instrument system levels. **Greg Kopp** [LASP] provided an overview of the Hyperspectral Imager for Climate Science (HYSICS) instrument. Recently, LASP demonstrated better than 0.2% accuracy within one standard deviation ($1-\sigma$) in the ratio of reflected (outgoing) to incoming solar radiation, achieving CLARREO-level accuracies. LASP is planning a high-altitude balloon flight in August 2013, which will demonstrate HYSICS under realistic flight conditions (i.e., TRL-7).

Use of CLARREO Spectrometers for Reference Intercalibration of Other Sensors in Orbit

Costy Lukashin [LaRC] discussed a practical demonstration of the CLARREO RS instrument using the ISS as a platform for intercalibration of other satellite instruments, thereby improving the accuracy of the Earth-observing system. Estimates of the number of samples useful for intercalibration using Sun-synchronous spacecraft (i.e., JPSS and MetOP³) revealed that the ISS orbit is well suited for performing intercalibration. **Lukashin** and **Dave Doelling** [LaRC] described the *multi-instrument intercalibration* (MIIC) framework, a streamlined approach for teams responsible for calibration and validation of target instrument data. Intercalibration events from multiple spacecraft for a given temporal window are automatically calculated from the specified sampling criteria and orbit crossings. For each event intercalibration algorithms are executed on remote servers using Open-source Project for Network Access Protocol (OPeNDAP⁴) server-side functions prior to delivery of the data to the instrument teams for further analysis. The approach has been shown to save months of effort that would have been required to download extraneous data; it also reduces local processing.

Climate Observing System Simulation Experiments

The SDT meeting highlighted several pioneering new methods for *observing system simulation experiments* (OSSEs) for climate observations. **Dan Feldman** [University of California-Berkeley] provided an overview of the first combined IR/RS OSSE—completed during 2012. The operational OSSE is being used to conduct observational tests for climate model response and to assess the utility of CLARREO-like hyperspec-

tral measurements, e.g., using shorter times to detect climate change trends. These measurements will provide a benchmark against which future measurements can be compared to detect and attribute climate change signals. Working in coordination with **Xu Liu** [LaRC] and **Zhonghai Jin** [Science Systems and Applications, Inc. (SSAI)], the Berkeley team (Dan Feldman and Bill Collins) has incorporated a new reflected solar Principle Component Radiative Transfer Model (PCRTM) to speed up the OSSEs by a factor of 30. In 2013 the team is moving toward incorporation of Coupled Model Intercomparison Project Phase 5 (CMIP5) datasets to provide OSSEs with varying climate sensitivity. **Zhonghai Jin** presented a cloud-based probability distribution function method, which provides a simple, fast, and effective option in obtaining the mean spectral reflectance in large climate domains using large volume of instantaneous satellite data. This new approach was applied to Moderate Resolution Imaging Spectroradiometer/Clouds and the Earth's Radiant Energy System (MODIS/CERES) data; the simulated spectral reflectance agreed well with Scanning Imaging Absorption Spectrometer for Atmospheric Chartography (SCIAMACHY) measurements.

Spectral Climate Change Fingerprints and Radio Occultation

A key CLARREO innovation is to add a new type of climate-change detection: “fingerprints” of IR and RS spectra. **Yolanda Roberts** [LASP] and **Peter Pilewskie** [LASP] described advances in this area, utilizing *principle component analysis* (PCA) to determine how the information content in short-wave hyperspectral radiances can be used to study changes in the Earth's climate. Results showed that six principal components could be used to explain 99% of the variance between the CLARREO climate OSSEs and SCIAMACHY datasets. Moreover, the PCA analysis helped identify key spectral patterns (e.g., water vapor, clouds, surface albedo, and sea ice). **Seiji Kato** [LaRC], **Xianglei Huang** [University of Michigan], and **Yi Huang** [McGill University] provided advanced results from IR *fingerprinting* using data from the Atmospheric Infrared Sounder on NASA's Aqua platform, climate model simulations, and CLARREO OSSE experiments. **Bill Smith** [UW] and **Larrabee Strow** [University of Maryland, Baltimore County] showed new climate-focused retrieval strategies for IR spectra. **Chi Ao** [NASA/Jet Propulsion Laboratory] showed results aimed at understanding and improving RO profile retrievals near the marine boundary layer, especially for climate applications.

Economic Value Studies

Bruce Wielicki [LaRC—*Mission Scientist*] summarized steps taken to combine the CLARREO *Science*

³ The Joint Polar Satellite System is a joint NASA–NOAA endeavor; MetOp-A and -B are the European Organization for the Exploitation of Meteorological Satellite's (EUMETSAT) operational meteorology satellites.

⁴ OPeNDAP is a common data transport protocol used by Earth-science researchers and practitioners.

SMAP Calibration/Validation Workshop

Thomas Jackson, U.S. Department of Agriculture, Agricultural Research Service, tom.jackson@ars.usda.gov

Peggy O'Neill, NASA's Goddard Space Flight Center, peggy.e.oneill@nasa.gov

Eni Njoku, NASA/Jet Propulsion Laboratory, California Institute of Technology, eni.g.njoku@jpl.nasa.gov

Introduction

NASA's Soil Moisture Active Passive (SMAP) mission is on schedule for launch in October 2014. SMAP will provide high-resolution, frequent-revisit, global mapping of soil moisture and freeze/thaw state that will enable a variety of hydrology, climate, and carbon-cycle science objectives and meteorological, agricultural, environmental, and ecological applications that are expected to have practical benefits for society—see *SMAP at a Glance* on page 36 to learn more. As with other space missions, the SMAP Project is required to implement a calibration/validation (cal/val) program to assess and minimize random errors and spatial and temporal biases in the soil moisture and freeze/thaw estimates, and demonstrate that SMAP retrievals meet the stated science requirements of the mission.

Up until now SMAP cal/val activities have primarily focused on prelaunch activities, seeking to insure that means are in place to fulfill mission objectives (e.g., acquiring and processing data with which to calibrate, test, and improve models and algorithms used to retrieve SMAP science data products). Now, however, with launch less than two years away, the focus has shifted to preparing for postlaunch activities, where the emphasis will be on validating the accuracies of the

SMAP science data products. A number of different methodologies have been proposed as part of the cal/val process—from the use of external calibration targets for the Level 1 (L1) instrument data (e.g., cold sky, ocean, forests, Antarctic scenes) to a combination of *in situ*, field campaign, satellite, and model data for the L2-4 geophysical data products—see **Table 1**.

SMAP will be the first of the missions proposed in the Earth Science Decadal Survey to launch. NASA Headquarters (HQ) has required that SMAP deliver fully calibrated instrument data and retrieved geophysical products to the SMAP Distributed Active Archive Centers (DAACs) for archive and public access within 15 months after launch (which is within 12 months of the start of SMAP routine science operations). SMAP radar data will be delivered to the Alaska Satellite Facility (ASF), while all other SMAP data will be sent to the National Snow and Ice Data Center (NSIDC). **Table 2** lists the SMAP baseline mission data products. *Beta versions* of L2-4 data products and validated L1 data products are due nine months after launch—see **Figure 1**. Due to the compressed timeline for the cal/val phase of the SMAP mission, it is essential that all the cal/val tools and methodologies are tested and in place by the launch date.

Table 1. SMAP Level 2-4 data product validation methodologies.

Methodology	Role	Constraints	Resolution
Core Validation Sites	Accurate estimates of products at matching scales for a limited set of conditions	<ul style="list-style-type: none"> • <i>In situ</i> sensor calibration • Limited number of sites 	<ul style="list-style-type: none"> • <i>In situ</i> testbed • Cal/val partners
Sparse Networks	One point in the grid cell for a wide range of conditions	<ul style="list-style-type: none"> • <i>In situ</i> sensor calibration • Up-scaling • Limited number of sites 	<ul style="list-style-type: none"> • <i>In situ</i> testbed • Scaling methods • Cal/val partners
Satellite Products	Estimates over a very wide range of conditions at matching scales	<ul style="list-style-type: none"> • Validation • Comparability • Continuity 	<ul style="list-style-type: none"> • Validation studies • Distribution matching
Model Products	Estimates over a very wide range of conditions at matching scales	<ul style="list-style-type: none"> • Validation • Comparability 	<ul style="list-style-type: none"> • Validation studies • Distribution matching
Field Campaigns	Detailed estimates for a very limited set of conditions	<ul style="list-style-type: none"> • Resources • Schedule conflicts 	<ul style="list-style-type: none"> • Simulators • Partnerships

Table 2. SMAP baseline mission data products.

Product	Description	Gridding (Resolution)	Latency†	Data
L1A_Radiometer	Radiometer data in time-order	–	12 hrs	Instrument
L1A_Radar	Radar data in time-order	–	12 hrs	
L1B_TB	Radiometer brightness temperature T_B in time-order	(36 x 47 km)	12 hrs	
L1B_S0_LoRes	Low-resolution radar σ_O in time-order	(5 x 30 km)	12 hrs	
L1C_S0_HiRes	High-resolution radar σ_O in half-orbits	1 km (1-3 km)*	12 hrs	
L1C_TB	Radiometer T_B in half-orbits	36 km	12 hrs	
L2_SM_A	Soil moisture (radar)	3 km	24 hrs	Science (Half-Orbit)
L2_SM_P	Soil moisture (radiometer)	36 km	24 hrs	
L2_SM_AP	Soil moisture (radar + radiometer)	9 km	24 hrs	
L3_FT_A	Freeze/thaw state (radar)	3 km	50 hrs	Science (Daily Composite)
L3_SM_A	Soil moisture (radar)	3 km	50 hrs	
S3_SM_P	Soil moisture (radiometer)	36 km	50 hrs	
L3_SM_AP	Soil moisture (radar + radiometer)	9 km	50 hrs	
L4_SM	Soil moisture (surface and root zone)	9 km	7 days	Science Value Added
L4_C	Carbon net ecosystem (NEE)	9 km	14 days	

* Over outer 70% of swath.

† The SMAP project will make a best effort to reduce the data latencies beyond those shown in this table.

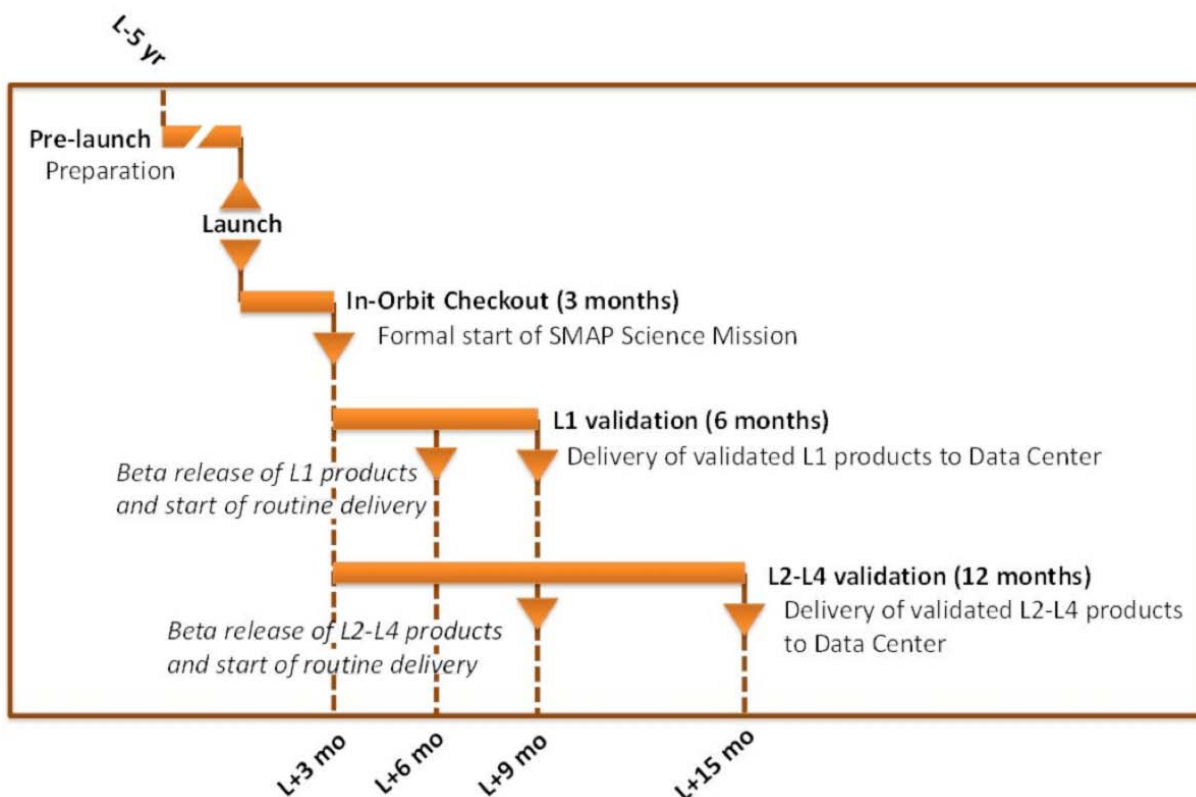


Figure 1. SMAP science data validation and delivery timeline.

Workshop Overview

To solicit science community input, the SMAP Project held its third community Cal/Val Workshop in Oxnard, CA, November 14-16, 2012. Participants included over 80 scientists and students, many of them from the SMAP Cal/Val Working Group—which is open to any interested individuals. For more detailed information on SMAP Working Groups, visit: smap.jpl.nasa.gov/science/wgroups. Summary information and presentations from the Cal/Val Workshop are posted at smap.jpl.nasa.gov/news/index.cfm?FuseAction=ShowNews&NewsID=121.

Workshop presentation topics included:

- An overview of project status;
- results of a formal panel review of the SMAP cal/val plan;
- L1 instrument data calibration;
- L2-4 retrieval algorithms and their cal/val requirements;
- ground-based and aircraft field campaigns with SMAP simulators;
- descriptions of core and sparse *in situ* measurement networks; and
- methods for upscaling sparse or point data to SMAP resolutions.

SMAP has been developing its *in situ* validation resources by establishing global Cal/Val Partners¹.

¹ To learn more about SMAP Cal/Val Partners, visit: smap.jpl.nasa.gov/science/Validation/solicitations.



Eni Njoku [NASA/Jet Propulsion Laboratory (JPL)—*SMAP Project Scientist*] and **Tom Jackson** [U.S. Department of Agriculture (USDA)—*SMAP Cal/Val Working Group Chair*] welcomed workshop participants on the first day. **Image credit:** **Alicia Joseph** [NASA's Goddard Space Flight Center (GSFC)]

The Partners provide data to SMAP on a no-exchange-of-funds basis in return for access to SMAP products during the early-mission cal/val phase. The Partners were selected primarily in response to a *Dear Colleague Letter* released by NASA HQ. **Figure 2** shows that a concerted effort has been made to distribute the SMAP cal/val sites spatially around the world and across a variety of major biomes. During the workshop, **Tom Jackson** [U.S. Department of Agriculture (USDA)—*SMAP Cal/Val Working Group Chair*] discussed how the process of becoming a Cal/Val Partner is being formalized and how new cal/val sites can be added. A poster session following this discussion provided an opportunity for Cal/Val Partners to present more information about their individual sites and measurement plans.

A major point of discussion at the workshop involved the design and implementation of *cal/val rehearsal*

Core Site Candidates

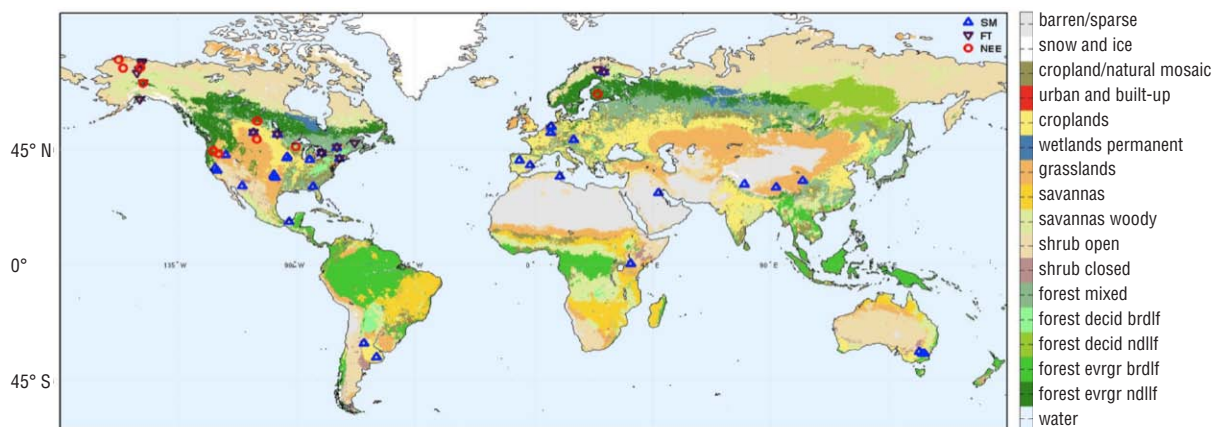


Figure 2. This map shows the global distribution of Cal/Val Partners (excluding the sparse networks), superimposed on a background image of land-cover types which are listed in the legend along the right side of the map. **Image credit:** **Andreas Colliander** [JPL]



Workshop participants interacting during the poster session.
Image credit: Peggy O'Neill [GSFC]



Installation of *in situ* sensors at MOISST.
Image credit: Michael Cosh [USDA]



Tom Jackson discussing results with Narendra Das [JPL].
Image credit: Alicia Joseph [GSFC]



Demonstration of the portable COSMOS Rover system.
Image credit: Alicia Joseph

*campaigns*² prior to the launch of SMAP, which is NASA's first soil moisture mission. The workshop consensus was that there should be two phases to a cal/val rehearsal campaign. The first phase will take place in summer 2013 and focus on the delivery and quality control of *in situ* ground truth data from SMAP's global Cal/Val Partners as well as the development of essential cal/val tools. The second phase will take place in summer 2014 and will be an end-to-end test of the SMAP science data processing system and cal/val tools.

The final day of the workshop began with a review of the Marena Oklahoma In Situ Sensor Testbed (MOISST)—a SMAP initiative to provide a basis for the integration and cross-calibration of the diverse *in situ* soil moisture measurement sensors and resources that will be used in cal/val activities—see top right photo above. This testbed includes instrumentation from many operational networks. Following the MOISST discussion, updates were presented on the Plate Boundary Observatories, Climate Reference

² Pre-launch cal/val rehearsal campaigns will ensure that the methodologies and tools are in place for the operational phase of the mission.

Network, and the COsmic-ray Soil Moisture Observing System (COSMOS³) network, as well as a demonstration of a portable version of COSMOS—called the COSMOS Rover [see bottom right photo above].

The workshop concluded with discussion and identification of action items to:

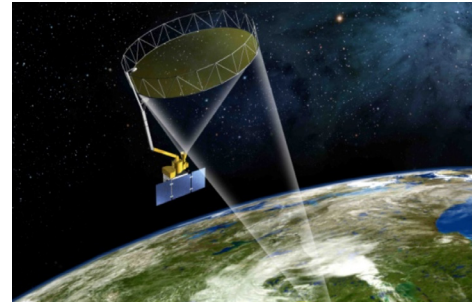
- define absolute calibration reference standards and procedures to be used for SMAP L1 radiometer and radar calibration;
- define the postlaunch *SMAP Validation Experiments* airborne campaigns planned for 2015 or 2016 (SMAPVEX15 or SMAPVEX16), including science objectives, site selection, desired airborne instruments, aircraft flight timing/duration, and a data analysis plan;
- complete agreements with Cal/Val Partners;

³ COSMOS is a National Science Foundation (NSF)-supported project to measure soil moisture on the horizontal scale of hectometers and depths of decimeters using cosmic-ray neutrons. For more information, visit: cosmos.hwr.arizona.edu.

SMAP at a Glance

Orbit Information

Type:	Near-polar, Sun-synchronous
Altitude (average geodetic):	685 km (~425.6 mi) Equator-crossing altitude
Equatorial Crossing Time:	18:00 hrs (6:00 PM local mean solar time; ascending node)
Inclination:	98.12°
Period:	98.5 min
Repeat Cycle:	8 days (exact orbit repeat)
Revisit	2-3 days



Spacecraft Specs

The SMAP spacecraft has been built in-house at NASA/Jet Propulsion Laboratory (JPL), leveraging avionics and power electronics derived from previous planetary missions. The spacecraft is designed to accommodate the unique needs of a large spinning instrument in a compact package that can fit within a small launch vehicle's fairing. The spacecraft structure is of aluminum construction and includes large reaction wheels that provide momentum compensation for the large, spinning 6-m- (~20-ft) diameter mesh reflector. The spacecraft has an S-band transponder to accommodate ground-based Doppler tracking for orbit determination rather than using the Global Positioning System (GPS) because the large spinning instrument antenna blocks GPS visibility. The solar array uses three fixed panels that are mounted to the spacecraft structure. The spacecraft design puts bounds on how the solar array, the large instrument reflector, and boom assembly are deployed, and the release of the spun instrument launch lock to allow the instrument to rotate. The spacecraft must also accommodate the large data volume generated by the SMAP synthetic aperture radar.

Length:	1.5 x 0.9 x 0.9 m (4.9 x 3 x 3 ft), spacecraft bus only
Mass:	1150 kg (~2535 lbs), including propellant and instrument
Power:	1450 W
Downlinks:	S-Band (satellite control and monitoring), X-Band (science data)
Design Life:	3 years

Launch Details

Date:	Late 2014
Location:	Vandenberg Air Force Base, Lompoc, CA
Vehicle:	United Launch Alliance Delta II 7320-10C

Instrument Summary

The instrument consists of an L-band radiometer and an L-band synthetic aperture radar (unfocused), sharing a rotating 6-m (~20-ft) mesh reflector and boom assembly. The spun instrument rotates continuously at rates from 13 to 14.6 rpm; antenna pointing is at a constant incidence angle of 40°. This arrangement produces a 1000-km (~621-mi) measurement swath that efficiently enables global coverage every two-to-three days. Radiometer antenna beam efficiency is > 87%, with an antenna temperature precision of < 0.5 K and a reflector emissivity of < 0.0035. Radar antenna gain is 35.5 dBi with a half-power beamwidth of 2.8°.

The 1.413-GHz radiometer is mounted on the spun-instrument platform (on the zenith-pointing spacecraft deck) to reduce losses between the instrument feed and the radiometer. The radiometer design mitigates radio frequency (RF) interference, and will acquire measurements in four channels [vertical (V) and horizontal (H) polarization, and third and fourth Stokes parameters¹], with a brightness temperature accuracy requirement of 1.3 K. The radiometer's spatial resolution is approximately 40 km (~25 mi) (real aperture). The fixed 1.26-GHz radar is mounted to the interior of the anti-Sun spacecraft panel (providing a good thermal field of view of deep space) to reduce spin momentum. The radar will acquire measurements in VV, HH, and HV² polarization channels, and uses various techniques to mitigate RF interference, e.g., frequency hopping. The radar has 1-3 km (~0.6-1.9 mi) spatial resolution over the outer 70% of the swath; its transmit power of 500 W is provided by a solid-state high-power amplifier, with a 9% duty cycle.

¹ Stokes parameters represent the polarization state of electromagnetic radiation.

² A radar transmits microwave radiation and measures the *backscatter* off a distant object—or radar cross section. The SMAP radar measures *polarized* radiation; each channel transmits and receives radiation in different orientations. HH stands for Horizontal Transmit, Horizontal Receive; VV stands for Vertical Transmit, Vertical Receive; and HV stands for Horizontal Transmit, Vertical Receive. The first two are copolarized; the third is cross polarized.

- decide on a subset of Cal/Val Partners to be designated as Core Validation Sites (CVS) to verify overall mission accuracy metrics;
- develop a “Rehearsal Plan” document for Phase I of the mission, based on discussions at the workshop;
- work with the European Space Agency’s Soil Moisture and Ocean Salinity (SMOS) mission and NASA’s Aquarius mission to converge on a reference standard for land calibration (warm brightness temperature), which will be extrapolated from the conventional cold sky/ocean/Antarctic calibration targets; and
- publish definitions of SMAP mission validation metrics.

All workshop presentations have been uploaded to the SMAP website at smap.jpl.nasa.gov/science/workshops/CalVal3WkshpPres. The next SMAP Cal/Val Workshop will be held on November 5-7, 2013, following the planned summer cal/val rehearsal campaign. ■



Kent Kellogg [JPL—SMAP Project Manager] and **Diane Evans** [JPL—Director for Earth Science and Technology] were pleased with the workshop presentations, discussions, and proposed actions. **Image credit: Alicia Joseph**

NASA Water Vapor Project–MEaSURES Dataset Release

The Atmospheric Science Data Center (ASDC) at NASA’s Langley Research Center, in collaboration with the NASA Water Vapor Project–Making Earth System Data Records for Use in Research Environments (MEaSURES) [NVAP-M] team, announce the release the following datasets:

- NVAP-M: Climate
- NVAP-M: Weather
- NVAP-M: Ocean

NVAP-M water vapor datasets comprise a combination of retrievals from the Atmospheric Infrared Sounder (AIRS) and the Special Sensor Microwave/Imager (SSM/I), radiosonde observations, High Resolution Infrared Sounder (HIRS) profiles, and Global Positioning System (GPS) observations. These datasets span 22 years (1988–2009) and contain total and precipitable water vapor from four layers.

The following are distinguishing features of the NVAP-M dataset:

- Global (land and ocean) data coverage;
- consistent, intercalibrated data sources;
- consistent, peer-reviewed algorithms;
- new data sources; and
- a three-tiered production format suitable for a variety of users.

The MEaSURES program creates stable, community-accepted Earth System Data Records (ESDRs) for a variety of geophysical time series, and is responsible for reanalysis and extension of NVAP-M data.

The datasets can be accessed from the ASDC at eosweb.larc.nasa.gov/content/nvap-m.

HyspIRI Science and Application Workshop Summary

Simon Hook, NASA/Jet Propulsion Laboratory, simon.j.hook@jpl.nasa.gov

Introduction

NASA's Hyperspectral Infrared Imager (HyspIRI) mission will observe the world's ecosystems and provide critical information on natural disasters such as volcanoes, wildfires, and drought. It will provide a benchmark on the state of the world's ecosystems against which future changes can be assessed, as the instruments will be capable of identifying vegetation type and health. The mission was recommended for implementation by the 2007 report from the U.S. National Research Council: *Earth Science and Applications from Space: National Imperatives for the Next Decade and Beyond*¹.

To address its objectives, HyspIRI's instrumentation manifest includes a visible-to-short-wave-infrared (VSWIR) imaging spectrometer that covers the range 380–2500 nm in 10-nm contiguous bands, and a multispectral imager that covers the range from 3–12 μm with 8 discrete bands across the mid- and thermal-IR (TIR) portion of the spectrum. Both instruments have a spatial resolution of 60 m (~197 ft) at nadir. The VSWIR instrument will have a revisit time of 19 days; the TIR instrument will have a revisit time of 5 days. HyspIRI also includes an Intelligent Payload Module (IPM) that will enable a subset of the data to be processed onboard the satellite and downlinked to the ground in near-realtime.

Meeting Overview

Approximately 190 scientists attended the fifth annual HyspIRI Science and Applications Workshop, held October 16–18, 2012, in Washington, DC.

The three-day workshop provided an open forum to present the mission's observational requirements and to assess its anticipated impact on scientific and operational applications. Participants had the opportunity to obtain feedback from the broader scientific community on the mission concept and to participate in a half-day session on HyspIRI-related science applications. There was a special session on coastal and inland water studies and how HyspIRI complements missions under development to look at deeper oceans.

Owing to the depth and breadth of information provided at the workshop, only an upper-level summary will be provided here. The full workshop agenda, presentations, and speakers list are available at hyspiri.jpl.nasa.gov/documents/2012-science-workshop.

Day 1

Michael Freilich [NASA Headquarters (HQ)—*Earth Science Division Director*], **Jack Kaye** [NASA

HQ—*Associate Director for Research, Earth Science Division*], and **Woody Turner** [NASA HQ—*Biological Diversity Program Manager*], provided the Headquarters perspective on the mission and how it fits into the “bigger picture” at NASA. In addition to discussing details specific to HyspIRI, they discussed the mission in the context of NASA's other Earth observing missions, the processes by which *Decadal Survey* missions (e.g., HyspIRI) were selected, and the steps involved in the mission development process. They also discussed how NASA's Science, Applied Sciences, and Technology programs contributed to the overall mission.

Dave Schimel [NASA/Jet Propulsion Laboratory (JPL)], **Dar Roberts** [University of Santa Barbara], **Michael Ramsey** [University of Pittsburgh], **Tom Painter** [JPL], and **Phil Dennison** [University of Utah] followed with presentations that highlighted the critical importance of HyspIRI science and applications. They discussed the use of HyspIRI data for ecosystem and volcano studies and some of the airborne precursor instrument development activities.

Steve Volz [HQ—*Associate Director for Flight Programs, Earth Science Division*] provided an update of NASA flight programs. **Carl Bruce** [JPL], **Marc Foote** [JPL] and **Dan Mandl** [NASA's Goddard Space Flight Center (GSFC)], provided updates on the two HyspIRI instruments (VSWIR, TIR) and the IPM. **Charles Norton** [JPL/Earth Science Technology Office (ESTO)] provided a description of ESTO activities in support of HyspIRI.

Simon Hook and **Robert Green** [JPL], rounded out the first day with presentations describing the Level-1 requirements² for the HyspIRI mission. Their presentation provided an opportunity for the community to fully understand the objectives for the mission. As with previous workshops, the community fully endorsed the requirements.

Day 2

The day's focus was on science applications and included a special session on the potential of HyspIRI data for studying coastal and inland waters—intended to provide key information not provided by the lower-spatial resolution missions designed to study deep oceans (e.g., Aqua). **Lawrence Friedl** [HQ—*Associate Director for Applied Sciences, Earth Science Division*] opened the second day with a presentation focusing on the NASA Applications Program. Many of the day's talks focused on applications of HyspIRI to operational uses. As there were over 30 technical presentations, individual presenters are not described here; full details,

² *Level-1 Requirements* represent project deliverables to NASA and the community.

¹ The report is also known as the Earth Science Decadal Survey and can be found online at www.nap.edu/catalog.php?record_id=13405.



Fifth annual HypsIRI Science and Application Workshop participants.

however, are available from the HypsIRI website—provided earlier in this article. These talks covered a wide range of topics and included updates from the studies funded by NASA solicitations, and updates on the key science questions that HypsIRI will address. The science questions were developed in conjunction with the Science Study Group, a group of scientists appointed by NASA to help guide the mission and to ensure that the measurements are of maximum benefit.

Day 3

The final day included discussions of related missions, partnership opportunities, and future plans. Of particular interest was the discussion of the HypsIRI Airborne Campaign³. As part of this preparatory airborne activity, NASA will fly the Airborne Visible Infrared Imaging Spectrometer (AVIRIS) and the MODIS/ASTER⁴ Airborne Simulator [MASTER] instruments on its ER-2 high-altitude aircraft to collect datasets in concert with other instruments for precursor science and applications research. These data will be used for HypsIRI-related science studies, to support HypsIRI mission development, and to prepare the community for HypsIRI-enabled science and applications research.

Woody Turner convened a wrap-up session, commenting that not only was the workshop a wonderful series of talks on the utility of VSWIR imaging spectrometer data and multispectral TIR imagery, but—more importantly—a demonstration of the fundamental groundbreaking science that could be performed by the combined capability provided by using both instruments. Further, the workshop clearly demonstrated the value of the data for use in operational systems.

Turner concluded by providing more details on the HypsIRI Airborne Campaign, which will provide simulation data from the Sierras to the coastal zone of California. He noted that the project would ensure that community would be able to evaluate the challenges of handling large datasets. While the airborne data are limited to AVIRIS and MASTER, it is hoped that

data from AVIRISng, PRISM, and HyTES⁵ will also be made available over selected sites. A planning meeting was scheduled for November with first flights in March–April 2013⁶. The goal of the planning meeting was to decide on the areas that would be covered and to ensure that the necessary field measurements were made to maximize the usefulness of the data.

As with previous workshops, the Preliminary Level 1 mission requirements were reviewed with the community to make sure they would meet the science needs. This year 39 posters were presented at a special early evening session. Participants commented on the usefulness of this session as a way to find more detail about particular activities and for the opportunity to network. Participants were particularly appreciative of the excellent opportunity to present results in a more interactive environment and to network with colleagues.

Summary

The participants concluded that the HypsIRI mission would provide a significant new capability to study ecosystems and natural hazards at spatial scales relevant to human resource use and would be particularly valuable for climate related studies. It was clear that the measurement requirements could be achieved with the reference instrument design concepts and be implemented through the use of current technology. The participants strongly endorsed the need for the HypsIRI mission and felt the mission, as defined, would accomplish the intended science goals. There was significant enthusiasm about the HypsIRI preparatory airborne campaign and for obtaining data from the slated instrumentation suite.

The participants confirmed that the Draft Preliminary HypsIRI Mission Level 1 Requirements were achievable within the mission concept presented and would provide the necessary data to address the science questions identified for the mission.

The next HypsIRI Science and Applications Workshop will be held in October 15-17 in Pasadena, CA. ■

³ The full name is HypsIRI Preparatory Airborne Activities and Associated Science and Applications Research; it is funded through the Research Opportunities in Space and Earth Science (ROSES) 2012 solicitation.

⁴ MODIS is the Moderate Resolution Imaging Spectroradiometer; ASTER is the Advanced Spaceborne Thermal Emissions and Reflection Radiometer.

⁵ AVIRISng is the Next Generation Airborne Visible/Infrared Imaging Spectrometer; PRISM is the Portable Remote Imaging Spectrometer; HyTES is the airborne Hyperspectral Thermal Emission Spectrometer.

⁶ **UPDATE:** This campaign is currently underway; the first (spring 2013) series of flights completed in May.

First Light for ISERV Pathfinder, Space Station's Newest 'Eye' on Earth

Janet Anderson, NASA's Marshall Space Flight Center, janet.l.anderson@nasa.gov

EDITORS NOTE: This article is taken from *nasa.gov*. While it has been modified slightly to match the style used in *The Earth Observer*, the intent is to reprint it with its original form largely intact.

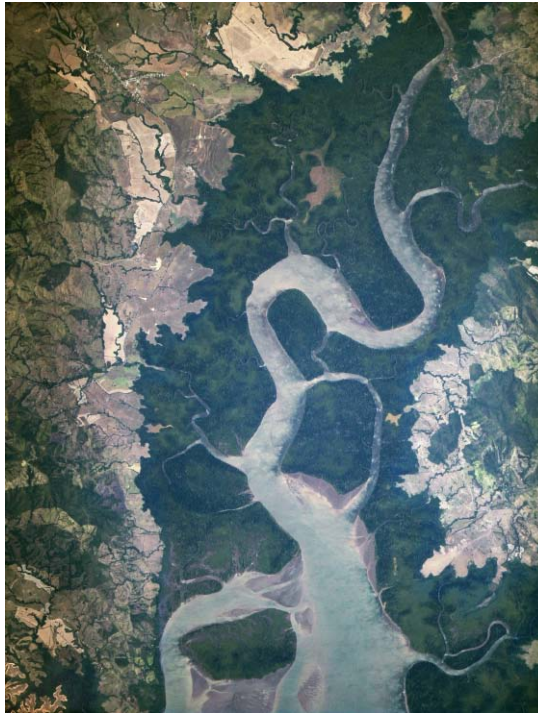
From the Earth-facing window of the International Space Station's (ISS) *Destiny* module, nearly 95% of the planet's populated area is visible during the station's orbit. This unique vantage point provides the opportunity to take photos of Earth from space. With the installation and activation of the ISS SERVIR¹ Environmental Research and Visualization System (ISERV), NASA will be able to provide even higher-resolution images of Earth.

The ISERV camera system's mission is to gain experience and expertise in automated data acquisition from the space station. ISERV is expected to provide useful images for disaster monitoring and assessment and environmental decision making. A system like ISERV could aid in delivering imagery and data to help officials in developing nations monitor impacts of disasters such as floods, landslides, and forest fires. Its images also could help decision makers address other environmental issues.

The instrument recently transmitted back its first images to scientists on Earth from its location in the Window Observational Research Facility (WORF²). ISERV is a commercial camera, telescope, and pointing system operated remotely from Earth by researchers at NASA's Marshall Space Flight Center (MSFC).

Acting on commands from the ground, ISERV can photograph specific areas of the Earth's surface as the ISS passes over them. The goal for ISERV is to help sci-

entists gain operational experience and expertise and to influence the design of a more capable system for future ISS expeditions. The ISS provides researchers a unique opportunity to develop ISERV's capability by conducting global observations from space.



This first-light image from ISERV, captured on February 16, shows the mouth of the Rio San Pablo in Veraguas, Panama, as it empties into the Gulf of Montijo. This wetland supports an important local fishery and provides habitat for many mammals and reptiles, as well as several species of nesting and wintering water birds. **Image credit:** NASA's Earth Observatory

“ISERV's full potential is yet to be seen, but we hope ISERV or a successor will really make a difference in people's lives,” said **Burgess Howell** [MSFC—*ISERV Principal Investigator*]. “For example, if an earthen dam gives way in Bhutan, we want to be able to show officials, via our images, where the bridge or a road is washed out, or where a power substation has been inundated. This kind of information is critical to focus and speed rescue efforts.”

An operational system with ISERV's optical characteristics could, in many cases, acquire near-real-time images of areas on the ground and transmit them within hours of the event. This would provide information that could shape disaster relief decisions and possibly prevent loss of life or injuries.

“ISERV could become a tool to enhance and expand NASA's hazard and disasters work across the whole disaster management cycle,” added **Frank Lindsay** [NASA Headquarters (HQ)—*Applied Sciences Disasters Program Manager*]. “The bottom line is that this camera opens up some opportunities we did not have before and clearly is a pathfinder for more assets on the space station for our applications.”

ISERV's software maintains knowledge of the space station's exact location and attitude in orbit at any given moment. With this information, it calculates the next chance to view a particular area. If there's a good viewing opportunity, the SERVIR team will send instructions to the camera. ISERV will take a series of high-resolution

¹ SERVIR is a decision support system that allows NASA satellite data to be analyzed and applied to a variety of issues with practical benefits for society—including disaster management. The name is derived from the Spanish word for “to serve.”

² The WORF was described in the October–November 2011 issue of *The Earth Observer* [Volume 23, Issue 3, pp. 25–27].

photographs of the area at rates of three to seven frames per second, totaling as many as 100 images per pass. “The camera’s nominal resolution is about 10 ft (~3 m),” Howell explained. “That’s about the size of a small car—and potentially valuable for disaster assessments.”

At first, the instrument will be used only by SERVIR and its existing hubs in Mesoamerica, East Africa, and the Hindu Kush-Himalaya region. After proving itself, ISERV could be made available to the broader disaster-response community and the NASA science community.

The team is assessing how the geometry of the window affects its imagery, how much sunlight the instrument needs to capture clear images, how the atmosphere affects that clarity, and more. This characterization phase will last from several weeks to a few months. The exposure, time of day, and location, as well as the land cover (e.g., savannah, rivers, forests) and other characteristics will be documented, catalogued, and archived for every scene acquired.

continued on page 43

Announcing a New Look for the EOS Project Science Office Website

NASA’s Earth Observing System Project Science Office (EOSPSO) recently launched an exciting redesign of the EOSPSO website at: eosps.nasa.gov. While the site has always included content that went beyond the original EOS missions, it now more strongly represents all of NASA’s Earth-observing satellite missions (many of which are joint endeavors with other nations and/or agencies), along with other elements of NASA’s Earth Science program.

The user interface has changed dramatically, with better content organization. Everything can now be more easily accessed via the main menu options listed across the top of the page. Potentially of interest to readers of this newsletter, *The Earth Observer Newsletter* menu option links to an index that dates back to the March-April 1999 issue. Color versions of the newsletter exist from January-February 2011 to present. A clickable table of contents, preview of the editorial, and PDF versions of the newsletter are available for each issue.

A standard *Google* search tool can be found in the top right corner of the page. Once a search is executed, users can categorize the results as “All results” or “Earth Observer” results. Clicking the “Earth Observer” option will focus the search to only *The Earth Observer Newsletter* pages.

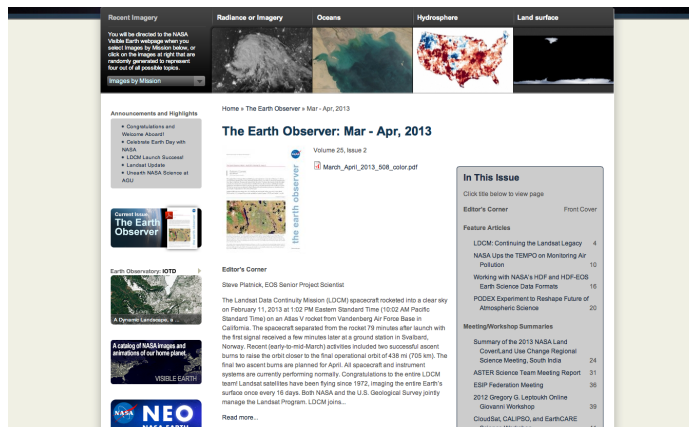
In addition to the redesigned interface, new features include:

- an *Announcements and Highlights* blog;
- a color-coded sliding chart that displays mission status and timelines; and
- recent imagery and prominent links to the Earth Observatory, Visible Earth, and NASA Earth Observations websites.

We hope you enjoy the new site!



Redesigned EOSPSO homepage.



The individual webpage for the March-April 2013 issue of *The Earth Observer* is displayed here.

2013 Wintertime Arctic Sea Ice Maximum Fifth Lowest on Record

Maria-Jose Vinas, NASA's Goddard Space Flight Center, maria-jose.vinasgarcia@nasa.gov

EDITORS NOTE: This article is taken from *nasa.gov*. While it has been modified slightly to match the style used in *The Earth Observer*, the intent is to reprint it with its original form largely intact.

Last September, at the end of the northern hemisphere summer, the Arctic Ocean's icy cover shrank to its lowest extent on record, continuing a long-term trend and diminishing to about half the size of the average summertime extent from 1979 to 2000.

During the cold and dark of Arctic winter, sea ice refreezes and achieves its maximum extent, usually in late February or early March. According to a NASA analysis, this year the annual maximum extent was reached on February 28 and it was the fifth lowest sea ice winter extent in the past 35 years.

The new maximum—5.82 million mi² (15.09 million km²)—is in line with a continuing trend in declining winter Arctic *sea ice extent*: nine of the ten smallest recorded maximums have occurred during the last decade. The 2013 winter extent is 144,402 mi² (374,000 km²) below the average annual maximum extent for the last three decades.

“The Arctic region is in darkness during winter and the predominant type of radiation is longwave—or infrared—which is associated with greenhouse warming,” said senior scientist

Joey Comiso [NASA's Goddard Space Flight Center (GSFC)—*Cryospheric Sciences Program Principal Investigator*]. “A decline in the sea ice cover in winter is thus a manifestation of the effect of the increasing greenhouse gases on sea ice.”

Satellite data retrieved since the late 1970s show that sea ice extent, which includes all areas of the Arctic Ocean where ice covers at least 15% of the ocean surface, is diminishing. This decline is occurring at a much faster pace in the summer than in the winter; in fact, some models predict that the Arctic Ocean could be ice-free in the summer in just a few decades.

The behavior of the winter sea ice maximum is not necessarily predictive of the following melt season. The record shows there are times when an unusually large maximum is followed by an unusually low minimum, and vice versa.

“You would think the two should be related, because if you have extensive maximum, that means you had an unusually cold winter and that the ice would have grown

thicker than normal. And you would expect thicker ice to be more difficult to melt in the summer,” Comiso said. “But it isn't as simple as that. You can have a lot of other forces that affect the ice cover in the summer, like the strong storm we got in August last year, which split a huge segment of ice that then got transported south to warmer waters, where it melted.”



An image of the Arctic sea ice when it reached the annual maximum extent of 5.82 million mi² (15.09 million km²) on February 28, 2013. **Image credit:** NASA

The sea ice maximum extent analysis produced at GSFC is compiled from passive microwave data from NASA's Nimbus-7 satellite and the U.S. Department of Defense's Defense Meteorological Satellite Program. The record, which began in November 1978, shows an overall downward trend of 2.1% per decade in the size of the maximum winter extent—a decline that accelerated after 2004.

The GSFC sea ice record is one of several analyses, along with those produced by the National Snow and Ice Data Center (NSIDC). The two institutions use slightly different methods in their sea ice tally, but overall, their trends show close agreement. NSIDC announced that Arctic sea ice reached its winter maximum on March 15, at an extent of 5.84 million mi² (15.13 million km²)—a difference of less than half a percent compared to the NASA maximum extent.

Another measurement that allows researchers to analyze the evolution of the sea ice maximum is *sea ice area*. The measurement of area, as opposed to extent, discards regions of open water among ice floes and only tallies the parts of the Arctic Ocean that are completely

covered by ice. The winter maximum area for 2013 was 5.53 million mi² (14.3 million km²), also the fifth lowest since 1979.

While the extent of winter sea ice has trended downward at a less drastic rate than summer sea ice, the fraction of the sea ice cover that has survived at least two melt seasons remains much smaller than at the beginning of the satellite era. This older, thicker *multi-year ice*—which buttresses the ice cap against more severe melting in the summer—grew slightly this past winter and now covers 1.03 million mi² (2.67 million km²), or about 39,000 mi² (101,010 km²) more than last winter. The extent, however, is still less than half of what it was in the early 1980s.

“I think the multi-year ice cover will continue to decline in the upcoming years,” Comiso said. “There’s a little bit of oscillation, so there still might be a small gain in some years, but it continues to go down and before you know it we’ll lose the multi-year ice altogether.”

This winter, the negative phase of the Arctic Oscillation kept temperatures warmer than average in the north-

ernmost latitudes. A series of storms in February and early March opened large cracks in the ice covering the Beaufort Sea along the northern coasts of Alaska and Canada, in an area of thin seasonal ice. The large cracks quickly froze over, but these new layers of thin ice might melt again now that the sun has re-appeared in the Arctic, which could split the ice pack into smaller ice floes.

“If you put a large chunk of ice in a glass of water, it is going to melt slowly, but if you break up the ice into small pieces, it will melt faster,” said **Nathan Kurtz**, [GSFC—*Sea Ice Scientist*]. “If the ice pack breaks up like that and the melt season begins with smaller-sized floes, that could impact melt.”

Kurtz will analyze data collected over the Beaufort Sea by NASA’s Operation IceBridge—an airborne mission that is currently surveying Arctic sea ice and the Greenland ice sheet—to see if the sea ice in the cracked area was abnormally thin. ■

2012 CLARREO Science Definition Team Meeting Summary

continued from page 31

Value Matrix concept with economic *integrated assessment models* for estimating climate change impact costs across an Intergovernmental Panel on Climate Change (IPCC)-like frequency distribution of climate sensitivity. The research creates a framework for *value of information* calculations, placing a dollar value on uncertainty reduction. It provides a new approach to more rigorously understand the economic value of NASA’s extensive range of climate science research.

David Young and **Bruce Wielicki** delivered a final wrap-up, followed by a team discussion of plans for publication of the science results and future collaborations among the team. The next meeting will be held in Hampton, VA in April 2013⁵. ■

⁵ **UPDATE:** This meeting took place on April 10-12, 2013.

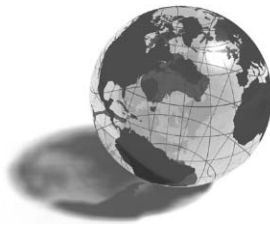
First Light for ISERV Pathfinder, Space Station’s Newest ‘Eye’ on Earth

continued from page 41

SERVIR consists of a coordination office and student research laboratory at MSFC, active hubs in Kenya and Nepal, and a network affiliate in Panama. The coordination office develops application prototypes for the SERVIR and integrates new and relevant technologies from NASA and other scientific research partner organizations to meet the needs of host countries. SERVIR’s primary technical work occurs at the hubs, which are staffed by local and regional experts from those countries. The hubs coordinate with other international and national organizations in their respective regions regarding climate change, environmental monitoring, disasters, weather, and mapping.

SERVIR, jointly funded by NASA and the U.S. Agency for International Development (USAID), operates within NASA’s Earth Sciences Division at HQ. Four other NASA centers work with MSFC on the program, including Goddard Space Flight Center, Ames Research Center, Langley Research Center, and the Jet Propulsion Laboratory.

Watch video highlights of SERVIR’s new camera system on the ISS at servirglobal.net/Globall/Articles/tabid/86/Article/1201/video-highlights-servirs-new-camera-system-on-iss.aspx. ■



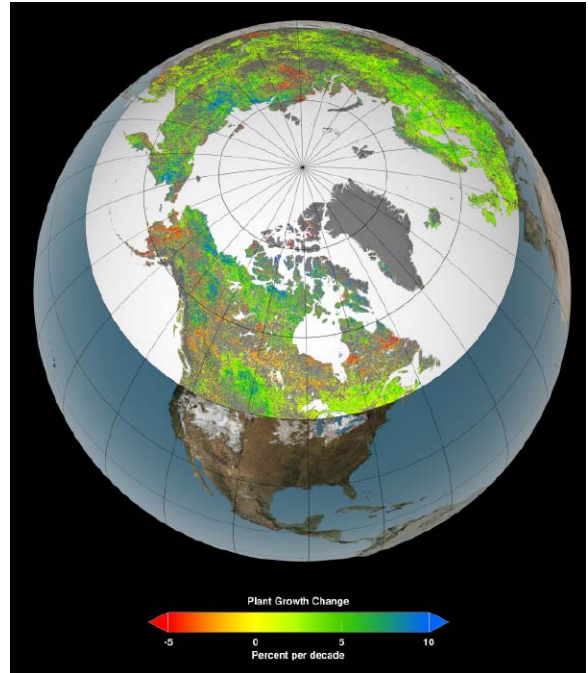
NASA Earth Science in the News

Patrick Lynch, NASA's Earth Science News Team, patrick.lynch@nasa.gov

***Visualized: First Photo Using ISS-mounted ISERV Pathfinder Zooms in on Panama**, March 7; *engadget.com*. The International Space Station (ISS) SERVIR Environmental Research and Visualization System [ISERV] Pathfinder—an imaging instrument that consists of a camera, telescope, and pointing system—was sent to the ISS in July 2012. The instrument was safely installed in the *Destiny* module on the ISS and captured its first image on February 16. The high-resolution image is of the Rio San Pablo, an ecological transition zone that's marked as a protected area by the National Environment Authority of Panama—see image on page 40.

Arctic Gets Greener as Climate Warms: NASA Study, March 11; *livescience.com*. Researchers report that higher temperatures and a longer growing season mean some of Earth's chilliest regions are looking increasingly green. According to a new study, the plant life found at northern latitudes today often looks like the vegetation researchers would have observed up to 430 mi (700 km) farther south in 1982. "It's like Winnipeg, Manitoba, moving to Minneapolis-Saint Paul, MN, in only 30 years," said **Compton Tucker** [NASA's Goddard Space Flight Center (GSFC)]. A team of university and NASA scientists looked at 30 years of satellite and land-surface data on vegetation growth from 45° N latitude to the Arctic Ocean. In this region large patches of lush vegetation now stretch over an area about the size of the continental U.S. and resemble what was found four-to-six latitude degrees to the south in 1982.

Large 2011 Arctic Ozone Hole Explained, March 11; *United Press International*. A combination of extremely cold temperatures, man-made chemicals, and a stagnant atmosphere caused a significant hole in the Arctic ozone layer in 2011. Although both the Earth's poles experience decreases in ozone during the winter, the ozone depletion over the Arctic tends to be milder and shorter-lived than that over Antarctica. Yet in 2011 ozone concentrations in the Arctic atmosphere were about 20% lower than average. While chlorine in the Arctic stratosphere and uncommon atmospheric conditions blocked wind-driven transport of ozone from the tropics, the main culprit was unusually low temperatures, said atmo-



Of the 10 million mi² (26 million km²) of northern vegetated lands, between 34 and 41% showed increases in plant growth (green and blue), 3 to 5% showed decreases in plant growth (orange and red), and 51 to 62% showed no changes (yellow) over the past 30 years. Satellite data in this image are from the Advanced Very High Resolution Radiometer (AVHRR) and Moderate Resolution Imaging Spectroradiometer (MODIS) instruments, which contribute to a vegetation index that allows researchers to track changes in plant growth over large areas. **Credit:** GSFC Scientific Visualization Studio

spheric scientist **Susan Strahan** [GSFC]. "You can safely say that 2011 was very atypical: In over 30 years of satellite records, we hadn't seen any time where it was this cold for this long," Strahan said.

Landsat's First LDCM Images Show Rocky Mountains in Stunning Detail, March 22; *gizmag.com*. The first batch of images from the NASA-U.S. Geological Survey Landsat Data Continuity Mission (LDCM) are part of a three-month testing period, and show the meeting of the Great Plains with the Front Ranges of the Rocky Mountains in Wyoming and Colorado. It's already a pretty spectacular scene when viewed from space by instruments on other platforms, but the images from LDCM managed to enhance it even further.

NASA Sends Fleet of Small Drones to Inspect Noxious Volcano Plumes, April 2; *Los Angeles Times*.

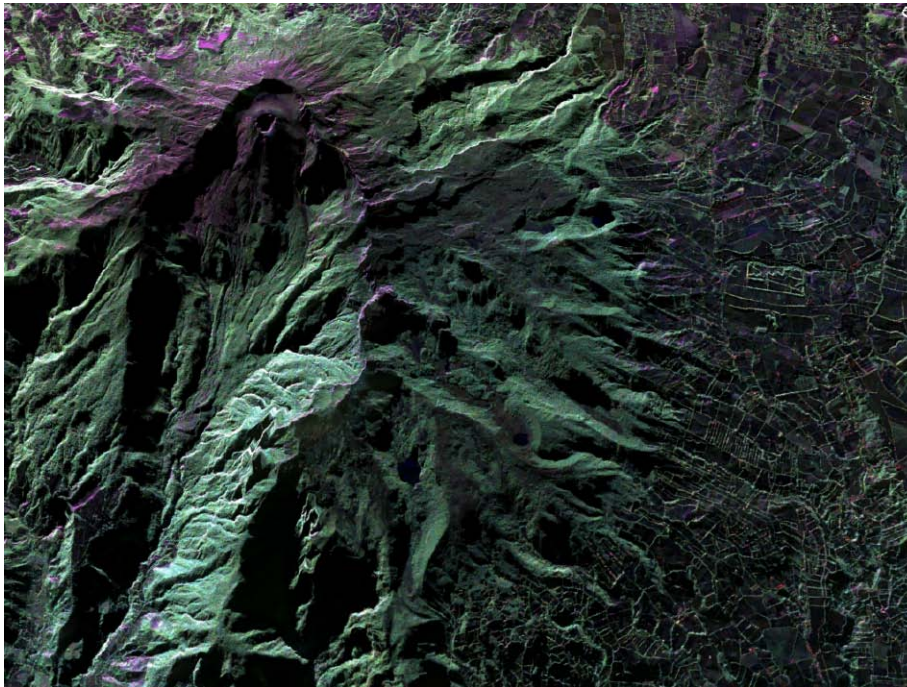
Last month a team of NASA researchers sent three repurposed military drones with special instruments into a sulfur dioxide plume emitted by Costa Rica's 10,500-ft (3200-m) Turrialba volcano. The team, led by principal investigator **David Pieri** [NASA/Jet Propulsion Laboratory (JPL)], launched 10 flights of the small, unmanned planes. The six-pound, twin-electric-engine planes, called Dragon Eyes, recorded video outside and inside the plume. Scientists think computer models derived from this study will contribute to safeguarding the National and International Airspace System, and will also improve global climate predictions and mitigate environmental hazards (e.g., sulfur dioxide volcanic smog, or *vog*) for people who live near volcanoes. The project was a collaboration among JPL and NASA's Ames Research Center and Wallops Flight Facility.

New Images from JPL's UAVSAR, the Radar that Sees through Trees, April 5; *Los Angeles Times*. In March, a manned, NASA-owned C-20A aircraft flew over the Americas carrying a powerful imaging radar system built and managed by the NASA/Jet Propulsion

Laboratory (JPL). The radar's name is the Uninhabited Aerial Vehicle Synthetic Aperture Radar (UAVSAR). What's special about UAVSAR is that it uses microwaves to acquire data rather than the light from the Sun. That means the radar is not befuddled by cloud cover, or stopped by a thick leaf canopy in a rainforest. It can collect data through these traditional barriers, which can be especially helpful in the tropics. "If you looked at a picture of a rainforest on *Google Earth*, you would only see a bunch of trees, but we would see that these forests are flooded, and that gives a lot of additional information," said **Naiara Pinto** [JPL—UAVSAR *Science Coordinator*].

*See news story in this issue for more details.

*Interested in getting your research out to the general public, educators, and the scientific community? Please contact **Patrick Lynch** on NASA's Earth Science News Team at patrick.lynch@nasa.gov and let him know of upcoming journal articles, new satellite images, or conference presentations that you think would be of interest to the readership of *The Earth Observer*. ■*



This image shows Colombia's highly active Galeras Volcano as acquired by UAVSAR on March 13, 2013. Galeras features a breached caldera and an active cone that produces numerous small-to-moderate explosive eruptions. UAVSAR will precisely fly the same flight path over the volcano in 2014. By comparing these camera-like images taken at different times, interferograms are generated that reveal changes in Earth's surface caused by volcanic deformation. **Credit:** NASA/Jet Propulsion Laboratory

NASA Science Mission Directorate – Science Education and Public Outreach Update

Theresa Schwerin, *Institute for Global Environmental Strategies, theresa_schwerin@strategies.org*

Morgan Woroner, *Institute for Global Environmental Strategies, morgan_woroner@strategies.org*

NASA Postdoctoral Fellowships

Deadline—July 1

The NASA Postdoctoral Program offers scientists and engineers unique opportunities to conduct research in space science, Earth science, aeronautics, exploration systems, lunar science, astrobiology, and astrophysics.

Awards: Annual stipends start at \$53,500—with supplements for specific degree fields and high cost-of-living areas. There is an annual travel budget of \$8000, a relocation allowance, and financial supplement for health insurance purchased through the program. Approximately 90 fellowships are awarded annually.

Eligibility: An applicant must be a U.S. citizen, lawful permanent resident, or foreign national eligible for J-1 status as a research scholar to apply. Applicants must have completed a Ph.D. or equivalent degree before beginning the fellowship, but may apply while completing the degree requirements. Fellowships are available to recent or senior-level Ph.D. recipients.

Fellowship positions are offered at several NASA centers. To obtain more information and to apply for this exciting opportunity, visit: nasa.orau.org/postdoc.

ESIP Teacher Workshop for Middle and High School Teachers

Date—July 9; Chapel Hill, NC

Middle- and high- school science teachers are invited to attend the 2013 Earth Science Information Partners (ESIP) Teacher Workshop on Tuesday, July 9, at the University of North Carolina at Chapel Hill. The workshop offers the opportunity to take an *iPad* on loan for an entire school year. The ESIP education committee invites regional science teachers to attend a one-day workshop, with an option to join ESIP members at an afternoon gathering at the North Carolina Museum of Natural History on Wednesday, July 10. The workshop theme will focus on Earth science education, with a strand on climate change education, featuring several hands-on sessions that demonstrate ways in which Earth science tools and data can be used in science classrooms. Space is limited to 20 teachers, so register now at cimss.ssec.wisc.edu/teacherworkshop/esip.

Presidential Awards for Excellence in Science, Mathematics, and Engineering Mentoring

Nominations Due—June 5

The Presidential Awards for Excellence in Science, Mathematics, and Engineering Mentoring (PAESMEM) were established by the White House to recognize U.S. citizens, permanent residents, and U.S. organizations that have demonstrated excellence in mentoring individuals from underrepresented groups in science, technology, engineering, and mathematics (STEM) education and career paths. Nominations, including self-nominations, are invited for individual and organizational PAESMEM awards. Each individual and organizational PAESMEM awardee will receive \$10,000 and a commemorative presidential certificate to be awarded at a special ceremony in Washington, DC. Up to sixteen nominees will be awarded. For full rules and to submit nominations, visit: 1.usa.gov/15EHbqC.

New Featured Products on NASA Wavelength

The NASA Wavelength home page at nasawavelength.org now offers a new round of forty featured products. This collection features educational resources from each of the NASA Science Mission Directorate's Education and Public Outreach Forums: astrophysics, Earth sciences, heliophysics, and planetary sciences. Resources cover a broad range of subject matter, and are appropriate for many different audiences.

NASA Solicitation: The GLOBE Program Implementation Office

NOIs Due—May 20; **Proposals Due**—July 19

The Global Learning and Observations to Benefit the Environment (GLOBE) Program is an important element of NASA's commitment to promoting STEM education among youth worldwide. The Earth Science Division of NASA's Science Mission Directorate solicits proposals for an organization or a consortium of organizations to host the GLOBE Implementation Office and to collaborate with NASA in implementing GLOBE, to strengthen programmatic support for GLOBE, and to enhance the value of GLOBE to its worldwide community of partners, students, teachers, and scientists. The GLOBE Implementation Office (GIO) shall perform functions related to GLOBE science, education, evaluation, and communication, as well as other functions necessary to support the GLOBE community. For more information and to view the full solicitation, visit: bit.ly/ZRU1uz. ■

EOS Science Calendar | Global Change Calendar

June 10–12, 2013

ASTER Science Team Meeting, Tokyo, Japan.

October 7, 2013

Ocean Surface Topography Science Team Meeting, Boulder, CO.

October 15–17, 2013

HypIRI Science and Applications Workshop, Pasadena, CA.

October 23–25, 2013

GRACE Science Team Meeting, Austin, TX.
www.csr.utexas.edu/grace/GSTM

November 5–7, 2013

SMAP Cal/Val Workshop, Oxnard, CA.
smap.jpl.nasa.gov/science/workshops

June 24–28, 2013

AGU Chapman Conference - Crossing the Boundaries in Planetary Atmospheres: From Earth to Exoplanets, Annapolis, MD. chapman.agu.org/planetaryatmospheres

July 21–26, 2013

2013 International Geoscience and Remote Sensing Symposium, Melbourne, Australia. www.igarss2013.org

October 27–30, 2013

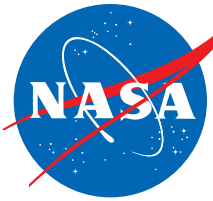
Geological Society of America, Denver, CO. community.geosociety.org/2013AnnualMeeting/Home

November 11–22, 2013

Conference of Parties (COP)-19, Warsaw, Poland.
www.cop19.org

December 9–13, 2013

American Geophysical Union, San Francisco, CA.
fallmeeting.agu.org/2013



Code 610
National Aeronautics and Space Administration

Goddard Space Flight Center
Greenbelt, MD 20771

PRSR STD
Postage and Fees Paid
National Aeronautics and Space Administration
Permit 396

Official Business
Penalty for Private Use: \$300

(affix mailing label here)

eos.nasa.gov

The Earth Observer

The Earth Observer is published by the EOS Project Science Office, Code 610, NASA Goddard Space Flight Center, Greenbelt, Maryland 20771, telephone (301) 614-5561, FAX (301) 614-6530, and is available in color at eospsa.nasa.gov/earth-observer-archive. Black and white hard copies can be obtained by writing to the above address.

Articles, contributions to the meeting calendar, and suggestions are welcomed. Contributions to the calendars should contain location, person to contact, telephone number, and e-mail address. Newsletter content is due on the weekday closest to the 15th of the month preceding the publication—e.g., December 15 for the January–February issue; February 15 for March–April, and so on.

To subscribe to *The Earth Observer*, or to change your mailing address, please call Cindy Trapp at (301) 614-5559, or send a message to Cynthia.trapp-1@nasa.gov, or write to the address above. If you would like to stop receiving a hard copy and be notified via email when future issues of *The Earth Observer* are available for download as a PDF, please send an email with the subject “**Go Green**” to Cynthia.trapp-1@nasa.gov. Your name and email address will then be added to an electronic distribution list and you will receive a bi-monthly email indicating that the next issue is available for download. If you change your mind, the email notification will provide an option for returning to the printed version.

The Earth Observer Staff

Executive Editor:	Alan B. Ward (alan.b.ward@nasa.gov)
Assistant/Technical Editors:	Heather H. Hanson (heather.h.hanson@nasa.gov) Mitchell K. Hobish (mkh@sciential.com)
Technical Editor:	Ernest Hilsenrath (hilsenrath@umbc.edu)
Design, Production:	Deborah McLean (deborah.f.mclean@nasa.gov)



JPL Publication 12-16



HyspIRI Thermal Infrared (TIR) Band Study Report

*Michael S. Ramsey
University of Pittsburgh
Pittsburgh, PA*

*Vincent J. Realmuto
Glynn C. Hulley
Simon J. Hook
Jet Propulsion Laboratory
Pasadena, CA*

**National Aeronautics and
Space Administration**

**Jet Propulsion Laboratory
California Institute of Technology
Pasadena, California**

Oct 2012

This research was carried out at the Jet Propulsion Laboratory, California Institute of Technology, and at the University of Pittsburgh under a contract with the National Aeronautics and Space Administration.

Reference herein to any specific commercial product, process, or service by trade name, trademark, manufacturer, or otherwise, does not constitute or imply its endorsement by the United States Government or the Jet Propulsion Laboratory, California Institute of Technology.

© 2012. California Institute of Technology. Government sponsorship acknowledged.

Revisions:

Version 1.0 draft by Glynn Hulley, 10/23/2012

Section 5 updated by Vince Realmuto, 10/25/2012

Minor edits and formatting by Peter Basch (JPL editor), 10/26/2012

Edits in all sections by Mike Ramsey, 11/1/2012

Notes:

Section 5 research was conducted by Realmuto at the Jet Propulsion Laboratory, California Institute of Technology.

Section 6 research was conducted by P.I. Ramsey at the University of Pittsburgh, PA.

Section 7.2 research and development of MAGI was conducted by Ramsey, P.I. Hall and the MAGI team at Aerospace Corporation, El Segundo, CA.

Section 7.1 development and research of HyTES was conducted by P.I. Hook and the HyTES team at the Jet Propulsion Laboratory, California Institute of Technology.

Contacts

Readers seeking additional information about this study may contact the following researchers:

Vincent J. Realmuto
MS 183-501
Jet Propulsion Laboratory
4800 Oak Grove Dr.
Pasadena, CA 91109
Email: vincent.j.realmuto@jpl.nasa.gov
Office: (818) 354-1824

Michael S. Ramsey
Department of Geology & Planetary Science
University of Pittsburgh
4107 O'Hara Street, room 200
Pittsburgh, PA 15260
Phone: (412) 624-8772; Fax: (412) 624-3914
Email: mramsey@pitt.edu

Glynn C. Hulley
MS 183-501
Jet Propulsion Laboratory
4800 Oak Grove Dr.
Pasadena, CA 91109
Email: glynn.hulley@jpl.nasa.gov
Office: (818) 354-2979

Simon J. Hook
MS 183-501
Jet Propulsion Laboratory
4800 Oak Grove Dr.
Pasadena, CA 91109
Email: simon.j.hook@jpl.nasa.gov
Office: (818) 354-0974

Abstract

One of the many science questions that will be addressed by the Hyperspectral Infrared Imager (HyspIRI) mission will be to help identify natural hazards such as volcanic eruptions and any associated precursor activity, and it will also map the mineralogical composition of the natural and urban land surface. To answer these questions, the HyspIRI satellite includes a thermal infrared (TIR) multispectral scanner with seven spectral bands in the thermal infrared (TIR) between 7 and 12 μm and one band in the mid-infrared between 3 and 5 μm designed to measure hot targets. The TIR bands have a NE Δ T of <0.2 K at 300 K and all bands have a spatial scale of 60 m. A critical aspect of HyspIRI being successful at answering the science questions associated with the HyspIRI science tractability matrix is placement of the 7 TIR bands in the 7–12 μm spectral region. In order to help determine the optimum positions for the TIR bands, a small team was assembled to conduct a study report based on laboratory, spaceborne, and airborne data.

Contents

Contacts	4
Abstract	5
1 Introduction	8
2 HypsIRI instrument characteristics	10
3 HypsIRI thermal infrared science objectives	14
4 Background	15
5 HypsIRI band positions for the detection of volcanic plumes	19
5.1 Mapping volcanic plume constituents	21
5.1.1 Conclusions	22
5.2 Case Study: Mount Etna eruption plume	22
5.2.1 Analysis	22
5.2.2 Conclusions	23
5.3 Case Study: Sarychev Peak volcano	24
5.3.1 Analysis	24
5.3.2 Conclusions	25
6 HypsIRI band positions for Earth surface compositional mapping	26
6.1.1 Case Study: Kelso Dunes	28
6.1.2 Case Study: Great Sands	33
6.1.3 Conclusions	35
7 Future work with airborne data	36
7.1 HyTES.....	36
7.2 MAGI.....	40
8 References	45

Figures

Figure 1. HypsIRI TIR instrument proposed spectral bands.	10
Figure 2. HypsIRI TIR scanning scheme.....	12
Figure 3. HypsIRI TIR conceptual layout.	12
Figure 4. HypsIRI TIR predicted sensitivity 200–500 K.....	13
Figure 5. HypsIRI TIR predicted sensitivity 300–1100 K.....	13
Figure 6. HypsIRI nominal band positions in the TIR region based on MODIS bands 28 and 32 (H1 and H7), and ASTER bands 10–12 (H2–H4). Bands H5 and H6 centered at 10.53 and 11.33 micron are similar to ASTER bands 13 and 14. Transmission features of H ₂ O, O ₃ and CO ₂ are also shown as reference.....	16
Figure 7. (a) ASTER nighttime TIR images of Augustine Volcano showing hot pyroclastic flow deposits (Bright in TIR) and eruption plume. Colors represent different materials entrained within plume. (b) SO ₂ map derived from ASTER data.....	17
Figure 8. ASTER decorrelation stretch (DCS) of Death Valley using bands 14, 12, and 10 as RGB respectively. Different colors in the image correspond to different mineral types, e.g., quartz features are red, carbonates are green, and quartz-poor regions are purple.	18
Figure 9. Heritage of the HypsIRI spectral response, showing (a) ASTER response vs. SO ₂ transmission, (b) MODIS response vs. SO ₂ transmission, (c) HypsIRI response vs. SO ₂ transmission, and (d) brightness temperature difference vs. SO ₂ concentration.	20
Figure 10. Transmission spectra expressed as brightness temperature difference spectra for three constituents of volcanic plumes and ash clouds. (a) SO ₂ , (b) silicate ash, and (c) SO ₄ aerosol at the spectral resolution of HyTES (thin line) and MASTER (thick line).....	21
Figure 11. (left) MODIS-Aqua band 28 (7.3 μm) image of the Mount Etna eruption on 28 October 2002, (right) thermal infrared responses of HypsIRI plotted with transmission curves for water vapor (top) and SO ₂ (right).....	23
Figure 12. Eruption of Sarychev Peak Volcano (Matua Island, Russian Kuril Islands). Top panels (a) true-color composite of MODIS-Terra data acquired at 00:50 UTC on 16 June 2006. (b) is a false-color composite of MODIS thermal infrared (TIR) channels 32, 31, and 29 displayed in red, green, and blue, respectively. Bottom panels show corresponding (a) MODIS band 28 (7.34 μm) and (b) band 33 (13.34 μm) brightness temperatures.	24
Figure 13. A selection of JPL mineral library spectra representing several classes shown as percent reflectance in the visible, shortwave infrared (0.38–2.5 μm) and infrared (2–14 μm) regions. Black circles in the infrared spectrum represent HypsIRI bands convolved to the library spectra. All spectra are offset for clarity.....	27
Figure 14. Decorrelation stretch (DCS) images of the Kelso Dunes, CA using MASTER data. The yellow indicates an equal abundance of quartz and microcline feldspar, while cyan is quartz and oligoclase feldspar. Increased magenta coloration in (B) shows improved feldspar detection using the 10.1 μm band instead of the 10.6 μm MASTER band.....	28
Figure 15. Thermal infrared (TIR) emissivity spectra of four mineral end-members acquired at Arizona State University (Oligoclase, Clay+Magnetite, Quartz and Microcline) and one spectrum (sample k24) of aeolian sand from the Kelso Dunes (Mojave Desert, CA). The spectra were degraded to the resolution of various TIR instruments: (A) Laboratory resolution (B) MASTER resolution (10 bands) (C) TIMS resolution (6 bands) (D) ASTER resolution (5 bands) (E) Current HypsIRI resolution (7 bands) and (F) Proposed new HypsIRI band alignment (7 bands). In this configuration, three of the bands have been moved for better gas and mineral detection. The 8.63 μm band has been shifted to 8.55 μm (centered over the SO ₂ absorption doublet). The 10.53 μm band has been moved to 10.05 μm for better detection and discrimination of feldspar minerals. The 11.33 μm band has been shifted slightly to 11.35 μm for more accurate carbonate detection.	29
Figure 16. Proposed HypsIRI version 2.0 band locations. Band modifications from version 1.0 are highlighted in red. The 8.63 μm band has been shifted to 8.55 μm, the 10.53 μm band has been moved to 10.05 μm, and the 11.33 μm band has been shifted slightly to 11.35 μm (see text for details).	30
Figure 17. Results of linear deconvolution of the Kelso sand sample (k24) at the various spectral resolution/band configurations shown in Fig 15. The laboratory resolution is assumed to be the most accurate and plotted as the dark blue line for each of the four mineral end-members. The closest match between the laboratory	

results and the other configurations are for the proposed new HypsIRI version 2.0 spectral bands shown in red (avg. error = 1.9%). 31

Figure 18. (left) Laboratory emissivity spectra of different silicate minerals including andesine, anorthoclase, microcline, and quartz, (right) silicate spectra convolved to HypsIRI v1.0 and v2.0 band positions. 32

Figure 19. HypsIRI TIR response functions showing band positions for v1.0 (left) and the proposed v2.0 modifications including narrowing of the proposed 10.05 μm and 11.35 μm bands (right). 33

Figure 20. Linear deconvolution results for ASTER, HypsIRI v1.0 and v2.0 band positions for three sand samples collected over the Gran Desierto dune system in Mexico (SAM94, SAM39, SAMG162). Bottom image shows a view of the dune system, which contains primarily a mixture of quartz and feldspars. 34

Figure 21. Laboratory spectra of feldspars, and carbonates, with HypsIRI v2.0 band positions shown as gray vertical bars. 35

Figure 22. (left) The model for the HyTES instrument, including a Dyson spectrometer, long, straight slit, curved diffraction grating and Quantum Well Infrared Photodetector (QWIP). (right) HyTES instrument specifications. 36

Figure 23. Test site locations on Google Earth. 37

Figure 24. (left) Cuprite, NV image acquired on 07-20-2012 with bands 150 (10.08 μm), 100 (9.17 μm), and 58 (8.41 μm) displayed as RGB respectively as image cube. A) Radiance at sensor for different locations at Cuprite, B) Noise equivalent Delta Temperature (NEDT) histogram (~ 0.2 K). 38

Figure 25. Comparisons between HyTES spectra convolved to HypsIRI TIR bands (blue circles) and laboratory spectra (red circles) of geologic samples collected in the Cuprite, NV region including basalt, carbonate, kaolinite, and silica. 39

Figure 26. (left) Heart of the MAGI sensor showing Dyson spectrometer, mounts, and optics bench. (right) Sensor dewar with external telescope (dewar diameter is 13 inches). 41

Figure 27. (left) Noise Equivalent Contrast (NEC) median ratio vs. number of channels (128, 64, 32, and 16) for 28 chemical compounds common in industrial gas plumes [Hall *et al.*, 2008]. Larger ratios suggest a lower sensitivity to the specific chemical. In most cases sensitivity loss from 128 channels to 32 is less than a factor of 2. However, note the significant penalty where the data is reduced to less than ~ 30 channels. (right) Similar plot for other materials and gases as well as the surface temperature retrieval error expected the in-scene atmospheric correction (ISAC). 42

Figure 28. MAGI level 2 atmospherically-corrected data (whisk 18) and emissivity spectral retrievals from the Salton Sea, CA. (top) MAGI band 10 (8.751 micrometers) showing the "sandbar" geothermal field in the center of the strip and the Salton Sea to the right (north is to the upper right in the image). (left) Gypsum emissivity spectrum. (right) Quartz emissivity spectrum. 43

Figure 29. (left) Four panel image showing SEBASS data acquired over the "sandbar" geothermal field at Salton Sea, CA on April 6, 2010. The mineral retrieval for the full spectral resolution of SEBASS (second panel) is compared to both HypsIRI TIR configurations. The fourth panel shows an oligoclase distribution (in red) more similar to the full spectral resolution. (right) Scatter plots of the oligoclase retrievals confirm that there is a more linear relationship between the full spectral resolution and the simulated HypsIRI TIR data with the shifted band centers. 44

Tables

Table 1. Preliminary TIR Measurement Characteristics 11

Table 2. Test sites and purpose for the HyTES test flights. 37

Table 3. MAGI instrument specifications. 41

1 Introduction

The Hyperspectral Infrared Imager (HypSIRI) mission will provide an unprecedented capability to assess how ecosystems respond to natural and human-induced changes. It will help us assess the status of biodiversity around the world and the role of different biological communities on land and within inland water bodies, as well as coastal zones and, at reduced resolution, in the ocean [*HypSIRI*, 2008]. Furthermore, it will help identify natural hazards—in particular, volcanic eruptions and any associated precursor activity—and it will map the mineralogical composition of the natural and urban land surface. The mission will advance our scientific understanding of how the Earth is changing as well as provide valuable societal benefit in understanding and tracking dynamic events such as volcanoes and wildfires.

HypSIRI includes two instruments: a visible shortwave infrared (VSWIR) imaging spectrometer operating between 380 and 2500 nm in 10-nm contiguous bands and a thermal infrared (TIR) multispectral scanner with eight spectral bands operating between 4 and 12 μm . Both instruments acquire data with a spatial resolution of 60 m from the nominal orbit altitude. The VSWIR and TIR instruments have revisit times of 19 and 5 days with swath widths of 145 and 600 km, respectively.

In terms of spectral and spatial resolution, the HypSIRI TIR measurement derives its heritage from the Advanced Spaceborne Thermal Emission and Reflection radiometer (ASTER) instrument, a five-channel multispectral TIR scanner that was launched on NASA's Terra spacecraft in December 1999 with a 90-m spatial resolution and revisit time of 16 days [*Yamaguchi et al.*, 1998]. The ASTER band positions in turn were derived from the NASA airborne Thermal Infrared Multispectral Scanner (TIMS), a precursor airborne instrument used in preparation for ASTER that had six TIR bands. One of the most important aspects of a TIR instrument's design is determining optimal number, positions, and detection thresholds of the TIR channels. Positions of the bands within the TIR region will influence the ability to better quantitatively map: 1) SO_2 from volcanic and anthropogenic sources, 2) minerals on the Earth's surface such as feldspars, carbonates, and silicates, as well as 3) urban materials.

The remainder of the document will detail case studies involving volcanic emissions and surface mineral mapping to optimize the HypSIRI TIR band positions in order to answer the

relevant Earth Science questions. The data used in this study include satellite, laboratory, and airborne data.

2 HypsIRI instrument characteristics

The TIR instrument will acquire data in eight spectral bands, seven of which are located in the thermal infrared part of the electromagnetic spectrum between 7 and 13 μm shown in Figure 1; the remaining band is located in the mid-infrared part of the spectrum around 4 μm . The center position and width of each band is provided in Table 1. The exact spectral location of each band has not been determined; the nominal locations provided here are based on the measurement requirements identified in the science-traceability matrices, which included recognition that related data was acquired by other sensors such as ASTER and the Moderate Resolution Imaging Spectroradiometer (MODIS). HypsIRI will contribute to maintaining a longtime series of these measurements. For example, the positions of three of the TIR bands closely match the first three thermal bands of ASTER, while two of the TIR bands match bands of ASTER and MODIS typically used for split-window type applications (ASTER bands 12–14 and MODIS bands 28, 31, 32). It is expected that small adjustments to the band positions will be made based on ongoing science activities.

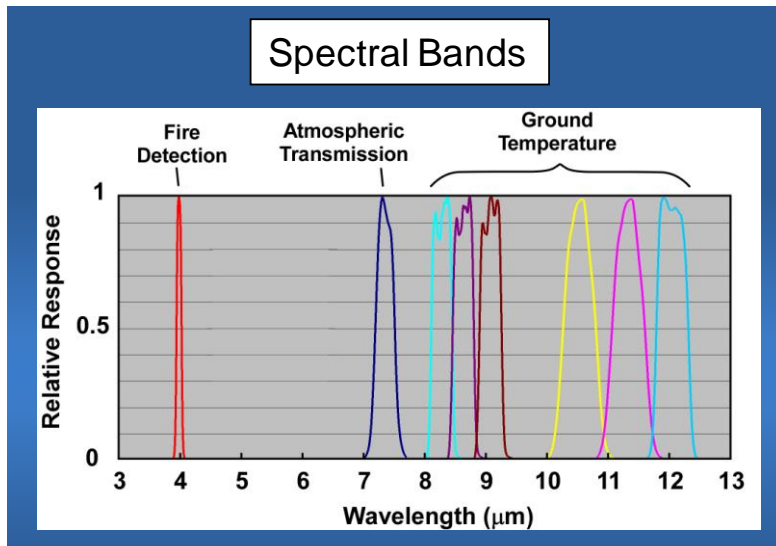


Figure 1. HypsIRI TIR instrument proposed spectral bands.

Table 1. Preliminary TIR Measurement Characteristics

Spectral	
Bands (8) μm	3.98 μm , 7.35 μm , 8.28 μm , 8.63 μm , 9.07 μm , 10.53 μm , 11.33 μm , 12.05 μm
Bandwidth	0.084 μm , 0.32 μm , 0.34 μm , 0.35 μm , 0.36 μm , 0.54 μm , 0.54 μm , 0.52 μm
Accuracy	<0.01 μm
Radiometric	
Range	Bands 2–8 = 200 K–500 K; Band 1 = 1200 K
Resolution	< 0.05 K, linear quantization to 14 bits
Accuracy	< 0.5 K 3-sigma at 250 K
Precision (NE Δ T)	< 0.2 K
Linearity	>99% characterized to 0.1 %
Spatial	
IFOV	60 m at nadir
MTF	>0.65 at FNy
Scan Type	Push-Whisk
Swath Width	600 km ($\pm 25.5^\circ$ at 623-km altitude)
Cross Track Samples	9,300
Swath Length	15.4 km (± 0.7 degrees at 623 km altitude)
Down Track Samples	256
Band to Band Co-Registration	0.2 pixels (12 m)
Pointing Knowledge	10 arcsec (0.5 pixels) (approximate value, currently under evaluation)
Temporal	
Orbit Crossing	11 a.m. Sun synchronous descending
Global Land Repeat	5 days at Equator
On Orbit Calibration	
Lunar views	1 per month {radiometric}
Blackbody views	1 per scan {radiometric}
Deep Space views	1 per scan {radiometric}
Surface Cal Experiments	2 (day/night) every 5 days {radiometric}
Spectral Surface Cal Experiments	1 per year
Data Collection	
Time Coverage	Day and Night
Land Coverage	Land surface above sea level
Water Coverage	Coastal zone minus 50 m and shallower
Open Ocean	Averaged to 1-km spatial sampling
Compression	2:1 lossless

A key science objective for the TIR instrument is the study of hot targets (volcanoes and wildfires), so the saturation temperature for the 4- μm channel is set high (1200 K) [Realmuto *et al.* 2011], whereas the saturation temperatures for the thermal infrared channels are set at 500 K.

The TIR instrument will operate as a whiskbroom mapper, similar to MODIS but with 256 pixels in the cross-whisk direction for each spectral channel (Figure 2). A conceptual layout for the instrument is shown in Figure 3. The scan mirror rotates at a constant angular speed. It

sweeps the focal plane image across nadir, then to a blackbody target and space, with a 2.2-second cycle time.

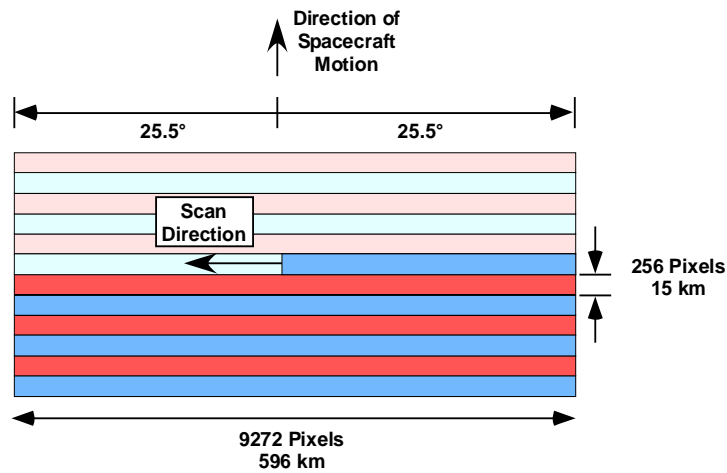


Figure 2. HypsIRI TIR scanning scheme.

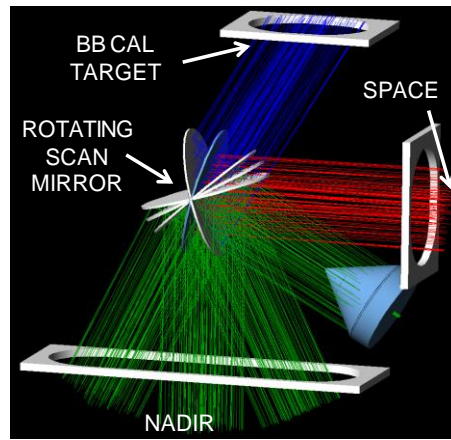


Figure 3. HypsIRI TIR conceptual layout.

The $f/2$ optics design is all reflective, with gold-coated mirrors. The 60-K focal plane will be a single-bandgap mercury cadmium telluride (HgCdTe) detector, hybridized to a CMOS readout chip, with a butcher-block spectral filter assembly over the detectors. Thirty-two analog output lines, each operating at 10–12.5 MHz, will move the data to analog-to-digital converters.

The temperature resolution of the thermal channels is much finer than the mid-infrared channel, which (due to its high saturation temperature) will not detect a strong signal until the target is above typical terrestrial temperatures at around 400 K. All the TIR channels are quantized at 14 bits. Expected sensitivities of the eight channels, expressed in terms on noise-equivalent temperature difference, are shown in the following two plots (Figures 4 and 5).

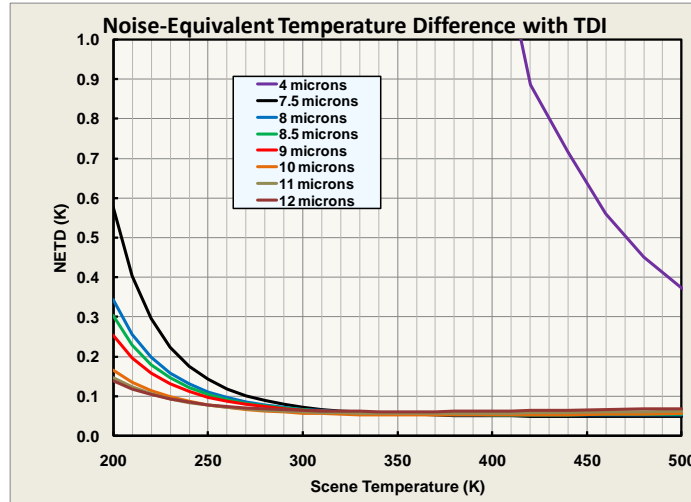


Figure 4. HyspIRI TIR predicted sensitivity 200–500 K.

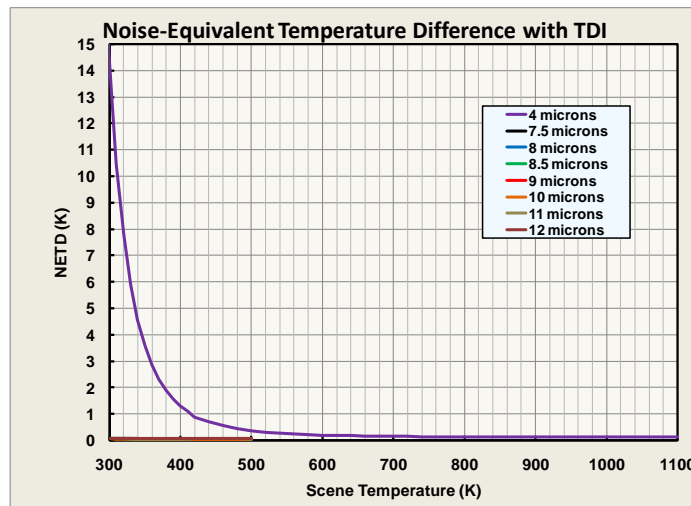


Figure 5. HyspIRI TIR predicted sensitivity 300–1100 K.

The TIR instrument will have a swath width of 600 km with a pixel spatial resolution of 60 m, resulting in a temporal revisit of 5 days at the equator. The instrument will be on both day and night, and it will acquire data over the entire surface of the Earth. Like the VSWIR, the TIR instrument will acquire full spatial resolution data over the land and coastal oceans (to a depth of <50 m) but, over the open oceans, the data will be averaged to a spatial resolution of 1 km. The large swath width of the TIR will enable multiple revisits of any spot on the Earth every week (at least one day view and one night view). This repeat period is necessary to enable monitoring of dynamic or cyclical events such as volcanic hotspots or crop stress associated with water availability.

3 HypsIRI thermal infrared science objectives

The HypsIRI mission is science driven by linking the measurement requirements for the mission to one or more science questions. HypsIRI has three top-level science questions related to 1) ecosystem function and composition, 2) volcanoes and natural hazards, and 3) surface composition and the sustainable management of natural resources [*HypsIRI*, 2008]. The NRC Decadal Survey called out these three areas specifically. These questions provide a scientific framework for the HypsIRI mission. NASA appointed the HypsIRI Science Study Group (SSG) to refine and expand these questions to a level of detail that was sufficient to define the measurement requirements for the HypsIRI mission. Five overarching thematic questions (TQ) were defined by the HypsIRI SSG for the TIR component:

- **TQ1: Volcanoes and Earthquakes:** How can we help predict and mitigate earthquake and volcanic hazards through detection of transient thermal phenomena?
- **TQ2: Wildfires:** What is the impact of global biomass burning on the terrestrial biosphere and atmosphere, and how is this impact changing over time?
- **TQ3: Water Use and Availability:** How is consumptive use of global freshwater supplies responding to changes in climate and demand, and what are the implications for sustaining water resources?
- **TQ4: Urbanization and Human Health:** How does urbanization affect the local, regional, and global environment? Can we characterize this effect to help mitigate its effects on human health and welfare?
- **TQ5: Earth Surface Composition and Change:** What are the composition and thermal properties of the exposed surface of the Earth? How do these factors change over time and affect land use and habitability?

For each of these questions, accurate retrieval of Land Surface Temperature and Emissivity plays a key role in defining the measurement objectives and requirements for these questions. The HypsIRI LST product, in particular, will be especially useful for studies of surface energy and water balance in agricultural regions at the crop scale (<100 m), where quantification of evapotranspiration processes are essential for helping land managers make important decisions relating to water use and availability. The HypsIRI emissivity product will

contain spectral/compositional information from rocks, soils, and vegetation at different wavelengths, which will provide a diagnostic tool for discriminating surface cover types at spatial scales of 60 m or less.

4 Background

In terms of TIR band positions, the HypsIRI TIR measurement will derive its heritage from the ASTER, MASTER, TIMS, and MODIS multispectral measurements. ASTER is a five-channel multispectral TIR scanner that was launched on NASA's Terra spacecraft in December 1999 with a 90-m spatial resolution and revisit time of 16 days. The TIR positions of ASTER bands 10–14 are placed in the so called atmospheric 'window' regions of the TIR region (8–12 μm) and centered on 8.3, 8.6, 9.1, 10.6 and 11.3 μm respectively. These positions allow accurate emissivity surface temperature retrievals which are used for mineralogic composition and mineral mapping studies [Hook *et al.*, 2005; Vaughan *et al.*, 2005; Scheidt, *et al.*, 2011]. The ASTER band positions are very similar to the NASA airborne Thermal Infrared Multispectral Scanner (TIMS), which has six spectral channels from 8–12 μm centered on 8.4, 8.8, 9.2, 9.9, 10.7, and 11.6 μm respectively.

MODIS is a multi-spectral imager onboard the Terra and Aqua satellites of NASA's Earth Observing System (EOS), and has been the flagship for land-surface remote sensing since the launch of Terra in December 1999 [Justice *et al.*, 1998]. MODIS scans $\pm 55^\circ$ from nadir and provides daytime and nighttime imaging of any point on the surface of the Earth every 1–2 days with a spatial resolution of ~ 1 km at nadir and 5 km at higher viewing angles at the scan edge [Wolfe *et al.*, 1998]. MODIS TIR bands include bands 28 (7.175–7.475 μm), 29 (8.4–8.7 μm), 30 (9.58–9.88 μm), 31 (10.78–11.28 μm), 32 (11.77–12.27 μm) and their placement include key uses such as upper tropospheric humidity, surface temperature, total ozone, cloud temperature, cloud height, and volcano monitoring. The MODIS/ASTER Airborne Simulator (MASTER) was developed to support scientific studies by ASTER and MODIS projects, including algorithm development and band placement studies [Hook *et al.*, 2001]. At present, the nominal HypsIRI TIR band placements are a hybrid between ASTER and MODIS TIR bands, and include MODIS bands 28, 32 and ASTER bands 10–12 shown in Figure 6.

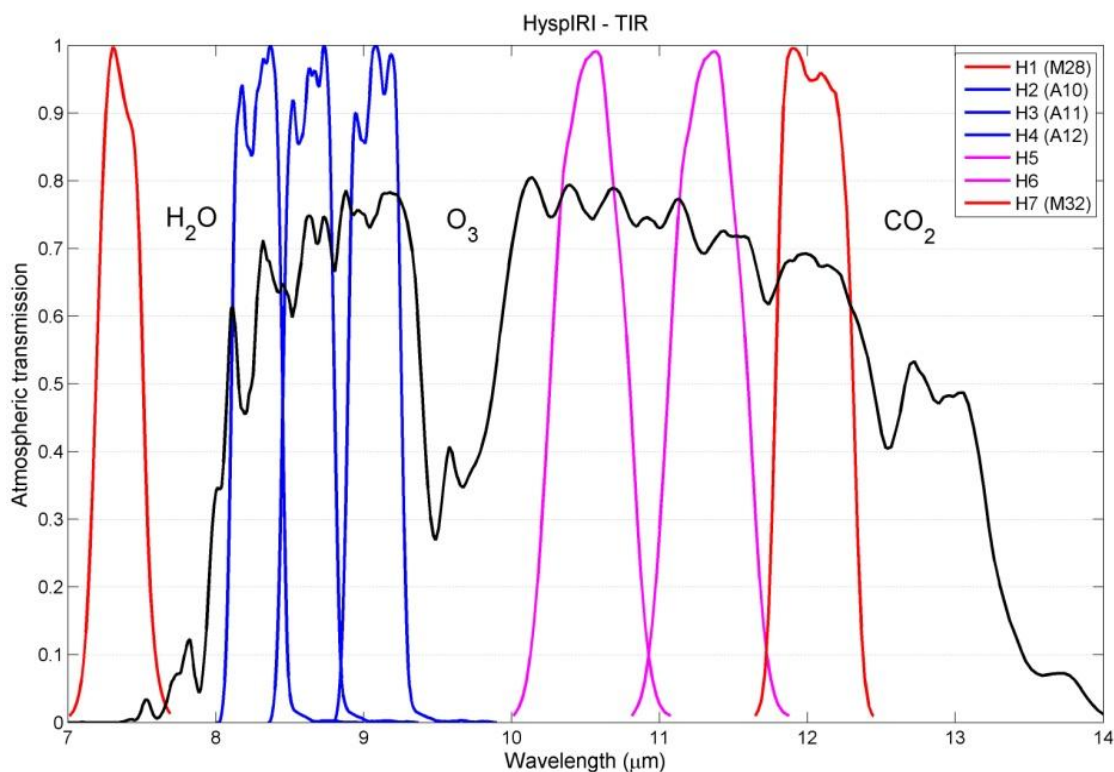


Figure 6. HypsIRI nominal band positions in the TIR region based on MODIS bands 28 and 32 (H1 and H7), and ASTER bands 10–12 (H2–H4). Bands H5 and H6 centered at 10.53 and 11.33 micron are similar to ASTER bands 13 and 14. Transmission features of H₂O, O₃ and CO₂ are also shown as reference.

The TQ1 HypsIRI overarching science question states: How can we help predict and mitigate earthquake and volcanic hazards through detection of transient thermal phenomena? It has been shown that transient thermal anomalies precede earthquakes and volcanic eruptions. TIR images from HypsIRI will allow us to monitor these phenomena in the hope of one day providing capability of predicting such disasters. Precursory behaviors of volcanoes can include increases in SO₂ emission, and therefore TIR data will allow us to detect not only SO₂, but also ash and water ice in the eruptive plumes [Realmuto and Worden, 2000; Realmuto et al., 1997]. Similarly, thermal anomalies such as crater lakes, fumaroles, domes, etc. typically precede an eruption [Ramsey and Harris, 2012; Rosi et al., 2006]. Remote monitoring of this activity provides crucial information that can lead to more accurate event predictions. SO₂ absorption primarily occurs in the 7.5 and 8.5 μm regions, and correct placement of bands around these regions is essential for quantitatively mapping SO₂ plumes.

Figure 7 (a) shows an ASTER nighttime multispectral TIR image of Augustine Volcano on 1 February 2006 showing hot pyroclastic flow deposits (bright in TIR) and eruption plume.

Colors represent different materials entrained within plume. For example, magenta indicates mixtures of water droplets (steam) and silicate ash; red, yellow, and orange indicate mixtures of ash and SO₂. Figure 7 (b) shows an SO₂ map of column abundance derived from ASTER data. The rapid acquisition of the high-resolution ASTER image was possible because of an integrated program of thermal anomaly detection, which uses lower spatial/higher temporal resolution TIR instruments to trigger ASTER TIR observations at a much higher temporal frequency [Duda *et al.*, 2009]. HypsIRI will provide both the high spatial and temporal TIR data to make this type of fire and volcano monitoring routinely possible.

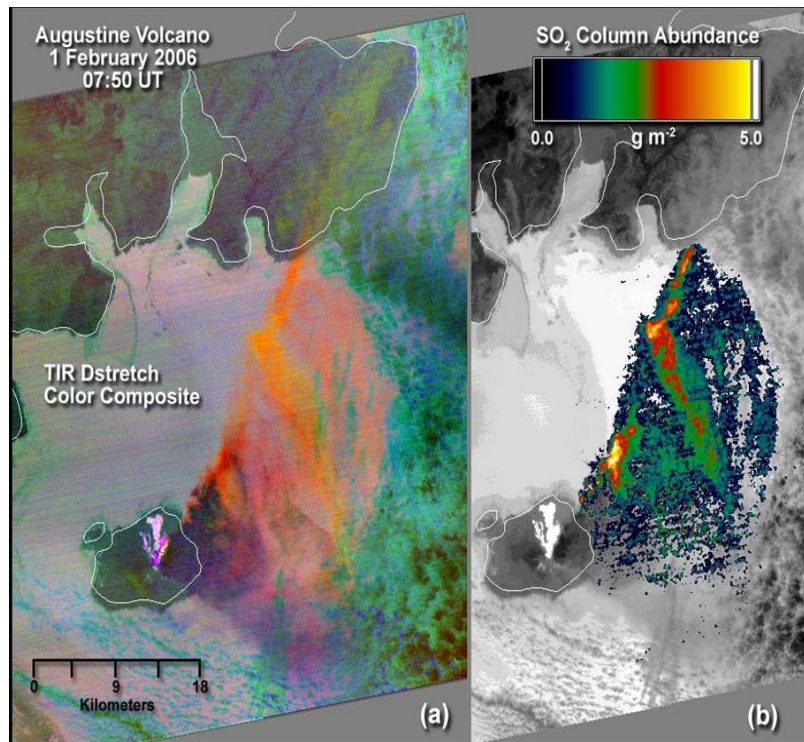


Figure 7. (a) ASTER nighttime TIR images of Augustine Volcano showing hot pyroclastic flow deposits (Bright in TIR) and eruption plume. Colors represent different materials entrained within plume. (b) SO₂ map derived from ASTER data.

The TQ5 HypsIRI overarching science question states: What are the composition and thermal properties of the exposed surface of the Earth, and how do these factors change over time and affect land use and habitability? The emissivity of the exposed terrestrial surface of the Earth can be uniquely helpful in discriminating between different rock, mineral, and soil types. Surface compositional studies hold clues to the origins of materials, the processes that transport/alter these materials, and also the geology and evolution of different rock types. Spaceborne measurements from HypsIRI will enable us to derive surface temperatures and

emissivities for a variety of Earth's surfaces. For example, different Si-O bonded structures vary in their interaction with energy in the thermal infrared region (8–12 μm). Framework silicates, such as quartz and feldspar (common in most continental rocks), show minimum emissivity at shorter wavelengths (8.5 μm), whereas pyroxene and olivine (common in many volcanoes) show minimum emissivity at progressively longer wavelength. Carbonate minerals have a diagnostic feature around between 11.2 and 11.4 μm , which moves from the shorter to the longer wavelengths as the atomic weight of the cation increases. Correct placement of the TIR bands in the 8–12 μm is critical for mapping and distinguishing between felsic and mafic rock compositions as well as positively identifying certain minerals, mineral classes, and urban materials. Figure 8 shows an example of an ASTER-derived decorrelation stretch (DCS) over Death Valley, CA. The DCS exploits inter-channel differences to enhance the color in images, resulting in an image where the pixels are distributed among the full range of possible colors. ASTER bands 14, 12, and 10 are plotted as red, green, and blue (RGB), respectively. Quartz-rich rocks are displayed in red and magenta, quartz-poor rocks in blues and purples, and carbonates in green. Temperature information is related to the brightness of the colors, i.e., areas of higher elevation (and cooler rocks) appear darker than lower elevation areas that have higher temperatures.

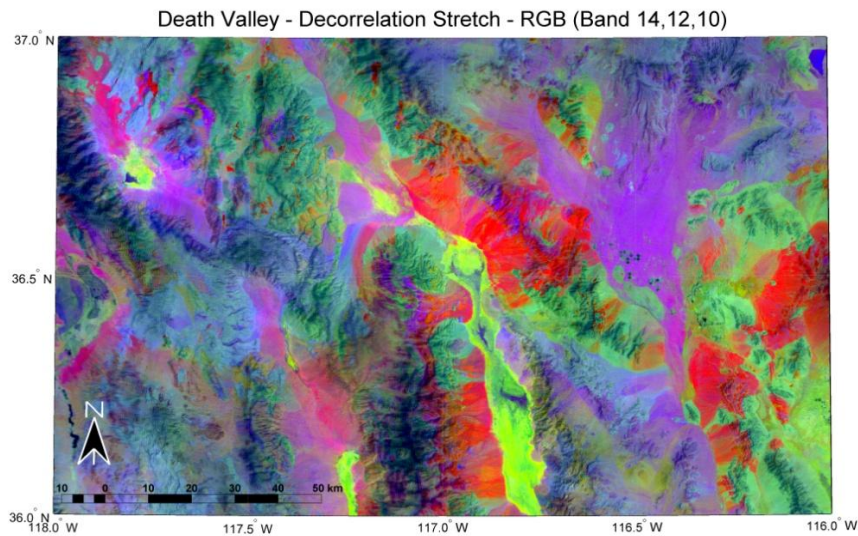


Figure 8. ASTER decorrelation stretch (DCS) of Death Valley using bands 14, 12, and 10 as RGB respectively. Different colors in the image correspond to different mineral types, e.g., quartz features are red, carbonates are green, and quartz-poor regions are purple.

5 HypsIRI band positions for the detection of volcanic plumes

TIR data will allow us to measure the emission rates of SO₂ from volcanoes. This in turn allows us to infer magma supply rates, contributions of volcanoes to the global SO₂ budget and emission rates of other amounts of gas (e.g., H₂O, CO₂, HCL, HF) and aerosols (ash, ice, sulfates) [Realmutto *et al.*, 1997; Watson *et al.*, 2004]. The frequent coverage and the higher spatial resolution of HypsIRI will allow us to more-accurately monitor passive SO₂ degassing from the world's active volcanoes. This input of emissions into the troposphere will affect local and regional climate around these persistently-active volcanoes, a capability not offered by existing moderate (~1 km) resolution instruments. Multispectral TIR data will also allow the identification of the mixture of ash, SO₂, and water vapor/ice in eruptive plumes, providing improved hazards warnings for aviation safety [Realmutto and Worden, 2000; Tupper *et al.*, 2006].

The use of multispectral TIR airborne data to map volcanic SO₂ plumes has been previously demonstrated with much success [Realmutto *et al.*, 1997; Realmutto *et al.*, 1994]. With the launch of NASA's Terra spacecraft in 1999, volcanic plume monitoring is now possible twice daily with MODIS data and at much higher spatial resolution with ASTER data. For example, MODIS will have sufficient resolution to monitor large-scale SO₂ plumes typical of those seen from Kilauea in Hawaii or Mount Etna in Italy [Realmutto *et al.*, 1994]. In contrast, ASTER has the ability to resolve smaller-scale plumes such as those from Pacaya in Guatemala or Soufrière Hills in Montserrat. Algorithms for detecting plumes rely on spectral attenuation of infrared radiation between 7–13 μm. ASTER band 11 and MODIS band 29 can be used to detect SO₂ burdens, whereas the 11-12 micron split-window bands can quantify silicate ash and water ice. The clarity of the Earth's atmosphere in these regions allow the detection of these plume constituents down to ground level. In contrast, the 7.3 micron absorption for SO₂ is much stronger, but is only effective if the plume is very large and/or enters the stratosphere due to the strong absorption of water vapor in this region. The heritage of the HypsIRI spectral response versus SO₂ transmission is shown in Figure 9, including the ASTER and MODIS band passes.

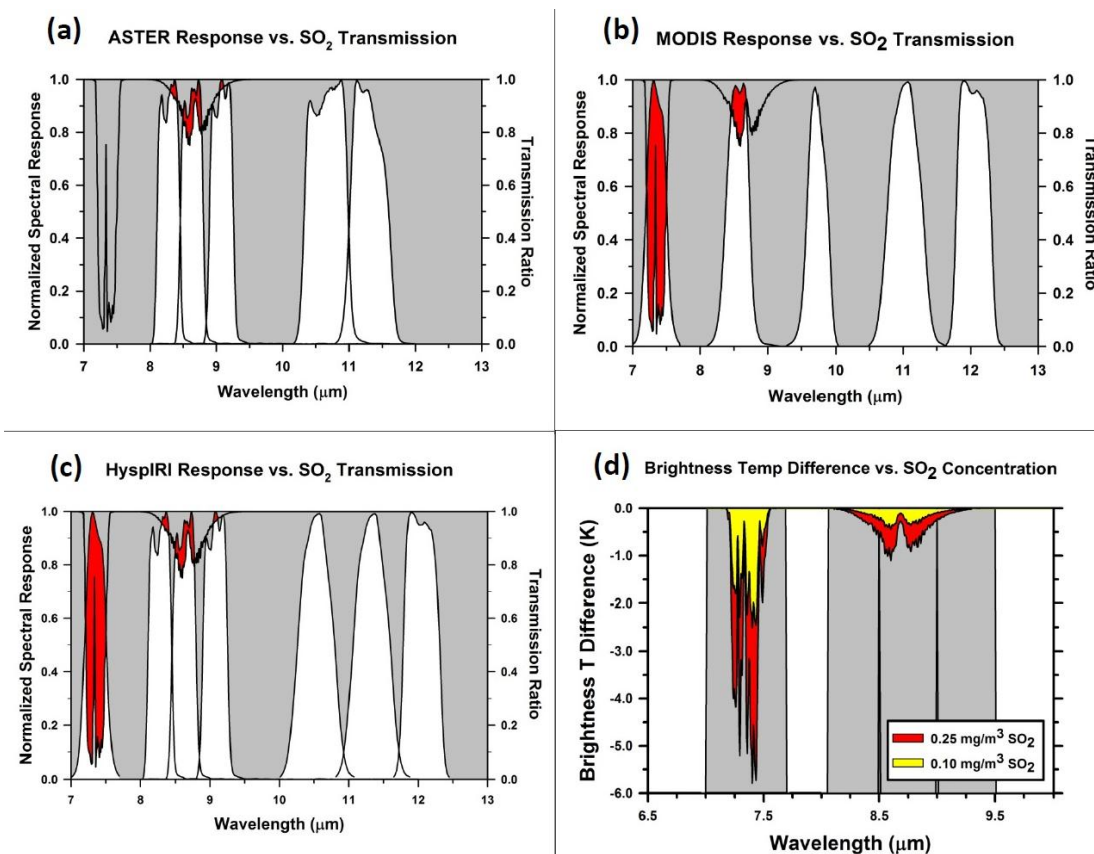


Figure 9. Heritage of the HypsIRI spectral response, showing (a) ASTER response vs. SO_2 transmission, (b) MODIS response vs. SO_2 transmission, (c) HypsIRI response vs. SO_2 transmission, and (d) brightness temperature difference vs. SO_2 concentration.

The retrieval of SO_2 concentrations from remote-sensing measurements relies on radiative transfer models that estimate the amount of atmospheric emission, and scattering and absorption of surface-leaving radiance. The recent introduction of high-resolution (0.1 cm^{-1}) band models in MODTRAN5 [Berk *et al.*, 2005] enables us to analyze hyperspectral TIR data. Hyperspectral radiance measurements improve our ability to discriminate the constituents of volcanic plumes. A limitation of radiative transfer models are their dependence on input atmospheric profiles such as temperature, relative humidity, and gas composition. Furthermore, the need for accurate atmospheric corrections increases with increasing spectral resolution. The improvement in our ability to model ambient atmospheric conditions, and thus improve atmosphere corrections, will increase our sensitivity to subtle changes in passive emissions of SO_2 and surface temperature, regardless of the spectral resolution of our radiance measurements.

5.1 Mapping volcanic plume constituents

Comparisons between multi- and hyperspectral remote sensing in the detection and mapping of plume constituents are illustrated in Figure 10, which shows the spectral signatures of SO₂ (Figure 10a), silicate ash (Figure 10b), and SO₄ aerosol (Figure 10c). These simulated spectra are plotted at the resolution of HyTES [Johnson *et al.*, 2009] and the airborne MODIS/ASTER Airborne Simulator, or MASTER [Hook *et al.*, 2001] instruments: ~0.02 μm (or 2 cm⁻¹) vs. 0.5–1.0 μm, respectively. In comparison, the thermal IR response of these corresponding constituents is shown on the right panels in Figure 10. We can readily

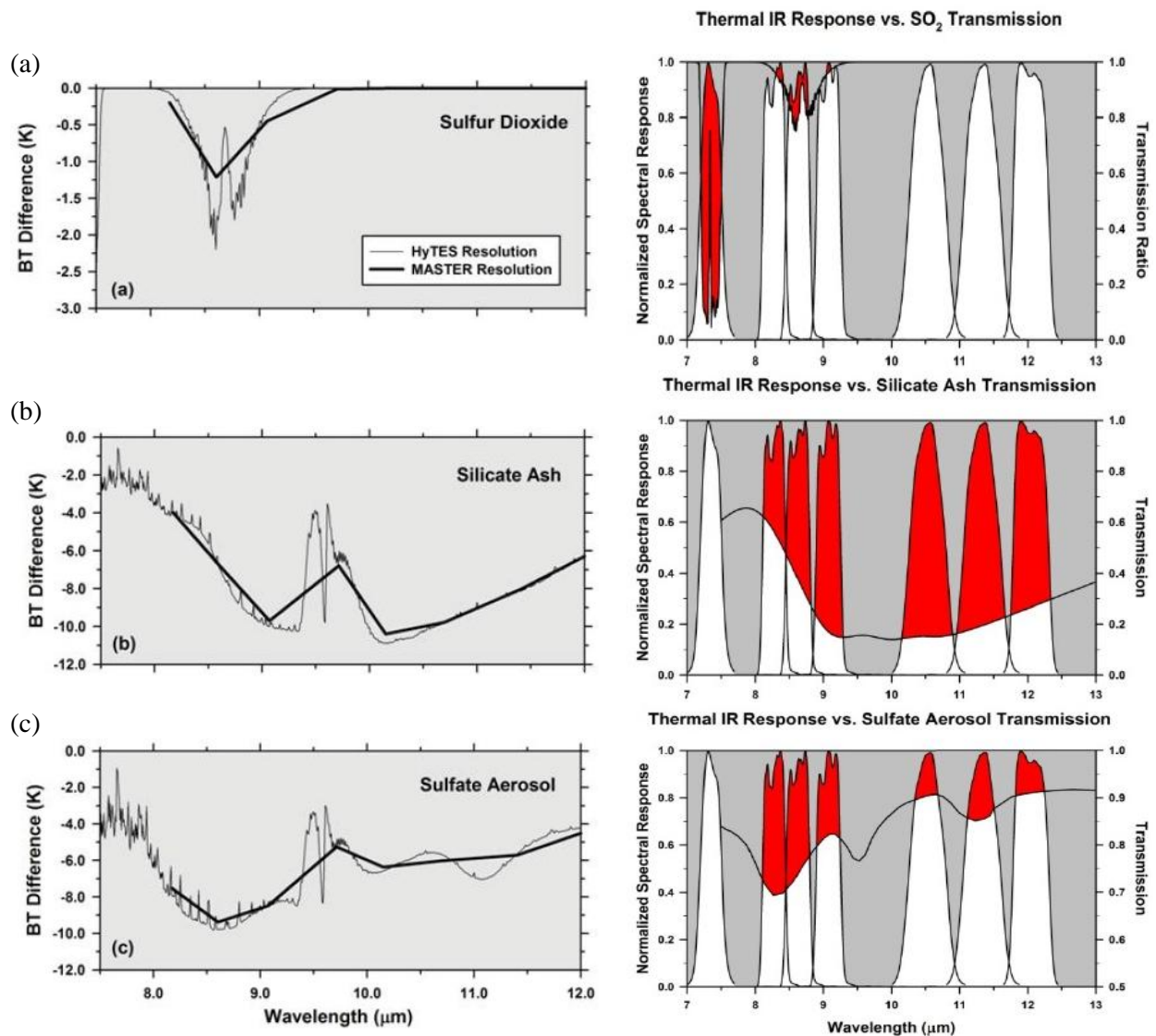


Figure 10. Transmission spectra expressed as brightness temperature difference spectra for three constituents of volcanic plumes and ash clouds. (a) SO₂, (b) silicate ash, and (c) SO₄ aerosol at the spectral resolution of HyTES (thin line) and MASTER (thick line)

discriminate the spectra of SO₂, ash, and SO₄ aerosols at the spectral resolution of HyTES (thin line), but the distinctions are more subtle at the resolution of MASTER (thick line). In real-world measurements, these distinctions are further muted by instrument noise and uncertainties in our knowledge of atmospheric and surface conditions. Given the MASTER spectra, we note the difficulties in discriminating SO₂ from SO₄ in the spectral range between 8 and 9.5 μm (Figures 10a and 10c), or ash from SO₄ in the range between 9.5 and 12 μm (Figures 10b and 10c).

The ability to discriminate SO₄ aerosols from SO₂ or ash is critical for climate and environmental studies; whereas the ability to discriminate ash from SO₄ (or SO₂) is critical to the mitigation of the aviation hazards posed by drifting ash clouds [Prata *et al.*, 2001; Tupper *et al.*, 2006].

5.1.1 Conclusions

SO₂ transmission in the longwave region (12–11 μm absorption difference) can be confused with sulfate aerosols and/or ash with current band positions. A suggestion would be to shift the HypsIRI 10.53 μm band between 9.5 and 10 μm in order to help discriminate sulfate aerosols from SO₂ or ash. Simulations will need to be run to investigate the effects of O₃ absorption in this region, and optimal placement of the 10.53 μm band. In terms of mineral mapping, moving the 10.53 μm band closer to 10 μm will also help to discriminate between feldspar and quartz minerals. This will be discussed in more detail in section 6. In any case, moving the 10.53 μm band to shorter wavelength region around the 10 μm band will be beneficial for both SO₂ and mineral mapping techniques.

5.2 Case Study: Mount Etna eruption plume

5.2.1 Analysis

Figure 11 shows a MODIS-Aqua visible (top) and thermal (bottom) image of a Mount Etna plume on the 28 Oct 2002 using band 28 (7.3 μm). The ground is not visible because at this wavelength the atmosphere is opaque due to strong H₂O and SO₂ absorption features. This is illustrated in Figure 11 (right panels) which shows that H₂O and SO₂ absorption strengths are of similar magnitude in the 7.3 μm band. This makes it difficult to separate their effective contributions to the total brightness temperature. In addition the 7.3 μm band is not suitable for mapping plumes below 5 km, and is therefore more useful for mapping large-scale eruptions where plumes persistent to higher altitudes in the stratosphere.

5.2.2 Conclusions

A more useful option for HypsIRI would be to move the 7.3 μm band closer to the 7.8–8 μm region in order to obtain more leverage from the water vapor absorption gradient that exists in this range (see Figure 11 top right panel). This would make simultaneous retrievals of SO_2 and H_2O easier in combination with the 8.6 μm SO_2 absorption feature.

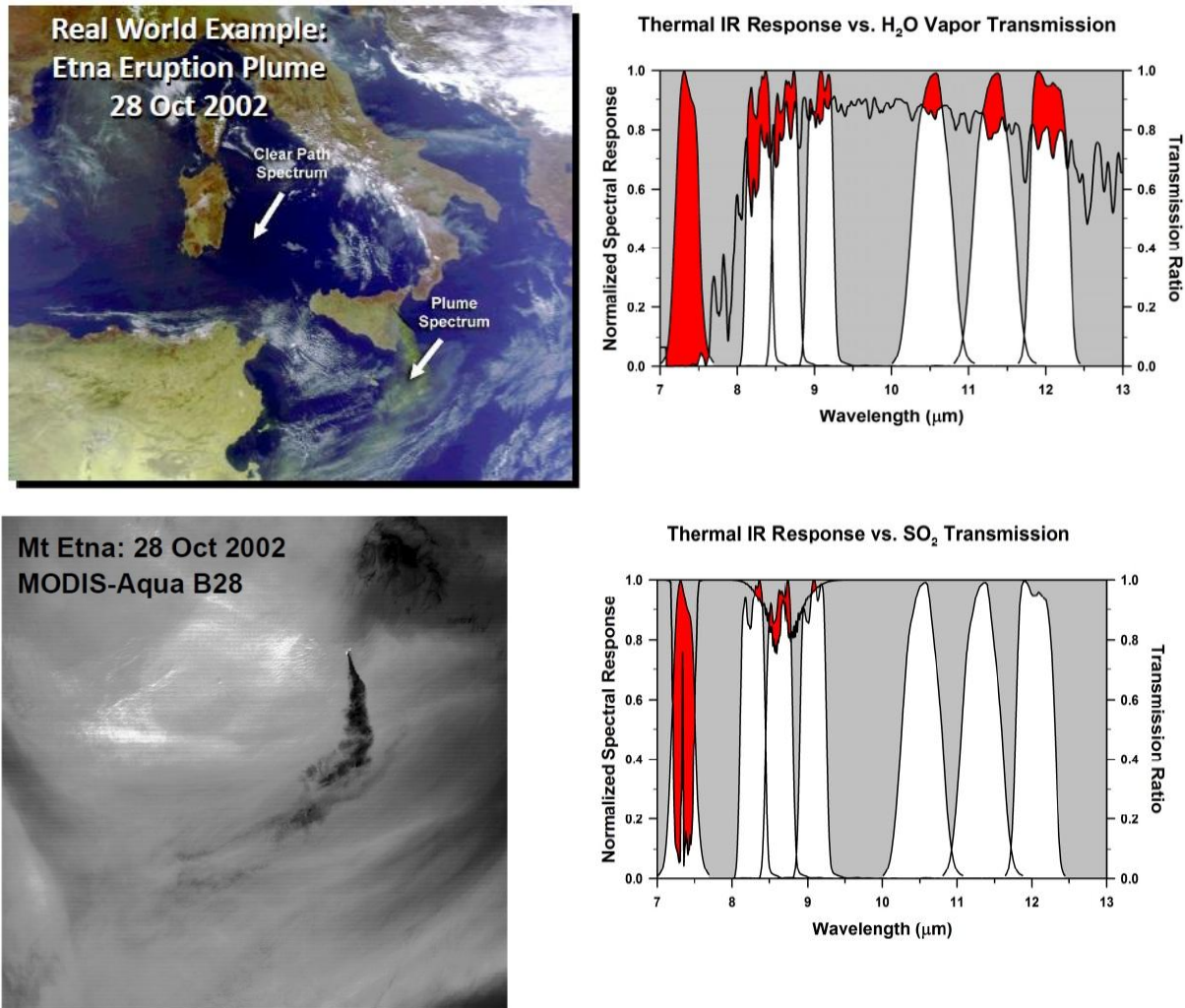


Figure 11. (left) MODIS-Aqua band 28 (7.3 μm) image of the Mount Etna eruption on 28 October 2002, (right) thermal infrared responses of HypsIRI plotted with transmission curves for water vapor (top) and SO_2 (right).

5.3 Case Study: Sarychev Peak volcano

5.3.1 Analysis

Figure 12 illustrates the complex dispersion of plumes and clouds during the recent eruptions of Sarychev Peak Volcano (Matua Island, Russian Kuril Islands). Figure 12(a) top panel is a true-color composite of MODIS-Terra data acquired at 00:50 UTC on 16 June 2006. We note the viewing conditions were cloudy, indicating unstable atmospheric conditions, and the

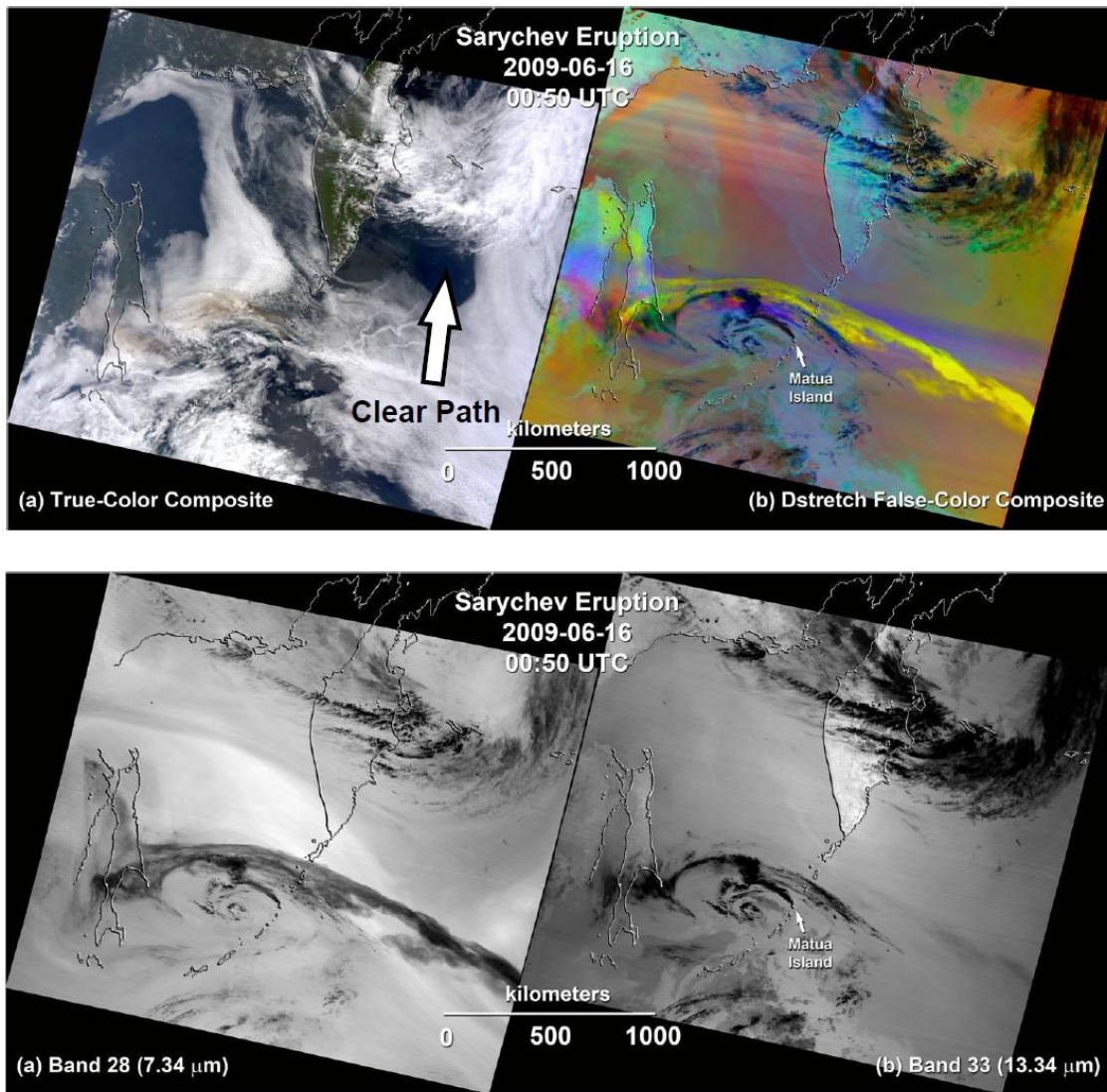


Figure 12. Eruption of Sarychev Peak Volcano (Matua Island, Russian Kuril Islands). Top panels (a) true-color composite of MODIS-Terra data acquired at 00:50 UTC on 16 June 2006. (b) is a false-color composite of MODIS thermal infrared (TIR) channels 32, 31, and 29 displayed in red, green, and blue, respectively. Bottom panels show corresponding (a) MODIS band 28 (7.34 μm) and (b) band 33 (13.34 μm) brightness temperatures.

eruption plume was obscured by the meteorological (met) clouds. Figure 12(b) top panel is a false-color composite of MODIS thermal infrared (TIR) channels 32, 31, and 29 displayed in red, green, and blue, respectively.

The radiance data were processed with the DCS. Due to distinctive features in the spectra of SO₂ and silicate ash [Watson *et al.*, 2004], SO₂-rich clouds appear yellow and ash-rich plumes and clouds appear in hues of red and purple. The portions of the volcanogenic and met clouds that are opaque to TIR radiance appear dark in Figure 12(b), signifying low radiometric temperatures.

The retrieval procedure for SO₂ requires profiles of atmospheric temperature, H₂O and O₃ as input to a radiative transfer model such as MODTRAN [Kneizys *et al.*, 1996]. Radiance spectra from a clear path (plume-free) shown in Figure 12(a) are used to first ‘tune’ the H₂O and O₃ profiles. Depending on the conditions, considerable spatial variations of H₂O within a scene may be present, which makes tuning a time-consuming process. Two candidate regions for better characterizing the H₂O distribution within a scene include the MODIS band 28 (7.34 μm) and band 33 (13.34 μm) channel. The brightness temperature plots in Figure 12(a) and (b) bottom panels show that strong H₂O absorption in the MODIS band 28 channel obscures the surface features, while in band 33, moderate H₂O absorption does not obscure the surface.

5.3.2 Conclusions

The 7.3 μm channel does not provide sufficient resolution to separate the effects of H₂O and SO₂ absorptions, despite the original proposal to add this channel for SO₂ detection and mapping. Characterizing spatial variations in H₂O within a scene will help to optimize the SO₂ retrievals and allow us to better characterize the atmosphere regardless of the ground target. For HypsIRI it is suggested to shift the 7.3 μm band closer to the 7.8–8 μm region in order to obtain more leverage from the water vapor absorption gradient that exists in this range, but a more definitive solution to the exact position requires higher spectral resolution data, such as HyTES and MAGI (see section 7). Adopting a longer wavelength band (e.g., MODIS band 33) for plume mapping will not be necessary for HypsIRI due to the three bands already positioned in the 8–9 μm SO₂ absorption feature.

6 HypsIRI band positions for Earth surface compositional mapping

Surface compositional studies hold clues to the origins of materials and also the geology and evolution of different rock types. Spaceborne measurements from HypsIRI will enable us to derive surface temperatures and emissivities of a variety of Earth's geologic surfaces. For example, different Si-O bonded structures vary in their interaction with energy in the thermal infrared region (8–12 μm). Framework silicates, such as quartz and feldspar, show minimum emissivity at shorter wavelengths (8.5 μm), whereas olivine and pyroxene minerals show minimum emissivity at progressively longer wavelengths [Hunt, 1980].

Primary rock-forming minerals exhibit major and diagnostic spectral absorption features in the infrared wavelength region of the electromagnetic spectrum, with only minor features in the visible/shortwave (VSWIR) infrared region (Figure 13). These features result from the selective absorption of photons with discrete energy levels and are dependent on the elemental composition, crystal structure, and chemical bonding characteristics of a mineral, and are therefore diagnostic of mineralogy [Hunt, 1980; Vaughan *et al.*, 2005]. For example, different Si-O bonded structures vary in their interaction with energy in the thermal infrared region (8-12 μm). Examples of reflectivity measurements from the ASTER spectral library (ASTlib) are shown in Figure 13 for six different rock types including metamorphic, sedimentary and igneous. The left panels show the VSWIR spectral range, whereas the right panels show the mid to-thermal infrared spectral range. The thermal spectra show original full resolution ASTlib spectra (solid lines) [Baldrige *et al.*, 2009] overlaid with the eight convolved HypsIRI preliminary TIR band placements (black circles). ASTlib includes spectra of rocks, minerals, terrestrial soils, lunar soils, manmade materials, vegetation, snow, and ice, covering spectral ranges from the visible to longwave infrared (0.4–15.4 μm).

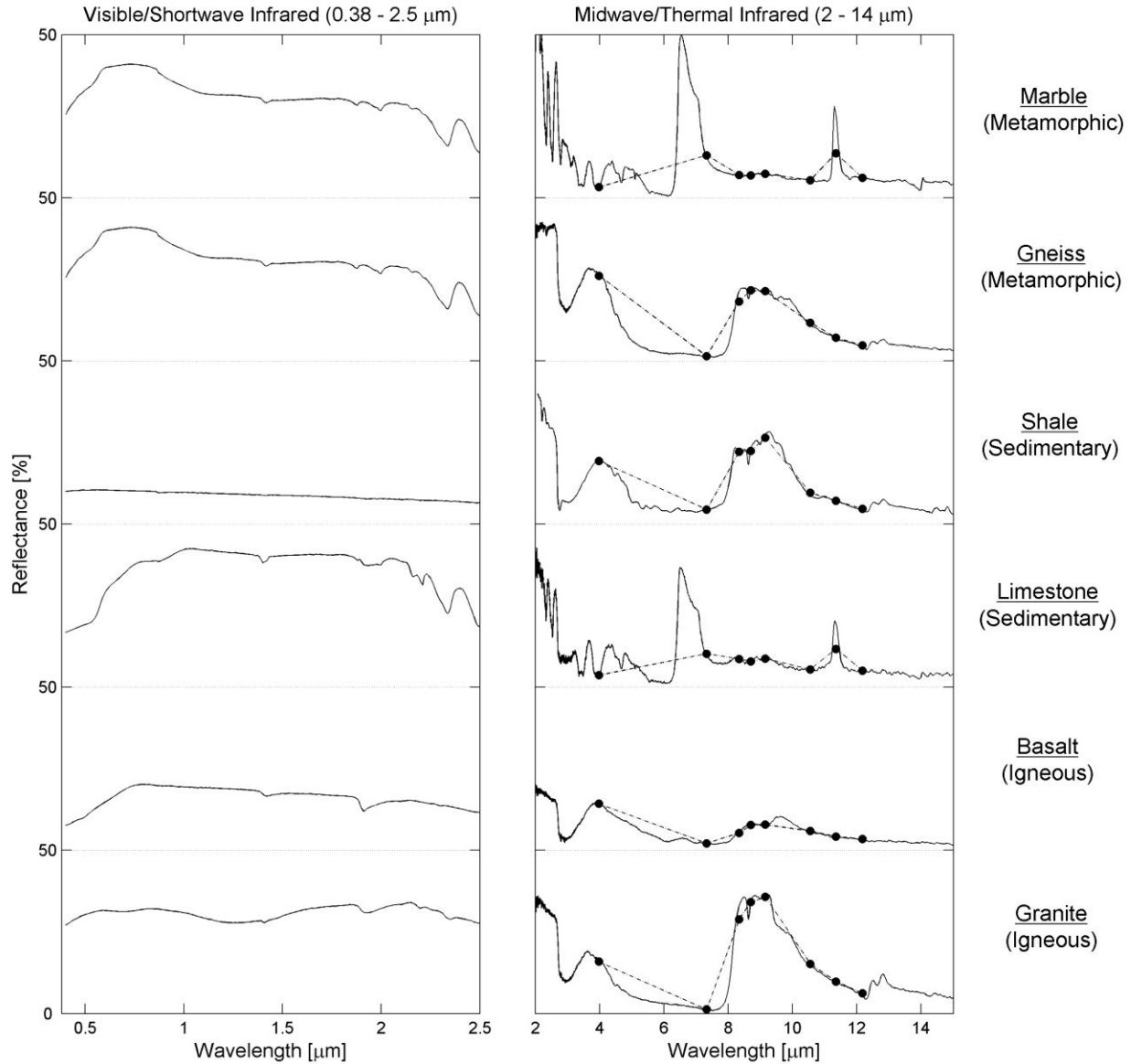


Figure 13. A selection of JPL mineral library spectra representing several classes shown as percent reflectance in the visible, shortwave infrared (0.38–2.5 μm) and infrared (2–14 μm) regions. Black circles in the infrared spectrum represent HyspIRI bands convolved to the library spectra. All spectra are offset for clarity.

The spectral features illustrated in Figure 13 result from the minerals that occur in these felsic to mafic igneous rock types. For example, emissivity minimums occur at 8.3 and 9.1 μm for granite, shale, and gneiss, whereas for basalt this feature is more subdued and shifted to longer wavelengths. Fundamental vibration modes for the CO_3 ion occur throughout the TIR region; in carbonate minerals (e.g., limestone in Figure 13), the most distinguishing features occur around 6.7 μm and 11.3 μm , with the former lying outside of the atmospheric window.

6.1.1 Case Study: Kelso Dunes

The Kelso Dunes are located in the Mojave National Preserve southeast of Baker, California. Sand from the Mojave River alluvial apron is driven approximately 35 miles by predominantly westerly winds, piling up at the base of the Granite and Providence mountains, which flank the south and southeast sides of the dune field. The westerly winds are counterbalanced by strong winds from other directions that result in a result in a variety of dune forms. The dune field covers an area of 115 km² and contains dunes that rise up to 195 m above the terrain. Large portions of the dunes have sparse vegetation cover that stabilizes areas of previously drifting sand. The dunes are composed predominately of quartz and feldspar eroded from granitics of San Bernardino Mountains to the south, but also contain a large proportion of lithic fragments [Edgett and Lancaster, 1993]. A later study by Ramsey *et al.* [1999] using TIMS data showed significant spectral variations within the active dunes, indicative of potential mineralogic heterogeneities, which was confirmed from results with a linear spectral retrieval algorithm. Further, petrographic techniques showed that the dunes were much less quartz rich than previously reported (90–100% quartz), indicating a more immature dune system than previously thought due to relatively higher percentages of feldspar minerals.

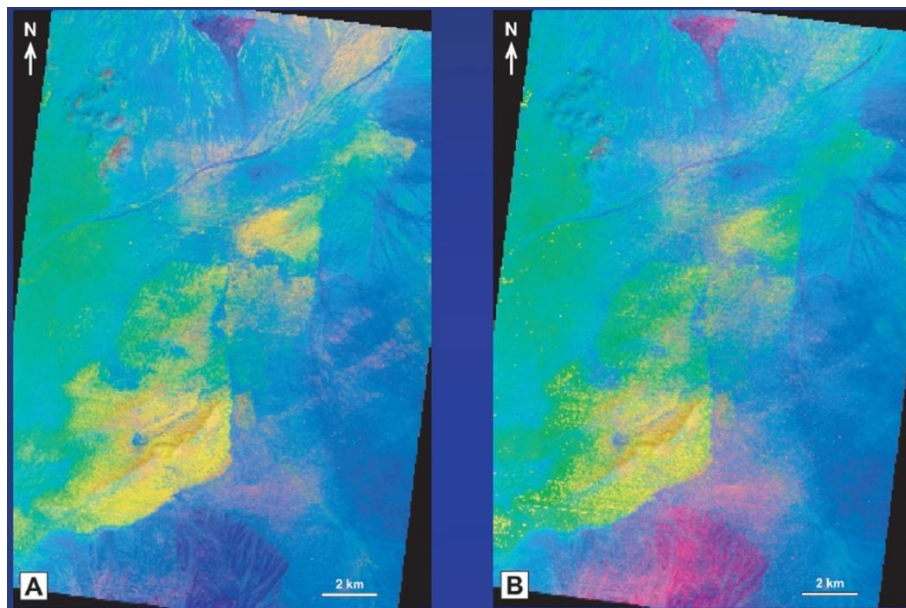


Figure 14. Decorrelation stretch (DCS) images of the Kelso Dunes, CA using MASTER data. The yellow indicates an equal abundance of quartz and microcline feldspar, while cyan is quartz and oligoclase feldspar. Increased magenta coloration in (B) shows improved feldspar detection using the 10.1 μm band instead of the 10.6 μm MASTER band.

Figure 15 shows TIR emissivities of four mineral end-members acquired at Arizona State University including oligoclase, clay+magnetite, quartz, and microcline together with one spectrum (sample k24) of aeolian sand from the Kelso Dunes [Ramsey and Rose, 2009]. The

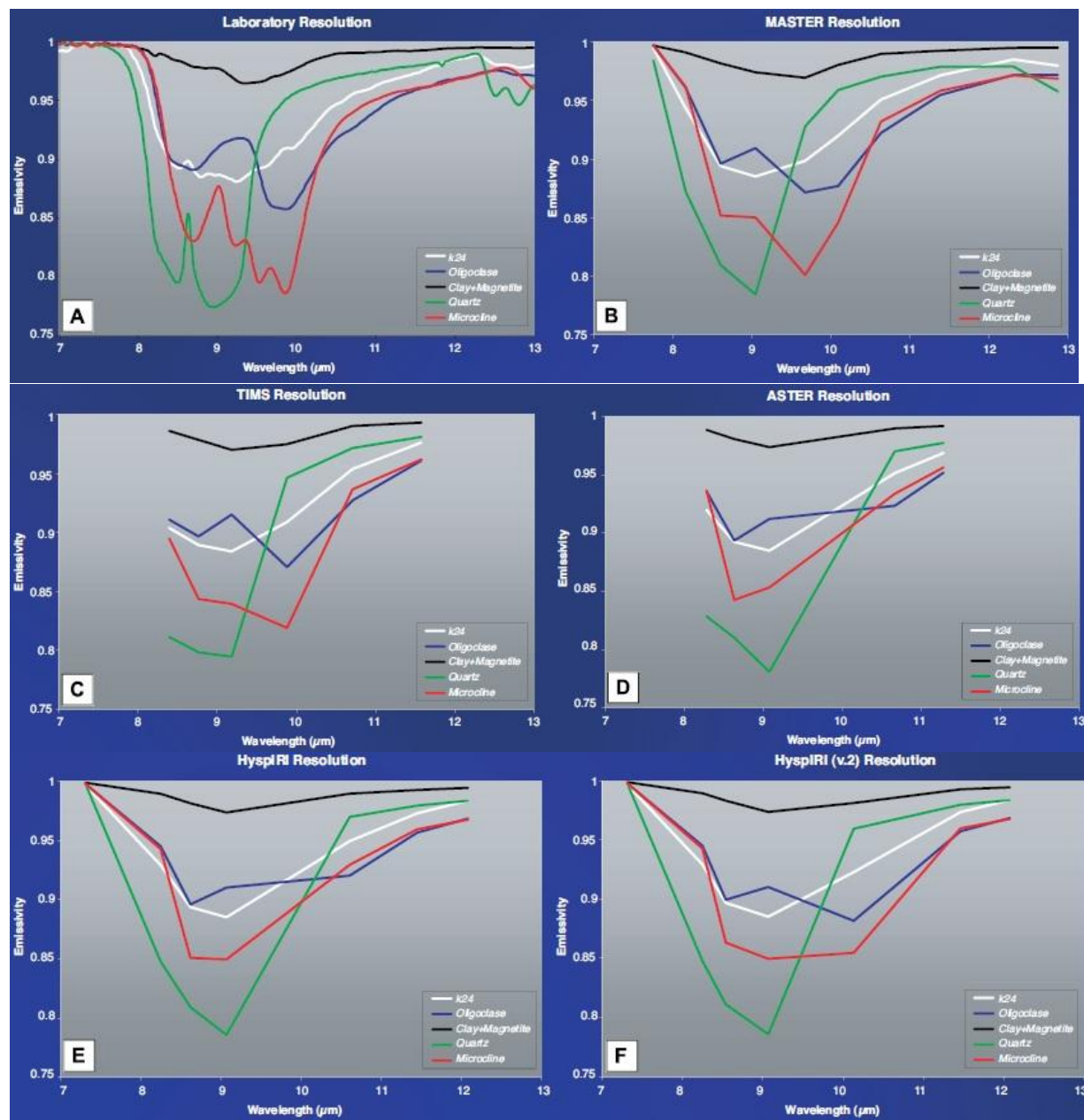


Figure 15. Thermal infrared (TIR) emissivity spectra of four mineral end-members acquired at Arizona State University (Oligoclase, Clay+Magnetite, Quartz and Microcline) and one spectrum (sample k24) of aeolian sand from the Kelso Dunes (Mojave Desert, CA). The spectra were degraded to the resolution of various TIR instruments: (A) Laboratory resolution (B) MASTER resolution (10 bands) (C) TIMS resolution (6 bands) (D) ASTER resolution (5 bands) (E) Current HypsIRI resolution (7 bands) and (F) Proposed new HypsIRI band alignment (7 bands). In this configuration, three of the bands have been moved for better gas and mineral detection. The 8.63 μm band has been shifted to 8.55 μm (centered over the SO_2 absorption doublet). The 10.53 μm band has been moved to 10.05 μm for better detection and discrimination of feldspar minerals. The 11.33 μm band has been shifted slightly to 11.35 μm for more accurate carbonate detection.

spectra were degraded to the resolution of various TIR instruments and used to analyze the compositional variation of the Kelso æolian system and argue for a more immature dune system because of the relatively high percentages of feldspar minerals. These include: (A) laboratory resolution; (B) MASTER resolution (10 bands); (C) TIMS resolution (6 bands); (D) ASTER resolution (5 bands); (E) current HypsIRI resolution (7 bands); and (F) a proposed new HypsIRI band alignment (7 bands). In the new proposed HypsIRI band configuration, three of the bands have been moved for better gas and mineral detection. The 8.63 μm band has been shifted to 8.55 μm (centered over the SO_2 absorption doublet), whereas the 10.53 μm band has been moved to 10.05 μm for better detection and discrimination of feldspar minerals. Lastly, the 11.33 μm band has been shifted slightly to 11.35 μm for more accurate carbonate detection. These modifications are highlighted in Figure 16 showing the band position changes in red. Of note in Figure 15(F) is the shape of the microcline and oligoclase feldspar spectra. The lower emissivity at 10.05 microns allows this class of minerals to be clearly distinguished from quartz, which is critical for accurate compositional analysis of geologic and urban surfaces.

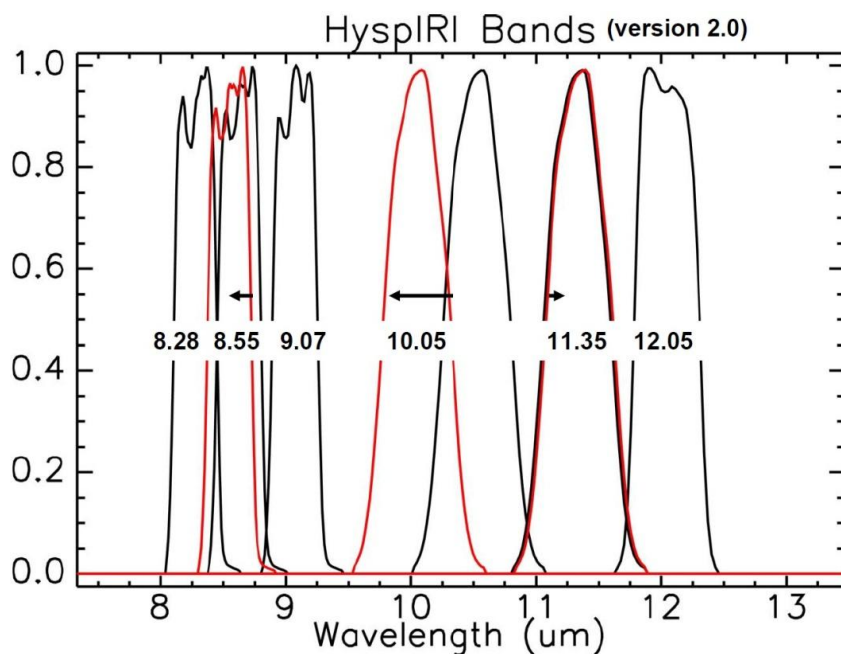


Figure 16. Proposed HypsIRI version 2.0 band locations. Band modifications from version 1.0 are highlighted in red. The 8.63 μm band has been shifted to 8.55 μm , the 10.53 μm band has been moved to 10.05 μm , and the 11.33 μm band has been shifted slightly to 11.35 μm (see text for details).

A method known as spectral deconvolution was then used to assess the ability of each band configuration to resolve the relative abundances of each mineral end member. The accurate

retrieval of mineralogy and abundance from surface materials requires the knowledge of how the radiated energy from each surface component interacts, as well as a model (spectral deconvolution) to separate that mixed energy for each end member [Ramsey and Christensen, 1998; Ramsey *et al.*, 1999]. This method relies on input end-member spectra to perform a best fit to the unknown (mixed) spectrum. The output is and a set of corresponding fractions, or abundances, that indicate the proportion of each end member present in the pixel. Analysis of Figure 15 using results of a linear deconvolution algorithm showed that the HypsIRI v2.0 band positions had the best agreement with laboratory derived end member percentages (Figure 17), with a lowest average error of 1.9%. The next closest match was MASTER, followed by ASTER, HypsIRI v1.0, and TIMS.

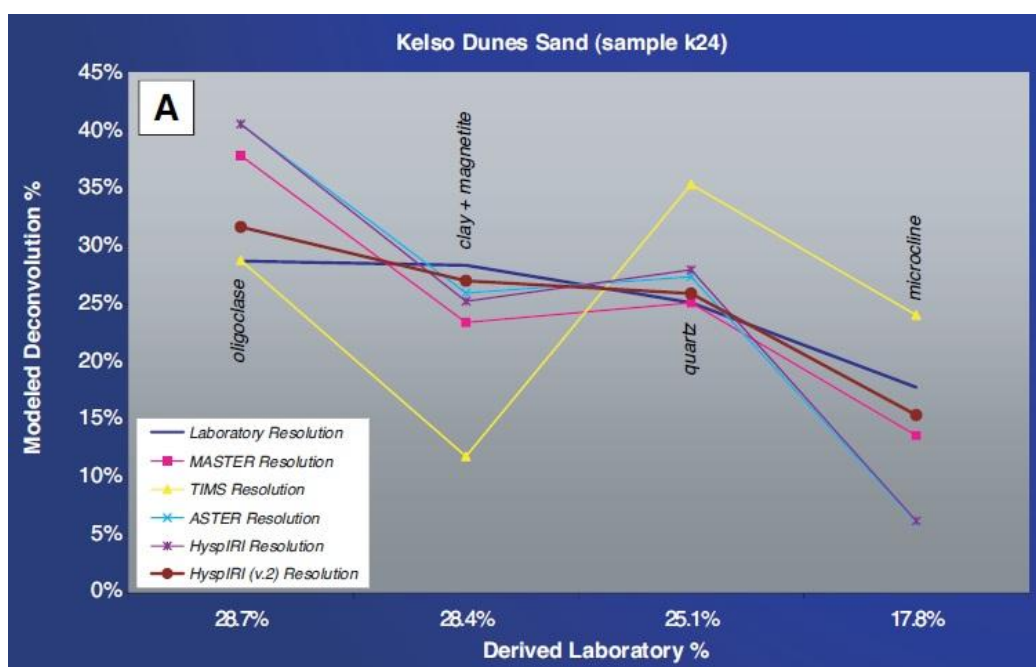


Figure 17. Results of linear deconvolution of the Kelso sand sample (k24) at the various spectral resolution/band configurations shown in Fig 15. The laboratory resolution is assumed to be the most accurate and plotted as the dark blue line for each of the four mineral end-members. The closest match between the laboratory results and the other configurations are for the proposed new HypsIRI version 2.0 spectral bands shown in red (avg. error = 1.9%).

Figure 18 shows laboratory emissivity spectra of different silicate minerals including andesine, anorthoclase, microcline, and quartz, with the current HypsIRI v1.0 band positions highlighted with blue vertical lines. From this image, it is clear that the current 10.53 μm band, situated longward of the ozone absorption features ($\sim 9.6 \mu\text{m}$) has marginal spectral variation for most silicate minerals including quartz and feldspars. This spectral variation reduces even more if these constituents are mixed, which is commonly the case for aeolian dune systems.

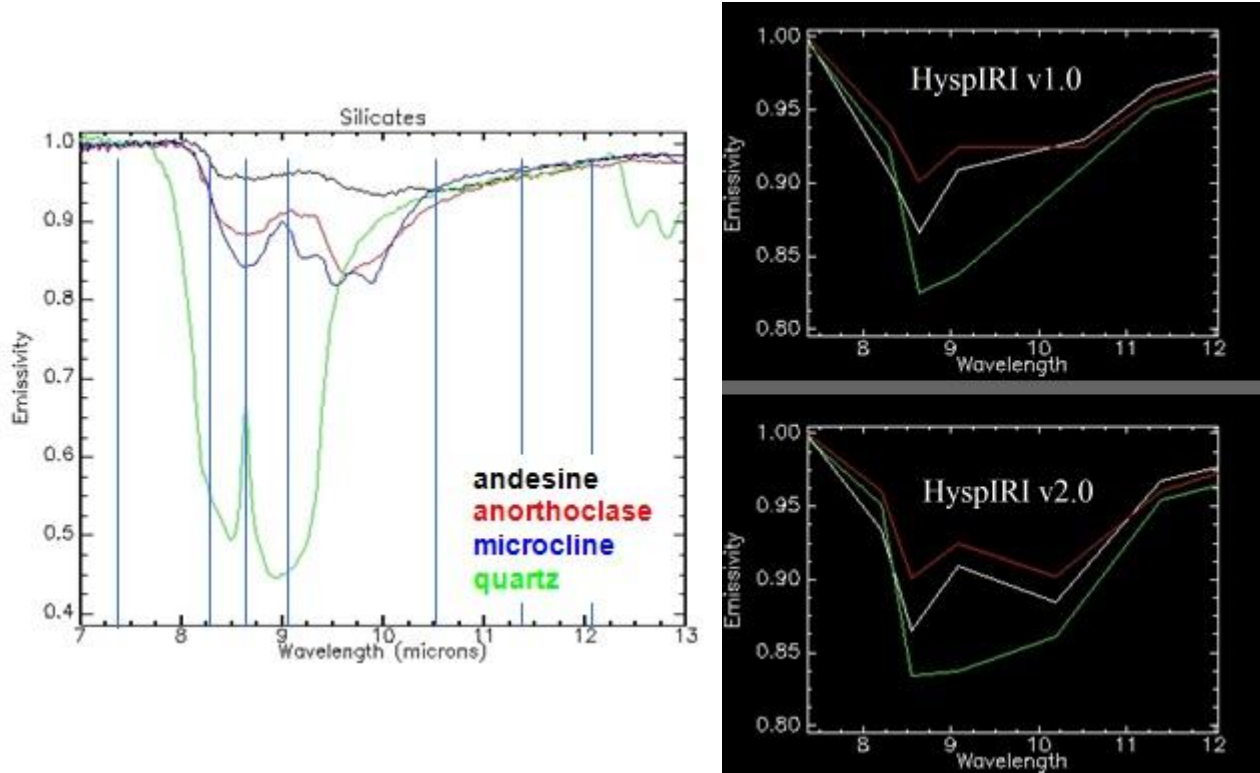


Figure 18. (left) Laboratory emissivity spectra of different silicate minerals including andesine, anorthoclase, microcline, and quartz, (right) silicate spectra convolved to HypsIRI v1.0 and v2.0 band positions.

The emissivity spectra on the right of Figure 18 show the silicate spectra convolved to the HypsIRI v1.0 and v2.0 band positions. This clearly shows an improvement in spectral contrast between the silicate spectra using v2.0 with the proposed shift of the 10.53 μm band shortward to 10.05 μm . An additional modification to the 10.05 μm band that could further increase spectral diversity between various silicate minerals and limit the amount of interference from the edge of the O_3 absorption region would be to narrow the response function itself. This modification is shown in Figure 19, including shifting of the 11.33 μm band to 11.35 μm for more accurate carbonate detection. Further simulations need to be performed in order to test the effects of narrowing the band response. These include possible issues with the sensitivity to O_3 absorption feature in this region, and possible degradation of the signal to noise of the detector response.

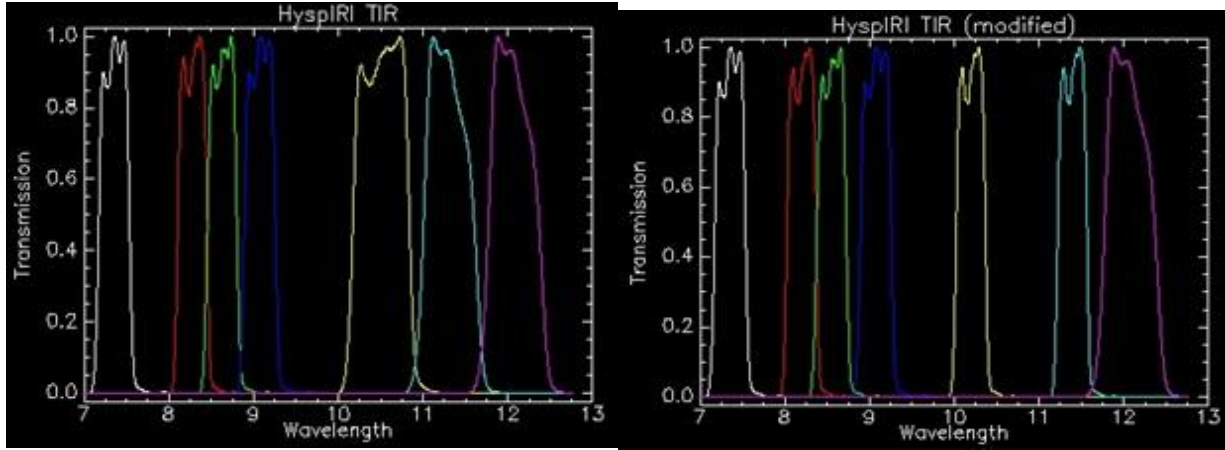


Figure 19. HypsIRI TIR response functions showing band positions for v1.0 (left) and the proposed v2.0 modifications including narrowing of the proposed 10.05 μm and 11.35 μm bands (right).

6.1.2 Case Study: Great Sands

The Gran Desierto dune system constitutes the largest portion of the Sonoran Desert in Mexico and the largest and most active sand sea in North America. *Scheidt et al.* [2011] showed that the central dune area consists of a mixture of approximately 90% quartz and 10% feldspar (plagioclase and potassium feldspar). The grain size, composition, texture, color and sorting have been well documented in previous studies [*Blount and Lancaster, 1990; Lancaster, 1992*]. Spatial variability in emissivity primarily occurs due to the distribution of quartz and feldspars across the central dune system via *æolian* deposits [*Scheidt et al., 2011*].

Figure 20 shows linear deconvolution results for ASTER, HypsIRI v1.0 and v2.0 band positions for three sand samples collected over the Gran Desierto dune system in Mexico (SAM94, SAM39, SAMG162). The emissivity spectra of the three sand samples are shown top left, in addition to band positions that were modified in HypsIRI v2.0 (vertical red bars), and the unchanged HypsIRI v1.0 band positions (vertical gray bars). The three end members chosen for the Desierto samples included carbonate, feldspar, and quartz for SAM94, and feldspar and quartz for SAM39 and SAMG162, respectively. The table (top right) shows results of the spectral unmixing, and, assuming the lab results are regarded as ‘truth’, HypsIRI v2.0 matched the lab results more closely for SAM94 and SAM39 than HypsIRI v1.0, whereas the results for SAMG162 were similar.

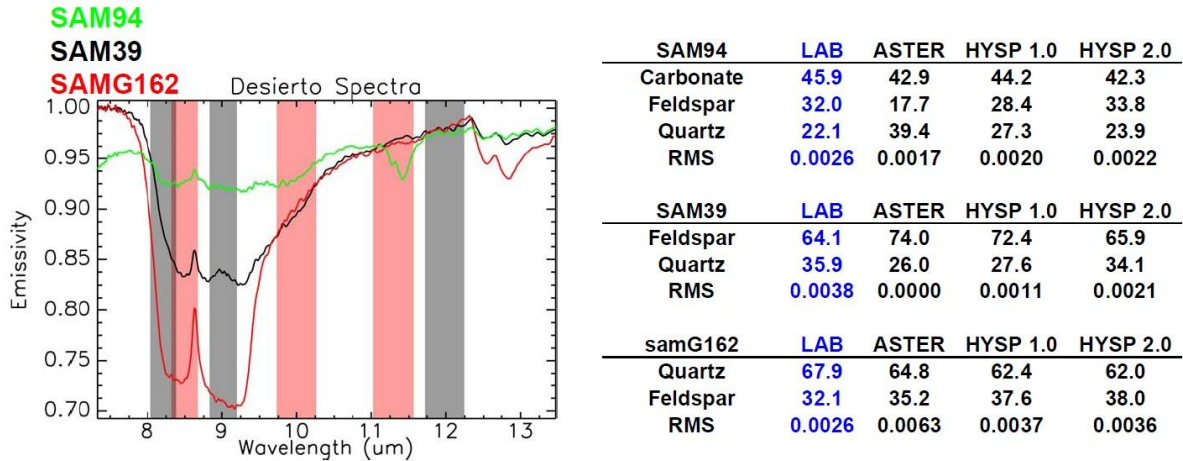


Figure 20. Linear deconvolution results for ASTER, HypsIRI v1.0 and v2.0 band positions for three sand samples collected over the Gran Desierto dune system in Mexico (SAM94, SAM39, SAMG162). Bottom image shows a view of the dune system, which contains primarily a mixture of quartz and feldspars.

Although the result for the carbonate end member were much the same for v1.0 and v2.0 for the SAM94 sample, it would still be useful to shift the current 11.33 μm band to a slightly higher position at 11.35 μm . This would allow more accurate resolution of a larger variety of different carbonate minerals. This is illustrated in Figure 21, which shows three different types of carbonate spectra from ASTlib including dolomite, calcite and siderite. Carbonates have a distinctive emissivity minimum in the 11–12 μm region. The gray bars show the modified v2.0 band positions, and it is clear that shifting the 11.33 μm band slightly to around 11.35–11.37 μm will better capture the response of all three different carbonate types in this region, especially dolomite.

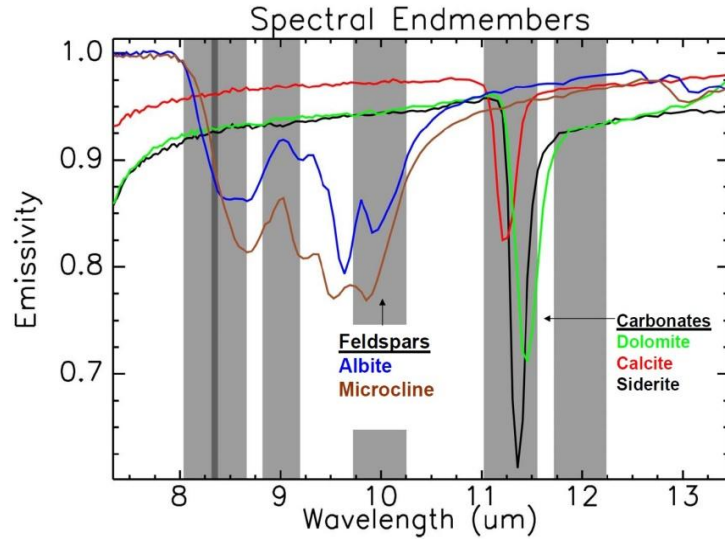


Figure 21. Laboratory spectra of feldspars, and carbonates, with HySPIRI v2.0 band positions shown as gray vertical bars.

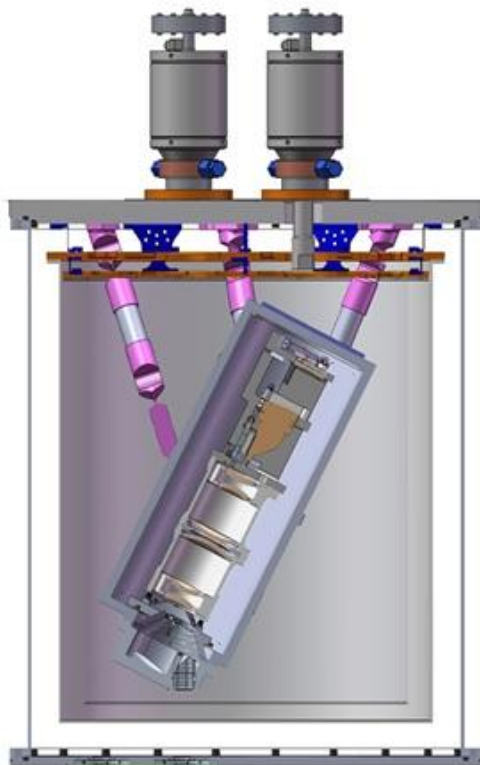
6.1.3 Conclusions

Preliminary research studies on the optimum TIR band placement for Earth surface compositional mapping in support of the HySPIRI mission suggest a new HySPIRI TIR band configuration. The major modification involves moving the 10.53 μm band closer to 10 μm in order to better discriminate between quartz and feldspar minerals. This was demonstrated using linear deconvolution results with both laboratory and airborne remote sensing data. An additional modification to the 10.05 μm band that could further increase spectral diversity between various silicate minerals and limit the amount of interference from the edge of the O_3 absorption region would be to narrow the response function of the 10.05 μm band. Lastly, the 11.33 μm band should be shifted slightly to 11.35 μm in order to better encompass the absorption feature of different types of carbonates including dolomite, calcite and siderite in this region.

7 Future work with airborne data

7.1 HyTES

The Hyperspectral Thermal Emission Spectrometer (HyTES) is an airborne imaging spectrometer with 256 spectral channels between 7.5 and 12 micrometers in the thermal infrared part of the electromagnetic spectrum and 512 pixels cross-track with pixel sizes in the range 5-50 m depending on aircraft altitude [Johnson *et al.*, 2011]. HyTES is being developed to support the HypsIRI mission and will provide precursor data at much higher spatial and spectral resolutions to help determine the optimum band positions for the HypsIRI-TIR instrument as well as provide precursor datasets for Earth Science research. HyTES completed its first flights during July 2012 and incorporates several new technologies including a Dyson spectrometer, long, straight slit, curved diffraction grating and Quantum Well Infrared Photodetector (QWIP) [Johnson *et al.*, 2009]. The model for the HyTES instrument is shown in Fig. 22.



Instrument Characteristic	HyTES
Mass (Scanhead) ¹	12kg
Power	400W
Volume	1m x 0.5m (Cylinder)
Number of pixels x track	512
Number of bands	256
Spectral Range	7.5-12 μm
Frame speed	35 or 22 fps
Integration time (1 scanline)	28 or 45 ms
Total Field of View	50 degrees
Calibration (preflight)	Full aperture blackbody
Detector Temperature	40K
Spectrometer Temperature	100K
Slit Length and Width	20 mm x 39 μm
IFOV	1.7066
Pixel Size/Swath at 2000 m flight altitude ²	3.41m/1868.33m
Pixel Size/Swath at 20,000 m flight altitude ²	34.13m/18683.31m

Figure 22. (left) The model for the HyTES instrument, including a Dyson spectrometer, long, straight slit, curved diffraction grating and Quantum Well Infrared Photodetector (QWIP). (right) HyTES instrument specifications.

Table 2. Test sites and purpose for the HyTES test flights.

Sitename	Purpose
La Brea Tarpits	Urban/Methane
Salton Sea	Calibration/Ammonia
Huntington Gardens	Ecosystems
Cuprite	Surface Composition
Death Valley	Surface Composition
Navajo Generating Station	Sulfur dioxide

Table 2 shows the test sites that HyTES flew over during July 2012 and their purpose, while Fig. 23 shows the site locations on a Google Earth image. The purpose of the different sites range from trace gas detection (e.g. methane, ammonia, sulfur dioxide), to calibration and surface composition mapping.



Figure 23. Test site locations on Google Earth.

An example of HyTES image acquired on 07-20-2012 over Cuprite, NV with bands 150 (10.08 μm), 100 (9.17 μm), and 58 (8.41 μm) displayed as RGB respectively and as image cube is shown in Fig. 24. Fig. 24 A shows the radiance at sensor for different locations at Cuprite, NV. Atmospheric features can be seen primarily in the 7.5-8.5 μm and $>11.5\mu\text{m}$ regions and are mostly due to water vapor absorption. Fig. 24 B shows the Noise Equivalent Delta Temperature (NEDT) histogram distribution was ~ 0.2 K for this image.

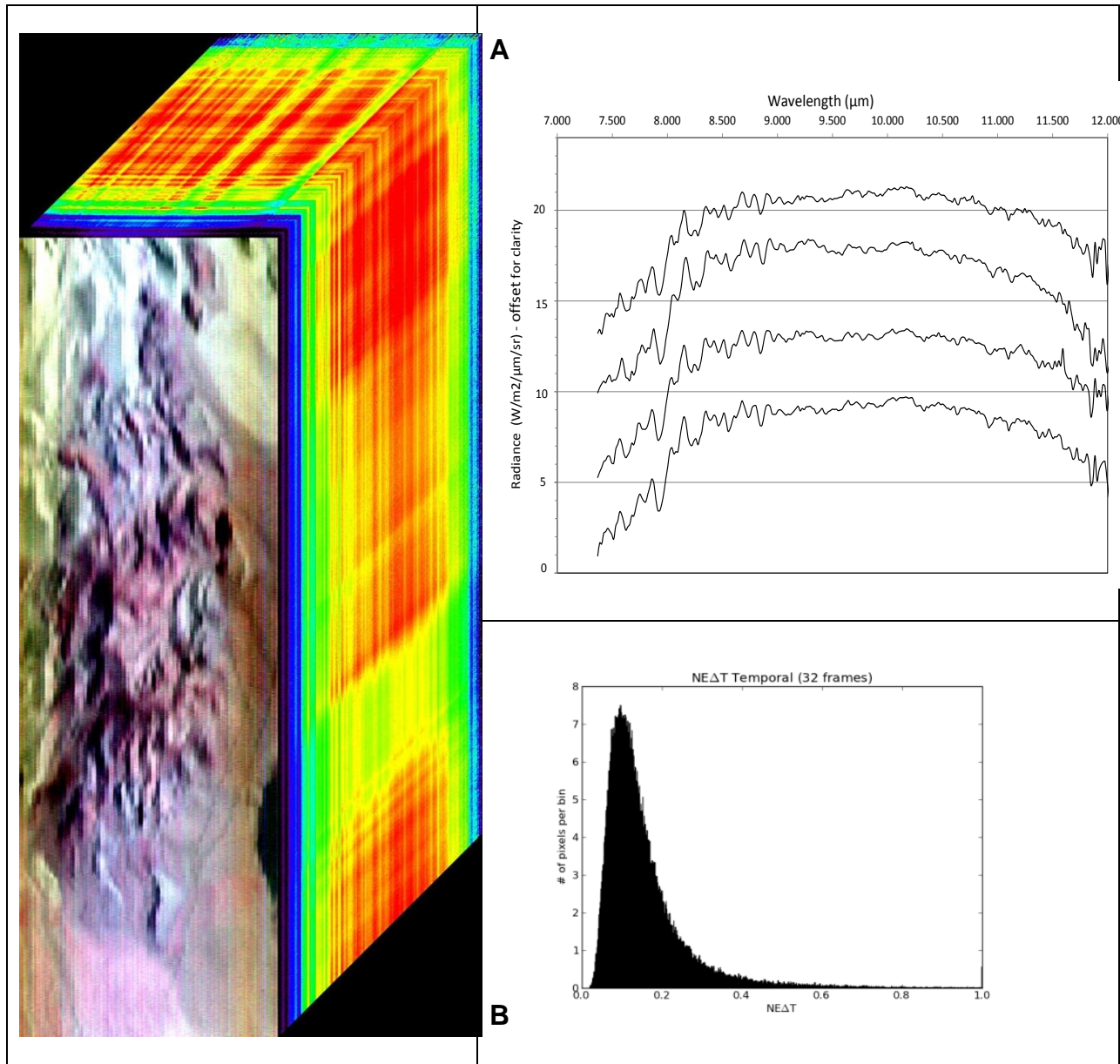


Figure 24. (left) Cuprite, NV image acquired on 07-20-2012 with bands 150 (10.08 μm), 100 (9.17 μm), and 58 (8.41 μm) displayed as RGB respectively as image cube. A) Radiance at sensor for different locations at Cuprite, B) Noise equivalent Delta Temperature (NEDT) histogram (~ 0.2 K).

Fig. 25 shows comparison between HyTES emissivity spectra and laboratory spectra of geologic samples collected over the Cuprite, NV site. The HyTES spectra were convolved to the nominal HypsIRI v1.0 band positions (blue circles) as well as the lab data (red circles) for comparison. The HyTES emissivity spectra were retrieved using the ASTER Temperature Emissivity Separation (TES) algorithm, and the calibration curve was modified for HypsIRI bands using a set of ~150 lab spectra consisting of rocks, sands, soils, vegetation, ice, water, and snow. Atmospheric correction was accomplished using MODTRAN 5.2 radiative transfer code with input atmospheric profiles of air temperature, relative humidity, and geopotential height from the NCEP-GDAS product. The spectra show comparisons at four sites with a variety of lithologies including areas of carbonate (Ca),

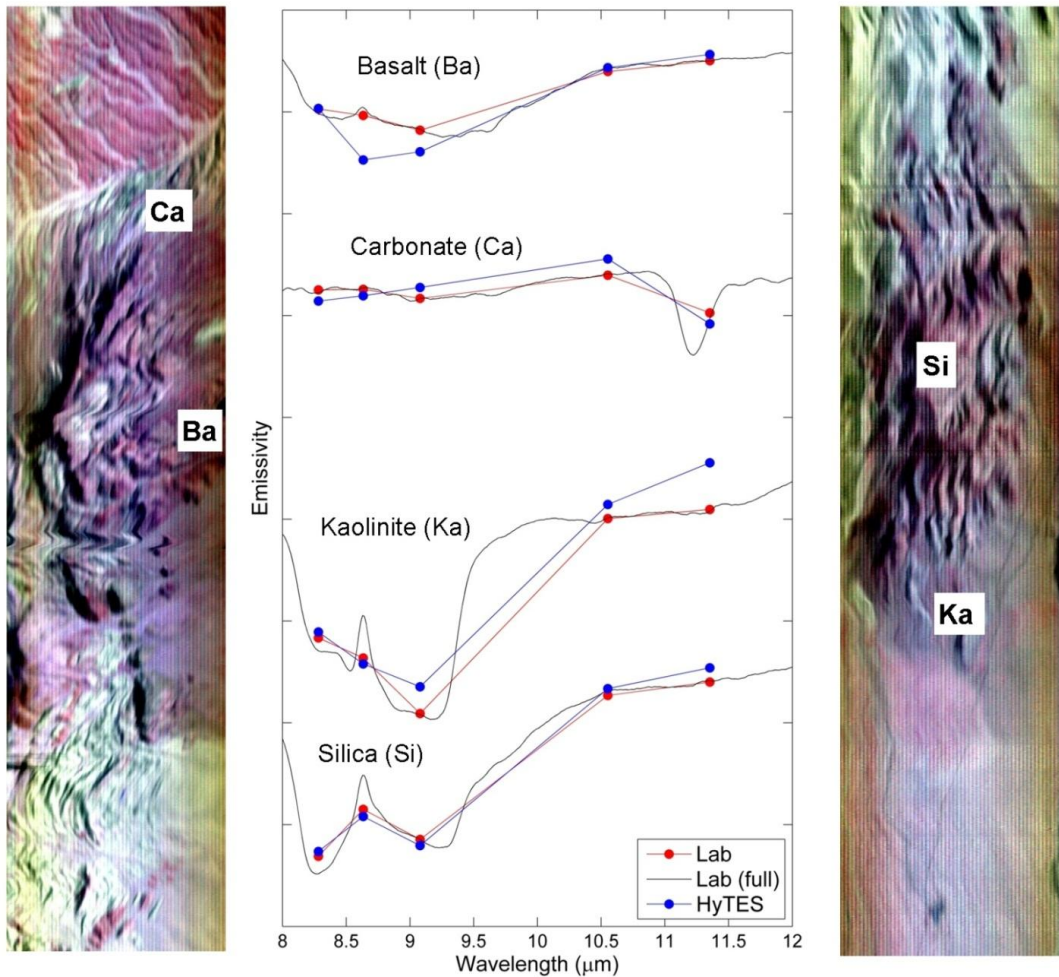


Figure 25. Comparisons between HyTES spectra convolved to HypsIRI TIR bands (blue circles) and laboratory spectra (red circles) of geologic samples collected in the Cuprite, NV region including basalt, carbonate, kaolinite, and silica.

basalt (Ba), kaolinite (Ka), and silica (Si). The lab spectra were obtained by measuring the reflectance of weathered surfaces of the field samples with the Jet Propulsion Laboratory Fourier Transform Infrared Spectrometer (JPL-FTIR). The reflectance measurements were converted to emissivity using Kirchoff's law, and then resampled to the HypsIRI response functions.

The laboratory spectra from the area of kaolinite have a strong broad emission minima across HypsIRI bands 8.3, 8.6, and 9.1 μm . This feature is typical of these clay minerals. The spectrum from the area of silica has two emission minima located in HypsIRI 8.3 and 9.1 μm bands. These are typical of fairly pure samples of quartz and result from Si-O stretching. In general, the shape of the image spectra retrieved from HyTES agrees well with the laboratory spectra. This gives confidence that band studies involving HyTES data will be possible in future work. Different band combinations and response shapes will be tested using the high spectral resolution data to assess the most optimal band positions for SO₂ mapping and associated atmospheric correction, as well as mineral mapping.

7.2 MAGI

The Mineral and Gas Identifier (MAGI) was recently developed and flown by The Aerospace Corporation with funding under the NASA Instrument Incubator Program (IIP). The airborne instrument has 32 channels in the thermal infrared (TIR) region spanning from 7.1 – 12.7 micrometers (Table 1). It consists of a whiskbroom design that can acquire up to 2800 pixels in the cross track direction by 128 pixels on the downtrack direction [Hall *et al.*, 2008]. Each of these scans constitute one "whisk" and the number of whisks is a function of the desired scan line length. This approach allows for wide crosstrack scanning over multiple channels, which is a significant improvement over previous hyperspectral TIR scanners such as the Spatially Enhanced Broadband Array Spectrograph System (SEBASS) sensor [Hackwell *et al.*, 1996]. For example, SEBASS is a pushbroom design and only acquires 128 pixels in the crosstrack direction resulting in limited areal coverage at the typical 1m/pixel spatial resolution.

Table 3. MAGI instrument specifications.

Number of spectral channels	32
Wavelength coverage	7.1 – 12.7 μm
Instantaneous pixel FOV	0.53 mrad
Frame rate	955 Hz
Integration Time	280 μsec
NEDT (single frame)	$\sim 0.12^\circ\text{C}$ at 10 μm
Number of along-track pixels	128
Maximum cross-track scan angle	$\pm 42^\circ$ (2800 pixels)
Max. number of cross-track scans	unlimited
Detector	HgCdTe
Detector Temperature	55 K
Optics Temperature	120 K
Calibration	Full aperture BB

MAGI was developed to test new TIR technologies and systems for future spaceborne TIR sensors such as HypsIRI. The sensor relies on a novel optical design that incorporates a Dyson spectrometer that has small optical distortion at low f-numbers. This spectrometer is mated to a HgCdTe focal plane array, which allows high frame rate data with very high signal to noise. Cryocoolers are used to cool the focal plane and optical bench, and an external telescope assembly sets the desired pixel IFOV (Figure 26).

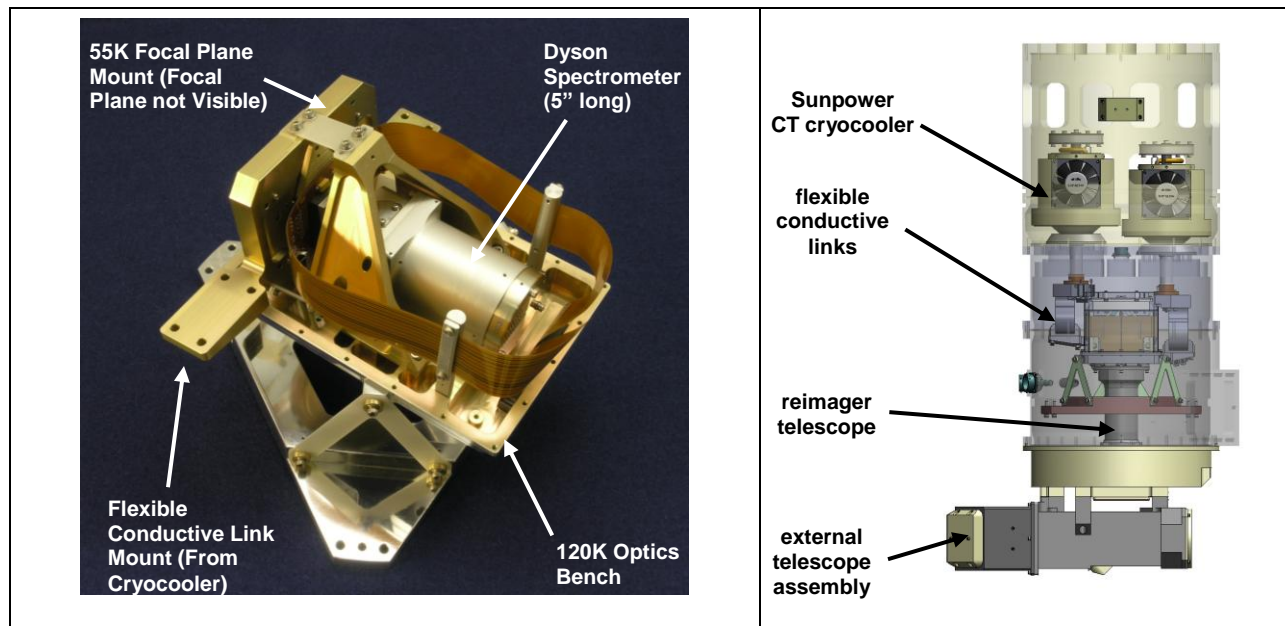


Figure 26. (left) Heart of the MAGI sensor showing Dyson spectrometer, mounts, and optics bench. (right) Sensor dewar with external telescope (dewar diameter is 13 inches).

The number of instrument channels was selected specifically to optimize the data return, span the entire wavelength region with no gaps, minimize spectral redundancy, and increase the signal to noise. Prior to building MAGI, trade studies were conducted using laboratory and SEBASS hyperspectral data to determine the optimal number of bands needed to discriminate most geologic and urban materials as well as common natural and anthropogenic gases. For both gas detection and mineral mapping studies, the spectral resolution of these hyperspectral datasets was iteratively degraded by factors of two to assess the point at which serious loss of detection fidelity sets in. The starting resolution was represented by the SEBASS configuration of 128 spectral channels spanning 7.65 to 13.55 μm . Degradations were then made to 64, 32, and 16 spectral channels across this same spectral range. Appropriate degradations were also made on the target end-member spectra chosen for the surface-mapping study and target gas spectra used for the gas detection study (Figure 27).

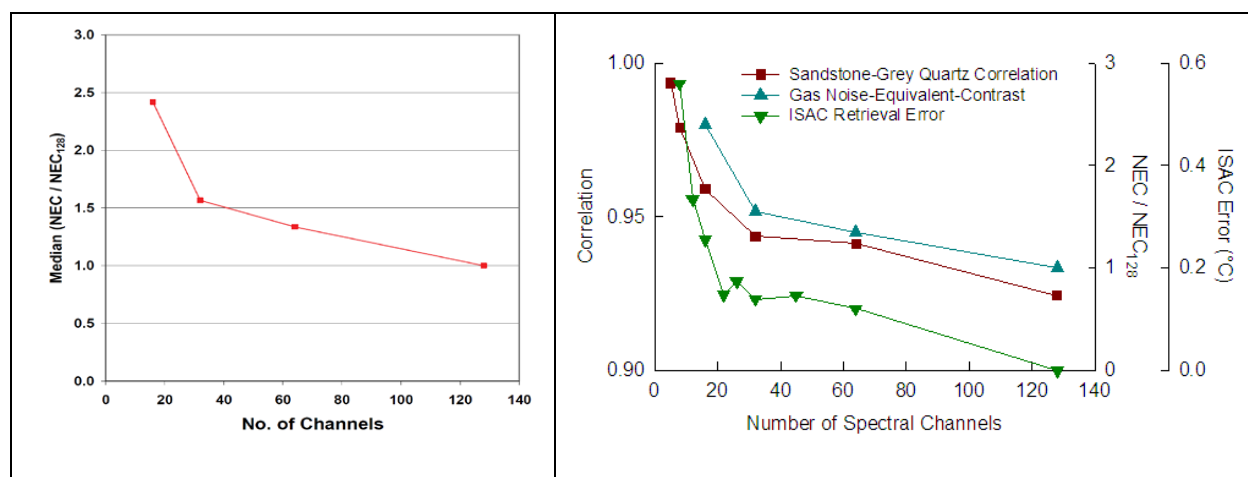


Figure 27. (left) Noise Equivalent Contrast (NEC) median ratio vs. number of channels (128, 64, 32, and 16) for 28 chemical compounds common in industrial gas plumes [Hall et al., 2008]. Larger ratios suggest a lower sensitivity to the specific chemical. In most cases sensitivity loss from 128 channels to 32 is less than a factor of 2. However, note the significant penalty where the data is reduced to less than ~ 30 channels. (right) Similar plot for other materials and gases as well as the surface temperature retrieval error expected the in-scene atmospheric correction (ISAC).

The initial flights of MAGI were conducted in December 2011 and include geologic targets such as the Salton Sea and Coso geothermal fields in CA and Cuprite in NV; agricultural targets such as portions of the Central Valley in CA; as well as urban targets in Los Angeles and El Segundo in CA. Atmospherically-corrected data from one whisk of the Salton Sea flight line is presented in Figure 28 and shows the excellent spatial and spectral quality of the data.

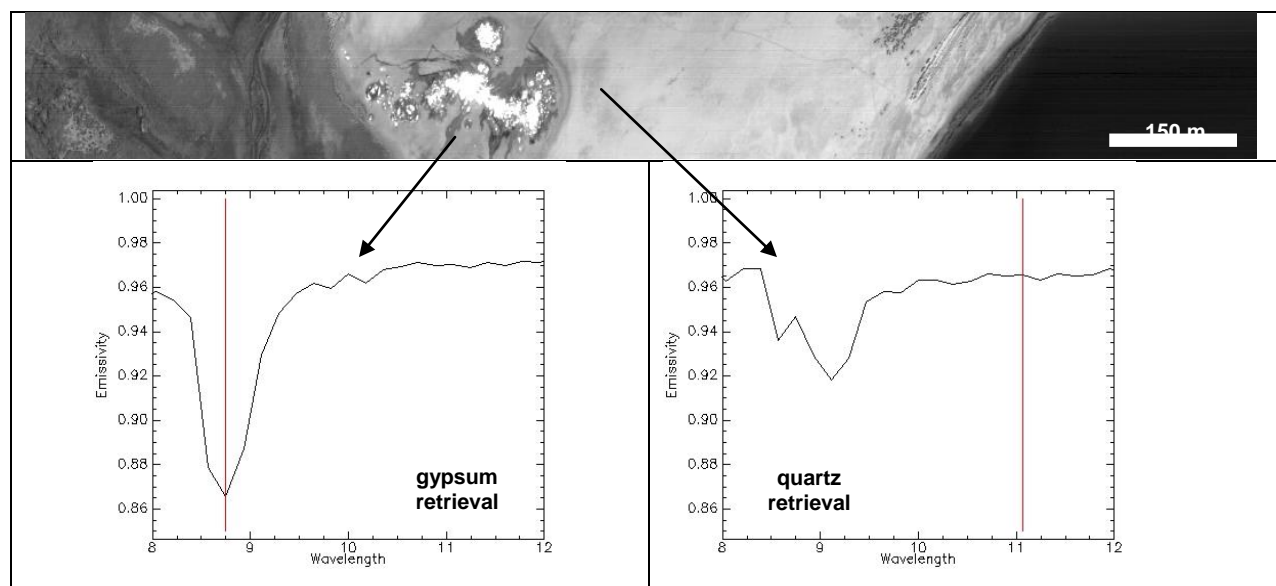


Figure 28. MAGI level 2 atmospherically-corrected data (whisk 18) and emissivity spectral retrievals from the Salton Sea, CA. (top) MAGI band 10 (8.751 micrometers) showing the "sandbar" geothermal field in the center of the strip and the Salton Sea to the right (north is to the upper right in the image). (left) Gypsum emissivity spectrum. (right) Quartz emissivity spectrum.

In order to test the accuracy of surface mineral retrievals using the currently-proposed HypsIRI TIR bandpasses, both MAGI TIR and the higher spectral resolution SEBASS TIR data were resampled to the six HypsIRI channels in the 8 – 12 micrometer region. The data were also resampled using the slightly altered band positions shown in Figure 19, which includes a narrower bandwidth at 10.05 micrometers. The resampled data were then subjected to linear spectral deconvolution using a library of common minerals known to occur in the region, including (but not limited to) quartz, gypsum, calcite, anhydrite, halite, oligoclase, microcline, and montmorillonite (a clay mineral). Of particular interest in this case study was the ability to detect the feldspar minerals (e.g., oligoclase and microcline) and carbonate minerals (e.g., calcite) in each bandpass configuration. Figure 29 shows the results for one of the mineral identification tests.

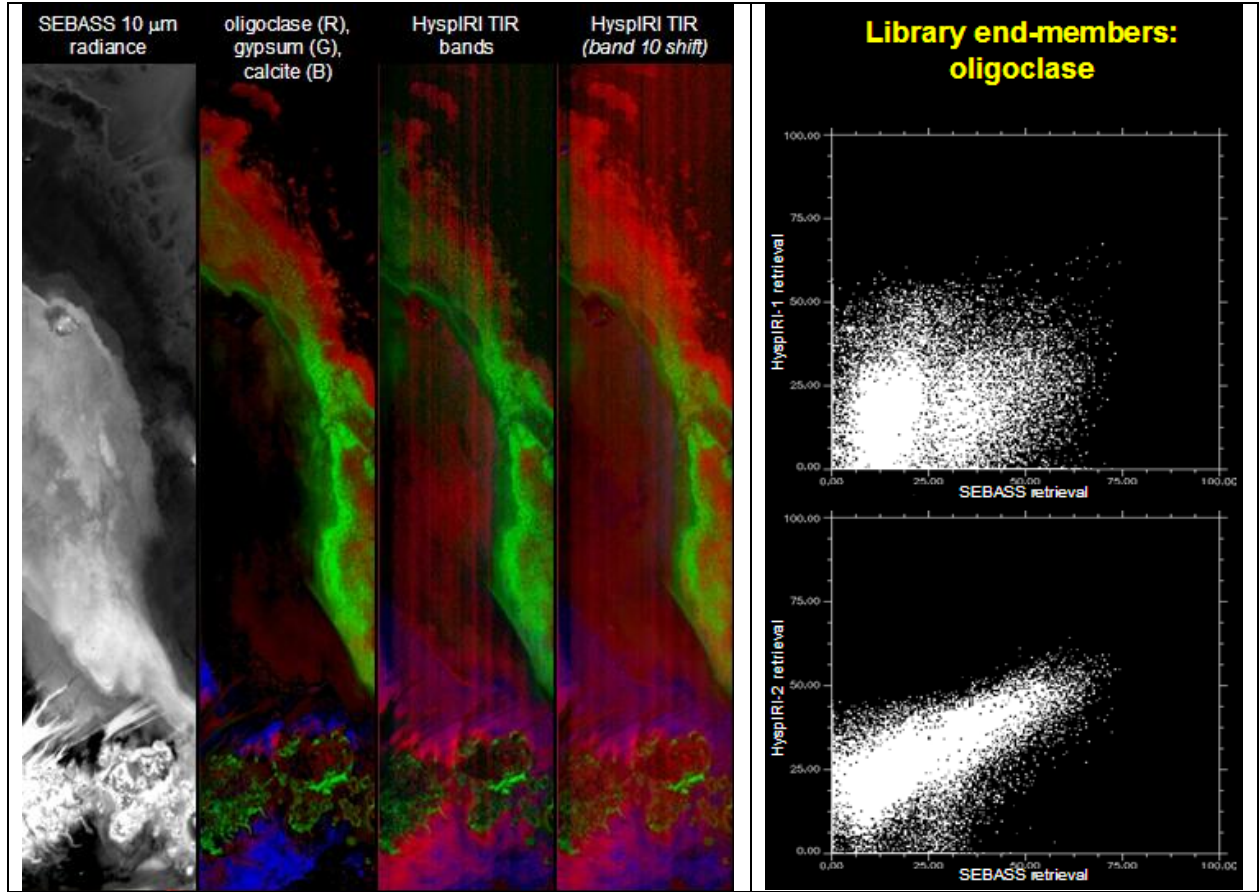


Figure 29. (left) Four panel image showing SEBASS data acquired over the "sandbar" geothermal field at Salton Sea, CA on April 6, 2010. The mineral retrieval for the full spectral resolution of SEBASS (second panel) is compared to both HypsIRI TIR configurations. The fourth panel shows an oligoclase distribution (in red) more similar to the full spectral resolution. (right) Scatter plots of the oligoclase retrievals confirm that there is a more linear relationship between the full spectral resolution and the simulated HypsIRI TIR data with the shifted band centers.

The initial results of the band position study using SEBASS and MAGI data both confirm that movement (and narrowing) of the 10 micron channel will greatly improve our ability to detect feldspar minerals and distinguish this class of minerals from other silicates. This will be important for surface change detection and mapping using a future HypsIRI TIR sensor. Furthermore, the proposed band shifts do not significantly change the ability to detect other minerals (e.g., quartz and calcite), which do not have emissivity features in the regions affected by the band position changes. Future work will be carried out using MAGI and SEBASS to assess the proposed position changes on other surface and gas detections.

8 References

- Baldrige, A. M., S. J. Hook, C. I. Grove, and G. Rivera (2009), The ASTER Spectral Library Version 2.0, *Remote Sensing of Environment*, 114(4), 711-715.
- Berk, A., et al. (2005), MODTRANTM 5, A Reformulated Atmospheric Band Model with Auxiliary Species and Practical Multiple Scattering Options: Update, in *Algorithms and Technologies for Multispectral, Hyperspectral, and Ultraspectral Imagery XI*, edited by S. S. Sylvia and P. E. Lewis, Proceedings of SPIE, Bellingham, WA.
- Blount, G., and N. Lancaster (1990), Development of the Gran Desierto Sand Sea, Northwestern Mexico, *Geology*, 18(8), 724-728.
- Duda, K. A., M. Ramsey, R. Wessels, and J. Dehn (2009), Optical satellite volcano monitoring: A multi-sensor rapid response system, in: P.P. Ho, (ed.), *Geoscience and Remote Sensing, INTECH Press, Vukovar, Croatia, ISBN 978-953-307-003-2*, 473-496.
- Campion, R., G.G. Salerno, P-F. Coheur, D. Hurtmans, L. Clarisse, K. Kazahaya, M. Burton, T. Caltabiano, C. Clerbaux, and A. Bernard (2010), Measuring volcanic degassing of SO₂ in the lower troposphere with ASTER band ratios, *J. Volcanol. Geotherm. Res.*, 194, 42-54.
- Corradini, S., L. Merucci, A. J. Prata, and A. Piscini (2010), Volcanic ash and SO₂ in the 2008 Kasatochi eruption: Retrievals comparison from different IR satellite sensors, *J. Geophys. Res.*, 115, D00L21, doi:10.1029/2009JD013634.
- Edgett, K. S., and N. Lancaster (1993), Volcanoclastic aeolian dunes: terrestrial examples and applications to martian sands, *Journal of Arid Environments*, 25, 271-297.
- Hackwell, J. A., D. W. Warren, R. P. Bongiovi, S. J. Hansel, T. L. Hayhurst, D. J. Mabry, M. G. Sivjee, and J. W. Skinner (1996), LWIR/MWIR imaging hyperspectral sensor for airborne and ground-based remote sensing, in *SPIE Imaging Spectrometry II, vol. 2819, M.R. Descour and J.M. Mooney, Eds.*, pp. 102-107.
- Hall, J. L., J. A. Hackwell, D. M. Tratt, D. W. Warren, and S. J. Young (2008), Space-based mineral and gas identification using a high-performance thermal infrared imaging spectrometer, *Proceedings of SPIE 7082, 70820M*. <http://dx.doi.org/10.1117/12.799659>.
- Hook, S. J., E. A. Abbott, C. Grove, A. B. Kahle, and F. D. Palluconi (1999), Use of multispectral thermal infrared data in geologic studies, *Remote Sensing for the Earth Sciences:*

- Manual of remote sensing, vol. 3 (E.N. Rencz ed.), (3rd ed.) (pp. 59-110). New York: John Wiley and Sons.*
- Hook, S. J., J. E. J. Myers, K. J. Thome, M. Fitzgerald, and A. B. Kahle (2001), The MODIS/ASTER airborne simulator (MASTER) - a new instrument for earth science studies, *Remote Sensing of Environment*, 76(1), 93-102.
- Hook, S. J., J. E. Dmochowski, K. A. Howard, L. C. Rowan, K. E. Karlstrom, and J. M. Stock (2005), Mapping variations in weight percent silica measured from multispectral thermal infrared imagery - Examples from the Hiller Mountains, Nevada, USA and Tres Virgenes-La Reforma, Baja California Sur, Mexico, *Remote Sensing of Environment*, 95(3), 273-289.
- Hunt, G. R. (1980), Electromagnetic radiation: the communication link in remote sensing, *Remote Sensing in Geology (B. S. Siegal and A.R. Gillespie, Eds.)*, Wiley, New York, pp. 5-45.
- HypIRI (2008), NASA 2008 HypIRI Whitepaper and Workshop Report, *Jet Propulsion Laboratory, California Institute of Technology, Pasadena, California*, May 2009.
- Johnson, W. R., S. J. Hook, P. Mouroulis, D. W. Wilson, S. D. Gunapala, C. J. Hill, J. M. Mumolo, and B. T. Eng (2009), Quantum well earth science testbed, *Infrared Physics & Technology*, 52(6), 430-433.
- Johnson, W. R., S. J. Hook, P. Mouroulis, D. W. Wilson, S. D. Gunapala, V. Realmuto, A. Lamborn, C. Paine, J. M. Mumolo, and B. T. Eng (2011), HyTES: Thermal imaging spectrometer development, AERO '11 Proceedings of the 2011 IEEE Aerospace Conference, pp 2011-2018, Washington DC, USA, 2011.
- Justice, C. O., et al. (1998), The Moderate Resolution Imaging Spectroradiometer (MODIS): Land remote sensing for global change research, *IEEE Transactions on Geoscience and Remote Sensing*, 36(4), 1228-1249.
- Kearney, C.S., K. Dean, V.J. Realmuto, I.M. Watson, J. Dehn, and F. Prata (2008), Observations of SO₂ production and transport from Bezymianny volcano, Kamchatka using the MODerate resolution Infrared Spectroradiometer (MODIS), *Int. J. Remote Sens.*, 29(22), 6647–6665.
- Kearney, C., I. M. Watson, G. J. S. Bluth, S. Carn, and V.J. Realmuto (2009), A comparison of thermal infrared and ultraviolet retrievals of SO₂ in the cloud produced by the 2003 Al-Mishraq State sulfur plant fire, *Geophys. Res. Lett.*, 36, L10807, doi:10.1029/2009GL038215.
- Kneizys, F. X., et al. (1996), The MODTRAN 2/3 Report & LOWTRAN 7 Model, F19628-91-C-0132, in *Phillips Lab*, edited, Hanscom AFB, MA.

- Lancaster, N. (1992), Relations between Dune Generations in the Gran Desierto of Mexico, *Sedimentology*, 39(4), 631-644.
- Prata, A. J., G. Bluth, B. Rose, D. Schneider, and A. Tupper (2001), Failures in detecting volcanic ash from a satellite-based technique - Comments, *Remote Sensing of Environment*, 78(3), 341-346.
- Prata, A. J., D. M. O'Brien, W.I. Rose, and S. Self (2003), Global, long-term sulphur dioxide measurements from TOVS data: a new tool for studying explosive volcanism and climate, *Geophysical Monograph 139*, 75 - 92.
- Prata, A. J., and C. Bernardo (2007), Retrieval of volcanic SO₂ column abundance from Atmospheric Infrared Sounder data, *J. Geophys. Res.*, 112, D20204, doi:10.1029/2006JD007955
- Pugnaghi, S., G. Gangale, S. Corradini, M.F. Buongiorno (2006), Mt. Etna sulfur dioxide flux monitoring using ASTER-TIR data and atmospheric observations, *J. Volcanol. Geotherm. Res.*, 152, 74-90.
- Ramsey, M., and S. Rose (2009), The complex effects of subpixel compositional, thermal and textural heterogeneities on spaceborne TIR data, in *The 2009 HypsIRI Science Workshop*, edited, Pasadena, CA.
- Ramsey, M. S., and P. R. Christensen (1998), Mineral abundance determination: Quantitative deconvolution of thermal emission spectra, *Journal of Geophysical Research-Solid Earth*, 103(B1), 577-596.
- Ramsey, M. S., P. R. Christensen, N. Lancaster, and D. A. Howard (1999), Identification of sand sources and transport pathways at the Kelso Dunes, California, using thermal infrared remote sensing, *Geological Society of America Bulletin*, 111(5), 646-662.
- Ramsey, M. S., and A. J. L. Harris (2012), Volcanology 2020: How will thermal remote sensing of volcanic surface activity evolve over the next decade?, *J. Volcanol. Geotherm. Res.*, 10.1016/j.jvolgeores.2012.05.011.
- Realmuto, V. J., and H. M. Worden (2000), Impact of atmospheric water vapor on the thermal infrared remote sensing of volcanic sulfur dioxide emissions: A case study from the Pu'u 'O'o vent of Kilauea Volcano, Hawaii, *Journal of Geophysical Research-Solid Earth*, 105(B9), 21497-21507.

- Realmuto, V. J., A. J. Sutton, and T. Elias (1997), Multispectral thermal infrared mapping of sulfur dioxide plumes: A case study from the East Rift Zone of Kilauea Volcano, Hawaii, *Journal of Geophysical Research-Solid Earth*, 102(B7), 15057-15072.
- Realmuto, V. J., M. J. Abrams, M. F. Buongiorno, and D. C. Pieri (1994), The Use of Multispectral Thermal Infrared Image Data to Estimate the Sulfur-Dioxide Flux from Volcanos - a Case-Study from Mount Etna, Sicily, July 29, 1986, *Journal of Geophysical Research-Solid Earth*, 99(B1), 481-488.
- Realmuto, V, S. Hook, M. Foote, I. Csiszar, P. Dennison, L. Giglio, M. Ramsey, R.G. Vaughan, M. Wooster, R. Wright (2011), HypsIRI High-Temperature Saturation Study, Jet Propulsion Laboratory, California Institute of Technology, Publication 11-2, April 2011, http://hyspiri.jpl.nasa.gov/downloads/2011_High_Temperature_Saturation_Report/Hyspiri_High-Temperature_Saturation_Report_110519.pdf
- Rose, W.I., Y. Gu, I. M. Watson¹, T. Yu¹, G. J. S. Bluth¹, A. J. Prata, A. J. Krueger, N. Krotkov, S. Carn, M. D. Fromm, D. E. Hunton, G. G. J. Ernst, A. A. Viggiano, T. M. Miller, J. O. Ballenthin, J. M. Reeves, J. C. Wilson, B. E. Anderson, and D. E. Flittner (2003), The February–March 2000 Eruption of Hekla, Iceland from a Satellite Perspective, *Geophysical Monograph 139*, 107-132.
- Rosi, M., A. Bertagnini, A. J. L. Harris, L. Pioli, M. Pistolesi, and M., Ripepe (2006), A case history of paroxysmal explosion at Stromboli: timing and dynamics of the April 5, 2003 event. *Earth and Planetary Science Letters 243*, 594–606.
- Rybin, A., M. Chibisova, P. Webley, T. Steensen, P. Izbekov, C. Neal, and V. Realmuto (2011), Satellite and ground observations of the June 2009 eruption of Sarychev Peak volcano, Matua Island, Central Kuriles, *Bull. Volcanol.*, doi: 10.1007/s00445-011-0481-0
- Scheidt, S., N. Lancaster, and M. Ramsey (2011), Eolian dynamics and sediment mixing in the Gran Desierto, Mexico, determined from thermal infrared spectroscopy and remote-sensing data, *Geological Society of America Bulletin*, 123(7-8), 1628-1644.
- Teggi, S., M.P Bogliolo, M.F. Buongiorno, S. Pugnaghi, and A. Sterni (1999), Evaluation of SO₂ emission from Mount Etna using diurnal and nocturnal multispectral IR and visible imaging spectrometer thermal IR remote sensing images and radiative transfer models, *J. Geophys. Res.*, 104(B9), 20,069-20,079.

- Thomas, H.E., I.M. Watson, C. Kearney, S.A. Carn, and S.J. Murray (2009), A multi-sensor comparison of sulphur dioxide emissions from the 2005 eruption of Sierra Negra volcano, Galápagos Islands, *Remote Sens. Environ.*, 113, 1331–1342.
- Tupper, A., J. Davey, P. Stewart, B. Stunder, R. Servranckx, and F. Prata (2006), Aircraft encounters with volcanic clouds over Micronesia, Oceania, 2002-03, *Aust Meteorol Mag*, 55(4), 289-299.
- Urai, M. (2004), Sulfur dioxide flux estimation from volcanoes using Advanced Spaceborne Thermal Emission and Reflection Radiometer – a case study of Miyakejima volcano, Japan, *J. Volcanol. Geotherm. Res.*, 134, 1-13.
- Vaughan, R. G., S. J. Hook, W. M. Calvin, and J. V. Taranik (2005), Surface mineral mapping at Steamboat Springs, Nevada, USA, with multi-wavelength thermal infrared images, *Remote Sensing of Environment*, 99(1-2), 140-158.
- Watson, I. M., V. J. Realmuto, W. I. Rose, A. J. Prata, G. J. S. Bluth, Y. Gu, C. E. Bader, and T. Yu (2004), Thermal infrared remote sensing of volcanic emissions using the moderate resolution imaging spectroradiometer, *Journal of Volcanology and Geothermal Research*, 135(1-2), 75-89.
- Wolfe, R. E., D. P. Roy, and E. Vermote (1998), MODIS land data storage, gridding, and compositing methodology: Level 2 grid, *IEEE Transactions on Geoscience and Remote Sensing*, 36(4), 1324-1338.
- Yamaguchi, Y., A. B. Kahle, H. Tsu, T. Kawakami, and M. Pniel (1998), Overview of Advanced Spaceborne Thermal Emission and Reflection Radiometer (ASTER), *IEEE Transactions on Geoscience and Remote Sensing*, 36(4), 1062-1071.



Approximately 180 scientists gathered from August 23-25, 2011 at the 4th NASA HypspIRI Science Workshop held in Washington, DC. PDF versions of the presentations given at the meeting are available from the HypspIRI website (<http://hypspiri.jpl.nasa.gov>).

Introduction and Meeting Overview

The HypspIRI mission was recommended for implementation by the 2007 report from the U.S. National Research Council *Earth Science and Applications from Space: National Imperatives for the Next Decade and Beyond* (also known as the Earth Science Decadal Survey or, simply, the Decadal Survey). The annual HypspIRI workshop provides an open forum to present the observational requirements for the mission and assess its anticipated impact on scientific and operational applications; the open forum also provides an opportunity to obtain feedback from the broader scientific community on the mission concept. This year's workshop had a greater emphasis on the science applications contribution from HypspIRI and included a full day on HypspIRI related science applications for water use and availability, wildland fires, volcanology and urban and environmental studies. The morning of the first day focused on providing an overview of the mission. The afternoon of the first day focused on the use of HypspIRI data for ecosystem studies and some of the airborne precursor instrument development activities. This included a discussion of the Airborne Visible/Infrared Imaging Spectrometer Next Generation (AVIRIS-ng) as well as the airborne Hyperspectral Thermal Emission Spectrometer (HyTES). The second day was focused on science applications together with science presentations, including discussion of the science questions that HypspIRI will address. The final day included discussions of related missions, partnership opportunities and plans for 2012 and beyond. Of particular interest was the discussion of a potential airborne campaign to acquire data for both science and algorithm testing beginning in the 2012-2013 timeframe. As with previous workshops, the Preliminary Level 1 mission requirements were reviewed with the community to make sure they would meet the science needs. This year there were over 24 posters which provided an excellent opportunity for more detailed discussions between talks. The workshop participants concluded that the HypspIRI mission would provide a significant new capability to study ecosystems and natural hazards at spatial scales relevant to human resource use and would be particularly valuable for climate related studies. The participants felt the measurement requirements could be achieved with the reference instrument design concepts and be implemented through the use of current technology. The workshop participants, like the Decadal Survey itself, strongly endorsed the need for the HypspIRI mission and felt the mission, as defined, would accomplish the intended science. Workshop participants were particularly enthusiastic about a dedicated airborne

campaign as well as obtaining data from the new AVIRIS-ng and HyTES airborne sensors.

Woody Turner [NASA Hq] started the meeting by welcoming the participants and outlining the goals and objectives for this year's meeting. He then provided an update on what we have achieved so far and what was planned for the future. Woody emphasized that HypsIRI is a global mission providing full spatial resolution data (60 m) of the land and coastal regions and lower spatial resolution (1 km) data over the deeper oceans. HypsIRI will obtain full global coverage with the TIR and VSWIR sensors every 5 and 19 days respectively. Woody welcomed the members of the newly formed HypsIRI International Science Group. This group will work with current Science Study Group to evaluate potential synergies between HypsIRI and other international missions. Woody noted the opportunity for community building especially given the strong attendance at the meeting as well as previous meetings. He was particularly looking forward to hearing more about the science applications work being done for HypsIRI. He indicated the need to continue to stay focused and conduct limited risk reduction and understand which products required low latency. He closed by reiterating that HypsIRI was a global mission with a broad user community that utilized mature technologies. He indicated we need to continue to retire risks, keep costs down, build the community and develop partnerships where appropriate.

Jack Kaye [NASA Hq] followed Woody's presentation and talked about how HypsIRI fits in with the bigger inter-agency picture. Jack indicated we need to continue to focus on calibration, algorithms and validation and make sure the data provide the maximum benefit to the community. Jack noted we have had a couple of HypsIRI calls and saw these as an excellent way to demonstrate the potential of HypsIRI data using existing precursor data. He indicated how his program had been able to support several airborne instrument activities such as HyTES and AVIRIS-ng which would help the community by providing data suitable for simulating HypsIRI. Jack indicated we need continue to emphasize the value of HypsIRI-like data at the local and regional level and the societal benefits. HypsIRI is considered to be very valuable for interdisciplinary studies supported by the US Global Climate Research Program and the upcoming airborne campaign would provide valuable data for the ongoing National Climate Assessment. During the questions and answers following his talk he encouraged the use of partnerships to reduce cost.

Mike Freilich [NASA Hq] presented slightly later in the meeting due to a conflict but his comments are included here since they were of programmatic relevance. Mike started by noting that the HypsIRI launch data is currently post 2020 but that Headquarters was undertaking HypsIRI-related activities to prepare for the mission. Mike noted that there were a large number of satellites in orbit which would help to inform the next set of missions as well as several missions due to launch soon. Aquarius had just had a successful launch before the HypsIRI meeting. Mike indicated that NASA earth science had a healthy budget but the costs estimated by the Decadal Survey were considerably lower than the subsequent estimates which would affect when missions were moved into Phase A. Mike also indicated that some missions were added in to those identified by the Decadal Survey to address Administration priorities that are not in the Decadal Survey.

Currently it is expected there will be about one launch per year for the next several years. Mike emphasized the new line of Venture Class missions which includes 3 strands: 1) Airborne investigations; 2) PI-led small spaceborne missions; and 3) Instruments for future opportunities. The EV-Instrument call is expected to be yearly. Mike indicated Hq was planning to continue to fund HypsIRI studies so we understand how to keep costs down and accomplish the mission science.

Rob Green and Carl Bruce [NASA/JPL] then summarized the instrument concept for the visible shortwave infrared (VSWIR) imaging spectrometer on HypsIRI. HypsIRI will have three main payload elements, a VSWIR imaging spectrometer, a multispectral thermal infrared (TIR) imager and an Intelligent Payload Module (IPM) henceforth referred to as the VSWIR, TIR and IPM. The VSWIR imaging spectrometer will obtain data covering the spectral range from 380 to 2500 nm with 10 nm sampling. VSWIR data will be acquired over the full terrestrial surface with a 19 day revisit, including shallow water regions. The deep oceans and ice sheets also will be acquired with a 19 day revisit but resampled to a spatial resolution of 1 km. Rob noted that we have developed a set of science objectives that HypsIRI will address and provided some examples of the science that could be accomplished. This included examples ranging from the Gulf of Mexico oil spill to determining canopy nitrogen content to estimating the impact of black carbon on snow and ice melt to mapping emergent and submerged aquatic vegetation. The VSWIR instrument concept was shown to have design heritage from instruments such as the Moon Mineralogy Mapper (M3). This heritage has allowed the VSWIR instrument to be far smaller and use less power than earlier designs such as Hyperion. In-flight, the instrument would be fully calibrated with an onboard solar panel, lunar looks and ground calibration experiments. Carl noted that the current point design had remained unchanged and the mass and power were now 55kg and 41 watts respectively. Carl highlighted the importance of accuracy and calibration and that the system was both highly linear with minimal polarization sensitivity and a large swath of 145 km. Several airborne instruments have been developed which demonstrate the approach used but nonetheless the project examined alternate approaches and found they did not meet the measurement requirements. Carl noted that due to some recent detector developments only two spectrometers were required instead of the original 4 spectrometers. Carl finished by illustrating the core technologies for the VSWIR instrument and how these technologies were mature.

Simon Hook [NASA/JPL] then summarized the instrument concept for the TIR multispectral imager on HypsIRI. The TIR imager will obtain data in eight spectral channels, one of the channels is located at 4 μm and the other seven channels are located between 7 and 12 μm . TIR data will be acquired over the full terrestrial surface with a 5-day revisit, including shallow water regions. The TIR instrument operates continuously, providing both a daytime and nighttime scene for the entire earth every 5 days at the equator. The deep oceans and ice sheets also will be acquired with a 5 day revisit but resampled to a spatial resolution of 1 km. Simon presented examples of how the TIR data would be used for a broad range of science and applications with particular emphasis on volcanoes, wildfires, and water use and availability. For each area, Simon provided examples of how the instrument concept was designed to address critical questions in

these areas. Simon showed how the revisit will be greater at higher latitudes and used an example from the recent Iceland eruption to highlight how the TIR would have been able to provide daily information on the composition and chemistry of the volcanic plume, of particular importance for aeronautics. The TIR instrument concept has design heritage from instruments such as ASTER and MODIS and is a mature concept that can be built and launched in the same timeframe as the VSWIR instrument. Simon highlighted risk reduction activities underway for the TIR including science risk reduction associated with the development of the HyTES and instrument risk reduction associated with the development of the Prototype HypsIRI Thermal Infrared Radiometer (PHyTIR). PhyTIR is a laboratory demonstration of key instrument capabilities including the focal plane assembly and scanning mechanism. HypsIRI-TIR data will be collected with a 2-sided scan mirror. The dwell time for any given pixel will be 32 microseconds. The system will use a Mercury Cadmium Telluride detector and the focal plane will be cooled to 60 Kelvin with an active cooler. A two point calibration (blackbody and deep space view) will be performed every 2 seconds. There also will be lunar looks and ground calibration using automated validation sites. The system will use a Cassegrain telescope with radiation from the instrument baffled away from the detector. There will be a single detector array, having 32 readout ports, with 256X16 pixels in each of the 8 spectral channels. The system will use time-delay-and-integration with each channel using 4 columns from the array; since each channel has extra columns, the best 4 columns can be used. Current testing of a prototype read out integrated circuit indicates compliance with noise and power specifications, and the instrument noise equivalent temperature difference should be less than 0.2 K in the seven thermal infrared channels, with ample signal from hot targets for the mid infrared channel. As part of the PHyTIR activity detector material will be added to the ROIC and tested with a scan mirror operating at the same speed as the spaceborne instrument. Various commercial cryocoolers are being studied with several available that meet the design requirement Simon closed by restating the TIR will provide essential data for reducing the uncertainties in land carbon flux together with data for a range of applications from volcano monitoring to wildfires.

Scott Ollinger [University of New Hampshire] presented the first science keynote on “Vegetation canopies in a whole new light: Measurements for New Understanding of the Earth's Carbon Cycle and Ecosystem-Climate Feedbacks”. Scott noted that plants process 15-20% of atmospheric carbon dioxide annually and are among the largest processors of carbon globally. Scott showed how the carbon and nitrogen cycles are linked and, to fully understand the carbon cycle, you also need to understand the nitrogen cycle. For example plant nitrogen concentrations help control both photosynthesis and respiration and in temperate deciduous regions, nitrogen is a more important driver of canopy photosynthesis than leaf area index. HypsIRI will enable the nitrogen in canopies to be mapped, a capability that is not currently available at broad spatial scales. The metabolism of plants and ecosystems is increasingly well understood at the local scale, but the lack of corresponding data at the global scale means there are still large uncertainties in future CO₂/climate predictions. Many land models do not include the nitrogen cycle and those that are working to incorporate it are limited by a lack of data on vegetation nitrogen status over broad scales. Despite these limitations, well calibrated imaging spectrometer data can be used to predict nitrogen response in plants and Scott is

currently using airborne data to test relationships over a wide range of sites in the Ameriflux network. The airborne data are at higher spatial resolutions than future HypsIRI data, but when resampled to HypsIRI resolution provide similar results. Scott noted our ability to characterize vegetation globally and its role in the carbon/climate system is limited and has been for decades. The role of the nitrogen cycle and vegetation nitrogen status represents a long-standing constraint. Global, high-resolution, high fidelity imaging spectrometer data will reduce substantially uncertainties in terrestrial carbon metabolism. Full spectral data may also help to reveal new processes that are unrecognized or presently underappreciated, and can also help to provide stepping stones between detailed field measurements and coarser resolution global data sets.

Bogdan Oaida [NASA/JPL] discussed the overall mission concept. HypsIRI is optimized to operate in a 626 km Sun synchronous orbit with a 10:30 am descending equatorial crossing time. Bogdan showed there are several other potential orbits that could support the 19-and 5-day revisit of the VSWIR and TIR respectively, including an orbit around 705 km used by many other spacecraft. Bogdan outlined the operations concept for HypsIRI which is very simple since both instruments are always turned on in order to provide global mapping. The VSWIR data are day-only and currently planned to be acquired when the local solar elevation is greater than 20 degrees, however, this constraint may be relaxed to 10 degrees to provide additional coverage in the Polar Regions. The HypsIRI payload can be accommodated by a number of commercially available spacecraft buses, some of which may require modifications to the power generation system to meet mission needs. Additional upgrades will likely include a solid state recorder with a 1 Tb capacity. HypsIRI is continuing to maintain compatibility with several Launch Vehicles, including the possibility of a shared launch. The ground systems and data management concept continues to be matured. As part of that effort and in a response to a Request For Information, KSAT has indicated they will have ample capacity to meet the downlink needs of HypsIRI with two polar downlink stations operating in the X-Band spectrum. The two polar stations are at Svalbard and Poker Flat, with additional stations available at both poles if needed.

Dan Mandl [NASA/GSFC] described the IPM. The IPM will provide low latency data which can be used for a wide range of applications such as near realtime monitoring of fires or floods. There will be two data streams on the spacecraft; one is downloaded through the normal route while a second identical stream goes to the IPM. The IPM will be able to subset and process this second stream and download the data in near realtime (NRT) via a direct broadcast antenna. The NRT data will be available over the internet. Work is currently underway benchmarking the Computer Processing Unit for IPM and developing delay tolerant network communication connectivity to handle any network disruption. The web coverage service will be used to automatically load algorithms so a custom algorithm can be loaded for a particular task or application and the data downloaded in NRT such as during a fire or flood. An IPM testbed for HypsIRI has been developed and is being used for testing algorithms such as automated atmospheric correction using existing Hyperion data.

Rob Green [NASA/JPL] and Simon Hook [NASA/JPL] then reviewed the Draft Level 1 Mission Requirements which serve as the top-level requirements for the HypsIRI mission and provide the basis for deriving the more detailed Level 2 requirements. These requirements were first presented at the 2008 Workshop and are reviewed at each workshop to make sure the community is fully aware of the data that HypsIRI will provide.

Jose Moreno [University of Valencia, Spain] then gave the second science keynote on the unique role for HypsIRI in Earth System Science Dynamical Global Vegetation Models. Jose began by summarizing the background and motivation for the presentation and then described the status of dynamical vegetation models and uniqueness of HypsIRI data. This was followed by a discussion of the different approaches for incorporating ecosystem information in the models. Currently three approaches are used: 1) assigned fixed tables of biophysical variables to classification maps, 2) retrieval of biophysical variables as direct inputs to a model and 3) direct assimilation of radiances/reflectances into the models. Finally Jose provided his perspectives on current trends and the way forward. Jose noted that we are now moving away from assigned biophysical variables for fixed vegetation types, obtained through approaches like land classification, towards the direct inputs to models of retrieved biophysical variables. Many of the key variables required can be obtained by a combination of visible to shortwave infrared imaging spectrometer data and thermal infrared data as will be provided by HypsIRI. Global data are available but the low spatial resolution and limited spectral information only allow indirect observation of the dynamical vegetation processes. HypsIRI will provide systematic global sampling at the appropriate spatial and spectral resolutions and complete spectral coverage. The key problem right now is the large number of parameters and large uncertainty in such parameters, which is limiting our ability to run predictive analyses based on perturbation of free model parameters to test future climate scenarios. We can undertake model intercomparisons to optimize existing parameterizations and limit parameter space but we need a reference dataset which is global, high spatial resolution and spectrally complete with good temporal resolution and covering several seasonal cycles – HypsIRI will provide that dataset.

Science Presentations

After the two keynote presentations the remainder of the first day, all of the second day and part of the third day was devoted to science and science applications talks. There were over 40 talks and most of the presentations associated with these talks are available from the HypsIRI website. The talks covered a wide range in topics and included updates from the studies funded by NASA solicitations as well as updates on the key science questions that HypsIRI will address. The science questions were developed in conjunction with the Science Study Group, a group of scientists appointed by NASA to help guide the mission and ensure the measurements are of maximum benefit. The science talks on the second day were dedicated to the use of HypsIRI data in science applications. The science applications talks covered many areas including water use and availability, wildland fires, volcanology and urban and environmental studies. The early part of the third day included several engineering presentations on the Intelligent Payload Module (IPM). The IPM includes onboard processing combined with direct broadcast

and will be available for a subset of the data. The remainder of the third day included both science talks as well as presentations from our international and domestic colleagues on related programs, for example the National Science Foundation supported NEON program.

Review of the Workshop and Next Steps

The final presentation reviewed the progress since the last meeting and future activities. Woody Turner began the wrap-up by commenting that not only was the workshop a wonderful series of talks on the utility of visible shortwave infrared imaging spectrometer data and multispectral thermal infrared imagery but more importantly a demonstration of the fundamental ground breaking science that could be performed by the combined capability from both instruments. Further, the Applications day had clearly demonstrated the value of the data for use in operational systems. Participants noted the large number of posters displayed at the meeting and asked that future meetings include an evening session dedicated to the posters. Of particular interest with the community was the possibility of an airborne campaign in California using the AVIRIS and MASTER sensors to acquire HypsIRI-like datasets for science development. Potential flight corridors were discussed together with how to ensure the necessary field measurements were made to maximize the usefulness of the data. There was also considerable interest in the follow-on airborne instruments AVIRIS-NG and HyTES and participants were eager to see data from both instruments at the next meeting. Lastly participants welcomed the greater international participation and are looking forward to additional presentations from the international community especially through the newly formed International Science Group.

In summary, the participants felt that the HypsIRI mission would provide a significant new capability to study ecosystems and natural hazards at spatial scales relevant to human resource use. The participants confirmed the Draft Preliminary HypsIRI Mission Level 1 Requirements were achievable within the mission concept presented and would provide the necessary data to address the science questions identified for the mission.



2011 HypIRI Science Symposium

Meeting Focus:

Identifying Potential Higher Level Products for HypIRI End Users and a Data Management Framework for Global HypIRI Products

Meeting Objectives:

Identify science/application data products to be derived from HypIRI measurements by users,
Discover/Discuss issues underlying data product processing/integration/fusion,
Prioritize the development of product prototypes

A Symposium Sponsored by NASA

Goddard Space Flight Center

May 17-18, 2011

Organizer: Dr. Elizabeth M. Middleton, 614.4

Day 1: May 17, 2011

8:00-9:00am *Registration/Coffee/Posters Hung*

9:00- 9:20am Meeting Welcome (*Nick White, Director 600*)

Status of HypsIRI Mission (*Woody Turner, HQ*)

Meeting Overview, Goals & Logistics (*Betsy Middleton, GSFC*)

Session I: Background & Framework-- Building on Past Experience

9:20-9:30am Update on HQ Perspective (*Jack Kaye, HQ*)

9:30-9:50am Short Summary of the HypsIRI VSWIR Spectrometer (*Rob Green, JPL*)

Short Summary of the HypsIRI TIR Instrument (*Simon Hook, JPL*)

9:50- 10:00am Challenges and Opportunities for the HypsIRI Community (*Betsy Middleton, GSFC*)

10:00-10:20am MODIS Science Algorithms and Data System-- Lessons Learned (*Robert Wolfe, GSFC*)

10:20-10:40am Lessons Learned from Three Decades of Landsat Collections (*Jeff Masek, GSFC*)

10:40-10:45am *Discussion*

10:45-11:00am *Coffee Break/Posters*

Session II: New Possibilities for Science with HypsIRI—General Ideas

11:00-11:20am Global/Seasonal Imaging Spectroscopy Measurements of the Terrestrial Earth System for Climate Feedback Process Understanding (*Rob Green, JPL*)

11:20-11:40am Scaling Biosphere-Atmosphere Fluxes from the Site-Level to the Globe Using Machine Learning Algorithms: Lessons for HypsIRI (*Hank Margolis, U Laval*)

11:40-12:00pm Societal Impacts: Agricultural Perspective (*Charlie Walthall, USDA*)

12:00-12:20pm CEOS-WGCV Land Product Validation Sub-Group Activities: Current and Potential Roles in Future Decadal Survey Missions (*Miguel Román, GSFC*)

12:20-12:30pm *Discussion*

12:30-1:30pm *Lunch [sandwiches/salad/sodas@\$9pp]*

Session III: New Possibilities for Science with HypsIRI—Examples

1:30-1:50pm Coral Reefs, Climate Change, and Remote Sensing (*Eric Hochberg, Nova SE U. Oceanog. Center*)

1:50-2:10pm The Conundrum of Impacts of Climate Change on Urbanization: Prospects for Using HypsIRI Data Products for Regional to Global Societal Impacts Analysis (*Dale Quattrochi, MSFC*)

2:10-2:30pm Mapping Coupled Carbon Assimilation and Transpiration Fluxes using TIR and Hyperspectral Imaging (*Martha Anderson, USDA*)

2:30-2:50pm Advancing the Use of Remote Sensing Information for Quantifying Photosynthetic Efficiency in Space and Time (*Rasmus Houborg, EU Joint Res. Centre, Italy*)

2:50-3:10pm Thermal Remote Sensing and the Thermodynamics of Ecosystem Development (*Jeffrey Luvall, MSFC*)

3:10-3:30pm Global Volcano Monitoring and Volcanic Hazard Assessment: How HypsIRI Improves Upon and Complements Results Obtained during the EOS Era (*Robert Wright, U. Hawai'i*)

3:30-3:50pm *Coffee Break/Posters*

Session IV: Data Volume Challenges & Solutions

3:50-4:10pm Managing NASA Satellite Data for Global Studies (*Ed Masuoka, GSFC*)

4:10-4:30pm Status of the Prototyping Efforts for the IPM & Low Latency Products (*Dan Mandl, GSFC*)

4:30-4:40pm *Topic Introduction for Panel Discussion* (*Bob Knox, GSFC*)

4:40-5:50pm *How do we handle HypsIRI data? What is the preferred Mission Model for the data processing chain? Panel Members: Bob Knox (Chair), Robert Wolfe, Ed Masuoka, Dan Mandl, Rob Green, Simon Hook*

5:50-6:00pm *Wrap-Up and Announcements*

6:00pm *Adjourn for the Day*

7:00-8:30pm *DINNER (at Ruby Tuesday – in alcove by bar; restaurant across from GSFC Main Gate)*

Day 2: May 18, 2011

8:00-9:00am Registration/Coffee/Posters Hung

8:15-9:00am Coffee/Posters

Session V: Context for Hyperspectral and TIR Data Products

9:00-9:20am Hyperspectral Remote Sensing of Vegetation: Knowledge Gain and Knowledge Gap after 40 years of research (*Prasad Thenkabail, USGS*)

9:20-9:40am How will remote sensing of volcanic activity evolve with HypsIRI? (*Mike Ramsey, U. Pittsburgh*)

9:40-10:00am Summary, 2010 HypsIRI Symposium on Higher Level Products (*Betsy Middleton, GSFC*)

10:00-10:20am Report on Two HypsIRI Workshops to Identify Climate Relevant Products at the Global Scale (*Susan Ustin, UC-Davis*)

Session VI: Data Issues

10:20-10:40am Sampling and Time Series Issues (*Bob Knox, GSFC*)

10:40-11:00am Coffee Break/Posters

11:00-11:15am Tagging and Retrieving Data for an Archive (*Dave Landis, Sigma Space*)

11:15-11:30am Data Processing Tools (*Vuong Ly, GSFC*)

11:30-11:45am Calibration & CEOS (*Steve Ungar, USRA*)

11:45-12:00pm AERONET (*Sasha Smirnov, Sigma Space*)

12:00-12:15pm Calibration and Validation Sensors for Next-Generation NASA Missions (*Stan Hooker, GSFC*)

12:15-12:35pm Use of HypsIRI Data with the Web Coverage Process Service (WCPS) for Environmental Monitoring – Pre-Launch Demonstrations Using SensorWeb Hyperion Data (*Robert Sohlberg, UMD*)

12:35-12:45pm Discussion

12:45-1:30pm Lunch [sandwiches/salad/sodas@\$9pp]

Session VII: Prototyping with EO-1, AVIRIS, Spectrometer, and MASTER/ASTER Data

1:30-1:50pm A Global Volcano Product for Thermal Emission and Effusion Rate (*Steve Chien/Ashley Davies, JPL*)

1:50-2:10pm NEON: Extending Site-based Observations to the Continental Scale Using Airborne and Satellite Remote Sensing (*Brian Johnson, NEON*)

2:10-2:30pm Estimation of Rangeland Changes & Evapotranspiration Using Multispectral Thermal Infrared Data (*Andy French, USDA*)

2:30-2:45pm Integration Photochemical Reflectance Index (PRI) and fAPARchl Products for Carbon Monitoring (*Yen-Ben Cheng, ERT*)

2:45-3:00pm Remote sensing estimates of ecosystem GEE using fAPARchl and PRI (*Qingyuan Zhang, USRA*)

3:00-3:15pm Spectral time series to monitor vegetation dynamics using EO-1 Hyperion (*Petya Campbell, UMBC*)

3:15-3:30pm Determining Ecosystem Carbon Flux from Spectral Reflectance for Multiple Sites: Implications for Global Sampling (*Fred Huemmrich, UMBC*)

3:30-3:45pm G-LiHT: Goddard's Lidar-Hyperspectral-Thermal airborne imager (*Bruce Cook, GSFC*)

3:45-3:50pm Topic Introduction for Break-Out Session Discussions (*Betsy Middleton, GSFC*)

3:50-4:05pm Coffee Break

Session VIII: Higher Level Regional/Global Products

4:05-5:00pm Two Break-Out Session Discussions: What are the Priority Higher Level Regional/Global Products?
Group 1 (*Prasad Thenkabail*) Group Two (*Petya Campbell*)

5:00-5:20pm Report from Break-out Session Discussions (*Prasad Thenkabail and Petya Campbell*)

5:20-5:40pm General Discussion

5:40-5:50pm Symposium Summary (*Woody Turner*)

5:50pm Adjourn Symposium

In addition to the Agenda, the following reports are included in this document:

1] Symposium Overview, written for the *Earth Observer*, to appear in August 2011, 4pp.

Elizabeth M. Middleton, NASA Goddard Space Flight Center, K. Fred Huemmrich, University of Maryland Baltimore County, and Yen-Ben Cheng, Earth Resources Technology, Inc.

2] Lessons Learned from Landsat, MODIS, EO-1, and Their Data Systems: A Summary of the HypsIRI Presentations by J. Masek, R. Wolfe, E. Masuoka, and D. Landis, *David Landis (GSFC/Sigma Space, Inc.)*, 3pp.

3] Panel Discussion: Data Volume Challenges & Solutions, with *Panel Members*: Bob Knox (Chair), Rob Green, Ed Masuoka, Dan Mandl, Karen Moe, *Bob Knox (GSFC)*, 2 pp.

4] Breakout Session Discussions: “*Priority HypsIRI Higher Level Regional/Global Products*”, *Petya Campbell (GSFC/UMBC)*, 5 pp.

APPENDIX 1: Higher Level Products for HypsIRI – *Discussions Summary*

2011 HypsIRI Science Symposium (*Earth Observer*, August 2011)

Elizabeth M. Middleton, NASA Goddard Space Flight Center, Elizabeth.M.Middleton@nasa.gov

K. Fred Huemmrich, University of Maryland Baltimore County, Karl.F.Huemmrich@nasa.gov

Yen-Ben Cheng, Earth Resources Technology, Inc., Yen-Ben.Cheng@nasa.gov



Illustration of the NASA Decadal Survey Mission HypsIRI in orbit

The Hyperspectral Infrared Imager (HypsIRI) mission is one of the missions recommended in the National Research Council (NRC) Earth Science Decadal Survey. HypsIRI will fly an imaging spectrometer measuring the visible to short wave infrared (VSWIR) spectrum and a multispectral thermal infrared (TIR) imager. HypsIRI data will be used to study terrestrial and coastal ecosystems and carbon cycle parameters, along with supporting geological studies, such as volcano observations. The 2011 HypsIRI Science Symposium on Ecosystem & Environmental Data Products was held at the NASA Goddard Space Flight Center (GSFC), Greenbelt, MD on May 17 - 18, 2011. Approximately 84 participants from academic institutes and government agencies joined us in the two-day event. Following the successful symposium held in 2010, this year's meeting focused on identifying potential higher level products for ecosystems and environment at regional and global scales, along with the requirements for a data management framework to process and deliver HypsIRI data. A total of 40 talks and 7 posters were presented. The presentations covered the background and activities of the HypsIRI mission, product integrity and availability, and science and applications from the user community. Potential higher level HypsIRI terrestrial ecology products were identified and proposed, and consensus discussions were initiated.

Background and Framework--Building on Past experience

Nick White [NASA GSFC] welcomed everyone to GSFC and commented on the Center's perspective to support the HypsIRI mission.

Woody Turner [NASA Headquarter (HQ)--Co-Program Scientist for HypsIRI] provided an update on the status of the HypsIRI mission. He noted the HypsIRI Summative Briefing to NASA HQ in 2010, and outlined the need for future work to enhance the maturity of the mission concept and advance the scientific case for the mission.

Betsy Middleton [NASA GSFC] presented the overall objectives and logistics of the meeting; identifying science and application data products from HypsIRI, discussing issues underlying data product processing and integration, and prioritizing the development of products and algorithms. She also pointed out an expected report summarizing the outcome of this symposium would be written.

Jack Kaye [NASA HQ--Associate Director for Research and Analysis, Earth Science Division] provided an update from HQ perspective on the status of the Decadal Survey missions and how the HypsIRI mission fits into the overall program.

Rob Green [NASA Jet Propulsion Laboratory (JPL)] summarized the HypsIRI VSWIR imaging spectrometer, which will provide observations over the 380-2500 nm spectral region with a 10 nm spectral resolution and a 19-day revisit time. With the global coverage and 60 m spatial resolution over the terrestrial surface, the HypsIRI VSWIR data will provide valuable observations for climate studies and ecosystem monitoring.

Simon Hook [NASA JPL] summarized the HypsIRI TIR instrument. The multispectral TIR imager on HypsIRI will acquire data in eight spectral bands between the spectral region of 4 -12 μm with a nominal 5-day revisit time. A wide range of science and application examples were given to show how the TIR data would be utilized, including studies of volcanoes, wildfires, and water use/availability.

Betsy Middleton [NASA GSFC] presented the opportunities and challenges of the HypsIRI mission, pointing out how the HypsIRI mission could contribute to NASA's strategic goal to advance Earth System Science and meet the challenges of understanding climate and environmental change. HypsIRI can provide key information for objectives of the NRC Decadal Survey and International Panel on Climate Change (IPCC) including ecosystem feedbacks for climate change, water resources management and sustainability, and critical volcano eruption parameters. Nevertheless, issues including data processing, calibration, and validation need further discussion and efforts.

Robert Wolfe [NASA GSFC] shared the successful experience and lessons learned from the Moderate Resolution Imaging Spectroradiometer (MODIS) mission. Wolfe pointed out the importance of leadership and communications within the community. Various issues including data systems, algorithm development, quality assurance, calibration and applications were reviewed. He examined issues that arose from each of the MODIS disciplines, oceans, atmosphere, and land, and how they were resolved.

Jeff Masek [NASA GSFC] reviewed the 40 years of the Landsat mission. He summarized the contributions that the continuous Landsat observations made to important science and application studies including land surveys, forest dynamics, disturbance and recovery. He emphasized the value of having frequent coverage and lessons from the development of Landsat global products that the HypsIRI mission can apply.

New Possibilities for Science with HypsIRI--General Ideas

Rob Green [NASA JPL] presented how the HypsIRI mission will provide unprecedented opportunity to monitor ecosystems and their responses and feedbacks to the changing climate since HypsIRI can provide information about vegetation species, functional types, biodiversity, plant chemical and physiological conditions from its measurements.

Hank Margolis [University of Laval] demonstrated the potential of using a machine learning algorithm to scale carbon exchange between ecosystems and the atmosphere from site level up to global level using remote sensing and meteorological data and the implications of this approach for potential HypsIRI global products. **Charlie Walthall** [USDA] discussed some challenges for agriculture including food safety, adaptation for climate change, and sustainability. Various measurements from local to global scale are needed and the HypsIRI mission can provide an opportunity to improve our current agricultural management. **Miguel Roman** [NASA GSFC] presented the Committee on Earth Observation Satellite (CEOS) Working Group on Calibration and Validation (WGCV) Land Product Validation (LPV) subgroup and their possible collaboration with the HypsIRI mission.

New Possibilities for Science with HypsIRI—Examples

Eric Hochberg [Nova Southeastern U] presented a summary of current coral reef studies, the connections with climate change, and how remote sensing and HypsIRI observations can be utilized. Because of its global coverage, HypsIRI will provide a unique opportunity to quantitatively assess the global status of coral reef ecosystems. **Dale Quattrochi** [NASA Marshall Space flight Center (MSFC)] discussed urbanization, its effects on human health, and responses to climate change. HypsIRI imagery, especially the TIR and day/night acquisitions, will provide measurements for products describing air quality, urban heat islands, and land cover/land use change. **Martha Anderson** [USDA] and **Rasmus Houborg** [EU Joint Research Centre, Italy] presented an algorithm that can utilize HypsIRI VSWIR and TIR data simultaneously to model carbon assimilation and transpiration. Results of test studies over multiple sites were described. **Jeffery Luvall** [NASA MSFC] presented the potential for using HypsIRI TIR measurements to evaluate ecosystem health and integrity through the connection between thermodynamics and ecosystem structural development. **Robert Wright** [U of Hawaii] discussed global volcano monitoring and hazard assessment with future HypsIRI data. The fine spatial and temporal resolution of HypsIRI data coupled with improved accuracy of surface temperature retrievals will significantly advance the ability to describe volcanic activity.

Data Volume Challenges & Solutions

Ed Masuoka [NASA GSFC] shared his experiences in managing the data from MODIS for the scientific community. The infrastructure of MODIS product development, processing, distribution, and response to the needs of the science community provide valuable lessons on how to handle the global coverage of HypsIRI data. **Dan Madl** [NASA GSFC] gave a status update on the intelligent payload module and low latency products. Current efforts focus on taking advantage of parallel processing for efficient computation power and rapid production of low latency data products. **Bob Knox** [NASA GSFC] led a panel discussion with **Rob Green** [NASA JPL], **Ed Masuoka** [NASA GSFC], Karen Moe (NASA HQ), and **Dan Madl** [NASA GSFC] focused on the preferred Mission Model for the data processing chain. Various framework and infrastructure approaches were introduced and discussed to achieve consistency, ensure availability, examine integrity, and maintain continuity of various HypsIRI data product types.

Context for Hyperspectral and TIR Data Products

Prasad Thenkabail [USGS] reviewed past research on hyperspectral remote sensing for vegetation, both natural and managed systems, and the status of our current knowledge. Potential HypsIRI VSWIR products on leaf biochemical and canopy biophysical properties were suggested.

Mike Ramsey [U of Pittsburgh] reviewed the past and current state-of-the-art remote sensing for volcanic activity. Capacities of volcanological remote sensing using TIR measurements have advanced rapidly over the last decade. Future observations, from HypsIRI, can be routinely used in monitoring, modeling, and hazard appraisals.

Betsy Middleton [NASA GSFC] reviewed the successful 2010 HypsIRI Science Symposium with a goal to identify and evaluate potential higher level products for end users of climate studies.

Susan Ustin [U of California, Davis] gave a summary of two workshops on HypsIRI global science products and their relevance for climate change research and modeling. The key message from the workshop was that the spatial resolution, temporal revisit, and spectral characteristics of HypsIRI will significantly advance ecosystem science and provide improved land surface parameterization for climate studies. Further, HypsIRI measurements can contribute critical information about ecosystem responses and feedbacks to climate change.

Data Issues

Dave Landis [Sigma Space] introduced the current design of tagging and developing metadata for the NASA Earth Observing-1 (EO-1) imagery and how this may lead to future approaches for searching HypsIRI data. **Vuong Ly** [NASA GSFC] presented current development of several data processing tools for the EO-1 mission and their potential for HypsIRI. **Steve Ungar** [Universities Space Research Association (USRA)] presented various CEOS activities and calibration topics with implications for HypsIRI. **Sasha Smirnov** [Sigma Space] reviewed AERONET activities. The HypsIRI mission can use AERONET measurements for calibration as well as learn from their successful international

network in the development of a calibration/validation network. **Stan Hooker** [NASA GSFC] reviewed various sensors for calibration and validation that were developed to support ocean color satellite missions. **Robert Sohlberg** [U of Maryland (UMD)] showed web-based data processing tools for environmental monitoring.

Prototyping with EO-1, AVIRIS, Spectrometer, and MASTER/ASTER Data

Steve Chien [NASA JPL] showed a global volcano product based on the current EO-1 Hyperion Volcano SensorWeb. **Brian Johnson** [National Ecological Observatory Network (NEON)] discussed data product prototyping by NEON and their activities to integrate data acquired at various spatial scales. **Andy French** [USDA] presented on the potential of using HypsIRI TIR data for estimates of rangeland changes and modeling energy fluxes. **Qingyuan Zhang** [USRA] gave an update on a potential HypsIRI science product, the Fraction of Absorbed Photosynthetic Active Radiation at Chlorophyll level (fAPARchl), a radiative transfer modeling based parameter that can help to improve the estimation of carbon fluxes over multiple sites of natural and managed ecosystems. **Yen-Ben Cheng** [Earth Resources Technology, Inc. (ERT)] presented an algorithm that integrated two of potential HypsIRI products; Photochemical Reflectance Index (PRI) and fAPARchl to estimate carbon assimilation with a discussion of possible effects due to spatial resolution. **Petya Campbell** [University of Maryland Baltimore County (UMBC)] utilized time series of EO-1 Hyperion imagery to demonstrate the use of multiple narrow spectral bands to monitor a range of ecosystems and their carbon exchange. **Fred Huemmrich** [UMBC] presented the concept of using PRI from MODIS narrow ocean bands for ecosystem carbon monitoring at multiple sites and implications for global sampling of HypsIRI. **Bruce Cook** [NASA GSFC] introduced a newly developed integration of multiple instruments, including an imaging spectrometer, thermal imager, and lidar, that can be flown on a light aircraft for carbon and ecosystem monitoring.

Break-out Session Discussions: Higher Level Regional/Global Products

Prasad Thenkabail [USGS] and **Petya Campbell** [UMBC] led two break-out discussion sessions. Various potential HypsIRI higher level products at regional and global scale were discussed. Other topics included enhancing communication about thermal sensing and imaging spectroscopy both within the scientific community and the general public, along with ideas on data and algorithm sharing within the HypsIRI community.

Summary

In general, participants recognized the planned HypsIRI mission will provide the science community with extremely valuable information on plant physiological condition and energy exchange between the atmosphere and terrestrial ecosystems. Potential higher level product at regional to global level will address science questions from various disciplines including ecosystem monitoring and modeling, biodiversity and climate change. Successful utilization of HypsIRI data will require the development of an information system that builds upon the lessons learned from past missions such as MODIS and Landsat.

Lessons Learned from Landsat, MODIS, EO-1, and Their Data Systems

A Summary of the HypSIRI Presentations by J. Masek, R. Wolfe, E. Masuoka, and D. Landis

Report prepared by David Landis (GSFC/Sigma Space, Inc.)

Product Availability

- Government-funded operation of both satellite and data system have enabled free and open distribution of data. Prices can be too high for scientists to purchase images at the levels required for commercial profitability.
- We have found that use of the data is inversely related to what users are charged for the data. The higher the cost, the fewer users. The lower the cost, the more users. The best price for data is free! Even minor charges (like processing fees) will inhibit the usage and distribution of data.

Data Product Processing and Formats

- Size standard products to facilitate processing, distribution and ease of use:
 - For MODIS products, sizes are 5 minutes of swath data (Level 1 and Level 2) and 10 degree x 10 degree tiles (Level 3)
 - Majority of products should be less than 500MB per file when compressed.
- Specialized products help meet emerging needs. Some products should be in Climate Modeling Grid for climate modelers. Others users need gap filled-products for their models.
- GIS-ready products and imagery and application specific formats are essential.
- The less customized encoding (HDF, NetCDF, etc.) the better. Power users should be able to reprocess the image data directly, not have to decode it first. This does not apply to standard compression routines (ZIP, Gzip, etc).
- A robust pre-processing approach is important. Prescreening the data for clouds, shadows, water, (etc.) makes processing the images much easier.
- Higher-level (Level 3+) products are more useful as standard products that can be compared across various satellite platforms.
- One map projection (grid spacing, etc.) will not work for all users (or even a majority).
- Advice on science testing of algorithms:
 - Don't bundle too many changes together – impacts of upstream algorithms are hard to untangle.
 - Storage is needed for multiple baselines and changes.
 - Maintain a basic set of science test days.
 - It is useful to have the same algorithms across multiple sensors. For example, adapting the heritage SeaWiFS Ocean Color algorithm for Aqua made it possible to produce a good quality product.
- Science team members should play a key role in development and maintenance of code, and they should remain responsible. The science team should lead the processing to ensure that the best products are generated and reprocessed with a workable schedule.
- Product development should be a well-defined process that allows for community feedback.
- Metadata for the images is critical to make it usable. The more that the images can be categorized by content, the better for future studies. Extra effort put into image categorization yield additional benefits later in the project.
- Keep the products simple and well-documented.

Image Reprocessing

- Reprocess the baseline data products as little as possible. Users want access to the original information, not data that has been averaged, smoothed, and otherwise massaged by unknown algorithms.
- Having Level 0 data on-line makes science testing and reprocessing much easier.
- If reprocessing is deemed necessary, it should be well-documented to allow users to understand what was done to the data, and to decide if the reprocessed data meets their needs. Alternatives to the reprocessed data should also be available.

Calibration and Cross-Platform Calibration

- Sensor calibration and cross-platform recalibration are critical for the record of satellite data.
- Cross-calibration with other sensors is vital to the integration of data products.

Data Systems and Distribution

- On-line products (including Level 0) greatly increase the speed and simplicity of data distribution.
- A robust data system enables processing-on-demand for tailoring products as well as Web services.
- The MODIS Adaptive Processing System (MAPS):
 - Scalable system for MODIS, AVHRR, VIIRS and Landsat processing were designed so that processing resources can be easily moved where needed.
 - Achieved significant savings (50% or more) purchasing servers in volume of 100+ but even greater savings in manpower by adding new missions and applications within the data center.
 - Building with commodity hardware makes it easier to scale, saves money, and is easier to do a technology refresh.
 - Built with open source components: Linux, Apache, Perl, Postgres, Subversion, FUSE.
 - Leveraging tools, procedures and staff experience for land product quality assessment from MODIS and VIIRS allowed us to meet schedule and cost targets.
 - Designed to run with limited staff:
 - “Lights out” processing outside of normal business hours
 - Months of processing can be queued up and execute without human intervention
 - Alerts emailed to system administrators when hardware components generate warnings or fail
 - Easy to use tools for monitoring the system (Ganglia) and investigating failed jobs
 - Rapid updating for provisioning of servers with science processing software, the operating system and applications (Depot and SATE).
 - Impact of Moore’s Law (increasing capability at decreasing cost) on computation and storage has made many things possible and allowed requirements to grow with increased capacity and performance.

Outreach (quick response, direct broadcast, disaster mode)

- A Near Real Time (NRT) data system is needed for application users:
 - A stand alone NRT system is needed to avoid gearing the entire production stream to the NRT constraints.
 - Direct Broadcast (DB) versions of code make it easier for broad product uptake and use – increases standardization.
 - DB encourages applications and regional algorithm development and has been a huge success with > 100 direct readout sites worldwide.
- Targeted outreach programs are needed:
 - Imagery support is needed for outreach.
 - Earth Observatory for one-stop shopping – must include good descriptions (captions) – this is a good way to deal with the Media.

Science Teams, Staffing

- Weekly team meeting should be held to keep everyone on same page.
- Full science team meetings should be held twice per year early in mission, once per year later.
- Discipline leaders and a core full-time group should be built around the data system. A close working relationship among data team and science team members is important.
- A core calibration group should have representation from the various science disciplines. Discipline representatives provide important feedback because they understand calibration and its impact on fundamental (upstream) science products (e.g., water leaving radiance, land surface temperature, land surface reflectance, aerosols).

Long-Term Advice

- Always build as much capability into the flight hardware as possible. Always assume that the satellite and instruments will last much longer than the original requirements.
- A small, dedicated data system is needed for algorithm refinement, integration/testing, and demonstration/evaluation of readiness in the years leading up to launch.
- Science team members should be funded before and through the life of the instrument – a long term commitment and experience base is critical.
- Time dedicated by science experts is the most valuable resource for making high quality products but hardest to fund over the long haul.
- Immortality of key personnel is not a viable alternative to succession planning. Always have new people coming into the project and learning about vital systems. Make sure no person is irreplaceable.

Panel Discussion: Data Volume Challenges & Solutions

Panel Members: Bob Knox (Chair), Rob Green, Ed Masuoka, Dan Mandl, Karen Moe

Report Prepared by Bob Knox (GSFC)

This discussion was framed by two over-arching questions: “How do we handle HypsIRI data?” and “What is the preferred Mission Model for the data processing chain?” Bob Knox offered a (blank) matrix of science data system functions (rows) and groups of HypsIRI data product types (columns). To help stimulate discussion he then offered a list of example architectures that might be used to support one or more functions for one or more groups of data products. The examples ranged from relatively established NASA models, such as, distributed active archive centers (DAAC), science investigator processing systems (SIPS), and direct broadcast of selected products; to less familiar potential architectures for serving mission science data, such as cloud-based virtual data centers (run by NASA and/or international partners), or peer-to-peer distribution of data subsets temporarily in high demand (*e.g.*, via a GeoTorrent protocol). Schedule conflicts with MODIS calibration meetings prevented two of the announced panel members from attending. Karen Moe of NASA’s Earth Science Technology Office (ESTO) generously agreed to participate. Knox concluded by briefly introducing the panel members.

Then the other panel members each spoke for a few minutes. Karen Moe noted several ESTO-supported technologies of relevance to the subject, including three included in the baseline concept for HypsIRI’s Intelligent Payload Module (addressed by Dan Mandl in a preceding talk). NASA has been supporting development of service oriented architectures, especially using the Open Geospatial Consortium specifications for web services (web map services, web coverage services, *etc.*). Semantic web technologies may make HypsIRI data more easily searched and found by potential users. This should reinforce importance of managing metadata and data provenance. Work on collaborative environments can help the community developing potential HypsIRI algorithms and products work together and capture findings of previous work. Also in the area of data intercomparison (*e.g.*, for product validation or change detection and measurement), there has been research on new methods of modeling and managing data uncertainty. Having spoken earlier on lessons learned from managing MODIS data for global studies, Ed Masuoka noted that HypsIRI will be generating long-term records—in the context of other operational and systematic missions, as well as potential follow-on missions providing global multispectral thermal and imaging spectrometer data. He also advised that HypsIRI may benefit from technologies that are coming down the pike, without our having to pay for them. Dan Mandl emphasized the value of flexible low-latency products (*e.g.*, reconfigurable direct broadcast) for certain user communities, and noted the potential for further use of the EO-1 mission as a test-bed for technologies relevant to HypsIRI.

On the topic of information technology clouds, discussions noted the flexibility clouds may offer for surges in processing, such as rapid re-processing of HypsIRI data with new or updated algorithms. On the other hand, communication bottlenecks in present and near-term information processing technology make it efficient to keep the processing as close to the data storage as feasible, whereas staging large parts of the HypsIRI archive into and out of clouds might impose unacceptable overhead. While noting that the HypsIRI mission data system concept is feasible now (much earlier than launch dates implied by the most recent NASA budget), Rob Green recalled the on-going rapid drops in prices for data storage media, noting that a generalized form of Moore’s Law continues to be true of much of the relevant technology of information processing and communication systems. For example, the data storage of imaging spectrometer data for the AVIRS lab approaches a Petabyte. Also recently Terrabit-per-second data links have been demonstrated over optical fiber.

A number of other issues and insights emerged during the open discussion period. There remains the question of when to distribute updated large-volume data products, analogous to MODIS numbered data collections, and when to provide updated algorithms to registered institutions or individuals mirroring or holding portions of the level 1 or level 2 HypsIRI archive. An important layer of a HypsIRI architecture, omitted from Knox’s list of examples, were other agency data centers, for example, some critical HypsIRI products could be served by a volcano center. In the area of spectral libraries that are essential for algorithm development and to produce some higher-level data products, HypsIRI

needs a mechanism for bringing together the piece-meal spectral libraries that exist now. Because we anticipate that more wide and diverse use of HypsIRI data sets could be enabled by regional and/or disciplinary centers, it may be appropriate to update our data system metaphors. While a NASA-funded archive may hold the most authoritative and complete set of HypsIRI data, analogous to holdings of the Library of Congress, individual data subsets (or books) might be more efficiently provided to users by a network of public and private libraries. The diversity of higher level products implied by the scientific and applications objectives recommended for HypsIRI suggests that many important products will be developed by global communities of scientists and land managers. HypsIRI and NASA will face decisions about what higher-level products to archive (as processed data or as validated algorithms) for long-term use. NASA and the evolving HypsIRI community will also need good mechanisms for tracking the provenance of community-developed data products. As anticipated by the organizers, this panel discussion generated more questions than answers. It can be hoped that it stimulates an on-going exploration of hybrid architectures that could be both cost effective for the NASA and the HypsIRI mission, and also engage diverse global communities of scientists, mission partners, and developers of applications of HypsIRI data.

Breakout Session Discussions: “Priority HypsIRI Higher Level Regional/Global Products”

Report prepared by Petya Campbell (GSFC/UMBC)

The two breakout discussion groups were led by Drs. Prasad Thenkabail and Petya Campbell. Each group consisted of approximately 20 participants. The summary below incorporates inputs from both discussion groups. Terrestrial and aquatic products require different inputs, so therefore, they were addressed separately. At the end of the discussion, the participants agreed that such discussions are very much needed and should continue. It was requested that the draft below be circulated among the listed participants for further input: Eric Hochberg, Jeff Morisette, Susan Ustin, Angela Mason, Michael Mercury, Fred Huemmrich, Bob Knox, Karen Moe, Dean Riley, Charles Norton, Steve Chien and Prasad Thenkabail.

The following EOS definitions for Level 3 and Level 4 Products were adapted for further use:

- **Level 3 Products:** Spectral or wavelength-dependent data (radiances, surface reflectance, temperature and emissions, etc.) mapped onto uniform space-time grids, usually with some completeness and consistency; terrain corrected products.
- **Level 4 Products:** Results from analyses of lower level (L1, L2) data, model outputs, data combinations, such as: (i) spectral indices applied to L2 or L3 data; (ii) variables derived from multiple measurements (e.g., time series) of same sensor; (iii) multi-sensor data fusion; and (iv) assimilation with other data types.

**1. Proposed HypsIRI Terrestrial products:
Included higher level products (L3 and L4), or L2 if they are not planned**

Product Level	Description	Maturity / Use
L2 VSWIR	Surface Reflectance Water vapor content Cloud masks TOA reflectance Surface radiance Incident PAR Albedo (nominal 19 days global albedo)	Mature products, available algorithms For model runs and simulations
L2 TIR	Surface Emissivity (local/regional) Surface radiance Sky irradiance	Mature products, Available from satellite
L3 VSWIR & TIR	Seasonally combined VSWIR&TIR Continuous fields vs. discriminate LC classes All MODIS and Landsat products Bio-indicators of vegetative function	The two data-sets need to be co-located Existing approaches need to be tested at larger scale Need to consider which to continue with HypsIRI Many algorithms available, some currently tested
L4 VSWIR & TIR	Mineral identification and mapping Urban and human landscapes: <ul style="list-style-type: none"> • 2/3 weeks thermal dynamics • Functional classifiers for urban landscapes New indicators of ecosystem function, diversity and disturbance	Mature, needs global spectral libraries for cal/val Include the urban elements of land cover. Some are currently tested but need further development. Currently developed with simulated HypsIRI data

Product Level	Description	Maturity / Use
L4 SWIR	Global Canopy Water Content Global Canopy Nitrogen Content Global Canopy Cellulose	Mature product Not global Mature algorithm, needs global testing and validation
L4 VSWIR	Global Canopy Chlorophyll Content	Needs further testing, many algorithms available, need to be reconciled for specific use
L4 VSWIR	Global fractional end members	Mature product
L4 TIR	Global ET	Need global testing and cal/val

2. Proposed HypsIRI Aquatic Products *(with a coral reef bias), prepared by Eric Hochberg, NOVA*

Product Level	Description	Maturity / Use
L2 VSWIR	Remote Sensing Reflectance (R_{rs} , units sr^{-1} , 400–800 nm) = water-leaving radiance (L_w) ÷ downwelling irradiance (E_d)	This is the result of atmosphere and glint corrections. There are well-developed and practically operational algorithms for atmospheric correction. Glint correction for shallow water imagery is nearing routine operational status.
L2 TIR	Sea Surface Temperature	Routine product from many satellites
L3 VSWIR	- Seafloor Spectral Reflectance (units %, 400–? nm) - Water Depth - Water Optical Properties - Retrieval Quality Flags	These are combined results from aquatic retrieval algorithms utilizing R_{rs} . There are several candidate algorithms in existence.
	- Fractional Cover	These are derived from Seafloor Spectral Reflectance. There are no existing algorithms, but there have been some basic investigations.
	- Light-Use Efficiencies for (1) Productivity and (2) Calcification - Dissolved Organic Mater (DOM) - Pigments (=chlorophyll)	There are no existing algorithms, and there have been (virtually) no investigations. There are developed algorithms
L3 TIR	Degree Heating Weeks	Routine product
L4 Combined VSWIR&TIR	- Productivity, Gross/Net - Calcification	There are no existing algorithms, and there have been (virtually) no investigations.

The following issues were considered critical for the success of the mission, to prepare the future users and broaden/expand the community (to be addressed ASAP):

- The need of broadly available non-proprietary (if possible) tools for spectral data processing and analysis.
- Establishing/promoting of consistent spectral (and temporal) libraries and depositories (ASAP).
- User pamphlet on spectral collection, and spectral library standards (101 round robin).
- Test Database of thermal and spectral data over the same geographical area, and preferably during the same timeframe: AVIRIS, Hyperion, MASTER, ASTER.
- Develop prototype *global* HypsIRI products, using MODIS and Hyperion imagery scaled to appropriate climate model scale(s) (for use in modeling activities, such as climate change, disturbance, fires, and MODIS/GOES data).
- HypsIRI Bio-Indicator prototypes:
- Compare broad band indices (Landsat and MODIS) vs. higher spectral resolution (various NDVI's, or versions of TM indices).
- Develop and test unique spectrometer spectral parameters/indicators that will be possible with HypsIRI (SWIR 1200:2500, VISWIR&TIR).

The group suggested that it is critical to bring HypsIRI “out” to the user communities, by starting user workshops at society meetings such as: ESA, USFS workshops, FLUXNET, etc. A question was raised if NASA funding may be available for this critical “outreach” activity.

APPENDIX 1: Higher Level Products for HypsIRI – Discussion Summary

#	Product	Level (L2/3/4)	Maturity	MODIS	Landsat	Models	Notes
Reflectance & TIR Products							
A. Global Products for Data Continuity							
1	Convolved Reflectance to other sensors (long term data records; narrowband/broadband)	3	yes	yes	progress	yes	R(%), LEDAPS, WELD algorithms
2	Symulated LST for other sensors (e.g. MODIS, LDCM/TIRS)	2	yes	yes	yes	yes	LST (T C°)
3	Fractional land cover type (FLC) [continuous fields, % of land cover: soil, water, vegetation, ice&snow]	3	yes	yes	yes	yes	for long term records continue MODIS product, test f(PV, NPV) for vegetation cover
4	Thermal Anomalies	4	yes		yes/limited	yes	
B. Terrestrial (veg. & soil)							
I. Spectral End-member Abundance							
	- mineral maps, veg type maps	3	in progress	no	no	no	Local Spectral libraries (cal/val) needed
II. Vegetation Spectral Bio-indicators (VIs)							
	- water, cellulose, chlorophyll, general stress	3/4	in progress	EVI, NDVI	TM 5/4, 4/3 etc.	progress	
	- nitrogen	3	in progress	yes/limited	no	no	
	- hot spots	4	in progress	no	no	yes	Local Spectral libraries and chemistry (cal/val)
	- LST per VFC and LC	4	in progress	yes/limited	yes	no	
	- LST per VFC and LC	4	in progress	yes/limited	in progress	no	
III. Canopy function Yield (CO2 sequestration, GPP, NEP)							
	- LUE, WUE	4	in progress		no	yes	
	- ET	4	in progress		no	yes	
IV. Classifications							
1	Fractional vegetation cover (FVC) [photosynthetic vegetation [PV] or non-photosynthetic vegetation [NPV], Soil]	3	yes	no	limited		AutoMCU or equivalent (SWIR and red-edge with tied spectra)
2	Fractional cover by plant functional type (PFTs)	4	in progress	see below	no	yes	Required by DVGM (dynamic global vegetation models) end ESM (Earth system models); At launch 26 types/km ² , goal 6-10 resolved
V. Terrestrial Products Supporting Long Term Data Records							
1 MODIS Vegetation Continuous Fields (VCF - cotext & Records							
	- life form (proportion of woody vegetation, herbaceous)	4	yes	yes		yes	
	- leaf type (proportion of woody vegetation that is needle)	4	yes			no	
	- leaf longevity (proportion of woody vegetation that is	4	yes			no	
2	Ecological disturbance (NPV increase)	4	yes, global on progress	Fire product	LEDAPS		Based on PV, spectral change diagnosing disturbance type; decline/recovery; for land history
	- Land cover conversions	4	yes, global in progress	yes	yes/limited	yes	Terrestrial ECVs: LC, permafrost, glaciers/ice, LAI, fire
	- Severe wind drought insect etc	4	in progress	yes	yes/limited	yes	False alarm a possibility
	- Fires (VISWIR detection, severity)	4	in progress	yes	yes/limited		
VI. Biodiversity							
	- Optical types diversity	4	initialized	no	no	yes	see publication on the topic by Usting and Gammon
	- Plant functional diversity	4	initialized	no	no	yes	see publication on the topic by Asner, Wright, et al.
	- Biodiversity indicators	4	in progress	no	no	yes	Spectral corelation with bio-diversity

Higher Level Products for HypIRI – Discussion Summary *(continued)*

#	Product	Level (L2/3/4)	Maturity	MODIS	Landsat	Models	Notes
C. <u>Aquatic [shallow water, rivers, lakes]</u>							
1	Remote Sensing Reflectance (Rrs)	2 or 3	yes, operational	yes	no		Remote Sensing Reflectance = water-leaving radiance (Lw) / downwelling irradiance (Ed); (Rrs, units sr-1, 400–800 nm) ; This is the result
2	Sea Surface Temperature	2-Jan	yes, operational	yes	no		Routine product from many satellites.
3	Seafloor Spectral Reflectance (units %, 400–???) nm)	3	in progress	no	no		Combined results from aquatic retrieval
4	Water Depth	3	in progress	no	no		There are several candidate algorithms in
5	Water Optical Properties	3	in progress	yes	no		-"
6	Retrieval Quality Flags	3	in progress	na	no		-"
7	Fractional Cover	3	in progress	na	no		Derived from Rrs, mixture decomposition methods need scaling to HypIRI data
8	Pigments (e.g. chlorophyll)	3	mature, work in progress to separate aquatic sources	yes	no		Derived from Rrs, work in progress to separate contributions of planktonic, submerged and emerged aquatic sources
9	Light-Use Efficiencies (for (1) Productivity and (2) Calcif	3	in progress	yes	no		There are few investigations for shallow
	- Productivity (Gross/Net)	4	in progress	yes	no		Investigations for fresh water bodies, needs synthesis of fresh, coastal and deep ocean
	- Calcification	4	not initialized	na	no		There are no existing algorithms, and there have been (virtually) no investigations
10	Water content Dissolved Organic Mater (DOM)	4	in progress	yes	no		Investigations for fresh water bodies, needs synthesis of fresh, coastal and ocean methods
11	Degree Heating Weeks	3	mature	yes	no		Routine product from many satellites.
D. <u>Snow/Ice [high latitudes, high</u>							
	Snow cover, Ice caps, Glaciers	3/4	no experts present				Input to be obtained from: Dorothy Hall, Jeff Dozier, Thomas Painter
<i>Top of Atmosphere and Localized Products, and By-products of Level 2 Processing</i>							
1	TOA Optical and TIR Radiance (bands)	1B	yes	yes/limited	yes/limited		
2	Volcanoes eruption, size, prognosis	4	yes	yes/limited	yes/limited	yes	
3	Clouds (masks)	3	yes	yes	yes/limited		
4	Incident PAR (direct, diffuse PAR)	3				yes	
5	Water vapor product	3	yes			yes	
6	Aerosol optical depth product	3	yes	no	no	no	
7	Albedo	4	in progress	yes	no		



HyspIRI Sun Glint Report

*E.J. Hochberg
Nova Southeastern University Oceanographic Center
Dania Beach, FL*

*C.F. Bruce
R.O. Green
B.V. Oaida
Jet Propulsion Laboratory*

*F.E. Muller-Karger
University of South Florida
Tampa, FL*

*C.D. Mobley
Sequoia Scientific, Inc.
Bellevue, WA*

*Y. Park
CSIRO
Clayton South VIC 3169, Australia*

*J. Goodman
University of Puerto Rico at Mayagüez
Mayagüez, Puerto Rico*

*R.G. Knox
E.M. Middleton
K.R. Turpie
S. Ungar
Goddard Space Flight Center
Greenbelt, MD*

*P.J. Minnett
University of Miami
Coral Gables, FL*

*C. Gentemann
Remote Sensing Systems
Santa Rosa, CA*

*R.C. Zimmerman
Old Dominion University
Norfolk, VA*

*W. Turner
NASA Headquarters
Washington, DC*

*B.-C. Gao
Naval Research Laboratory
Washington, DC*

**National Aeronautics and
Space Administration**

**Jet Propulsion Laboratory
California Institute of Technology
Pasadena, California**

Part of this work was carried out at the Jet Propulsion Laboratory, California Institute of Technology, under a contract with the National Aeronautics and Space Administration.

Reference herein to any specific commercial product, process, or service by trade name, trademark, manufacturer, or otherwise, does not constitute or imply its endorsement by the United States Government or the Jet Propulsion Laboratory, California Institute of Technology.

© 2011. All rights reserved.

Executive Summary

The basic objective of the Hyperspectral Infrared Imager (HypIRI) mission is to provide high-quality imaging spectrometer global observations to characterize a baseline of multiple Earth-surface processes at timescales ranging from seasonal to multi-annual. Among the HypIRI science objectives, several questions address aquatic ecosystems. Several factors confound easy interpretation of aquatic remote-sensing data. Reflectance of sunlight and skylight off the water surface, or glint, is one potential obstacle to HypIRI's successful application to study of aquatic systems.

To address this issue, the HypIRI Sun Glint Subgroup was formed during the fall of 2009. The Subgroup had three main objectives:

- (1) Quantitatively characterize the glint problem;
- (2) Determine glint impacts to HypIRI mission aquatic science objectives; and
- (3) Provide advice on a way forward to address the glint issue.

To achieve these objectives, the Subgroup initiated a series of weekly teleconferences, beginning in October 2009 and extending into April 2010. The Subgroup first developed a plan of action to address the objectives. Figure 1 provides a brief outline of the steps taken by the Subgroup. The general plan was first to quantitatively characterize glint primarily using radiative transfer models, including both basic analytical equations and HydroMod. The characterization was supplemented with examination of actual remote sensing image data. To assess glint impacts on HypIRI aquatic science objectives, the Subgroup relied on radiative transfer modeling, using both HydroLight and HydroMod. Various glint correction procedures were assessed using both modeled and real-world data. Finally, the Subgroup agreed on a short list of recommendations for future activities.

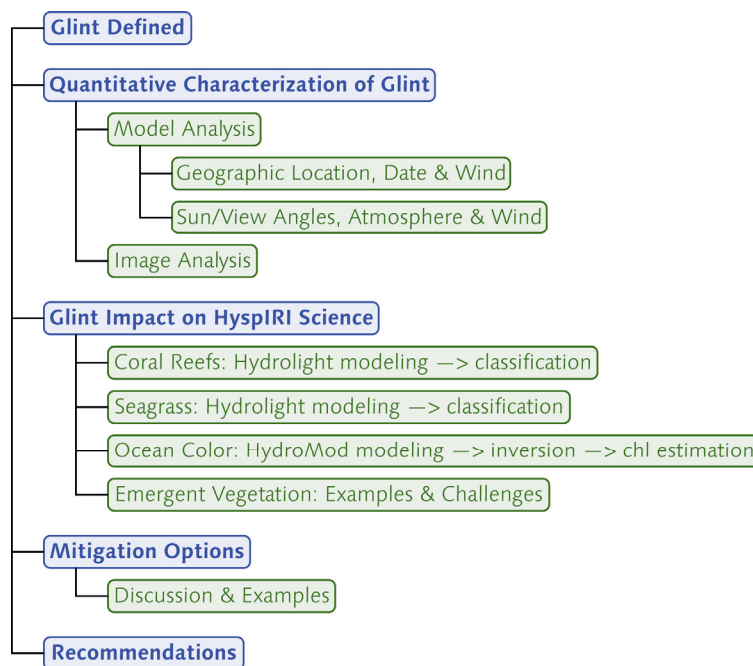


Figure 1. HypIRI Sun Glint Subgroup Activities Overview

The Subgroup's investigations point to several summary observations:

- Quantitative Characterization of Glint
 - Because HypsIRI views from near zenith, glint has a stronger effect where the sun is also near-zenith.
 - Glint effects are present in a latitudinal band that is 50° to 100° wide, depending on wind speed and the across-track pixel location.
 - Glint at the east edge of the HypsIRI scan line is consistently higher (by a factor of two to five) than at the west edge.
 - HypsIRI glint is sensitive to wind speed at moderate-to-high sun zenith angles, which correspond with low-to-moderate glint in the absence of wind, but it is less sensitive to wind speed at low sun zenith angles, which correspond to high glint in the absence of wind.
 - Glint radiance is a function of incident irradiance.
 - Glint reflectance can surpass that of water-leaving reflectance.
 - Glint reflectance at the sea surface, to first order, is spectrally flat across the visible, near infrared and short-wave infrared.
- Glint Impact on HypsIRI Aquatic Science
 - Results from two basic HypsIRI science objectives, to investigate glint impacts on retrievals for coral reefs and seagrass, showed that expected levels of glint do not appear to dramatically affect classification retrievals.
 - Glint has the greatest impact when retrieval conditions are already marginal, for example, when water column optical properties limit penetration depth.
 - For the open ocean, with very low suspended chlorophyll levels, it is clear that glint correction must be tied to correction for atmospheric aerosols.
 - The impact of glint on retrievals of emergent vegetation is less clear, as measurement and modeling capabilities for these systems lag those for shallow and deep oceans.
- Mitigation Options
 - Avoidance is the simplest method for glint mitigation, but it is often not an option for nearshore and benthic applications.
 - Empirical corrections based on the linear relationship between visible and near-infrared radiances have been demonstrated to perform very well at correcting for glint, but these techniques have yet to be automated.
 - Computation glint reflectance in the near infrared, followed by subtraction of that value in the visible, has also been demonstrated to be very effective at correcting for glint.
 - Discrimination between aerosol and glint reflectance may lead to better determination of near-infrared reflectance.
- Recommendations
 - Glint correction algorithms should be refined and tested using real-world data sets.
 - Further sensitivity analyses should be conducted to investigate glint impacts on other aspects of HypsIRI aquatic science objectives.
 - Field measurements are required to validate model results for select HypsIRI aquatic science objectives.

- In the longer term, a glint “toolbox” of computer code should be developed that would allow a user to select among a suite of glint correction techniques.
- In the longer term, a comprehensive data set of oceanic and atmospheric radiometric parameters would be very valuable for validation of radiative transfer models; this would not only benefit HypIRI, but would also benefit all remote-sensing missions that observe the ocean.

Table of Contents

1	HyspIRI Sun Glint Subgroup.....	1
1.1	Background and Rationale.....	1
1.2	Glint.....	2
1.3	Tasks.....	5
1.3.1	Quantitatively Characterize Glint.....	5
1.3.2	Determine Glint Impacts on HyspIRI Science.....	5
1.3.3	Suggest Options for Way Forward.....	6
1.4	Participants.....	6
1.5	Timeline.....	7
2	Literature Review.....	8
3	Quantitative Characterization of Glint.....	10
3.1	Modeling.....	10
3.1.1	Glint Reflectance: Geographic Location, Date, and Wind.....	10
3.1.2	Glint Reflectance: Sun/View Angles, Atmosphere, and Wind.....	18
3.2	Glint Reflectance: Image Analysis.....	23
3.3	Summary.....	26
4	Glint Impact on HyspIRI Science.....	27
4.1	Coral Reefs.....	27
4.2	Seagrass.....	36
4.3	Station ALOHA Simulation.....	41
4.3.1	Forward Modeling.....	41
4.3.2	Radiometric Inversion of Simulation Data.....	42
4.3.3	Estimating Chlorophyll from Simulated and Inverted Data.....	48
4.4	Emergent Vegetation and Coastal Wetlands.....	51
4.5	Summary.....	53
5	Mitigation Options.....	54
5.1	Avoidance.....	54
5.2	NIR-VIS Empirical Linear Relationships.....	54
5.3	Subtraction of NIR Reflectance.....	57
5.4	Uniform Spectral Offset Approach.....	58
5.5	Glint-Aerosol Discrimination.....	59
6	Recommendations.....	60
6.1	Algorithms Showing Promise.....	60
6.2	Priorities for Phase A.....	60
6.2.1	Further Sensitivity Analyses.....	60
6.2.2	Field Glint Observations.....	60
6.3	Longer-Term Priorities.....	60
6.3.1	Comprehensive Oceanic and Atmospheric Data Set.....	60
6.3.2	Glint Toolbox.....	61
7	References.....	62
Appendix A	Global Wind Fields: 2-Parameter Weibull Distribution.....	65
Appendix B	Global Distribution of Coral Reefs.....	67

1 HypsIRI Sun Glint Subgroup

1.1 Background and Rationale

HypsIRI data and products are designed to address a set of key science questions initially identified by the National Research Council (NRC) in its Decadal Survey *Earth Science and Applications from Space: National Imperatives for the Next Decade and Beyond*. The general questions identified by the NRC Decadal Survey are consistent with those posed by the HypsIRI Science Study Groups and support a broad set of terrestrial, limnological, and marine research communities, as well as resource management efforts. The questions are grouped into three areas: (1) questions primarily requiring visible-to-shortwave infrared (VSWIR) data; (2) questions primarily requiring thermal infrared (TIR) data; and (3) questions requiring a combination of VSWIR and TIR data.

The HypsIRI mission will include two instruments mounted on a satellite in low-Earth orbit: a VSWIR imaging spectrometer and a TIR multispectral imager. The VSWIR and TIR instruments will both have a spatial resolution of 60 m at nadir. The VSWIR instrument will have a temporal revisit of approximately three weeks (19 days), and the TIR instrument will have a temporal revisit of approximately one week (5 days).

Among the HypsIRI science objectives, several questions address aquatic ecosystems. Among these are as follows:

- How do inland, coastal, and open ocean aquatic ecosystems change due to local and regional thermal climate, land-use change, and other factors? (Combined VSWIR+TIR Question 1)
- What are the seasonal expressions and cycles for terrestrial and aquatic ecosystems, functional groups, and diagnostic species? How are these being altered by changes in climate, land use, and disturbance? (VSWIR Question 2)
- What is the land surface soil/rock and shallow water substrate composition? (VSWIR Question 6)

The unique HypsIRI design allows unprecedented high-quality imaging spectrometer observations in marine and inland aquatic environments. Although the mission will collect data globally, the data over ocean areas deeper than 50 m is planned to be binned into 1-km pixels. Over the coastal ocean and inland aquatic ecosystems, the higher resolution VSWIR and TIR image data can provide excellent information about the composition, distribution, and functional status of aquatic ecosystems. VSWIR data are particularly important for optically shallow waters, such as coral reefs and seagrass beds, and for sandy, rocky or other bottoms from the tropics to high latitudes, where the problem of determining benthic community structure and processes is confounded by unknown water depths and unknown water column optical properties.

That said, there are several well-documented difficulties inherent to satellite-based VSWIR imaging of the ocean (and other aquatic systems). Chief among these is proper correction for atmospheric path radiance contributions to the remotely sensed signal. For shallow waters, there is also the previously mentioned conundrum of correcting for unknown water depth and optical properties to derive bottom composition. These issues are well studied, and they continue to be the focus of ongoing research.

The issue of sea surface glint (also referred to as “glitter” or “clutter”) has received somewhat less investigative attention. In fact, in existing ocean color missions, the primary method to mitigate for glint is avoidance, rather than correction. However, for researchers utilizing higher-resolution imagery (1–10 m, as opposed to 1 km) to study the coastal zone, glint avoidance is generally not an option. Of necessity, these coastal researchers have developed various approaches to correct for glint impacts where possible. Many published approaches for glint mitigation in high-spatial-resolution remote sensing rely on in-scene statistics, but these methods are not suitable for automated global remote sensing. While mitigation has been repeatedly demonstrated, and such mitigation has been further demonstrated to improve quality of retrievals of subsurface features, the issue is devising a method that can be automated. Many of these approaches are straightforward, but they are typically unrefined in terms of ability to be applied to a variety of imagery on a general basis.

Because several aquatic science questions are central to the HypSPIRI mission, the issue of glint and glint mitigation must be investigated. The HypSPIRI Sun Glint Subgroup was formed to provide preliminary assessment of the impact of glint on HypSPIRI aquatic science objectives. It is important to note that HypSPIRI is not the sole owner of the glint problem: glint is an issue for any VSWIR remote sensing of aquatic systems. Thus, the analysis and results of the HypSPIRI Sun Glint Subgroup are useful for other current and future mission.

1.2 Glint

In remote sensing of any water body, some of the measured signal arises from light reflected from the water surface. This light does not penetrate into the water column and thus does not provide information about submerged materials. There are two sources for this light: the direct solar beam and skylight. Reflection of the direct solar beam into the remote sensing signal is termed *sun glint*, while reflection of skylight is termed *sky glint*. Together, the sun glint and sky glint contribution constitutes *glint radiance* in the remotely sensed signal. The directionality, distribution, and magnitude of glint are a function of sun angle, view angle, and the state of the water surface. Glint can adversely affect the remote-sensing retrieval of subsurface features (Wang and Bailey 2001; Hochberg et al. 2003). Qualitative examples of sun glint and sky glint scales, derived from Quickbird imagery, are given in Figures 1.2-1 through 1.2-4.

In traditional remote sensing of ocean color, glint mitigation is achieved largely by avoidance: the radiometer is simply pointed in a direction away from the glint pattern on the sea surface (Wang and Bailey 2001). The remotely sensed portion of the ocean is presumed to include some small glint contribution; this contribution is modeled using Cox-Munk wind-wave statistics (Cox and Munk 1954) and then subtracted from the total signal. These corrections are designed for the open ocean, where wind waves are assumed to be mono-directional, and for low-resolution data (≥ 1 km), where glint effects occur at a scale much smaller than pixel dimensions. For nearshore or shallow environments, because of the varied topography, the assumption of mono-directionality of waves (Borrego 1993) is generally not valid. Moreover, ocean color algorithms (Fraser et al. 1997; Wang and Bailey 2001) are designed for low-resolution data (≥ 1 km), where glint effects occur at a scale much smaller than pixel dimensions.



Figure 1.2-1. Quickbird scene of Tampa Bay, Florida. (Left) Wide-area scene to provide context. Yellow box shows location of close-up detail scene. (Right) Close-up scene to show detail (if any) of glint distribution. Wind conditions are very calm, resulting in virtually no capillary waves. This is a sheltered embayment, so there are also no surface gravity waves. In this case, there is sky glint but no sun glint.

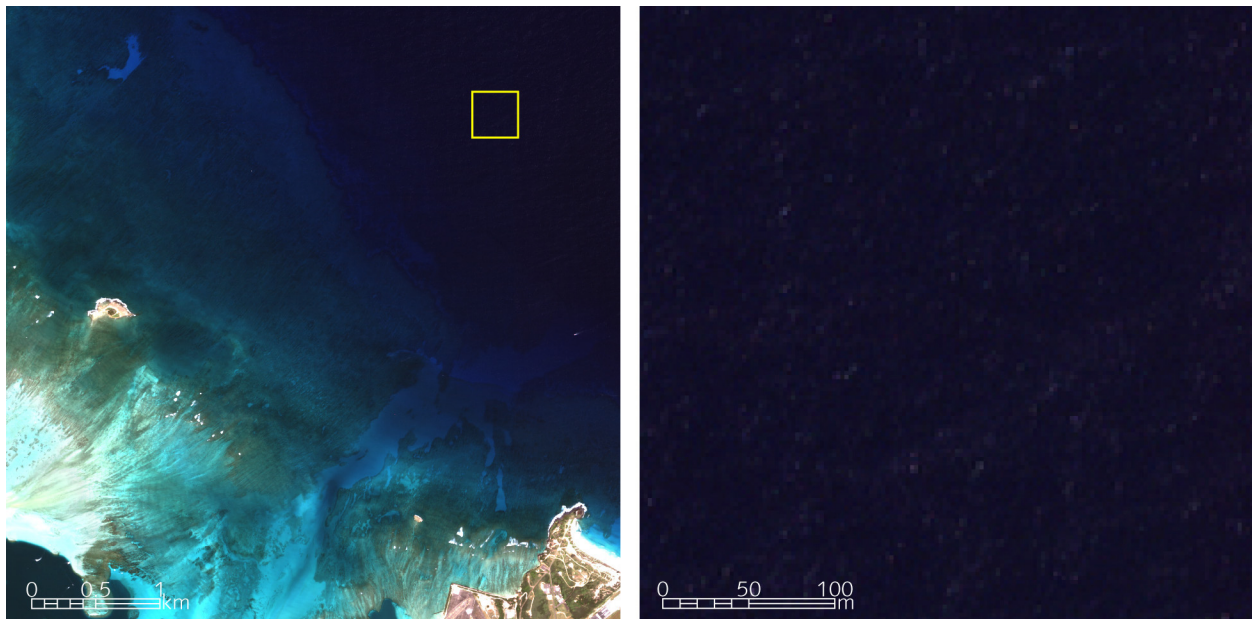


Figure 1.2-2. Quickbird scene of Kaneohe Bay, Hawaii. (Left) Wide-area scene to provide context. Yellow box shows location of close-up detail scene. (Right) Close-up scene to show detail of glint distribution. Wind speed is low, but non-zero, resulting in some capillary waves. Small (~0.5 m) surface gravity waves generated at distance are also present. In this case, there are both sky glint and sun glint, although sun glint intensity is minimal.

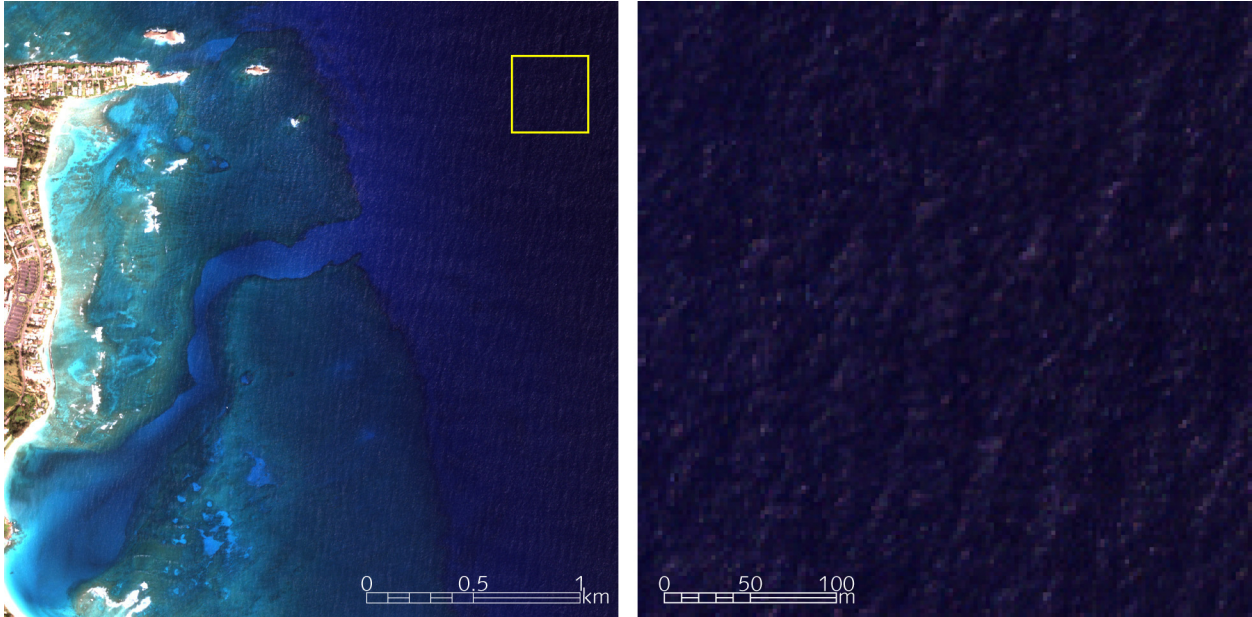


Figure 1.2-3. Quickbird scene of Punaluu, Hawaii. (Left) Wide-area scene to provide context. Yellow box shows location of close-up detail scene. (Right) Close-up scene to show detail of glint distribution. Typical trade wind speed is about $5\text{--}10\text{ m s}^{-1}$. Trade wind waves ($\sim 2\text{ m}$) are also present. Sun glint is readily apparent on the faces of surface gravity waves.

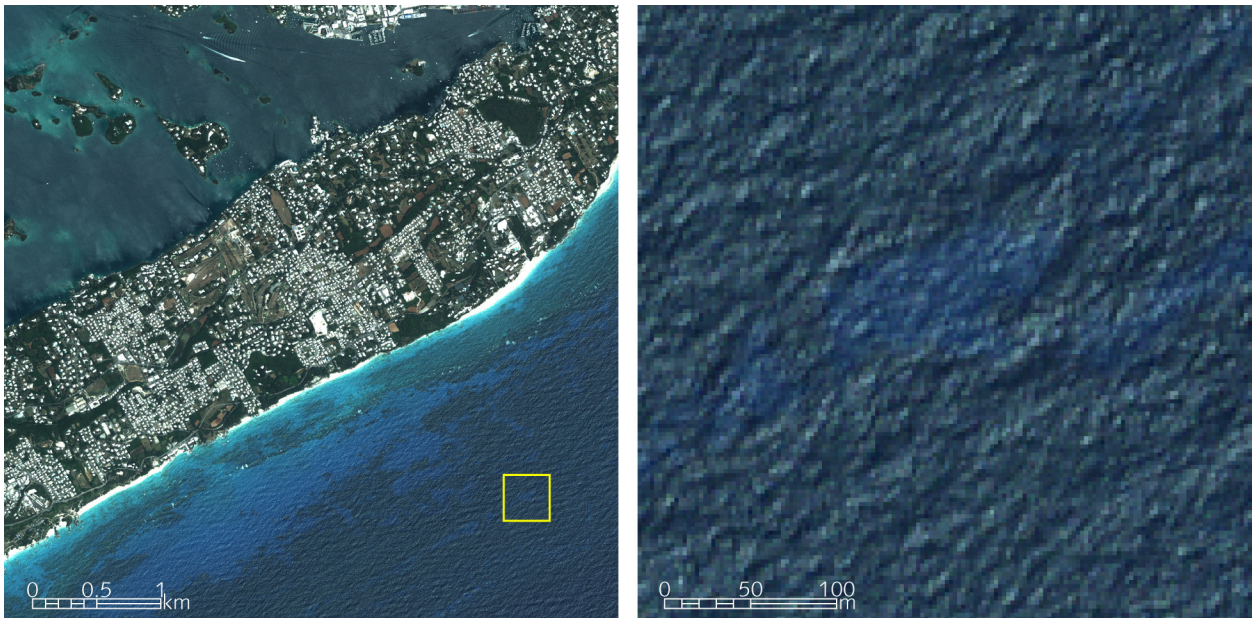


Figure 1.2-4. Quickbird scene of Bermuda. (Left) Wide-area scene to provide context. Yellow box shows location of close-up detail scene. (Right) Close-up scene to show detail of glint distribution. This scene illustrates a nearly stochastic sea surface; wind chop is convolved with small surface gravity waves. In this case, sensor view angle also increases sun glint intensity.

HyspIRI has a nominal ground sample distance of 60 m , which is roughly equivalent to the scale of gravity waves on the ocean surface. Thus, if the ocean is not flat, any given HyspIRI pixel is subject to glint, whether or not the sensor is pointed away from the main glint pattern. The

average amount of glint will vary statistically by latitude as a function of the time of the year, but any given pixel can contain more or less glint.

1.3 Tasks

The objective of the Sun Glint Subgroup is to characterize the potential impact of sun glint on aquatic science applications and to develop a mitigation approach for removing or reducing the impact of sun glint. The approaches to glint should be quantitative, physically based, and traced to work that is supported by the refereed literature. Glint results must be linked to the relevant HypsIRI science questions.

The original tasks for the Subgroup are as follows:

- Define sun glint plan for HypsIRI;
- Characterize sun glint effects of different orbits/crossing times and view angles for inclusion in plan;
- Outline Phase A process for developing HypsIRI-specific algorithm(s) to mitigate and/or remove sun glint building on existing and future published techniques;
- Engage different disciplines of the coastal and marine communities to assess percentages of additional radiance from sun glint, aerosols, and other atmospheric effects they can tolerate and still achieve their science—assessments included in the Sun Glint Plan; and
- Prepare an initial draft Sun Glint Plan to be ready for the HypsIRI Mission Concept Review (MCR) and complete a final plan with algorithm(s) to address glint and other during HypsIRI mission Phase A/B, including plans to test the algorithm(s).

1.3.1 Quantitatively Characterize Glint

The first component of this report is a quantification of glint levels across the range of conditions that HypsIRI will be imaging aquatic systems. Important parameters that determine glint magnitude include sun zenith and azimuth angles, sensor (view) zenith and azimuth angles, atmosphere gas and aerosol conditions, and state of the sea surface. Additional subsurface parameters are required to characterize aquatic science objectives, e.g., water depth, water optical properties, and nature of the sea floor. Aquatic bodies are complex optical systems, and complete characterization would require a concerted effort beyond the current scope of work. The objective of the HypsIRI Sun Glint Subgroup has been characterization of glint primarily through computer-based modeling (Section 3.1), as well as through examination of existing remote-sensing data (Section 3.2).

1.3.2 Determine Glint Impacts on HypsIRI Science

The second component of this report is an investigation into the impacts of glint on representative HypsIRI science objectives. These objectives were initially defined by the NRC Decadal Survey and fall under the key science questions identified by the HypsIRI Science Study Groups and the wider research community. Of importance is to examine the magnitude and errors in surface reflectance to assess whether the signal introduced by glint renders accurate retrieval of subsurface radiance reflectance impossible. For the current report, the Sun Glint

Subgroup has chosen to investigate glint impacts on retrievals for coral reef (Section 4.1), seagrass (Section 4.2) and optically deep-water (Section 4.3) science. Emergent vegetation is another important objective, but neither suitable models nor data were available to the Subgroup, and analysis has been deferred. Because appropriate radiometric data sets are also not available to investigate the three HypsIRI science questions that are addressed, the Subgroup has decided to rely on modeling using HydroLight and/or HydroMod to generate the necessary data.

1.3.3 Suggest Options for Way Forward

The final component of this report is a discussion of options for the “way forward.” This includes the Subgroup’s collective suggestions for glint mitigation approaches that currently seem most promising (Section 5), as well as recommended directions for future investigations (Section 6). This discussion is not exhaustive, but it does reflect the consensus of the Subgroup.

1.4 Participants

Table 1.4-1 lists the individuals nominally in the HypsIRI Sun Glint Subgroup and their institutions. The Subgroup initiated weekly teleconferences in October 2009. These individuals receive weekly email reminders about the teleconferences, as well as copies of all documents circulated within the Subgroup.

Table 1.4-1. HypsIRI Sun Glint Subgroup email distribution list.

Name	Institution
Paul Bisset	Florida Environmental Research institute
Paula Bontempi	NASA Headquarters Ocean Biology and Biogeochemistry
Vittorio Brando	Australia Commonwealth Scientific and Industrial Research Organisation
Carl Bruce	NASA Jet Propulsion Laboratory
Kyle Cavanaugh	University of California at Santa Barbara
Arnold Dekker	Australia Commonwealth Scientific and Industrial Research Organisation
Heidi Dierssen	University of Connecticut
Bo-Cai Gao	Naval Research Laboratory
James Goodman	University of Puerto Rico at Mayagüez
Robert Green	NASA Jet Propulsion Laboratory
Eric Hochberg	National Coral Reef Institute, Nova Southeastern University
Robert Knox	NASA Goddard Space Flight Center
Fred Lipschultz	NASA Headquarters Ocean Biology and Biogeochemistry
Betsy Middleton	NASA Goddard Space Flight Center
Peter Minnet	Rosenstiel School of Marine and Atmospheric Science, University of Miami
Curtis Mobley	Sequoia Scientific, Inc.
Frank Muller-Karger	College of Marine Science, University of South Florida
Bogdan Oaida	NASA Jet Propulsion Laboratory
Youngje Park	Australia Commonwealth Scientific and Industrial Research Organisation
Thomas Schroeder	Australia Commonwealth Scientific and Industrial Research Organisation
Dave Siegel	University of California at Santa Barbara
Woody Turner	NASA Headquarters Biological Diversity
Kevin Turpie	NASA Goddard Space Flight Center
Stephen Ungar	NASA Goddard Space Flight Center
Richard Zimmerman	Old Dominion University

1.5 Timeline

The timeline for Subgroup activities is short. Discussion began in late September 2009, with an initial date for the draft report at the end of January 2010. The current timeline has the draft report being completed in June 2010.

September 2009	Initiate Sun Glint Subgroup
October 2009	Begin teleconferencing Begin modeling of glint intensities
November 2009	Continued modeling of glint intensities Continued discussions
December 2009	Begin modeling of glint impact on science Continued discussions
January 2010	Continued modeling of glint impact on science Continued discussions Begin draft outline of report
April 2010	Continued modeling Continued discussions Completion of draft report
May 2010	Feedback/Review of draft report
June 2010	Revise draft report
June–July 2010	Pre-Phase A HyspIRI Sun Glint Subgroup Report

2 Literature Review

Glint has been recognized as a potentially confounding factor from the outset of ocean remote sensing. Correspondingly, there has been a fair amount of research into the subject. Kay et al. (2009) provide a thorough review of the physical processes that engender glint, as well as existing mitigation strategies.

Approaches to glint mitigation follow the strategies of avoidance and correction. Avoidance refers to physically pointing the remote sensor toward the ocean at an angle that minimizes specular reflection at the sea surface. The actual pointing angle is determined by the position of the sensor relative to the position of the sun, generally assuming the ocean is smooth. This is a fundamental component of the SeaWiFS glint mitigation strategy, which was possible since SeaWiFS was designed solely for ocean color.

Even in cases where the bulk of direct specular reflection can be avoided, sky-glint contamination remains, as does sun glint that arises due to deviations from the level-surface ocean, i.e., waves. As a result, glint correction is also a central component of ocean remote sensing. There are two basic approaches to glint correction: (1) statistical modeling of sea surface state to infer glint contribution and (2) direct estimation of glint contribution from the remote-sensing image data. Statistical modeling of sea surface state can be traced to Cox and Munk (1954), who analyzed aerial photographs of sun glint to infer statistics of the sea surface wave slope distribution as a function of wind speed. This is the basis for ocean color glint correction: knowledge of wind speed can be used to estimate the sea surface wave slope distribution, which in turn can be used to estimate the combined sky- and sun-glint radiances.

An alternative correction approach is to estimate the glint signal directly from remote-sensing data. This approach is based on the common assumption that there is no water-leaving radiance in the near infrared (NIR) due to strong absorption of light by water at these wavelengths, especially greater than 900 nm (Figure 2-1). This means that top-of-atmosphere NIR signals can arise only from the atmosphere or sea surface. After atmosphere corrections, the only remaining NIR signals must originate from the sea surface, i.e., glint.

Based on these principles, several researchers have developed interactive, empirical approaches to glint correction (Tassan 1994; Hochberg et al. 2003; Hedley et al. 2005; Lyzenga et al. 2006). These correction techniques all rely on the linear relationship between glint radiances at visible and near-infrared wavelengths. In addition, these correction techniques generally require human interaction to develop necessary statistics describing that linear relationship.

It is important to note that the linear relationship between VIS and NIR glint radiances has a physical basis: the index of refraction of seawater is (nearly) the same at VIS and NIR wavelengths (Figure 2-2). As a result, the reflectance of the water surface is (nearly) spectrally flat, i.e., glint has the same reflectance at VIS and NIR wavelengths. This is the basis for an empirical correction that does not require human interaction (Gao et al. 2000). Simply, after atmospheric correction, any remaining NIR reflectance is due to glint. This glint reflectance can simply be subtracted from VIS wavelengths, leaving only water-leaving reflectance.

For moderate- and low-spatial-resolution remote sensing, it is often sufficient to mitigate for glint via simple avoidance coupled with statistical estimation of sub-pixel glint content. Published methods for glint mitigation in high-spatial-resolution remote sensing all rely on in-scene statistics. Such methods are not suitable for automated global remote sensing. It is important to note that mitigation has been repeatedly demonstrated, and such mitigation has been further demonstrated to improve quality of retrievals of subsurface features. However, the issue is devising a method that can be automated.

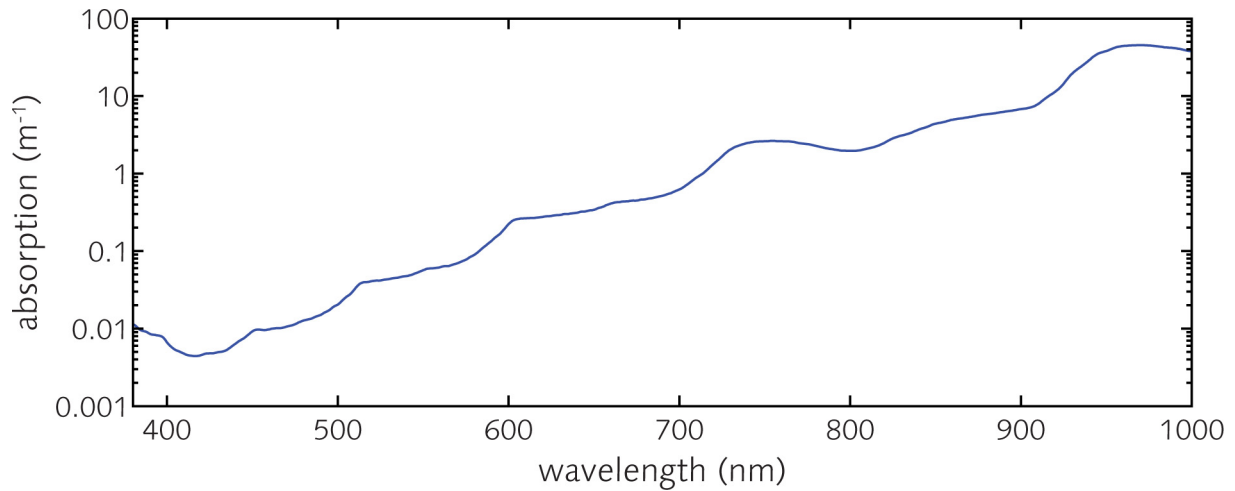


Figure 2-1. Water absorbs light very strongly at NIR wavelengths, especially >900 nm. Water-leaving radiance at these wavelengths is negligible. Data at VIS wavelengths from Pope and Fry (1997); data at NIR wavelengths from Kou et al. (1993).

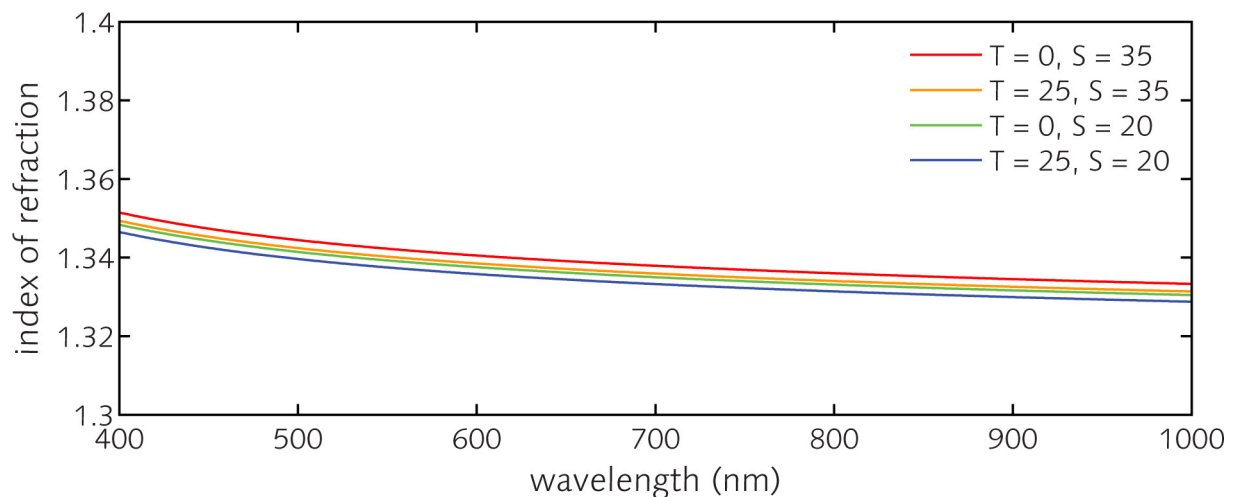


Figure 2-2. Index of refraction of water. Values are calculated following empirical model of Quan and Fry (1995), which is valid for wavelength range 400–700 nm, temperature range 0°–30°, and salinity range 0‰–35‰. Values are modeled for four combinations of temperature (T, °C) and salinity (S, ‰).

3 Quantitative Characterization of Glint

3.1 Modeling

The HypsIRI Sun Glint Subgroup has adopted computer-based radiative transfer modeling as the primary route to characterize glint for two reasons. First, modeling provides exact numerical determination of light fluxes that can be partitioned based on their sources (e.g., subsurface vs. glint). Second, there are no existing comprehensive data sets that contain the entire suite of radiometric and environmental measurements necessary to investigate both varying degrees of glint and the impact of glint on remote sensing science retrievals.

Two modeling approaches are utilized in this report. The first approach, performed by Youngje Park of Australia’s Commonwealth Scientific and Industrial Research Organisation (CSIRO), utilizes analytical and empirical equations to determine glint reflectance as a function of latitude for four key dates in the HypsIRI orbit (March 21, June 21, September 21, and December 21). These simulations describe the approximate high, low and average glint values that can be expected for HypsIRI. Details of the model approach and results are provided in Section 3.1.1.

The second approach, performed by Curtis Mobley of Sequoia Scientific, Inc., utilizes HydroMod, a coupled HydroLight-MODTRAN radiative transfer model. HydroLight computes in-water and water-leaving spectral radiance distributions, while MODTRAN computes radiance distributions in and above the atmosphere. HydroMod simulations are used here to investigate glint under specific coupled atmosphere-water column conditions. Chosen conditions do not necessarily cover extremes that HypsIRI may encounter but are representative of “typical” conditions. Details of the model approach and results are provided in Section 3.1.2.

3.1.1 Glint Reflectance: Geographic Location, Date, and Wind

In order to investigate seasonal variability of glint reflectance, computations were made for four key dates (March 21, June 21, September 21, December 21) for which HypsIRI orbits have been simulated. Model computations differentiated the east edge, middle point, and west edge of the HypsIRI swath to examine variability within a cross-track line. Wind data were taken from global wind speed climatology.

In this model estimation, the nondimensional sun glint reflectance at the surface (ρ_g^{0+}) is defined by

$$\rho_g^{0+} = \frac{\pi L_g^{0+}}{E_d^{0+}}, \quad (3.1.1-1)$$

where L_g^{0+} is the radiance at surface due to sun glint and E_d^{0+} is the downward irradiance (due to direct sun) at the surface. This definition is equivalent to

$$\rho_g^{0+} = \pi BRDF(a, w; \theta_0, \phi_0 \rightarrow \theta_v, \phi_v), \quad (3.1.1-2)$$

where θ_0 , ϕ_0 , θ_v , and ϕ_v are the solar zenith angle, the solar azimuth angle, the sensor zenith angle and the sensor azimuth angle, respectively; and $BRDF(a, w; \theta_0, \phi_0 \rightarrow \theta_v, \phi_v)$ is the bidirectional

reflectance distribution function (with units sr^{-1} ; Nicodemus et al. 1977) for reflectance by the air-water surface itself (not including the water below the surface), including the effects of sea surface roughness. Equation (3.1.1-2) shows that the nondimensional reflectance of equation (3.1.1-1) is the surface BRDF normalized by the BRDF of a perfectly reflecting (white) Lambertian surface, for which the BRDF is $1/\pi$. By purely geometrical consideration, it is related to the surface slope distribution (Cox and Munk 1954):

$$\rho_g^{0+} = \frac{\pi \rho_F(\omega) P_s(\theta_0, \phi_0, \theta_v, \phi_v; W)}{4 \mu_v \mu_0 \cos^4(\theta_n)}, \quad (3.1.1-3)$$

where $\rho_F(\omega)$ is the Fresnel reflectance; $P_s(\theta_0, \phi_0, \theta_v, \phi_v; W)$ is the probability of surface slope for which the incident ray with direction (θ_0, ϕ_0) is reflected to the direction (θ_v, ϕ_v) ; W is the wind speed about 10 m above sea surface; ω is half of the angle between the vectors of surface to sun and surface to sensor; and μ_v and μ_0 are the cosines of θ_v and θ_0 . This formula for the sun glint reflectance at sea surface (equation [3.1.1-3]) can be found in Viollier et al. (1980) and is used for ocean color image processing (Montagner et al. 2003; Gordon and Voss 2004). Equation (3.1.1-3) considers the highly pointing incident solar beam reflected to the sensor, and thus it excludes the sky glint effect. In fact, Cox and Munk (1954) removed sky glint and water-leaving radiances in their analysis of aerial photographs.

The wind-direction-independent (azimuthally isotropic) surface slope distribution function, $P_s(\theta_0, \phi_0, \theta_v, \phi_v; W)$ is approximated by

$$P_s(\theta_0, \phi_0, \theta_v, \phi_v; W) = \frac{1}{\pi \sigma^2} \exp\left(-\frac{\tan^2 \theta_n}{\sigma^2}\right), \quad (3.1.1-4)$$

where $\sigma^2 = 0.003 + 0.512W$.

The wind-direction-dependent (azimuthally anisotropic) model for the slope distribution is expressed as follows:

$$P_s(\theta_0, \phi_0, \theta_v, \phi_v; W, X) = \frac{1}{2\pi\sigma_c\sigma_u} \exp\left(-\frac{\xi^2 + \eta^2}{2}\right) \cdot \left\{ \begin{aligned} &1 - \frac{1}{2}c_{21}(\xi^2 - 1)\eta - \frac{1}{6}c_{03}(\eta^3 - 3\eta) + \frac{1}{24}c_{40}(\xi^4 - 6\xi^2 + 3) \\ &+ \frac{1}{4}c_{22}(\xi^2 - 1)(\eta^2 - 1) + \frac{1}{24}c_{04}(\eta^4 - 6\eta^2 + 3) \end{aligned} \right\}, \quad (3.1.1-5)$$

where

$$\sigma_c^2 = 0.003 + 0.00192 \times W;$$

$$\sigma_u^2 = 0.00316 \times W;$$

$$\xi = z_c / \sigma_c;$$

$$\eta = z_u / \sigma_u;$$

$$z_c = \tan \beta \sin \alpha : \text{surface slope in crosswind direction};$$

$z_u = \tan \beta \cos \alpha$: surface slope in upwind direction;
 $\alpha = \phi_n - X$: azimuth of surface normal vector, ϕ_n from upwind direction, X ;
 $\beta = \theta_n$: zenith of surface normal vector;
 $c_{21} = 0.01 - 0.0086 \times W$;
 $c_{03} = 0.04 - 0.033 \times W$;
 $c_{40} = 0.40$;
 $c_{22} = 0.12$; and
 $c_{04} = 0.23$.

The sun-glint reflectance is determined from sun-sensor angles and wind speed according to equation (3.1.1-3). Sun zenith varies with season and latitude. Sensor-viewing angles are determined by pixel position within a cross-track line. To examine seasonal effects on sun glint, HypsIRI orbits are simulated by latitude, altitude, sun zenith angle, and sun azimuth angle for four key dates: March 21, June 21, September 21, and December 21.

Sun azimuth angles were measured counterclockwise from spacecraft flight direction. Sensor azimuth seen from the ground is 90° (or -90°) measured counterclockwise from spacecraft flight direction toward west (or east) edge of the ground track. By pointing 4° west, the sensor-viewing zenith at scene edges is 10° (or 2°) at the western (or eastern) edge. Within a cross-track line, the minimum glint reflectance would occur at the west edge (sensor azimuth 90° and zenith 10°), while the maximum would occur at the east edge (sensor azimuth -90° and zenith 2°). To highlight this cross-track variability, sun-glint reflectance was computed separately for east edge, middle point and west edge.

Glint Global Longitudinal Variability

The global wind climatology is given as Weibull parameters as function of location (latitude and longitude) for each month, which are converted to the mean and standard deviation. (Details on the global wind speed climatology are described in Appendix A.) Here, the wind climatology is used to estimate (1) global longitudinal variability for given latitude and month and (2) local (temporal) variability for given latitude, longitude, and month. Since wind direction information is not available in this climatology, we use the wind-direction-independent glint model (equation [3.1.1-4]). In this section, we assume the index of refraction of seawater relative to air to be a constant 1.34, although the index of refraction does, in fact, vary slightly with wavelength. Medium, minimum, and maximum wind speeds at each latitude and month were extracted from the mean wind speed field, which is converted from the Weibull parameters. These numbers provide a rough estimate of the medium, low and high bounds of the wind speed for each latitude and month; they are used as input to the sea surface slope model as described above.

Figures 3.1.1-1 through 3.1.1-4 illustrate the simulated global longitudinal variability of sun-glnt reflectance for the simulated HypsIRI orbits for the four key dates. Table 3.1.1-1 provides the expected range (min ~ max) of the sun-glnt reflectances for the east and west edges of the HypsIRI field of view.

Table 3.1.1-1. Summary table for global longitudinal variability of the sea-surface sun-glint reflectance for the east and west edges of the HypSIIRI field of view.

Lat	March 21		June 21		September 21		December 21	
	West edge	East edge						
70°N	< 0.001	< 0.001	0.000 ~ 0.001	0.000 ~ 0.005	< 0.001	< 0.001	< 0.001	< 0.001
60°N	< 0.001	0.000 ~ 0.002	0.000 ~ 0.007	0.001 ~ 0.021	< 0.001	0.000 ~ 0.001	< 0.001	< 0.001
50°N	0.000 ~ 0.002	0.000 ~ 0.005	0.000 ~ 0.018	0.005 ~ 0.047	0.000 ~ 0.001	0.000 ~ 0.003	< 0.001	< 0.001
40°N	0.000 ~ 0.005	0.000 ~ 0.015	0.005 ~ 0.030	0.037 ~ 0.083	0.000 ~ 0.003	0.000 ~ 0.010	< 0.001	0.000 ~ 0.001
30°N	0.000 ~ 0.007	0.004 ~ 0.025	0.011 ~ 0.036	0.076 ~ 0.108	0.000 ~ 0.008	0.003 ~ 0.029	0.000 ~ 0.000	0.000 ~ 0.002
20°N	0.000 ~ 0.015	0.010 ~ 0.044	0.011 ~ 0.035	0.059 ~ 0.104	0.001 ~ 0.019	0.015 ~ 0.054	0.000 ~ 0.003	0.000 ~ 0.008
10°N	0.001 ~ 0.021	0.020 ~ 0.055	0.002 ~ 0.031	0.016 ~ 0.065	0.002 ~ 0.028	0.044 ~ 0.075	0.000 ~ 0.006	0.000 ~ 0.017
0°	0.000 ~ 0.019	0.021 ~ 0.055	0.000 ~ 0.019	0.001 ~ 0.037	0.005 ~ 0.028	0.060 ~ 0.076	0.000 ~ 0.010	0.002 ~ 0.034
10°S	0.001 ~ 0.012	0.014 ~ 0.048	0.000 ~ 0.007	0.000 ~ 0.015	0.001 ~ 0.025	0.020 ~ 0.064	0.001 ~ 0.017	0.016 ~ 0.052
20°S	0.001 ~ 0.009	0.005 ~ 0.030	0.000 ~ 0.002	0.000 ~ 0.006	0.000 ~ 0.019	0.006 ~ 0.041	0.002 ~ 0.021	0.043 ~ 0.059
30°S	0.000 ~ 0.005	0.002 ~ 0.015	< 0.001	0.000 ~ 0.001	0.001 ~ 0.009	0.004 ~ 0.021	0.007 ~ 0.021	0.041 ~ 0.058
40°S	0.000 ~ 0.001	0.000 ~ 0.004	< 0.001	< 0.001	0.000 ~ 0.003	0.000 ~ 0.008	0.003 ~ 0.015	0.018 ~ 0.044
50°S	0.000 ~ 0.001	0.000 ~ 0.002	< 0.001	< 0.001	0.000 ~ 0.002	0.000 ~ 0.004	0.002 ~ 0.011	0.009 ~ 0.028
60°S	< 0.001	0.000 ~ 0.001	< 0.001	< 0.001	< 0.001	0.000 ~ 0.001	0.000 ~ 0.005	0.001 ~ 0.013
70°S	< 0.001	< 0.001	< 0.001	< 0.001	< 0.001	< 0.001	< 0.001	0.000 ~ 0.002

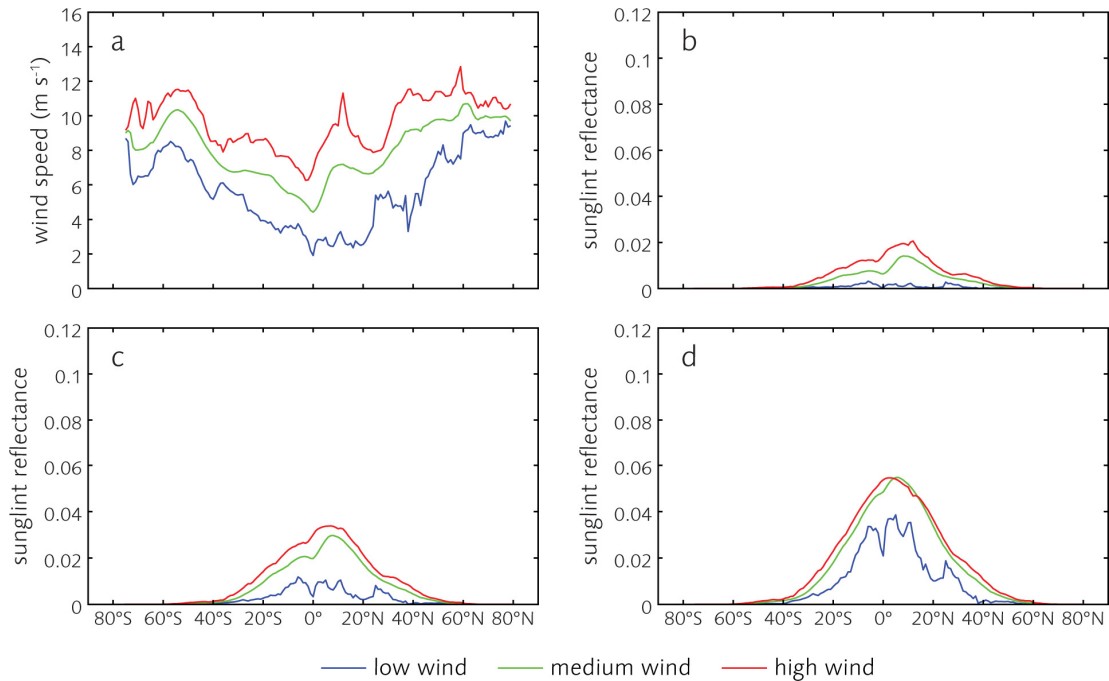


Figure 3.1.1-1. Global longitudinal variability of sea-surface sun-glint reflectance for the **March 21** HypSIIRI orbit for (a) three levels of wind speed, which were used to compute sea-surface glint at (b) the west edge, (c) the middle point, and (d) the east edge of the HypSIIRI field of view.

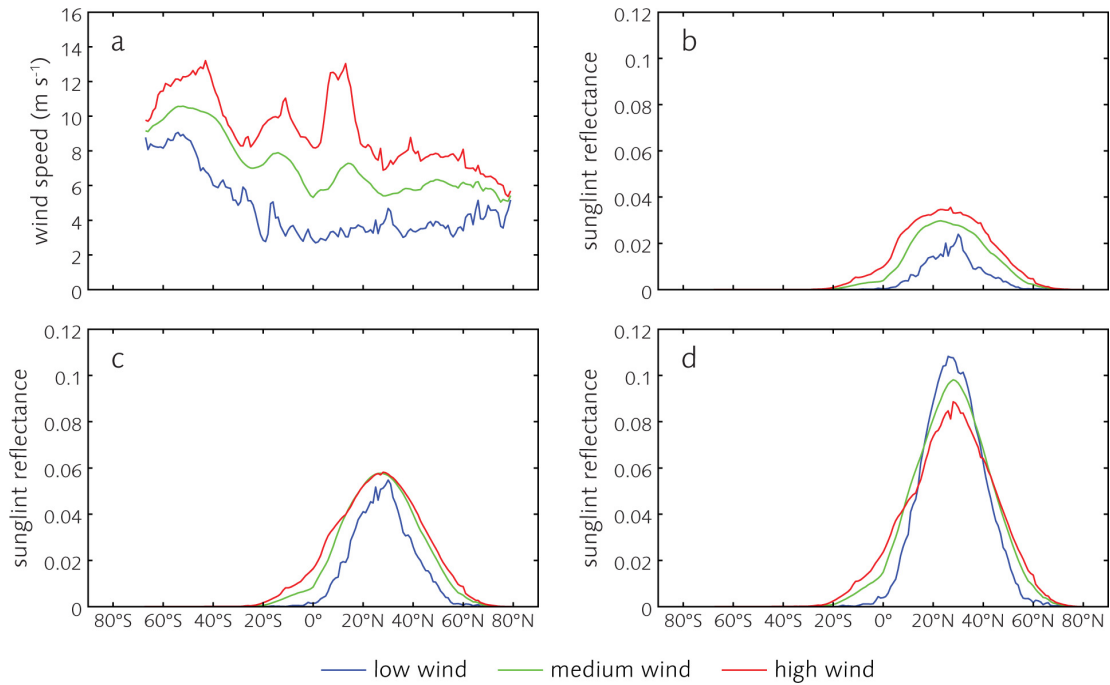


Figure 3.1.1-2. Global longitudinal variability of sea-surface sun-glint reflectance for the **June 21** HyspIRI orbit for (a) three levels of wind speed, which were used to compute sea-surface glint at (b) the west edge, (c) the middle point, and (d) the east edge of the HyspIRI field of view.

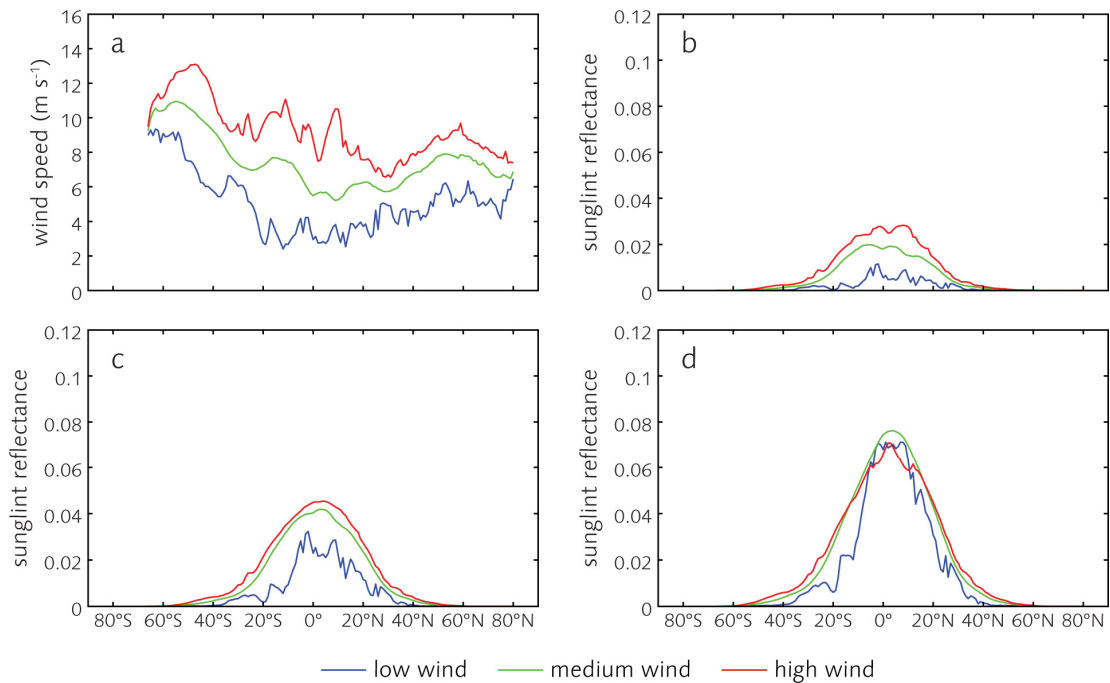


Figure 3.1.1-3. Global longitudinal variability of sea-surface sun-glint reflectance for the **September 21** HyspIRI orbit for (a) three levels of wind speed, which were used to compute sea-surface glint at (b) the west edge, (c) the middle point, and (d) the east edge of the HyspIRI field of view.

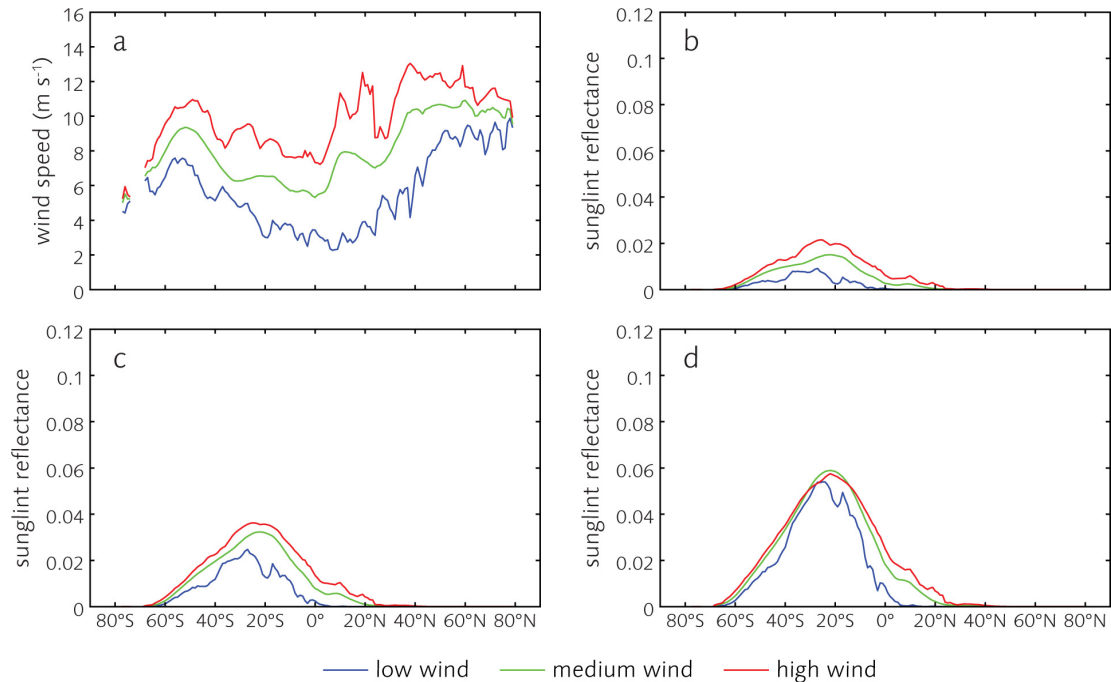


Figure 3.1.1-4. Global longitudinal variability of sea-surface sun-glint reflectance for the **December 21** HypsIRI orbit for (a) three levels of wind speed, which were used to compute sea-surface glint at (b) the west edge, (c) the middle point, and (d) the east edge of the HypsIRI field of view.

Glint Regional Temporal Variability

By this model, the glint reflectance is given as function of solar angles, view angles, and wind speed. Wind speed climatology varies across the world's oceans. To further examine glint intensities at a regional scale, we used the wind speed climatology for the longitude band 165°W – 150°W . Again, we estimated three wind speed levels: medium, low, and high. The medium wind speed is computed as an arithmetic mean of the mean wind field within the longitude zone for each latitude. The high and low wind speeds were computed as the arithmetic mean plus/minus one sigma, respectively. The sigma was taken as a mean of the standard deviation (computed from the Weibull parameters) over the given longitude range.

Figures 3.1.1-5 through 3.1.1-8 illustrate example results from modeling sun-glint reflectance in the specific longitude range (165°W – 150°W) for the same four key dates as previously modeled. Note the y-axis scale for sun-glint reflectance varies depending on date. Table 3.1.1-2 summarizes the expected range of the sun-glint reflectances for the east and west edges of the HypsIRI field of view.

Table 3.1.1-2. Summary table for local temporal variability of the sea-surface sun-glint reflectance for the longitude band 165°W–150°W.

	March 21		June 21		September 21		December 21	
	West edge	East edge						
70°N	< 0.001	< 0.001	< 0.001	< 0.001	< 0.001	< 0.001	< 0.001	< 0.001
60°N	0.000 ~ 0.001	0.000 ~ 0.003	0.000 ~ 0.009	0.000 ~ 0.023	0.000 ~ 0.001	0.000 ~ 0.002	< 0.001	< 0.001
50°N	0.000 ~ 0.003	0.000 ~ 0.008	0.000 ~ 0.022	0.005 ~ 0.047	0.000 ~ 0.002	0.000 ~ 0.006	< 0.001	< 0.001
40°N	0.000 ~ 0.007	0.001 ~ 0.016	0.004 ~ 0.030	0.036 ~ 0.084	0.000 ~ 0.005	0.000 ~ 0.014	< 0.001	0.000 ~ 0.001
30°N	0.000 ~ 0.011	0.004 ~ 0.029	0.008 ~ 0.037	0.075 ~ 0.107	0.000 ~ 0.011	0.002 ~ 0.032	0.000 ~ 0.001	0.000 ~ 0.003
20°N	0.002 ~ 0.018	0.016 ~ 0.044	0.024 ~ 0.037	0.061 ~ 0.098	0.003 ~ 0.022	0.021 ~ 0.055	0.000 ~ 0.003	0.000 ~ 0.010
10°N	0.010 ~ 0.022	0.043 ~ 0.055	0.005 ~ 0.030	0.025 ~ 0.066	0.004 ~ 0.025	0.055 ~ 0.075	0.000 ~ 0.007	0.003 ~ 0.019
0	0.005 ~ 0.020	0.042 ~ 0.055	0.001 ~ 0.014	0.005 ~ 0.035	0.011 ~ 0.025	0.063 ~ 0.077	0.002 ~ 0.011	0.011 ~ 0.035
10°S	0.001 ~ 0.015	0.011 ~ 0.048	0.000 ~ 0.006	0.001 ~ 0.014	0.007 ~ 0.024	0.035 ~ 0.064	0.002 ~ 0.016	0.027 ~ 0.052
20°S	0.000 ~ 0.009	0.004 ~ 0.030	0.000 ~ 0.002	0.000 ~ 0.005	0.002 ~ 0.018	0.009 ~ 0.041	0.003 ~ 0.022	0.041 ~ 0.059
30°S	0.000 ~ 0.006	0.000 ~ 0.017	< 0.001	0.000 ~ 0.001	0.000 ~ 0.010	0.001 ~ 0.022	0.002 ~ 0.022	0.029 ~ 0.058
40°S	0.000 ~ 0.002	0.000 ~ 0.007	< 0.001	0.000 ~ 0.001	0.000 ~ 0.005	0.000 ~ 0.011	0.002 ~ 0.017	0.013 ~ 0.044
50°S	0.000 ~ 0.001	0.000 ~ 0.003	< 0.001	< 0.001	0.000 ~ 0.002	0.000 ~ 0.004	0.001 ~ 0.012	0.004 ~ 0.028
60°S	< 0.001	0.000 ~ 0.001	< 0.001	< 0.001	0.000 ~ 0.001	0.000 ~ 0.002	0.000 ~ 0.006	0.000 ~ 0.015
70°S	< 0.001	< 0.001	< 0.001	< 0.001	< 0.001	< 0.001	0.000 ~ 0.002	0.000 ~ 0.005

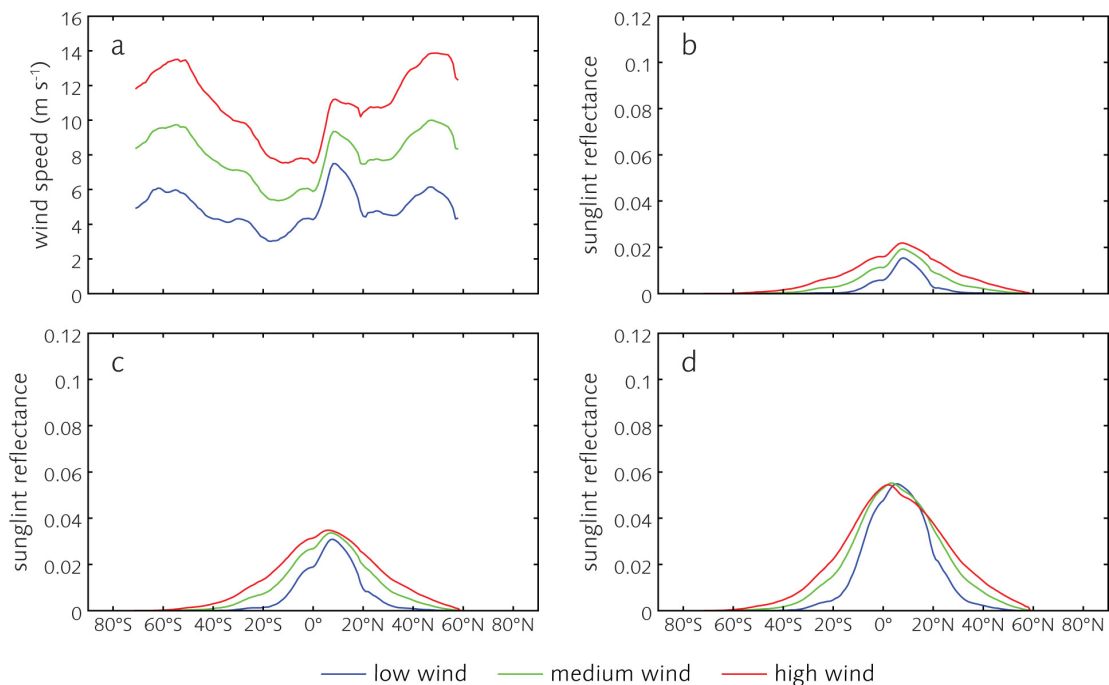


Figure 3.1.1-5. Example sea-surface sun-glint reflectance variability in a 15° longitudinal band (165°W–150°W) for the **March 21** HypSIRe orbit at (a) three levels of wind speed, which were used to compute sea-surface glint at (b) the west edge, (c) the middle point, and (d) the east edge of the HypSIRe field of view.

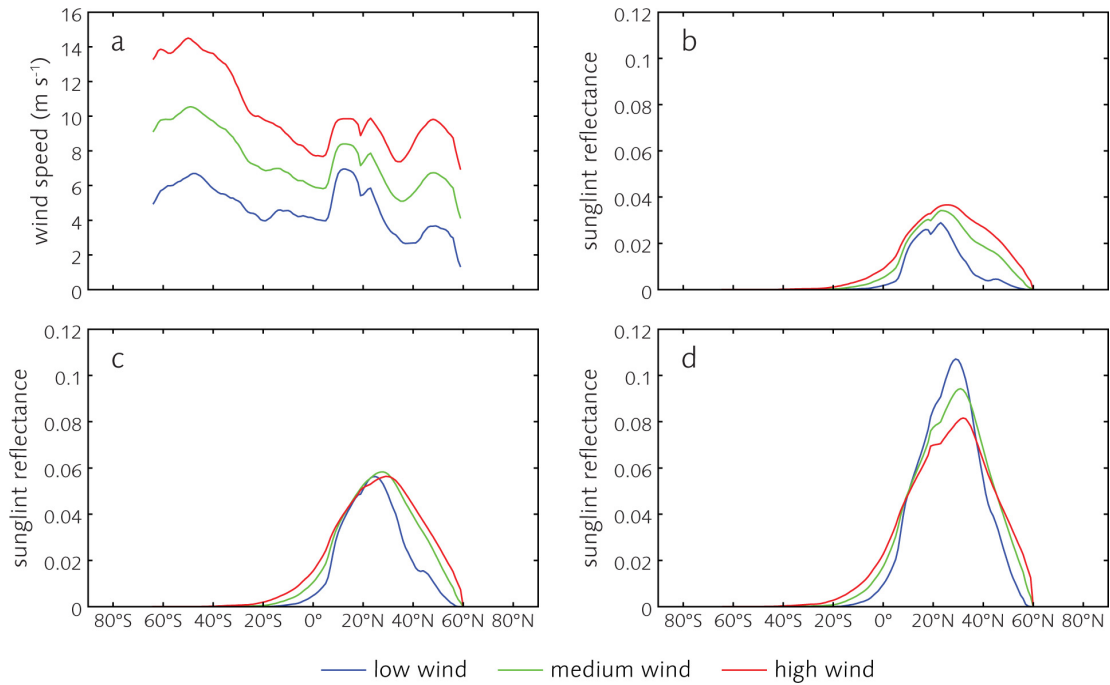


Figure 3.1.1-6. Example sea-surface sun-glint reflectance variability in a 15° longitudinal band (165°W–150°W) for the **June 21** HySpIRI orbit at (a) three levels of wind speed, which were used to compute sea-surface glint at (b) the west edge, (c) the middle point, and (d) the east edge of the HySpIRI field of view.

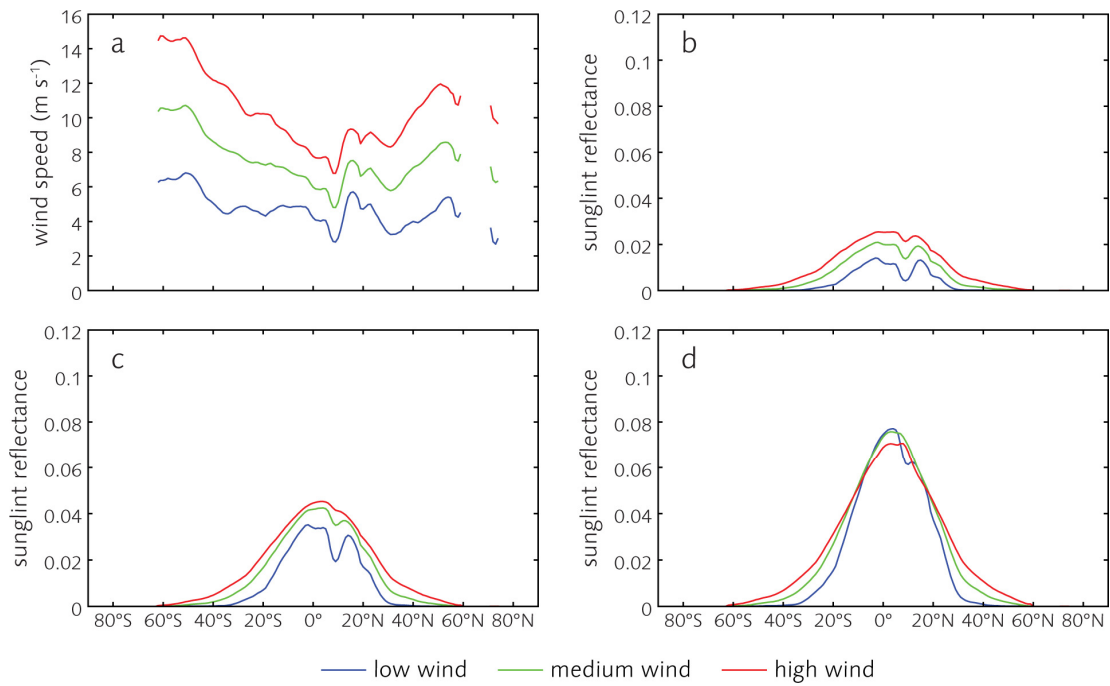


Figure 3.1.1-7. Example sea-surface sun-glint reflectance variability in a 15° longitudinal band (165°W–150°W) for the **September 21** HySpIRI orbit at (a) three levels of wind speed, which were used to compute sea-surface glint at (b) the west edge, (c) the middle point, and (d) the east edge of the HySpIRI field of view.

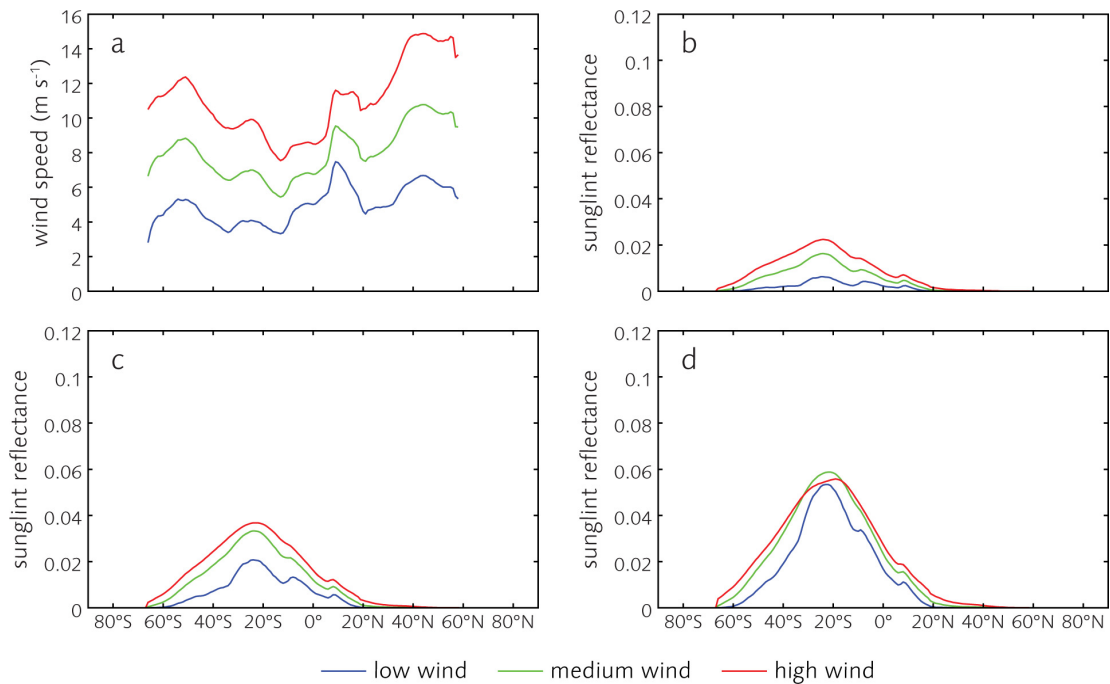


Figure 3.1.1-8. Example sea-surface sun-glint reflectance variability in a 15° longitudinal band (165°W–150°W) for the **December 21** HypSIIRI orbit at (a) three levels of wind speed, which were used to compute sea-surface glint at (b) the west edge, (c) the middle point, and (d) the east edge of the HypSIIRI field of view.

Several summary observations can be made from the model results:

- The effect of latitude is very clear. Sun glint is stronger where the sun is high, because HypSIIRI looks almost straight down. Sun-glint effects are apparent across a latitude band of 50° to 100° (i.e., 25°S–25°N to 50°S–50°N), depending on wind speed and the across-track pixel location.
- Sun glint is sensitive to wind speed for low to moderate glint strength and less sensitive for high glint.
- Sun glint at the east edge is consistently stronger (a factor of two) than at the west edge.
- Sun glint is high in summer due to high sun and low in winter due to low sun. At the equator in the middle point of the swath, sun-glint reflectance takes values of 0.025, 0.01, 0.04, and 0.01 for March, June, September, and December, respectively.
- Regional temporal variability appears similar to global longitudinal variability in magnitude.

3.1.2 Glint Reflectance: Sun/View Angles, Atmosphere, and Wind

This modeling activity utilizes HydroMod (integrated HydroLight and Modtran radiative transfer codes) to model the coupled water column and atmosphere system. Results provide information on glint reflectance intensity but also crucial information about water-leaving reflectance intensities. Importantly, HydroMod accurately models light fields for both optically shallow and

optically deep waters. Thus, it is possible to investigate the combined effects of atmospheric conditions, solar angles, view angles, water optical properties, and seafloor conditions (where desired) on the water-leaving signal and the potentially confounding glint signal.

The HydroLight radiative transfer model (Mobley et al. 1993, 1994; see www.hydrolight.info) computes radiance distributions and derived quantities for natural water bodies. In brief, HydroLight solves the scalar radiative transfer equation to compute the time-independent radiance distribution as a function of depth, direction, and wavelength within and leaving any plane-parallel water body. The upwelling radiance just above the sea surface includes both the water-leaving radiance and that part of the incident direct and diffuse sky radiance that is reflected upward by the wind-blown sea surface (glint radiance). The water-leaving and reflected-sky radiances are computed separately in order to isolate the water-leaving radiance, which is the quantity of interest in most remote sensing applications. Input to the model consists of the absorbing and scattering properties of the water body, the wind speed, the BRDF of the bottom of the water column, and the sun and sky radiance incident on the sea surface.

Modtran (Acharya et al. 1998; www.kirtland.af.mil/library/factsheets/factsheet.asp?id=7915) similarly computes spectral radiances within the atmosphere, given detailed information about the atmospheric constituents, the solar and viewing geometry, and the BRDF of the earth or sea surface at the lower boundary of the atmosphere.

In its standard form, HydroLight uses approximate semi-analytical models to obtain the incident spectral radiance onto the sea surface for a given solar zenith angle and atmospheric conditions. The incident radiance so computed is sufficiently accurate for most purposes of optical oceanography, such as computing remote-sensing reflectances or in-water irradiances. However, HydroLight's simple atmospheric models can neither simulate the full range of atmospheric conditions, nor can HydroLight propagate its water-leaving or surface-reflected radiances upward through the atmosphere. Modtran allows the user to select the BRDF of the land or water at the lower boundary of the atmosphere from several options defined by idealized analytic BRDFs. The only option for an ocean as the lower boundary is a Lambertian BRDF with a user-specified spectral irradiance reflectance. Modtran cannot compute the non-Lambertian BRDF corresponding to particular ocean conditions. Although both HydroLight and Modtran are considered industry standards for solving the unpolarized radiative transfer equation (RTE) with great accuracy within their respective oceanic and atmospheric domains, each is limited by its simplifying assumptions about the other domain.

To overcome the limitations of HydroLight and Modtran when run as separate codes, C. Mobley previously coupled HydroLight and Modtran into one package, called HydroMod. HydroMod is able to make round-trip radiative transfer simulations beginning with sunlight entering the top of the atmosphere, propagating through the atmosphere and into the ocean, propagating within and leaving the ocean, and finally returning to the top of the atmosphere. One complete HydroMod run generates the total radiance as measured for a single viewing direction and altitude, as seen by a satellite or aircraft-imaging sensor viewing a particular spot on the ocean. The at-sensor radiance includes ocean water-leaving and surface-reflected radiances transmitted through the atmosphere and atmospheric path radiance resulting from sunlight being scattered into the viewing direction between the sea surface and the sensor. These three contributions to the total

radiance are separately computed so that the total radiance can be partitioned into these contributions. All of the scattering and absorption effects within the ocean and atmosphere are computed just as in the separate codes. HydroMod is thus well suited for evaluation of airborne and satellite ocean color sensors.

The primary limitation of HydroMod is that it does not include polarization effects. Including polarization would require development of a vector version of HydroLight, then coupling that code with a vector atmospheric code such as 6SV (Kotchenova et al. 2006; <http://6s.ltdri.org/>). This would be a major project far beyond the scope of the Subgroup. Note that the lack of polarization code is an issue for many radiative transfer models that are routinely used for ocean and atmosphere studies. Thus, the Subgroup’s use of HydroMod is in line with current practices of the wider research community.

The HypsIRI equatorial crossing data for March 21 were used to determine the sun and sensor geometry for the east and west edges of the HypsIRI scan (sensor off-nadir angles of 2° E and 10° W, perpendicular to the sensor flight direction; the solar zenith angle was 24.33°). The wind speed was 5 m s⁻¹. Modtran’s default tropical atmosphere was used, with its various default values for marine aerosols, humidity, etc. The water index of refraction was a function of wavelength, although this is a small effect in the visible and near-IR wavelength range. These runs covered the range 350–1500 nm at 5-nm resolution.

Geometry of model input and output is an important consideration: incorrect geometries would produce much less meaningful results. Figure 3.1.2-1 illustrates the geometry used in the HydroMod simulations.

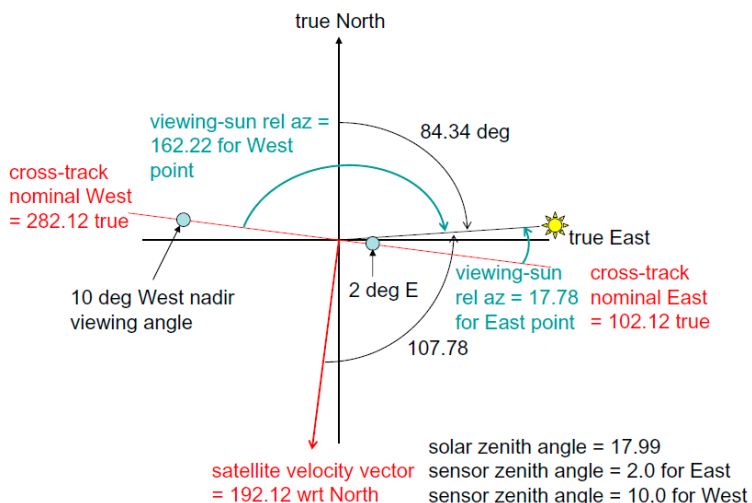


Figure 3.1.2-1. Example geometry used in HydroMod simulations, in this case for Station ALOHA on June 21.

Two cases were simulated for in-water and bottom conditions:

1. Shallow-water, coral and sand bottom: Case 1 water with chlorophyll concentration of 0.3 mg m⁻³ in the “new Case 1” inherent optical properties (IOP) model of HydroLight version 5 (based on recent publications by Bricaud and Morel; see Mobley and Sundman

2008). In this model, all IOPs are determined by the chlorophyll value alone. The bottom was 50% sand and 50% coral at 5 m depth. This gives a large water-leaving radiance because of the clear water and relatively bright bottom.

2. Deep, dark ocean: Case 1 water with chlorophyll concentration of 5 mg m^{-3} and infinitely deep water. The high chlorophyll value and optically deep water together result in a much smaller water-leaving radiance.

Figure 3.1.2-2 shows the results for the shallow-water case, east edge of the HypsIRI field of view. The green line shows the water-leaving reflectance at the sea surface. This curve depends on both the water column optical properties and the bottom reflectance. The teal curve shows how much of the water-leaving reflectance (i.e., water-leaving radiance) actually reaches the top of the atmosphere (TOA). The red line shows the sea-surface glint reflectance (including both sun glint and sky glint, which are not separated in HydroMod). Note that the glint reflectance is almost independent of wavelength. (The small kinks near 1360 nm are due to Modtran numerical inaccuracies in the opaque atmospheric window where surface radiances are extremely small.) The purple curve shows how much of the surface glint makes it to the TOA. The orange curve shows the atmospheric path radiance at the TOA. This curve includes both Rayleigh and aerosol scattering contributions to the TOA path radiance. Finally, the blue curve shows the total TOA reflectance as would be measured by HypsIRI. (This curve is π times the TOA radiance divided by the TOA solar plane irradiance E_d .) The TOA ρ_u curve is the sum of the atmospheric and TOA glint and water-leaving curves.

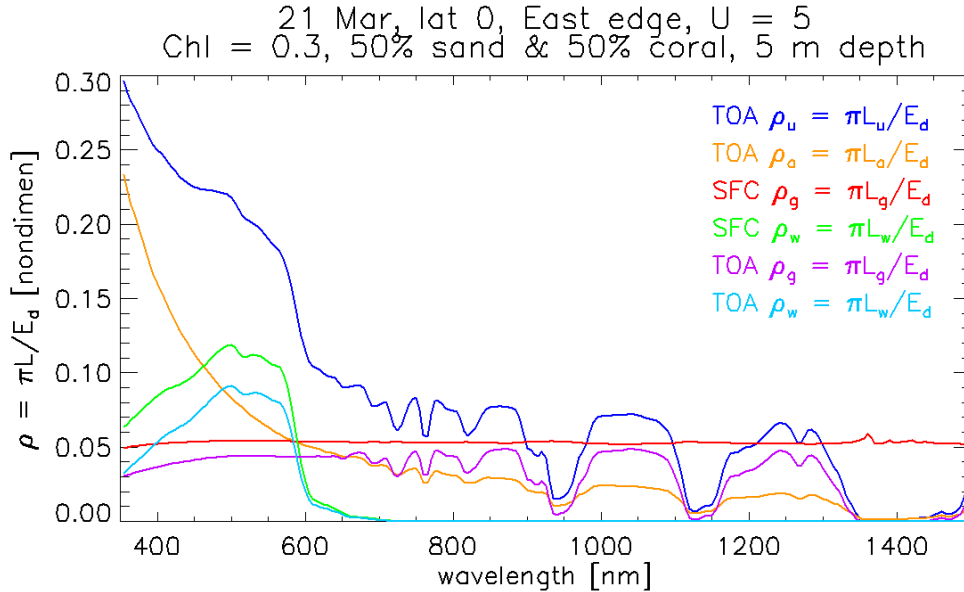


Figure 3.1.2-2. HydroMod results for the equator, March 21, shallow water, east-edge simulation.

Figure 3.1.2-3 compares the east and west edges of the HypsIRI field of view, with all other conditions the same as in Figure 3.1.2-2. It should be noted that the water-leaving reflectances are almost identical. However, the surface glint is much less for the west edge of the field of view because that viewing geometry picks up much less direct sun glint than the east edge. The

atmospheric contribution for the west edge is slightly greater than for the east edge, owing to the slightly longer atmospheric path length and different scattering angles from the sun's direct beam direction into the sensor.

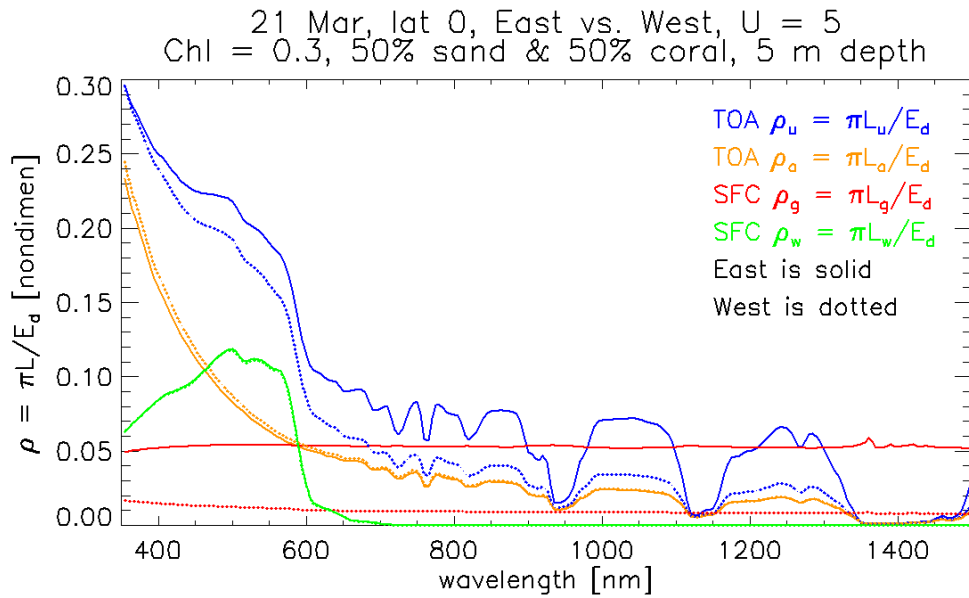


Figure 3.1.2-3. Same conditions as Figure 3.1.2-2 but including the west edge of the HypSIPI field of view.

Figure 3.1.2-4 corresponds to Figure 3.1.2-2, except that the chlorophyll concentration is 5.0 mg m^{-3} and the water is infinitely deep. The surface glint and atmospheric reflectances are almost identical. However, the water-leaving reflectance is now much less for the deep, high-chlorophyll ocean than for the shallow, clear water case.

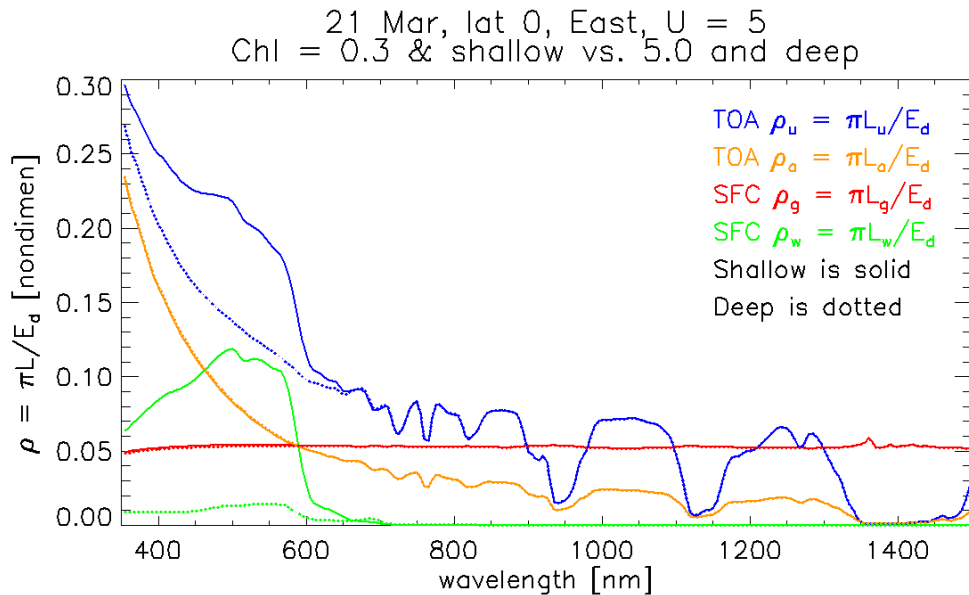


Figure 3.1.2-4. Same conditions as Figure 3.1.2-2 but including the high chlorophyll, optically deep case.

In summary, Figure 3.1.2-3 shows the large differences in glint reflectance that can occur from the east to the west edges of the HypSIIRI field of view for moderate wind speeds in equatorial regions. Figure 3.1.2-4 shows the range of water-leaving reflectances that can occur for shallow clear waters with a mixed coral and sand bottom compared to deep, high-chlorophyll waters. In all of the examples, the remote-sensing problem is to start with any of the blue curves and retrieve the corresponding green curves after atmospheric and glint correction.

3.2 Glint Reflectance: Image Analysis

The objective here is to estimate glint radiances using remote-sensing imagery. This analysis utilizes seven scenes of AVIRIS high-altitude spectral imagery from the 2000 campaign in Hawaii (Figure 3.2-1).

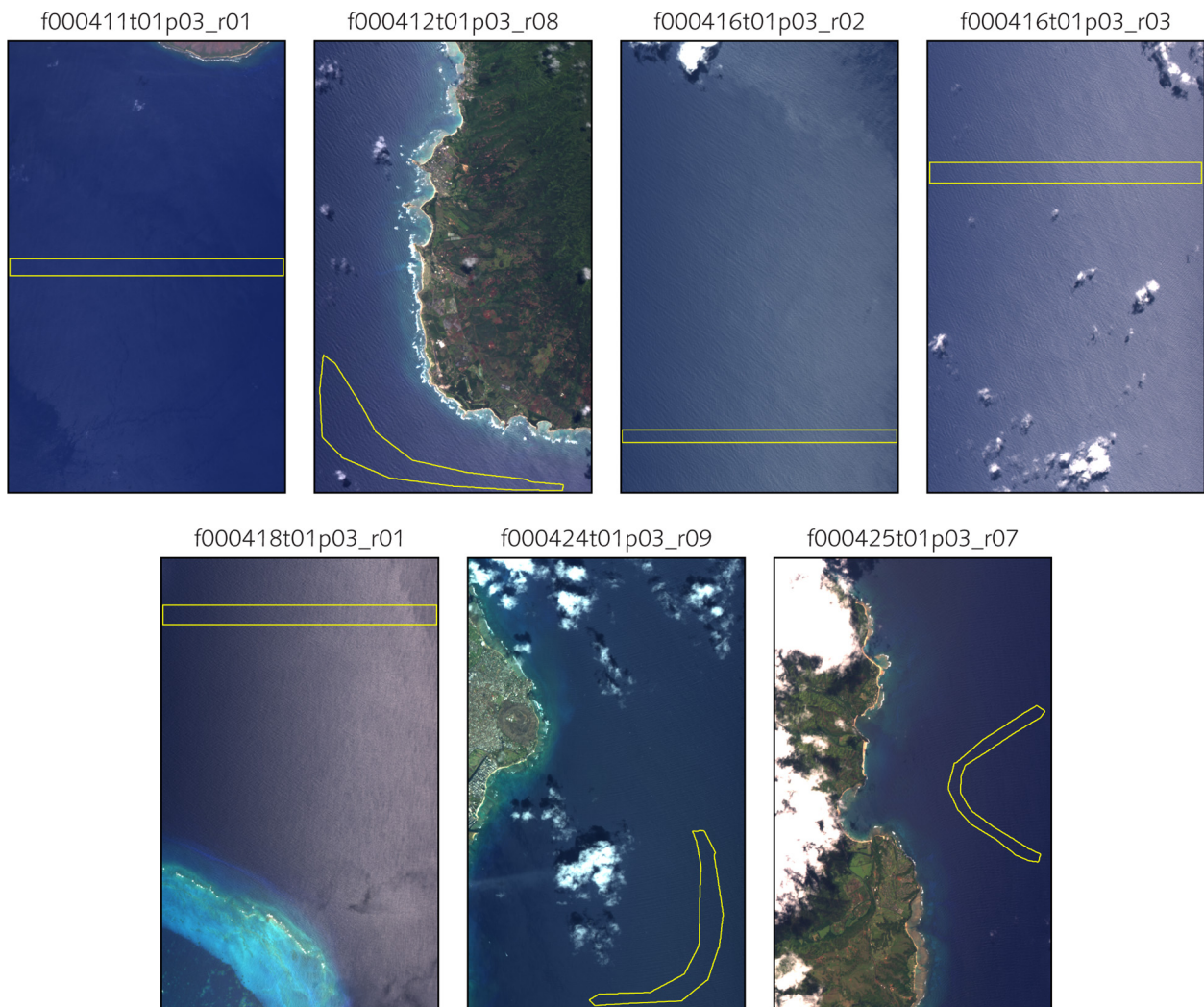


Figure 3.2-1. AVIRIS scenes used to estimate glint radiance for comparison with modeled values. These scenes are from the 2000 campaign in Hawaii. Yellow regions are deep-water areas used to extract glint statistics.

Assuming that a small area of deep ocean has uniform water-leaving reflectance, and also assuming that the same small area has uniform atmospheric absorbance and transmittance properties, then the variability in TOA measured reflectances must be due to variations in glint intensity in that small area. For this analysis, deep ocean areas were identified in each of the seven AVIRIS scenes, and TOA reflectance spectra were extracted for all pixels in the areas.

Within each area, the spectrum with the highest values represents the maximum observed glint intensity, and the spectrum with the lowest values represents the minimum observed glint intensity. Note that these maximum and minimum intensities are not globally absolute; they are only relative to the current area of interest. The difference between the maximum and minimum spectra represents the maximum range of glint reflectance in the area of interest, as observed at the TOA. Figure 3.2-2 shows this range for each of the seven AVIRIS scenes.

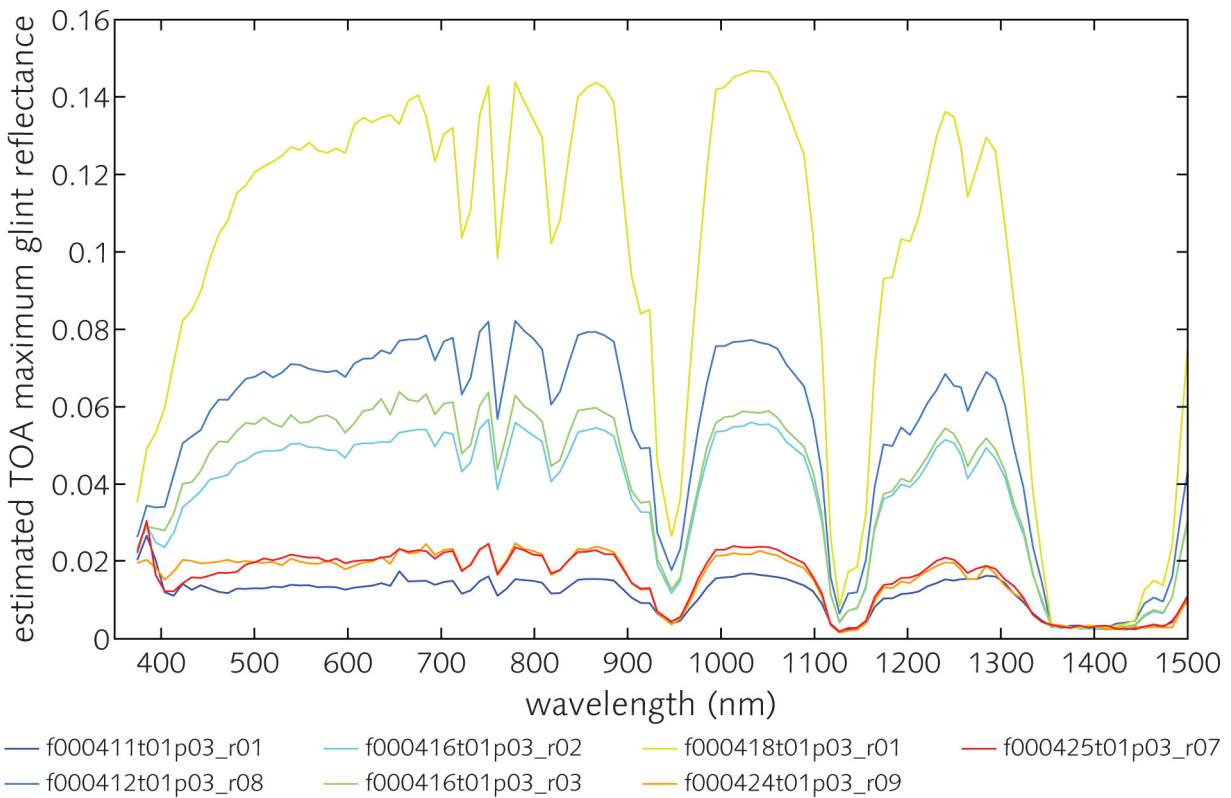


Figure 3.2-2. Estimated maximum glint reflectances for seven AVIRIS scenes.

The magnitude of glint reflectance varies with visually apparent sea surface glint intensity (see Figure 3.2-1). The high level of glint seen in AVIRIS scene f000418t01p03_r01 is demonstrative of the impact of sun and view angles on the glint signal.

TOA ρ_g can be separated from TOA ρ_a via simple algebraic decomposition (see Sections 4.3.2 and 5.5). In the NIR, the spectral shape of ρ_a is considerably steeper than that of ρ_g , which is nearly spectrally flat. At NIR wavelength λ , where water-leaving radiance is zero, the total reflectance minus Rayleigh reflectance gives the reflectance due to aerosol and glint (and their interaction):

$$\rho_{ga}(\lambda) = \rho_g(\lambda) + \rho_a(\lambda).$$

Assuming constant but different spectral shapes for the glint and aerosol components, glint and aerosol reflectances at one wavelength can be expressed as a function of their respective reflectances at a reference wavelength:

$$\rho_g(\lambda_1) = G \cdot \rho_g(\lambda_0) \text{ and } \rho_a(\lambda_1) = A \cdot \rho_a(\lambda_0),$$

where G and A are constants. Thus, with reflectances at two bands, the glint and aerosol reflectances can be solved by simple algebra.

Based on radiative transfer simulations of the conditions in AVIRIS scene f000418t01p03_r01, the following constants are set for analysis of that scene: $G = 0.95$, $A = 0.65$, $\lambda_0 = 1042$ nm and $\lambda_1 = 1553$ nm. Figure 3.2-3 shows the location of a cross-track sample extracted from the scene, and Figure 3.2-4 shows the ratio $\rho_{ga}(1042 \text{ nm}) / \rho_{ga}(1553 \text{ nm})$ along the cross-track line, as well as $\rho_g(1042)$ and $\rho_g(1553)$ along the cross-track line.

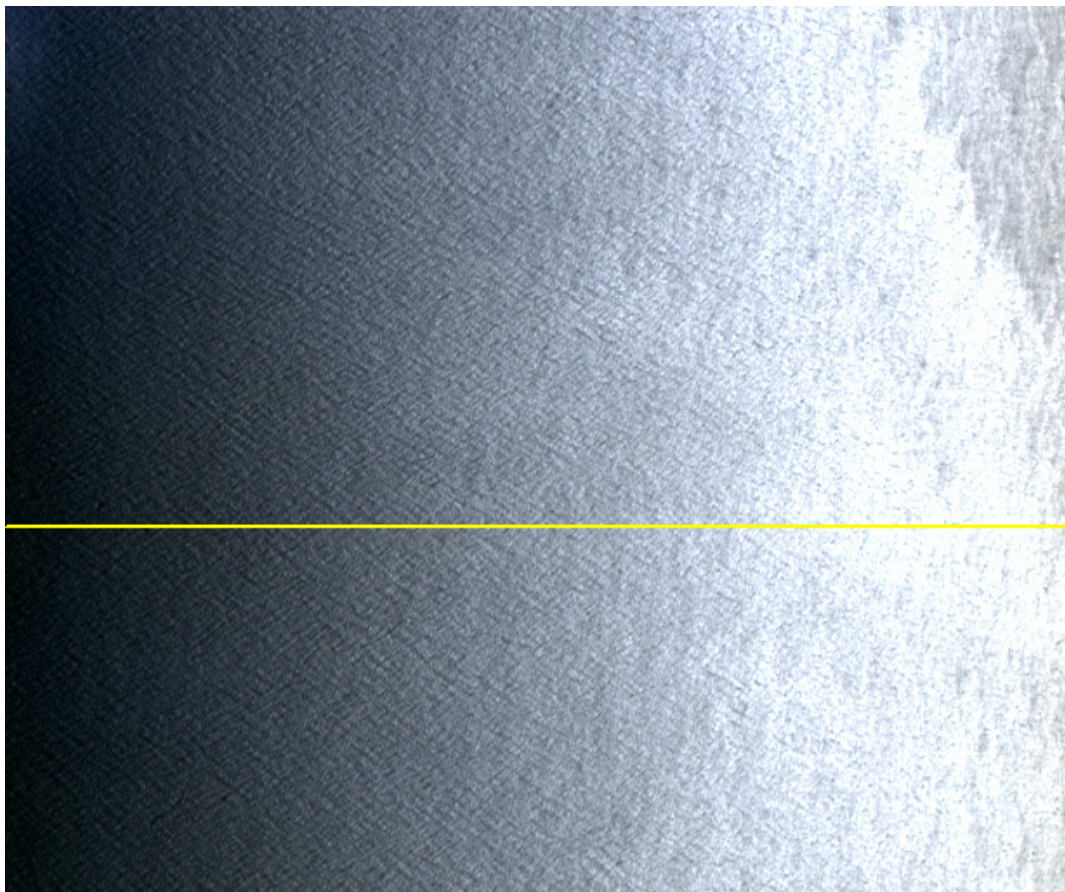


Figure 3.2-3. AVIRIS scene f000418t01p03_r01. The yellow line shows the location of the cross-track sample analyzed in Figure 3.2-4.

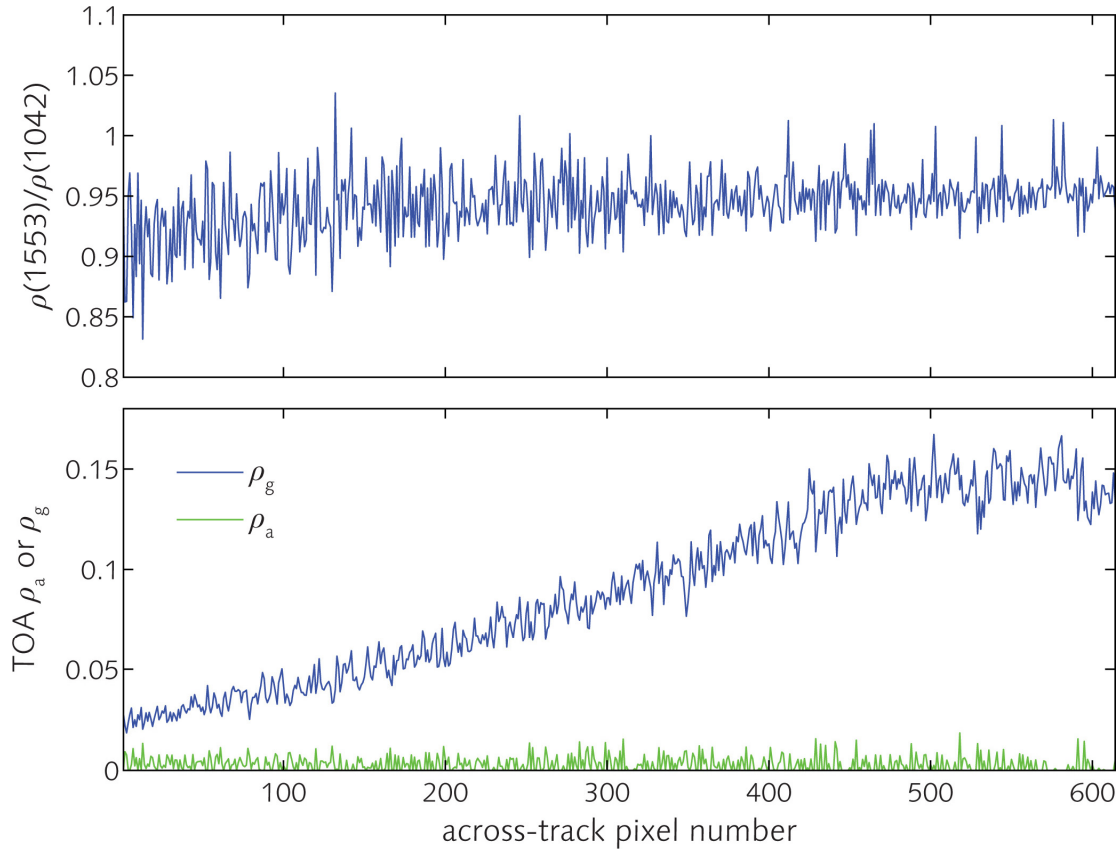


Figure 3.2-4. Discrimination between ρ_g and ρ_a . (Top) Ratio of TOA apparent reflectance at 1553 nm to TOA apparent reflectance at 1042 nm. (Bottom) Extracted ρ_g and ρ_a .

The reflectance ratio $\rho_{ga}(1553) / \rho_{ga}(1042)$ ranges from 0.9 at the left edge of the scene and quickly rises to ~ 0.95 , where glint dominates over aerosol reflectance. The value 0.95 is consistent with radiative transfer simulations (not shown). ρ_a has a value ~ 0.003 , while ρ_g ranges 0.02–0.15 in this scene: at least an order of magnitude higher than ρ_a . Note that a noisy reflectance ratio generates a noisy ρ_a . The noise level 0.005 in reflectance corresponds to $0.005 \times 65 \div \pi = 10 \mu\text{W cm}^{-2} \text{ nm}^{-1} \text{ sr}^{-1}$ at 1042 nm. In practical image processing, since ρ_a varies at a much larger spatial scale than ρ_g , ρ_a can and should be smoothed first by spatial averaging. Then, the smoothed ρ_a can be used to derive ρ_g .

3.3 Summary

There are several key points to be taken from the model and image analysis:

- (1) Glint intensity can surpass that of water-leaving radiance;
- (2) Glint radiance is function of incident irradiance;
- (3) Glint reflectance is a function of the index of refraction of the water body; and
- (4) Glint reflectance at the sea surface, to the first order, is spectrally flat.

Point (4) is particularly important, because it is the basis for virtually all glint-correction strategies.

4 Glint Impact on HypsIRI Science

4.1 Coral Reefs

One science question for HypsIRI, as stated repeatedly in the NRC Decadal Survey (2007), is to determine the health and extent of coral reefs. The most common scientific approach to the question of coral reef health is to quantify the areal coverage of a reef by corals, various algae, and sediment. From the perspective of HypsIRI, the issue becomes one of accurate spectral discrimination between coral, algae, and sand (the predominant sediment on reefs). To investigate the impact of glint on retrievals of coral, algae, and sand, we conducted a modeling exercise using HydroLight.

The preferred method to evaluate spectral discrimination is through classification analysis. In classification analysis, a data set is used to train a classifier, which is then applied to the same or another data set to make predictions about class membership. The idea is to find the rates that spectra are predicted to belong to the correct class, as well as the rates that spectra are predicted to belong to the wrong class. These rates are very readily interpretable. For example, it is possible to say that coral is correctly predicted to be coral $X\%$ of the time, and coral is incorrectly predicted to be algae $Y\%$ of the time. The problem is obtaining the necessary data. At a minimum, the training data must have as many spectra as wavebands. Ideally, there should be hundreds to thousands of spectra for each class.

It is not reasonable to make tens of thousands of HydroLight runs in the short time available to the HypsIRI Sun Glint Subgroup. So, an approximation was employed: run HydroLight for several different conditions with spectrally flat bottom reflectance, then interpolate between modeled values as needed. In all, HydroLight was run 5,832 times. In each run, one of the following parameters was varied among the listed values:

- Bottom reflectance: 0, 5, 10, 25, 65, 100%; spectrally flat
- Suspended chlorophyll: 0.05, 0.5, 1 mg m^{-3}
- $a_{\text{CDOM}(440)}$: 0, 0.15, 0.3 m^{-1}
- Suspended sand: 0, 0.5, 1 g m^{-3}
- Water depth: 0.5, 2, 5, 10 m
- Wind speed: 0, 5, 10 m s^{-1}
- Sun zenith: 20°, 30°, 40°

Output was taken for the following wavelengths and geometries:

- Wavelength: 355–995 nm in steps of 10 nm
- Sun azimuth wrt to along-track: 30°, 45°, 60°, 75°, 90°, 105°, 120°, 135°, 150°, 165°
- View zenith: 0°, 10°, 20°

Thus, there are values for water-leaving radiance (L_w), glint radiance (L_g), and downwelling irradiance (E_d) at each of the conditions specified by the 10 parameters (11,372,400 total values for each radiometric quantity).

The L_w , L_g , and E_d values have been assembled into three separate 10-dimensional arrays. These arrays are essentially look-up tables. With these arrays, it is possible to specify any bottom reflectance spectrum, suspended chlorophyll level, $a_{CDOM}(440)$, etc., then interpolate to get L_w , L_g , and E_d for the desired conditions and geometries. Several comparisons between interpolated values and explicitly modeled HydroLight values showed that results are nearly identical. However, for the present purposes, the aim is only to interpolate between bottom reflectances at condition values already in the arrays, not to interpolate between (for example) chlorophyll values.

Using the interpolation technique, it is possible to derive L_w , L_g and E_d under, for example, specific chlorophyll, CDOM, and sand conditions for 10,000 different bottom spectra in about 30 seconds. This affords the ability to use true multivariate analyses (namely, classification analysis) to explore the impact of glint on spectral separability of the classes. The current analysis utilizes reflectance spectra measured *in situ* for coral ($n = 4,005$), algae ($n = 5,500$), and sand ($n = 642$), and explores spectral separability of these bottom types under two different water and sun conditions, both without and with glint.

The first step is to interpolate at specified water, sun, and bottom reflectance conditions to generate appropriate L_w , L_g , and E_d spectra. In the coral reef case, each interpolation included coral, algae, and sand, for a total of 10,147 spectra. For each water/sun condition, interpolations were performed at four seafloor depths (0.5, 2, 5, and 10 m). The interpolation result for a single set of water/sun conditions totals 40,588 spectra. This is equivalent to running HydroLight 40,588 times, once for each bottom spectrum under the given water, sun, and depth conditions.

The next step is to build the classification functions. The objective here is not explicit radiative transfer inversion, where water column effects are derived and then subtracted from above-water spectra. Rather, we follow the implicit inversion approach put forward by Mobley and colleagues (Louchard et al. 2003; Mobley et al. 2005; Lesser and Mobley 2007) and Lee and colleagues (Lee et al. 1998, 1999, 2001, 2007). In this approach, above-water spectra are classified directly as combinations of bottom-type, water depth, and water optical properties. The difference is that, in the present case, classifications utilize class covariances and are based on statistical comparison with large samples, whereas the previous workers made single spectrum-to-spectrum comparisons. Thus, classes are not simply *coral*, *algae*, and *sand* but, rather, *coral-at-2-m-depth*, *algae-at-10-m-depth*, and so on.

Classification functions were based on remote-sensing reflectance, defined as

$$R_{rs} = L_w / E_d.$$

The classification functions were built without glint. Two coral reef scenarios were explored separately. Each scenario had coral, algae, and sand at four depths, resulting in 12 classes per scenario and 144 possible classification outcomes, as shown in Table 4.1-1.

Table 4.1-1. Matrix of possible classification outcomes. Cells labeled with a “C” indicate that the outcome is a correct classification. All other outcomes are incorrect classifications.

		ACTUAL CLASSES											
		coral 0.5 m	algae 0.5 m	sand 0.5 m	coral 2 m	algae 2 m	sand 2 m	coral 5 m	algae 5 m	sand 5 m	coral 10 m	algae 10 m	sand 10 m
PREDICTED CLASSES	coral 0.5 m	C											
	algae 0.5 m		C										
	sand 0.5 m			C									
	coral 2 m				C								
	algae 2 m					C							
	sand 2 m						C						
	coral 5 m							C					
	algae 5 m								C				
	sand 5 m									C			
	coral 10 m										C		
	algae 10 m											C	
	sand 10 m												C

The same R_{rs} spectra were used to test the classification. (Resubstitution has the potential to favorably bias the results, but with large data sets such as this, the bias is negligible.) Each spectrum was identified as belonging to one of the 144 outcomes, and the total count in each outcome was tallied in an error matrix similar to Table 4.1-1. Classification rates were calculated by dividing the number of spectra predicted to belong in a given class by the total number of spectra in the actual class (i.e., counts divided by column totals). To simplify interpretation, the 12×12 table was partitioned into nine 4×4 tables, arranged by actual and predicted classes. The idea is to more clearly show rates between the same bottom-type at different depths, as well as to highlight rates of misclassification.

Next, the same classification functions were applied to remote-sensing reflectance with glint, defined as

$$R_{rs,glint} = (L_w + L_g) / E_d.$$

That is, the $R_{rs,glint}$ data were classified using classification functions derived from R_{rs} . The objective is to see how glint impacts the classification. As before, results were tallied, converted to rates, then partitioned into 4×4 tables.

Again, this was done for two coral reef scenarios. The results for scenario #1 (clear water, sun zenith 20° , wind 5 m s^{-1} , sun azimuth 90°) are shown in Tables 4.1-2 and 4.1-3 for R_{rs} and $R_{rs,glint}$, respectively. The results for scenario #2 (turbid water, sun zenith 40° , wind 10 m s^{-1} , sun azimuth 30°) are shown in Tables 4.1-4 and 4.1-5 for R_{rs} and $R_{rs,glint}$, respectively. The complete conditions for each scenario are listed at the top of each table.

Summary interpretations of each table are as follows:

Table 4.1-2: Clear water, small sun zenith angle, no glint. Coral and algae are reasonably well separated. Interestingly, rates of correct classification increase with depth. Most misclassification is between depths within coral or algae, not between coral and algae. There is virtually no confusion with sand.

Table 4.1-3: Clear water, small sun zenith angle, glint. Correct classifications increase in spots and decrease markedly in others. Again, rates of correct classification are high at 10 m. Most confusion appears between 2-m and 5-m depths within coral or algae, not between coral and algae. There is virtually no confusion with sand. It is important to recall that classification functions were trained using glint-free R_{rs} .

Table 4.1-4: Turbid water, large sun zenith angle, no glint. Coral and algae are reasonably well separated to 5 m. At 10 m, coral/algae discrimination fails. Misclassification between algae and coral is higher than clear water (Table 4.1-2), especially at 5 m. There is virtually no confusion with sand.

Table 4.1-5: Turbid water, large sun zenith angle, glint. Coral and algae separation is very similar to the glint-free scenario (Table 4.1-4) to 5 m. At 10 m, coral is misclassified almost entirely as algae. Confusion with sand increases, but not markedly.

Tables are shown separately on the following pages.

Table 4.1-2. Classification rates in percent.

R_{rs} model: L_w / E_d
 wavebands: 405–695 nm at 10 nm intervals
 suspended chl: 0.05 mg m^{-3}
 $a_{CDOM}(440)$: 0 m^{-1}
 suspended sand: 0 g m^{-3}
 sun azimuth wrt along track: 90°
 sun zenith: 20°
 view zenith: 10°
 wind: 5 m s^{-1}

		ACTUAL CLASS						ACTUAL CLASS						ACTUAL CLASS					
		coral 0.5 m	coral 2 m	coral 5 m	coral 10 m			coral 0.5 m	coral 2 m	coral 5 m	coral 10 m			coral 0.5 m	coral 2 m	coral 5 m	coral 10 m		
PREDICTED CLASS	coral 0.5 m	84.3	0	0	0			algae 0.5 m	1.9	0	0	0			sand 0.5 m	0	0	0	0
	coral 2 m	7.7	93.7	0	0			algae 2 m	0.1	1.6	0	0			sand 2 m	0	0	0	0
	coral 5 m	0.1	1	90.5	1.6			algae 5 m	3.3	2.7	2.8	0			sand 5 m	0	0	0	0
	coral 10 m	0.2	0.5	4.7	94.2			algae 10 m	2.4	0.5	2	4.1			sand 10 m	0	0	0	0
		algae 0.5 m	algae 2 m	algae 5 m	algae 10 m			algae 0.5 m	algae 2 m	algae 5 m	algae 10 m			algae 0.5 m	algae 2 m	algae 5 m	algae 10 m		
PREDICTED CLASS	coral 0.5 m	2.1	0	0	0			algae 0.5 m	82	0	0	0			sand 0.5 m	0.1	0	0	0
	coral 2 m	0.1	1.6	0	0			algae 2 m	7.6	89.3	0.4	0			sand 2 m	0	0.1	0	0
	coral 5 m	0	0.2	3.9	0.1			algae 5 m	8.1	8.7	94.7	0.7			sand 5 m	0	0	0.1	0
	coral 10 m	0	0	0.7	6			algae 10 m	0	0	0.1	93.1			sand 10 m	0	0	0	0.1
		sand 0.5 m	sand 2 m	sand 5 m	sand 10 m			sand 0.5 m	sand 2 m	sand 5 m	sand 10 m			sand 0.5 m	sand 2 m	sand 5 m	sand 10 m		
PREDICTED CLASS	coral 0.5 m	0	0	0	0			algae 0.5 m	0	0	0	0			sand 0.5 m	100	0	0	0
	coral 2 m	0	0	0	0			algae 2 m	0	0	0	0			sand 2 m	0	100	0	0
	coral 5 m	0	0	0	0			algae 5 m	0	0	0	0			sand 5 m	0	0	100	0
	coral 10 m	0	0	0	0			algae 10 m	0	0	0	0			sand 10 m	0	0	0	100

Table 4.1-3. Classification rates in percent.

R_{rs} model: $(L_w + L_g) / E_d$
 wavebands: 405–695 nm at 10 nm intervals
 suspended chl: 0.05 mg m^{-3}
 $a_{CDOM}(440)$: 0 m^{-1}
 suspended sand: 0 g m^{-3}
 sun azimuth wrt along track: 90°
 sun zenith: 20°
 view zenith: 10°
 wind: 5 m s^{-1}

		ACTUAL CLASS						ACTUAL CLASS						ACTUAL CLASS			
		coral	coral	coral	coral			coral	coral	coral	coral			coral	coral	coral	coral
		0.5 m	2 m	5 m	10 m			0.5 m	2 m	5 m	10 m			0.5 m	2 m	5 m	10 m
PREDICTED CLASS	coral	95	0.4	0	0	PREDICTED CLASS	algae	1.5	0	0	0	PREDICTED CLASS	sand	0	0	0	0
	coral	0	80.2	0	0		algae	0	0.2	0	0		sand	0	0	0	0
	coral	0.5	15.4	90.8	1.5		algae	0.1	0.5	0.7	0		sand	0	0	0	0
	coral	0	1.6	7.7	97.3		algae	2.9	1.6	0.7	1.1		sand	0	0	0	0
PREDICTED CLASS	algae	3.1	0	0	0	PREDICTED CLASS	algae	96.2	15.5	0	0	PREDICTED CLASS	sand	0.1	0	0	0
	algae	0	3	0	0		algae	0	31.7	0	0		sand	0	0.1	0	0
	algae	0.1	2.1	8	0.2		algae	0.4	47.2	75.1	0.3		sand	0	0	0.1	0
	algae	0	0.3	1.3	9.5		algae	0	0.2	15.5	89.9		sand	0	0	0	0.1
PREDICTED CLASS	sand	0	0	0	0	PREDICTED CLASS	algae	0	0	0	0	PREDICTED CLASS	sand	100	0	0	0
	sand	0	0	0	0		algae	0	0	0	0		sand	0	100	0	0
	sand	0	0	0	0		algae	0	0	0	0		sand	0	0	100	0
	sand	0	0	0	0		algae	0	0	0	0		sand	0	0	0	100

Table 4.1-4. Classification rates in percent.

R_{rs} model: L_w / E_d
 wavebands: 405–695 nm at 10 nm intervals
 suspended chl: 1 mg m^{-3}
 $a_{CDOM}(440)$: 0.3 m^{-1}
 suspended sand: 0.5 g m^{-3}
 sun azimuth wrt along track: 30°
 sun zenith: 40°
 view zenith: 10°
 wind: 10 m s^{-1}

		ACTUAL CLASS						ACTUAL CLASS						ACTUAL CLASS			
		coral 0.5 m	coral 2 m	coral 5 m	coral 10 m			coral 0.5 m	coral 2 m	coral 5 m	coral 10 m			coral 0.5 m	coral 2 m	coral 5 m	coral 10 m
PREDICTED CLASS	coral 0.5 m	93.3	0	0	0	PREDICTED CLASS	algae 0.5 m	4.8	0	0	0	PREDICTED CLASS	sand 0.5 m	0	0	0	0
	coral 2 m	1.2	94.4	0	0		algae 2 m	0.4	4.9	0	0		sand 2 m	0	0	0	0
	coral 5 m	0	0.5	79.8	0		algae 5 m	0	0	18.4	0		sand 5 m	0	0	0	0
	coral 10 m	0	0	0.6	48.2		algae 10 m	0.2	0	0	51.8		sand 10 m	0	0	1.2	0
PREDICTED CLASS	algae 0.5 m	1.5	0	0	0	PREDICTED CLASS	algae 0.5 m	98.4	0	0	0	PREDICTED CLASS	algae 0.5 m	0.1	0	0	0
	coral 2 m	0	2	0	0		algae 2 m	0.1	97.5	0	0		sand 2 m	0	0.1	0	0
	coral 5 m	0	0.1	4.4	0		algae 5 m	0	0.4	91.2	0		sand 5 m	0	0	0.1	0
	coral 10 m	0	0	0.1	8.5		algae 10 m	0	0	2.7	91.3		sand 10 m	0	0	1.5	0.2
PREDICTED CLASS	sand 0.5 m	0	0	0	0	PREDICTED CLASS	sand 0.5 m	0.3	0	0	0	PREDICTED CLASS	sand 0.5 m	99.5	0	0	0
	coral 2 m	0	0	0	0		algae 2 m	0	0	0	0		sand 2 m	0	100	0	0
	coral 5 m	0	0	0	0		algae 5 m	0	0	0	0		sand 5 m	0.2	0	100	0
	coral 10 m	0	0	0	0		algae 10 m	0	0	0	0		sand 10 m	0	0	0	100

Table 4.1-5. Classification rates in percent.

R_{rs} model: $(L_w + L_g) / E_d$
 wavebands: 405–695 nm at 10 nm intervals
 suspended chl: 1 mg m^{-3}
 $a_{CDOM}(440)$: 0.3 m^{-1}
 suspended sand: 0.5 g m^{-3}
 sun azimuth wrt along track: 30°
 sun zenith: 40°
 view zenith: 10°
 wind: 10 m s^{-1}

		ACTUAL CLASS						ACTUAL CLASS						ACTUAL CLASS			
		coral	coral	coral	coral			coral	coral	coral	coral			coral	coral	coral	coral
		0.5 m	2 m	5 m	10 m			0.5 m	2 m	5 m	10 m			0.5 m	2 m	5 m	10 m
PREDICTED CLASS	coral	94	0	0	0	PREDICTED CLASS	algae	3.6	0	0	0	PREDICTED CLASS	sand	0	0	0	0
	coral	2	98.2	0	0		algae	0	0.8	0	0		sand	0	0	0	0
	coral	0	0.9	79.8	0		algae	0	0.1	15	0		sand	0	0	0	0
	coral	0	0	1.4	3.2		algae	0.3	0	0.5	96.7		sand	0	0	3.2	0
PREDICTED CLASS	algae	1.6	0	0	0	PREDICTED CLASS	algae	98.2	0	0	0	PREDICTED CLASS	algae	0.1	0	0	0
	algae	0	4.6	0	0		algae	0	93.8	0	0		algae	0	0.1	0	0
	algae	0	0.1	4	0		algae	0	1.3	86	0		algae	0	0	0.2	0
	algae	0	0	0	0		algae	0	0	6.9	99.6		algae	0	0	2.9	0.4
PREDICTED CLASS	sand	0	0	0	0	PREDICTED CLASS	sand	0.2	0	0	0	PREDICTED CLASS	sand	99.7	0	0	0
	sand	0	0	0	0		algae	0	0	0	0		sand	0	99.7	0	0
	sand	0	0	0	0		algae	0	0	0	0		sand	0.2	0.3	100	0
	sand	0	0	0	0		algae	0	0	0	0		sand	0	0	0	100

Another interpretation approach is to consider that the predicted depth does not matter—only the predicted bottom type matters. This amounts to simply computing the column totals of the 4×4 partitioned tables. Thus, for example, it is possible to see how often *coral-0.5-m* is classified as *coral*. Those results are shown in Figures 4.1-1 and 4.1-2; for brevity, and because there is no problem with its discrimination, sand is not included in the figures.

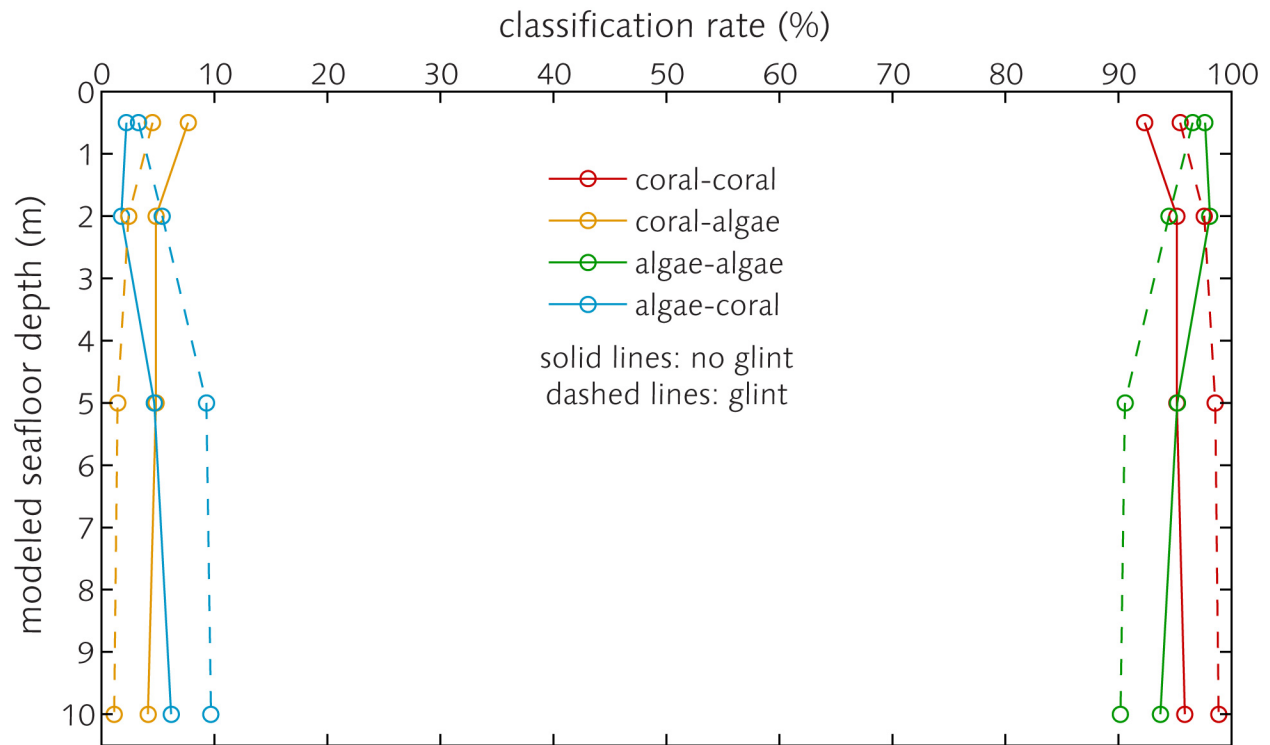


Figure 4.1-1. Classification rates for coral reef scenario #1 (conditions in Tables 4.1-2 and 4.1-3). Values indicate classification rates for specific bottom-type/depth combinations classified as bottom-type at any depth. Thus, for example, *coral-at-0.5-m* is classified as *coral-at-any-depth* approximately 92% of the time. Solid lines show results of R_{rs} modeled without glint (Table 4.1-2). Dashed lines show results of R_{rs} modeled with full glint (Table 4.1-3). Under the given water column and view conditions, glint actually increases the correct classification rate of coral at all depths, but it also increases the misclassification of algae as coral at all depths.

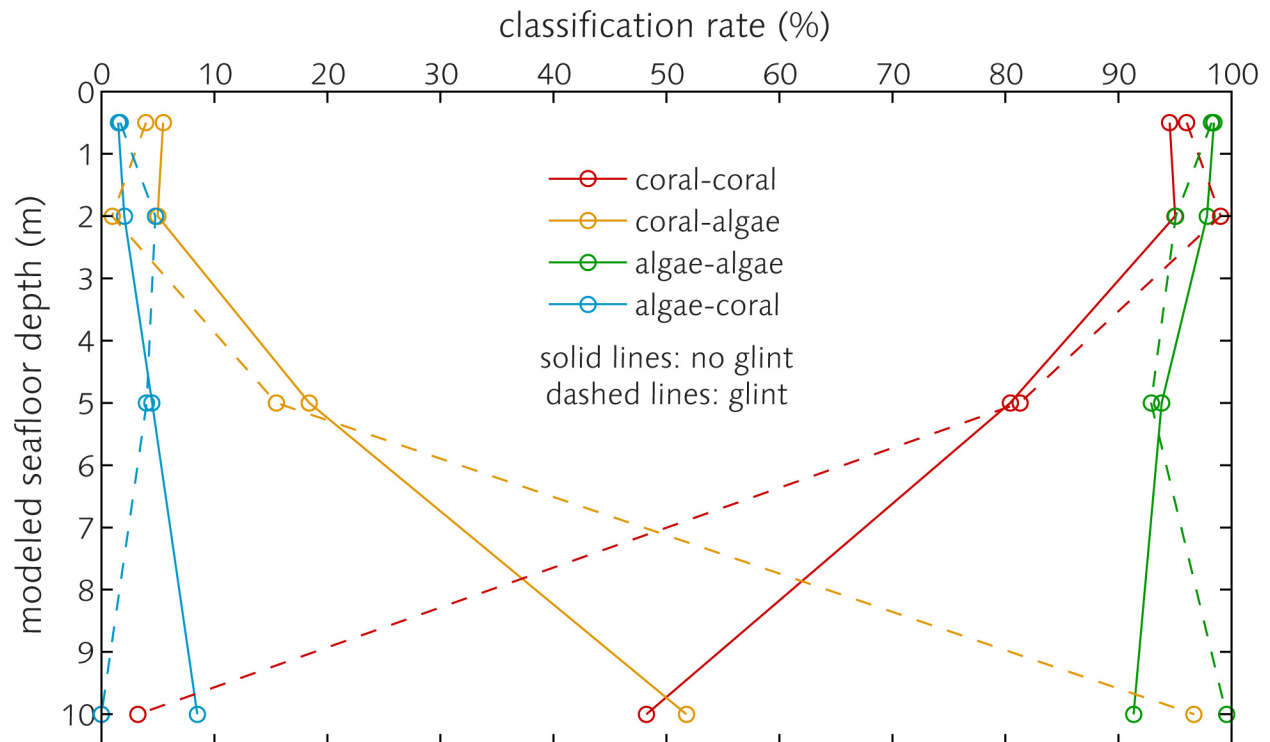


Figure 4.1-2. Classification rates for coral reef scenario #2 (conditions in Tables 4.1-4 and 4.1-5). Values indicate classification rates for specific bottom-type/depth combinations classified as bottom-type at any depth. Thus, for example, *coral-at-0.5-m* is classified as *coral-at-any-depth* approximately 93% of the time. Solid lines show results of R_{rs} modeled without glint (Table 4.1-4). Dashed lines show results of R_{rs} modeled with full glint (Table 4.1-5). Under these more turbid water column conditions, glint increases the correct classification rate of coral at 0.5 and 2 m, but greatly reduces correct coral classifications at 10 m.

The general conclusion, based on these simulations, is that glint does not markedly impact coral reef retrievals. Water clarity (or lack thereof) has a much greater impact.

4.2 Seagrass

Another important aquatic science focus for HypIRI is detection and status of seagrass. In this case, the technical issue for HypIRI reduces to discrimination between seagrass and sand. Since seagrass ecosystems often occur in the same regions as coral reefs, the same modeling approach as in Section 4.1 was used to investigate glint effects on seagrass retrievals. This analysis utilizes reflectance spectra measured *in situ* for sand ($n = 642$) and seagrass ($n = 263$). Results are detailed in Tables 4.2-1 through 4.2-2 on the following pages.

Table 4.2-1. Classification rates in percent.

R_{rs} model: L_w / E_d
 wavebands: 405–695 nm at 10 nm intervals
 suspended chl: 0.05 mg m^{-3}
 $a_{CDOM}(440)$: 0 m^{-1}
 suspended sand: 0 g m^{-3}
 sun azimuth wrt along track: 90°
 sun zenith: 20°
 view zenith: 10°
 wind: 5 m s^{-1}

		ACTUAL CLASS				ACTUAL CLASS			
		seagr 0.5 m	seagr 2 m	seagr 5 m	seagr 10 m	seagr 0.5 m	seagr 2 m	seagr 5 m	seagr 10 m
PREDICTED CLASS	seagr 0.5 m	94.7	0	0	0	0	0	0	0
	seagr 2 m	4.6	97.7	0	0	0	0	0	0
	seagr 5 m	0	1.5	95.8	0.8	0	0	0	0
	seagr 10 m	0.8	0.8	4.2	99.2	0	0	0	0

		ACTUAL CLASS				ACTUAL CLASS			
		sand 0.5 m	sand 2 m	sand 5 m	sand 10 m	sand 0.5 m	sand 2 m	sand 5 m	sand 10 m
PREDICTED CLASS	seagr 0.5 m	0	0	0	0	100	0	0	0
	seagr 2 m	0	0	0	0	0	100	0	0
	seagr 5 m	0	0	0	0	0	0	100	0
	seagr 10 m	0	0	0	0	0	0	0	100

Table 4.2-2. Classification rates in percent.

R_{rs} model: $(L_w + L_g) / E_d$
 wavebands: 405–695 nm at 10 nm intervals
 suspended chl: 0.05 mg m^{-3}
 $a_{CDOM}(440)$: 0 m^{-1}
 suspended sand: 0 g m^{-3}
 sun azimuth wrt along track: 90°
 sun zenith: 20°
 view zenith: 10°
 wind: 5 m s^{-1}

		ACTUAL CLASS				ACTUAL CLASS			
		seagr 0.5 m	seagr 2 m	seagr 5 m	seagr 10 m	seagr 0.5 m	seagr 2 m	seagr 5 m	seagr 10 m
PREDICTED CLASS	seagr 0.5 m	98.9	0	0	0	0	0	0	0
	seagr 2 m	1.1	96.6	0	0	0	0	0	0
	seagr 5 m	0	3.4	100	23.2	0	0	0	0
	seagr 10 m	0	0	0	76.8	0	0	0	0

		ACTUAL CLASS				ACTUAL CLASS			
		sand 0.5 m	sand 2 m	sand 5 m	sand 10 m	sand 0.5 m	sand 2 m	sand 5 m	sand 10 m
PREDICTED CLASS	seagr 0.5 m	0	0	0	0	100	0	0	0
	seagr 2 m	0	0	0	0	0	100	0	0
	seagr 5 m	0	0	0	0	0	0	100	0
	seagr 10 m	0	0	0	0	0	0	0	100

Table 4.2-3. Classification rates in percent.

R_{rs} model: L_w / E_d
 wavebands: 405–695 nm at 10 nm intervals
 suspended chl: 1 mg m^{-3}
 $a_{CDOM}(440)$: 0.3 m^{-1}
 suspended sand: 0.5 g m^{-3}
 sun azimuth wrt along track: 30°
 sun zenith: 40°
 view zenith: 10°
 wind: 10 m s^{-1}

		ACTUAL CLASS				ACTUAL CLASS			
		seagr 0.5 m	seagr 2 m	seagr 5 m	seagr 10 m	seagr 0.5 m	seagr 2 m	seagr 5 m	seagr 10 m
PREDICTED CLASS	seagr 0.5 m	95.4	0	0	0	0	0	0	0
	seagr 2 m	4.6	99.6	0	0	0	0	0	0
	seagr 5 m	0	0.4	97.7	0	0	0	0	0
	seagr 10 m	0	0	1.9	100	0	0	0.4	0

		ACTUAL CLASS				ACTUAL CLASS			
		sand 0.5 m	sand 2 m	sand 5 m	sand 10 m	sand 0.5 m	sand 2 m	sand 5 m	sand 10 m
PREDICTED CLASS	seagr 0.5 m	0	0	0	0	100	0	0	0
	seagr 2 m	0	0	0	0	0	100	0	0
	seagr 5 m	0	0	0	0	0	0	100	0
	seagr 10 m	0	0	0	0	0	0	0	100

Table 4.2-4. Classification rates in percent.

R_{rs} model: $(L_w + L_g) / E_d$
 wavebands: 405–695 nm at 10 nm intervals
 suspended chl: 1 mg m^{-3}
 $a_{CDOM}(440)$: 0.3 m^{-1}
 suspended sand: 0.5 g m^{-3}
 sun azimuth wrt along track: 30°
 sun zenith: 40°
 view zenith: 10°
 wind: 10 m s^{-1}

		ACTUAL CLASS				ACTUAL CLASS			
		seagr 0.5 m	seagr 2 m	seagr 5 m	seagr 10 m	seagr 0.5 m	seagr 2 m	seagr 5 m	seagr 10 m
PREDICTED CLASS	seagr 0.5 m	97	0	0	0	0	0	0	0
	seagr 2 m	3	100	0	0	0	0	0	0
	seagr 5 m	0	0	99.6	0	0	0	0	0
	seagr 10 m	0	0	0.4	100	0	0	0	0

		ACTUAL CLASS				ACTUAL CLASS			
		sand 0.5 m	sand 2 m	sand 5 m	sand 10 m	sand 0.5 m	sand 2 m	sand 5 m	sand 10 m
PREDICTED CLASS	seagr 0.5 m	0	0	0	0	100	0	0	0
	seagr 2 m	0	0	0	0	0	100	0	0
	seagr 5 m	0	0	0	0	0	0	100	0
	seagr 10 m	0	0	0	3	0	0	0	97

The only confusion between seagrass and sand occurs under turbid water conditions at the greatest depth modeled (10 m) with glint included. However, the confusion rate is very small: only 3%. *The general conclusion is that glint does not impact seagrass retrievals, even under turbid water conditions.*

4.3 Station ALOHA Simulation

4.3.1 Forward Modeling

Further HydroMod simulations were performed to investigate the impact of glint on retrieval of suspended chlorophyll concentrations. This exercise was based on very clear oligotrophic oceanic conditions typically encountered at Station ALOHA, north of Oahu, Hawaii. The idea is simply to model conditions at Station ALOHA along the west and east edges of the HypIRI scan-line, then attempt to retrieve subsurface chlorophyll values in the presence of glint, as well as after performing a glint-correction procedure. This represents somewhat of a worst-case scenario in that the target (clear, deep ocean) is very dark, which means that glint reflectance can be greater than the water-leaving reflectance signal.

HydroMod was parameterized as follows:

- Location: Station ALOHA, 22°45'N, 158°W
- Date: June 21
- Sun Azimuth wrt Along Track: 107.78°
- Sun Zenith: 17.99°
- Suspended Chlorophyll: 0.05 $\mu\text{g l}^{-1}$
- Wind Speed: two values modeled, 0 and 10 m s^{-1}
- Atmosphere Conditions: Clear sky with marine aerosols
- Bottom Boundary: Infinitely deep ocean

To generate water column IOPs for HydroLight, the “new Case 1” IOP model in HydroLight v. 5 was used. Atmospheric conditions were modeled as Modtran’s defaults for tropical atmosphere with marine aerosols. The geometry in these HydroMod simulations was similar to the previous glint characterization simulations illustrated in Figures 3.1.2-1 through 3.1.2-4.

The HydroMod runs were chosen to show the extremes of viewing direction (east and west edges of the HypIRI field of view) and wind speed (calm and rough sea surface, $U = 0 \text{ m s}^{-1}$ and $U = 10 \text{ m s}^{-1}$, respectively). The results of these four simulations are shown in Figure 4.3.1-1.

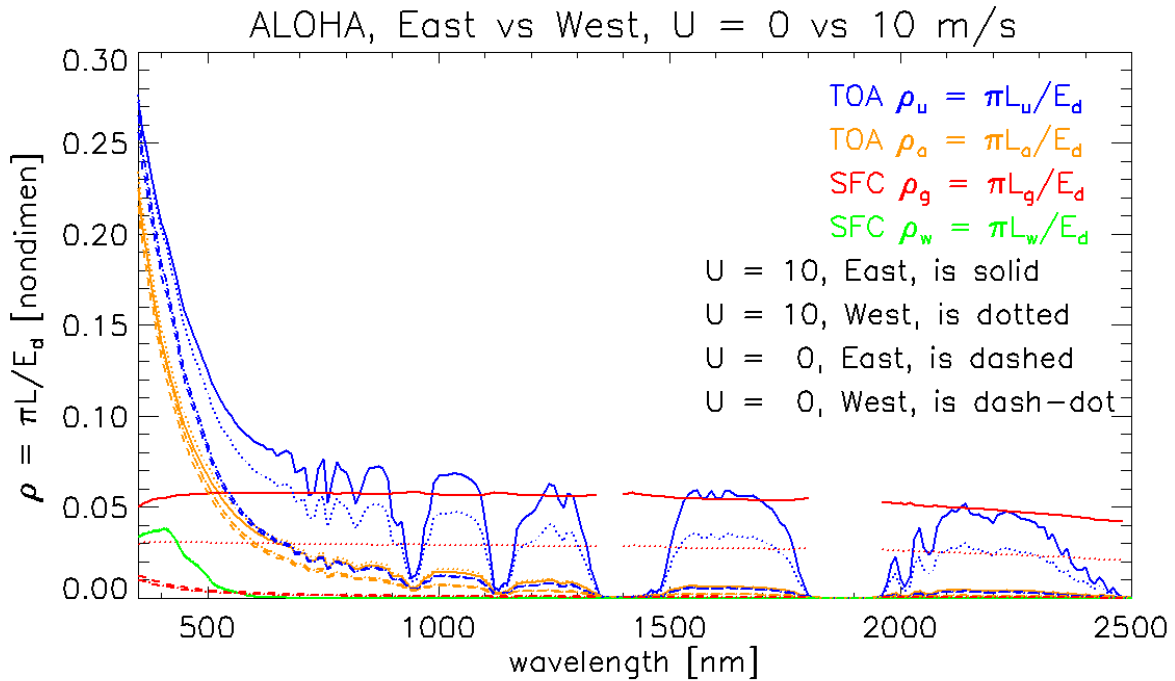


Figure 4.3.1-1. HydroMod simulations for station ALOHA.

There are several notable features in Figure 4.3.1-1. First, the water-leaving reflectances (green lines) at the sea surface are almost indistinguishable because apparent optical properties like ρ_w are insensitive to external environmental conditions such as sun angle and wind speed. The glint reflectances (red) for $U = 0 \text{ m s}^{-1}$ (a level surface) are small and almost identical because these are background sky reflectances with no direct sun glint. However, for $U = 10 \text{ m s}^{-1}$, the glint reflectances are large because the sea surface is rough, which means that some wave facets will produce direct sun glint. The east edge of the HypsIRI field of view (solid red) has roughly twice the glint as the west edge because the east edge is looking closer to the center of the glitter pattern. The surface glint reflectances are not plotted in the opaque atmospheric regions near 1350, 1800, and 2500 nm because the extremely low irradiances reaching the sea surface in these bands makes the Modtran calculations at the sea surface inaccurate. The TOA atmospheric path reflectances (orange) do not depend strongly on the atmospheric path differences in the east vs. west viewing directions (solid vs. dotted and dashed vs. dash-dot curves). However, the atmospheric reflectances do depend somewhat on the wind speed (upper pair of orange curves vs. lower pair) because of differences in the aerosols in the atmosphere, which depend on the 24-hour wind speed. The blue curves show the total TOA reflectances as would be measured by HypsIRI. Note that, as shown previously in Figure 3.1.2-2, the surface ρ_w and ρ_g curves plotted in Figure 4.3.1-1 are not the contributions of ρ_w and ρ_g to the TOA reflectances ρ_u because of atmospheric effects as the surface radiances are transmitted to the TOA.

4.3.2 Radiometric Inversion of Simulation Data

The HydroMod simulation data for Station ALOHA are used to investigate a possible implementation of a glint correction algorithm in a per-pixel atmospheric correction procedure.

The atmosphere-glint correction methodology is described and its application to the simulated data follows below.

Satellite-measured reflectance at the top of the atmosphere (ρ_t) is decomposed as follows:

$$\rho_t = \rho_{atm}^{TOA} + \rho_{glint}^{TOA} + \rho_w^{TOA}, \quad (4.3.2-1)$$

where ρ_{atm}^{TOA} is atmospheric path reflectance; ρ_{glint}^{TOA} is the glint reflectance due to photons reflecting off the sea surface; and ρ_w^{TOA} is the water-leaving radiance contribution to the TOA reflectance (Gao et al. 2000). It is often useful to distinguish the Rayleigh (ρ_r) and aerosol (ρ_a , which includes Rayleigh-aerosol interaction) reflectances since the Rayleigh contribution is estimated with given atmospheric pressure while the aerosol contribution is unknown *a priori*:

$$\rho_{atm}^{TOA} = \rho_r + \rho_a. \quad (4.3.2-2)$$

Direct sun glint at the surface is highly variable, depending on the sea surface slope distribution (or wind speed) and viewing geometry as described in Section 3.1. In contrast, sky glint at the TOA varies depending on atmospheric molecules and aerosols with almost no dependency on the sea surface slope distribution. Sky glint is expected to be much less variable than sun glint, and therefore it can be reasonably estimated using radiative transfer simulations. Taking advantage of this *a priori* estimation of the sky glint contribution, it can be eliminated from the TOA reflectance. To do this, the two glint components are separated:

$$\rho_{glint}^{TOA} = \rho_g^{TOA} + \rho_{sky}^{TOA}. \quad (4.3.2-3)$$

The TOA water-leaving reflectance (ρ_w^{TOA}) is related to the sea surface water-leaving reflectance (ρ_w^{SFC}) as follows (Gao et al. 2000):

$$\rho_w^{TOA} = \frac{\rho_w^{SFC} \cdot T_{gas} \cdot t_d \cdot t_u}{1 - s \cdot \rho_w^{SFC}}, \quad (4.3.2-4)$$

where T_{gas} is a two-way atmospheric gas transmittance; t_d and t_u are the downward and upward transmittances, respectively, due to the atmosphere; and s is the spherical albedo of the atmosphere for upward radiance. Combining the above equations produces

$$\rho_t = \rho_r + \rho_a + \rho_{sky}^{TOA} + \rho_g^{TOA} + \frac{\rho_w^{SFC} \cdot T_{gas} \cdot t_d \cdot t_u}{1 - s \cdot \rho_w^{SFC}}. \quad (4.3.2-5)$$

The goal of the atmosphere-glint correction procedure is to derive ρ_w^{SFC} from ρ_t . All other variables in equation (4.3.2-5) must be determined. Some variables (T_{gas} , ρ_r) are computed by radiative transfer simulations with ancillary inputs such as ozone, water vapor, and atmospheric pressure. Other variables such as ρ_{sky}^{TOA} , t_d , t_u , and s vary with aerosols to a certain degree. These variables are assumed to be known in this exercise; in practice, these may need to be refined by

an iterative approach. The remaining two terms, ρ_a and ρ_g^{TOA} are highly dependent on aerosols and sea surface slope distribution and, therefore, these are key parameters to be determined in the atmosphere-glint correction procedure.

The aerosol and glint retrieval here is performed on wavelengths longer than 1000 nm, then extrapolated to visible wavelengths. At wavelengths longer than 1000 nm, where water-leaving reflectance is negligible, equation (4.3.2-5) reduces to

$$\rho_t - \rho_r - \rho_{sky}^{TOA} = \rho_a + \rho_g^{TOA}. \quad (4.3.2-6)$$

The left-hand side can be easily computed as described above, while the right-hand side (aerosol and glint reflectances) must be derived. A simple approach is given here to spectrally decompose the aerosol and glint contribution. The glint reflectance spectral shape, $G(\lambda)$, and the aerosol reflectance spectral shape, $A(\lambda)$, are defined by normalization at a reference wavelength λ_0 :

$$\rho_a(\lambda) = \rho_{a0} \cdot A(\lambda) \quad \text{and} \quad \rho_g^{TOA}(\lambda) = \rho_{g0} \cdot G(\lambda), \quad (4.3.2-7)$$

where ρ_{a0} and ρ_{g0} are the aerosol and glint reflectances at wavelength, λ_0 . $A(\lambda)$ and $G(\lambda)$ are obtained using radiative transfer simulations. Then, equations (4.3.2-6) and (4.3.2-7) can be solved for ρ_a and ρ_{g0} from two-band data by simple algebraic manipulation. The aerosol and glint reflectances are extrapolated to the visible and subtracted from the total reflectance according to equation (4.3.2-5).

Youngje Park applied the above-described atmospheric-glint correction algorithm to the HydroMod simulated TOA data for the ALOHA-East edge case. Figure 4.3.2-1 shows the input spectra for the atmospheric correction for the ALOHA-East edge, $U = 10 \text{ m s}^{-1}$ simulation, which includes HydroMod-generated TOA reflectance and some pre-computed atmospheric correction variables: Rayleigh reflectance, sky glint reflectance, and aerosol and glint reflectance shapes. The Rayleigh reflectance and the aerosol spectra were computed using MODTRAN5 (Berk et al. 2008) with almost identical input conditions as the forward modeling (see Section 4.3.1) to minimize errors due to differences in the Rayleigh reflectance and aerosol models. All other parameters were computed using the 6Sv1 code (Vermote et al. 1997) with the following input conditions:

- Solar zenith/azimuth: 17.99°/107.78°
- Sensor zenith/azimuth: 2°/-90°
- Atmosphere profile: tropical
- Aerosols: optical thickness 0.2 at 550 nm, maritime model with 70% relative humidity
- Wind speed: 5 m s⁻¹ (different from the forward modeled $U = 10 \text{ m s}^{-1}$)

$A(\lambda)$ and $G(\lambda)$ are different and vary smoothly in the NIR-SWIR range. Aerosol reflectance decreases with wavelength, while glint reflectance is rather flat.

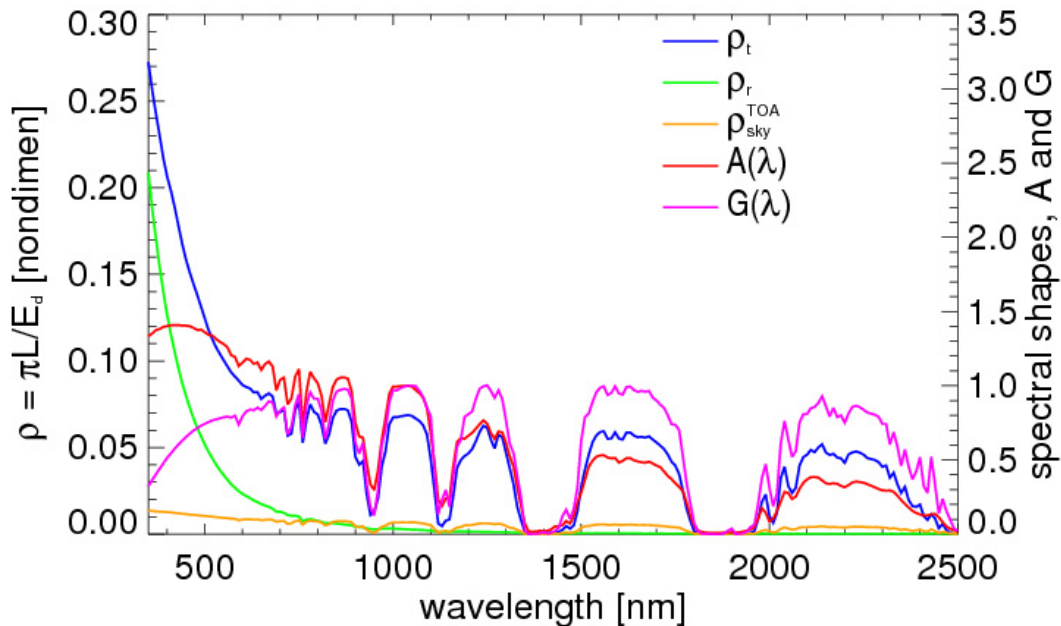


Figure 4.3.2-1. Input spectra for the atmospheric and glint correction for the ALOHA-East edge simulation. HydroMod-generated TOA reflectance (ρ_t), Rayleigh reflectance (ρ_r), sky glint reflectance (ρ_{sky}^{TOA}), and the spectral shape of the aerosol reflectance [$A(\lambda)$] and glint reflectance [$G(\lambda)$]. $A(\lambda)$ and $G(\lambda)$ are normalized at 1040 nm.

Figure 4.3.2-2 shows the glint and aerosol correction for the ALOHA-East, $U = 10 \text{ m s}^{-1}$ simulation. In this high-glint scenario, glint reflectance at 1040 nm is 0.047, which is more than three times that of aerosol reflectance at the same wavelength (0.013). As expected, the sum of the retrieved aerosol and glint reflectances well match the TOA reflectance corrected for Rayleigh and sky glint in the atmospheric transparent windows of the NIR-SWIR spectral range. The difference at visible wavelengths is attributable to the water-leaving reflectance contribution, which is shown in Figure 4.3.2-3. The retrieved water-leaving reflectance compares very well to the true water-leaving reflectance from the HydroMod simulation at the atmospheric window wavelengths.

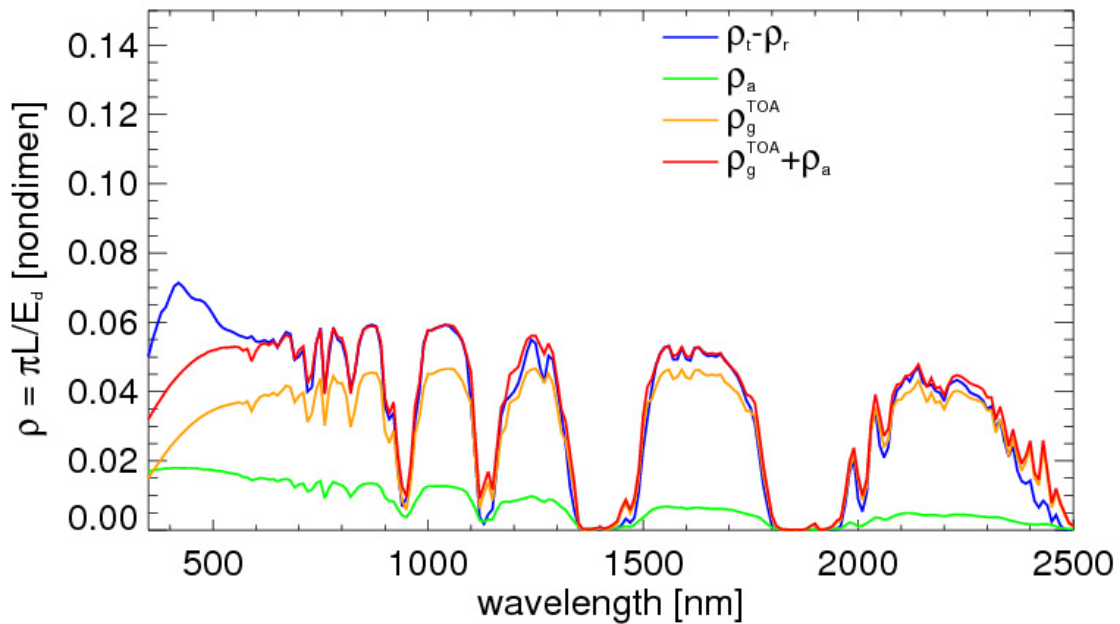


Figure 4.3.2-2. Aerosol and glint correction for the ALOHA-East edge, $U = 10 \text{ m s}^{-1}$ case.

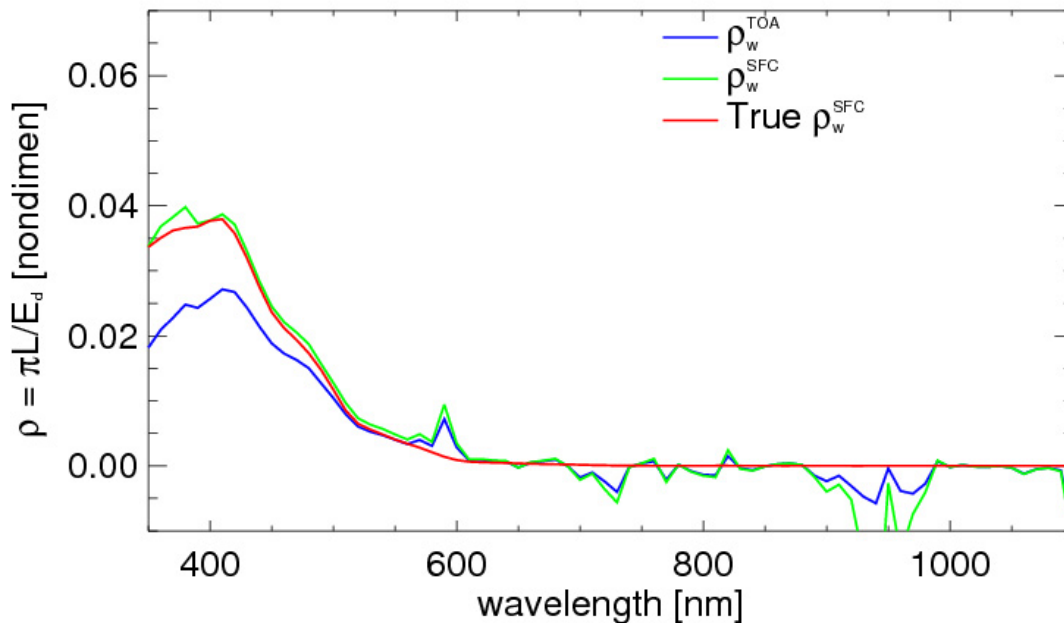


Figure 4.3.2-3. Water-leaving reflectance spectra for the ALOHA-East edge, $U = 10 \text{ m s}^{-1}$ case, including retrieved TOA spectrum (ρ_w^{TOA}), retrieved surface spectrum (ρ_w^{SFC}), and true surface spectrum.

For comparability, comparisons of water-leaving reflectance between true and retrieved are provided for other three cases in Figures 4.3.2-4 through 4.3.2-6. The ALOHA-West edge, $U = 10 \text{ m s}^{-1}$ case (Figure 4.3.2-4) again shows an excellent retrieval of water-leaving reflectance. However, two $U = 0 \text{ m s}^{-1}$ cases (Figures 4.3.2-5 and 4.3.2-6) show significantly higher retrievals

of the water-leaving reflectance in the visible range. The $U = 0 \text{ m s}^{-1}$ cases represent sun-glint-free conditions with a flat ocean surface. The estimated sun glint (not shown here) is zero for both cases. The errors are presumably due to incorrect computations of the Rayleigh reflectance, the aerosol reflectance shape, or a combination of the two.

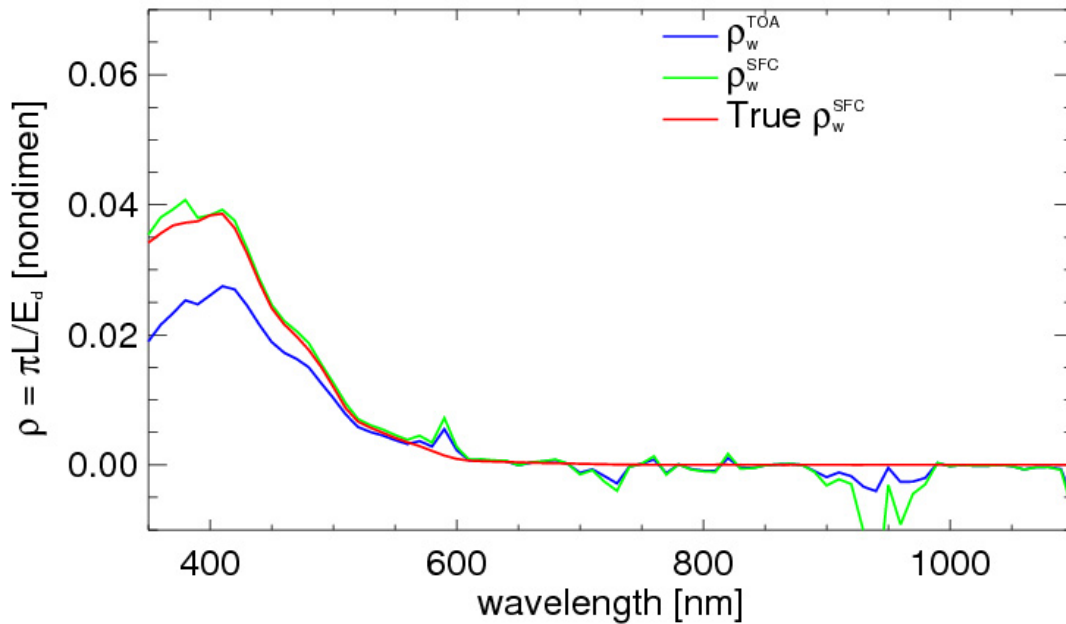


Figure 4.3.2-4. Water-leaving reflectance spectra for the ALOHA-West edge, $U = 10 \text{ m s}^{-1}$ case, including retrieved TOA spectrum (ρ_w^{TOA}), retrieved surface spectrum (ρ_w^{SFC}), and true surface spectrum.

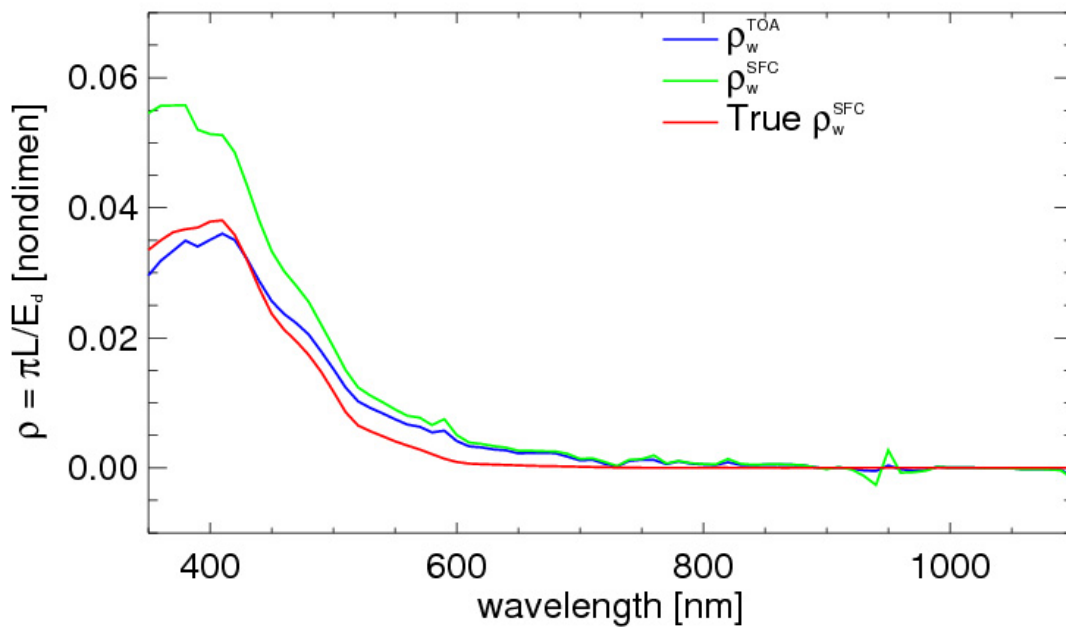


Figure 4.3.2-5. Water-leaving reflectance spectra for the ALOHA-East edge, $U = 0 \text{ m s}^{-1}$ case, including retrieved TOA spectrum (ρ_w^{TOA}), retrieved surface spectrum (ρ_w^{SFC}), and true surface spectrum.

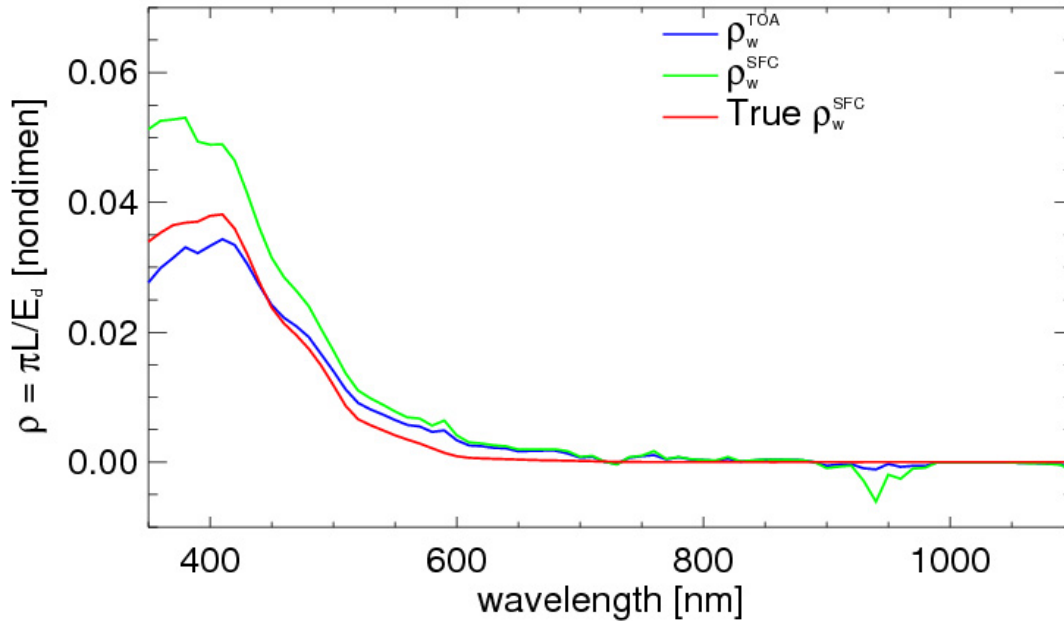


Figure 4.3.2-6. Water-leaving reflectance spectra for the ALOHA-West edge, $U = 0 \text{ m s}^{-1}$ case, including retrieved TOA spectrum (ρ_w^{TOA}), retrieved surface spectrum (ρ_w^{SFC}), and true surface spectrum.

This atmosphere-glint correction exercise for the Station ALOHA simulation demonstrates that a glint correction technique can be implemented systematically on a per-pixel basis, coupled with an atmospheric correction procedure. This glint correction relies on the separation of the TOA glint reflectance from the aerosol reflectance. Successful glint correction therefore requires accurate estimation of the spectral shape of aerosol reflectance and the Rayleigh reflectance.

4.3.3 Estimating Chlorophyll from Simulated and Inverted Data

Standard ocean color algorithms OC4 (SeaWiFS) and OC3M (MODIS) were applied to the forward-modeled radiance and inverted water-leaving reflectance data. To produce appropriate wavebands for use in OC4, HydroMod output and radiometrically inverted spectra at 10-nm intervals was spline-interpolated to 1-nm intervals then convolved with SeaWiFS relative spectral response (oceancolor.gsfc.nasa.gov/DOCS/RSR/SeaWiFS_RSRs.txt). To produce appropriate wavebands for use in OC3M, HydroMod output and radiometrically inverted spectra at 10-nm intervals was spline-interpolated to 1-nm intervals then convolved with MODIS Aqua relative spectral response (oceancolor.gsfc.nasa.gov/DOCS/RSR/Aqua_RSRs.txt).

To explore the impact of glint on chlorophyll retrievals, varying proportions of surface glint radiance were added to the water-leaving reflectance values (only for the HydroMod forward-modeled simulation data). For forward-modeled data, remote-sensing reflectance (R_{rs}) was calculated as

$$R_{rs} = (L_w + xL_g) / E_d, \quad (4.3.3-1)$$

where L_w is water-leaving radiance computed by HydroMod; L_g is glint radiance computed by HydroMod; E_d is downwelling plane irradiance computed by HydroMod; and x is the proportion of glint radiance included in the calculation, varying between 0 and 1. For the radiometrically inverted data, nondimensional reflectance values were divided by a factor of π to produce remote-sensing reflectance (R_{rs}) in units of sr^{-1} .

Table 4.3.3-1 lists chlorophyll values retrieved from the HydroMod simulation data, both for OC4 and OC3M. For detailed explanation of model runs, see Section 4.3.1. The concentration of suspended chlorophyll used in the forward model was 0.05 mg m^{-3} , a typical value at Station ALOHA. The values are plotted in Figure 4.3.3-1.

Table 4.3.3-1. Chlorophyll values (mg m^{-3}) retrieved using OC4 and OC3M algorithms applied to R_{rs} modeled by HydroMod for conditions at Station ALOHA on June 21. Values for x refer to proportion of glint included in calculation of $R_{rs} = (L_w + xL_g) / E_d$. Actual chlorophyll concentration used in HydroMod bio-optical model is 0.05 mg m^{-3} .

Algorithm	Edge	$U \text{ (m s}^{-1}\text{)}$	Value of x in $R_{rs} = (L_w + xL_g) / E_d$				
			0.0	0.25	0.5	0.75	1.0
OC4	West	0	0.066	0.081	0.094	0.106	0.117
OC4	East	0	0.065	0.084	0.101	0.115	0.128
OC4	West	10	0.065	0.22	0.355	0.484	0.603
OC4	East	10	0.064	0.354	0.613	0.833	1.013
OC3M	West	0	0.063	0.077	0.089	0.101	0.111
OC3M	East	0	0.063	0.08	0.095	0.109	0.122
OC3M	West	10	0.062	0.21	0.337	0.454	0.559
OC3M	East	10	0.062	0.336	0.567	0.754	0.903

Even with no glint, OC4 and OC3M overestimate chlorophyll by 20%: retrievals are $\sim 0.06 \text{ mg m}^{-3}$. This is likely because HydroMod, OC4 and OC3M all rely on empirical best fits of various data sets to relate chlorophyll to absorption and scattering (HydroMod) or to R_{rs} (OC4, OC3M). Thus, the observed 20% error reflects that the IOP models and retrieval algorithms are based on different data sets, for which the optical properties were different for the same chlorophyll values.

The retrieval does vary with wind speed and position on the HypsIRI scan line. When wind speed is zero, there is not much difference in retrievals between the west and east edges of the scan line. When wind speed is 10 m s^{-1} , there is strong dependency on position in the scan line. Although angles associated with the west end of the swath perform better than those associated with the east edge, providing about half as large an overestimate, only in the zero-wind-speed cases do chlorophyll overestimates in the presence of large glint contributions stay within $\sim 2\times$ the glint-free estimate. Therefore, an effective glint correction (or some fundamentally different, full-spectral algorithm) would be required for accurate chlorophyll retrievals under all wind conditions and would be especially important in the presence of moderate-to-high wind speeds. This result differs from bottom-type discrimination, which appears more robust to glint than turbidity and worked well under a range of view-illumination geometries and water depths relevant to the HypsIRI concept (see Sections 4.1 and 4.2). A useful feature of the observed retrievals is that consistent systematic gradients across the HypsIRI VSWIR swath in chlorophyll estimated by these algorithms (i.e., higher means and/or variances towards the east edge), in the

presence of light-to-moderate winds, might provide an indicator of ineffective or incomplete glint removal.

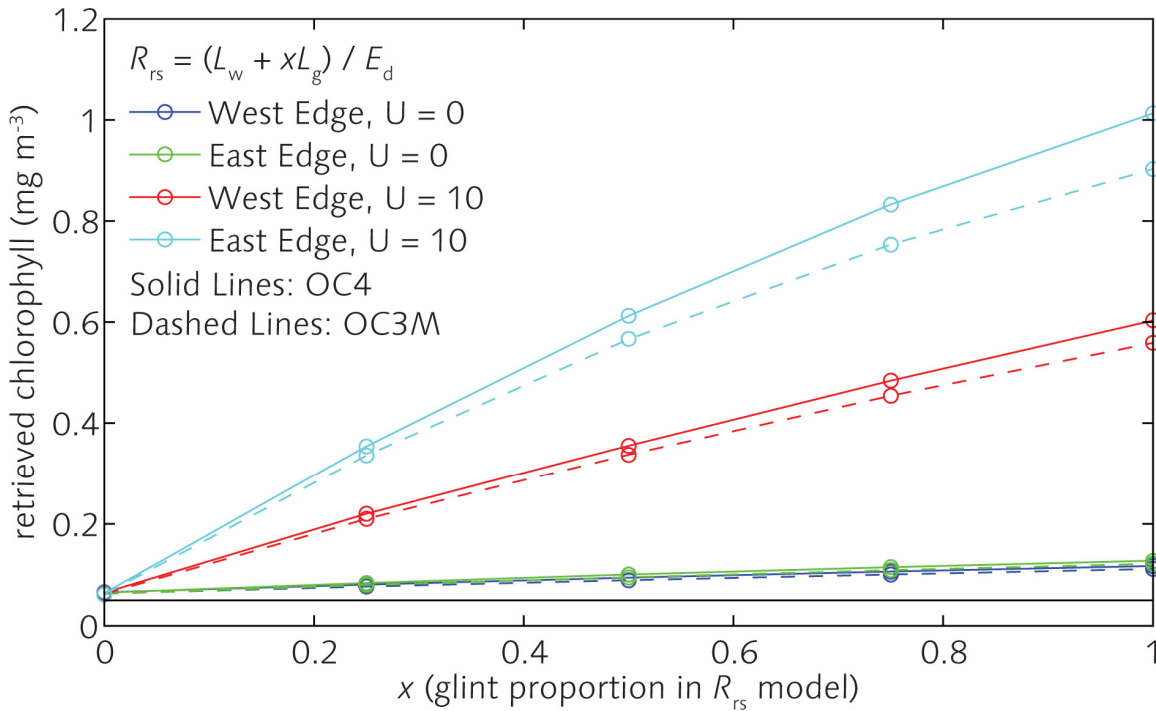


Figure 4.3.3-1. Chlorophyll values retrieved using OC4 (solid lines) and OC3M (dashed lines) algorithms, as applied to R_{rs} modeled by HydroMod for conditions at Station ALOHA on June 21. Horizontal black line is 0.05 mg m^{-3} , the chlorophyll value used in HydroMod’s Case 1 bio-optical model.

Figure 4.3.3-2 shows ρ_w^{SFC} as retrieved in Section 4.3.2. When the modeled wind speed is 10 m s^{-1} , the inverted ρ_w^{SFC} closely matches the “true” ρ_w^{SFC} for both the west and east edges of the HypIRI field of view. For the no-wind condition, however, inversion results overestimate “true” ρ_w^{SFC} by almost 0.02 (nondimensional reflectance units) at blue wavelengths, also for both the west and east edges of the HypIRI field of view. This indicates that the coupled atmosphere-glint correction procedure noticeably under-corrects glint for the zero-wind case.

Table 4.3.3-2 lists the retrieved chlorophyll values using OC4 and OC3M and the inverted ρ_w^{SFC} spectra shown in Figure 4.3.3-2. For the zero-wind scenario, both algorithms significantly overestimate suspended chlorophyll concentrations, while for the 10 m s^{-1} wind scenario, retrievals are closer to “truth.”

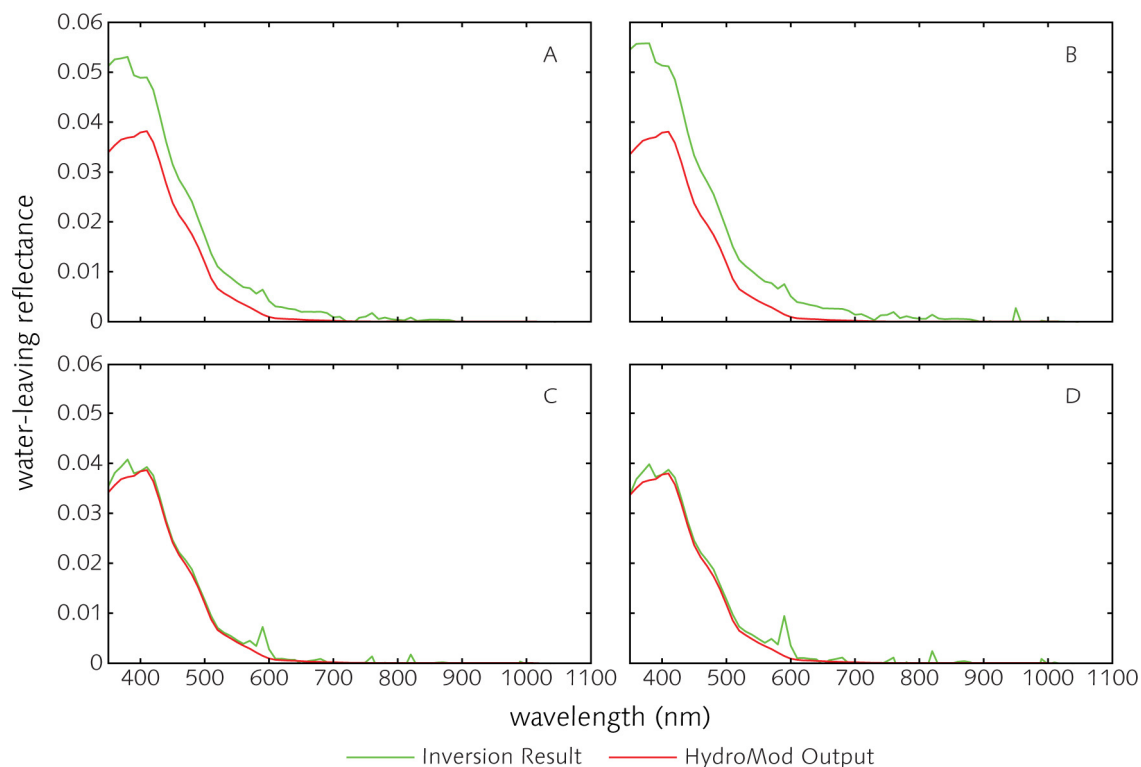


Figure 4.3.3-2. Radiometrically inverted, water-leaving reflectance spectra for Station ALOHA June 21 simulation. (A) West edge of HypSIIRI field of view, $U = 0 \text{ m s}^{-1}$; (B) east edge, $U = 0 \text{ m s}^{-1}$; (C) west edge, $U = 10 \text{ m s}^{-1}$; and (D) east edge, $U = 10 \text{ m s}^{-1}$.

Table 4.3.3-2. Chlorophyll values (mg m^{-3}) retrieved using OC4 and OC3M algorithms applied to R_{rs} data derived from Figure 4.3.3-2. Actual chlorophyll concentration used in HydroMod bio-optical model is 0.05 mg m^{-3} .

Edge	$U (\text{m s}^{-1})$	Algorithm	
		OC4	OC3M
West	0	0.12	0.12
East	0	0.14	0.13
West	10	0.08	0.07
East	10	0.08	0.08

4.4 Emergent Vegetation and Coastal Wetlands

For coastal emergent vegetation, the glint issue becomes much more complex. For example, in salt marshes, tidal emergent vegetation is typically erectophile, with small pools of water interspersed (Figure 4.4-1). At higher tides, water encroaches on the vegetation itself, such that the soil becomes submerged, but the blades of marsh grass remain subaerial. In these systems, glint undoubtedly contributes to the remotely sensed signal and, as in open waters, the effect varies with sun and view angles. However, suitable models or measurement techniques have yet to be developed to quantify this effect.



Figure 4.4-1. Examples of salt marsh vegetation and interspersed water in Fishing Bay Wildlife Management Area, Maryland. Two species of salt marsh grass are labeled. Photos: K. Turpie.

Qualitatively, it is possible to infer glint effects from multi-angle satellite images acquired by CHRIS/Proba. Figure 4.4-2 illustrates an example of glint in the wetlands shown in Figure 4.4-1. With a nominal view zenith angle of 0° , glint is visually apparent in water bodies amongst the vegetated areas (Figure 4.4-2a). This glint is likely caused by capillary waves patterned by the local wind field. With a nominal view zenith angle of 55° , glint is much less visually apparent (Figure 4.4-2b).

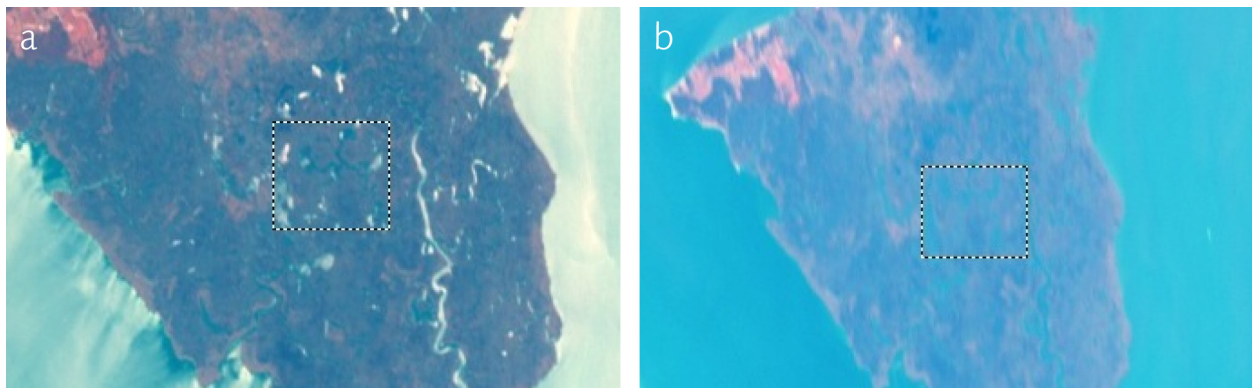


Figure 4.4-2. Multi-angle CHRIS/Proba images of Fishing Bay Wildlife Management Area, Maryland. (a) At 0° nominal view, zenith-angle glint is visually apparent on water bodies interspersed amongst subaerial vegetation. (b) At 55° nominal view, zenith-angle glint is much less apparent. Boxes cover the same ground area in (a) and (b). This region is extracted for statistics shown in Figure 4.4-3.

These visual glint patterns are supported by sample spectra. For the same region of wetland, the 0° nominal view angle spectra (Figure 4.4-3a) have higher values and are more variable than the 55° view angle spectra (Figure 4.4-3b).

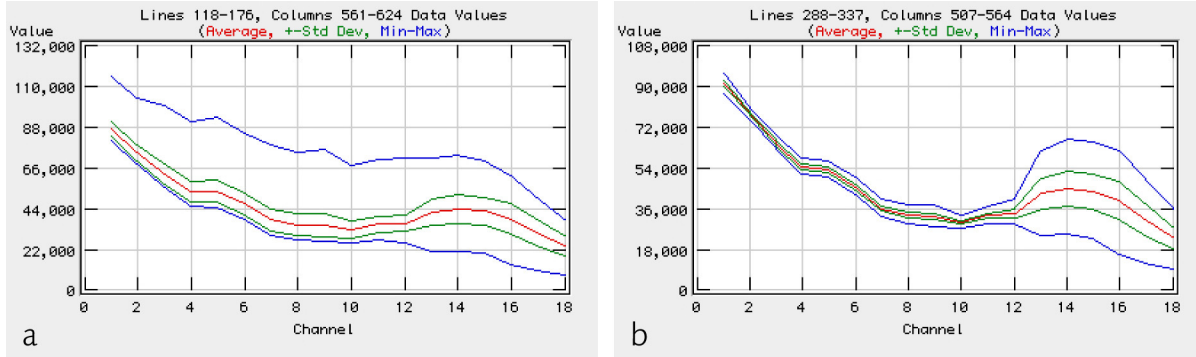


Figure 4.4-3. Spectra extracted from regions highlighted by boxes in Figure 4.4-2. (a) At 0° nominal view zenith angle, glint produces very high values across the spectrum, evidenced by the maximum spectral curve. (b) At 55° nominal view zenith angle, the glint effect is greatly reduced.

The impact of glint on emergent vegetation retrievals is unknown. Because this vegetation is subaerial, NIR and SWIR wavebands are viable for detection and characterization. This may help offset glint effects that would otherwise negatively impact retrievals based solely on VIS wavebands. The issue of emergent vegetation is possibly the most in need of focused investigation.

4.5 Summary

Results from two basic HypIRI science objectives, to investigate glint impacts on retrievals for coral reefs and seagrass, showed that expected levels of glint do not appear to dramatically affect classification retrievals. Glint has the greatest impact when retrieval conditions are already marginal, for example, when water column optical properties limit penetration depth. Potential for improvement via mitigation for glint was not investigated.

For the open ocean, with very low suspended chlorophyll levels, it is clear that glint correction must be tied to correction for atmospheric aerosols. Thus, both are fundamental requirements for accurate retrieval of spectral remote-sensing reflectance.

The situation is less clear for glint effects in emergent vegetation. Measurement and modeling capabilities for these systems lag those for shallow and deep oceans. At the same time, emergent vegetation has the benefit of usefully observable NIR and SWIR spectral features.

5 Mitigation Options

5.1 Avoidance

Avoidance is the simplest method for mitigation of glint impacts, and it is the method of choice in operational ocean color. It is a viable option for this application because ocean color satellites have very wide fields of view and very short revisit times. As a result, any portions of imagery that exhibit significant glint can merely be ignored, then re-imaged on subsequent satellite overpasses.

Nearshore and benthic applications typically require higher spatial resolution than do scientific efforts to assess deep-ocean, offshore aquatic reflectance for the purpose of estimating inherent and apparent optical properties and parameters such as chlorophyll concentration from ocean color, i.e., 1–100 m vs. 1 km. The higher spatial resolution required closer to shore is offset by narrower fields of view and longer revisit times. The data rate for a given area of Earth surface is much lower, and it is generally not possible to ignore image data that exhibit glint effects. Thus, glint avoidance is a luxury not often afforded to nearshore and benthic applications.

Several glint correction techniques have been proposed in the peer-reviewed literature. Virtually all of them rely on the NIR to derive glint levels in the VIS. The following subsections describe the general basis for a few of these techniques.

5.2 NIR-VIS Empirical Linear Relationships

Upwelling radiance just above the sea surface $L_u(\lambda)$ is the sum of the water-leaving radiance $L_w(\lambda)$ and the glint radiance $L_g(\lambda)$:

$$L_u(\lambda) = L_w(\lambda) + L_g(\lambda). \quad (5.2-1)$$

At NIR wavelengths, especially those longer than ~900 nm, water-leaving radiance is negligible due to very strong absorption by water (see Figure 2-1), such that

$$L_w(\text{NIR}) \approx 0. \quad (5.2-2)$$

Thus, for NIR wavelengths, equation (5.2-1) reduces to

$$L_u(\text{NIR}) \approx L_g(\text{NIR}). \quad (5.2-3)$$

Because the index of refraction of water is nearly identical at VIS and NIR wavelengths (see Section 2), the relative amount of downwelling radiance reflected upward is solely a function of geometry and is independent of wavelength (see Section 3). $L_g(\text{VIS})$ and $L_g(\text{NIR})$ have very strong positive correlation.

If there are several remote-sensing pixels, each with the same $L_w(\lambda)$, then variability in $L_u(\lambda)$ is equivalent to variability in $L_g(\lambda)$. For NIR wavelengths, this situation arises *a priori* through equation (5.2-3). For VIS wavelengths, this situation arises when the underwater light field is the

same for each of the given pixels, as might occur for a small area of optically deep water. The slope $\beta_1(L_u)$ of the least-squares linear regression line of $L_u(\text{VIS})$ on $L_u(\text{NIR})$ is

$$\beta_1(L_u) = r(L_u) \times s[L_u(\text{VIS})] \div s[L_u(\text{NIR})], \quad (5.2-4)$$

where $r(L_u)$ is the correlation coefficient between $L_u(\text{VIS})$ and $L_u(\text{NIR})$, and s refers to the sample standard deviation. Because the variability in $L_u(\lambda)$ is equivalent to the variability in $L_g(\lambda)$, $s[L_g(\text{VIS})] = s[L_u(\text{VIS})]$, and $s[L_g(\text{NIR})] = s[L_u(\text{NIR})]$. Thus, the slope $\beta_1(L_g)$ of the least-squares linear regression line of $L_g(\text{VIS})$ on $L_g(\text{NIR})$ is

$$\beta_1(L_g) = r(L_u) \times s[L_u(\text{VIS})] \div s[L_u(\text{NIR})]. \quad (5.2-5)$$

$L_g(\text{VIS})$ is related to $L_g(\text{NIR})$ by

$$L_g(\text{VIS}) = \beta_1(L_g) \times L_g(\text{NIR}). \quad (5.2-6)$$

Once $\beta_1(L_g)$ has been determined for the few pixels where $L_w(\lambda)$ is constant, it is applicable to the entire scene. $L_w(\text{VIS})$ for the entire scene is determined by substitution of equation (5.2-6) into equation (5.2-1):

$$L_w(\text{VIS}) = L_u(\text{VIS}) - \beta_1(L_g) \times L_g(\text{NIR}). \quad (5.2-7)$$

Figure 5.2-1 shows regression lines for three VIS wavebands against a NIR waveband for an AVIRIS scene of French Frigate Shoals, Hawaii (f000418t01p03_r01). Figure 5.2-2 shows the scene before and after application of equation (5.2-7). The yellow box highlights the deep-ocean region from which glint statistics were derived.

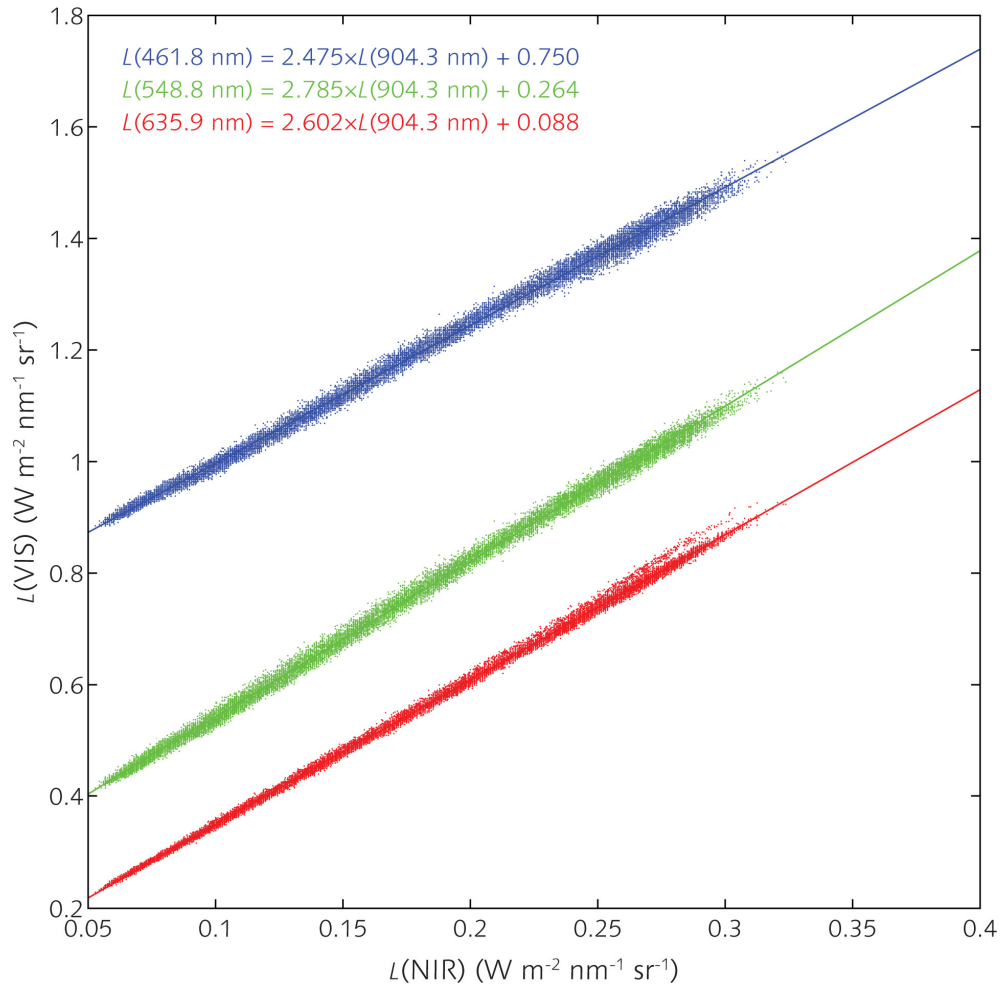


Figure 5.2-1. Empirical linear relationships between three VIS wavebands and a NIR waveband for the AVIRIS scene shown in Figure 5.2-2.

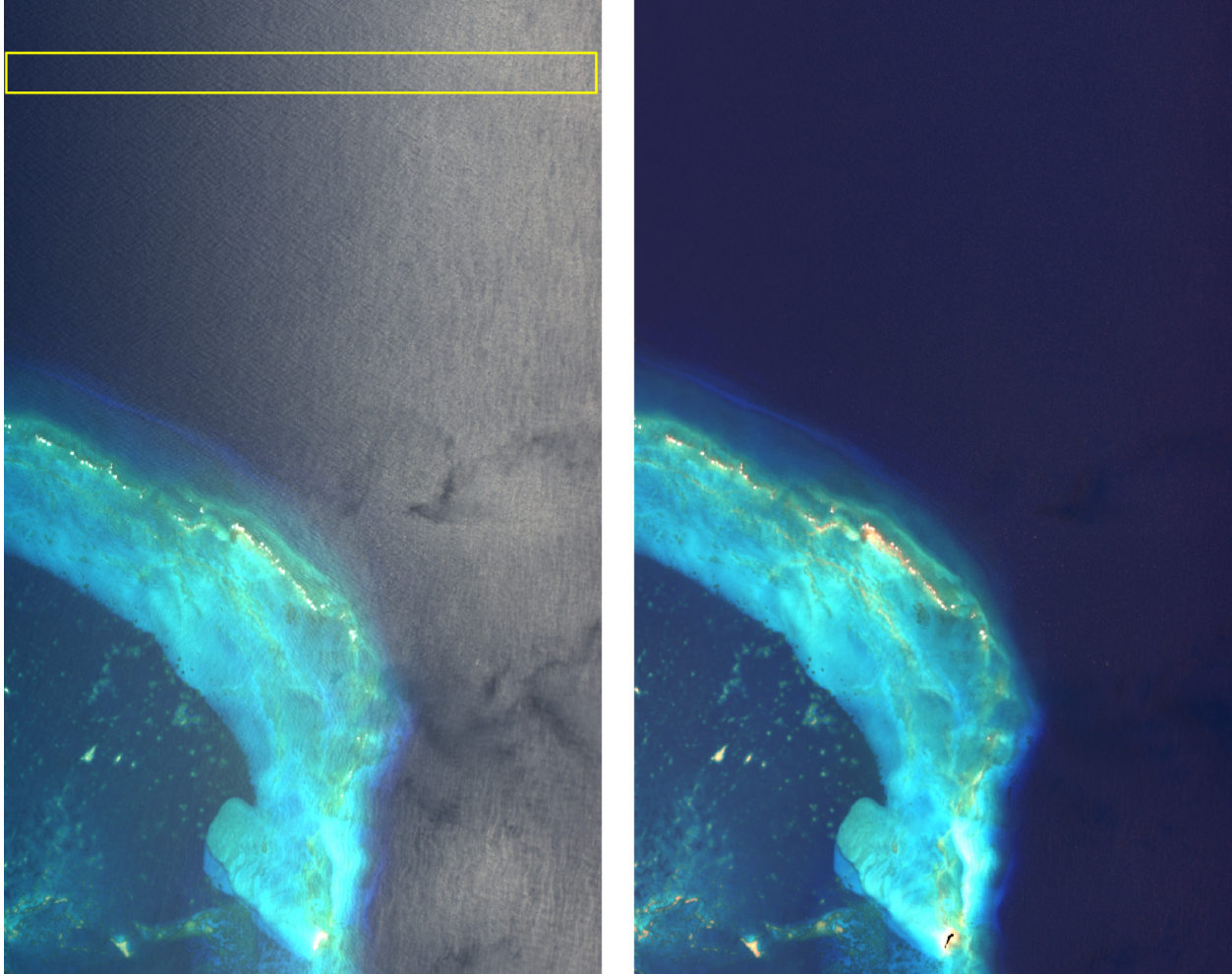


Figure 5.2-2. AVIRIS scene f000418t01p03_r01 covering the southeast portion of French Frigate Shoals, Hawaii and surrounding deep ocean. Image is rotated so that north is to the left of the scene. (Left) Original scene shows very strong glint effects. The yellow box highlights the region from which empirical linear relationships in Figure 5.2-1 were derived. (Right) The scene after application of equation (5.2-7). Glint effects are very effectively removed.

5.3 Subtraction of NIR Reflectance

Another empirical approach to correcting for glint effects makes use of the fact that glint reflectance is nearly spectrally flat throughout the VIS and NIR regions of the spectrum. Following Gao et al. (1993, 2000, 2007), the remote sensing imagery is first converted to TOA apparent reflectance and corrected for atmospheric effects. The result of the atmospheric correction is apparent reflectance at the sea surface. Because of the relationship in equation (5.2-2), any reflectance value at NIR wavelengths must arise from glint. Because glint reflectance is the same at VIS and NIR wavelengths, the NIR-derived glint reflectance can simply be subtracted from the VIS reflectance, leaving a de-glintoned scene. Figure 5.3-1 shows an example of the de-glintoning result.

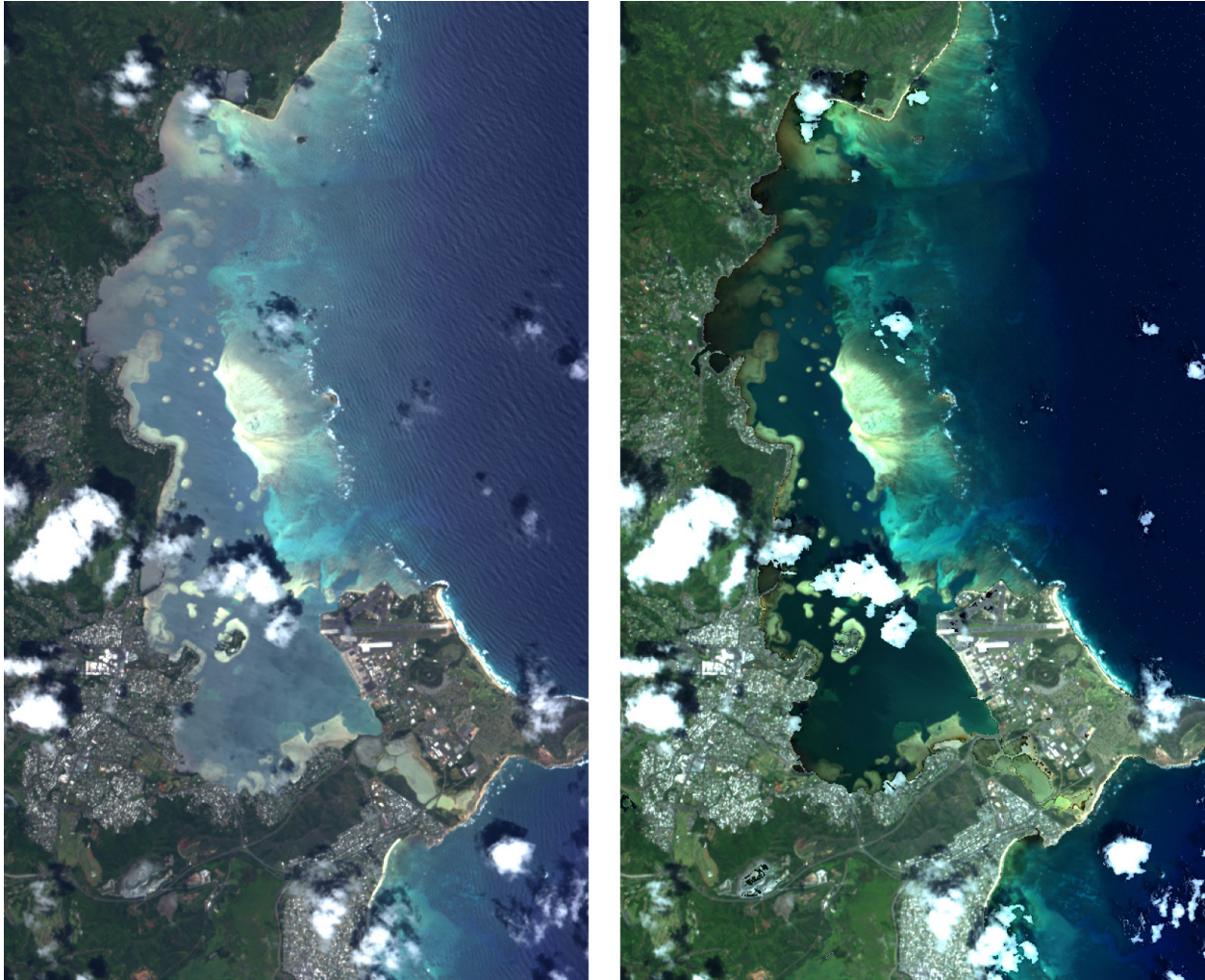


Figure 5.3-1. Example of glint correction using subtraction of NIR reflectance. (Left) Original AVIRIS scene of Kaneohe Bay, Hawaii (f000412t01p03_r08). (Right) The scene after atmosphere and glint correction. Clouds and some sea surface features remain; this is due to automated masking. Overall, glint correction performs quite well.

5.4 Uniform Spectral Offset Approach

Goodman and Ustin (2007) and Goodman et al. (2008) describe a slightly modified version of the approach in Section 5.3. The algorithm is implemented following atmospheric correction using values of surface remote-sensing reflectance (R_{rs} , units sr^{-1}). A uniform spectral offset is calculated for each pixel such that the resulting reflectance at 750 nm is equal to a derived constant, Δ . Rather than assuming the same offset applies for all pixels or that reflectance is zero at all wavelengths greater than 750 nm, the offset in this algorithm allows reflectance to be greater than zero in areas of optically shallow water with bright substrates (e.g., sand). Using the reflectance output generated from atmospheric correction, $R_{rs}^*(\lambda)$, the sun-glint corrected surface reflectance, $R_{rs}(\lambda)$, is calculated as

$$R_{rs}(\lambda) = R_{rs}^*(\lambda) - R_{rs}(750) + \Delta, \quad (5.4-1)$$

where

$$\Delta = 0.00019 + 0.1[R_{rs}^*(640) - R_{rs}^*(750)]. \quad (5.4-2)$$

5.5 Glint-Aerosol Discrimination

The objective of this approach is simultaneous determination of the aerosol and glint components from the TOA reflectance spectrum itself. This approach would fit an automated pixel-by-pixel atmospheric correction procedure as outlined in Section 4.3. The spectral decomposition relies on the distinct shapes of the TOA glint and aerosol reflectance spectra in the NIR-SWIR bands. Aerosol reflectance has a steeper slope, while glint reflectance is rather flat across NIR-SWIR wavelengths.

The preliminary inversion of modeled Station ALOHA TOA spectra in Section 4.3 demonstrates the approach using two SWIR bands and a constant aerosol model. Results are promising, but further investigation is necessary. It would be especially useful to develop a model that can accommodate aerosol variability. Figure 5.5-1 shows variability in spectral shapes of aerosol reflectance simulated using 6S code (Vermeete et al. 1997; Kotchenova et al. 2006) for three aerosol types for the Station ALOHA geometry used in Section 4.3. Since the variability primarily arises due to different aerosol types, the aerosol slope (or model) should also be retrieved in the glint-aerosol separation step. To retrieve three parameters—aerosol intensity, glint intensity, and aerosol slope—three or more bands are required for spectral decomposition. Least squares error optimization could be employed to find a matched spectrum.

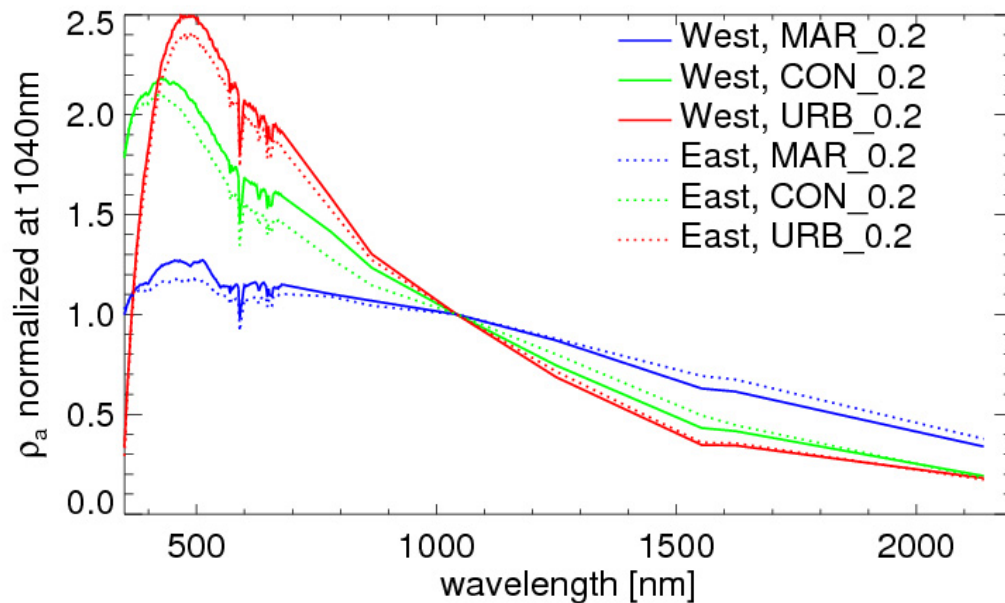


Figure 5.5-1. Variability of the aerosol reflectance spectral shapes. Computation was made using 6S code for three aerosol types—maritime, continental and urban. Aerosol optical thickness is 0.2 at 550 nm. Sun-sensor geometries are the same as ALOHA simulations in Section 4.3. For wavelengths >700nm, only atmospheric transparent window channels are shown for clarity.

6 Recommendations

6.1 Algorithms Showing Promise

The literature and the examples from Section 5 demonstrate that glint correction is feasible. The examples in Section 4 further demonstrate that key HypsIRI science objectives are achievable even in the presence of glint. Therefore, it is very reasonable to deduce that active glint correction can be a part of a successful HypsIRI processing flow; that is, glint avoidance is unnecessary, except possibly in the most extreme cases.

Each of the approaches described in Sections 5.2, 5.3, 5.4 and 5.5 has good potential for routine glint correction. Each also requires further refinement. The Empirical Linear Relationship (Section 5.2) method is insensitive to spectral variations in the reflectance of the sea surface and thus provides very good glint correction. However, in its current form, this method relies on human interaction to identify image regions of constant $L_w(\lambda)$. This precludes automated implementation. The remaining correction methods are all fully automated, so they are more readily implemented in an automated processing flow. However, they all rely on the assumption that sea surface reflectance is spectrally flat across the VIS–NIR. This assumption is valid only to first-order; deviations result in over- or under-correction. The deviations, though, would arise from differences in the index of refraction of seawater, the spectral shape of which is predictable. Thus, it should be possible to refine these methods to provide consistently reliable results.

6.2 Priorities for Phase A

6.2.1 Further Sensitivity Analyses

This report is not exhaustive. The presented analyses have touched on some key points about glint and its impact on remote-sensing retrievals of certain biophysical parameters. These issues could certainly benefit from deeper investigation. There are technical issues yet to be investigated, including (among others) the convolution of sensor noise and its impact on glint detection and correction. These technical issues, a wider variety of environmental conditions, and additional science objectives can all be addressed through continued modeling exercises.

6.2.2 Field Glint Observations

It would be very desirable to validate model results of selected, important HypsIRI science objectives. This validation can be performed on a relatively small scale with *in situ* measurements of relevant optical and biophysical parameters. Airborne measurements could also be useful, but then the scope of the validation becomes larger and less constrained. For this type of validation, see Section 6.3.1.

6.3 Longer-Term Priorities

6.3.1 Comprehensive Oceanic and Atmospheric Data Set

Forward radiative transfer models have been validated to the extent possible with incomplete data sets. Model inputs have relied on available IOP measurements plus reasonable assumptions about the missing pieces. Model predictions have been compared with available radiometric or AOP measurements. However, there are always enough missing inputs and outputs that rigorous

and complete model validation remains elusive. The same is true for inverse algorithms—there are always too many missing pieces requiring assumptions. Thus, comprehensive oceanic and atmospheric data sets are needed for validation of radiative transfer forward models (e.g., HydroLight, Monte Carlo, Modtran, HydroMod) and development and validation of remote-sensing inverse models/algorithms (e.g., TOA radiance → atmospheric correction algorithms → Rrs → in-water algorithms → IOPs, chlorophyll, water depth, bottom-type, etc.).

Environmental optics would be greatly advanced by the collection of a few comprehensive data sets for selected water and atmospheric conditions. In addition to collecting the data needed for model and algorithm validation, such a program should be viewed as an opportunity to compare various instruments and methodologies for making the same kind of measurement. Measurement redundancy is absolutely necessary in a field experiment.

Such a program must include measurements for all inputs needed to solve the radiative transfer equation (RTE) as well as the outputs from the RTE. To validate a coupled ocean-atmosphere optical model at one point in space and time, the measurements should be simultaneous and co-located. In addition to all pertinent optical parameters for solution of the RTE, ancillary measurements should be made for evaluation of various retrieval algorithms (e.g., chlorophyll, water depth, and bottom type).

The program as described would be both ambitious and expensive, but it would not be for the sole benefit of HypSIIRI. This program would benefit all remote-sensing missions that observe the ocean. Thus, this program should be jointly developed by the broader oceanic and atmospheric optical science communities.

6.3.2 Glint Toolbox

Glint correction algorithms are in a state of ongoing development. Even as they become codified and implemented in routine processing, it still may be advantageous to utilize different algorithms, depending on the situation at hand. Thus, it would be useful to have a glint toolbox utility from which a user could select among a suite of glint correction techniques. Such a toolbox could easily be incorporated as a module in existing image processing software applications that rely on high-level computer languages such as IDL (e.g., ENVI and SeaDAS).

7 References

- Acharya PK, Berk A, Bernstein LS, Matthew MW, Adler-Golden SM, Robertson DC, Anderson GP, Chetwynd JH, Kneizys FX, Shettle EP, Abreu LW, Gallery WO, Selby JEA, Clough SA (1998) *MODTRAN User's Manual, Versions 3.7 and 4.0*. Air Force Research Laboratory, Space Vehicles Directorate, Hanscom Air Force Base, Mass. 79 pages
- Berk A, Anderson GP, Acharya PK, Shettle EP (2008) *MODTRAN5.2.0.0 User's Manual*. Spectral Sciences, Inc., MA & Air Force Research Laboratory, MA. pages
- Borrego JA (1993) Wave height spectrum from sun glint patterns - an inverse problem. *J Geophys Res-Oceans* 98:10245-10258
- Cox C, Munk W (1954) Statistics of the sea surface derived from sun glitter. *Journal of Marine Research* 13:198-227
- Earth Science and Applications from Space: National Imperatives for the Next Decade and Beyond (2007). Committee on Earth Science and Applications from Space: A Community Assessment and Strategy for the Future (2007). National Research Council, National Academies Press. Referred to as the Decadal Survey or NRC 2007.
- Fraser RS, Mattoo S, Yeh EN, McClain CR (1997) Algorithm for atmospheric and glint corrections of satellite measurements of ocean pigment. *J Geophys Res-Atmos* 102:17107-17118
- Gao BC, Heidebrecht KB, Goetz AFH (1993) Derivation of scaled surface reflectances from AVIRIS data. *Remote Sens Environ* 44:165-178
- Gao BC, Montes MJ, Ahmad Z, Davis CO (2000) Atmospheric correction algorithm for hyperspectral remote sensing of ocean color from space. *Appl Optics* 39:887-896
- Gao BC, Montes MJ, Li RR, Dierssen HM, Davis CO (2007) An atmospheric correction algorithm for remote sensing of bright coastal waters using MODIS land and ocean channels in the solar spectral region. *IEEE Trans Geosci Remote Sens* 45:1835-1843
- Goodman JA, Ustin SL (2007) Classification of benthic composition in a coral reef environment using spectral unmixing. *Journal of Applied Remote Sensing* 1
- Goodman JA, Lee ZP, Ustin SL (2008) Influence of atmospheric and sea-surface corrections on retrieval of bottom depth and reflectance using a semi-analytical model: a case study in Kaneohe Bay, Hawaii. *Applied Optics* 47:F1-F11
- Gordon HR, Voss KJ (2004) MODIS normalized water-leaving radiance algorithm theoretical basis document (MOD 18) version 5
- Hedley JD, Harborne AR, Mumby PJ (2005) Simple and robust removal of sun glint for mapping shallow-water benthos. *Int J Remote Sens* 26:2107-2112
- Hochberg EJ, Andréfouët S, Tyler MR (2003) Sea surface correction of high spatial resolution Ikonos images to improve bottom mapping in near-shore environments. *IEEE Trans Geosci Remote Sens* 41:1724-1729
- Kay S, Hedley JD, Lavender S (2009) Sun glint correction of high and low spatial resolution images of aquatic scenes: a review of methods for visible and near-infrared wavelengths. *Remote Sensing* 1:697-730
- Kotchenova SY, Vermote EF, Matarrese R, Klemm FJ (2006) Validation of a vector version of the 6S radiative transfer code for atmospheric correction of satellite data. Part I: Path radiance. *Appl Optics* 45:6762-6773
- Kou LH, Labrie D, Chylek P (1993) Refractive-indexes of water and ice in the 0.65- μm to 2.5- μm spectral range. *Appl Optics* 32:3531-3540

- Lee Z, Carder KL, Chen RF, Peacock TG (2001) Properties of the water column and bottom derived from Airborne Visible Infrared Imaging Spectrometer (AVIRIS) data. *J Geophys Res-Oceans* 106:11,639-611,651
- Lee ZP, Carder KL, Mobley CD, Steward RG, Patch JS (1998) Hyperspectral remote sensing for shallow waters. 1. A semianalytical model. *Appl Optics* 37:6329-6338
- Lee ZP, Carder KL, Mobley CD, Steward RG, Patch JS (1999) Hyperspectral remote sensing for shallow waters: 2. Deriving bottom depths and water properties by optimization. *Appl Optics* 38:3831-3843
- Lee ZP, Casey B, Arnone R, Weidemann A, Parsons R, Montes MJ, Gao BC, Goode W, Davis CO, Dye J (2007) Water and bottom properties of a coastal environment derived from Hyperion data measured from the EO-1 spacecraft platform. *Journal of Applied Remote Sensing* 1:DOI: 10.1117/1111.2822610
- Lesser MP, Mobley CD (2007) Bathymetry, water optical properties, and benthic classification of coral reefs using hyperspectral remote sensing imagery. *Coral Reefs* 26:819-829
- Louchard EM, Reid RP, Stephens FC, Davis CO, Leathers RA, Downes TV (2003) Optical remote sensing of benthic habitats and bathymetry in coastal environments at Lee Stocking Island, Bahamas: A comparative spectral classification approach. *Limnol Oceanogr* 48:511-521
- Lyzenga DR, Malinas NR, Tanis FJ (2006) Multispectral bathymetry using a simple physically based algorithm. *IEEE Trans Geosci Remote Sens* 44:2251-2259
- Mobley CD (1994) *Light and Water: Radiative Transfer in Natural Waters*. Academic Press, San Diego
- Mobley CD, Sundman LK (2008) *HydroLight 5 EcoLight 5 Technical Documentation*. Sequoia Scientific, Inc. 95 pages
- Mobley CD, Gentili B, Gordon HR, Jin ZH, Kattawar GW, Morel A, Reinersman P, Stamnes K, Stavn RH (1993) Comparison of numerical models for computing underwater light fields. *Applied Optics* 32:7484-7504
- Mobley CD, Sundman LK, Davis CO, Bowles JH, Downes TV, Leathers RA, Montes MJ, Bissett WP, Kohler DDR, Reid RP, Louchard EM, Gleason A (2005) Interpretation of hyperspectral remote-sensing imagery by spectrum matching and look-up tables. *Appl Optics* 44:3576-3592
- Montagner F, Billat V, Bélanger S (2003) MERIS ATBD 2.13 - Sun glint flag algorithm, issue 4, revision 2
- Nicodemus FE, Richmond JC, Hsia JJ, Ginsburg IW, Limperis T (1977) *Geometrical Considerations and Nomenclature for Reflectance*. National Bureau of Standards Monographs National Bureau of Standards. 52 pages
- Pope RM, Fry ES (1997) Absorption spectrum (380-700 nm) of pure water .2. Integrating cavity measurements. *Appl Optics* 36:8710-8723
- Quan XH, Fry ES (1995) Empirical equation for the index of refraction of seawater. *Appl Optics* 34:3477-3480
- Tassan S (1994) Removal of the effect of sun-glitter from Thematic Mapper imagery of the sea. *Int J Remote Sens* 15:719-723
- Vermote EF, Tanre D, Deuze JL, Herman M, Morcrette J-J (1997) Second Simulation of the Satellite Signal in the Solar Spectrum, 6S: An Overview. *IEEE Trans Geosci Remote Sens* 35:675-686

Viollier M, Tanré D, Deschamps PY (1980) An algorithm for remote sensing of water color from space. *Boundary-Layer Meteorology* 18:247-267

Wang MH, Bailey SW (2001) Correction of sun glint contamination on the SeaWiFS ocean and atmosphere products. *Appl Optics* 40:4790-4798

Appendix A Global Wind Fields: 2-Parameter Weibull Distribution

An 18-year time series of wind speeds was constructed using SSM/I-10, SSM/I-11, SSM/I-13, and SSM/I-14 data from January 1, 1988, through September 1, 2006. SSM/I-11 and SSM/I-14 are polar orbiters, with afternoon equatorial crossovers. SSM/I-10 and SSM/I-13 have morning equatorial crossovers. Wind speed is calculated for all valid retrievals, except in the presence of rain.

From the 18-year SSM/I data set, monthly Weibull parameters were calculated using maximum likelihood estimation (MLE). The shape and scale parameters were found via a multidimensional, unconstrained, nonlinear minimization of the log-likelihood function using the downhill simplex method (Nelder and Mead).

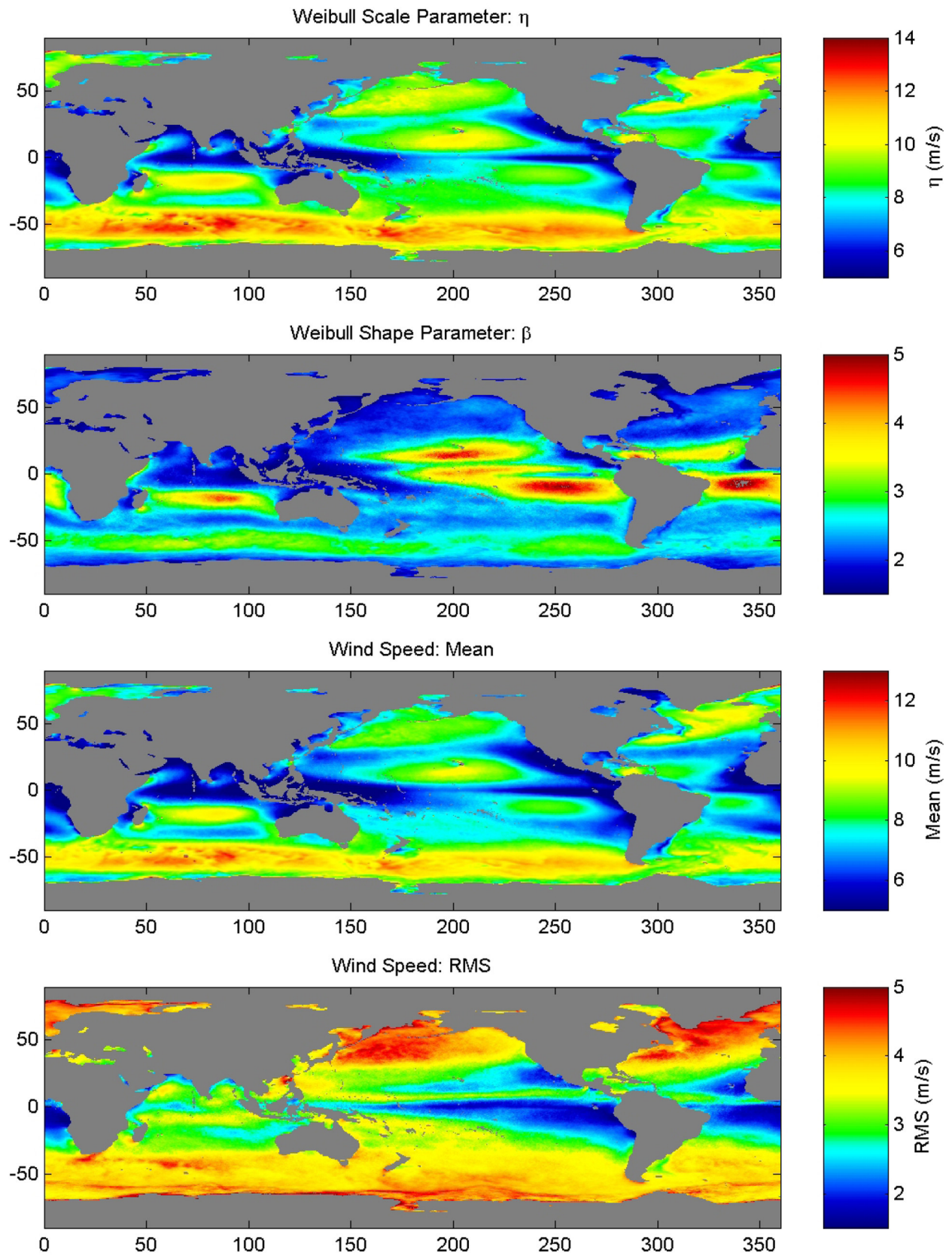
$$f(x) = \frac{\beta}{\eta} \left(\frac{x}{\eta} \right)^{\beta-1} e^{-\left(\frac{x}{\eta} \right)^\beta}$$

The Weibull distribution, $f(x)$, is greater than or equal to zero; the shape parameter, β , is greater than zero; and the scale parameter, η , is also greater than zero.

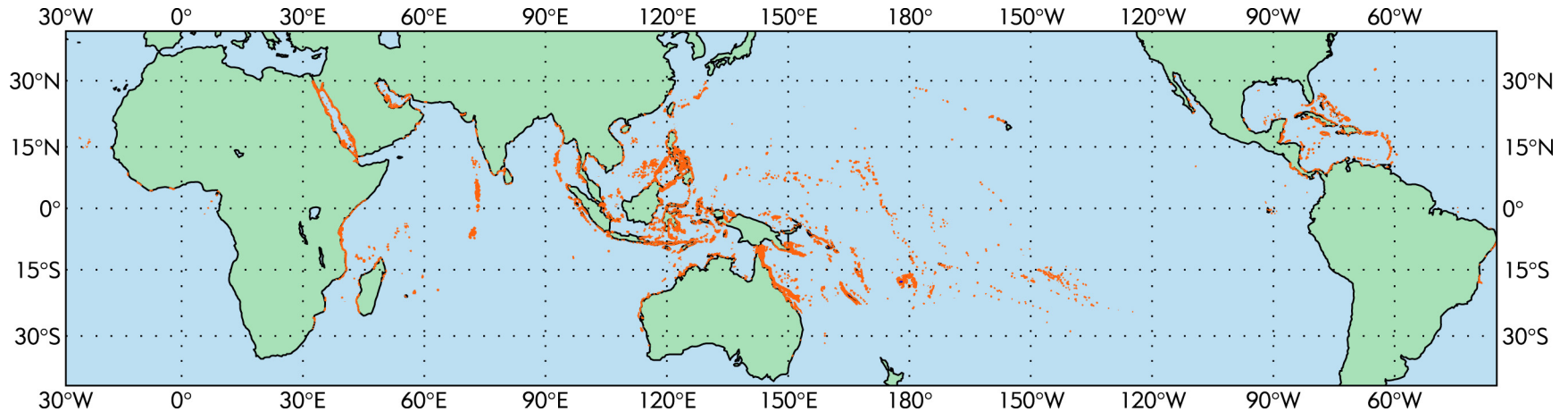
$$\text{Mean of } f(x) = \eta \Gamma\left(\frac{1}{\beta} + 1\right)$$

$$\text{STD of } f(x) = \eta \sqrt{\Gamma\left(\frac{2}{\beta} + 1\right) - \Gamma\left(\frac{1}{\beta} + 1\right)^2}$$

The 2-parameter Weibull distribution is commonly used in probability analysis of wind speeds as it can parameterize unimodal skewed probability density functions (PDFs) of non-negative random variables. While the Weibull PDF accurately parameterizes wind-speed PDF over much of the ocean, it can fail to accurately describe very calm regions (it does not allow for any probability of zero-wind speed).



Appendix B Global Distribution of Coral Reefs



Global distribution of coral reefs (data from UNEP-WCMC). Reefs exist in the waters of over 100 countries, with an estimated area of 500,000 km². However, reefs are spread across 200,000,000 km² of ocean. Satellite remote sensing is the only feasible means of acquiring uniform scientific data across these spatial scales. Based on several previous concept studies, HypSIRI has characteristics ideally suited to global reef survey, including spatial, spectral and orbital parameters. HypSIRI will be the first ever survey to directly and uniformly assess global reef status.



HyspIRI High-Temperature Saturation Study

*V. Realmuto
S. Hook
M. Foote
Jet Propulsion Laboratory*

*I. Csiszar
NOAA/NESDIS Center for Satellite Applications and Research
Camp Springs, MD*

*P. Dennison
University of Utah
Salt Lake City, UT*

*L. Giglio
University of Maryland
College Park, MD*

*M. Ramsey
University of Pittsburgh
Pittsburgh, PA*

*R.G. Vaughan
USGS Astrogeology Science Center
Flagstaff, AZ*

*M. Wooster
King's College London
London*

*R. Wright
University of Hawaii at Manoa
Honolulu, HI*

**National Aeronautics and
Space Administration**

**Jet Propulsion Laboratory
California Institute of Technology
Pasadena, California**

This research was carried out at the Jet Propulsion Laboratory, California Institute of Technology, under a contract with the National Aeronautics and Space Administration.

Reference herein to any specific commercial product, process, or service by trade name, trademark, manufacturer, or otherwise, does not constitute or imply its endorsement by the United States Government or the Jet Propulsion Laboratory, California Institute of Technology.

© 2011. All rights reserved.

Contents

1	SUMMARY	1-1
2	INTRODUCTION.....	2-1
2.1	Heritage Instruments.....	2-4
3	THE REMOTE ESTIMATION OF TEMPERATURE	3-1
3.1	The MODIS Fire Detection Algorithm.....	3-4
3.2	The MODVOLC Algorithm	3-6
3.3	Sub-Pixel Temperature Models	3-8
3.4	Minimized Multi-Component Modeling.....	3-9
3.5	Spectral Endmember Mapping	3-10
3.6	Fire Radiant Power	3-12
4	CASE STUDIES	4-1
4.1	Published Studies.....	4-1
4.2	Team Studies.....	4-2
4.2.1	AMS Survey of Southern California Wildfires.....	4-2
4.2.2	AGEMA Camera Data for Sharpsand Creek Fire.....	4-10
4.2.3	AVIRIS Survey of the Indians Fire.....	4-13
4.2.4	ASTER Surveys of Klyuchevskoy and Kilauea Volcanoes.....	4-15
4.2.5	Hyperion Surveys of Nyamuragira and Eyjafjallajökull Volcanoes.....	4-18
5	CONCLUSION	5-1
6	SELECTED BIBLIOGRAPHY	6-1

1 Summary

As part of the precursor activities for the HypsIRI mission, a small team was assembled to determine the optimum saturation level for the mid-infrared (4- μm) channel, which is dedicated to the measurement of hot targets. Examples of hot targets include wildland fires and active lava flows. This determination took into account both the temperature expected for the natural phenomena and the expected performance of the mid-infrared channel as well as its overlap with the other channels in the thermal infrared (7.5–12 μm) designed to measure the temperature of lower temperature targets. Based on this work, the hot target saturation group recommends a saturation temperature of 1200 K for the mid-infrared channel. The saturation temperature of 1200 K represents a good compromise between the prevention of saturation and sensitivity to ambient temperature.

2 Introduction

In 2004, the National Aeronautics and Space Administration (NASA), the National Oceanic and Atmospheric Administration (NOAA), and the U.S. Geological Survey (USGS) requested that the National Research Council (NRC) identify and prioritize the satellite platforms and associated observational capabilities that should be launched and operated over the next decade for Earth observation. In addition to providing information for the purpose of addressing scientific questions, the committee identified the need to ensure that the measurements helped benefit society and provide policymakers with the necessary information to make informed decisions on future policies affecting the Earth.

The resulting NRC study *Earth Science and Applications from Space: National Imperatives for the Next Decade and Beyond*, also known as the Earth Science Decadal Survey (NRC 2007), recommended launching 15 missions in three time phases. These three time phases are referred to as Tier 1, Tier 2, and Tier 3. The Hyperspectral Infrared Imager (HypIRI) mission is one of the Tier 2 missions recommended for launch in the 2013–2016 timeframe. The mission will advance our scientific understanding of how the Earth is changing as well as provide valuable societal benefit, particularly in understanding and tracking dynamic events such as volcanoes and wildfires.

The HypIRI mission includes two instruments: a Visible-Shortwave Infrared (VSWIR) imaging spectrometer and a Thermal Infrared (TIR) multispectral scanner. The VSWIR instrument will measure the radiance in 212 channels between 0.38 and 2.5 micrometers (μm) at a spatial resolution of 60 m. The VSWIR ground track will have a swath width of 145 km and revisit time of 19 days at the equator. The TIR instrument will measure the radiance in 8 channels between 4 and 12 μm at a spatial resolution of 60 m. The TIR ground track will have a swath width of 600 km and revisit time of 5 days at the equator.

The current specifications for the HypIRI TIR channels, with the exception of a proposed channel centered at 7.5 μm , are shown in Figure 1. These channels include a mid-infrared (MIR) channel, positioned near 4 μm , for investigations of high-temperature phenomena such as wildland fires and active lava flows and domes. The channels are superimposed on the radiance spectra of blackbodies at temperatures of 300, 500, and 700 K (Fig. 1). We present a detailed discussion of the fundamentals of blackbody radiation in Section 3; Figure 1 is an explanation for the positions of the HypIRI TIR channels. The channels between 8 and 12 μm are well positioned to measure the radiance of a blackbody at 300 K (Fig. 1), the average temperature of the Earth's surface. The HypIRI channels between 8 and 12 μm are designed to saturate at temperatures near 500 K, the approximate cross-over temperature at which the blackbody radiance at 4 and 8 μm is roughly equivalent (Fig. 1). The radiance of a blackbody at 700 K peaks near the center of the proposed 4- μm channel.

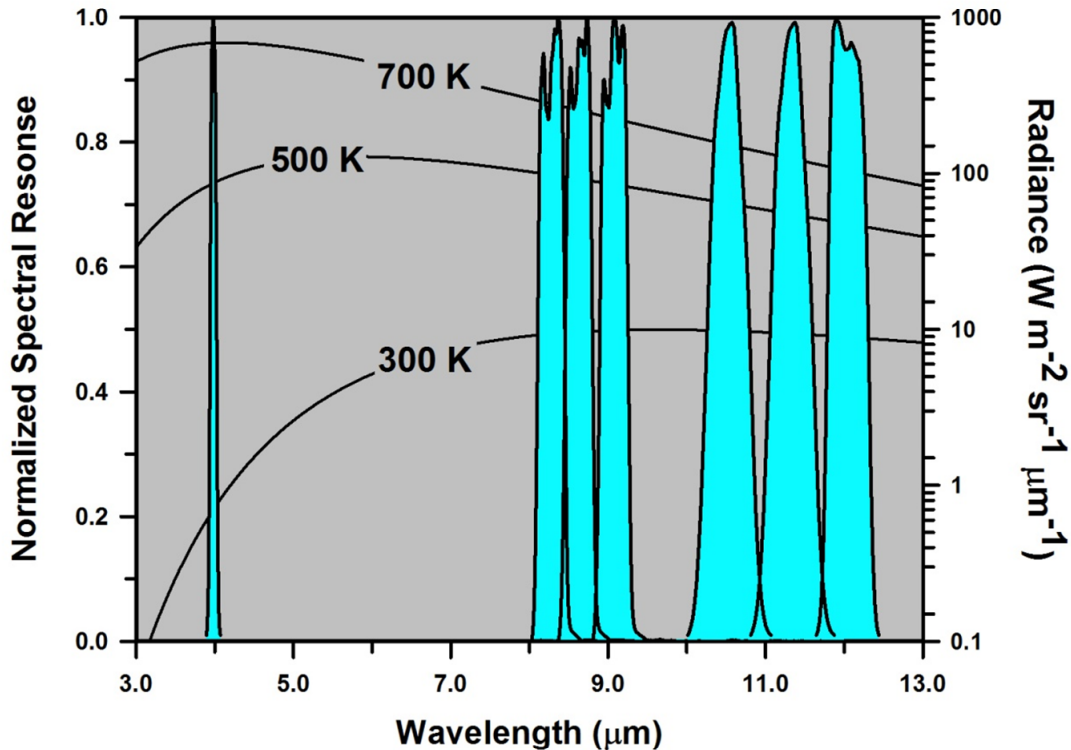


Figure 1. Normalized Spectral Response of HypsIRI Channels in the Mid (4 μm) and Thermal Infrared (8 – 12 μm). The Spectral Response Functions (shown in blue) are Superimposed on Blackbody Radiance Spectra for Temperatures of 300, 500, and 700 K.

The importance of the 4- μm channel to the HypsIRI science objectives is evident in the number of science questions that require high-temperature measurements. The science questions are listed below; the information in brackets denotes the relevant pages of the NRC Decadal Survey.

- TQ1:** How can we help predict and mitigate earthquake and volcanic hazards through detection of transient thermal phenomena?
- What do changes in the rate of lava effusion tell us about the maximum lengths that lava flows can attain and the likely duration of lava flow-forming eruptions? [DS 226]
- TQ2:** What is the impact of global biomass burning on the terrestrial biosphere and atmosphere, and how is this impact changing over time?
- How are global fire regimes changing in response to, and driven by, changing climate, vegetation, and land use practices? [DS 198]
 - Is regional and local scale fire frequency changing? [DS 196]
 - What is the role of fire in global biogeochemical cycling, particularly trace gas emissions? [DS 195]
 - Are there regional feedbacks between fire and climate change?

- CQ2:** How are fires and vegetation composition coupled?
- How do the timing, temperature, and frequency of fires affect long-term ecosystem health?
 - How do vegetation composition and fire temperature impact trace gas emissions?
 - How do fires in coastal biomes affect terrestrial biogeochemical fluxes into estuarine and coastal waters and what is the subsequent biological response? [DS 198]
 - What are the feedbacks between fire temperature and frequency and vegetation composition and recovery?
 - How does vegetation composition influence wildfire severity?
- CQ3:** Do volcanoes signal impending eruptions through changes in the temperature of the ground, rates of gas and aerosol emission, temperature and composition of crater lakes, or health and extent of vegetation cover?
- What do comparisons of thermal flux and SO₂ emission rates tell us about the volcanic mass fluxes and the dynamics of magma ascent? [DS 227; 230]
 - Can measurements of the rate at which lava flows cool allow us to improve forecasts of lava flow hazards? [DS 50; 226]
 - Do changes in the health and extent of vegetation cover indicate changes in the release of heat and gas from crater regions? [DS 230; 231]

The goal of this study was to identify an optimum temperature setting that prevents saturation of the 4- μ m measurements over targets of interest while providing useful overlap with measurements made with the remaining TIR channels (Fig. 1). The TIR channels will saturate between 450 and 500 K, leading us to evaluate the impact of the 4- μ m saturation temperature on the sensitivity of the MIR channel to scene temperatures less than 500 K. One metric for sensitivity is the noise-equivalent temperature difference (NE Δ T), which is the smallest difference in temperature that can be measured in the presence of noise.

Figure 2 shows the anticipated NE Δ T as a function of saturation and scene temperature. For scene temperatures \geq 500 K the saturation temperature does not have much effect on the NE Δ T. The sensitivity decreases (i.e., NE Δ T increases) with decreasing scene temperature, regardless of the saturation temperature. For a given scene temperature, the sensitivity will decrease with an increase in saturation temperature. At a scene temperature of 340 K, for example, saturation temperature settings of 800 and 1400 K will result in NE Δ T values of 1.5 and 7.0 K, respectively (Fig. 2).

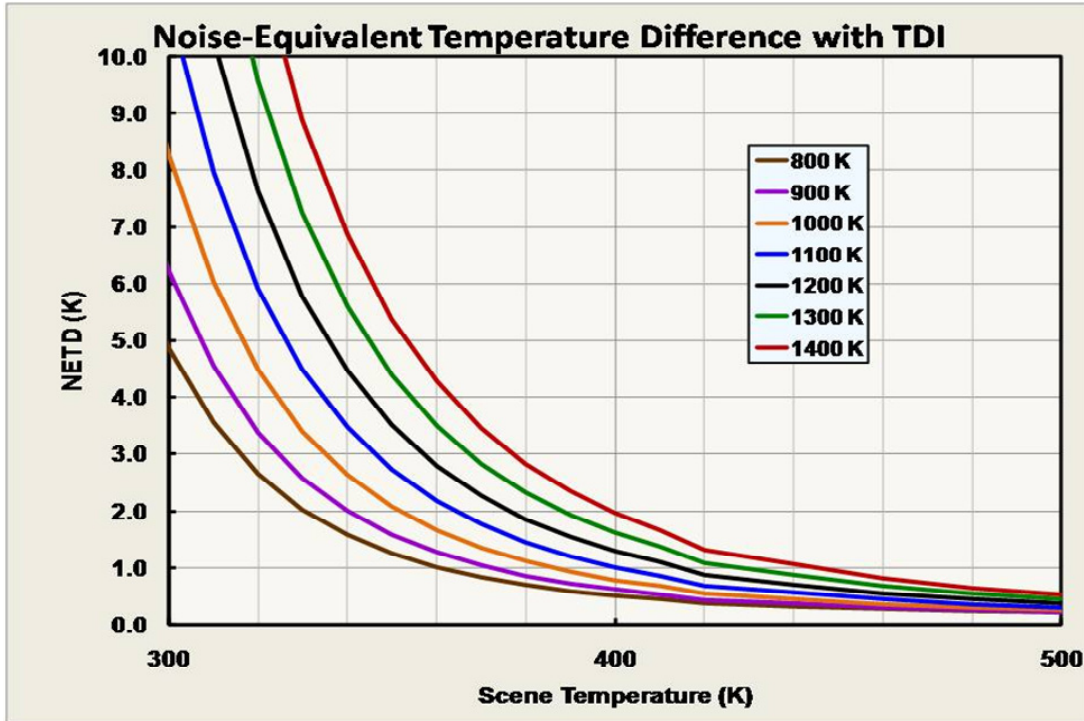


Figure 2. Simulated sensitivity of the HypsIRI 4- μ m Channel to scene temperatures between 300 and 500 K. The sensitivity is expressed as Noise Equivalent Temperature Difference (NEAT). For a scene temperature of 340 K a saturation temperature of 800 K results in an NEAT of 1.5 K, while a saturation temperature of 1400 K results in an NEAT of 7 K.

2.1 Heritage Instruments

Table 1 lists current and recent satellite instruments equipped with MIR channels positioned near 4 μ m. The data from all of these instruments have been applied to studies of high-temperature phenomena (cf. Selected Bibliography), but only MODIS and the Hot Spot Recognition System (HSRS) on board the Bi-spectral Infrared Detection (BIRD) satellite, designed and operated by DLR, were designed specifically to measure high temperatures.

The column highlighted in yellow lists the spatial resolution of the heritage instruments (Table 1). The 60-m spatial resolution of HypsIRI represents a significant improvement over that of the heritage instruments. For example, one HSRS pixel, with a resolution of 370 meters, would enclose 36 HypsIRI pixels.

Table 1. HypsIRI Heritage: Imaging Instruments with MIR Channels

Instrument	Central Wavelength	Spatial Resolution (at nadir)	Temporal Coverage (daytime)	Saturation Temperature
AVHRR	3.7 μm	1.1 km	Daily (NOAA 18 + 19)	~ 321.5 K
VIRS (TRMM)	3.75 μm	2.4 km	2 day revisit	321K
ATSR/AATSR	3.7 μm	1 km /1.5 x 2 km	3 day revisit	311 K
MODIS	3.95 μm	1 km	Daily (Terra + Aqua)	478 K /506 K (Ch. 21); 330 K (Ch. 22)
GOES Imager	3.9 μm	2.3 x 4 km	3 hr/15-30 min	335 K
SEVIRI (MSG)	3.9 μm	3 km	15 min	335 K
HSRS (BIRD)	3.4 – 4.2 μm	370 m	Targeted	600 K

The data acquired with MODIS Channels 21 and 22 provide a real-world example of the relationship between saturation temperature and sensitivity. The channels have the same spectral response, but Channel 21, the so-called “Fire Channel,” was designed with a higher saturation temperature than Channel 22 (500 vs. 330 K). As a consequence of the higher saturation temperature, Channel 21 is less sensitive to scene temperatures ~300 K than Channel 22 (NE Δ T of 0.8 K for Ch. 21 vs. 0.03 K for Ch. 22). As noted by Gao et al. (2007), the Channel 21 data have proven to be too noisy for use in an operational estimation of fire temperature. In addition, the use of Channel 21 data in the operational MODIS fire detection algorithm is limited to cases when the Channel 22 data are saturated.

To re-evaluate the saturation temperature for MODIS Channel 21, Gao et al. derived temperature estimates for pixels flagged by the MODIS fire detection algorithm from over 40 sets of Channel 21 data acquired by MODIS-Terra and MODIS-Aqua. Figure 3 shows histograms of these temperature estimates. The cumulative histogram (Fig. 3[b]) indicates that 90% of the temperatures were less than 350 K. Given that the great majority of temperature estimates fell within the range of low Channel 21 sensitivity, Gao et al. recommended a saturation temperature \leq 450 K for any future instruments with 4- μm channels with a spatial resolution of 1 km.

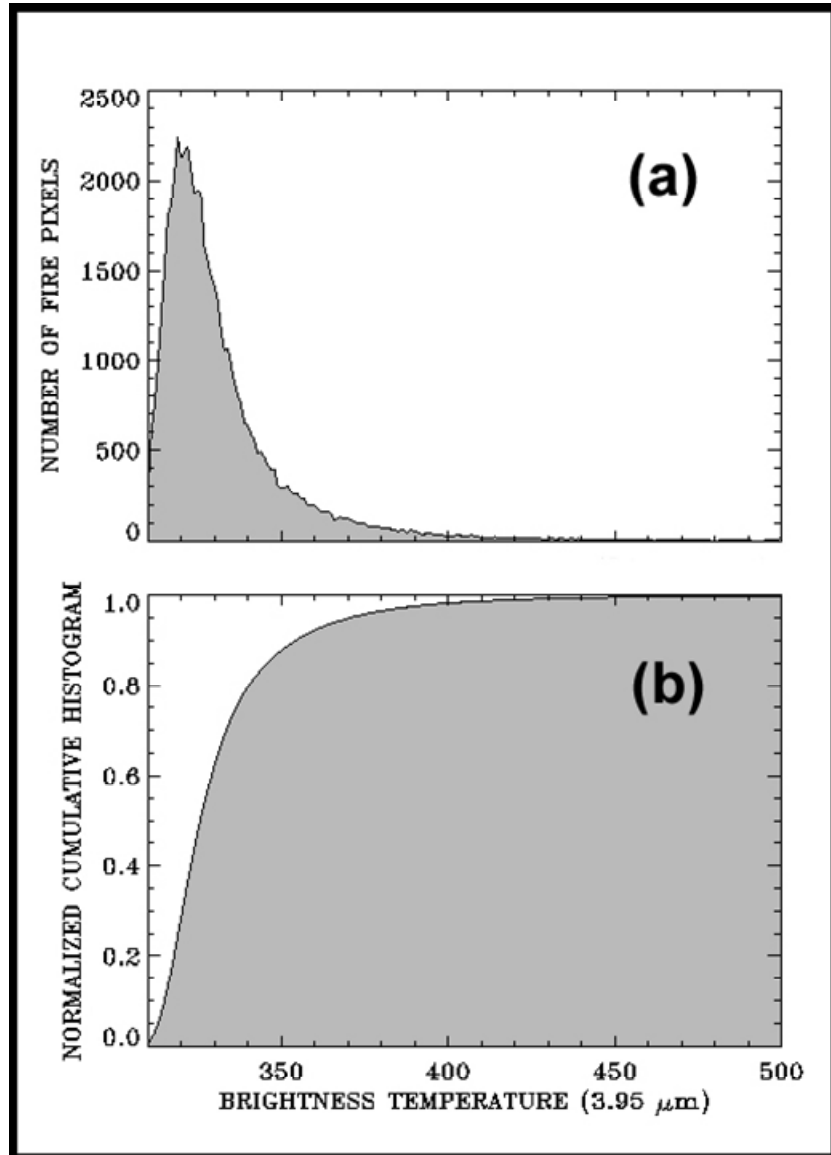


Figure 3. Fire pixels histograms compiled by Gao *et al.* [2007].
 (a) Relative frequency plot; (b) cumulative probability plot.
 Note that 90% of the 4-μm temperatures were ≤ 350 K.

The recommendation of Gao et al. (2007) is the result of a probability-based approach, in which the saturation temperature was set to the highest scene temperature that we are likely to encounter. However, many of the high-temperature phenomena identified in the HypsIRI science questions are the result of unique events, which, by definition, have low probabilities of occurrence. In Figure 4 we show rank-order plots of brightness temperatures for three volcanoes—Kilauea, Etna, and Nyamuragira (Figs. 4[a], [b], and [c], respectively)—accumulated over the period 2000–2009. We see that all three volcanoes produced temperatures in excess of 478 K, the saturation temperature of MODIS-Terra Channel 21 (Xiong et al. 2009), while Etna and Nyamuragira produced temperatures in excess of 506 K, the saturation temperature of MODIS-Aqua Channel 21. In all three cases, a saturation temperature of 450 K would preclude measurements of such high-temperature events.

For another argument against a 4- μm saturation temperature of 450 K, we recall that the HypsIRI TIR channels centered between 8 and 13 μm will have saturation temperatures of 500 K. Therefore, in the case of HypsIRI, a 4- μm channel with a saturation temperature less than 500 K will provide no additional information about high-temperature phenomena relative to the TIR channels.

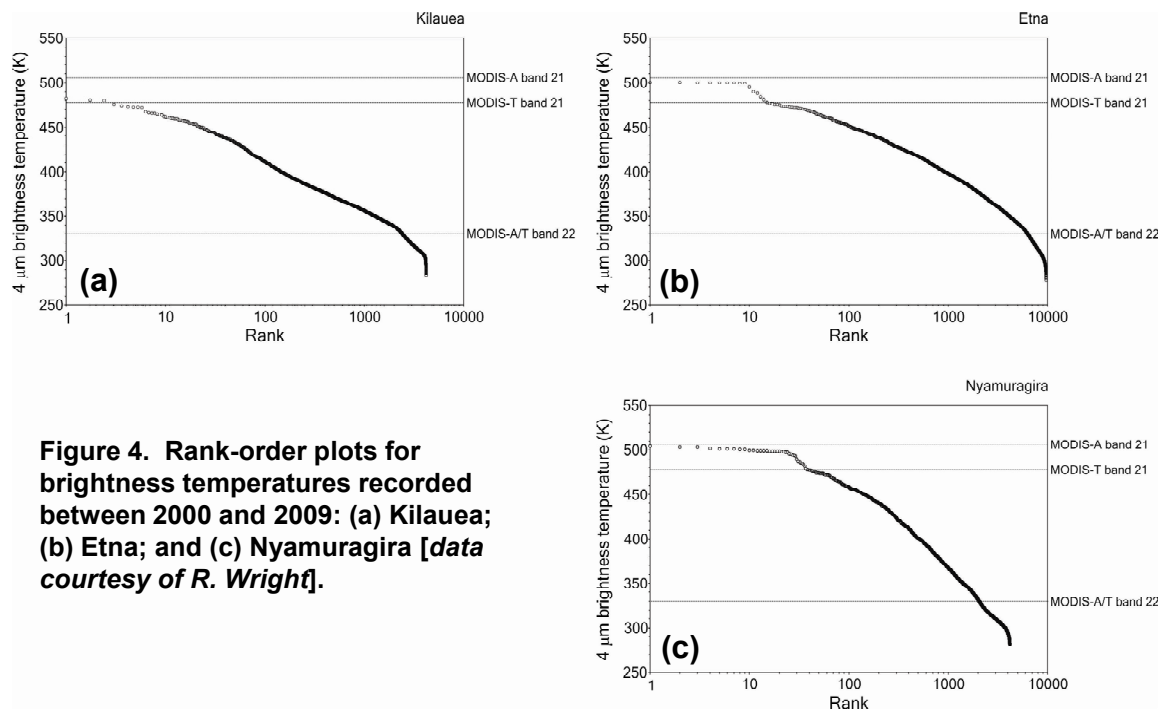


Figure 4. Rank-order plots for brightness temperatures recorded between 2000 and 2009: (a) Kilauea; (b) Etna; and (c) Nyamuragira [data courtesy of R. Wright].

3 The Remote Estimation of Temperature

In the following sections, we will present airborne and satellite observations to support our recommendation for saturation temperature. We note that neither HypsIRI nor any of the heritage instruments from Table 1 make direct measurements of surface temperature. The instruments measure scene radiance, and we must derive estimates of temperature from these radiance measurements. The 4- μm channel will be designed for a maximum level of radiance, and the saturation temperature will correspond to the maximum radiance.

We do not have radiance data at the spatial resolution and spectral response of HypsIRI, so we must work with radiance measured at spatial resolutions and spectral responses different from the notional HypsIRI parameters. As we demonstrate below, temperature estimates depend strongly on the spatial resolution and spectral response of the corresponding radiance measurements. To discuss these dependences, we first present a brief review of the theory and practice of remote estimates of temperature.

The relationship between the temperature of a surface and spectral radiance emitted from the surface is described by the Planck blackbody law:

$$B_{\lambda}(T) = \frac{C_1}{\pi \lambda^5 \left[\exp\left(\frac{C_2}{\lambda T}\right) - 1 \right]},$$

where T and λ represent temperature in Kelvins (K) and wavelength in micrometers (μm), respectively. The resulting units of radiance are Watts per unit area, solid angle, or steradian, and wavelength ($\text{W m}^{-2} \text{sr}^{-1} \mu\text{m}^{-1}$). C_1 and C_2 are the first and second radiation constants, defined as

$$C_1 = 3.74151 \times 10^8 \text{ W m}^2 \mu\text{m}^4 \text{ (or } 3.74151 \times 10^{-16} \text{ W m}^2\text{) and} \\ C_2 = 1.43879 \times 10^4 \mu\text{m K (or } 1.43879 \times 10^{-2} \text{ m K).}$$

The Planck Law describes an idealized perfect radiator. The relationship between the radiance of a real-world surface and that of a blackbody is given by:

$$L(\lambda, T) = \varepsilon(\lambda)B(\lambda, T),$$

where $\varepsilon(\lambda)$ represents the spectral emissivity of the surface. By definition, the emissivity of a blackbody is constant and equal to 1.0. A graybody is an idealized radiator with a constant emissivity less than 1.0. The emissivity of most real-world surfaces varies with wavelength, and emissivity spectra are used to identify materials and estimate material properties.

Given a radiance spectrum, we can invert the Planck law to derive an estimate of temperature. If we assume that the surface is a blackbody, then the resulting temperature estimate is known as a brightness temperature. We may also assign an emissivity spectrum to the surface before deriving temperature estimates. In either situation, we will obtain temperature estimates that vary with wavelength if our knowledge of emissivity is not perfect.

In practice, the estimation of temperature from remote sensing measurement is more complicated than the theory discussed previously. For the purposes of this study, the most important consideration is the non-uniform distribution of surface temperatures within the instantaneous field of view of a sensor. Here we discuss this sub-pixel mixing of temperatures in greater detail.

Figure 5 illustrates the radiance spectra for surface temperatures ranging from 300 to 700 K. We note that the peak radiance, signified by the solid circles (Fig. 5), shifts to shorter wavelengths as the temperature increases. Wien's Displacement Law describes the relation between the wavelength of the peak radiance and temperature as $\lambda_{max} = b/T$, where $b \sim 3 \times 10^{-3} \text{ m}\cdot\text{K}$. The radiance at 300 K peaks near $10 \mu\text{m}$ (Fig. 5), the approximate center of the wavelength range covered by the HypsIRI TIR channels ($8\text{--}12 \mu\text{m}$). The radiance at 700 K peaks near $4 \mu\text{m}$, highlighting the need for a $4\text{-}\mu\text{m}$ channel to study high-temperature phenomena.

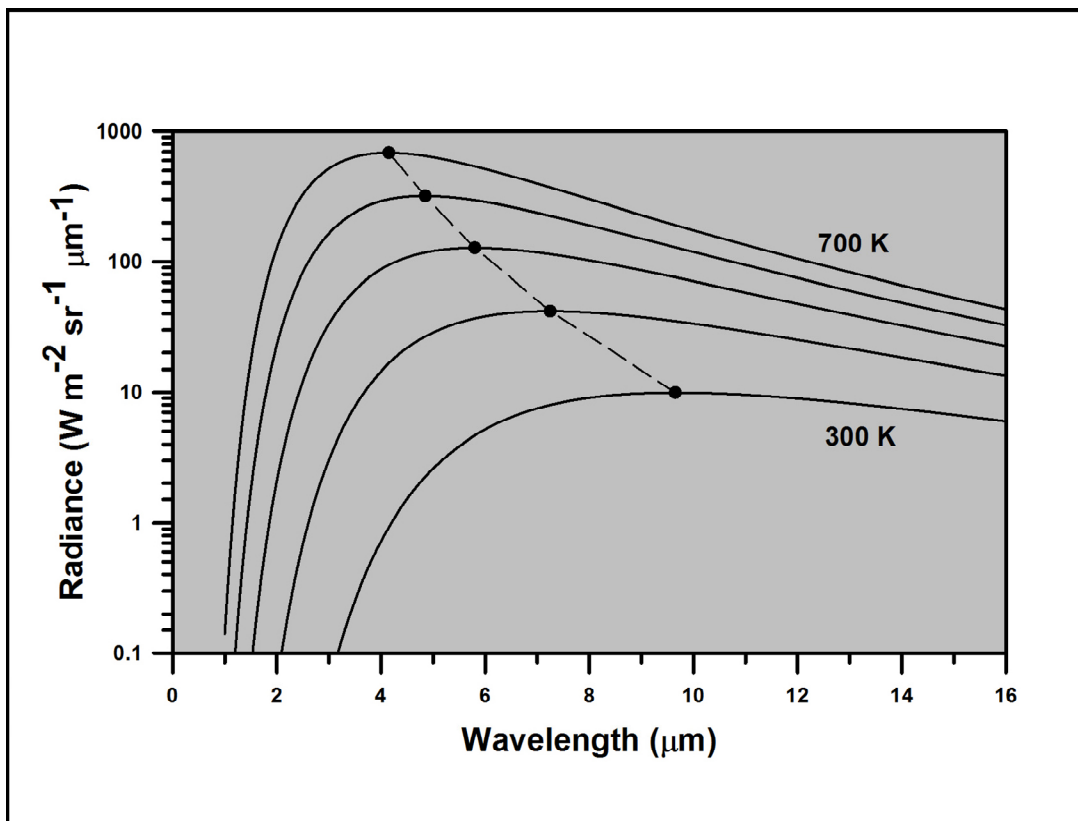


Figure 5. Illustration of Wien's Displacement Law for surface temperatures between 300 – 700 K. The solid circles indicate the peak radiance of each spectrum.

Figure 6 illustrates the radiance spectra resulting from sub-pixel mixing of two temperature components (Wright et al. 2002). The solid line represents the spectrum of a surface at a uniform temperature of 300 K. The dashed line represents the spectrum resulting from a mixture of components at 300 and 1200 K temperatures, with the hot component occupying 0.005% of the surface area. In accordance with Wien's Displacement Law (Fig. 5), the presence of this hot component increases radiance at wavelengths $< 6.0 \mu\text{m}$, relative to the isothermal spectrum, and has less effect on the radiance at longer wavelengths (Fig. 6). The broken line represents the spectrum resulting from an increase in the size of the 1200 K component to 0.03% of the surface area. The presence of this larger hot component increases the radiance at all wavelengths, relative to the isothermal spectrum, with the greatest increase occurring at the shorter wavelengths. Accordingly, the difference between brightness temperatures calculated at short and long wavelengths, such as 4 and $11 \mu\text{m}$, will increase with increases in the area and/or temperature of the hot fraction. The detection of such variation from isothermal radiance is the foundation of the operational MODIS fire and MODVOLC hot-spot detection algorithms, which we discuss in the next section.

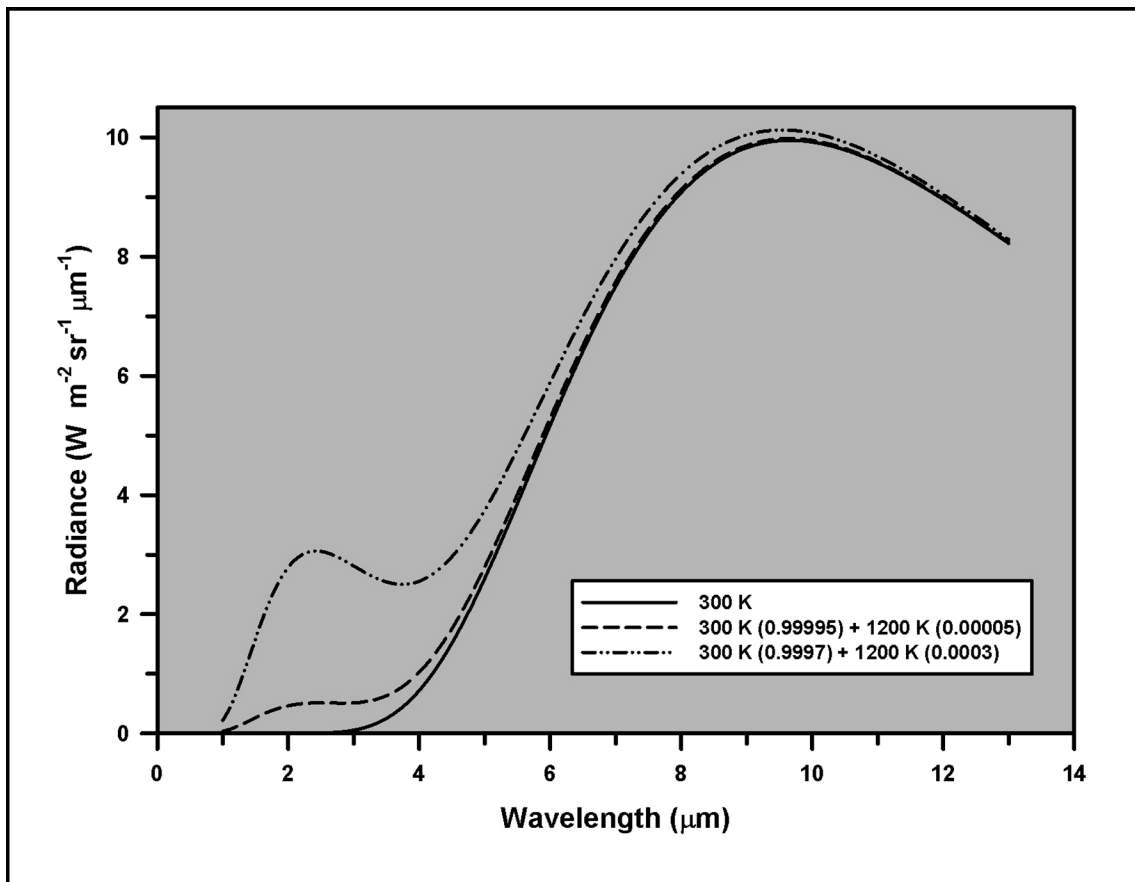


Figure 6. Compound radiance spectra resulting from sub-pixel mixture of two temperature components [after Wright et al., 2002].

3.1 The MODIS Fire Detection Algorithm

The MODIS project generates fire detection maps in Level 2 (MOD14/MYD14) and Level 3 daily (MOD14A1/MYD14A1) and 8-day (MOD14A2/MYD14A2) formats. The maps show the locations of pixels classified as “active” fire. The fire detection algorithm (Justice et al. 2002; Kaufman et al. 2003) uses brightness temperatures derived from radiance measurements at 4 and 11 μm , denoted by T_4 and T_{11} , respectively. T_4 is derived from Channel 22 whenever possible, as this channel has smaller quantization errors (0.03 vs. 0.8 K for a surface temperature of 300 K). When Channel 22 saturates, or these data are missing, T_4 is derived from Channel 21. T_{11} is derived from Channel 31, which was designed to saturate at 400 and 340 K for MODIS-Terra and MODIS-Aqua, respectively.

The fire detection algorithm operates in two modes. The absolute, or spectral, mode is based on pre-defined thresholds on T_4 and the difference between T_4 and T_{11} ($T_4 - T_{11}$). If the derived values fall below these thresholds, the detection algorithm switches to the relative, or context, mode in which the values of T_4 and ($T_4 - T_{11}$) at a pixel are compared to the values from surrounding pixels. The region of interest surrounding the pixel under consideration increases in area until a pre-defined number of fire-free pixels are identified.

The metrics for the accuracy of the detection include probabilities of detection and commission/omission error rates. These metrics are based on ground truth data at the scale of the MODIS footprint and ASTER data acquired coincidentally with MODIS-Terra data (Csiszar et al. 2006; Morisette et al. 2005a, 2005b). Figure 7 shows an ASTER scene, acquired over a fire in Siberia, superimposed with the corresponding output of the MODIS fire detection algorithm. Such comparisons between MODIS and ASTER data products have revealed that a MODIS pixel must enclose 45 to 60 contiguous ASTER fire pixels in order to have a 50% probability of being classified as fire. Similarly, a MODIS pixel must enclose at least 50 contiguous ASTER fire pixels to achieve omission, or false negative, probabilities below 40%. The probability of commission errors, or false positives, is typically $<0.1\%$, due to the fact that MODIS does not, in general, detect fires that are not detected in the corresponding ASTER data.

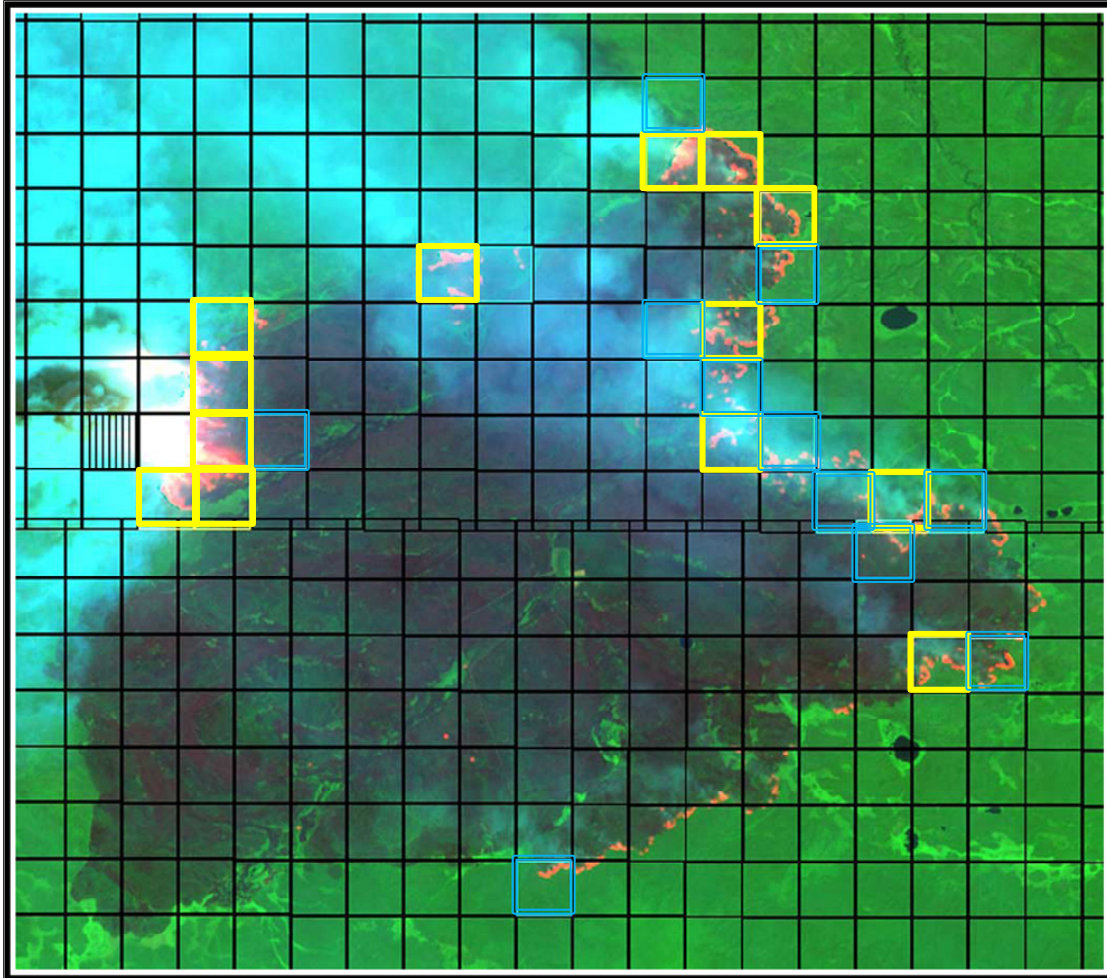


Figure 7. MODIS 1-km grid superimposed over ASTER color-composite scene depicting a fire in Siberia (62.57 °N, 125.72 °E). Yellow and blue grid cells correspond to MODIS fire pixels identified with high and nominal confidence, respectively [Csiszar et al., 2006].

The potential contribution of HypsIRI to fire detection programs is illustrated in Figure 8, which is a plot of the theoretical limit, or threshold, of detection for the MODIS fire algorithm as a function of the size and temperature of a fire (Giglio et al. 1999; Csiszar et al. 2006). Fires with areas of 100 and 10,000 m² would require temperatures of at least 1200 and 500 K, respectively, to be detected. The temperatures 1200 and 500 K represent the upper and lower thresholds for flaming and smoldering fires, respectively, in the MODIS fire algorithm (e.g., Kaufman et al. 1998b). Figure 8 also shows the predicted detection threshold for HypsIRI, and we see that the high spatial resolution of HypsIRI, relative to MODIS (60 m vs. 1 km at nadir, respectively), will improve our detection of small fires. For a fire at 500 K, the necessary area threshold drops from 10,000 m² (MODIS) to 30 m² (HypsIRI).

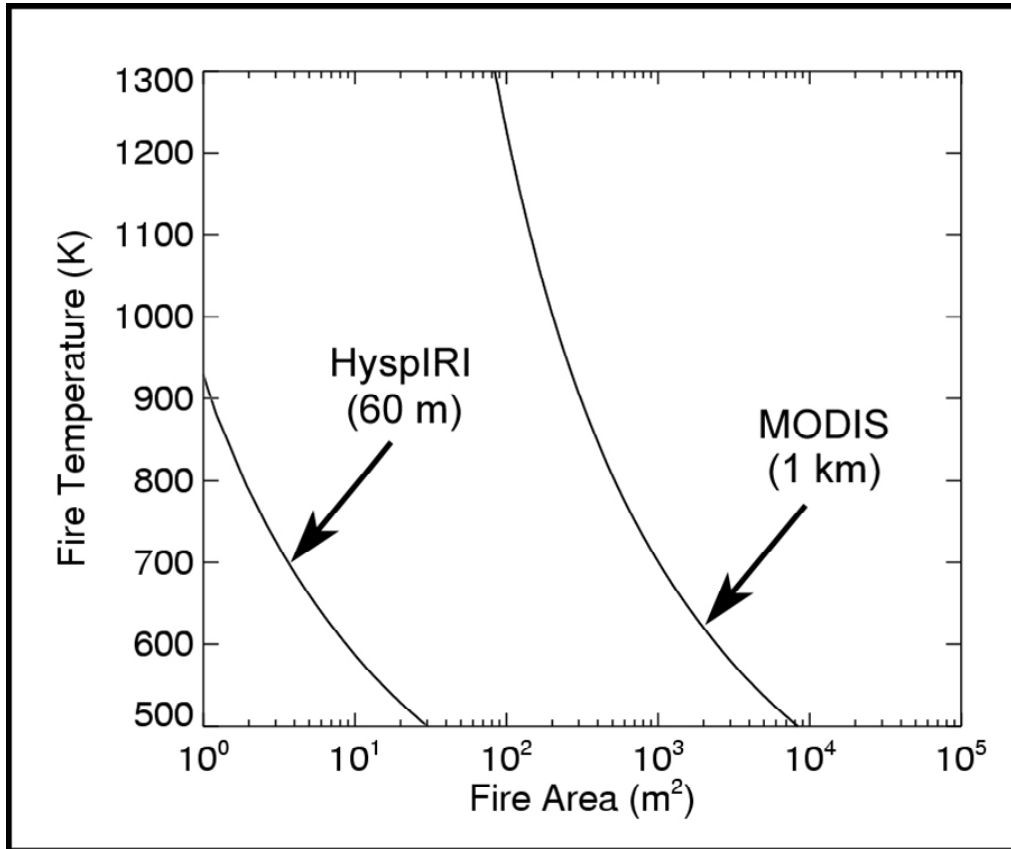


Figure 8. Detection thresholds for the MODIS fire algorithm at the spatial resolution of MODIS and HyspIRI [data courtesy of L. Giglio].

3.2 The MODVOLC Algorithm

MODVOLC is an automated hot-spot detection system developed and operated by the University of Hawaii (Wright et al. 2002, 2004). The algorithm is run on every MODIS scene, but MODVOLC is not part of the standard MODIS product generation system. Consequentially, the MODVOLC algorithm operates under strict resource restrictions. The algorithm has no context mode and is limited to eight mathematical operations on the radiance measured in five MODIS channels.

The limited computational resources available to MODVOLC preclude the conversion of radiance to brightness temperature, and the detection algorithm is based on characteristic changes in the shape of radiance spectra due to the presence of sub-pixel hot spots (Fig. 6). The increase in the radiance at 4 μm (MODIS Ch. 21/22) relative to that at 12 μm (Ch. 32) will decrease the difference between the radiance measured in these channels. As with the MODIS fire detection algorithm, MODVOLC makes use of Ch. 22 data preferentially, switching to Ch. 21 when Ch. 22 data are saturated.

However, the difference in radiance at 4 and 12 μm ($L_4 - L_{12}$) is also sensitive to isothermal surface temperature. As shown in Figure 9, a plot of $L_4 - L_{12}$ vs. temperature, this relationship is not unique. For example, a radiance difference of $-10 \text{ W m}^{-2} \text{ sr}^{-1} \mu\text{m}^{-1}$ can result from surface

temperatures of 40 or 140°C (Fig. 9). To remove this ambiguity the radiance differences are normalized by the sum of the radiances, which increases with an increase in L_4 . The resulting normalized temperature index, or NTI, is weighted to surfaces with sub-pixel hot fractions.

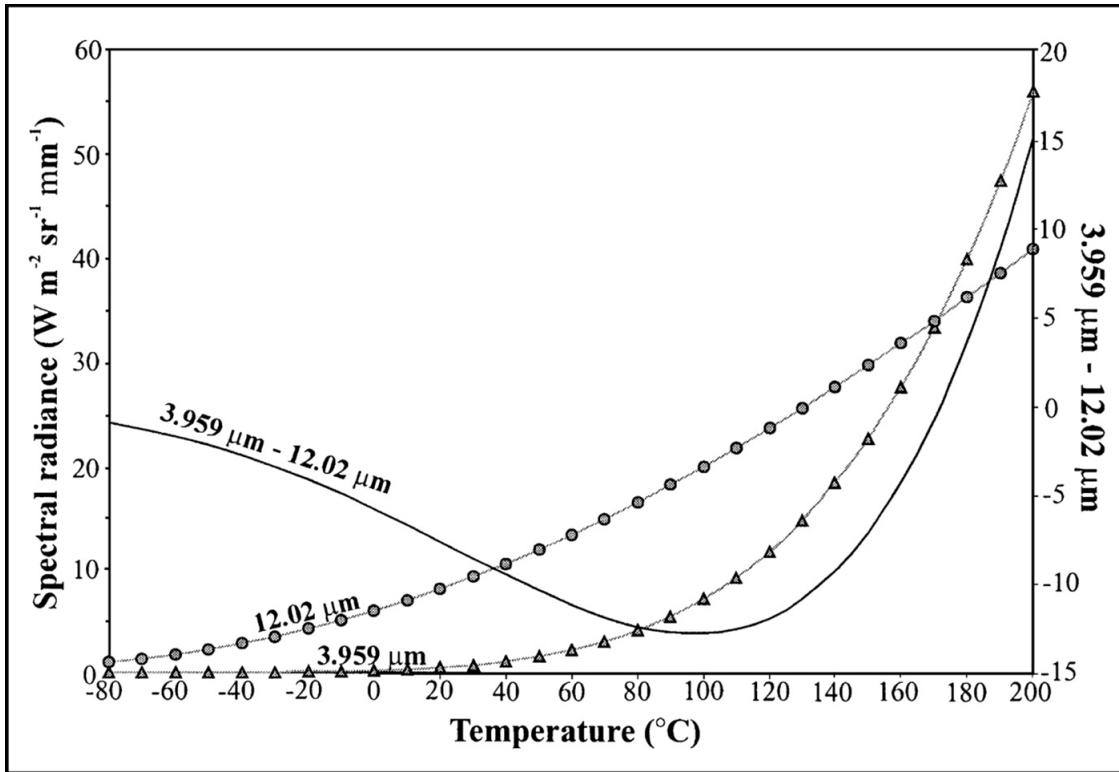


Figure 9. Difference in radiance at 4- and 12-μm as a function of temperature [Wright et al., 2002].

3.3 Sub-Pixel Temperature Models

Dozier (1981) and Matson and Dozier (1981) pioneered the use of two-component temperature mixing models to estimate the temperature and area of the hot component. This technique was originally developed for the AVHRR instrument, utilizing the radiance measured in Channels 3 (3.55 – 3.93 μm) and 4 (10.5 – 11.5 μm). Denoting the radiance at 4 μm (AVHRR Ch. 3) and 11 μm (AVHRR Ch. 4) as L_4 and L_{11} , respectively, the relative contributions of the high-temperature (T_h) and background (T_b) components to the radiance may be modeled as:

$$\begin{aligned} L_4 &= pB_4(T_h) + (1 - p)B_4(T_b) \\ L_{11} &= pB_{11}(T_h) + (1 - p)B_{11}(T_b), \end{aligned}$$

where p is the fraction of the pixel occupied by the high-temperature component and B_4 and B_{11} represent the blackbody radiance at 4 and 11 μm , respectively. In most applications, the background temperature (T_b) is estimated from pixels surrounding the pixel of interest. Two-component temperature models have been applied to numerous studies of fires and volcanic phenomena, incorporating data from the following instruments: ASTER (Eckmann et al. 2009), AVHRR (e.g., Langaas 1993; Giglio et al. 1999; Harris et al. 1997a,b), Landsat (e.g., Wooster and Kanako 2001; Wright et al. 2001), ATSR (Wooster and Rothery 1997), and BIRD (Oertel et al. 2004; Siegert et al. 2004; Wooster et al. 2003), as well as the airborne AVIRIS (e.g., Oppenheimer et al. 1993b; Dennison et al. 2006) and Digital Airborne Imaging Spectrometer (DAIS; Lombardo et al. 2006).

However, most high-temperature events involve more than two sub-pixel temperature components, and the resulting estimates of the high-temperature component are too low. To evaluate the impact of such additional components on two-channel temperature retrievals of fire temperatures, Giglio and Kendall (2001) introduced components representing smoldering fire, at a temperature intermediate to the flaming and background temperatures, and a burned area component, at a temperature above the background temperature. Similarly, Harris et al. (1997a) introduced a third component representing hot crust, at a temperature intermediate to the melt and background temperatures, to an analysis of AVHRR data acquired during the 1991–1993 eruption of Mt. Etna. In both investigations, these additional model components provided insight into the radiative process but were not constrained by the observed data. Giglio and Kendall found that the addition of the smoldering component resulted in a systematic underestimate of the area of the flaming component. Their four-component model led to systematic underestimates of fire temperature and overestimates of fire area. The following conclusion by Giglio and Kendall is a prelude to the role of HypsIRI in studies of wildland fires:

In order to reliably determine instantaneous fire temperature and area over a wide range of active fire sizes using Dozier’s two-component model, it would be necessary to observe fire activity with sensors having much higher spatial resolution (~100 m) and very high (>1000 K) middle infrared band saturation.

Various investigators have explored the use of multiple spectral channels in temperature-mixing models. Oppenheimer et al. (1993b) applied curve-fitting techniques to AVIRIS data to obtain estimates of the temperature and size of hot spots at Stromboli volcano. Harris et al. (1999) applied a three-component model to triplets of Landsat TM channels to study the temperature structure of lava lakes. Wright and Flynn (2003) and Wright et al. (2010) present a non-linear

minimization approach for estimating the temperature and fractional area of multiple sub-pixel components from Hyperion data. Dennison et al. (2006) and Eckmann et al. (2008) demonstrated that spectral mixing analysis could be used to estimate fire temperatures and area from AVIRIS and MODIS data, respectively. We employed the approaches of Wright et al. and Dennison et al. to help define the HypsIRI saturation temperature, and we discuss these approaches in greater detail in the following sections.

3.4 Minimized Multi-Component Modeling

The multi-component approach developed by Wright and Flynn (2003) is based on the extension of the two-component model to three or more components. To address the problem of resolving the temperature and fractional area of the additional components, the multi-component model was developed for analysis of hyperspectral V-SWIR data acquired with the Hyperion instrument. This approach allowed Wright and Flynn to treat the temperature and fractional area of each component as free parameters, in contrast to the multi-component models from Oppenheimer (1993b), Giglio and Kendall (2001), and Harris et al. (1997a,b and 1999). The strategy of the Wright and Flynn approach is to minimize the number of sub-pixel components required to fit the observed radiance spectrum.

Figure 10 illustrates the concepts behind minimized multi-component modeling. The FLIR-based temperature map represents the distribution of temperatures found within a pixel from a hypothetical satellite image data acquired over an active lava flow. The histograms to the right of the FLIR map show the temperature distribution. Superimposed on the histograms are gray bars representing the temperature components estimated by the conventional two-component, or dual-band, model and multi-component models with 2, 3, and 6 components. The height of a bar indicates the area fraction occupied a component.

For the dual-band model (Fig. 10[a]) the temperature of the hot component was fixed at 1100°C (1373 K), and the best solution to the model was a single temperature component at 500°C (773 K). The two-component solution (Fig. 10[b]) yielded components at 425 °C (700 K) and 700°C (973 K), with fractional areas (f_i) of 0.9 and 0.1, respectively. Increasing the number of temperature components to 3 and 6 (Figs. 10[c] and 10[d], respectively) improved the fit to the observed temperature distribution. In practice, however, instrument noise limits the maximum number of free components to 3.

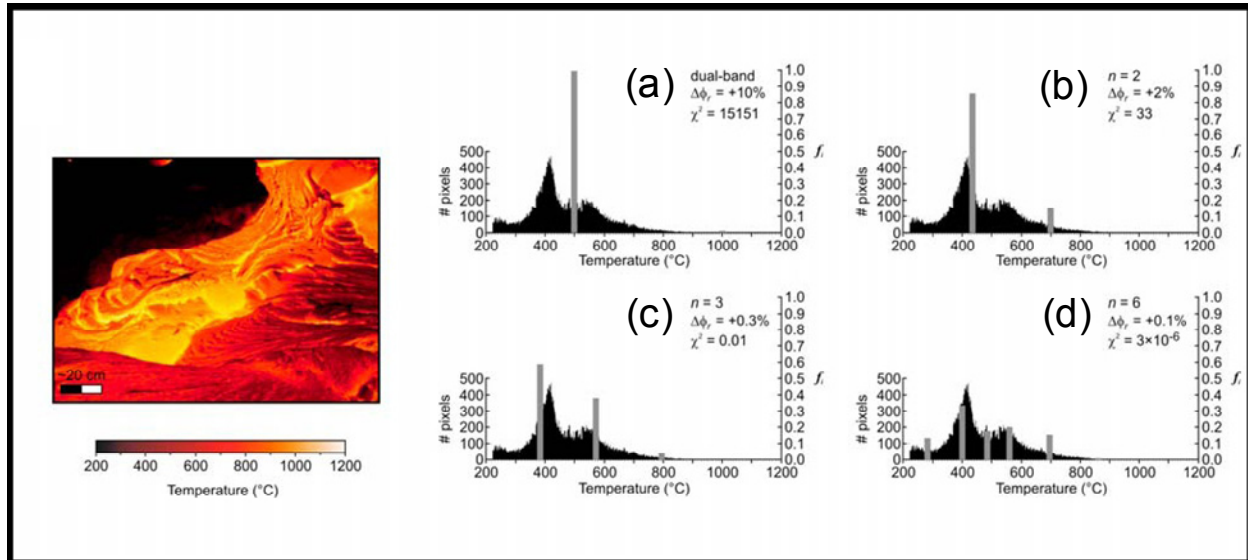


Figure 10. Illustration of the Minimized Multi-Component Modeling technique. The FLIR image (at left) represents the distribution of temperatures within a Hyperion pixel. The histograms (at right) show the temperature distribution, together with fits of the dual-band and multi-component model results to the observed temperature distribution. The six-component model ($n = 6$) yields the best fit, in the Chi-Squared (χ^2) sense, to the observations [Wright et al., 2010].

3.5 Spectral Endmember Mapping

Multiple endmember spectral mixture analysis (MESMA), as described by Roberts et al. (1998), fits observed spectra with linear combinations, or mixtures, of endmember spectra selected from spectral libraries. The endmember spectra, and relative contribution of the spectra to the spectral mixture, are treated as free parameters and may vary from pixel to pixel. Dennison et al. (2006) demonstrated that the MEMSA concept could be extended to map fire temperatures and fractional areas. The investigators introduced a new spectral library of emitted radiance, containing synthetic spectra generated for representative ground cover types and temperatures between 500 and 1500 K. The observed radiance was modeled as a combination of solar reflected radiance, emitted radiance, and shade (or zero radiance). The solar-reflected radiance endmembers were selected from the image data under consideration.

Figure 11 contains the fire temperature and fractional area estimates derived from AVIRIS data acquired over the 2003 Simi Fire, which burned $\sim 44,000$ ha (440 km^2) in the Santa Susana Mountains of Ventura County, California. Figure 11(a), a false-color composite of AVIRIS data collected at 1.682, 1.107, and 0.655 μm , displayed in red, green, and blue, respectively, shows the locations of the active fire fronts. Figure 11(b), the map of fire temperature, indicates that temperatures along the active fronts were as high as 1100 K. Figure 11(c), the map of fire fractional areas, indicates that the highest temperatures shown in Figure 11(b) corresponded with fractional areas as high as 95%.

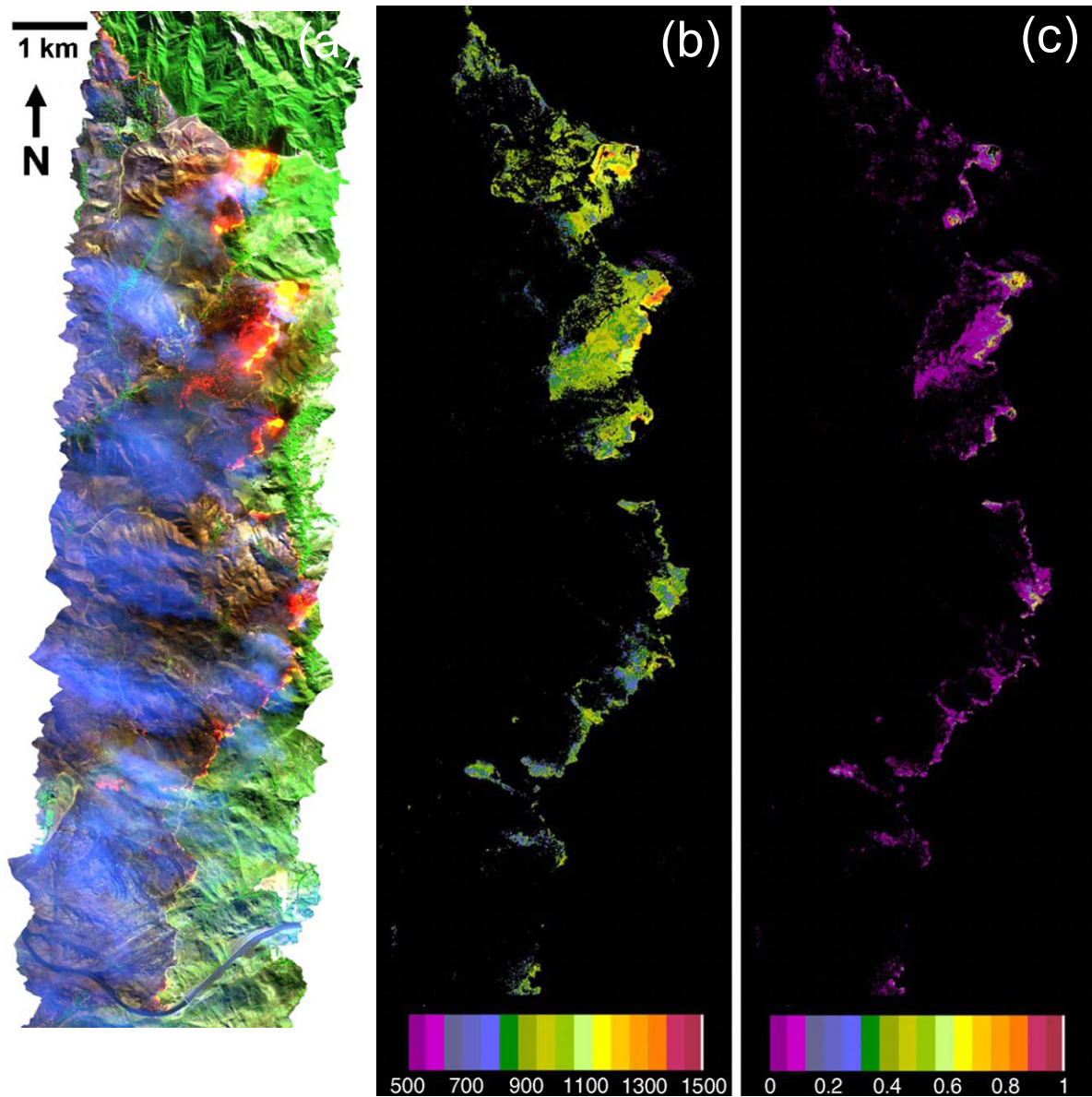


Figure 11. Results of the application of Multiple Endmember Spectral Mixture Analysis (MEMSA) to AVIRIS data from the 2003 Simi Fire. (a) Color-composite of data from the 1.682, 1.107, and 0.655 μm channels of AVIRIS; (b) map of fire temperatures; and (c) map of fractional areas corresponding to the fire temperatures [Dennison *et al.*, 2006].

3.6 Fire Radiant Power

While the sizes and temperatures of hot spots are important information for studies of wildfires, these parameters tell us little about the amount of fuel (biomass) consumed, or mass of carbon volatilized, by a fire. The fire radiant power (FRP) is an instantaneous measure of the radiant energy released by combustion, per unit area, that can be derived via remote sensing. The integral of FRP over the life of a fire gives us the fire radiant energy (FRE), which is proportional to the total amount of biomass consumed by the fire (Kaufman et al. 1998a,b,c; Wooster et al. 2003 and 2005; Roberts et al. 2005).

The theoretical form of FRP is based on the Stefan-Boltzmann Law, which is the integration of the Planck Law over wavelength and solid angles. The Stefan-Boltzmann Law describes the radiant flux per unit area (W m^{-2}) corresponding to a temperature T :

$$M = \sigma T^4,$$

where σ is the Stefan-Boltzmann constant ($5.67 \times 10^{-18} \text{ J s}^{-1} \text{ m}^{-2} \text{ K}^{-4}$). For a fire with multiple temperature components, the FRP may be expressed as:

$$FRP = \varepsilon \sigma \sum_{i=1}^n A_i T_i^4,$$

where n is the total number of temperature components, A_i and T_i are the fractional area and temperature, respectively, of the i^{th} component, and ε is the (broadband) emissivity of the fire. If there are only two temperature components, fire plus background, then the standard two-component temperature retrieval techniques can be used to estimate A_i and T_i . In practice, however, the FRP is derived via empirical functions of the 4- μm temperature (T_4), such as the approximation developed by the MODIS Fire Team (e.g., Kaufman et al. 1998a and 1998b):

$$FRP \approx 4.34 \times 10^{-19} (T_{4,f}^8 - T_{4,b}^8),$$

where $T_{4,f}$ and $T_{4,b}$ indicate the 4- μm temperatures of the fire and background, respectively. The difference between the fire and background temperatures provides an approximation of the “excess radiance” generated by the fire.

The chief advantage of the MODIS FRP estimation technique is its simplicity—the estimation is based on radiance measured in one spectral channel. To extend this advantage to data acquired with other instruments, Wooster et al. (2003 and 2005) have developed a more generalized estimation procedure. The first step in the development of this technique was to approximate the 4- μm radiance (L_4) with a simple power law:

$$L_4 \approx aT^4$$

that holds for temperatures in the range between 650 and 1300 K. The coefficient a is a function of the band-pass of the 4- μm channel and, with the notable exception of the BIRD HSRS ($a = 3.33$), this coefficient may be approximated as 3×10^{-9} (Wooster et al. 2005). The use of the

power law approximation for radiance results in a simplified model that does not require knowledge of the fire or background temperatures:

$$FRP \approx \frac{A\sigma}{(3 \times 10^{-9})} (L_{4,f} - L_{4,b}),$$

where A is the projection of the instrument IFOV onto the surface, σ is the Stefan-Boltzman constant, and $L_{4,f}$ and $L_{4,b}$ are the radiance of the fire and background, respectively, at 4 μm . Applications of the simplified FRP model to BIRD, SEVIRI, and GOES data are found in Wooster et al. (2003), Roberts et al. (2005), and Pereira et al. (2009), respectively. We use the FRP approach to help define the HypSPIRI saturation temperature, and we will return to our discussion of this approach in a later section.

4 Case Studies

Our specification of saturation temperature is based on a review of the literature and analyses of airborne and satellite data from five case studies. As discussed in the previous sections, the presence of multiple temperature components within a pixel results in temperature estimates that depend strongly on the spatial and spectral resolution of the radiance measurements. Our case studies are based on radiance measurements at spatial resolutions < 60 m aggregated to 60-m, or HypsIRI, resolution prior to the estimation of temperature. This strategy gave us explicit knowledge of the extent of sub-pixel mixing. For the published temperature estimates, we gave preference to estimates derived from radiance measurements at spatial resolutions > 60 m that included estimates of the area of the hot component. This strategy allowed us to determine if the hot component would fill a HypsIRI pixel.

4.1 Published Studies

Without access to the original radiance data, we cannot aggregate the published temperature estimates derived from radiance measurements at high spatial resolution (< 60 m) to HypsIRI resolution. However, such estimates provide a useful perspective on the variability of high-temperature phenomena. For example, Wooster et al. (2005) reported temperature estimates up to 1650 K for an experimental fire beneath an 11.5-m observation tower. These temperature estimates were derived from data acquired with a non-imaging spectro-radiometer. Riggan et al. (1993 and 2004) described the use of an airborne IR scanner to measure temperatures in the range 1400–1600 K for leading edges of controlled burns in the Brazilian savanna. Temperatures within the fires were in the range 900–1200 K, and the trailing edges were < 900 K. Dennison et al. (2006) applied spectral endmember mapping to AVIRIS data acquired over a wildland fire in Southern California and estimated fire temperatures as high as 1500 K, with the majority of temperatures in the range 750–950 K. Eckmann et al. (2009) estimated fire temperatures up to 1500 K through an application of spectral endmember mapping to ASTER data.

Examples of temperature estimates for volcanic phenomena include Rose and Ramsey (2009), who derived temperature estimates of ~ 1080 K from ASTER VNIR data acquired over open-channel lava flows from Klyuchevskoy Volcano. Wooster et al. (2000) reported temperatures up to ~ 1100 K for the active lava dome at Unzen lava dome, derived from Landsat TM data acquired in 1991 and 1992. Vaughan et al. (2008) estimated temperatures up to ~ 825 K for carbonate-rich lava flows at Oldoinyo Lengai Volcano based on analysis of ASTER data.

Turning to surveys conducted at low spatial resolution, Harris et al. (1995a) found that 240,000 m² of a lava flow emplaced during the 1984 eruption of Krafla Volcano was at a temperature of ~ 1325 K. This expansive hot spot, mapped with AVHRR data, would contain over 65 HypsIRI pixels. The two-component temperature modeling performed by Harris et al. is similar to the dual-band approach discussed by Wright and Flynn (2003) and Wright et al. (2010); the temperature of the hot component was fixed at 1325 K, and the area of this component and the background temperature were estimated from the observed radiance. Eckmann et al. (2008) applied spectral endmember mapping to MODIS data acquired over wildland fires in the Ukraine and found several pixels containing components at 500 K that were large enough to fill a HypsIRI pixel. The investigators validated the size of the hot components through comparison with coincident ASTER SWIR data.

As shown in Table 1 and Figure 2, the BIRD HSRS provided 4- μm radiance measurements with the highest spatial resolution (370 m) and saturation temperature (600 K) of the heritage instruments. Based on these attributes, the published results from HSRS are strong predictors of the potential results from HypsIRI. The lifespan of the BIRD mission was brief—BIRD was launched on October 22, 2001, and operations ceased on December 31, 2005.

Table 2 is a summary of HSRS results drawn from Briess et al. (2003), Oertel et al. (2004), Siegert et al. (2004), and Zhukov et al. (2006). The areas corresponding to the high-temperature features are given in hectares; for the purpose of comparison with HypsIRI, we note that a 60-m HypsIRI pixel (3600 m²) is equal to 0.36 hectares. All of the features listed in Table 3 were large enough to fill at least one HypsIRI pixel. The largest feature in this table, a lava flow of Mt. Etna, would fill 69 HypsIRI pixels. The HSRS results suggest that the HypsIRI saturation temperature should be no lower than 1000 K.

Table 2. Temperature Estimates Derived from BIRD HSRS Data

Australia Fire 2002-01-05		Kalimantan Fire 2002-08-24/25		Lake Baikal Fire 2003-06-16		Etna Lava Flow 2002-11-02	
T _f (K)	A _f (Ha)	T _f (K)	A _f (Ha)	T _f (K)	A _f (Ha)	T _f (K)	A _f (Ha)
815	0.48	860	2.5	800 - 920	4.4 - 8.4	540	25
715	2.3	740	1.9	668 - 771	0.7 - 1.5	-	-
893	0.59	650	4.6	716 - 868	1.2 - 3.1	-	-
852	0.92	520	2.1	740 - 839	0.38 - 0.71	-	-
957	1.0	720	1.1	771 - 988	0.23 - 0.70	-	-
796	0.39	690	3.0	819 - 913	1.4 - 2.3	-	-
-	-	590	3.3	694 - 882	0.36 - 1.21	-	-
-	-	560	0.7	-	-	-	-

4.2 Team Studies

4.2.1 AMS Survey of Southern California Wildfires

In this section, we present an analysis of data acquired with the Autonomous Modular Sensor (AMS) during the Southern California Firestorm of October 2007. The AMS, which is operated by the NASA/Ames Research Center (ARC), was deployed on the Ikhana UAV platform. Figure 12 lists the specifications for the AMS, which was configured in high-temperature mode for the Southern California missions. This configuration included spectral channels between 3.60 and 3.79 (Channel 11) and 10.26 and 11.26 μm (Channel 12). The AMS data were acquired between October 24 and 28; there were no flights on October 27 due to cloudy weather conditions.

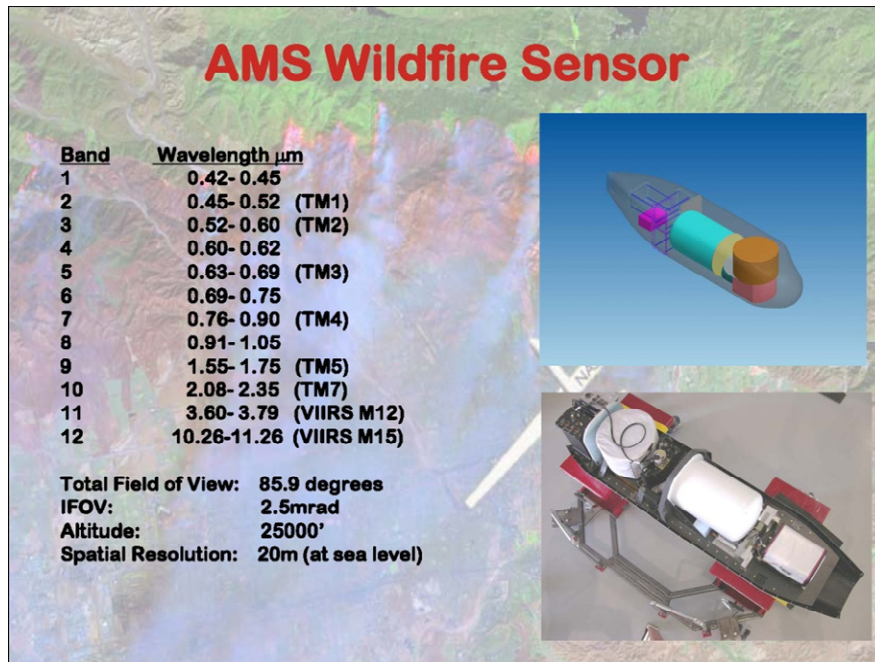


Figure 12. Characteristics of the Autonomous Modular Sensor (AMS), together with photograph showing instrument as mounted in a wing pod [courtesy NASA ARC/ASF].

Figure 13 is a map showing the locations of Southern California fires as of November 9, 2007, following the final containment of the fires. The text boxes outlined in red describe the five fires studied in this report. Table 3 summarizes this information, together with the number of AMS flights over the study areas. Listed from north to south, our study included the Grass Valley, Santiago, Poomacha, Witch, and Harris Fires (Fig. 13). The Witch Fire was the largest and most destructive fire; the Grass Valley Fire was the smallest, in terms of burn area, but the damage to structures was large in proportion to the small size of this fire.

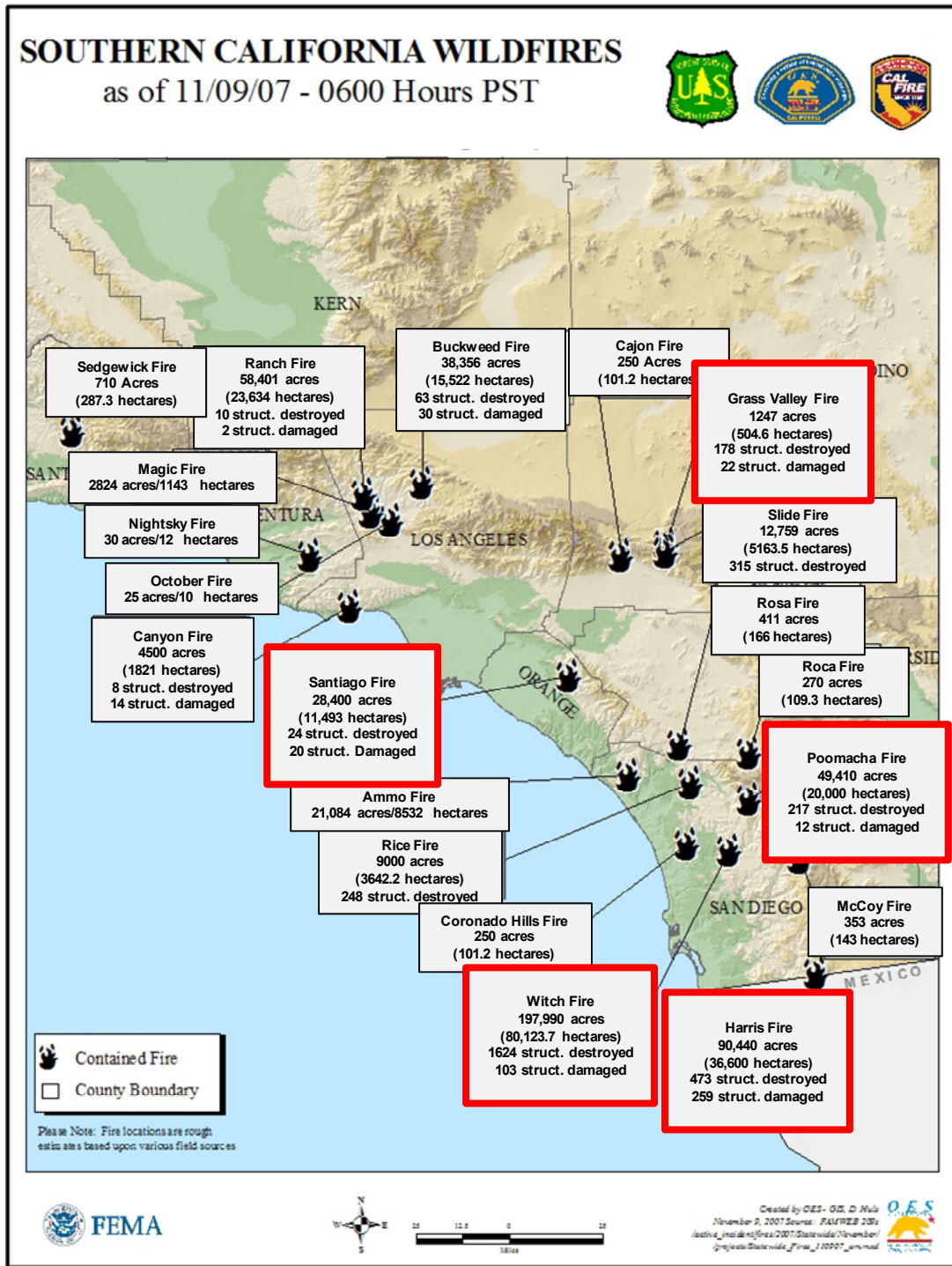


Figure 13. Locations of Southern California Wildfires as of 9 November 2007, following the final containment of these fires. The text boxes outlined in red describe the fires studies in this report.

Table 3. Statistics for the Wildfires Described in Case Study

Name	Burn Area		Structures Damaged or Destroyed	AMS Flight Line Count
	Acres	Hectares		
Grass Valley	1247	505	200	25
Santiago	28,000	11,500	44	9
Poomacha	49,000	20,000	229	19
Witch	198,000	80,000	1727	26
Harris	90,000	37,000	732	15

Analysis Procedure

We obtained the AMS data from the Airborne Sensor Facility (ASF) at ARC. These data are available as HDF files, containing several data fields in addition to the radiance data. For this study we extracted the longitude, latitude, surface elevation (DEM) and sensor zenith angles for each image pixel from the ancillary data fields.

The first step in our analysis was a visual inspection of the radiance data to identify the flight lines that covered active fire fronts, with an emphasis on flight lines that were centered on fire fronts. This emphasis was necessitated by the difference between the total Field of View (FOV) of AMS (85°) and HypsIRI (51°). To approximate the effects of atmospheric absorption and emission on HypsIRI measurements, we restricted our analysis to AMS pixels within ± 26° of nadir.

We used the pixel latitude and longitude data to project the AMS data into UTM coordinates and then aggregated the radiance data to the 60-m spatial resolution of HypsIRI. The map projection and aggregation operations were applied to floating point values to minimize the effects of re-sampling and interpolation on the simulated radiance. Finally, we converted the simulated HypsIRI radiance to brightness temperature.

Figure 14 demonstrates of the impact of spatial resolution on our temperature estimates. At high spatial resolution, the probability that the surface, or target, within a pixel is isothermal is also high. With decreasing spatial resolution, there is an increase in the probability of sub-pixel temperature mixing and a decrease in the fractions of a pixel occupied by hot components. If sub-pixel hot spots are present, the general effect of decreasing spatial resolution is a decrease in the pixel-integrated temperature.

The data depicted in Figure 14 were acquired over the Santiago Fire on October 26, 2007. Figure 14(b) is a map of 3.7- μm (Channel 11) brightness temperatures at a spatial resolution of 8.3 m (following the re-projection to UTM coordinates). Figures 14(c) and (d) show the results of re-sampling the AMS data to the 60-m spatial resolution of HypsIRI and 1-km resolution of MODIS, respectively. We note that the high-temperature estimates at HypsIRI resolution (Fig. 14[c]) are approximately 25 K lower than the original estimates (Fig. 14[b]), but the relative distribution of temperature within the active fire fronts are preserved in the simulated HypsIRI scene. At the 1-km spatial resolution of MODIS (Fig. 14[d]), the high-temperature estimates are 100 K lower than the original estimates (Fig. 14[b]), and we have lost any information regarding the spatial distribution of temperature with the fire fronts.

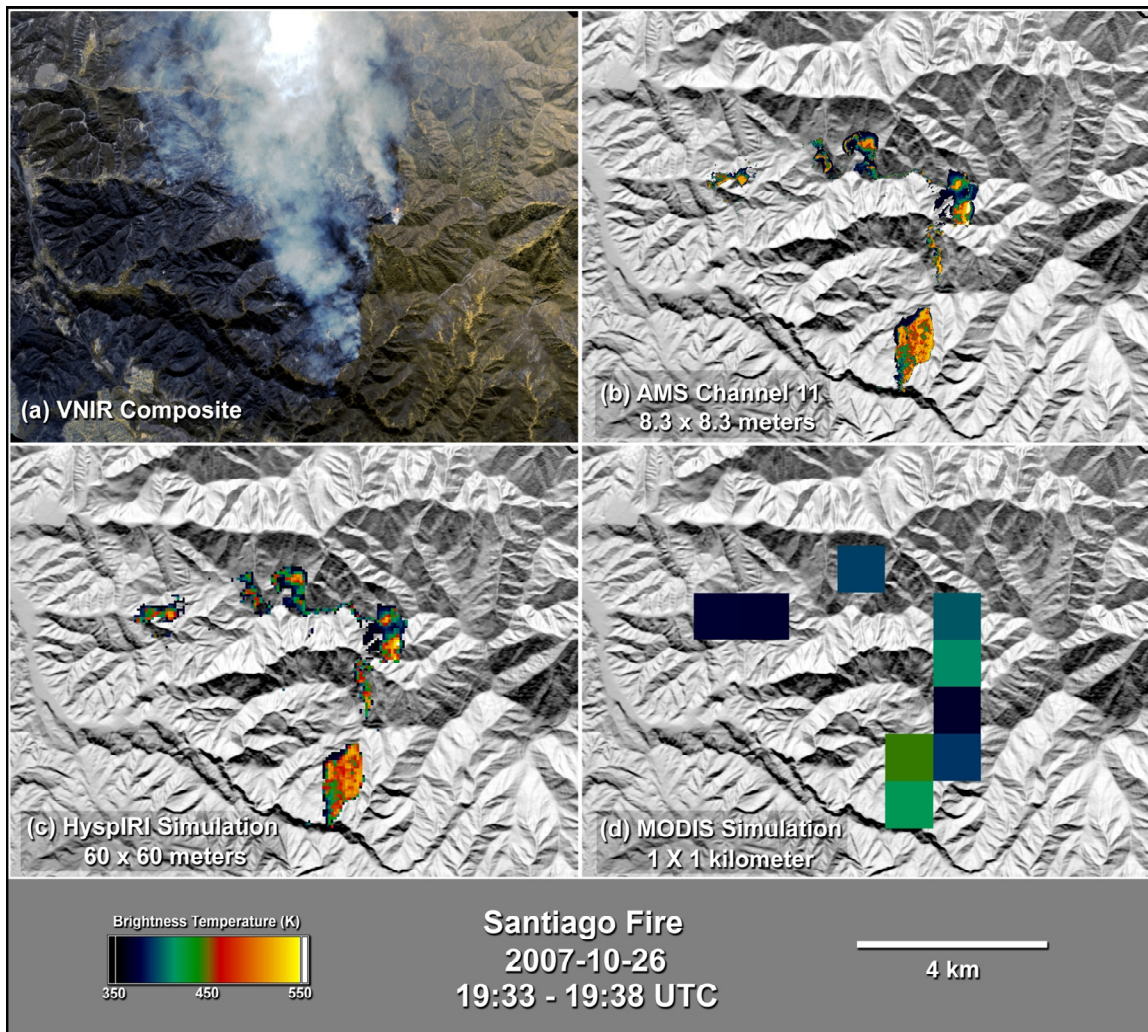


Figure 14. Impact of spatial resolution on the perceived temperature of a pixel. (a) Color-composite of AMS VNIR data; (b) 4- μm temperature at native AMS resolution (8.3 meters); (c) temperature at HypsIRI resolution (60 meters); and (d) temperature at MODIS resolution (1 km).

Our original intent for this case study was to use the aggregated AMS 3.7- μm radiance data to predict the maximum 4- μm radiance that HypsIRI might encounter over a wildland fire. However, we could not follow this approach due to saturation of the 3.7- μm (Channel 11) radiance data. As shown in Figure 15, a scatterplot of brightness temperatures for the 3.7- and 10.5- μm channels (Channels 11 and 12, respectively), the 3.7- μm temperatures did not exceed 530 K. However, the scatterplot results suggested that we could use the 10.5- μm (Channel 12) data to measure temperatures up to 800 K. Laboratory calibration of AMS, performed in 2008 (Fig. 16), confirmed the saturation of the 3.7- μm channel and the lack of saturation in the 10.5- μm channel. The calibration of the 10.5- μm channel revealed a temperature-dependent bias that we accommodated with the following linear correction: $T_{true} = (T_{est} - 71\text{K})/0.8175$.

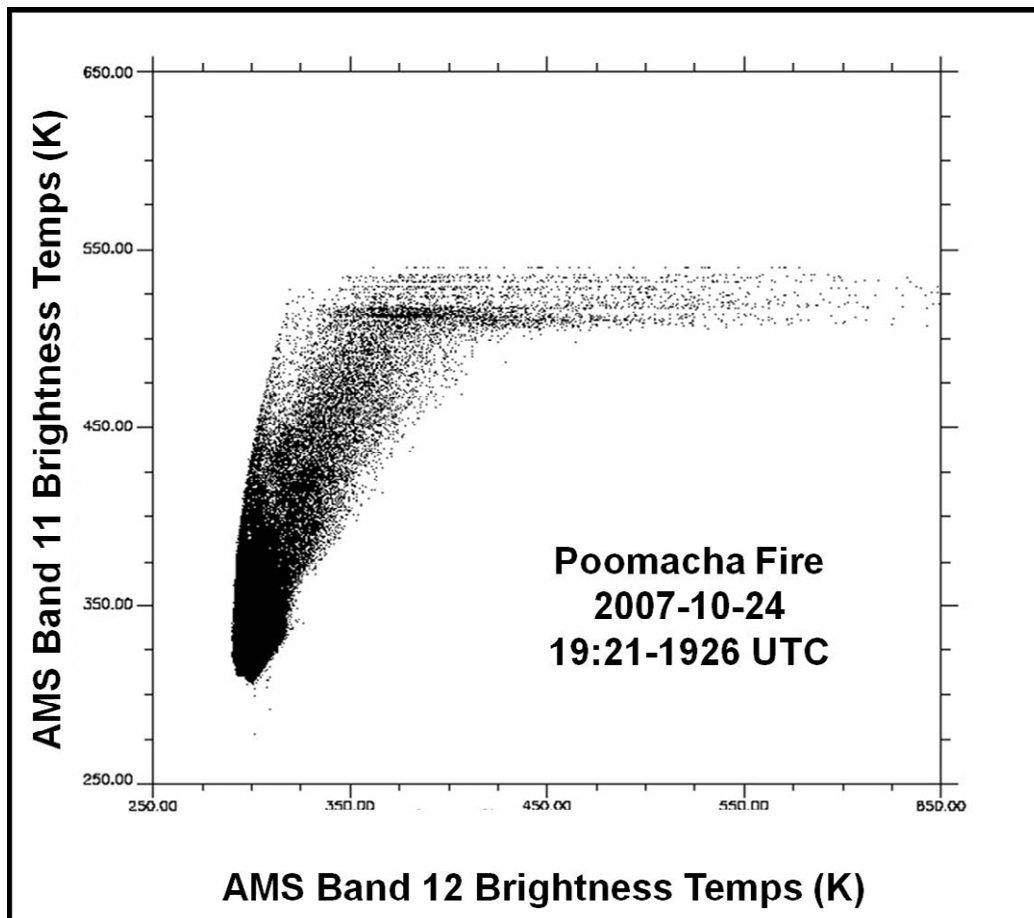


Figure 15. Scatterplot of brightness temperatures in AMS Channel 11 (3.7 μm) vs. Channel 12 (10.5 μm)

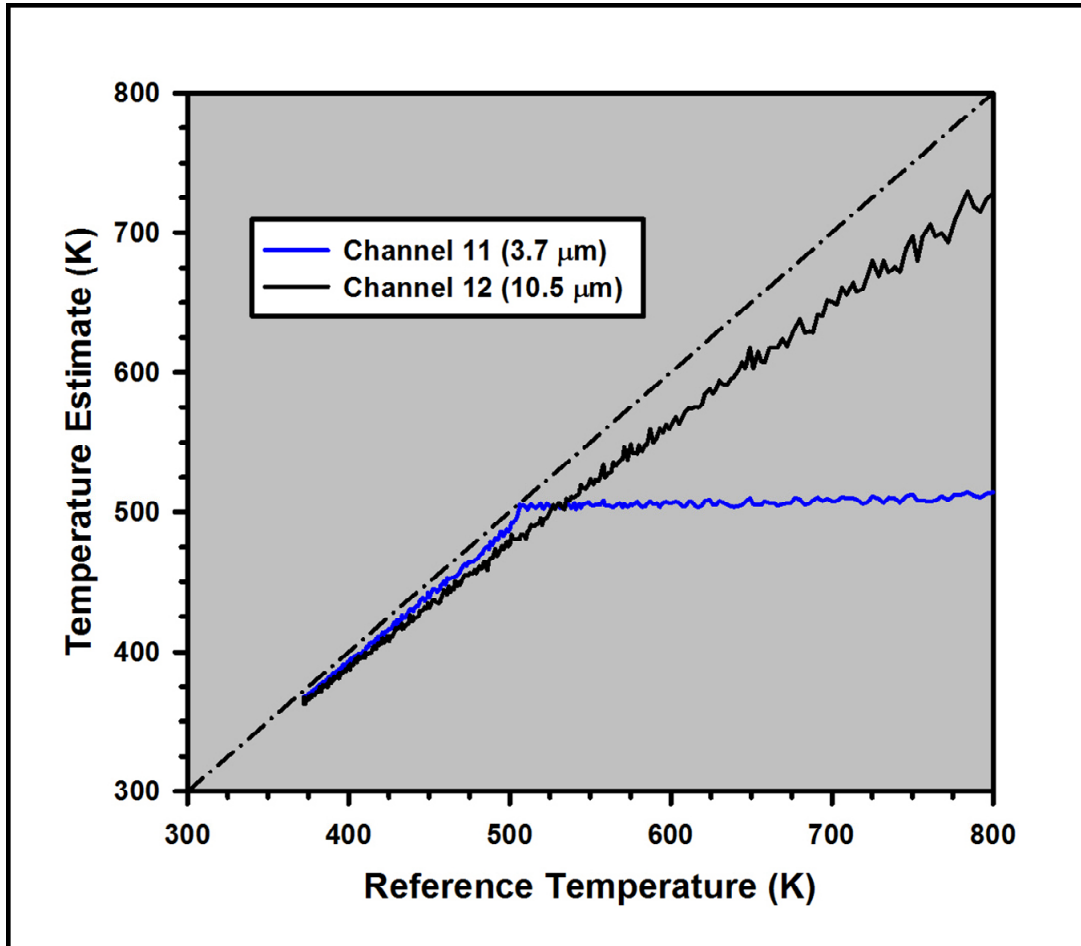


Figure 16. Laboratory calibration of AMS Channels 11 and 12. Dashed line indicates perfect agreement between reference and estimated temperatures. Temperature-dependent bias in the Channel 12 response modeled as $T_{ref} = (T_{est} - 71K)/0.8175$ [courtesy NASA/ARC ASF].

Figure 17 is a collection of histograms showing the probability distribution of the hot temperatures ($330 \leq T \leq 730$ K) for each study area, following aggregation of the 10.5- μm radiance data from native resolution to 60-m HypsIRI-scale pixels. We see that the probability distribution for all fires (Fig. 17[a]), is dominated by the Poomacha Fire (Fig. 17[b]), which contributed approximately 60% of the pixels to the total. We note that the Witch Fire (Fig. 17[e]) contributed only 7.4% of the pixels to the total. The sizes of these contributions appear to be counterintuitive, as the area burned by the Witch Fire was more than four times larger than the area burned by the Poomacha Fire. Fire science is beyond the scope of this report, and additional research will be required to determine if this negative correlation between total burn area and fire temperature was the result of environmental factors, such as available fuel loads or local topography, or a bias imposed by the logistics of deploying the Ikhana UAV platform. For example, the Ikhana may not have surveyed the hottest portions of the Witch Fire due to scheduling or airspace restrictions.

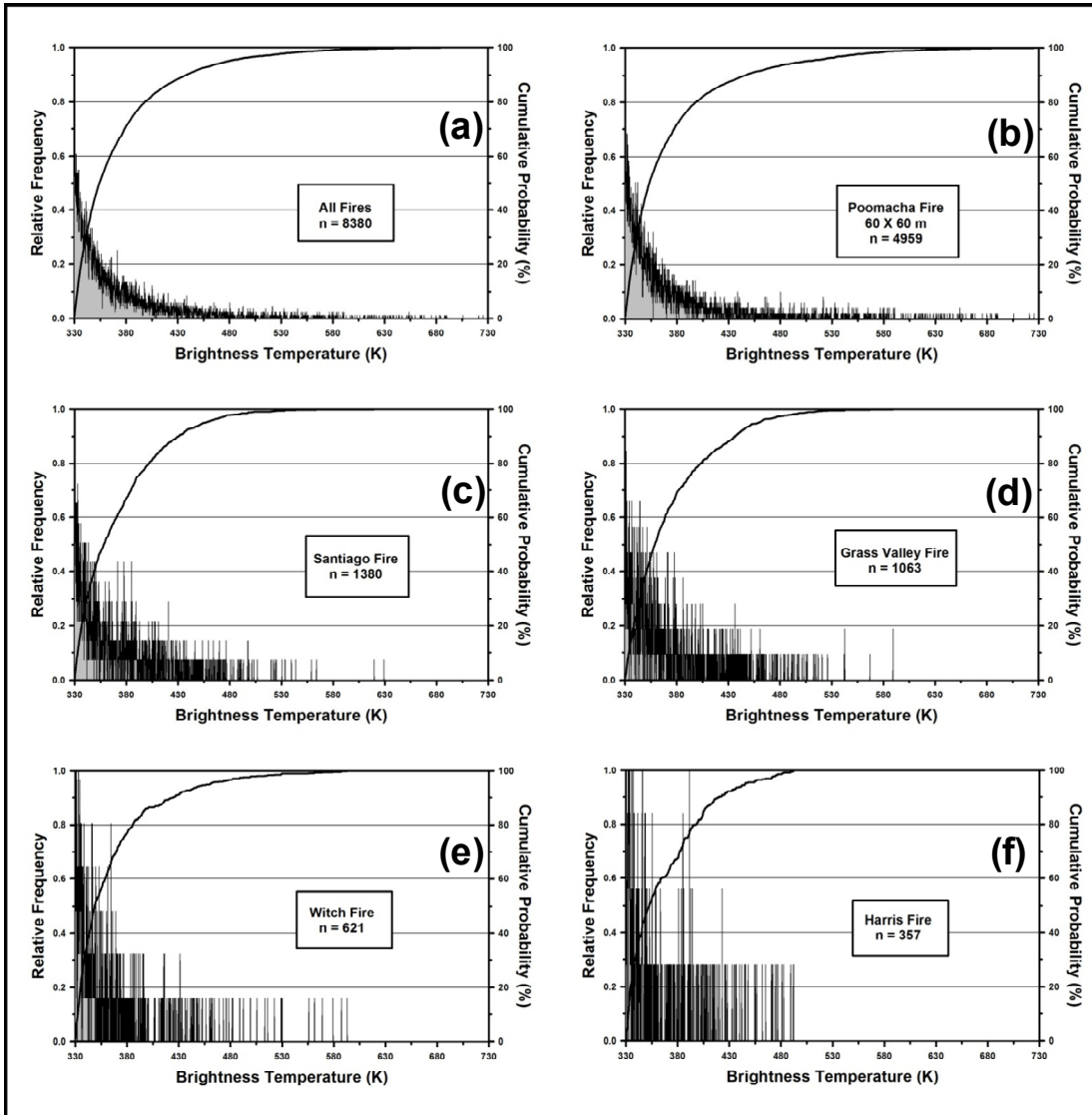


Figure 17. Relative frequency and cumulative histograms of high temperatures estimates (330 – 730 K), following aggregation of the Channel 12 (10.5 μm) radiance from native resolution into 60-m HypsIRI pixels. (a) Histogram for all fires; (b) Poomacha Fire histogram, (c) Santiago Fire histogram; (d) Grass Valley Fire histogram; (e) Witch Fire histogram; and (f) Harris Fire histogram.

We will focus our attention on the Poomacha data since the data depicted in Figure 17 suggest that the Poomacha histogram could be used as a proxy for the all-fire histogram. The maximum temperature at 60-m resolution was 795 K, following the application of our linear correction. As we saw in Figure 14, the high spatial resolution of HypsIRI will minimize the effects of sub-pixel temperature mixing.

To evaluate the impact of sub-pixel mixing on the maximum temperature estimate, we compared the cumulative histograms of the temperatures at native and aggregated (60-m) resolution. This comparison is found in Figure 18, where Figs. 18(a) and 18(b) are the histograms for the native and aggregated 60-m resolution, respectively, and Fig. 18(c) is the comparison of cumulative histograms. We see that the cumulative histograms diverge for temperatures higher than 380 K, corresponding to a cumulative probability of 60%. For temperatures higher than 380 K, the native-resolution temperatures are higher than the corresponding 60-m temperatures at probabilities greater than 60%, although the separation between the cumulative histograms is less than 5%.

The agreement between the cumulative histograms (Fig.18[c]) indicates that the 60-m temperature distribution maintained much of the structure of the native distribution, but sub-pixel temperature mixing was a factor for pixel-integrated temperatures greater than 380 K. Therefore, the maximum aggregated temperature of 795 K must be a lower bound on the HypsIRI saturation temperature.

4.2.2 AGEMA Camera Data for Sharpsand Creek Fire

The Sharpsand Creek fire was a prescribed burn conducted via collaboration between the Canadian Forest Service and the Ministry of Natural Resources, with scientists from King's College London, University of Edinburgh, and University of Leicester attending from the UK. The burn site was 1 hectare (approximately 100 m x 100 m square) of Jack Pine forest located approximately 60 km north of Thessalon, Ontario, Canada (latitude 46° 47' N, longitude 83° 20' W). Smith et al. (2009) describe the Sharpsand Creek site and the prescribed burn, which occurred on May 13, 2007.

The plot was lit with a perimeter ignition pattern, which resulted in some extreme fire behavior, including flames estimated to be > 100-m high at the maximum. During the fire, a helicopter hovered above and slightly to the side of the plot, and IR imagery of the fire was collected using an AGEMA-550 thermal imaging camera equipped with a 3.9- μ m narrowband filter. The pixel brightness temperature measurements were used to calculate FRP per pixel, using the MIR approximations discussed previously (Wooster et al. 2003 and 2005). Detailed discussions of the use of AGEMA-550 data in FRP calculations are provided by Wooster et al. (2005) and Freeborn et al. (2008).

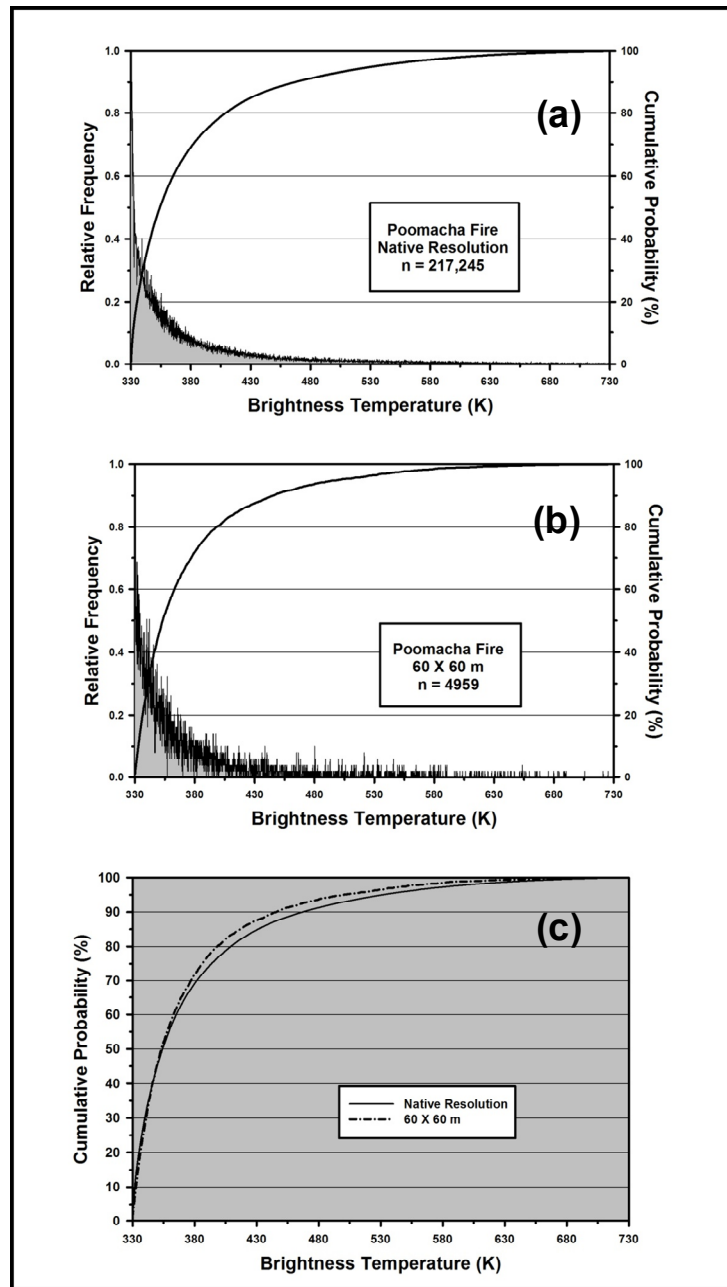


Figure 18. Comparison of Poomacha Fire temperatures at the spatial resolutions of AMS and HyspIRI. (a) histograms for temperatures at native (AMS) resolution; (b) histograms for temperatures at aggregated 60-m (HyspIRI) resolution; and (c) comparison of the cumulative histograms for native-resolution (solid line) and aggregated (dashed line) temperatures.

Figure 19 shows the spatial distribution of FRP generated from the AGEMA-550 data. We evaluated the potential HypsIRI response to this fire with two approaches. In the first approach, we aggregated the FRP over a 60 x 60-m (3600 m²) region of interest centered over the hottest portion of the fire. Recalling the similarity between FRP and the Stefan-Boltzmann Law, we can convert the aggregated FRP, ~ 430 MW, into an apparent temperature of ~1205 K. Our second approach was to aggregate the radiance measurements over the same region of interest and convert this aggregated radiance to an apparent temperature. The aggregated radiance, ~7454 W m⁻² sr⁻¹ μm⁻¹, corresponds to an apparent temperature of ~1260 K. The two temperature estimates are within 5% of each other, and this close agreement is a validation of the approximations entailed in the FRP approach.

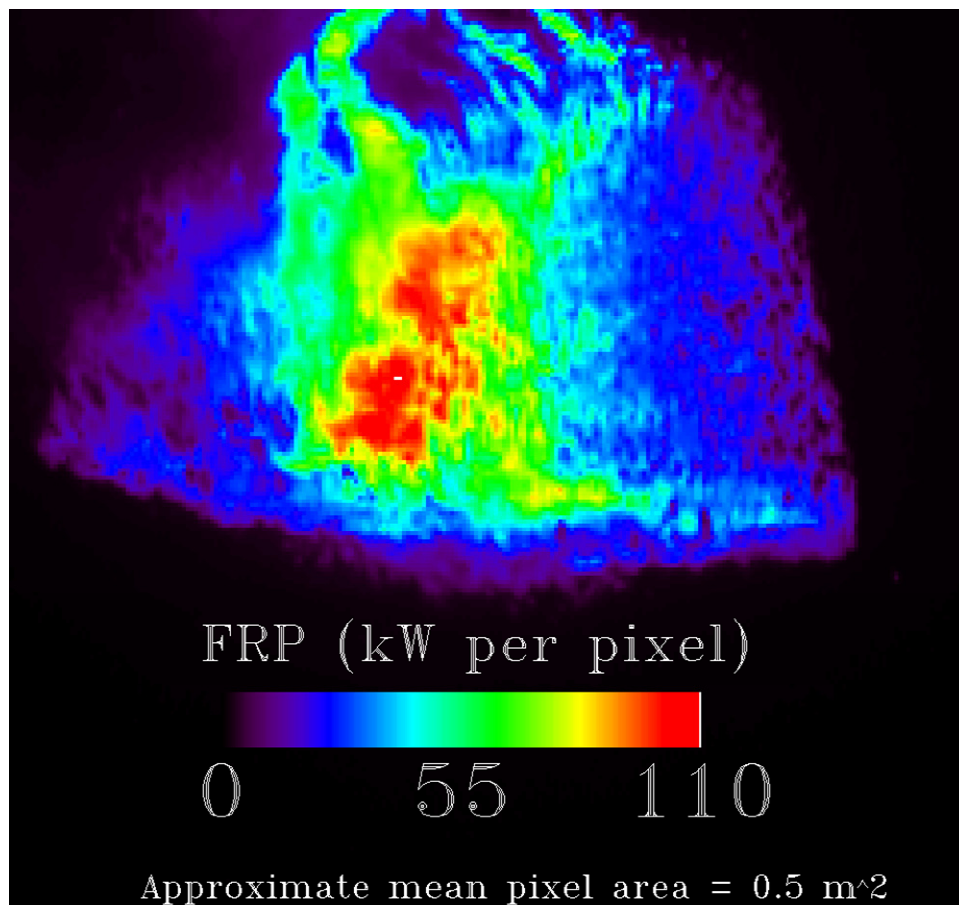


Figure 19. Map of Fire Radiant Power (FRP) estimated for the Sharpsand Creek (Ontario, Canada) prescribed burn. Temperature estimates of 1205 and 1260 K obtained by aggregating the FRP and radiance, respectively, over a 60X60 m region of interest centered on the hottest portion of the fire [data courtesy of M. Wooster].

4.2.3 AVIRIS Survey of the Indians Fire

The Indians Fire burned a 300-km² area of Santa Lucia Mountains, Los Padres National Forest (Monterey County, California). The fire began on June 8, 2008, with final containment on July 10, 2008, and was imaged by AVIRIS and the MODIS/ASTER (MASTER) airborne simulator on June 11. Dennison and Matheson (2011) present a detailed analysis of these AVIRIS and MASTER data.

Figure 20 depicts fire temperatures and corresponding fractional areas derived through the application of the MESMA procedure to the AVIRIS data. The AVIRIS radiance data were aggregated to a spatial resolution of 64 m from the native spatial resolution of 16 m. Following the procedure established by Dennison et al. (2006), the aggregated radiance was modeled as a combination of solar-reflected radiance, emitted radiance, and shade (or zero radiance). The emitted radiance library represented temperatures between 500 and 1500 K, with each spectrum corresponding to a single temperature.

Figure 20(a) is a color-composite of the AVIRIS data acquired at 1.672, 0.957, and 0.655 μm , displayed in red, green, and blue, respectively. The color-composite scene shows the AVIRIS data at native (16-m) resolution. Figures 20(b) and 20(c) are the maps of fire temperature and corresponding area fraction, respectively. Using the area fraction map as a guide, we identified the pixels with an area fraction of 1.0 as well as the temperatures corresponding to these isothermal pixels. Figure 20(d) plots the temperatures of the 14 isothermal pixels found in our analysis. There were six pixels with temperatures greater than 760 K, including a single pixel at of 860 K. A visual inspection of Figures 20(b) and 20(c) suggests that there were a large number of pixels with area fractions only slightly less than 1.0, and many of these pixels were at temperatures between 750 and 1000 K.

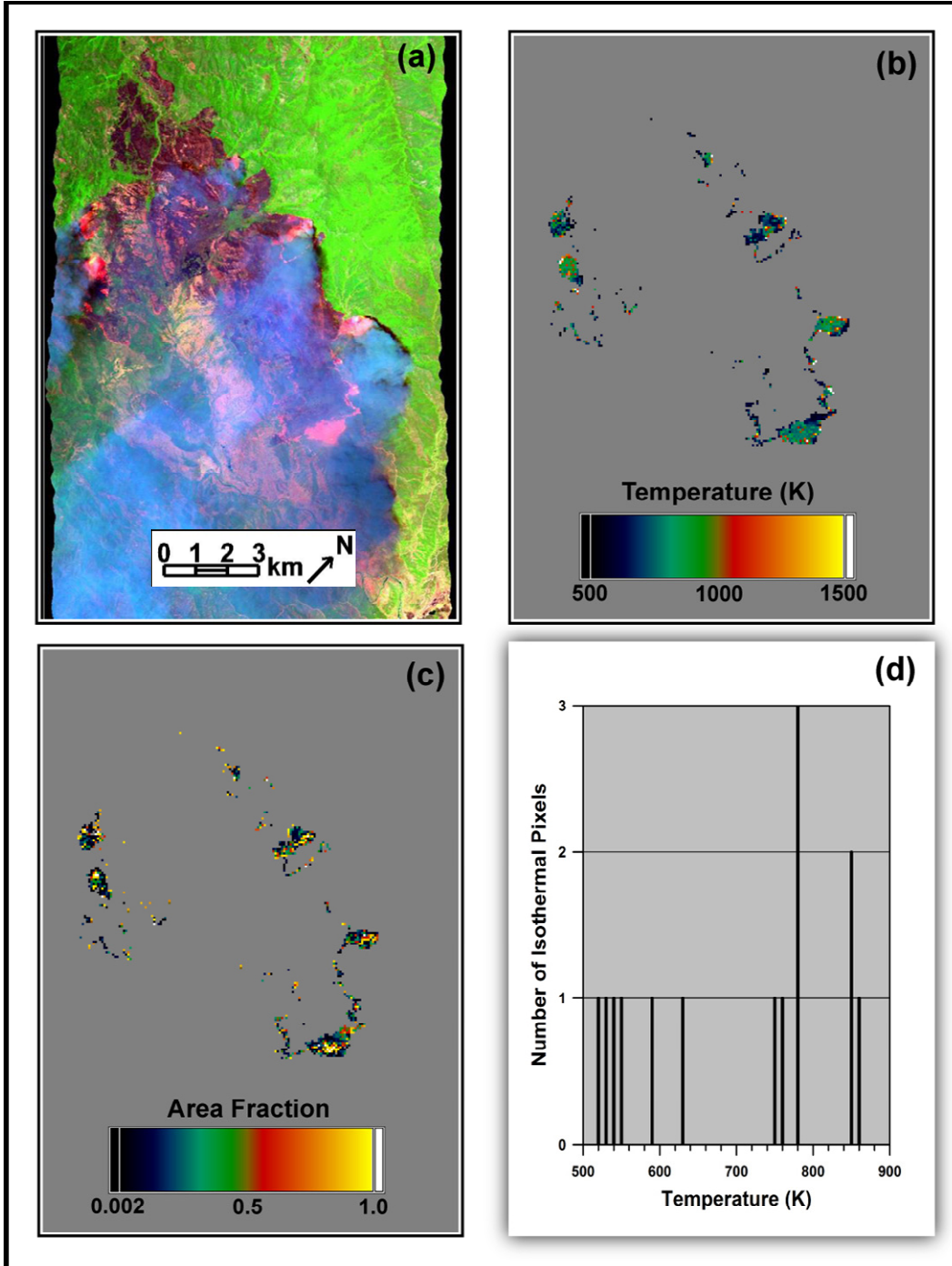


Figure 20. Analysis of AVIRIS data acquired over the 2008 Indians Fire, Monterey County, California. (a) Color-composite of AVIRIS data from the 1.672, 0.957, and 0.655 μm channels; (b) fire temperature derived from application of the MESMA procedure to aggregated AVIRIS pixels; (c) area fractions corresponding to the fire temperatures; and (d) plot of the temperatures of isothermal pixels (area fraction = 1) [data courtesy of P. Dennison].

4.2.4 ASTER Surveys of Klyuchevskoy and Kilauea Volcanoes

ASTER data acquired by the VNIR and SWIR subsystems feature spatial resolutions of 15 and 30 m, respectively, and radiance measurements in the VNIR and SWIR may be aggregated into HypsIRI-scale pixels. Figure 21 contains ASTER data acquired over Klyuchevskoy Volcano (Kamchatka Peninsula, Russia) on May 28, 2007, during an eruption episode that began on February 15, 2007, and ended on July 15, 2007. The color-composite of VNIR data (Fig. 21[a]) reveals an incandescent lava flow within the shadow cast by an eruption plume. This lava flow was hot enough to saturate the SWIR measurements. Fortunately, the aforementioned shadow minimized the reflection of incident solar irradiance and thus facilitated the estimation of lava flow temperatures from the VNIR data. We applied an additional correction for reflected solar irradiance, following the procedure of Wooster and Kaneko (2001).

The twin panels below the VNIR color-composite are maps of lava flow temperatures derived from radiance measured in ASTER Channel 3 (centered at $0.807\ \mu\text{m}$). Figure 21(b) shows the temperatures derived from the radiance at the native spatial resolution (15 m), and Figure 21(c) shows the temperatures derived from radiance aggregated to HypsIRI-scale (60-m) pixels. As shown in these temperature maps, the aggregation of radiance resulted in a decrease of $\sim 60\ \text{K}$ in the maximum observed temperature: 1101 vs. 1043 K.

Figure 22 depicts ASTER data acquired over Kilauea Volcano, Hawaii, on November 25, 2007, during an outbreak of surface activity. These data were acquired during a nighttime overpass to eliminate the contributions of reflected solar irradiance to the temperature estimates. The active flow field is prominent Figure 22(a), an example of ASTER TIR data. The high temperatures of the active flows resulted in saturation of the TIR and SWIR data. The twin panels below the TIR scene are temperature maps derived from Channel 3 radiance. Figure 22(b) shows the temperatures derived from radiance at the native spatial resolution, and Figure 22(c) shows the temperatures derived from Channel 3 radiance aggregated to HypsIRI-scale pixels. The aggregation resulted in a decrease of $\sim 130\ \text{K}$ in the maximum observed temperature: 1122 vs. 993 K. This large reduction in maximum temperature, relative to the aggregation-based reduction in the maximum temperature of the Klyuchevskoy flow (Figs. 21[b] and 21[c]), is a consequence of the smaller size and isolated nature of the Kilauea hot spots (Figs. 22[b] and 22[c]).

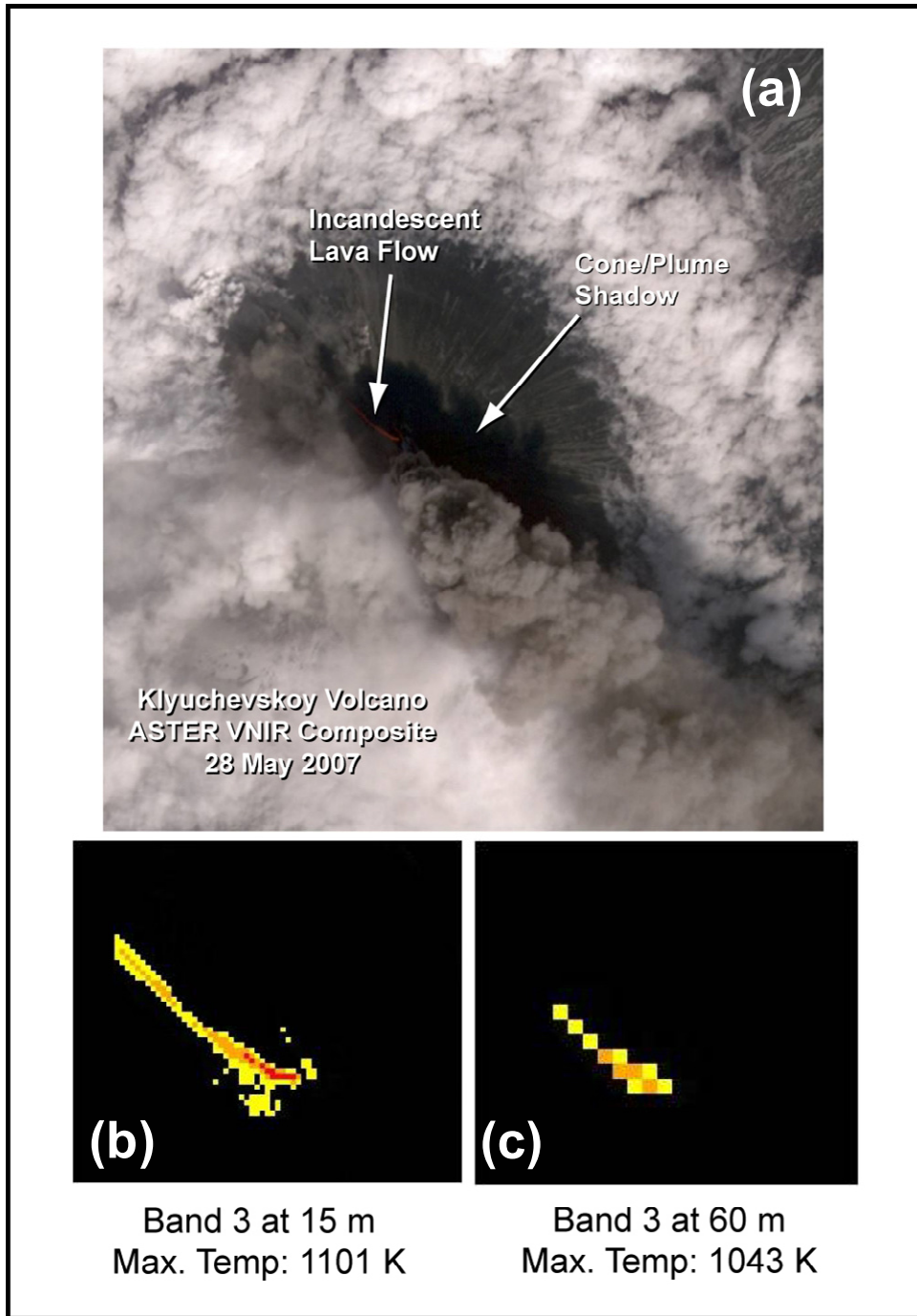


Figure 21. ASTER data acquired over Klyuchevskoy Volcano. (a) Color-composite of ASTER VNIR data showing incandescent lava flow in the shadow cast by an eruption plume; (b) lava flow temperatures derived from Channel 3 (0.807 μm) radiance measurements; (c) lava flow temperatures derived from Channel 3 radiance following aggregation to 60-m pixels [data courtesy of M. Ramsey].

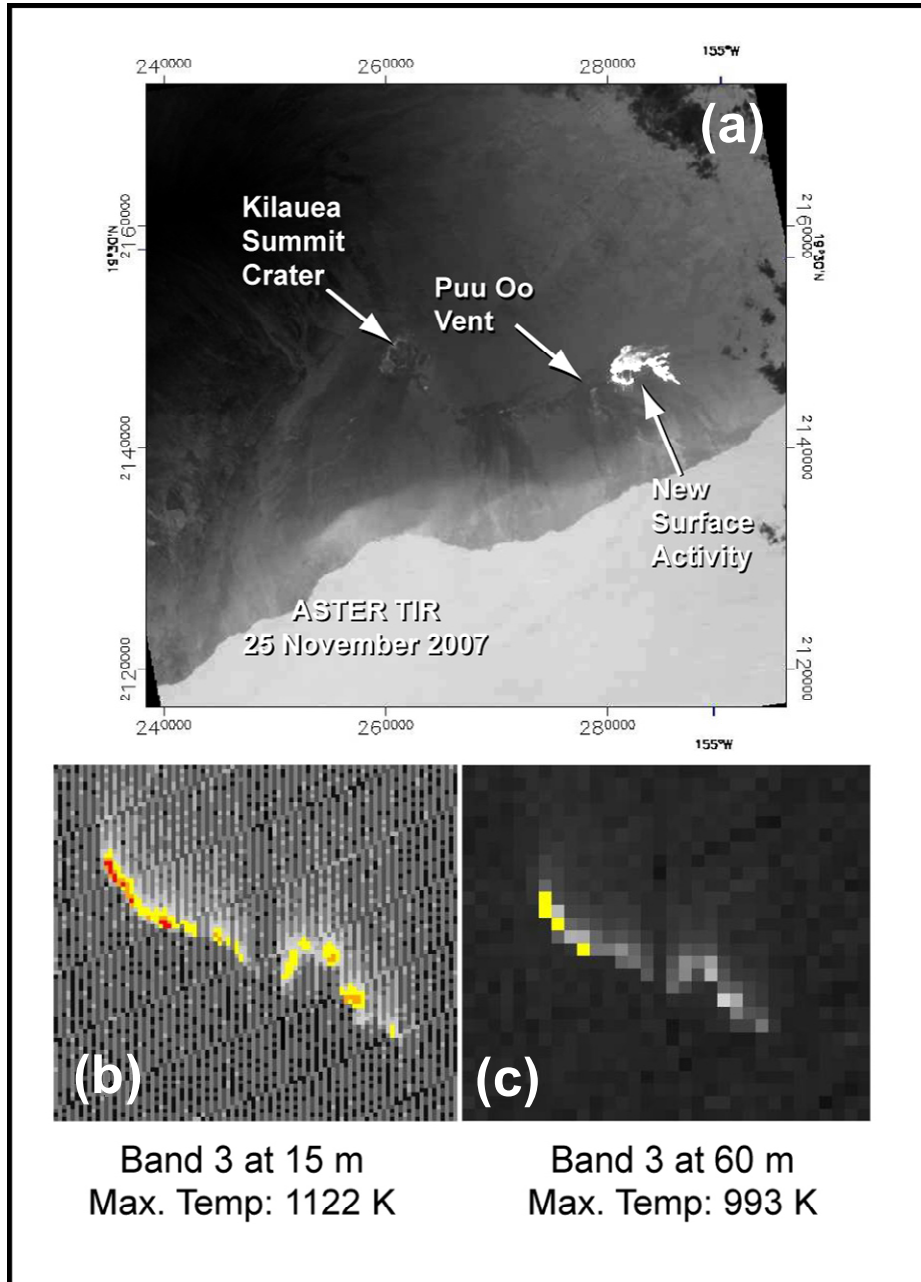


Figure 22. ASTER data acquired over Kilauea Volcano, Hawaii. (a) Night-time TIR data, showing active lava flow field; (b) lava flow temperatures derived from Channel 3 (0.807 μm) radiance measurements; (c) temperatures derived from Channel 3 radiance following aggregation to 60-m pixels [data courtesy of M. Ramsey].

4.2.5 Hyperion Surveys of Nyamuragira and Eyjafjallajökull Volcanoes

Figures 23 and 24 feature 4- μm temperature maps for Nyamuragira (DR-Congo) and Eyjafjallajökull (Iceland) Volcanoes as simulated from hyperspectral V-SWIR radiance spectra measured with Hyperion. The Hyperion data were acquired at night to eliminate the contributions of reflected solar irradiance to the temperature estimates. At the time the Nyamuragira data were acquired, May 21, 2004, the activity at the volcano was near the end of an eruption episode that began on May 8, 2004 and ended sometime between May 25 and 31, 2004. The Eyjafjallajökull data were acquired on April 1, 2010, during an eruption that began with the opening of a fissure on March 20, 2010. The data acquisition coincided with the opening of a new fissure on March 31, and the data depict lava fountains from both fissures.

The temperature maps (Figs. 23 and 24) are the results of a multi-step analysis procedure. For each pixel in the Hyperion data, we derived sub-pixel temperature components and corresponding area fractions through an application of the minimized multi-component procedure (see Figure 10). The resulting temperature distribution was used to calculate a continuous (VIS through TIR) radiance spectrum, which we convolved with the notional spectral response of the HypsIRI 4- μm channel to simulate radiance measured in this channel. Figures 23(a) and 24(a) are maps of the temperatures derived from this simulated radiance at the native (30-m) spatial resolution of Hyperion. Figures 23(b) and 24(b) are maps of temperatures derived from radiance aggregated to HypsIRI-scale pixels. The aggregation resulted in a reductions of approximately 150 and 350 K in the maximum temperatures for the Nyamuragira flow field (1100 vs. 950 K) and Eyjafjallajökull fissures (1100 vs. 750 K), respectively.

The bottom set of panels indicate the pixels that would be saturated with 4- μm saturation temperature settings of 800–1000 K (Figs. 23[c], [d], and [e]) in the case of Nyamuragira and 700–900 K in the case of Eyjafjallajökull (Figs. 24[c], [d], and [e]). We see that saturation temperature settings of 1000 and 900 K, respectively, would be required to prevent saturation of HypsIRI data acquired during Nyamuragira- and Eyjafjallajökull-class eruptions.

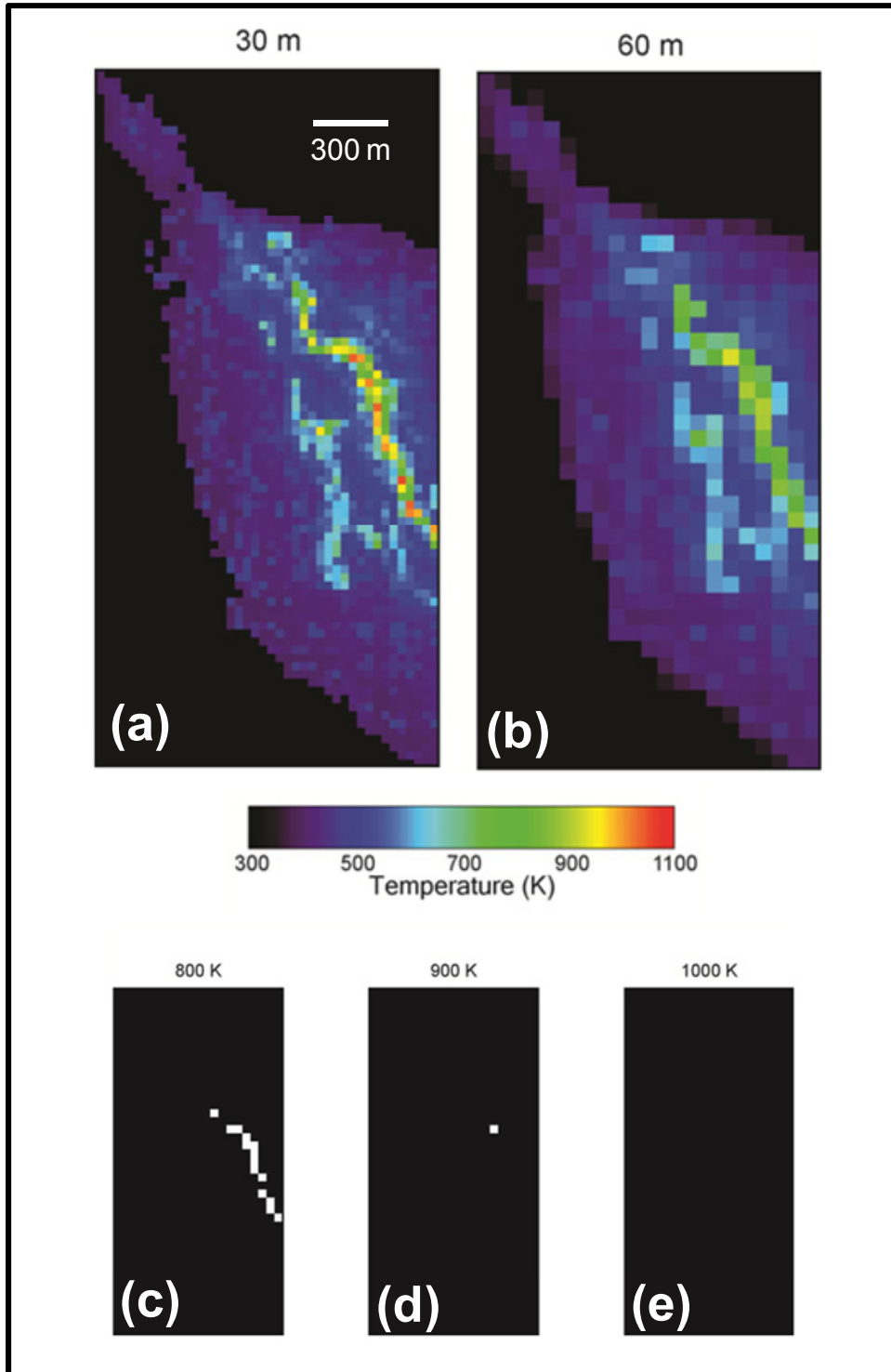


Figure 23. Analysis of Hyperion data acquired over Nyamuragira Volcano on 21 May 2004. (a) Simulated 4- μm temperatures at native (30 m) spatial resolution of Hyperion; (b) simulated 4- μm temperatures for aggregated, HyspIRI-scale pixels; (c) – (e) maps of pixels saturated for saturation temperature settings of 800, 900, and 1000 K, respectively [data courtesy of R. Wright].

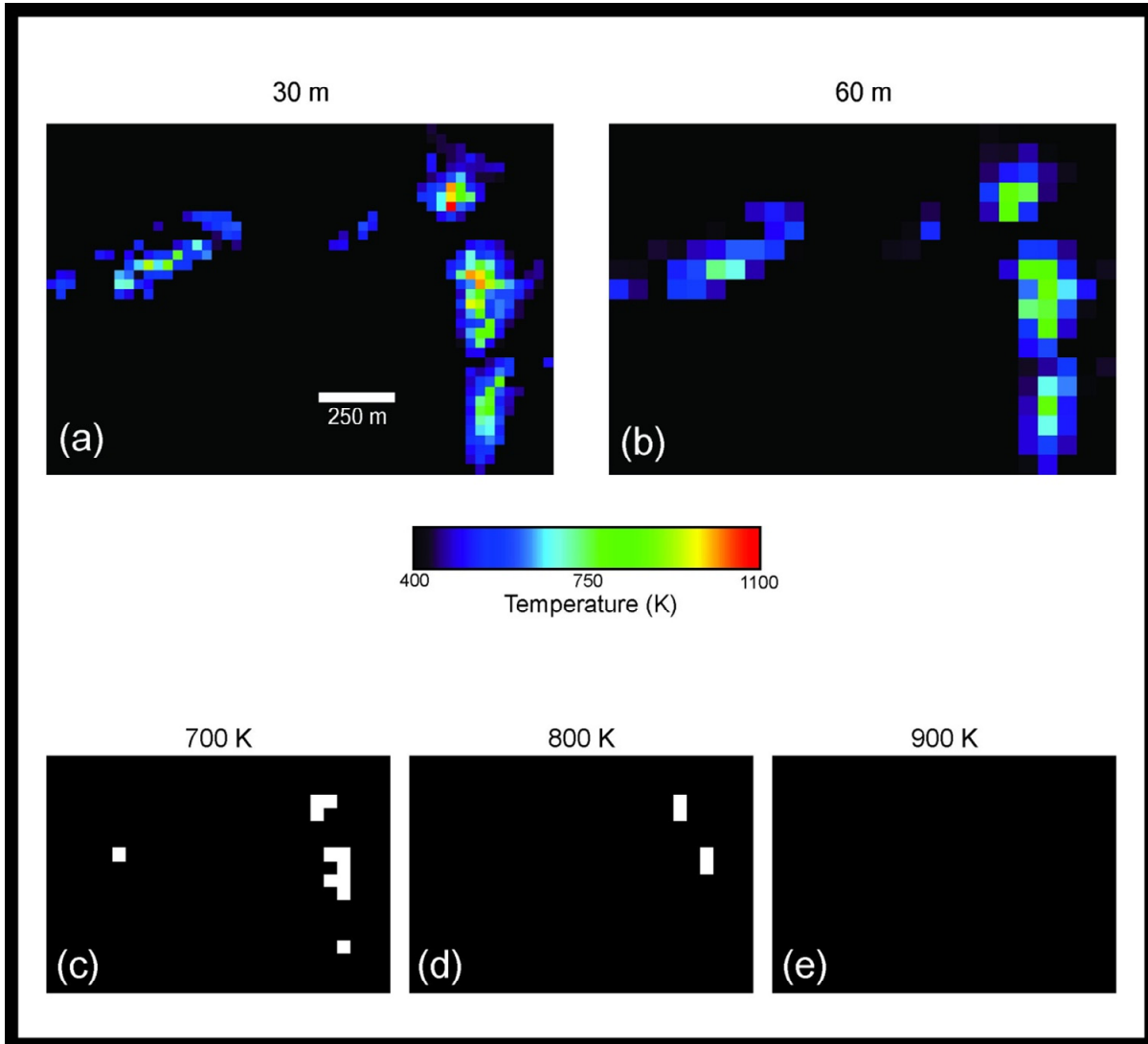


Figure 24. Analysis of Hyperion data acquired over Eyjafjallajökull Volcano on 1 April 2010. (a) Simulated 4-mm temperatures at native (30 m) spatial resolution of Hyperion; (b) simulated 4-mm temperatures for aggregated, HypsIRI-scale pixels; (c) – (e) maps of pixels saturated for saturation temperature settings of 700, 800, and 900 K, respectively [data courtesy of R. Wright].

5 Conclusion

Table 4 summarizes the results of our case studies, together with the highest temperature estimates published for the Lake Baikal Fire of 2003 (Zhukov et al. 2006) and Krafla eruption of 1984 (Harris et al. 1995a). Based on these results we recommend a 4- μm saturation temperature setting of 1200 K. This setting will prevent saturation for all of the temperatures found in our studies with the exception of the Sharpsand Fire (and we note that the lower of our simulated HypsIRI temperatures for this fire was 1205 K) and the Krafla Eruption of 1984.

Referring to Figure 2, a saturation temperature of 1200 K will result in NEAT levels of 8–4.5 K for scene temperatures in the range 320–340 K, respectively. The proposed NEAT levels are too high for land- and sea-surface temperature studies with the HypsIRI 4- μm channel, but the TIR channels between 8 and 12 μm (Fig. 1) will be well-suited for studies of ambient surface temperatures. In addition, we note that HypsIRI data acquired over the oceans will be aggregated into 960-m pixels (representing a 16 x 16 block of 60-m pixels) with a corresponding 16 times improvement in NEAT. The aggregated 4- μm radiance data may fit the needs of the sea-surface temperature community.

The trade-off between saturation temperature and sensitivity is particularly acute for fire and hotspot detection techniques, and the full impact of the proposed NEAT on such algorithms has yet to be determined. For example, the Fire Radiant Power (FRP) algorithm will require us to measure fire temperatures together with temperatures adjacent to the active fire fronts. A smoldering fire at 700 K occupying 1% (36 m²) of a HypsIRI pixel at an ambient temperature of 320 K would increase the 4- μm temperature to ~380 K. Given an NEAT of 8 K, we could calculate the FRP of this modest fire with an uncertainty of $\pm 6\%$. An increase in the 4- μm saturation temperature setting from 1200 to 1300 K would increase the NEAT by 25% (10 K vs. 8 K), with a corresponding increase in uncertainty for the FRP estimation.

The trade-off between saturation at scene temperatures > 1200 K, as encountered during the Krafla eruption, and increased sensitivity to smoldering (~700 K) fires is acceptable, given the high probability of observing such fires over the life of a HypsIRI mission relative to the probability of observing another Krafla-scale eruption. With regard to volcanic phenomena, we note that the proposed saturation temperature of 1200 K is higher than the Klyuchevskoy (Fig. 21[b]), Kilauea (Fig. 22[b]), Nyamuragira (Fig. 23[a]), or Eyjafjallajökull (Fig. 24[a]) temperatures estimated at the native spatial resolution of ASTER or Hyperion.

Table 4. Summary of Maximum Temperatures from Team and Published Studies

Case Study	Instrument	Maximum Temperature
Sharpsand Fire, 2007	AGEMA Thermal Camera	1205/1260 K
Klyuchevskoy Volcano, 2007	ASTER VNIR	1043 K
Kilauea Volcano, 2007	ASTER VNIR	990 K
Nyamuragira Volcano, 2004	Hyperion SWIR	950 K
Indians Fire, 2008	AVIRIS SWIR	860 K
Poomacha Fire, 2007	AMS TIR	795 K
Published Study	Instrument	Maximum Temperature
Krafla Eruption, 1984 (Harris et al. 1995)	AVHRR MIR	1325 K
Lake Baikal Fire, 2003 (Zhukov et al. 2006)	HSRS MIR	988 K

6 Selected Bibliography

- Boschetti, L., and D. P. Roy (2009), Strategies for the fusion of satellite fire radiative power with burned area data for fire radiative energy derivation, *J. Geophys. Res.*, *114*, D20302, doi:10.1029/2008JD011645
- Briess, K., H. Jahn, E. Lorenz, D. Oertel, W. Skrbek, and B. Zhukov (2003), Fire recognition potential of the bi-spectral Infrared detection (BIRD) satellite, *Int. J. Remote Sens.*, *24*(4), 865-872.
- Carter, A.J., O. Girina, M.S. Ramsey, and Y.V. Demyanchuk (2008), ASTER and field observations of the 24 December 2006 eruption of Bezymianny Volcano, Russia, *Remote Sens. Environ.*, *112*, 2569-2577.
- Carter, A.J., and M.S. Ramsey (2009), ASTER- and field-based observations at Bezymianny Volcano: focus on the 11 May 2007 pyroclastic flow deposit, *Remote Sens. Environ.*, *113*, 2142-2151.
- Csiszar, I., and J. Sullivan (2002), Recalculated pre-launch saturation temperatures of the AVHRR 3.7 μm sensors on board the TIROS-N to NOAA-14 satellites, *Int. J. Remote Sens.*, *23*(24), 5271-5276.
- Csiszar, I.A., J.T. Morisette, and L. Giglio (2006), Validation of active fire detection from moderate-resolution satellite sensors: the MODIS example in northern Eurasia, *IEEE Trans. Geosci. Remote Sens.*, *44*(7), 1757-1764, doi: 10.1109/TGRS.2006.875941.
- Dennison, P.E., K. Charoensiri, D.A. Roberts, S.H. Peterson, and R.O. Green (2006), Wildfire temperature and land cover modeling using hyperspectral data, *Remote Sens. Environ.*, *100*(2), 212-222.
- Dennison, P.E., and D.S. Matheson (2011), Comparison of fire temperature and fractional area modeled from SWIR, MIR, and TIR multispectral and SWIR hyperspectral airborne data, *Remote Sens. Environ.*, *115*(3), 876-886.
- Dozier, J. (1981), A method for satellite identification of surface temperature fields of subpixel resolution, *Remote Sens. Environ.*, *11*, 221-229.
- Earth Science and Applications from Space: National Imperatives for the Next Decade and Beyond, 2007. Committee on Earth Science and Applications from Space: A Community Assessment and Strategy for the Future (2007). National Research Council, National Academies Press. Referred to as the Decadal Survey or NRC 2007.
- Eckmann, T.C., D.A. Roberts, and C.J. Still (2008), Using multiple endmember spectral mixture analysis to retrieve subpixel fire properties from MODIS, *Remote Sens. Environ.*, *112*, 3773-3783.
- Eckmann, T.C., D.A. Roberts, and C.J. Still (2009) Estimating subpixel fire sizes and temperatures from ASTER using multiple endmember spectral analysis, *Int. J. Remote Sens.*, *30*(22), 5851-5864.
- Ellicott, E., E. Vermote, L. Giglio, and G. Roberts, Estimating biomass consumed from fire using MODIS FRE (2009), *Geophys. Res. Lett.*, *36*, L13401, doi:10.1029/2009GL038581.

- Freeborn, P.H., M.J. Wooster, W.M. Hao, C.A. Ryan, B.L. Nordgren, S.P. Baker, and C. Ichoku (2008), Relationships between energy release, fuel mass loss, and trace gas and aerodol emissions during laboratory biomass fires, *J. Geophys. Res.*, *113*, D01301, doi:10.1029/2007JD008679.
- Gao, B-C, X. Xiong, R-R Li, and D-Y Wang (2007), Evaluation of the Moderate Resolution Imaging Spectrometer special 3.95-mm fire channel and implications on fire channel selections for future satellite instruments, *J. Appl. Remote Sens.*, *1*, 013516, doi: 10.1117/1.2757715.
- Giglio, L., J.D. Kendall, and C.O. Justice (1999), Evaluation of global fire detection algorithms using simulated AVHRR infrared data, *Int. J. Remote Sens.*, *20*(10), 1947-1985.
- Giglio, L., J.D. Kendall, and C.J. Tucker (2000), Remote sensing of fires with the TRMM VIRS, *Int. J. Remote Sens.*, *21*(1), 203-207.
- Giglio, L. and J. D. Kendall (2001), Application of the Dozier retrieval to wildfire characterization - a sensitivity analysis, *Remote Sens. Environ.*, *77*, 34-49.
- Giglio, L., J. Desloîtres, C.O. Justice, and Y.J. Kaufman (2003), An enhanced contextual fire detection algorithm for MODIS, *Remote Sens. Environ.*, *87*, 273-282, doi:10.1016/S0034-4257(03)00184-6.
- Giglio, L. and C.O. Justice (2003), Effects of wavelength selection on characterization of fire size and temperature, *Int. J. Remote Sens.*, *24*(17), 3515-3520, doi:10.1080/0143116031000117056.
- Giglio, L., J.D. Kendall, and R. Mack (2003), A multi-year active fire dataset for the tropics derived from the TRMM VIRS, *Int. J. Remote Sens.*, *24*(22), 4505-4525.
- Giglio, L., I. Csiszar, A. Restas, J.T. Morisette, W. Schroeder, D. Morton, and C.O. Justice (2008), Active fire detection and characterization with the advanced spaceborne thermal emission and reflection radiometer (ASTER), *Remote Sens. Environ.*, *112*, 3055-3063, doi:10.1016/j.rse.2008.03.003.
- Giglio, L., T. Loboda, D.P. Roy, B. Quayle, and C.O. Justice (2009), An active-fire based burned area mapping algorithm for the MODIS sensor, *Remote Sens. Environ.*, *113*, 408-420, doi:10.1016/j.rse.2008.10.006.
- Harris, A.J.L., and C.R. Thornber (1999), Complex effusive events at Kilauea as documented by the GOES satellite and remote video cameras, *Bull. Volcanol.*, *61*, 382-395.
- Harris, A.J.L., L.P. Flynn, D.A. Rothery, C. Oppenheimer, and S.B. Sherman (1999), Mass flux measurements at active lava lakes, *J. Geophys. Res.*, *104*(B4), 7117-7136.
- Harris, A.J.L., R.A. Vaughan, and D.A. Rothery (1995a), Volcano detection and monitoring using AVHRR data: the Krafla eruption, 1984, *Int. J. Remote Sens.*, *16*(6), 1001-1020.
- Harris, A.J.L., D.A. Rothery, R.W. Carlton, S. Langaas, and H. Mannstein (1995b), Non-zero saturation of AVHRR thermal channels over high temperature targets: evidence from volcano data and a possible explanation, *Int. J. Remote Sens.*, *16*(1), 189-196.
- Harris, A.J.L., S. E. J. Swabey, and J. Higgins (1995c), Automated thresholding of active lavas using AVHRR data, *Int. J. Remote Sens.*, *16*, 3681-3686.

- Harris, A. J. L., L. Keszthelyi, L. P. Flynn, P. J. Mougini-Mark, C. Thornber, J. Kauahikaua, D. Sherrod, F. Trusdell, M. W. Sawyer, and P. Flament (1997a), Chronology of the episode 54 eruption at Kilauea volcano, Hawaii, from GOES-9 satellite data, *Geophys. Res. Lett.*, *24*, 3281–3284.
- Harris, A.J.L., S. Blake, D. A. Rothery, and N.F. Stevens (1997b), A chronology of the 1991 to 1993 Etna eruption using advanced very high resolution radiometer data: Implications for real-time thermal volcano monitoring, *J. Geophys. Res.*, *102*, 7985–8003.
- Harris, A. J. L., et al., Real-time monitoring of volcanic hot spots with satellites, in Remote Sensing of Active Volcanism, Geophys. Monogr. Ser., vol. 116, edited by P. J. Mougini-Mark, J. A. Crisp, and J. H. Fink, pp. 139–159, AGU, Washington, D. C., 2000.
- Harris, A. J. L., E. Pilger, L. P. Flynn, H. Garbeil, P. J. Mougini-Mark, J. Kauahikaua, and C. Thornber (2001), Automated, high temporal resolution, thermal analysis of Kilauea volcano, Hawai'i, using GOES satellite data, *Int. J. Remote Sens.*, *22*, 945–967.
- Justice, C.O., L. Giglio, S. Korontzi, J. Owens, J.T. Morisette, D. Roy, J. Descloitres, S. Alleaume, F. Petitcolin, and Y. Kaufman (2002), The MODIS fire products, *Remote Sens. Env.*, *83*, 244 – 262.
- Kaufman, Y.J., R.G. Kleidman, and M.D. King (1998a), SCAR-B fires in the tropics: properties and remote sensing from EOS-MODIS, *J. Geophys. Res.*, *103(D24)*, 31,955-31,968.
- Kaufman, Y.J., C.O. Justice, L.P. Flynn, J.D. Kendall, E.M. Prins, L. Giglio, D.E. Wards, W.P. Menzel, and A.W. Setzer (1998b), Potential global fire monitoring from EOS-MODIS, *J. Geophys. Res.*, *103(D24)*, 32,215-32,238.
- Kaufman, Y.J., C. Ichoku, L. Giglio, S. Korontzi, D.A. Chu, W.M. Hao, R.R. Li, and C. Justice (2003), Fire and smoke observed from Earth Observing System MODIS instrument – products, validation, and operational use, *Int. J. Remote Sens.*, *24(8)*, 1765-1781.
- Langaas, S. (1993) A parameterised bispectral model for savanna fire detection using AVHRR night images, *Int. J. Remote Sens.*, *14(12)*, 2245-2262.
- Lombardo, V., M.F. Buongiorno, and S. Amici (2006), Characterization of volcanic thermal anomalies by means of sub-pixel temperature distribution analysis, *Bull. Volcanol.*, *68*, 641-651.
- Matson, M., and J. Dozier (1981), Identification of subresolution high temperature sources using a thermal IR sensor, *Photogram. Eng. Remote Sens.*, *47(9)*, 1311-1318.
- Morisette, J.T., L. Giglio, I. Csiszar, and C.O. Justice (2005a), Validation of the MODIS active fire product over Southern Africa with ASTER data, *Int. J. Remote Sens.*, *26(10)*, 4239-4264.
- Morisette, J.T., L. Giglio, I. Csiszar, A. Setzer, W. Schroeder, D. Morton, and C.O. Justice (2005b), Validation of MODIS active fire detection products derived from two algorithms, *Earth Interact.*, *9(9)*, 1-25.
- Oertel, D., B. Zhulov, H-P Thamm, J. Roehrig, and B. Orthmann (2004) Space-borne high resolution fire remote sensing in Benin, West Africa, *Int. J. Remote Sens.*, *25(11)*, 2209-2216.

- Oppenheimer, C., P.W. Francis, D.A. Rothery, and R.W.T. Carlton (1993a), Infrared Image Analysis of Volcanic Thermal Features: Lascar Volcano, Chile, 1984-1992, *J. Geophys. Res.*, *98(B3)*, 4269-4286.
- Oppenheimer, C., D.A. Rothery, D.C. Pieri, D.C. Pieri, M.J. Abrams, and V. Carrere (1993b), Analysis of Airborne Visible/Infrared Imaging Spectrometer data of volcanic hot spots, *Int. J. Remote Sens.*, *14(16)*, 2919-2934.
- Pereira, G., S.R. Freitas, E.C. Moraes, N.J. Ferreira, Y.E. Shiombukuro, V.B. Rao, and K.M. Longo (2009), Estimating trace gas and aerosol emissions over South America: relationship between fire radiative energy released and aerosol optical depth observations, *Atmos. Environ.*, *43*, 6388-6391.
- Ramsey, M., and J. Dehn (2004), Spaceborne observations of the 2000 Bezymianny, Kamchatka eruption: the integration of high-resolution ASTER data into near real-time monitoring using AVHRR, *J. Volcanol. Geotherm. Res.*, *135*, 127-146.
- Riggan, P.J., J.A. Brass, and R.N. Lockwood (1993), Assessing fire emissions from tropical savanna and forest of central Brazil, *Photogram. Eng. Remote Sens.*, *59(6)*, 1009-1015.
- Riggan, P.J., R.G. Tissell, R.N. Lockwood, J.A. Brass, J.A.R. Pereira, H.S. Miranda, A.C. Miranda, T. Campos, and R. Higgans (2004), *Ecolog. Appl.*, *14(3)*, 855-872.
- Roberts, D.A., M. Gardner, R. Church, S. Ustin, G. Scheer, and R.O. Green (1998), Mapping chaparral in the Santa Monica Mountains using multiple endmember spectral mixture models, *Remote Sens. Environ.*, *65*, 267-279.
- Roberts, G., M. J. Wooster, G. L. W. Perry, N. Drake, L.-M. Rebelo, and F. Dipotso (2005), Retrieval of biomass combustion rates and totals from fire radiative power observations: Application to southern Africa using geostationary SEVIRI imagery, *J. Geophys. Res.*, *110*, D21111, doi:10.1029/2005JD006018.
- Roberts, G.J., and M.J. Wooster (2008) Fire detection and fire characterization over Africa using Meteosat SEVIRI, *IEEE Trans. Geosci. Remote Sens.*, *46(4)*, 1200-1218.
- Rose, S., and M. Ramsey (2009) The 2005 eruption of Kliuchevskoi volcano: chronology and processes derived from ASTER spaceborne and field-based data, *J. Volcanol. Geotherm. Res.*, *184*, 367-380.
- Siegert, F., B. Zhukov, D. Oertel, S. Limin, S.E. Page, J.O. Rieley (2004) Peat fires detected by the BIRD satellite, *Int. J. Remote Sens.*, *25(16)*, 3221-3230.
- Smith, D.R., J.D. Kaduk, et al., (2010), Soil surface CO₂ flux increases with successional time in a fire scar chronosequence of Canadian boreal jack pine forest, *Biogeosci.*, *7*, 1375-1381, doi:10.5194/bg-7-1375-2010.
- Vaughan, R.G., M. Kervyn, V. Realmuto, M. Abrams, and S.J. Hook (2008), Satellite measurements of recent volcanic activity at Oldoinyo Lengai, Tanzania, *J. Volcanol. Geotherm. Res.*, *173*, 196-206.
- Wooster, M. J., and D. A. Rothery (1997), Thermal monitoring of Lascar Volcano, Chile, using infrared data from the along-track scanning radiometer: a 1992–1995 time series, *Bull. Volcanol.*, *58*, 566–579.

- Wooster, M.J., T. Kaneko, S. Nakada, and H. Shimizu (2000), Discrimination of lava dome activity styles using satellite-derived thermal structures, *J. Volcanol. Geotherm. Res.*, *102*, 97-118.
- Wooster, M.J., and T. Kaneko (2001), Testing the accuracy of solar-reflected radiation corrections applied during satellite shortwave infrared thermal analysis of active volcanoes, *J. Geophys. Res.*, *106(B7)*, 13,381-13,393.
- Wooster, M.J., B. Zhukov, and D. Oertel (2003), Fire radiative energy for quantitative study of biomass burning: derivation from the BIRD experimental satellite and comparison to MODIS fire products, *Remote Sens. Environ.*, *86*, 83-107, doi:10.1016/S0034-4257(03)00070-1.
- Wooster, M.J., G. Roberts, G.L.W. Perry, and Y.J. Kaufman (2005), Retrieval of biomass combustion rates and totals from fire radiant power observations: FRP derivation and calibration relationship between biomass consumption and fire radiative energy release, *J. Geophys. Res.*, *110*, D24311, doi:10.1029/2005JD006318.
- Wright, R., L.P. Flynn, and A.J.L. Harris (2001), Evolution of lava flow-fields at Mount Etna, 27-28 October 1999, observed by Landsat ETM+, *Bull. Volcanol.*, *63*, 1-7.
- Wright, R., L. P. Flynn, H. Garbeil, A. J. S. Harris, and E. Pilger (2002), Automated volcanic eruption detection using MODIS, *Remote Sens. Environ.*, *82*, 135-155
- Wright, R., and L.P. Flynn (2003), On the retrieval of lava-flow surface temperatures from infrared satellite data, *Geology*, *31*, 893-896, doi:10.1130/G19645.1
- Wright, R., L.P. Flynn, H. Garbeil, A. J. L. Harris, and E. Pilger (2004), MODVOLC: near-real-time thermal monitoring of global volcanism, *J. Volcanol. Geothermal Res.*, *135*, 29- 49
- Wright, R., H. Garbeil, and A.G. Davies (2010), Cooling rate of some active lavas determined using an orbital imaging spectrometer, *J. Geophys. Res.*, *115*, B06205, doi:10.1029/2009JB006536
- Xiong, X., B.N. Wenny, A. Wu, W.L. Barnes, and V.V. Salmonson (2009), Aqua MODIS thermal emissive band on-orbit calibration, characterization, and performance, *IEEE Trans. Geosci. Remote Sens.*, *47(3)*, 803-814, doi: 10.1109/TGRS.2008.2005109
- Xu, W., M.J. Wooster, G. Roberts, and P. Freeborn (2010), New GOES imager algorithms for cloud and active fire detection and fire radiative power assessment across North, South, and Central America, *Remote Sens. Env.*, *114*, 1876-1895.
- Zhukov, B., K. Briess, E. Lorenz, D. Oertel, and W. Skrbek (2005), Detection and analysis of high-temperature events in the BIRD mission, *Acta Astro.*, *56*, 65-71.
- Zhukov, B., E. Lorenz, D. Oertel, M. Wooster, and G. Roberts (2006), Spaceborne detection and characterization of fires during the bi-spectral infrared detection (BIRD) experimental small satellite mission (2001-2004), *Remote Sens. Environ.*, *100*, 29-51.

HyspIRI Science Workshop Summary

Simon J. Hook, NASA/Jet Propulsion Laboratory/ California Institute of Technology, Simon.J.Hook@jpl.nasa.gov

Approximately 180 scientists gathered from August 24–26, 2010, at the 3rd NASA Hyperspectral Infrared Imager (HyspIRI) Science Workshop held in Pasadena, CA. PDF versions of the presentations given at the meeting are available from the HyspIRI website (hyspiri.jpl.nasa.gov).

Introduction and Meeting Overview

The HyspIRI mission was recommended for implementation by the 2007 report from the U.S. National Research Council *Earth Science and Applications from Space: National Imperatives for the Next Decade and Beyond* (also known as the Earth Science Decadal Survey or, simply, the Decadal Survey). The annual HyspIRI workshop provides an open forum to present the observational requirements for the mission and assess its anticipated impact on scientific and operational applications; the open forum also provides an opportunity to obtain feedback from the broader scientific community on the mission concept. This year's workshop had a greater emphasis on the science contribution from HyspIRI and, in particular, its contribution to climate science. There also was more emphasis on the potential contribution to science applications with recent examples from the oil spill in the Gulf and the volcanic erup-

tion in Iceland. The morning of the first day focused on providing an overview of the mission. The afternoon of the first day focused on climate related talks. The second day was primarily science presentations, including discussion of the science questions that HyspIRI will address. The final day included discussions of related missions, partnership opportunities and plans for 2011 and beyond. Of particular interest was the discussion of a potential airborne campaign to acquire data for both science and algorithm testing beginning in the 2011-2012 timeframe. As at last year's meeting, there was a review of the Preliminary Level 1 mission requirements. This year there were over 25 posters which provided an excellent opportunity for more detailed discussions between talks. The workshop participants concluded that the HyspIRI mission would provide a significant new capability to study ecosystems and natural hazards at spatial scales relevant to human resource use. The participants felt the measurement requirements could be achieved with the reference instrument design concepts and be implemented through the use of current technology. The workshop participants endorsed the recommendation of the Decadal Survey itself, and reiterated the need for the HyspIRI mission; they felt the mission, as defined, would accomplish the intended science.



HyspIRI Science Workshop Participants

Woody Turner [NASA Headquarters (HQ)—*Co-Program Scientist for HypsIRI*] started the meeting by welcoming the participants and outlining the goals and objectives for this year's meeting. Turner noted that the science focus this year would be on climate but there would also be several key talks on the potential of using HypsIRI for applications research, and in particular, disaster response—illustrated by talks on the recent Gulf oil spill and volcanic eruption in Iceland. He noted that since the last workshop we have had a symposium at Goddard Space Flight Center (GSFC) that focused on higher level ecosystem products as well as largely completed two reports addressing certain critical aspects of the mission (i.e., sun glint and hot target saturation). Turner also highlighted the opportunities for international partnerships and welcomed the large number of international investigators present at the workshop. He closed by stating that the mission concept is clearly defined, utilizes mature technologies and is low cost, and is ready to go!

Jack Kaye [HQ—*Associate Director for Research and Analysis, Earth Science Division*] further emphasized the importance of climate observations. Kaye noted that there will be a National Climate Assessment in 2013 and NASA would play a key role. He discussed the possibility of the acquisition of a HypsIRI-like airborne dataset for NASA science and HypsIRI algorithm testing which also could contribute to the climate assessment.

HypsIRI will have three main payload elements, a Visible Shortwave Infrared imaging spectrometer (VSWIR), a multispectral thermal infrared (TIR) imager, and an Intelligent Payload Module (IPM). The next series of presentations gave details on these elements.

Rob Green [NASA/Jet Propulsion Laboratory (JPL)] identified how HypsIRI would provide critical climate observations and noted that the Decadal Survey had explicitly cited the need for HypsIRI for climate. He also summarized the instrument concept for the VSWIR. The VSWIR imaging spectrometer will obtain data covering the spectral range from 380–2500 nm with 10 nm sampling. VSWIR data will be acquired over the full terrestrial surface with a 19-day-revisit, including shallow water regions. The deep oceans and ice sheets also will be acquired with a 19-day-revisit but resampled to a spatial resolution of 1 km. Green presented examples of how the VSWIR data would be used for a range of science challenges, primarily focused on ecology, including mapping species and canopy chemistry. **The VSWIR system will provide the same level of spectrometer coverage in 1 year that it would take current and future full solar reflected range imaging spectrometers 100 years to provide.** The VSWIR instrument concept was shown to have design heritage from instruments such as the Moon Mineralogy Mapper (M3). This heritage has allowed the VSWIR instrument

to be far smaller and use less power than earlier designs such as Hyperion on the Earth Observing-1 mission. In-flight, the instrument would be fully calibrated with an onboard solar panel, lunar looks, and ground calibration experiments. Green closed by reiterating that the VSWIR concept was mature and ready to go.

Simon Hook [JPL] summarized the instrument concept for the thermal infrared (TIR) multispectral imager on HypsIRI. The TIR imager will obtain data in eight spectral channels; one of the channels is located at 4 μm and the other seven channels are located between 7–12 μm . TIR data will be acquired over the full terrestrial surface with a 5-day-revisit, including shallow water regions. The deep oceans and ice sheets also will be acquired with a 5-day-revisit but resampled to a spatial resolution of 1 km. Hook presented examples of how the TIR data would be used for a broad range of science and applications with particular emphasis on volcanoes, wildfires, and water use and availability. For each area, Hook provided examples of how the instrument concept was designed to address critical questions in that area. The TIR instrument operates continuously, providing both a daytime and nighttime scene for the entire Earth every five days at the equator. He showed how the revisit will be greater at higher latitudes and used an example from the recent Iceland eruption to highlight how the TIR would have been able to provide daily information on the composition and chemistry of the volcanic plume—of particular importance for aeronautics. The TIR instrument concept has design heritage from instruments such as the Advanced Spaceborne Thermal Emission and Reflection Radiometer (ASTER) and the Moderate Resolution Imaging Spectroradiometer (MODIS) and is a mature concept that can be built and launched in the same timeframe as the VSWIR instrument. In-flight, the instrument will be calibrated with a two-point calibration, obtained by viewing an onboard blackbody and deep space every scan. There also will be lunar looks and ground calibration using automated validation sites. Hook closed by restating that the TIR will provide essential data for reducing the uncertainties in land carbon flux together with data for a range of applications from volcano monitoring to wildfires.

Carl Bruce [JPL] provided more detail on the VSWIR reference design concept. Bruce stated that this year's effort had focused on checking the mass and power requirements and confirming the instrument met certain key requirements. This included numerical modeling of the signal to noise and uniformity. He noted the VSWIR system will be a high data rate system with no new technology needing to be developed as the critical parts are at Technology Readiness Level (TRL) 6. Antecedent data are available from the MARS instrument, a similar design to the VSWIR instrument, and together with data from the upcoming Airborne Visible/Infra-

red Imaging Spectrometer—Next Generation (AVIRIS-NG) will provide valuable information on the nominal design concept. Current plans call for ground control points in order to meet the 30-m geolocation accuracy requirement. There are some differences between the HypsIRI concept and the M3; for example, the VSWIR instrument will use two identical spectrometers, have a larger radiator and use four detectors compared to a single detector in M3. These differences will not impact the reference design concept which continues to be optimized. The VSWIR instrument is possible because of several key technologies that have been developed over the last decade such as curved electron-beam fabricated gratings and uniform slits which enable a highly uniform imaging spectrometer to be built.

Marc Foote [JPL] then provided more information on the TIR reference design concept. The TIR instrument will be a whiskbroom scanner with a 51° total field of view and ground resolution of 60 m. The data will be collected with a two-sided scan mirror. The dwell time for any given pixel will be 32 microseconds. The system will use a Mercury Cadmium Telluride detector and the focal plane will be cooled to 60 K with an active cooler. The scan mirror will use a lower resolution controller combined with a higher resolution interferometric encoder for high pointing knowledge. A two point calibration (viewing a blackbody and deep space) will be performed every two seconds. The system will use a Cassegrain telescope with radiation from the instrument baffled away from the detector. There will be a single detector array, having 32 readout ports, with 256 x 16 pixels in each of the eight spectral channels. The system will use time delay and integration with each channel using four columns from the array—since each channel has extra columns, the best four columns can be used. Current testing of a prototype read-out integrated circuit indicates compliance with noise and power specifications, and the instrument noise-equivalent temperature difference should be less than 0.2 K in the seven thermal infrared channels, with ample signal from hot targets for the mid-infrared channel. Various commercial cryocoolers are being studied with several available that meet the design requirement.

Dan Mandl [NASA/Goddard Space Flight Center (GSFC)] described the Intelligent Payload Module (IPM) that will provide low-latency data, which can be used for a wide range of applications such as near-real-time (NRT) monitoring of fires or floods. There will be two data streams on the spacecraft; one is downloaded through the normal route while a second identical stream goes to the IPM. The IPM will be able to subset and process this second stream and download the data in NRT via a direct-broadcast antenna. The NRT data will be available over the internet. Work is currently underway on benchmarking the Computer Processing Unit for IPM and developing delay tolerant network

communication connectivity to handle any network disruption. The web coverage service will be used to automatically load algorithms so a custom algorithm can be loaded for a particular task or application and the data downloaded in NRT such as during a fire or flood. An IPM testbed for HypsIRI has been developed and is being used for testing algorithms such as automated atmospheric correction using existing Hyperion data.

Bogdan Oaida [JPL] discussed the overall mission concept. HypsIRI is planned to be in a 626 km Sun-synchronous orbit with a 10:30 AM descending equatorial crossing time. Oaida showed there are several other potential orbits that could support the 19- and 5-day revisit of the VSWIR and TIR respectively, including an orbit around 705 km used by many other spacecraft—e.g., the A-Train. He outlined the operations concept for HypsIRI, which is very simple since both instruments are always turned on in order to provide global mapping. The VSWIR data are day-only data and currently planned to be acquired when the solar elevation is greater than 20°, however, this constraint may be relaxed to 10° to provide additional coverage in the polar regions. This year the results from the 2009 concept study were reviewed and the mass confirmed to meet the design principle for JPL. Multiple spacecraft solutions are available which would be modified to add power and an onboard recorder. Several launch vehicles are available which would meet the requirements. The ground systems and data management concept continues to mature. In a response to a Request For Information, Norway's Kongsberg Satellite Services (KSAT) has indicated they will have ample capacity to meet the downlink needs of HypsIRI with two polar downlink stations.

Rob Green and **Simon Hook** reviewed the Draft Level 1 Mission Requirements that serve as the top-level requirements for the HypsIRI mission and provide the basis for deriving the more detailed Level 2 requirements. These requirements were first presented at the 2008 Workshop and are reviewed at each workshop to make sure the community is fully aware of the data that HypsIRI will provide.

Greg Asner [Carnegie Institution for Science, Stanford University] then gave the first of two keynote presentations highlighting the key climate contributions of HypsIRI. Asner began by noting that biospheric and cryospheric feedbacks are two major uncertainties that need to be resolved to understand and predict climate change. Changes in greenhouse gas emissions are controlled by biospheric feedbacks, and although the different biospheric processes are known, we do not understand their relative contributions. For example, temperature changes can result in a large re-shuffling of plant functional types, including changes in invasive species and nitrogen fixing plants. This re-shuffling

results from drier and warmer conditions, which then leads to new feedbacks. Invasive species may grow faster but only if higher temperatures and light are available with sufficient nutrients and moisture. Invasive plants and other changes in plant functional types can result in significant changes in nitrogen cycling and thus levels of the greenhouse super-gas nitrous oxide. New plant functional types may store less carbon or have a different albedo which in turn can result in a new feedback. Studies have shown that by combining imaging spectrometer data with model data, e.g. the Carnegie Ames Stanford Approach (CASA), these fluxes can be obtained. This information cannot be obtained from current coarse spatial and spectral resolution measurements. Asner noted that the Intergovernmental Panel on Climate Change (IPCC) is currently trying to determine whether a biospheric feedback is taking place in the Amazon, which in recent years has been getting ~1% drier every 3 years. A recent paper using MODIS data suggested the Amazon became greener during droughts but subsequent studies suggested this was an artifact in the MODIS data. HypsIRI will provide the measurements needed to observe and understand this shift in plant functional types that coarser spatial and spectral resolution instruments cannot provide. He also reported that HypsIRI will provide valuable information on albedo feedbacks, fire emissions, and evapotranspiration. Asner noted that current sensors are underestimating fire emissions since they do not resolve the contribution from many agricultural and forest fires that are typically smaller than large wildfires. The global mapping capability of HypsIRI is critical to fully understand these feedbacks. (Other missions provide detail on local processes but HypsIRI will provide the core measurements for understanding what is happening globally.) HypsIRI measurements would be even more powerful when coupled with data from other systems which provide plant structural information such as the Deformation, Ecosystem Structure and Dynamics of Ice (DESDynI) mission. Finally, Asner emphasized that the IPCC needs this information as soon as possible to understand what changes are happening now and to better predict what will happen in the future.

Tom Painter [JPL] gave the second keynote presentation on albedo feedbacks associated with dust and black carbon (BC) in snow. As noted in the recent IPCC reports albedo changes can have a radical effect on climate, but at present our knowledge of albedo feedback is very limited. This lack of knowledge occurs because *in situ* radiation measurements are expensive and sparse, and quantitative retrievals from current remote-sensing technology are not possible. Information about changes in snow albedo is critical but more improved measurements are needed to understand the impact of BC and dust. A key area where such knowledge is important

is the *down wasting*¹ of Himalayan glaciers due to increasing warming and a combination of BC and dust. We know that down wasting is taking place but do not understand how much of this down wasting comes from changes in climate and radiative forcing by BC and dust. Likewise, changes in snowmelt have a critical impact on water resources such as in the Southwest U.S. In the Upper Colorado River basin, point models indicate that increasing dust from land-use/land-cover change in the desert southwest has reduced snow cover by 28–50 days. Current data from coarse spectral resolution sensors such as MODIS does not provide information where the albedo differences are greatest and easiest to measure. The higher spatial and spectral resolution of HypsIRI allows the retrieval of radiative forcing by dust and black carbon, fractional snow cover, snow grain size, and albedo.

Science Presentations

After the two keynote presentations the remainder of the first day, all of the second day, and part of the third day were devoted to science talks. There were over 40 talks and the presentations associated with these talks are available from the HypsIRI website listed earlier. The talks covered a wide range in topics and included updates from the studies funded by NASA solicitations as well as updates on the key science questions that HypsIRI will address. The science questions were developed in conjunction with the Science Study Group, a group of scientists appointed by NASA to help guide the mission and ensure the measurements are of maximum benefit. The science talks included multiple presentations related to the application of the science data, in particular, recent results from the Gulf oil spill. HypsIRI-like imaging spectrometer data from the Gulf oil spill were obtained with the AVIRIS instrument. These data were used to determine the surface oil thickness and oil-to-water ratio, a new technique that greatly aided the response because to date there have been no technologies to derive oil slick thickness other than human observation and measurement. Thus, coarse spatial and spectral resolution sensors and Synthetic Aperture Radar (SAR) sensors can determine the presence of oil on the surface but are unable to determine if a thin film (i.e., sub-micron) is present or a thick (i.e., cm-scale) oil layer. The high spectral resolution of AVIRIS and HypsIRI will allow quantification of the amount of oil to guide response efforts, and to improve predictive capabilities. AVIRIS data also were acquired over the coastal wetlands for the entire Gulf region both before oil washed onshore and afterwards. These data will be used in ongoing studies to better understand the impact of the oil spill and remediation techniques on the fauna and flora of the wetlands around the Gulf.

¹ *Down wasting* is the stationary thinning of the glacial ice.

The third and final day of the workshop began with a short report on the recent HypsIRI Symposium arranged by **Betsy Middleton** [GSFC] and colleagues. The focus of the symposium was the higher-level data products, especially those related to ecosystem studies. Middleton highlighted the plethora of products that HypsIRI could potentially produce and noted such products will be critical in understanding the carbon budget. She also identified that more frequent revisits in the northern latitudes will be particularly advantageous given these regions are undergoing rapid change.

Middleton's presentation preceded a series of talks from our international colleagues and included presentations from Germany, Italy, Japan, Argentina, and Australia, each of which highlighted the capabilities within each country and how their respective efforts would dovetail with the unique HypsIRI global mapping mission. These included downlink opportunities as well as joint calibration and validation experiments.

The remainder of the morning and early part of the afternoon included a mixture of science and engineering presentations. These included more detailed presentations on the orbits, coverage, and downlink procedures. For example, **Bob Knox** [GSFC] discussed the benefit of the increased number of opportunities with latitude and noted how the TIR sensor would provide daily coverage in the northern latitudes. **Alexander Berk** [Spectral Sciences, Inc.] described updates to the MODTRAN⁹² radiative transfer model and how these would benefit the HypsIRI mission. For example a recent update for modeling gas plumes could be used for

modeling volcanic eruption plumes. **Susan Ustin** [University of California Davis] gave a short presentation on a small workshop she is organizing on developing global HypsIRI data products.

Review of the Workshop and Next Steps

The final presentation reviewed the progress since the last meeting and future activities. Excellent progress has been made since the last meeting with additional reports such as the sunglint and hot target saturation reports that provide invaluable feedback on the measurement requirements for the instruments. Participants noted the large number of posters displayed at the meeting and asked that future meetings included an evening session dedicated to the posters. Of particular interest with the community was the possibility of an airborne campaign in California using the AVIRIS and the MODIS/ASTER Airborne Simulator (MASTER) sensors to acquire HypsIRI-like datasets for both science and algorithm development. Potential flight corridors were discussed together with how to ensure the necessary field measurements were made to maximize the usefulness of the data.

In summary, the participants felt that the HypsIRI Level 1 Mission would provide a significant new capability to study ecosystems and natural hazards at spatial scales relevant to human resource use. The participants confirmed the Draft Preliminary HypsIRI Mission Level 1 Requirements were achievable with the mission concept presented and would provide the data necessary to address the science questions identified for the mission.

² MODTRAN computer software is a registered trademark owned by the United States Government as represented by the Secretary of the Air Force.

JPL Publication 10-3

NASA 2009 HypIRI Science Workshop Report

HypIRI Group

Prepared for
**National Aeronautics and
Space Administration**

by

**Jet Propulsion Laboratory
California Institute of Technology
Pasadena, California**

Jan 2010

JPL Publication 10-3

NASA 2009 HypsIRI Science Workshop Report

HypsIRI Group



Prepared for
**National Aeronautics and
Space Administration**

by

**Jet Propulsion Laboratory
California Institute of Technology
Pasadena, California**

Jan 2010

The work described in this publication was performed at a number of organizations, including the Jet Propulsion Laboratory, California Institute of Technology, under a contract with the National Aeronautics and Space Administration (NASA). Compilation and publication support was provided by the Jet Propulsion Laboratory, California Institute of Technology, under a contract with NASA.

Reference herein to any specific commercial product, process, or service by trade name, trademark, manufacturer, or otherwise, does not constitute or imply its endorsement by the United States Government or the Jet Propulsion Laboratory, California Institute of Technology.

© 2010. All rights reserved.

Abstract

From August 11-13, 2009, NASA held a three-day workshop to consider the Hyperspectral Infrared Imager (HyspIRI) mission recommended for implementation by the 2007 report from the U.S. National Research Council Earth Science and Applications from Space: National Imperatives for the Next Decade and Beyond (also known as the Earth Science Decadal Survey or, simply, the Decadal Survey). The open workshop provided a forum to present the observational requirements for the mission and assess its anticipated impact on scientific and operational applications; the open forum also offered the opportunity to obtain feedback from the broader scientific community on the mission concept.

The workshop participants concluded that the HyspIRI mission would provide a significant new capability to study ecosystems and natural hazards at spatial scales relevant to human resource use. In addition, participants reviewed the Draft Preliminary HyspIRI Mission Level 1 Requirements and confirmed that they were achievable with the mission concept presented and would provide the necessary data needed to address the science questions identified for the mission and by the Decadal Survey. These requirements could be met using the reference instrument designs and be implemented through the use of current technology.

The workshop participants, like the Decadal Survey itself, strongly endorsed the need for the HyspIRI mission and felt the mission, as defined, would accomplish the intended science.

Document Contacts

Many researchers provided Inputs for this workshop report. Readers seeking more information about particular details and contacting researchers in certain areas may access that information through the following two individuals.

- Simon J. Hook
MS 183-503
Jet Propulsion Laboratory
4800 Oak Grove Dr.
Pasadena, CA 91109
Email: Simon.J.Hook@jpl.nasa.gov
Office: (818) 354-0974
Fax: (818) 354-5148
- Bogdan V. Oaida
MS 301-165
Jet Propulsion Laboratory
4800 Oak Grove Dr.
Pasadena, CA 91109
Email: Bogdan.Oaida@jpl.nasa.gov
Office: (818) 354-5517
Mobile: (626) 375-5398
Fax: (818) 393-9815

Preface

In 2004, the National Aeronautics and Space Administration (NASA), the National Oceanic and Atmospheric Administration (NOAA), and the U.S. Geological Survey (USGS) requested that the National Research Council (NRC) identify and prioritize the satellite platforms and associated observational capabilities that should be launched and operated over the next decade for Earth observation. In addition to providing information for the purpose of addressing scientific questions, the committee identified the need to ensure that the measurements helped benefit society and provide policymakers with the necessary information to make informed decisions on future policies affecting the Earth.

The resulting NRC study *Earth Science and Applications from Space: National Imperatives for the Next Decade and Beyond* (also known as the *Earth Science Decadal Survey* or, simply, the *Decadal Survey*) (NRC, 2007) recommended launching 15 missions in three time phases. These three time phases are referred to as Tier 1, Tier 2, and Tier 3, respectively. The Hyperspectral Infrared Imager (HypspIRI) mission is one of the Tier 2 missions recommended for launch in the 2013–2016 timeframe. This global survey mission provides an unprecedented capability to assess how ecosystems respond to natural and human-induced changes. It will help us assess the status of elements of biodiversity around the world and the role of different biological communities on land, within inland water bodies, and in shallow coastal zones, as well as on the surface of the deep ocean (but at reduced spatial resolution for the latter). Furthermore, the mission will help characterize natural hazards, with an emphasis on volcanic eruptions and associated precursor activities. HypspIRI will also map the mineralogical composition of the exposed land surface. The mission will advance our scientific understanding of how the Earth is changing as well as provide valuable societal benefit through an enhancement of our understanding of dynamic events, such as volcanoes and wildfires.

The HypspIRI mission concept includes two instruments: 1) a visible shortwave infrared (VSWIR) imaging spectrometer operating between 0.38 and 2.5 μm at a spatial scale of 60 m with a swath width of 145 km and 2) a co-aligned thermal infrared (TIR) multispectral scanner operating between 4 and 12 μm at a spatial scale of 60 m with a swath width of 600 km. The VSWIR and TIR instruments have revisit times of 19 and 5 days, respectively. Several of the other Tier 1 and Tier 2 missions provide complementary measurements for use with HypspIRI data; for example, the DesDynI, ACE, ICESat-II, and GEO-CAPE Decadal Survey missions, each of which measures very different properties or spatial scales compared to the features observable at local and landscape scales with HypspIRI. Note that, while the synergy between HypspIRI and other sensors, including those on operational satellites, benefits all missions and would support relevant scientific endeavors, the ability of HypspIRI to achieve its primary mission goals is not dependent on data from the other instruments.

This report documents a NASA-sponsored three-day workshop held in Pasadena, California, in August 2009 to refine the scientific questions, objectives, and requirements of the HypspIRI mission and to identify the priority near-term investments to mature the HypspIRI concept towards a possible Mission Concept Review (MCR) by mid 2010. Initially, some background on the NRC Decadal Survey is provided. This is followed by a discussion of the science, measurement requirements, mission concept, Level 1 requirements, and associated science as presented and discussed at the workshop, along with recommendations for future activities.

Executive Summary

NASA held a three-day workshop on August 11–13, 2009, to consider the Hyperspectral Infrared Imager (HyspIRI) mission recommended for implementation by the 2007 NRC Earth Science and Applications from Space: National Imperatives for the Next Decade and Beyond (also known as the Earth Science Decadal Survey or, simply, the Decadal Survey) ((NRC, 2007). The workshop was open to the research community as well as members of other communities with an interest in the HyspIRI mission. The workshop provided a forum for the HyspIRI Science Study Group (SSG) to present their observational requirements, assess the anticipated impact of HyspIRI on scientific and operational applications, and obtain feedback from the broader scientific community.

As part of the ongoing preparatory studies for the HyspIRI mission, the SSG has developed sets of measurement requirements tied to addressing a particular set of science questions. These requirements, together with those already provided by the Decadal Survey, were first presented at the 2008 Workshop and were updated at the 2009 Workshop. The requirements form the basis for the overall instrument and mission requirements. At the 2009 Workshop, participants reviewed the Draft Preliminary HyspIRI Mission Level 1 Requirements and confirmed that a mission developed to address these requirements would enable the science to be addressed by the HyspIRI mission. Breakout sessions provided a forum for participants to review the science questions, as well as measurement requirements, and to suggest additional opportunities for enhanced science or applications that might be achieved through synergies with other planned missions and/or with augmentations to the current mission.

Several key conclusions resulted from the workshop:

- The Preliminary HyspIRI Mission Level 1 Requirements would enable HyspIRI to address the science questions identified for the mission.
- HyspIRI provides a unique capability to address a set of specific scientific questions about local and global ecosystems, habitats, biodiversity, and hazards and their response to anthropogenic or natural changes.
- The reference instrument designs are capable of meeting the scientific measurement requirements.
- There is a stable set of instrument measurement requirements for HyspIRI; these requirements are traceable to the science questions for the mission.
- Significant heritage exists, from both a design and risk-reduction standpoint, for both instruments. This heritage includes missions such as the Moon Mineralogy Mapper and the Advanced Spaceborne Thermal Emission and Reflection Radiometer as well as the associated algorithms to deliver the Level 0 through Level 2 data products.
- There do not appear to be any significant technology “show stoppers,” and the mission is ready for implementation at the earliest opportunity.
- HyspIRI complements measurements from the DesDynI, ACE, and GEO-CAPE missions, each of which measures very different properties or spatial scales compared to the local and landscape scale features observable with HyspIRI.

The research community, like the Decadal Survey, strongly endorsed the need for the HyspIRI mission. There was a strong consensus that the HyspIRI mission, as defined, would accomplish the intended science.

Contents

Abstract	iii
Document Contacts	iii
Preface	v
Executive Summary	vi
Contents	vii
Figures	ix
Tables	ix
1 Introduction	1-1
1.1 The Decadal Survey	1-1
1.2 The HypsIRI Workshop.....	1-1
2 Measurement Requirements and Point Designs	2-1
2.1 VSWIR Instrument Concept.....	2-1
2.1.1 VSWIR Measurement Calibration Approach and Traceability	2-1
2.2 TIR Instrument Concept	2-2
2.2.1 TIR Measurement Calibration Approach and Traceability	2-4
3 Mission Concept	3-1
4 DRAFT Preliminary HypsIRI Mission Level 1 Requirements	4-1
5 Science Questions and Presentations	5-1
6 Data Products and Algorithms	6-1
6.1 VSWIR Level 2 Products.....	6-1
6.1.1 Introduction	6-1
6.1.2 Terrestrial Surface Reflectance	6-2
6.1.3 Aquatic Surface Reflectance	6-2
6.2 TIR Level 2 Products	6-3
6.2.1 Introduction	6-3
6.2.2 Surface Radiance.....	6-3
6.2.3 Surface Temperature and Emissivity	6-3
6.3 Low Latency Data Products.....	6-4
6.3.1 Hardware investigation.....	6-4
6.3.2 Science and Applications	6-4
6.3.3 Operations Concepts.....	6-4
7 Conclusions and Recommendations	7-1
8 References	8-1
9 Appendices	9-1
Appendix A – Acronyms	9-1
Appendix B - Workshop Agenda.....	9-3
Appendix C – List of Participants.....	9-9

Appendix D – Science-Traceability Matrices..... 9-17

Figures

Figure 1: HypsIRI-VSWIR key signal-to-noise and uniformity requirements	2-1
Figure 2: HypsIRI TIR instrument proposed spectral bands	2-2
Figure 3: HypsIRI TIR scanning scheme	2-3
Figure 4: HypsIRI TIR conceptual layout	2-3
Figure 5: HypsIRI TIR predicted sensitivity 200-500 K	2-3
Figure 6: HypsIRI TIR predicted sensitivity 300-1100 K	2-3
Figure 7: Number of image acquisitions in 19 days	3-1
Figure 8: Illustration of the Sun illumination at the winter solstice.....	3-1

Tables

Table 1 Preliminary VSWIR Measurement Characteristics	2-5
Table 2: Preliminary TIR Measurement Characteristics.....	2-6
Table 3: HypsIRI Data Volume, includes illumination constraints for VSWIR, compression and overhead	3-2
Table 4: The SA-200HP bus can meet the HypsIRI needs with minimum modifications.....	3-2
Table 5 Summary of payload accommodations.....	3-3
Table 6 Summary of resource margins.....	3-3

1 Introduction

1.1 The Decadal Survey

In 2004, NASA, NOAA, and the USGS commissioned the National Research Council (NRC) to conduct a ten-year survey for Earth science and applications from Space. The 2007 report resulting from that survey is titled: *Earth Science and Applications from Space: National Imperatives for the Next Decade and Beyond* (herein referred to as the Decadal Survey). The objective of the survey was to generate consensus recommendations from the Earth and environmental science and applications communities regarding an integrated approach to future space-based and ancillary observations.

The NRC appointed a committee to undertake the Decadal Survey. The committee participated in—and synthesized work from—seven thematically organized study panels:

- 1) Earth-science applications and societal benefits;
- 2) Land-use change, ecosystem dynamics, and biodiversity;
- 3) Weather;
- 4) Climate variability and change;
- 5) Water resources and the global hydrologic cycle;
- 6) Human health and security, and
- 7) Solid-Earth hazards, resources, and dynamics.

Each of these thematic areas identified key science measurements, justified these measurements, and recommended a small number of missions. The Decadal Survey committee consolidated the recommendations from each theme into a short list of prioritized missions. Included in this list as a high priority was the Hyperspectral Infrared Imager (HyspIRI) mission, which would provide global observations of multiple key surface attributes at local and landscape spatial scales (tens of meters to hundreds of kilometers) for a wide array of Earth-system studies,

including: integrating assessments of local and landscape changes key to understanding biodiversity in both terrestrial and aquatic (inland, coastal, and shallow oceanic) ecosystems; measuring the condition and types of vegetation on the Earth's surface, and changes in the mineralogical composition of the surface in order to understand the distribution of geologic materials. The mission would help map volcanic gases and surface temperatures, which were identified as indicators of impending volcanic hazards, as well as plume ejecta that pose risks to aircraft and people and property downwind.

The committee recommended that HyspIRI be launched in the 2013–2016 timeframe and include a hyperspectral visible shortwave infrared (VSWIR) imaging spectrometer and a multispectral thermal infrared (TIR) scanner. The mission would provide global coverage from low Earth orbit with a high temporal frequency, especially in the case of the TIR instrument, which would have a revisit time of 6 days or less.

The NRC Decadal Survey participants recognized that both instruments had strong spaceborne heritage through the Hyperion Instrument on the Earth Observing-1 (EO-1) platform, the Moon Mineralogy Mapper (M3) instrument on the Chandrayaan-1 platform, and the Advanced Spaceborne Thermal Emission and Reflection Radiometer (ASTER) instrument on the Terra platform.

1.2 The HyspIRI Workshop

On October 21-23, 2008, NASA held a three-day workshop to consider the HyspIRI mission. The workshop participants, like the Decadal Survey, strongly endorsed the need for the HyspIRI mission and felt the mission, as defined, would accomplish the intended science.

A second HypsIRI workshop was held on August 11–13, 2009 in Pasadena, California. This workshop was open to all interested parties (US and international). The goals of the workshop were to:

- Review and validate the HypsIRI science questions;
- Review and validate the Draft Preliminary HypsIRI Mission Level 1 requirements;
- Review the list of Level 2 HypsIRI Mission data products;
- List potential Level 3 HypsIRI user data products (with on-line tools), and
- Address and consider options for resolving key issues affecting HypsIRI science, including: Sun glint, spatial resolution in the coastal zone, data processing (on board and ground), partnership opportunities, and identification of key pre-launch science activities.

The workshop agenda is provided in Appendix B. The morning of the first day of the 2009 workshop focused on providing background information on the Decadal Survey and NASA’s approach to the HypsIRI mission. This was followed by descriptions of the measurement requirements, which included point designs for the instruments as well as the current science measurement acquisition baseline during normal and low latency operations. Next was a discussion of the Draft Preliminary HypsIRI Mission Level 1 Requirements. The measurement requirements, acquisition baseline, and Draft Preliminary HypsIRI Mission Level 1 requirements are described in sections 2-4.

The remainder of the first day and most of the second day were focused on a series of science presentations and discussions concerning the HypsIRI science questions and associated Science Traceability Matrices as well as potential products and uses for HypsIRI data. The Science Traceability

Matrices aim to directly link the science questions to instrument and mission requirements. The start of the second day involved discussion of potential funding opportunities for HypsIRI-related activities, including possible airborne campaigns. There was also a talk on the Intelligent Payload Module as a means to address needs for low-latency data. Section 5 describes the science questions and presentations.

The morning of the third and final day of the workshop began with a review of partnership opportunities with presentations of related international missions. There are several international missions that complement the global mapping provided by the HypsIRI mission. The remainder of the final morning and early afternoon included a discussion of ground data processing and data products (Level 1 and Level 2). The rest of the afternoon included additional science presentations followed by a discussion of the key outcomes of the workshop and next steps. A key outcome of the workshop was a consensus that the Draft Preliminary HypsIRI Mission Level 1 requirements clearly articulated the mission requirements.

Approximately 220 people participated in the workshop, with representatives from academia and industry, including participants from Australia, Canada, India, Japan, and Europe. Presentations given by NASA and academia addressed key aspects of the mission, with additional time for open discussion when appropriate. All the oral presentations can be found on the HypsIRI website at: <http://hyspiri.jpl.nasa.gov>.

2 Measurement Requirements and Point Designs

The Science Traceability Matrices (STMs) helped determine the system-level requirements for the HypsIRI instruments. The system-level requirements for the VSWIR and TIR instruments are presented in Table 1 and Table 2, respectively.

2.1 VSWIR Instrument Concept

The VSWIR instrument will acquire data between 380 and 2500 nm in 10-nm, contiguous bands. The instrument signal to noise ratio (SNR) was modeled for several different input radiances (see Figure 1). The current instrument model includes representative reflectances and transmissions for all surfaces in the instrument optical train. The model also includes the baseline geometry for the instrument and accounts for thermally generated, instrument background photon flux. The read noise and dark current of the sensor is also included. The instrument design minimizes polarization sensitivity and scattered light. The baseline data collection scenario involves observing the land and shallow (< 50m) water habitats at full spatial and spectral resolution and transmitting these data to the ground.

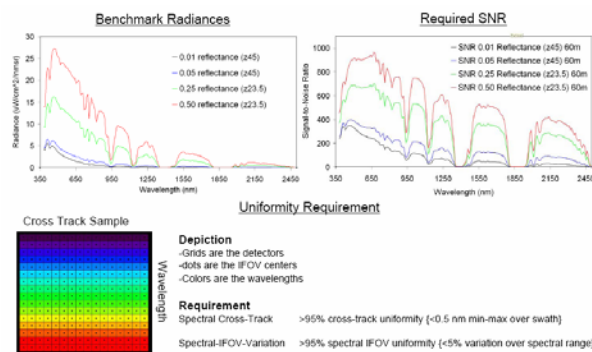


Figure 1: HypsIRI-VSWIR key signal-to-noise and uniformity requirements.

In addition, although not driven by the L1 requirements, the VSWIR will provide data over the deep, open ocean. These data will be summed to a spatial resolution of 1 km

and be transmitted to the ground. All data will be quantized at 14 bits. The instrument will have a swath width of 145 km, with a ground data sample of 60 m, resulting in a temporal revisit of 19 days at the equator. The nominal overpass time is 10:30 a.m.; this might, however, be adjusted by as much as ± 30 minutes to help manage certain effects, such as Sun glint on aquatic targets. Note that this swath width and repeating orbit provide timely coverage without frequent pointing maneuvers (cf. DS 2007: HypsIRI concept with 90 km VSWIR swath and rapid pointing). This approach resolves a trade-off between pixel resolution and frequent observation, which was recommended for further study in designing the Ecosystem Function mission recommended by the study panel on land use change, ecosystem dynamics, and biodiversity (DS, 2007), while also limiting the complexity of mission operations.

The absolute radiometric accuracy requirement is greater than 95% this will be maintained by using a variety of approaches, as is described below.

2.1.1 VSWIR Measurement Calibration Approach and Traceability

The VSWIR will be calibrated using an onboard solar reflectance calibration panel as well as monthly lunar views and periodic surface calibration experiments. VSWIR's spectral, radiometric, and spatial calibration characteristics will be determined and reported prior to launch. Spectral response functions will be determined for each spectral channel by recording VSWIR's output as calibrated laboratory monochromator scans from 350 to 2550 nm in 0.5 nm steps. Radiometric response and linearity will be determined by viewing an absolute radiometric source over a range of intensities. The radiometric source is

a known reflectance panel illuminated by a National Institute of Standards and Technology (NIST) irradiance lamp. This provides an absolute radiometric calibration for VSWIR with low uncertainties that are traceable to NIST. Spatial response functions will be determined by recording the output of VSWIR as a white light slit is “translated” across the field of view (FOV) in two orthogonal directions. A uniform spatial response with wavelength is required to provide a spectrum where all wavelengths measured originate from the same spatial sample area. For each field of view of the VSWIR instrument, the range, sampling, accuracy and precision (spectrally, radiometrically and spatially) will be determined.

During the course of the mission, the VSWIR spectral, radiometric, and spatial calibration will be assessed, monitored, and updated. Spectral calibration will be assessed by comparing the solar-atmospheric absorption features in measured spectra of the Earth’s atmosphere. A spectral fitting algorithm will be used to determine and report the optimal spectral calibration.

Radiometric calibration will be periodically assessed using a small calibration target on the VSWIR cover. Sunlight will be reflected from this surface into the VSWIR FOV. VSWIR measurements will be corrected to reflectance using a ratio of the measured target spectrum to a measured reference spectrum with a known bi-directional reflectance distribution function.

Less frequently, the spacecraft will orient the VSWIR for scans of the Sun-lit lunar surface. These data will provide a basis for tracking long-term changes to the instrument calibration.

2.2 TIR Instrument Concept

The TIR instrument will acquire data in eight spectral bands: seven of these bands are located in the thermal infrared part of the

electromagnetic spectrum between 7 and 12 μm ; the remaining band is located in the mid infrared part of the spectrum around 4 μm . The center position and width of each band is given in Table 2. The exact spectral location of each band was based on the measurement requirements identified in the Science Traceability Matrices, which included recognition that related data was acquired by other sensors, such as ASTER and Moderate Resolution Imaging Spectroradiometer (MODIS). HypsIRI will contribute to maintaining a long-time series of these measurements. For example, the positions of three of the TIR bands closely match the first three thermal bands of ASTER, while two of the TIR bands match bands of ASTER and MODIS typically used for split-window type applications (ASTER bands 12–14 and MODIS bands 31 and 32). It is expected that small adjustments to the band positions will be made based on ongoing science activities.

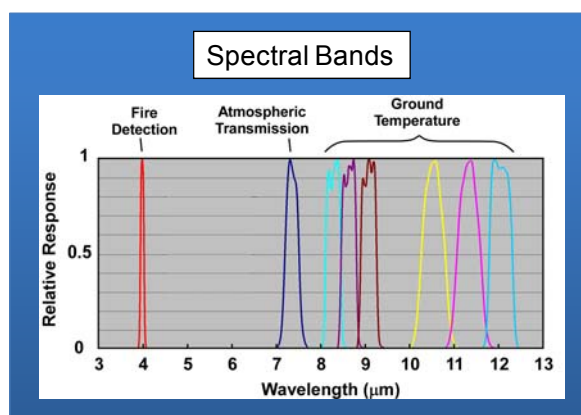


Figure 2: HypsIRI TIR instrument proposed spectral bands.

A key science objective for the TIR instrument is the study of hot targets (volcanoes and wildfires); therefore, the saturation temperature for the 4- μm channel is set high (1200 K) and the saturation temperatures for the thermal infrared channels are set at 500 K.

The TIR instrument will operate as a push-whisk mapper, similar to MODIS but

with 256 pixels in the cross-whisk direction for each spectral channel (Figure 3).

A conceptual layout for the instrument is shown in Figure 4. The scan mirror rotates at a constant angular speed. The mirror sweeps the focal plane image across nadir, then to a blackbody target and space, with a 2.2 seconds cycle time.

The f/2 optics design is all reflective, with gold-coated mirrors. The 60-K focal plane will be single-bandgap mercury cadmium telluride, hybridized to a Complementary Metal–Oxide–Semiconductor (CMOS) readout chip, with a butcher block spectral filter assembly over the detectors. Thirty-two analog output lines, each operating at 10-12.5 MHz, will move the data to analog-to-digital converters.

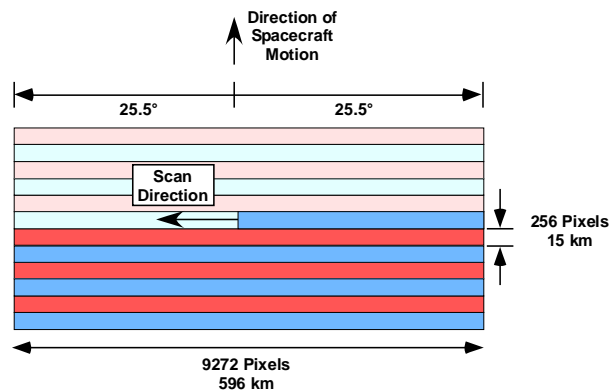


Figure 3: HypsIRI TIR scanning scheme.

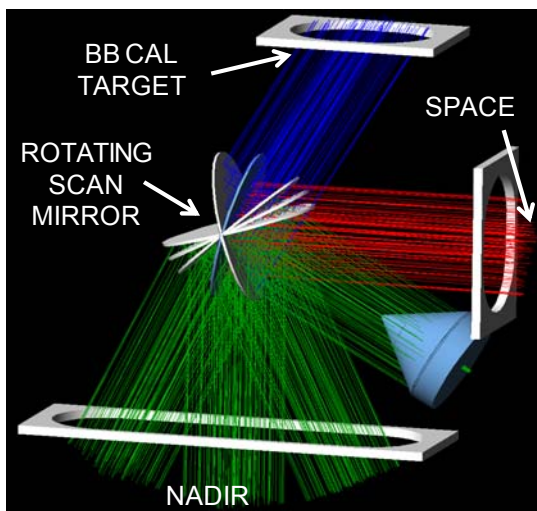


Figure 4: HypsIRI TIR conceptual layout.

The temperature resolution of the thermal channels is much finer than the mid-infrared channel, which (due to its high saturation temperature) will not detect a strong signal until the target is above typical terrestrial temperatures. All the TIR channels are quantized at 14 bits. Expected sensitivities of the eight channels, expressed in terms of noise-equivalent temperature difference, are shown in the following two plots.

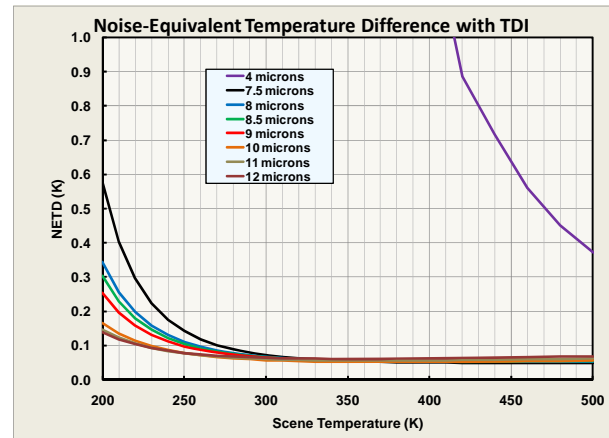


Figure 5: HypsIRI TIR predicted sensitivity 200-500 K.

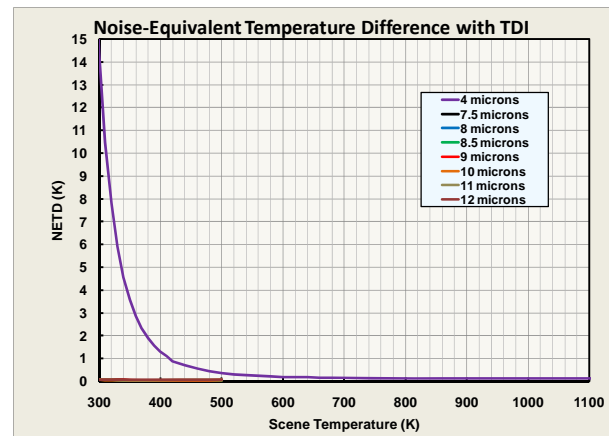


Figure 6: HypsIRI TIR predicted sensitivity 300-1100 K.

The TIR instrument will have a swath width of 600 km, with a pixel spatial resolution of 60 m, resulting in a temporal revisit of 5 days at the equator. The instrument will be on both day and night and will acquire data over the entire surface of the Earth. Like the VSWIR, the TIR instrument will acquire

full spatial resolution data over the land and coastal oceans (to a depth of < 50 m); over the open oceans, however, the data will be averaged to a spatial resolution of 1 km. The large swath width of the TIR will enable multiple revisits of any spot on the Earth every week (at least 1 day view and 1 night view). This repeat period is necessary to enable monitoring of dynamic or cyclical events, such as volcanic hotspots or crop stress associated with water availability.

geolocation calibration will be performed in flight by matching maps generated by this instrument to known features on the ground.

2.2.1 TIR Measurement Calibration Approach and Traceability

The radiometric accuracy and precision of the instrument are 0.5 K and 0.2 K, respectively. This radiometric accuracy will be ensured by using an on-board blackbody and view to space included as part of every 2.2 second sweep (15.4 km × 600 km on the ground). There will also be periodic surface validation experiments and monthly lunar views. The instrument will be calibrated before launch using a cold blackbody to simulate space and with a scene black body that will be varied in temperature from 200 K to more than 400 K. The temperature of both the ground-calibration blackbody and the in-flight blackbody will be measured with NIST-traceable temperature sensors.

Spectral calibration will be performed before launch using a monochromator, which will be calibrated against standards with known spectral features. A Fourier Transform Interferometer (FTIR) system might also be used to measure response over a broad spectral range.

Spatial (field-of-view) calibration will be performed before launch using a target projector with both in-track and cross-track slits. Pointing knowledge will be obtained from theodolite measurements that will measure the angular location of both the target projector slit and a reference cube on the instrument. This cube will then be used to determine the exact orientation of the instrument on the spacecraft. Additional

Table 1 Preliminary VSWIR Measurement Characteristics

Visible Shortwave Infrared Measurement Characteristics	
Spectral	
Range	380 to 2500 nm in the solar reflected spectrum
Sampling	10 nm {uniform over range}
Response	< 15 nm (full-width-at-half-maximum) {uniform over range}
Accuracy	< 0.5 nm
Radiometric	
Range & Sampling	0 to 1.5 × max benchmark radiance, 14 bits measured
Accuracy and stability	> 95% absolute radiometric, 98% on-orbit reflectance, 99.5%
Precision (SNR)	See spectral plots at benchmark radiances
Linearity	> 99% characterized to 0.1 %
Polarization	< 2% sensitivity, characterized to 0.5 % in sensitive regions
Scattered Light	< 1:100 characterized to 0.1% (next nearest neighbor)
Spatial	
Swath Width	> 145 km
Cross-Track Samples	> 2400
Sampling	60 m (GSD)
Response	70 m (FWHM)
Uniformity	
Spectral Cross-Track	> 95% cross-track uniformity {<0.5 nm min-max over swath}
Spectral-IFOV-Variation	> 95% spectral IFOV uniformity {<5% variation over spectral range}
Temporal	
Orbit Crossing	10:30 am Sun synchronous descending
Global Land Coast Repeat	19 days at equator
Rapid Response Revisit	3 days (cross-track pointing)
Cross Track Pointing	4 degrees in backscatter direction
On Orbit Calibration	
Lunar View	1 per month {radiometric}
Solar Cover Views	1 per week {radiometric}
Surface Cal Experiments	3 per year {spectral & radiometric}
Data Collection	
Land Coverage	Land surface above sea level excluding ice sheets
Water Coverage	Shallow water habitat – 50 m and shallower
Solar Elevation	20 degrees or greater
Open Ocean	Averaged to approximately 1-km spatial sampling
Compression	3:1 lossless

Table 2: Preliminary TIR Measurement Characteristics

Thermal Infrared Measurement Characteristics	
Spectral	
Bands (8) μm	3.98 μm , 7.35 μm , 8.28 μm , 8.63 μm , 9.07 μm , 10.53 μm , 11.33 μm , 12.05 μm
Bandwidth	0.084 μm , 0.32 μm , 0.34 μm , 0.35 μm , 0.36 μm , 0.54 μm , 0.54 μm , 0.52 μm
Accuracy	<0.01 μm
Radiometric	
Range	Bands 2–8 = 200 K – 500 K; Band 1= 1200 K
Resolution	< 0.05 K, linear quantization to 14 bits
Accuracy	< 0.5 K 3-sigma at 250 K
Precision (NEdT)	< 0.2 K
Linearity	> 99% characterized to 0.1 %
Spatial	
IFOV	60 m at nadir
MTF	> 0.65 at FNy
Scan Type	Push-Whisk
Swath Width	600 km
Cross Track Samples	9,300
Swath Length	15.4 km
Down Track Samples	256
Band to Band Co-Registration	0.2 pixels (12 m)
Pointing Knowledge	10 arcsec (0.5 pixels)
Temporal	
Orbit Crossing	10:30 a.m. Sun synchronous descending
Global Land Repeat	5 days at equator
On Orbit Calibration	
Lunar views	1 per month {radiometric}
Blackbody views	1 per scan {radiometric}
Deep Space views	1 per scan {radiometric}
Surface Cal Experiments	2 (day/night) every 5 days {radiometric}
Spectral Surface Cal Experiments	1 per year
Data Collection	
Time Coverage	Day and Night
Land Coverage	Land surface above sea level
Water Coverage	Coastal zone minus 50 m and shallower
Open Ocean	Averaged to approx 1-km spatial sampling
Compression	2:1 lossless

3 Mission Concept

The HypsIRI satellite will be put in a Sun-synchronous, low-Earth orbit. The local time of the descending node is expected to be 10:30 a.m. \pm 30 minutes, due to the benefits it offers in terms of observation geometry and signal to noise ratio at the instrument. As noted in Table 1 and Table 2, the VSWIR has a 19-day revisit at the equator, and the TIR has a 5-day revisit at the equator. Since the TIR is on both day and night, it acquires one daytime image every 5 days and one nighttime image every 5 days for a given ground location. The current altitude for the spacecraft is 626 km at the equator. The number of acquisitions for different parts of the Earth in a 19-day cycle is shown in Figure 2.

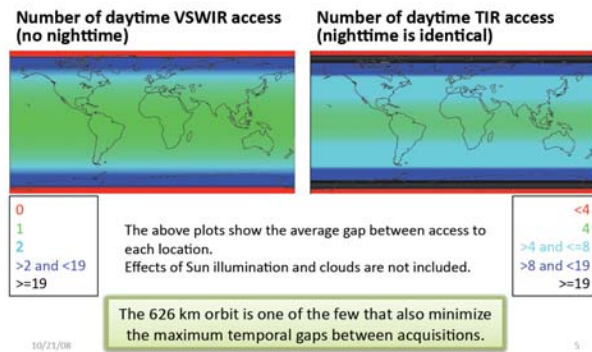


Figure 7: Number of image acquisitions in 19 days.

The figure is color-coded such that areas that are green meet the requirement and areas that are light blue, dark blue, and black exceed the requirement. Examination of the TIR map indicates that as one moves towards the poles the number of acquisitions exceeds the requirements with daily coverage at the poles. Because HypsIRI will travel an inclined orbit, no data will be acquired above and below 83° N and 83° S, respectively, in the VSWIR. Similarly, no data are acquired poleward of 85° N and 85° S in the TIR. The slightly more poleward

extension of the TIR instrument is due to its larger swath width.

VSWIR data acquisitions are also limited by the Sun illumination conditions, with no data being acquired when the Sun elevation angle is less than 20 degrees (Figure 8).

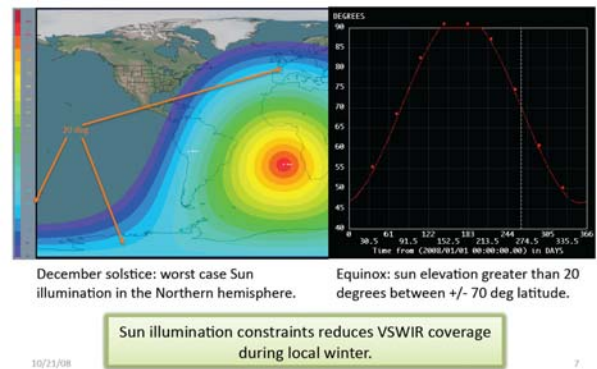


Figure 8: Illustration of the Sun illumination at the winter solstice.

The acquisition scenario for the HypsIRI mission is driven by target maps, with pre-defined maps controlling the acquisition mode. As noted earlier, the instruments are always on; however, they store data at either high-resolution mode (maximum spatial and spectral) or low-resolution mode. High-resolution mode data are acquired over the land and coastal waters shallower than 50 m. Low-resolution mode data are acquired over the rest of the oceans. The low-resolution mode return data are averaged or sub-sampled to about 1 km. This target-map-driven strategy combined with high- and low-resolution modes minimizes the cost of mission operations, allowing the instruments to acquire data in a near-autonomous fashion.

The satellite also includes an Intelligent Payload Module (IPM) with a direct broadcast capability that taps into the data feed from the instruments and allows a small subset of the data to be broadcasted in

near real time. The IPM is independent of the onboard data recording and storage system and connects to the data stream to pull out the desired spatial and spectral information for direct broadcast. The IPM is also independent of the spacecraft telecommunications system, as it features its own X-Band antenna designed to maximize the real-time broadcast footprint. The IPM has no significant data storage capacity.

The main spacecraft onboard data recording and storage system takes the data acquired in either low- or high-resolution mode and downlinks them to Earth. These data are then sent to the appropriate Distributed Active Archive Center (DAAC) for further processing into the different data products.

Table 3 shows the HypsIRI data volume, including the rate reduction associated with the VSWIR illumination requirement, compression, and overhead; note, however, that the table excludes the contribution from the low-resolution targets, which represent a minor addition to the total volume.

Table 3: HypsIRI Data Volume, includes illumination constraints for VSWIR, compression and overhead.

	VSWIR	TIR	Combined
Raw Instrument Data (Mbps)	804	130	934
Compression Factor	3	2	-
Compressed Data Rate (Mbps)	268	65	333
Year long averaged Duty Cycle	11.3%	34.6%	-
Compressed Data Rate (average) (Mbps)	30	23	53
Data Volume Per Orbit (average) (Gb)	177	131	308
Daily Data Volume (average) (Gb)	2623	1945	4568
Overhead	10%	10%	-
Packetized Daily Data Volume (Gb)	2,886	2,140	5,026
Cloud Obscuration	20%	0%	-
Usable Daily Data Volume (Gb)	2,309	2,140	4,449
TOTAL DAILY DATA VOLUME (Tb)	2.89	2.14	5.03

The continuous averaged, compressed data rate is 53 Mbps, which results in a data volume of 308 Gb/orbit and 5.03 Tb/day. Compared to the current Earth Observing System (EOS) missions, the HypsIRI data rates are higher, but they are comparable to other, more recently launched satellite

missions, such as WorldView-1, which has a data volume of 331 Gb/orbit. The HypsIRI satellite will have an onboard storage capacity of 3 Tb (WorldView-1 has 2.2 Tb of onboard storage). In the current configuration, HypsIRI data will be downloaded using dual-pole X-Band, which will be capable of download rates of upwards of 700 Mbps. Other options, such as Ka-Band, are also being considered. The Ka-Band option has a projected maximum downlink rate of 1 Gbps. This capability, however, is not currently operational.

The mission is currently carrying a three-ground-station solution for down linking the data, with facilities located at Svalbard, Norway; Poker Flats, Alaska; and U. of Tasmania, Australia.

The HypsIRI Flight System is made up of the two scientific instruments, the IPM, and an industry-provided spacecraft bus. The RSDO Catalog SA-200HP (option 6) bus was used in the 2008 TeamX study as an example of a potential bus to identify and cost needed modifications. A summary of the required modifications for this particular example is shown in Table 4.

Table 4: The SA-200HP bus can meet the HypsIRI needs with minimum modifications

	Requirements	RSDO SA-200HP	Modifications
Orbit	626 km 10:30 LTDN	✓	-
Mission duration	3 years, selective redundancy	✓	-
Pointing Knowledge	2 arcsec (3 σ /axis)	.5 arcsec (3 σ)	Ball CT-602 star tracker to protect against deformation between bus and payload
Pointing Accuracy	165 arcsec (3 σ /axis)	16 arcsec (3 σ)	
Pointing Stability	5 arcsec/sec (3 σ)	0.1 arcsec/sec (3 σ)	
Thermal	Passive architecture	✓	-
Downlink	740 Mbps	80Mbps	Dual-pol X-band
Propellant	42 m/s	131 m/s	-
Onboard recorder	3 Tb	100 Gbits	SEAKR SSP-R
Payload mass	132kg	666 kg	-
Payload + SSR power	217 W	650 W	Single wing configuration

The current design calls for HypsIRI to be launched on a Taurus 3210. This launch vehicle provides the closest fit in terms of capabilities among currently NASA-approved launchers. Insertion into a

mapping orbit can be achieved through daily launch windows.

The existing baselined point design provides sufficient margin in all significant areas of interest. Tables 5 and 6 summarize the payload accommodation and resource margins.

Table 5 Summary of payload accommodations

Accommodations	VSWIR	TIR
Mass (CBE)	66 kg	85 kg
Mass (w/ contingency)	81 kg	99 kg
Volume	1.6 x 1.6 x 1 m	1.2 x 0.5 x 0.4 m
Power	38 W	78 W
Data Rate (raw)	804 Mbps	130 Mbps
Data Rate (compressed)	268 Mbps	65 Mbps
Avg. Daily Data Volume	2.89Tbits	2.14 Tbits

Table 6 Summary of resource margins

	Required	Design (CBE)	Margin (D-R)/D
Swath width VSWIR	140 km	145 km	4%
Swath width TIR	558 km	600 km	7%
Recorder capacity	1.4 Tb	3 Tb	53%
Downlink capacity	5.0 Tb/day	8.4 Tb/day	31%
Power	217 W	650 W	66%
LV mass capability	561 <small>(includes propellant for (OL maneuver))</small>	790 kg	29%

Future efforts aimed at advancing the maturity of the mission concept will include: the development of a higher-fidelity data budget to allow for optimization of system resources, such as storage space and downlink times; the affect of Sun illumination constraints, and support for a second TeamX study in early 2010.

4 DRAFT Preliminary HypsIRI Mission Level 1 Requirements

A key part of the 2009 workshop was the presentation and discussion of the Draft Preliminary HypsIRI Mission Level 1 Requirements. These mission requirements are ultimately kept by NASA Headquarters and serve as the top-level requirements for the HypsIRI mission. They are the basis for deriving Level 2 requirements, which provide more detail.

The Draft Preliminary HypsIRI Mission Level 1 Requirements document contains several sections. Certain key sections that were discussed in detail at the workshop are summarized below and presented in italic text.

The Mission Imperative comes from the Decadal Survey and summarizes certain key deliverables as well as the communities that the mission will support. The Science Objectives identify what the mission will deliver. In the case of HypsIRI, they are the surface reflectance and water leaving radiance from the VSWIR instrument and the surface radiance, surface emissivity, and surface temperature from the TIR instrument. The Implementation Approach summarizes a point design that will meet the science objectives and provides more detail on the instruments and measurement range, such as the 60-m spatial resolution. The implementation approach also gives the lifetime (3 years) and indicates that both a calibration and validation plan will be developed for the mission. The remaining key section discussed at the workshop was the Requirements and Mission Success Criteria for the Baseline and Minimum Science Mission. Key differences between the baseline and minimum missions relate to the coverage and availability of data; these items are underlined in the text.

Mission Imperative

HYSPIRI is one of the missions recommended by the National Research Council's Committee on Earth Science and Applications from Space, (Earth Science and Applications from Space: National Imperatives for the Next Decade and Beyond, Space Studies Board, National Academies Press, 2007). HYSPIRI data have both high scientific value and high applications value. The high accuracy, resolution, and global coverage of HYSPIRI solar reflectance, temperature and thermal emissivity measurements are invaluable across many science and applications disciplines including ecology, biogeochemistry, biodiversity, coastal ocean and inland water research, geology, natural hazards, hydrology, climate, studies of the carbon cycle, and related applications.

Science Objectives

The HypsIRI Project will implement a spaceborne Earth observation mission designed to collect and provide global imaging measurements for surface reflectance, water leaving radiance, thermal emissivity, and surface radiance and temperature that will enable science and applications users to advance the current understanding of the Earth's ecology, biogeochemistry, biodiversity, coastal and inland waters, geology, natural hazards, hydrology, climate, and studies of the carbon cycle.

Implementation Approach

The HypsIRI observatory employs a dedicated spacecraft with a pair of instruments that will be launched into a 10:30 a.m., sun-synchronous orbit on an expendable launch vehicle. The baseline HypsIRI instruments include a visible to

shortwave infrared imaging spectrometer operating between 380 nm and 2500 nm, and a multiband thermal infrared imaging radiometer operating in the 4 – 12 micron range. Observations made with these instruments will be analyzed to yield estimates of surface reflectance, water leaving radiance, thermal emissivity and surface radiance and temperature at a nominal ground sample distance of 60 m. The measurements will be acquired for a period of three years. A Calibration and Validation Plan will be developed and implemented to assess random errors, and spatial and temporal biases in the data.

Requirements: Baseline Science Mission

a) VSWIR: To address the Decadal Survey and community identified science and application questions related to terrestrial and coastal ocean ecosystem composition, function, and change as well as surface composition (Decadal Survey pp. 113-115), the baseline science mission shall provide global mapping measurements of the surface reflectance and water leaving radiance (for persistently water covered regions) across the solar reflected spectrum from 380 to 2500 nm at ≤ 10 nm sampling at the specified signal-to-noise ratio and accuracy with $>95\%$ spectral/spatial uniformity at ≤ 60 m spatial sampling with <20 day revisit to provide $>60\%$ seasonal and $>80\%$ annual coverage of the terrestrial and shallow water regions of the Earth for at least three years with a subset of measurements available near-real-time for designated science and applications.

b) TIR: To address the Decadal Survey and community-identified science and application questions related to volcanoes, wild fires, water usage, urbanization and surface composition (Decadal Survey pp. 113-115), the baseline science mission shall provide global mapping measurements of the surface radiance, temperature and

emissivity with 8 spectral bands from the 3-5 micron and 7-12 micron regions of the spectrum at the specified noise-equivalent-delta-temperature and accuracy at ≤ 60 m spatial sampling with ≤ 5 day revisit to provide $>60\%$ monthly, $>70\%$ seasonal and $>85\%$ annual coverage of the terrestrial and shallow water regions of the Earth for at least three years with a subset of measurements available near-real-time for designated science and applications.

c) Combined Sensors: To address Decadal Survey and community-identified science and application questions (DS113-115), requiring combined reflectance, emissivity and temperature measurements, the baseline mission shall provide combined global mapping data sets with both reflectance from 380 to 2500 nm at ≤ 10 nm and emissivity, temperature and surface radiance from the 3-5 and 7-12 micron regions each at ≤ 60 m spatial sampling with <20 day revisit to provide $>60\%$ seasonal and $>80\%$ annual coverage of the terrestrial and shallow water regions of the Earth for at least three years with a subset of measurements available near-real-time for designated science and applications.

Requirements: Minimum Science Mission

a) VSWIR: To address the Decadal Survey and community-identified science and application questions related to terrestrial and coastal ocean ecosystem composition, function, and change as well as surface composition (Decadal Survey pp. 113-115), the minimum science mission shall provide global mapping measurements of the surface reflectance and water leaving radiance (for persistently water covered regions) across the solar reflected spectrum from 380 to 2500 nm at ≤ 10 nm sampling at $>90\%$ of the specified signal-to-noise ratio and accuracy with $>90\%$ spectral/spatial uniformity at ≤ 60 m spatial sampling with <20 day revisit to provide $>50\%$ seasonal

and >70% annual coverage of the terrestrial and shallow water regions of the Earth for at least two years.

b) TIR: To address the Decadal Survey and community identified science and application questions related to volcanoes, wild fires, water usage, urbanization and surface composition (DS113-115), the minimum science mission shall provide global mapping measurements of the surface temperature as well as emissivity and surface radiance in 8 spectral bands from the 3-5 micron and 7-12 micron regions of the spectrum at >90% the specified noise-equivalent-delta-temperature and accuracy at ≤ 60 m spatial sampling with ≤ 5 day revisit to provide >40% monthly, 60% seasonal and >70% annual coverage of the terrestrial and shallow water regions of the Earth for at least two years.

c) Combined Sensors: To address Decadal Survey and community identified science and application questions requiring combined reflectance, emissivity and temperature measurements, the minimum mission shall provide combined global mapping data sets with both reflectance from 380 to 2500 nm at ≤ 10 nm and emissivity, temperature and surface radiance from the 3-5 and 7-12 micron regions each at ≤ 60 m spatial sampling with <20 day revisit to provide >50% seasonal and >70% annual coverage of the terrestrial and shallow water regions of the Earth for at least two years.

These requirements were thoroughly discussed with the workshop participants. It was concluded they met the mission as described by the Decadal Survey and supported by the HypsIRI Science Study Group and were fully endorsed by the workshop participants.

5 Science Questions and Presentations

The HypsIRI mission is science driven by linking the measurement requirements for the mission to one or more science questions. HypsIRI has three top-level science questions related to 1) ecosystem function and composition, 2) volcanoes and natural hazards, and 3) surface composition and the sustainable management of natural resources. The NRC Decadal Survey called out these three areas. The top-level science questions for the HypsIRI mission are:

Ecosystem function and composition

What is the global distribution and status of terrestrial and shallow-aquatic ecosystems and how are they changing?

Volcanoes and natural hazards

How do volcanoes, fires, and other natural hazards behave; and do they provide precursor signals that can be used to predict future activity?

Surface composition and the sustainable management of natural resources

What is the composition of the land surface and coastal shallow water regions, and how can they be managed sustainably under natural and human-induced change?

These questions provide a scientific framework for the HypsIRI mission. NASA appointed the HypsIRI Science Study Group (SSG) to define and expand these questions to a level of detail that was sufficient to provide the measurement requirements for the HypsIRI mission. In 2007, the first SSGs were formed; note that there was a separate SSG for each instrument (VSWIR and TIR). These groups were then merged in 2008, their overall membership reassessed, and the HypsIRI SSG formed. The SSG represents the scientific community and domestic agencies interested in HypsIRI data, including the

NASA centers. Terrestrial and marine ecologists, geologists, geophysicists and atmospheric scientists participate in this group.

The SSG developed a more detailed set of overarching thematic questions that were separated into three groups. The first two groups deal with overarching questions that may be addressed by only one of the two instruments. The third group requires data from both instruments. All three groups may require supporting measurements from other instruments, whether spaceborne, airborne, or ground. The three question groups are referred to as the 1) VSWIR questions (VQ), 2) TIR questions (TQ) and 3) Combined questions (CQ), respectively (Table 7). For each of these overarching thematic questions, there are a set of thematic subquestions; it is these subquestions that provide the necessary detail to understand the measurement requirements (see the 2008 Workshop report).

As noted in Section 1, the 2009 HypsIRI Workshop included a large number of science-related presentations. These began with two parallel sessions in the afternoon of the first day focused on the VSWIR and TIR, respectively. The VSWIR and TIR sessions examined each of the overarching science questions in sequence (see Table 7). Each speaker presented the science sub questions and applications associated with the overarching question and discussed enabling data products and the associated Science Traceability Matrix. There were very few substantive updates to the Science Traceability Matrices presented in 2008, which the community felt accurately summarized that science that would be addressed by the HypsIRI mission. At the end of each session the Level 1 measurement calibration approach and traceability was described followed by the Level 2 products. The Level 1 measurement

calibration approach and traceability is described in Section 2 of the report; the Level 2 data products are described in Section 6. The second day also included two parallel sessions that addressed the Combined questions and followed a similar format to the VSWIR and TIR questions, with the exception that there are no Science Traceability Matrices for the combined questions since their requirements are consistent with requirements captured in the VSWIR and TIR Science Traceability Matrices. The second and third days included several presentations by individuals or groups of individuals that highlighted key science applications with HypsIRI data, such as characterizing geothermal resources or assessing change in coral reef ecosystems.

Table 7: Overarching Thematic Science Questions

Question #	Area	Question	Lead and Co-Lead
VQ1	Pattern and Spatial Distribution of Ecosystems and their Components	What is the global spatial pattern and diversity of ecosystems and how do ecosystems differ in their composition or biodiversity?	Roberts, Middleton
VQ2	Ecosystem Function, Physiology, and Seasonal Activity	What are the seasonal expressions and cycles for terrestrial and aquatic ecosystems, functional groups, and diagnostic species? How are these being altered by changes in climate, land use, and disturbance?	Gamon
VQ3	Biogeochemical Cycles	How are the biogeochemical cycles that sustain life on Earth being altered/disrupted by natural and human-induced environmental change? How do these changes affect the composition and health of ecosystems, and what are the feedbacks with other components of the Earth system?	Ollinger
VQ4	Changes in and Responses to Disturbance	How are disturbance regimes changing, and how do these changes affect the ecosystem processes that support life on Earth?	Asner, Knox
VQ5	Ecosystem and Human Health	How do changes in ecosystem composition and function affect human health, resource use, and resource management?	Townsend, Glass
VQ6	Earth Surface and Shallow-Water Substrate Composition	What is the land surface soil/rock and shallow-water substrate composition?	Green, Dierssen
TQ1	Volcanoes and Earthquakes	How can we help predict and mitigate earthquake and volcanic hazards through detection of transient thermal phenomena?	Abrams, Freund
TQ2	Wildfires	What is the impact of global biomass burning on the terrestrial biosphere and atmosphere, and how is this impact changing over time?	Giglio
TQ3	Water Use and Availability	How is consumptive use of global freshwater supplies responding to changes in climate and demand, and what are the implications for sustainable management of water resources?	Anderson, Allen
TQ4	Urbanization and Human Health	How does urbanization affect the local, regional, and global environment? Can we characterize this effect to help mitigate its impact on human health and welfare?	Quattrochi, Glass
TQ5	Surface Composition and Change	What is the composition and temperature of the exposed surface of the Earth? How do these factors change over time and affect land use and habitability?	Prakash, Mars
CQ1	Coastal, ocean, and inland aquatic environments	How do inland, coastal, and open-ocean aquatic ecosystems change due to local and regional thermal climate, land-use change, and other factors?	Muller-Karger
CQ2	Wildfires	How are fires and vegetation composition coupled?	Giglio
CQ3	Volcanoes	Do volcanoes signal impending eruptions through changes in the temperature of the ground, rates of gas and aerosol emission, temperature and composition of crater lakes, or health and extent of vegetation cover?	Wright, Realmuto
CQ4	Ecosystem Function and Diversity	How do species, functional type, and biodiversity composition within ecosystems influence the energy, water, and biogeochemical cycles under varying climatic conditions?	Roberts, Anderson
CQ5	Land surface composition and change	What is the composition of the exposed terrestrial surface of the Earth, and how does it respond to anthropogenic and non anthropogenic drivers?	Mars, Prakash
CQ6	Human Health and Urbanization	How do patterns of human environmental and infectious diseases respond to leading environmental changes, particularly to urban growth and change and the associated impacts of urbanization?	Quattrochi, Glass

6 Data Products and Algorithms

The product-level definitions for the HypsIRI mission are very similar to those currently in use by EOS missions. These data product levels are briefly summarized below.

- Level 0 - Reconstructed unprocessed instrument/payload data at full resolution; any and all communications artifacts (e.g., synchronization frames, communications headers) removed.
- Level 1A - Reconstructed unprocessed instrument data at full resolution, time-referenced, and annotated with ancillary information, including radiometric and geometric calibration coefficients and georeferencing parameters (i.e., platform attitude and ephemeris) computed and appended, but not applied, to the Level 0 data.
- Level 1B - Level 1A data that have been processed to sensor units.
- Level 2 - Derived geophysical variables at the same resolution and location as the Level 1 source data.
- Level 3 - Variables mapped on uniform space-time grid scales, usually with some completeness and consistency.
- Level 4 - Model output or results from analyses of lower-level data (i.e., variables derived from multiple measurements).

For the HypsIRI mission, it is anticipated that the project will provide the Level 0 through Level 2 data; the Level 3 and above data will be provided by the scientific community. The Level 1B data for HypsIRI will be geolocated radiance at sensor. Note that the data will not be orthorectified. In other words, we will know the latitude and longitude for any given pixel, but the image

pixels will not be resampled to be on a defined grid and of equal size. The Level 2 data will include surface radiance, surface reflectance (land and water), surface temperature, and surface emissivity. There will also be two cloud masks: one for the VSWIR and one for the TIR. Two masks are necessary due to the difference in the swath width of the VSWIR and TIR sensors. The size of data granules has not been determined yet; they will, however, be selected to make it straightforward to work with both the VSWIR and TIR products. The Level 0 through Level 2 products will be treated as standard products (i.e., produced for all scenes). The Level 3 and above products will be considered as special products (i.e., produced for a specified time-frame or region).

It is expected that the Level 0 through Level 2 data will be produced at the Science Data System and will be stored at a Distributed Active Archive Center (DAAC). The Science Data System will be developed later in the project.

The VSWIR and TIR Level 2 products, together with the low latency data products, are described in more detail below

6.1 VSWIR Level 2 Products

6.1.1 Introduction

HypsIRI will produce two Level-2 VSWIR products: Terrestrial and Aquatic Surface Reflectances.

There is growing interest in hyperspectral remote sensing for research and applications in a variety of fields, including geology, agriculture, forestry, coastal and inland water studies, environment hazards assessment, and urban studies (Gao et al. 2009).

In order to study surface properties using hyperspectral data, accurate removal of atmospheric absorption and scattering effects

is required. This process, called atmospheric correction, is essential to convert radiances measured by the sensors to reflectances of surface materials (Gao et al. 2009).

6.1.2 Terrestrial Surface Reflectance

The solar radiation on the Sun-surface-sensor path is affected by absorption and scattering effects from atmospheric gases and aerosols. Accurate modeling of these effects is required to derive surface reflectance spectra from VSWIR data.

An operational version of Atmosphere Removal Algorithm (ATREM) developed by Gao et al. (1993) is the current choice for hyperspectral VSWIR data. The algorithm is based on approximate radiative transfer calculations and a look-up table procedure and does not require field measurements of reflectance spectra. The ATREM was distributed to more than 300 researchers worldwide and has been extensively used for land surface reflectances (Gao et al. 2000; Gao et al. 2009).

ATREM uses a theoretical radiative transfer modeling technique that simulates explicitly the absorption and scattering effects of atmospheric gases and aerosols, as follows: 1) the integrated water vapor amount is derived on a pixel by pixel basis using a channel ratio technique (Gao et al., 1993); a fast line-by-line atmospheric transmittance model (Gao & Davis, 1997) and the HITRAN2000 line database (Rothman et al., 2003, 2005) are used to calculate atmospheric gaseous absorption; 2) the scattering effect due to atmosphere and aerosols is modeled using 6S computer code (Tanre et al., 1986; Gao et al., 2009).

The measured radiances are divided by solar irradiances above the atmosphere to obtain the apparent reflectances. The scaled surface reflectances are derived from the apparent reflectances using the simulated atmospheric gaseous transmittances and the simulated molecular and aerosol scattering data. The “absolute” surface reflectance is

obtained from the scaled surface reflectance multiplied by a combined factor of the slope and aspect of the surface (Gao et al. 2009).

The standard output from the ATREM code includes a water vapor image and a surface reflectance data cube.

More advanced features, such as spectral smoothing, topographic adjacency effect (Richter, 1998) correction, and atmospheric adjacency effect (Tanre et al., 1979) correction are not mature enough to be added to the current ATREM code during the development phase but will be considered once they are mature.

6.1.3 Aquatic Surface Reflectance

The ATREM algorithm designed for hyperspectral data over land is not suitable for that over shallow aquatic regions. Because aquatic surfaces are much darker than land surfaces and the air/water interface is not Lambertian, very accurate modeling of atmospheric absorption and scattering effects and the specular aquatic surface reflection effects is required to derive the aquatic surface reflectance or water leaving reflectance (Gao et al., 2009).

The current choice for the atmospheric correction of hyperspectral remote sensing data for water leaving radiance is the Tafkaa algorithm developed at the Naval Research Laboratory in the late 1990s (Gao et al., 2000).

The algorithm uses lookup tables, corresponding to various aerosol models, generated with a vector radiative transfer code (Ahmad & Fraser, 1982) and uses a spectral matching technique based on gaseous transmission spectra generated from ATREM code ported over for data processing. Tafkaa has been successfully demonstrated with hyperspectral imaging data acquired with the Portable Hyperspectral Imager for Low Light Spectroscopy (PHILLS) (Davis et al., 2002), the AVIRIS, and the Hyperion instrument on EO-1 (Ungar, 1997).

6.2 TIR Level 2 Products

6.2.1 Introduction

HyspIRI will produce three Level-2 Thermal Infrared (TIR) products: surface radiance, land surface temperature, and emissivity. The surface radiance product is used for temperature emissivity separation and requires an atmospheric correction using a radiative transfer model. The atmospheric correction is necessary to isolate land surface features from the effects of atmospheric emission, scattering, and absorption in the Earth's atmosphere. Once the surface radiance is known, the ASTER Temperature Emissivity Separation (TES) algorithm will be implemented to estimate the land surface temperature and emissivity (Gillespie et al. 1998).

6.2.2 Surface Radiance

The radiance leaving the surface is a combination of two terms: self emission from the Earth's surface and reflected downward irradiance from the sky and surroundings. The approach for computing surface radiance involves two steps. First, the atmosphere must be characterized by obtaining profiles of temperature, water vapor, and ozone at the HyspIRI observation time and location of the measurement. Ideally the profiles should be obtained from a validated, mature product with sufficient spatial resolution and close enough in time with the HyspIRI observation to avoid interpolation errors. Second, the atmospheric profiles need to be input to a radiative transfer model to estimate three atmospheric parameters necessary for atmospheric correction: the path radiance, transmittance, and downward sky radiance. The current choice of radiative transfer model is the latest version of the Moderate Resolution Atmospheric Radiance and Transmittance Model (MODTRAN) (Kneizys et al. 1996). MODTRAN has been sufficiently tested and validated and meets the speed requirements necessary for high spatial

resolution data processing. The latest version (5.3) uses an improved molecular band model (SERTRAN), with much finer spectroscopy from previous versions — down to 0.1 cm⁻¹ — resulting in more accurate modeling of band absorption features in the longwave TIR window regions. Furthermore, validation with Line-by-Line (LBL) models have shown good accuracy.

6.2.3 Surface Temperature and Emissivity

Land surface temperature and emissivity (LST&E) products are essential for a wide range of global climate change studies that include the Earth's radiation budget, surface-atmosphere interactions, climate modeling, cryospheric research, and land cover, land use change monitoring. Knowledge of the surface emissivity is also critical for accurately recovering the surface skin temperature, a key climate variable in many scientific studies, from climatology to hydrology and modeling the greenhouse effect.

The Temperature-Emissivity-Separation algorithm (TES) is applied to the land-leaving TIR radiances that are estimated by atmospherically correcting the at-sensor radiance on a pixel-by-pixel basis using the MODTRAN radiative transfer code. TES uses an empirical relationship to predict the minimum emissivity that would be observed from a given spectral contrast, or Minimum-Maximum Difference (MMD) (Kealy and Hook 1993; Matsunaga 1994). The empirical relationship is referred to as the calibration curve and is derived from a subset of spectra in the ASTER spectral library. A new calibration curve, applicable to HyspIRI TIR bands will be computed with the latest version of the ASTER spectral library. TES has been shown to accurately recover temperatures within 1.5 K and emissivities within 0.015 for a wide range of surfaces (Gillespie et al. 1998). The ASTER TES algorithm is well established, produces seamless images with no artificial discontinuities; emissivities in the

North American ASTER Land Surface Emissivity Database (NAALSED) (Hulley and Hook, 2009) have been validated at nine validation sites with mean differences for all five ASTER TIR bands of 0.016 (1.6 %), equivalent to ~ 1 K error in surface temperature for a material at 300 K (Hulley et al. 2009). Accurate atmospheric correction, particularly in humid atmospheric conditions, is critical for retrieving accurate TES LST&E products over graybody surfaces. As a consequence, the Water Vapor Scaling (WVS) method will be used to improve the water vapor atmospheric profiles on a band-by-band basis for each observation (Tonooka, 2005). The WVS method results in improved atmospheric corrections, and resulting emissivities have better accuracy and reduced spectral contrast over vegetation and waterbodies.

6.3 Low Latency Data Products

The current HypsIRI mission concept includes a direct broadcast capability, which will allow any user with the appropriate antenna to download a subset of the HypsIRI data stream to a local ground station. It is expected that distributed software will be developed to mimic the software that produces the standard products. This will enable direct broadcast users access to some HypsIRI data in near real time. The data latency for the standard products has not been determined, but it is anticipated that it will be on the order of a few days to one week.

6.3.1 Hardware investigation

A number of onboard processing algorithms used on Earth Observing One (EO-1) have been benchmarked on a range of hardware platforms, including the Mongoose M5, Rad750, Leon, SpaceCube (Vertex) and Opera (Tilera) platforms. These benchmarks are quite preliminary, but indicate that the more than conventional flight processor options (e.g., SpaceCube, Opera, Iboard, and

FPGA) options are the most promising in terms of being able to provide the necessary computing to keep up with the large (roughly 934 Mbits per second raw) data rate from the HypsIRI instruments. Current work involves refining benchmarks as well as solidifying a baseline datapath and transmission (e.g., antenna, transmitter) design. These further efforts are targeting formulation of a baseline hardware design with options and costs for design trades. Current transmission options are based on existing heritage direct broadcast designs with a potential for 15 Megabit/s downlink rates; note, however, that effective rates might be less (refining this number is an area of current work).

6.3.2 Science and Applications

On the software/science/applications side, a number of applications and users groups have been discussed among members of the HypsIRI Science Study Group. With these groups, a range of options have been discussed including: (1) specific bands common to other successful missions, (2) downlink of a spectral subset based on pre-defined spatial masks, and (3) derivation of selected low latency data products onboard. Fundamentally, the data can be reduced spatially, spectrally, or in context based on analysis. The primary applications for the rapid data delivery are wildfires and volcanoes. For active fire mapping and volcanic thermal detection, well understood temperature inversion methods can be used to detect activity and trigger downlink of low-latency data products. Rapid delivery of other products would support applications identified in the Decadal Survey (DS, 2007). For example, vegetation products based on plant color and thermal data can be used for drought and crop yield products and modeling disease vectors.

6.3.3 Operations Concepts

The HypsIRI study team has developed a preliminary operations concept for the IPM

option (Chien, 2009). In this concept, the science team would have the ability to specify regions of interest that can be spatially and temporally restricted and have an associated priority. For example, coastal masks might specify downlink of shallow water habitat information. Land masks might specify downlink of selected vegetation information. Depending on the product type, reduced spatial resolution data of specific bands might be downlinked (e.g., sea surface temperature information) or an algorithm might be run searching for specific signatures (volcanic activity, drought stress) and, when the signature is found in a region of interest, full spectral information for the triggered pixels downlinked. Based on the operations

constraints of onboard computing, onboard computing setup, and downlink, the highest priority requests for each overpass of an area that can be accommodated are scheduled. In most cases, multiple low-latency data products could be supported; however, for some high-contention areas, where the swath covers a range of targets, prioritization might be needed to resolve oversubscription (e.g., a coastal region could easily include: forest fire areas, coastal sediment plumes, shallow ocean algal blooms, and drought-stressed crops). The HyspIRI science and applications team would provide or review criteria for prioritizing targets.

7 Conclusions and Recommendations

The HypsIRI workshop re-affirmed the importance and desirability of the HypsIRI mission concept to conduct new science targeted at 1) ecosystem function and composition, 2) volcanoes and natural hazards, and 3) surface composition and sustainable management of natural resources.

The concept would provide high spatial, spectral, and temporal resolution visible through thermal infrared data of the land surface of the Earth and aquatic regions (defined by a water depth of < 50m). Data with the same spectral and temporal resolution but lower spatial resolution would be provided for the open ocean with a depth of > 50m. The measurements would be used to extract the surface radiance, spectral reflectance, emissivity, and temperature that would be used to address a core set of scientific questions related to research, applications, and their associated societal benefits. The concept study has found that the mission recommended by the Decadal Survey could be readily implemented with some minor modifications that optimize the science return from the mission.

Several key conclusions resulted from the workshop:

- HypsIRI provides a unique capability to address a set of specific scientific questions about global ecosystems, habitats, biodiversity, and hazards and their response to anthropogenic or natural changes.
- HypsIRI will help integrate terrestrial and aquatic (inland, coastal, and shallow oceanic) ecosystem studies and allow assessments at spatial scales relevant to resource use by humans.
- The reference instrument designs are capable of meeting the initial science measurement requirements.

- There is an initial set of instrument measurement requirements for HypsIRI that are traceable to the maturing scientific requirements for the mission.
- Significant heritage exists from both a design and risk-reduction standpoint for both candidate instruments. This heritage includes missions, such as the Moon Mineralogy Mapper and EO-1, and the Advanced Spaceborne Thermal Emission and Reflection Radiometer (ASTER), as well as the associated algorithms to deliver the Level 0 through Level 2 data products.
- There are no technology “show stoppers,” and the mission is ready for implementation at the earliest opportunity.
- The Draft Preliminary HypsIRI Mission Level 1 Requirements would enable HypsIRI to address the science questions identified for the mission. These requirements were evaluated and fully endorsed by the workshop participants and, by extension, the research community.
- HypsIRI complements measurements from the DesDynI, ACE, and GEO-CAPE missions, each of which addresses very different properties or spatial scales compared to the local and landscape scale features observable with HypsIRI.

Next steps identified by the Science Study Group and affirmed at the workshop include:

- Defining the requirements for *in situ*, tower, and aircraft instrumentation to support HypsIRI;

- Developing spectral libraries to support the reduction and analysis of HypsIRI data;
- Developing simulated HypsIRI data sets for algorithm development and testing;
- Evaluating how data from HypsIRI can be used synergistically with data from other instruments;
- Preparing for the Mission Concept Review (MCR) planned for June of 2010.
- Undertaking studies to evaluate:
 - Sun glint,
 - Saturation of mid and thermal channels,
 - The TIR band positions to determine the optimum band placement, and
 - Compression algorithms for VSWIR/TIR;
- Develop 3-5 key questions that we can take to the public (questions of obvious importance to people);
- Start to define metadata for Level 1 and 2 data products;
- Start to define level 3 products, and
- Develop validation approaches for products.

There was a strong consensus that the HypsIRI mission as recommended by the Decadal Survey would enable the intended science. The mission is clearly defined and ready for implementation at the first available opportunity.

8 References

[*DS, Decadal Survey; titles used informally*] *Earth Science and Applications from Space: National Imperatives for the Next Decade and Beyond, 2007. Committee on Earth Science and Applications from Space: A Community Assessment and Strategy for the Future (2007)*. National Research Council, National Academies Press. Referred to as the Decadal Survey or NRC 2007.

Steve Chien, Dorothy Silverman, Ashley Gerard Davies, Daniel Mandl, "Onboard Science Processing Concepts for the HypsIRI Mission," *IEEE Intelligent Systems*, vol. 24, no. 6, pp. 12-19, Nov./Dec. 2009, doi:10.1109/MIS.2009.120

Ahmad, Z., and Fraser, R. S., "An iterative radiative transfer code for ocean atmosphere systems", *Journal of Atmospheric Science*, 39, pp.656–665, 1982.

Bo-Cai Gao, Kathleen B. Heidebrecht, and Alexander F. H. Goetz, "Derivation of Scaled Surface Reflectances from AVIRIS Data", *Remote Sens. Environ.*, 44, pp.165-178, June 1993

Davis, C. O., Bowles, J., Leathers, R. A., Korwan, D., Downes, T. V., Snyder, W. A., Rhea, W. J., Chen, W., Fisher, J., Bissett, W. P., and Reisse, R. A., "Ocean PHILLS hyperspectral imager: design, characterization, and calibration", *Optics Express*, 10, pp. 210–221, 2002

Gao, B. -C., and Davis, C. O., "Development of a line-by-line-based atmosphere removal algorithm for airborne and spaceborne imaging spectrometers", *SPIE Proceedings*, vol. 3118, pp. 132–141, 1997.

Gao, B. -C., Montes, M. J., Ahmad, Z., and Davis, C. O., "Atmospheric correction algorithm for hyperspectral remote sensing of ocean color from space", *Applied Optics*, 39, 887–896, 2000.

Bo-Cai Gao, Marcos J. Montes, Curtiss O. Davis, Alexander F.H. Goetz, "Atmospheric correction algorithms for hyperspectral remote sensing data of land and ocean", *Remote Sens. Environ.*, 113 (2009), pp. S17-S24, Sept. 2009, doi:10.1016/j.rse.2007.12.015

Gillespie, A., Rokugawa, S., Matsunaga, T., Cothorn, J. S., Hook, S., & Kahle, A. B. (1998). A temperature and emissivity separation algorithm for Advanced Spaceborne Thermal Emission and Reflection Radiometer (ASTER) images. *Ieee Transactions on Geoscience and Remote Sensing*, 36(4), 1113–1126.

Hulley, G. C., and S. J. Hook (2009), The North American ASTER Land Surface Emissivity Database (NAALSED) version 2.0, *Remote Sens. Environ.*, 113(9), 1967– 1975, doi:10.1016/j.rse.2009.1005.1005.

Hulley, G. C., et al. (2009), Validation of the North American ASTER Land Surface Emissivity Database (NAALSED) version 2.0 using pseudo-invariant sand dune sites, *Remote Sens. Environ.*, 113(10), 2224–2233, doi:10.1016/j.rse.2009.06.005.

Kealy, P. S., & Hook, S. (1993). Separating temperature and emissivity in thermal infrared multispectral scanner data: Implication for recovering land surface temperatures. *Ieee Transactions on Geoscience and Remote Sensing*, 31(6), 1155–1164.

Kneizys, F. X., Abreu, L. W., Anderson, G. P., Chetwynd, J. H., Shettle, E. P., Berk, A., et al. (1996). The MODTRAN 2/3 Report and LOWTRAN 7 Model. In P. Lab (Ed.), F19628-91-C-0132 MA: Hanscom AFB.

Matsunaga, T. (1994). A temperature-emissivity separation method using an empirical relationship between the mean, the maximum, and the minimum of the thermal infrared emissivity spectrum, in Japanese with English abstract. *Journal of the Remote Sensing Society of Japan*, 14(2), 230–241.

Rothman, L. S., Jacquemart, D., Barbe, A., Benner, D. C., Birk, M., Brown, L. R., et al., “The HITRAN 2004 molecular spectroscopic database”, *Journal of Quantitative Spectroscopy and Radiative Transfer*, 96, pp. 139–204, 2005

Rothman, L. S., Barbe, A., Benner, D. C., Brown, L. R., Camy-Peyret, C., Carleer, M. R., et al., “The HITRAN molecular spectroscopic database: edition of 2000 including updates through 2001”, *Journal of Quantitative Spectroscopy and Radiative Transfer*, 82, 5–44, 2003

Tanre, D., Deschamps, P. Y., and de Lefte, A., “Atmospheric modeling for space measurements of ground reflectances, including bidirectional properties”, *Applied Optics*, 18, pp.3587–3594, 1979.

Richter, R., “Correction of satellite imagery over mountainous terrain”, *Applied Optics*, 37, pp. 4004–4015, 1998.

Tanre, D., Deroo, C., Duhaut, P., Herman, M., Morcrette, J. J., Perbos, J., and Deschamps, P. Y., “Simulation of the Satellite Signal in the Solar Spectrum (5S)”, *User's Guide*, U.S.T. de Lille, 59655 Villeneuve d'Ascq, France: Laboratoire d'Optique Atmospherique, 1986

Tonooka, H. (2005). Accurate atmospheric correction of ASTER thermal infrared imagery using the WVS method. *Ieee Transactions on Geoscience and Remote Sensing*, 43(12), 2778–2792.

Ungar, S. G., “Technologies for future Landsat missions”, *Photogrammetric Engineering & Remote Sensing*, 63, pp. 901–905, 1997.

9 Appendices

Appendix A – Acronyms

abs cal: Absolute Calibration
AC: Coastal Aquatic
ACE: Aerosol-Cloud-Ecosystems (Mission)
ALEXI/DisALEXI: Atmosphere-Land Exchange Inverse / Disaggregated Atmosphere-Land Exchange Inverse
ASTER: Advanced Spaceborne Thermal Emission and Reflection Radiometer
AVHRR: Advanced Very High Resolution Radiometer
AVIRIS: Airborne Visible Infrared Imaging Spectrometer
cal/val: Calibration/Validation
CCSP: Climate Change Science Program
CDOM: Colored Dissolved Organic Matter
CQ: Combined Question(s)
DAAC: Distributed Active Archive Center
DesDynI: Deformation, Ecosystems Structure, and Dynamics of Ice
DS: Decadal Survey
EO-1 Earth Observing-1
EOS : Earth Observing System
ET: Evapotranspiration
FG: Functional Group
FRP: Fire Radiative Power
FWHM: Full Width at Half Maximum
GDP: Gross Domestic Product
GEO: Group on Earth Observations
GEO-CAPE: Geostationary Coastal and Air Pollution Events
GEOSS: Global Earth Observation System of Systems
GOES: Geostationary Operational Environmental Satellite
HAB: Harmful Algal Bloom
HyspIRI: Hyperspectral Infrared Imager
HyTES: Hyperspectral thermal emission spectrometer
ICESat-II: Ice, Cloud, and Land Elevation Satellite II
IDP : Intelligent Data Payload
IFOV: Instantaneous Field of View
InSAR: Interferometric Synthetic Aperture Radar
IOOS: Integrated Ocean Observing System
IPM: Intelligent Payload Module
IR: Infrared
IOOS: Integrated Ocean Observing System
LDCM: Landsat Data Continuity Mission
LEO: Low Earth Orbit
LST: Land Surface Temperature
M3: Moon Mineralogy Mapper
MASTER: MODIS/ASTER Airborne Simulator
MCR: Mission Concept Review
MODIS: Moderate Resolution Imaging Spectroradiometer

NAS: National Academy of Sciences
NASA: National Aeronautics and Space Administration
NDVI: Normalized Difference Vegetation Index
NE: Noise-Equivalent
NE Δ T: Noise-Equivalent Delta Temperature
NPOESS/VIIRS: National Polar-orbiting Operational Environmental Satellite System / Visible Infrared Imaging Radiometer Suite
NOAA: National Oceanographic and Atmospheric Administration
NPV: Non-Photosynthetic Vegetation
NRC: National Research Council
PET: Potential Evapotranspiration
PFT: Plant Functional Type
PV: Photosynthetic Vegetation
NPV: Non photosynthetic vegetation
ROSES: Research Opportunities in Space and Earth Sciences
SAV: Submerged Aquatic Vegetation
SCOPE: Scientific Organization on Problems of the Environment
SEVIRI: Spinning Enhanced Visible and InfraRed Imager
SNR: Signal-to-Noise Ratio
SSG: (HyspIRI) Science Study Group
STM: Science Traceability Matrix
SWIR: Short-Wave Infrared
T-E Separation: Temperature-Emissivity Separation
TIR: Thermal Infrared
TM: (Landsat) Thematic Mapper
TQ: Thermal Infrared Question(s)
UHI: Urban Heat Island
UNIS: United Nations Information Service
USCOP: U.S. Commission on Ocean Policy
VIIRS: Visible Infrared Imager Radiometer Suite
VNIR : Visible and Near Infrared
VQ : Visible Shortwave Infrared Question(s)
VSWIR: Visible Shortwave Infrared
WGA: Western Governors Association

Appendix B - Workshop Agenda

11 Aug 2009 =====

8:00 Registration

8:45 Welcome and Objectives of HyspIRI Science Workshop

- Woody Turner, John LaBrecque

9:00 Overview of Decadal Survey Missions and Context for HyspIRI

- John LaBrecque

Review of Current Baseline HyspIRI Science Measurements Characteristics

9:30 - VSWIR Current Science Measurement Baseline - Rob Green

9:45 - TIR Current Science Measurement Baseline - Simon Hook

10:00 Break

10:30 Review of HyspIRI Mission Characteristics with HyspIRI Mission Current Science Measurement Acquisition Baseline (VSWIR, TIR) - Carl Bruce, Marc Foote, Bogdan Oaida

11:10 - Low latency (Dan Mandl, Steven Chien)

11:30 Draft Preliminary HyspIRI Mission Level 1 Requirements - Robert Green, Simon Hook

12:00 Lunch

VSWIR and TIR Parallel Sessions

VSWIR Afternoon Session

1:00 VQ1 – Pattern and Spatial Distribution of Ecosystems and their Components - John Gamon, Phil Townsend Dar Roberts

- Science Questions & Applications, Enabling Data Products, Science Traceability Matrix review

1:30 VQ2 – Ecosystem Function, Physiology and Seasonal Activity - Susan Ustin

- Science Questions & Applications, Enabling Data Products, Science Traceability Matrix review

2:00 VQ3 - Biogeochemical Cycles - Scott Ollinger, John Gamon

- Science Questions & Applications, Enabling Data Products, Science Traceability Matrix review

on hold at authors request

2:30 VQ4 - Ecosystem Response to Disturbance - Dar Roberts, Greg Asner

- Science Questions & Applications, Enabling Data Products, Science Traceability Matrix review

3:00 Break

3:30 VQ5 – Ecosystems and Human Well-being - Betsy Middleton

- Science Questions & Applications, Enabling Data Products, Science Traceability Matrix review

4:00 VQ6 - Earth Surface and Shallow Water Benthic Composition - Robert Green, Heidi Dierssen

- Science Questions & Applications, Enabling Data Products, Science Traceability Matrix review

4:30 VSWIR Special Topics

- Level 1 Measurement (Radiance) Calibration Approach and Traceability - Michael Eastwood

- Level 2 Product, terrestrial and aquatic surface reflectance - Bo-Cai Go

5:30 VSWIR Session Close

TIR Afternoon Session

1:00 TQ1 – Volcanoes - Mike Abrams

- Science Questions & Applications, Enabling Data Products, Science Traceability Matrix review

1:30 TQ2 – Wildfires - Ivan Csiszar

- Science Questions & Applications, Enabling Data Products, Science Traceability Matrix review

2:00 TQ3 – Water Use and Availability- Rick Allen

- Science Questions & Applications, Enabling Data Products, Science Traceability Matrix review

2:30 TQ4 – Human Health and Urbanization - Dale Quattrochi

- Science Questions & Applications, Enabling Data Products, Science Traceability Matrix review

3:00 Break

3:30 TQ5 – Earth surface composition and Change - Anupma Prakash

- Science Questions & Applications, Enabling Data Products, Science Traceability Matrix review

4:00 TIR Special Topics

- Measurement (Radiance) Calibration Approach and Traceability - Marc Foote

- Level 2 Product, surface radiance, temperature, emissivity - Glynn Hulley

5:30 TIR Session Close

7:00 Social Gathering

12 Aug 2009 =====

8:00 HypsIRI Data Analysis ROSES call Status and Upcoming HypsIRI Science Research Opportunities -
Woody Turner

8:20 HypsIRI related airborne campaigns - Woody Turner, Simon Hook, Robert Green

8:40 Science Prototype Activities using Hyperion Data and Existing Airborne and Spaceborne Data Sets - Betsy
Middleton

9:00 Mapping Floating Aquatic Vegetation (Kelp) with Imaging Spectroscopy at Spatial Scales from 4 to 60 m
using Linear Spectral Mixture Modeling - Phil Dennison

9:20 Biogeochemistry measurements for HypsIRI - Scott Ollinger

10:00 Break

10:30 Intelligent Payload Module for low latency measurements and parameters - Dan Mandl, Steven Chien

11:00 Characterization and Monitoring of Geothermal Resources Using Simulated HypsIRI Data - Fred Kruse

11:20 Assessing change in coral reef ecosystems using hyperspectral remote sensing - James Goodman

11:40 HypsIRI Spatial Scale for Coastal Ocean Science - Richard Zimmerman

12:00 Lunch

12:30 Space Grant Students Presentation (30 min)

Combined Question Parallel Sessions

CQ 1-3 Afternoon Session 12 Aug 2009

1:00 CQ1 – Coastal, ocean, and inland aquatic environments - Frank Muller-Karger

- Science Questions & Applications, Enabling Data Products, Science Traceability Matrix review

1:30 CQ2 – Wildfires - Ivan Csizsar

- Science Questions & Applications, Enabling Data Products, Science Traceability Matrix review

2:00 CQ3 – Volcanoes - Rob Wright

- Science Questions & Applications, Enabling Data Products, Science Traceability Matrix review

2:30 Break

CQ 4-6 Afternoon Session 12 Aug 2009

1:00 CQ4 – Ecosystem Function and Diversity - Dar Roberts

- Science Questions & Applications, Enabling Data Products, Science Traceability Matrix review

1:30 CQ5 – Land surface composition and change - Lyle Mars

- Science Questions & Applications, Enabling Data Products, Science Traceability Matrix review

2:00 CQ6 – Human Health and Urbanization - Mike Ramsey

- Science Questions & Applications, Enabling Data Products, Science Traceability Matrix review

2:30 Break

Return to Combined Session

3:00 - Shallow benthic habitat mapping opportunities in both continental nearshore and remote marine park islands; spatial-spectral and temporal scale issues of benthic health and processes - Arnold Dekker, CSIRO, Australia

3:20 Remote Sensing of Volcanic Thermal Features with HyspIRI - Greg Vaughan

3:40 Use of Imaging Spectroscopy to Detect Plant Physiological Traits - Phil Townsend

4:00 Use of VIS/NIR/SWIR/TIR Remote Sensing for U.S. Wildland Fire Characterization and Management: Potential for HyspIRI - Rob Sohlberg

4:20 Imaging spectroscopy for coastal benthic ecosystems: algae and seagrass - Heidi Dierssen

4:40 Evapotranspiration Estimation with ASTER & MASTER over the Jornada Experiment Range, New Mexico, USA - Andy French

5:00 Utility of HyspIRI for Coral Reef Studies and a Case Study of Sun Glint Correction in a Coral Reef Environment - Eric Hochberg

5:20 Close, 7:00 Social Gathering

13 Aug 2009 =====

Partnership Discussion (International and Domestic)

8:00 - Australia - Alex Held

8:20 - Canada - Alan Hollinger

no slides

Related International Missions

8:40 - ENMAP, Germany - Hermann (Charly) Kaufmann

9:00 - PRISMA, Italy - Cristina Ananasso

9:20 - APEX - Michael Schaepman

9:40 - ISRO Imaging Spectroscopy Plans - AS Kiran Kumar

10:00 - JAPAN imaging spectroscopy plans

10:20 Break

10:40 HypsIRI Ground Data Processing Baseline and Options - Robert Knox and Bogdan Oaida

Level 1 Validation of on orbit Radiance Calibration

11:00 - VSWIR - Carol Bruegge, Sven Geier, Robert O. Green

11:20 - TIR - Simon Hook

11:40 - Hyperion lessons learned - Steve Ungar

12:00 Lunch

Level 2 Product Validation and discussion

1:00 - VSWIR - Kevin Turpie, Robert O. Green

1:20 - TIR - Glynn Hulley, Simon Hook

1:40 Canopy small scale variability from HypsIRI for ecological applications - Yuri Knyazikhin

2:00 Anticipated Contributions of HypsIRI to the Remote Sensing of Volcanic Plumes - Vince Realmuto

2:20 Towards an assessment of photosynthetic light use efficiency from space: Upscaling PRI reflectance using an automated multi-angular spectroradiometer - Thomas Hilker

2:40 Deriving soil moisture and sediment mobility using future HypsIRI-derived thermal inertia - Mike Ramsey

3:00 Break

3:20 Use of ASTER Images to Study the Outbreak of West Nile Virus and its Relations with Environmental Variables in Indianapolis, Indiana: Implications for HyspIRI - Qihao Weng

3:40 The NEON Project and Potential Parameter/Algorithm Validation for HyspIRI - Tom Kampe

4:00 Key results and discussion Simon Hook, Robert O. Green

5:00 Review and Discussion of Draft Preliminary HyspIRI Mission Level 1 Requirements -Robert O. Green and Simon Hook

5:20 Review of Workshop and Next Steps - Woody Turner, John LaBrecque, Robert O. Green, Simon J. Hook

5:40 Close

Appendix C – List of Participants

HyspIRI Science Workshop 2009 Attendance Rpt.		
Last	First	Institution
Abbott	Elsa	JPL
Abrams	Michael	JPL
Algiers, Jr.	Joseph G.	NPS
Allen	Richard G.	U of Idaho
Amici	Stefania	Istituto Nazionale de Geofifica e Vulcanologia (INGV)
Ananasso	Christina	Italian Space Agency
Armstrong	Edward	
Arroyo-Mora	J. Pablo	McGill University
Bagheri	Sima	New jersey institute of technology
Baldauf	Brian	
Baldrige	Alice M.	JPL
Bauer	David	Northrop Grumman
Bernard	William L.	SpectIR
Binder	Holly	JPL
Block	Gary L.	JPL
Bontempi	Paula	NASA/HQ
Bowen	Jacob A.	JPL
Bradley	Eliza S.	UCSB
Bras	Rafael L.	UC Irvine
Brown	Jacob	JPL
Bruce	Carl F.	JPL
Bruce	Lori	Mississippi State University
Bruegge	Carol	JPL
Buckner	Janice L.	GSFC
Campbell	Petya	UMBC, Earth Science Technology Office
Carlson	Jennifer	
Castle	John	
Cavanaugh	Kyle	UCSB
Cetinic	Ivona	University of Southern California
Cheng	Samuel R.	JPL
Chien	Steve A.	JPL/California Institute of Technology

HyspIRI Science Workshop 2009 Attendance Rpt.

Last	First	Institution
Chilenski	Mark A.	JPL
Christensen	Phil	Arizona State University
Chull	Mitch	
Cristo	Alejandro	U of Extremadura
Csiszar	Ivan A.	NESDIS Center for Satellite Applications & Research (NOAA)
Corp	Lawrence A.	GSFC
Crippen	Robert E.	JPL
Cristina	Ananasso	Italian Space Agency
Czapla-Myers	Jeff	University of Arizona
Dalton	James B.	JPL
David	Valencia	U of Extremadura
Dawson	Jason	JPL
Dekker	Arnold G.	CSIRO / Land & Water
De Jong	Steven M.	Utrecht University/Faculty of Geosciences
Dennison	Philip e.	University of Utah
Dierssen	Heidi	
Domanguez Larios	Nieves	U of Extremadura
Donnallen	Andrea	Jet Propulsion Laboratory
Dungan	Jennifer L.	NASA/Ames Research Center
Eastwood	Cathleen	Jet Propulsion Laboratory
Eastwood	Michael	Jet Propulsion Laboratory
Estrada	Miguel	
Farmer-Toro	Gerardo	University of Southern California
Farrand	William H.	(SSI) Space Science Institute
Fitch	Robert A.	(DLR) German Space Agency
Fladeland	Matthew	NASA/Ames
Flatley	Tom	NASA/GSFC Research Center
Foote	Marc C.	Jet Propulsion Laboratory
Frederick	Christina A.	UT Austin
Freeman	Anthony	Jet Propulsion Laboratory/Cal Tech
French	Andrew N.	USDA/ARS
Freund	Friedemann T.	NASA ARC/SETI
Gamon	John A.	U of Alberta

HyspIRI Science Workshop 2009 Attendance Rpt.

Last	First	Institution
Gao	Bo-Cai	Naval Research Lab.
Garcia	Luz	
Geller	Gary	
Geier	Sven	Jet Propulsion Laboratory
Goodman	James	Univ. Puerto Rico & Mayaguez
Goulden	Michael L.	UC Irvine
Green	Robert O.	Jet Propulsion Laboratory
Guild	Liane	NASA Ames Research Center
Guess	Abigail	RSAC
Gunapala	Sarath	Jet Propulsion Laboratory
Gunderson	Adam K.	Jet Propulsion Laboratory
Habib	Shahid	NASA/GSFC
Hall	Gavin	Jet Propulsion Laboratory
Hall	Jeff L.	The Aerospace Corp.
Hamilin	Louise	Jet Propulsion Laboratory
Handley	Timothy A.	Santa Monica Mountains NRA
Harris	Sarah L.	Jet Propulsion Laboratory
Hartzell	Christine	Univ. Colorado
Held	Andrew A.	
Henebry	Geoffrey M.	S Dakota State University
Hengemihle	Jerry T.	Microtel LLC
Hepner	George	University of Utah
Hernandez	Luz M.	U of Extremadura
Hernandez	Marco	Jet Propulsion Laboratory
Hartzell	Christnie	JPL/University of Colorado, Boulder
Hill	Michael J.	Univ. N. Dakota
Hiker	Thomas	University of British Columbia
Ho	Shen-Shyang	Jet Propulsion Laboratory/Cal Tech
Hochberg	Eric J.	Nova Southeastern Univ.
Hollinger	Allan	Canadian Space Agency
Hook	Simon J.	Jet Propulsion Laboratory
Houborg	Rasmus	NASA/GSFC
Huete	Alfredo	U of Arizona

HyspIRI Science Workshop 2009 Attendance Rpt.

Last	First	Institution
Hulley	Glynn	Jet Propulsion Laboratory
Hunt	Raymond E.	USDA-ARS Hydrology & Remote Sensing Lab.
Hurst	Ken	Jet Propulsion Laboratory
Hyon	Jason J.	Jet Propulsion Laboratory
Jacob	Joseph C.	Jet Propulsion Laboratory
Johnson	Brad	NASA/GSFC
Johnson	Brian R.	
Johnson	William R.	Jet Propulsion Laboratory
Kampe	Thomas	National Ecological Observatory Network (NEON)
Kaufmann	Hermann J.	German Research Centre (GFZ)
Keely	Roth	UCSB
Kiang	Nancy Y.	Goddard Institute for Space Studies (GISS)
Knyazikhin	Yuri	Boston Univ.
Kroll	Lenley	Jet Propulsion Laboratory
Kruse	Fred A.	UNR
Kumar	Kiran Sedin A	ISRO Space Applications Centre
Kurzweil	Charlie	Jet Propulsion Laboratory
Kwoun	Oh-ig	Jet Propulsion Laboratory
LaBrecque	John L.	NASA Hq
Lapez	Mara	U of Extremadura
Larios	Niezes	
Lau	Gary K.	Jet Propulsion Laboratory
Leathers	Robertt	U. S. Naval Research Lab.
Lee	Krista R.	Naval Postgraduate School
Leifer	Ira S.	University of California @ Santa Barbara (UCSB)
Leung	Kon	Jet Propulsion Laboratory
Lieuallen	Athena E.	Oregon State University/JPL
Lopez	Maria P.	University of Extremadura
Lopez-Carrasco	Picar	
Lundeen	Sarah R.	Jet Propulsion Laboratory
Mandl	Daniel	NASA/GSFC
Mann	Lauri Bruce	Mississippi State University
Margolis	Jack S.	Prakash Institut

HyspIRI Science Workshop 2009 Attendance Rpt.

Last	First	Institution
Marraco	Hugo G.	Comision Nacional de Actividades Espaciales (CONAE)
Mars	John C.	USGS
Matsunaga	Tsuneo	National Institute of Environmental Studies
McCorke	Joel	NEON/U of Arizona
Merino	Jesus Mr.	U of Extremadura
Meyer	David	
Myers	Lynn	NASA/GSFC
Middleton	Elizabeth M.	NASA/GSFC
Moersch	Jeffrey	U of Tennessee
Mouroulis	Pantazis	Jet Propulsion Laboratory
McCubbin	Ian B.	DRI/Storm Peak Laboratory
Muller-Karger	Frank E.	University of South Florida (USF)/Marine Science
Myers	Jeff	UC Santa Cruz
Myers	Lynn	NASA/GSFC
Myneni	Ranga	Boston University
Navaro	Robert	NASA Dryden Flight Research Center
Nightingale	Joanne M.	NASA/GSFC
Njoku	Eni G.	Jet Propulsion Laboratory
Nuding	Danielle L.	Jet Propulsion Laboratory
Oaida	Bogdan	Jet Propulsion Laboratory
Ollinger	Scott V.	University of New Hampshire
Ong	Lawrence	NASA/GSFC - SSAI
Otero	Richard E.	Jet Propulsion Laboratory
Paine	Christopher G.	Jet Propulsion Laboratory
Painter	Thomas H.	U of Utah
Pestak	Christopher	Battelle Memorial Institute
Pieri	David C.	Jet Propulsion Laboratory
Policelli	Fritz S.	NASA/GSFC
Porter	David	
Porter	Michael	
Prakash	Anupma	Univ. of Alaska, Fairbanks/Geophysical Institute
Prasad	Lela C.	Arizona State University
Prasad	Saurabh	Mississippi State University

HyspIRI Science Workshop 2009 Attendance Rpt.

Last	First	Institution
Quattrochi	Dale A.	NASA/MSFC
Quirk	Bruce K.	USGS
Radocinski	Robert G.	Jet Propulsion Laboratory
Ramsey	Michael	Univ. Pittsburgh
Realmuto	Vincent J.	Jet Propulsion Laboratory
Rice	Joseph P.	NIST
Richardson	Brandon S.	Jet Propulsion Laboratory
Rivera	Geraldo	JPL/Test
Roberts	Dar A.	University of California @ Santa Barbara (UCSB)
Ross	Arwen E.	Naval Postgraduate School
Roth	Keely L.	University of California @ Santa Barbara (UCSB)
Sarde	Uday s.	Government of Maharashtra, India
Sarture	Charles M.	Jet Propulsion Laboratory
Savelyev	Alexander A.	Univ. Northern Iowa
Schaepman	Michael e.	Remote Sensing Lab/Univ. of Zurich
Schneider	Philipp	Jet Propulsion Laboratory
Schoenung	Susan M.	Ames Research Center
Schull	Mitchell	
Schulze	William	Jet Propulsion Laboratory
Seelin	Karen	
Serbin	Shawn P.	U of Wisconsin-Madison
Shu	Peter K.	NASA/GSFC
Silverman	Dorothy L.	Jet Propulsion Laboratory
Singh	Aditya	U of Wisconsin
Sohlberg	Robert A.	University of Maryland
Staenz	Karl	U of Lethbridg
Stone	Tom	US Geological Survey (USGS)
Su	Yi	(ICET) Mississippi State University
Takahashi	Duke	
Thomas	Alys C.	University of California @ Irvine (UCI)
Thomas	Valeria A.	Virginia Tech.
Tratt	David M.	The Aerospace Corp.
Tao	Tony s.	Jet Propulsion Laboratory

HyspIRI Science Workshop 2009 Attendance Rpt.

Last	First	Institution
Thome	Kurtis	NASA/GSFC
Townsend	Phil	U of Wisconsin
Tran	Daniel	Jet Propulsion Laboratory
Tulaczyk	Slawek	University of California @ Santa Cruz
Turmon	Michael	Jet Propulsion Laboratory
Turner	Woody	NASA Hq
Turpie	Kevin R.	NASA/GSFC
Ungar	Stephen	NASA/GSFC
Ustin	Susan L.	UC Davis
Van Gorp	Brian	
Vande Castle	John R.	University of New Mexico
Vasudevan	Gopal	
Vatsavai	Ranga R.	Oak Ridge Nat. Lab.
Vaughan	Greg	USGS
Valencia	David	
Valerie	Thomas	Virginia Tech
Velez-Reyes	Miguel	UPRM-IRISE
Wang	Jingfeng	University of California
Wang	Jinxue	Raytheon Vision Systems (RVS)
Wang	Kaicun	U of Maryland, College Park
Watson	Gail	Jet Propulsion Laboratory
Weng	Qihao	Marsospace
Wessels	Rick	USGS Alaska Volcano Observatory
West	Terrance R.	Mississippi State University
Wilcox	Eric	NASA/GSFC
Witter	Marti	National Park Service (NPS)
Woodruff	Robert A.	Lockheed Martin
Wright	Robert	Hawaii Institute of Geophysics & Planetology (HIGP)
Wu	Dong L.	Jet Propulsion Laboratory
Wiberg	Dean Y.	Jet Propulsion Laboratory
Wynne	Randolph	Virginia Tech
Xiao	Xiangming	University of Oklahoma
Xu	Liang	

HyspIRI Science Workshop 2009 Attendance Rpt.

Last	First	Institution
Yang	Wenze	Hunter College Dept of Geography
Zhang	Qingyuan	GEST/UMBC
Zimmerman	Richard C.	Old Dominion University

Appendix D – Science-Traceability Matrices

The DS cross-references in the Science Objectives column (first column includes the page number(s) of relevant material in the 2007 Decadal Survey)

Pattern and Spatial Distribution of Ecosystems and their Components: What is the global spatial pattern of ecosystem and diversity distributions and how do ecosystems differ in their composition or biodiversity? [DS 195]			
<p>How are ecosystems organized within different biomes associated with temperate, tropical, and boreal zones, and how are these changing? [DS 191, 203]</p>	<p>Measure globally vegetation covered regions seasonally and on a multi-year scale.</p> <p>Derive Fractional Cover of Plant Functional Types and Species where possible (terrestrial): e.g. tree, shrub, herbaceous, cryptogam; thick/thin leaves; broad/needle leaves; deciduous/evergreen; nitrogen-fixer/non-fixer; C3/C4 physiology.</p>	<p>Measure diagnostic spectral signature (400-2500@10nm) with high precision and accuracy to derive plant functional type and species where possible.</p> <p>Selected wavelengths (760+/-20 - oxygen for surface pressure and atm aerosols; 940 +/- 50 and 1150+/-50 - for water vapor; 1380 +/-20 for cirrus clouds) to allow for atmospheric correction for terrestrial and aquatic observations.</p> <p>Measure patch scales of <100 m.</p> <p>Measure seasonally (90 day revisit) through several (3) years to observe the seasonal regional occurrence and trends.</p> <p>Measure regionally-important Plant Functional Type with a revisit time of at most 20 days.</p>	<p>Surface reflectance in the solar reflected spectrum for elevation angles >20; rigorous cal/val program; Monthly lunar calcs; Daily solar calcs; 6 per year vcalcs; >3X zero-loss compression; ~10:30 am sun sync LEO orbit; Radiometric calibration; Atmospheric Correction; AC validation; Parameter Ground Validation; Geolocation; Pointing strategy to minimize sun glint; Avoid terrestrial hot spot; Ground processing; latency: seasonal, multi-year; 30m (3s) Pointing knowledge;</p>
<p>How do similar ecosystems differ in size, species composition, fractional cover and biodiversity across terrestrial and aquatic biomes? [DS 195]</p>	<p>Measure globally fraction of dominant Plant Functional Types and Species where possible (terrestrial): e.g. tree, shrub, herbaceous, cryptogam; thick/thin leaves; broad/needle leaves; deciduous/evergreen; nitrogen-fixer/non-fixer; C3/C4 physiology.</p> <p>Sample globally dominant aquatic phytoplankton functional types e.g. phytoplankton (diatoms, dinoflagellates, coccolithophores, N-fixers)</p> <p>Measure dominant submerged aquatic communities (i.e., coral, sea grass, kelp)</p> <p>Sample aquatic biogeochemical constituent: (phytoplankton, sediment, CDOM, benthos)</p>	<p>Measure diagnostic spectral signature (400-2500@10nm) with high precision and accuracy to derive terrestrial functional groups, species and critical measurable</p> <p>Selected wavelengths (760+/-20 - oxygen for surface pressure and atm aerosols; 940 +/- 50 and 1150+/-50 - for water vapor; 1380 +/-20 for cirrus clouds) to allow for atmospheric correction for terrestrial and aquatic observations.</p> <p>Measure diagnostic spectral signature (380-900@10nm) to derive aquatic functional groups, species and critical measurable abiotic components.</p> <p>Selected wavelengths in the short wavelength infrared (1250, 1650, 2250) to enable atmospheric correction for aquatic observations.</p> <p>Measure with spatial resolution of <100 m.</p> <p>Measure seasonally (90 day revisit) through several (3) years to capture baseline</p> <p>Measure regionally-important Plant Functional Type with a revisit time of at most 20 days.</p>	<p>Surface reflectance in the solar reflected spectrum for elevation angles >20; Rigorous cal/val program; Monthly lunar calcs; Daily solar calcs; 6 per year vcalcs; >3X zero-loss compression; ~10:30 AM sun sync LEO orbit; Radiometric calibration; Atmospheric Correction; AC validation; Parameter Ground Validation; Geolocation; Pointing strategy to minimize sun glint; Avoid terrestrial hot spot; Ground processing; latency: seasonal, multi-year; 30m (3s) Pointing knowledge ;</p>
<p>What is the current spatial distribution of ecosystems, functional groups, or key species within major biomes including agriculture, and how are these being altered by climate variability, human uses, and other factors?</p>	<p>Measure Fractional Cover of Plant Functional Types and Species where possible (terrestrial): e.g. tree, shrub, herbaceous, cryptogam; thick/thin leaves; broad/needle leaves; deciduous/evergreen; nitrogen-fixer/non-fixer; C3/C4 physiology.</p>	<p>Measure diagnostic spectral signature (400-2500@10) with high precision and accuracy to derive plant functional type and species.</p> <p>Selected wavelengths (760+/-20 - oxygen for surface pressure and atm aerosols; 940 +/- 50 and 1150+/-50 - for water vapor; 1380 +/-20 for cirrus clouds) to allow for atmospheric correction for terrestrial and aquatic observations.</p> <p>Measure patch scales of <100 m.</p> <p>Measure seasonally (90 day revisit) through several (3) years to observe the seasonal regional occurrence and trends.</p> <p>Measure regionally-important Plant Functional Type with a revisit time of at most 20 days.</p>	<p>Surface reflectance in the solar reflected spectrum for elevation angles >20; Rigorous cal/val program; Monthly lunar calcs; Daily solar calcs; 6 per year vcalcs; >3X zero-loss compression; ~10:30 AM sun sync LEO orbit; Radiometric calibration; Atmospheric Correction; AC validation; Parameter Ground Validation; Geolocation; Pointing strategy to minimize sun glint; Avoid terrestrial hot spot; Ground processing; latency: seasonal, multi-year; 30m (3s) Pointing knowledge</p>

VQ1

Science Question	Scientific (Measurement) Objective	Scientific Measurement Requirement	Mission Functional Requirement
Pattern and Spatial Distribution of Ecosystems and their Components: What is the global spatial pattern of ecosystem and diversity distributions and how do ecosystems differ in their composition or biodiversity? [DS 195]			
What are the extent and impact of invasive species in terrestrial and aquatic ecosystems? [DS 192, 194, 196, 203, 204, 214]	<p>Measure globally vegetation covered regions seasonally and on a multi-year scale.</p> <p>Derive Fractional Cover of Plant Functional Types and Species where possible focusing on invasive species types (terrestrial and aquatic)</p>	<p>Measure diagnostic spectral signature (400-2500@10nm) with high precision and accuracy to derive terrestrial functional groups, species and critical measurable abiotic components.</p> <p>Selected wavelengths (760+/-20 - oxygen for surface pressure and atm aerosols; 940 +/- 50 and 1150+/-50 - for water vapor; 1380 +/-20 for cirrus clouds) to allow for atmospheric correction for terrestrial and aquatic observations.</p> <p>Measure diagnostic spectral signature (380-900@10nm) to derive aquatic functional groups, species and critical measurable abiotic components.</p> <p>Selected wavelengths in the short wavelength infrared (1250, 1650, 2250) to enable atmospheric correction for aquatic observations.</p> <p>Measure with spatial resolution of <100 m.</p> <p>Measure seasonally (90 day revisit) through several (3) years to observe the seasonal regional occurrence and trends in the coastal regions.</p> <p>Measure regionally-important Plant Functional Type with a revisit time of at most 20 days.</p>	<p>Surface reflectance in the solar reflected spectrum for elevation angles >20; Rigorous cal/val program; Monthly lunar cals; Daily solar cals; 6 per year vcal; >3X zero-loss compression; ~10:30 am sun sync LEO orbit; Radiometric calibration; Atmospheric Correction; AC validation; Parameter Ground Validation; Geolocation; Pointing strategy to minimize sun glint; Avoid terrestrial hot spot; Ground processing; latency: seasonal, multi-year; 30m (3s) Pointing knowledge;</p>
What is the spatial structure and species distribution in a phytoplankton bloom? [DS 201, 208]	<p>Sample globally algal blooms (including harmful) species and spatial structure in the coastal regions and in the deep oceans with reduced spatial resolution.</p>	<p>Measure diagnostic spectral signature (380-900@10) with high precision and accuracy of aquatic vegetation in coastal regions.</p> <p>Selected wavelengths in the short wavelength infrared (1250, 1650, 2250) to allow atmospheric correction.</p> <p>Measure deep ocean with spatial resolution of <1000 m.</p> <p>Measure coastal aquatic with spatial resolution of <100 m.</p> <p>Measure seasonally (90 day revisit) through several (3) years to observe the seasonal regional occurrence and trends in the coastal regions.</p> <p>Measure regionally-important Plant Functional Type with a revisit time of at most 20 days.</p>	<p>Surface reflectance in the solar reflected spectrum for elevation angles >20; Rigorous cal/val program; Monthly lunar cals; Daily solar cals; 6 per year vcal; >3X zero-loss compression; ~10:30 am sun sync LEO orbit; Radiometric calibration; Atmospheric Correction; AC validation; Parameter Ground Validation; Geolocation; Pointing strategy to minimize sun glint; Avoid terrestrial hot spot; Ground processing; latency: seasonal, multi-year; 30m (3s) Pointing knowledge;</p>
How do changes in coastal morphology and surface composition impact coastal ecosystem composition, diversity and function [DS 41]?	<p>Measure coastal ecosystem functional characteristics and diversity at the seasonal and multiyear time scale.</p>	<p>Measure diagnostic spectral signature (400-2500@10) with high precision and accuracy of terrestrial vegetation in coastal regions.</p> <p>Selected wavelengths (760+/-20 - oxygen for surface pressure and atm aerosols; 940 +/- 50 and 1150+/-50 - for water vapor; 1380 +/-20 for cirrus clouds) to allow for atmospheric correction for terrestrial and aquatic observations.</p> <p>Measure diagnostic spectral signature (380-900@10) with high precision and accuracy of aquatic ecosystems in coastal regions.</p> <p>Selected wavelengths in the short wavelength infrared (1250, 1650, 2250) to enable atmospheric correction for aquatic observations.</p> <p>Measure with spatial resolution of <100 m.</p> <p>Measure seasonally (90 day revisit) through several (3) years to observe the seasonal regional occurrence and trends in the coastal regions.</p> <p>Measure regionally-important Plant Functional Type with a revisit time of at most 20 days.</p>	<p>Surface reflectance in the solar reflected spectrum for elevation angles >20; Rigorous cal/val program; Monthly lunar cals; Daily solar cals; 6 per year vcal; >3X zero-loss compression; ~10:30 am sun sync LEO orbit; Radiometric calibration; Atmospheric Correction; AC validation; Parameter Ground Validation; Geolocation; Pointing strategy to minimize sun glint; Avoid terrestrial hot spot; Ground processing; latency: seasonal, multi-year; 30m (3s) Pointing knowledge;</p>

VQ1

Science Question	Scientific (Measurement) Objective	Scientific Measurement Requirement	Mission Functional Requirement
Ecosystem Function, Physiology and Seasonal Activity: What are the seasonal expressions and cycles for terrestrial and aquatic ecosystems, functional groups and diagnostic species? How are these being altered by changes in climate, land use, and disturbances? [DS 191, 195, 203]			
How does the seasonal activity of ecosystems and functional types vary across biomes, geographic zones, or environmental gradients between the equator and the poles? How are seasonal patterns of ecosystem function being affected by climate change? [DS 205, 206, 210] (include agriculture?)	Measure the functional type composition of ecosystems at spatial scales that capture regional and global distributions and temporal scales that capture seasonal and multi-year trends.	Measure surface reflectance in the VSWIR region (400-2500@10nm) at high precision and accuracy. Selected wavelengths (760+/-20 - oxygen for surface pressure and atm aerosols; 940 +/- 50 and 1150+/-50 - for water vapor; 1380 +/-20 for cirrus clouds) to allow for atmospheric correction for terrestrial and aquatic observations. Measure diagnostic spectral signature (380-900@10) with high precision and accuracy of aquatic ecosystems in coastal regions. Selected wavelengths in the short wavelength infrared (1250, 1650, 2250) to enable atmospheric correction for aquatic observations. Measure globally at spatial resolution patch scale relevant for ecosystem 10^4 to 10^6 m^2. Measure seasonally (90 day revisit) through several (3) years to observe the seasonal regional occurrence and trends in the coastal regions. Measure regionally-important Plant Functional Type with a revisit time of at most 20 days.	Surface reflectance in the solar reflected spectrum for elevation angles >20; Rigorous cal/val program; Monthly lunar calcs; H42Daily solar calcs; 6 per year vcalcs; ~700mbs downlink; >3X zero loss compression; ~10:30 AM sun sync LEO orbit; Radiometric calibration; Atmospheric Correction; AC validation; Geolocation; Pointing strategy to minimize sun glint; Avoid terrestrial hot spot; Ground processing; Seasonal latency; 30m (3s) Pointing knowledge
How do seasonal changes affect productivity, carbon sequestration, and hydrological processes across ecosystems and agriculture? [DS 195, 205, 210]	Measure seasonal changes and status of natural ecosystem and agricultural lands over the seasonal and multiyear scale.	Measure surface reflectance in the VSWIR region (400-2500@10nm) at high precision and accuracy. Selected wavelengths (760+/-20 - oxygen for surface pressure and atm aerosols; 940 +/- 50 and 1150+/-50 - for water vapor; 1380 +/-20 for cirrus clouds) to allow for atmospheric correction for terrestrial and aquatic observations. Measure globally at spatial resolution patch scale relevant for ecosystem 10^4 to 10^6 m^2. Measure seasonally (90 day revisit) through several (3) years to observe the seasonal regional occurrence and trends in the coastal regions. Measure regionally-important Plant Functional Type with a revisit time of at most 20 days.	Surface reflectance in the solar reflected spectrum for elevation angles >20; Rigorous cal/val program; Monthly lunar calcs; Daily solar calcs; 6 per year vcalcs; ~700mbs downlink; >3X zero loss compression; ~10:30 AM sun sync LEO orbit; Radiometric calibration; Atmospheric Correction; AC validation; Geolocation; Pointing strategy to minimize sun glint; Avoid terrestrial hot spot; Ground processing; Seasonal latency; 30m (3s) Pointing knowledge
How do environmental stresses affect the physiological function of water and carbon exchanges at the seasonal time scale within ecosystems (including agriculture)? [DS 203, 206, 210]	Measure the physiological function indicators of ecosystems related to water and carbon exchange over the seasonal and multiyear time frame.	Measure diagnostic spectral signature (380-900@10) with high precision and accuracy of aquatic ecosystems in coastal regions. Selected wavelengths in the short wavelength infrared (1250, 1650, 2250) to enable atmospheric correction for aquatic observations. Measure globally at spatial resolution patch scale relevant for ecosystem 10^4 to 10^6 m^2. Measure seasonally (90 day revisit) through several (3) years to observe the seasonal regional occurrence and trends in the coastal regions. Measure regionally-important Plant Functional Type with a revisit time of at most 20 days.	Surface reflectance in the solar reflected spectrum for elevation angles >20; Rigorous cal/val program; Monthly lunar calcs; Daily solar calcs; 6 per year vcalcs; ~700mbs downlink; >3X zero loss compression; ~10:30 AM sun sync LEO orbit; Radiometric calibration; Atmospheric Correction; AC validation; Geolocation; Pointing strategy to minimize sun glint; Avoid terrestrial hot spot; Ground processing; Seasonal latency; 30m (3s) Pointing knowledge
What is the environmental impact of aquatic plants and coral in inland and coastal water environments at the seasonal time scale? [DS 201, 208]	Measure the distribution and type of algal bloom in a sampling sense globally over the seasonal and multiyear timescale.	Measure diagnostic spectral signature (380-900@10) with high precision and accuracy of aquatic ecosystems in coastal regions. Selected wavelengths in the short wavelength infrared (1250, 1650, 2250) to enable atmospheric correction for aquatic observations. Measure globally at spatial resolution patch scale relevant for ecosystem 10^4 to 10^6 m^2. Measure seasonally (90 day revisit) through several (3) years to observe the seasonal regional occurrence and trends in the coastal regions. Measure regionally-important Plant Functional Type with a revisit time of at most 20 days.	Surface reflectance in the solar reflected spectrum for elevation angles >20; Rigorous cal/val program; Monthly lunar calcs; Daily solar calcs; 6 per year vcalcs; ~700mbs downlink; >3X zero loss compression; ~10:30 AM sun sync LEO orbit; Radiometric calibration; Atmospheric Correction; AC validation; Geolocation; Pointing strategy to minimize sun glint; Avoid terrestrial hot spot; Ground processing; Seasonal latency; 30m (3s) Pointing knowledge

Science Question	Scientific (Measurement) Objective	Scientific Measurement Requirement	Mission Functional Requirement
Biogeochemical Cycles : How are the biogeochemical cycles that sustain life on Earth being altered/disrupted by natural and human-induced environmental change? How do these changes affect the composition and health of			
How do changes in climate and atmospheric processes affect the physiology and biogeochemistry of ecosystems? [DS 194, 201] ["Physiology" considered elsewhere (VQ2) so may not be needed here]	Measure absorption and scattering properties related to biogeochemistry of photosynthetic and non-photosynthetic vegetation.	<p>Measure surface reflectance in the VSWIR region (400-2500@10nm) that is shown to be sensitive to vegetation canopy chemistry at high precision and accuracy.</p> <p>Selected wavelengths (760+/-20 - oxygen for surface pressure and atm aerosols; 940 +/- 50 and 1150+/-50 - for water vapor; 1380 +/-20 for cirrus clouds) to allow for atmospheric correction for terrestrial and aquatic observations.</p> <p>Measure diagnostic spectral signature (380-900@10) with high precision and accuracy of aquatic ecosystems in coastal regions.</p> <p>Measure Nitrogen and other components in the spectral region 1300 to 2500 nm at 10 nm.</p> <p>Selected wavelengths in the short wavelength infrared (1250, 1650, 2250) to enable atmospheric correction for aquatic observations.</p> <p>Measure globally at spatial resolution patch scale relevant for ecosystem 10^4 to 10^6 m^2.</p> <p>Measure seasonally (90 day revisit) through several (3) years to observe the seasonal regional occurrence and trends.</p> <p>Measure with a revisit time of at most 20 days.</p>	Surface reflectance in the solar reflected spectrum for elevation angles >20; Rigorous cal/val program; Monthly lunar calcs; Daily solar calcs; 6 per year vcalcs; >3X zero-loss compression; ~10:30 AM sun sync LEO orbit; Radiometric calibration; Atmospheric Correction; AC validation; Geolocation; Pointing strategy to minimize sun glint; Avoid terrestrial hot spot; Ground processing; Seasonal latency; 30m (3s) Pointing knowledge;
What are the consequences of uses of land and coastal systems, such as urbanization, agriculture, and resource extraction, for the carbon cycle, hydrological cycle, nutrient fluxes and biodiversity functional composition [DS 196, 197] [We need to broaden this to include other uses (e.g. agriculture and related soil and water issues) and other cycles (e.g. water cycle). Biodiversity per se (as biologists define it) may not be the right word; "functional composition" or some other term may be more appropriate here.]	<p>Measure biological component and state of land and coastal ecosystems globally at the seasonal to several year time scale.</p> <p>Relate these to sources, conduits and sinks of relevant elements.</p>	<p>Measure surface reflectance in the VSWIR region (400-2500@10) with high precision and accuracy that allows mapping of land ecosystem elements.</p> <p>Selected wavelengths (760+/-20 - oxygen for surface pressure and atm aerosols; 940 +/- 50 and 1150+/-50 - for water vapor; 1380 +/-20 for cirrus clouds) to allow for atmospheric correction for terrestrial and aquatic observations.</p> <p>Measure diagnostic spectral signature (380-900@10) with high precision and accuracy that allows mapping of coastal ecosystem elements.</p> <p>Selected wavelengths in the short wavelength infrared (1250, 1650, 2250) to enable atmospheric correction for aquatic observations.</p> <p>Measure globally at spatial resolution patch scale relevant for ecosystem 10^4 to 10^6 m^2.</p> <p>Measure seasonally (90 day revisit) through several (3) years to observe the seasonal regional occurrence and trends.</p> <p>Measure with a revisit time of at most 20 days.</p>	Surface reflectance in the solar reflected spectrum for elevation angles >20; Rigorous cal/val program; Monthly lunar calcs; Daily solar calcs; 6 per year vcalcs; >3X zero-loss compression; ~10:30 AM sun sync LEO orbit; Radiometric calibration; Atmospheric Correction; AC validation; Geolocation; Pointing strategy to minimize sun glint; Avoid terrestrial hot spot; Ground processing; Seasonal latency; 30m (3s) Pointing knowledge;
What are the consequences of increasing nitrogen deposition for carbon cycling and biodiversity in terrestrial and coastal ecosystems? [DS 195, 196] ["Biodiversity" may not be the right term here (biodiversity is treated elsewhere, and we may not be assessing biodiversity per se. Perhaps "functional composition" might be a better term. Also, we might want to rephrase the aquatic terminology to "marine, coastal and inland waterways" since coastal marine ecosystems are not the only aquatic concern.]	<p>Measure ecological components of terrestrial and coastal ecosystem including elements of biodiversity.</p> <p>Measure ecological signatures closely tied to nitrogen deposition.</p>	<p>Measure surface reflectance in the VSWIR region (400-2500@10) with high precision and accuracy that allows mapping of land ecosystem elements.</p> <p>Selected wavelengths (760+/-20 - oxygen for surface pressure and atm aerosols; 940 +/- 50 and 1150+/-50 - for water vapor; 1380 +/-20 for cirrus clouds) to allow for atmospheric correction for terrestrial and aquatic observations.</p> <p>Measure diagnostic spectral signature (380-900@10) with high precision and accuracy that allows mapping of coastal and aquatic ecosystem elements.</p> <p>Selected wavelengths in the short wavelength infrared (1250, 1650, 2250) to enable atmospheric correction for aquatic observations.</p> <p>Measure globally at spatial resolution patch scale relevant for ecosystem 10^4 to 10^6 m^2.</p> <p>Measure seasonally (90 day revisit) through several (3) years to observe the seasonal regional occurrence and trends.</p> <p>Measure with a revisit time of at most 20 days.</p>	Surface reflectance in the solar reflected spectrum for elevation angles >20; Rigorous cal/val program; Monthly lunar calcs; Daily solar calcs; 6 per year vcalcs; >3X zero-loss compression; ~10:30 AM sun sync LEO orbit; Radiometric calibration; Atmospheric Correction; AC validation; Geolocation; Pointing strategy to minimize sun glint; Avoid terrestrial hot spot; Ground processing; Seasonal latency; 30m (3s) Pointing knowledge;

VQ3

Science Question	Scientific (Measurement) Objective	Scientific Measurement Requirement	Mission Functional Requirement
<p>Biogeochemical Cycles : How are the biogeochemical cycles that sustain life on Earth being altered/disrupted by natural and human-induced environmental change? How do these changes affect the composition and health of</p> <p>How do changes in hydrology, pollutant inputs and sediment transport affect freshwater and coastal marine ecosystems? [DS 196]</p>	<p>Measure diagnostic elements of freshwater and coastal marine ecosystem including sediments, chlorophyll, algal communities, and CDOM.</p>	<p>Measure at high accuracy and precision the spectral signatures (380-900@10nm) that allow derivation of key elements of freshwater and coastal marine ecosystems.</p> <p>Selected wavelengths in the short wavelength infrared (1250, 1650, 2250) to enable atmospheric correction for aquatic observations.</p> <p>Measure globally at spatial resolution patch scale relevant for ecosystem 10⁴ to 10⁶ m².</p> <p>Measure seasonally (90 day revisit) through several (3) years to observe the seasonal regional occurrence and trends.</p> <p>Measure with a revisit time of at most 20 days.</p>	<p>Surface reflectance in the solar reflected spectrum for elevation angles >20; Rigorous cal/val program; Monthly lunar cals; Daily solar cals; 6 per year vcal; >3X zero loss compression; ~10:30 AM sun sync LEO orbit; Radiometric calibration; Atmospheric Correction; AC validation; Geolocation; Pointing strategy to minimize sun glint; Avoid terrestrial hot spot; Ground processing; Seasonal latency; 30m (3s) Pointing knowledge;</p>
<p>How do changing water balances affect carbon storage by terrestrial ecosystems? [DS 196]</p>	<p>Measure water content of canopies.</p> <p>Measure signals of evapotranspiration.</p>	<p>Measure at high accuracy and precision the surface reflectance in the VSWIR region (400-2500@10nm) that allow derivation of canopy liquid water.</p> <p>Selected wavelengths (760+/-20 - oxygen for surface pressure and atm aerosols; 940 +/-50 and 1150+/-50 - for water vapor; 1380 +/-20 for cirrus clouds) to allow for atmospheric correction for terrestrial and aquatic observations.</p> <p>Measure at high accuracy and precision the spectral region (380-900@10nm) where liquid water and water vapor are expressed.</p> <p>Selected wavelengths in the short wavelength infrared (1250, 1650, 2250) to enable atmospheric correction for aquatic observations.</p> <p>Measure globally at spatial resolution patch scale relevant for ecosystem 10⁴ to 10⁶ m².</p> <p>Measure seasonally (90 day revisit) through several (3) years to observe the seasonal regional occurrence and trends.</p> <p>Measure with a revisit time of at most 20 days.</p>	<p>Surface reflectance in the solar reflected spectrum for elevation angles >20; Rigorous cal/val program; Monthly lunar cals; Daily solar cals; 6 per year vcal; >3X zero loss compression; ~10:30 AM sun sync LEO orbit; Radiometric calibration; Atmospheric Correction; AC validation; Geolocation; Pointing strategy to minimize sun glint; Avoid terrestrial hot spot; Ground processing; Seasonal latency; 30m (3s) Pointing knowledge;</p>
<p>What are the key interactions between biogeochemical cycles and the composition and diversity of ecosystems? [195, 196]</p>	<p>Measure biogeochemistry elements as well as composition and diversity of ecosystems.</p>	<p>Measure at high accuracy and precision the surface reflectance in the VSWIR region (400-2500@10nm) that is shown to be sensitive to vegetation canopy chemistry and ecosystem composition.</p> <p>Selected wavelengths (760+/-20 - oxygen for surface pressure and atm aerosols; 940 +/-50 and 1150+/-50 - for water vapor; 1380 +/-20 for cirrus clouds) to allow for atmospheric correction for terrestrial and aquatic observations.</p> <p>Measure Nitrogen and other components in the spectral region 1300 to 2500 nm at 10 nm.</p> <p>Measure globally at spatial resolution patch scale relevant for ecosystem 10⁴ to 10⁶ m².</p> <p>Measure seasonally (90 day revisit) through several (3) years to observe the seasonal regional occurrence and trends.</p> <p>Measure with a revisit time of at most 20 days.</p>	<p>Surface reflectance in the solar reflected spectrum for elevation angles >20; Rigorous cal/val program; Monthly lunar cals; Daily solar cals; 6 per year vcal; >3X zero loss compression; ~10:30 AM sun sync LEO orbit; Radiometric calibration; Atmospheric Correction; AC validation; Geolocation; Pointing strategy to minimize sun glint; Avoid terrestrial hot spot; Ground processing; Seasonal latency; 30m (3s) Pointing knowledge;</p>
<p>How do changes in biogeochemical processes feed back to climate and other components of the Earth system? [DS 190, 192, 195]</p>	<p>Measure global biogeochemical constituents related to processes involved in feedback to climate and other environmental factors.</p>	<p>Measure at high accuracy and precision the surface reflectance in the VSWIR region (400-2500@10nm) that is shown to be sensitive to vegetation canopy chemistry and ecosystem composition.</p> <p>Selected wavelengths (760+/-20 - oxygen for surface pressure and atm aerosols; 940 +/-50 and 1150+/-50 - for water vapor; 1380 +/-20 for cirrus clouds) to allow for atmospheric correction for terrestrial and aquatic observations.</p> <p>Measure Nitrogen and other components in the spectral region 1300 to 2500 nm at 10 nm.</p> <p>Measure globally at spatial resolution patch scale relevant for ecosystem 10⁴ to 10⁶ m².</p> <p>Measure seasonally (90 day revisit) through several (3) years to observe the seasonal regional occurrence and trends.</p> <p>Measure with a revisit time of at most 20 days.</p>	<p>Surface reflectance in the solar reflected spectrum for elevation angles >20; Rigorous cal/val program; Monthly lunar cals; Daily solar cals; 6 per year vcal; >3X zero loss compression; ~10:30 AM sun sync LEO orbit; Radiometric calibration; Atmospheric Correction; AC validation; Geolocation; Pointing strategy to minimize sun glint; Avoid terrestrial hot spot; Ground processing; Seasonal latency; 30m (3s) Pointing knowledge;</p>

Science Question	Scientific (Measurement) Objective	Scientific Measurement Requirement	Mission Functional Requirement
Changes in Disturbance Activity : How are disturbance regimes changing and how do these changes affect the ecosystem processes that support life on Earth?			
How do patterns of abrupt (pulse) disturbance vary and change over time within and across ecosystems?	<p>Measure changes (<10%) in fractional cover (from clearing, logging, wetland drainage, fire, weather related, etc.) at the seasonal and multiyear time scales, to characterize disturbance regimes in global ecosystems (e.g., conditional frequencies and/or return intervals for VQ1 ecosystem classes).</p> <p>Measure the seasonal and multi-year change in abundance and fractions of biotic and abiotic components of the aquatic environment.</p>	<p>Measure surface reflectance in the VSWIR region (400-2500@10nm) at high precision and accuracy (for spectral mixture algorithms to give insight to subpixel events).</p> <p>Selected wavelengths (760+/-20 - oxygen for surface pressure and atm aerosols; 940 +/- 50 and 1150+/-50 - for water vapor; 1380 +/-20 for cirrus clouds) to allow for atmospheric correction for terrestrial and aquatic observations.</p> <p>Measure diagnostic spectral signature (380-900@10nm) of biotic and abiotic components of the aquatic environment with high precision and accuracy.</p> <p>Selected wavelengths in the short wavelength infrared (1250, 1650, 2250) to enable atmospheric correction for aquatic observations.</p> <p>Measure globally at spatial resolution patch scale relevant for ecosystem 10⁴ to 10⁶ m².</p> <p>Measure seasonally (90 day revisit) through several (3) years to observe the seasonal regional occurrence and trends.</p> <p>Measure with a revisit time of at most 20 days.</p>	<p>Surface reflectance in the solar reflected spectrum for elevation angles >20; Rigorous cal/val program; Monthly lunar cals; Daily solar cals; 6 per year vcal; ~700mbs downlink; >3X zero loss compression; ~10:30 AM sun sync LEO orbit; Radiometric calibration; accurate enough to simulate historical satellite data through band synthesis; Atmospheric Correction; AC validation; Geolocation: 10 m (1 sigma); Ground processing; Seasonal latency; 30m (3s) Pointing knowledge ;</p>
How do climate changes affect disturbances such as fire and insect damage? [DS 196]	<p>Measure changes in vegetation canopy cover, pigments, and water content in ecosystems globally at the seasonal and multiyear time scale.</p> <p>Make measurements in such a way that they are backward compatible with pre-existing estimates and algorithms (e.g., band synthesis for historical vegetation indexes), as well as allowing more advanced algorithmic approaches.</p> <p>(Measure PV, NPV and Soil (+/- 5%) using full VSWIR and SWIR algorithms.)</p> <p>(Measure characteristic changes or differences in plant pigments (10% changes in total chlorophyll),</p>	<p>Measure surface reflectance in the VSWIR region (400-2500@10nm) at high precision and accuracy (for spectral mixture algorithms to give insight to subpixel events).</p> <p>Selected wavelengths (760+/-20 - oxygen for surface pressure and atm aerosols; 940 +/- 50 and 1150+/-50 - for water vapor; 1380 +/-20 for cirrus clouds) to allow for atmospheric correction for terrestrial and aquatic observations.</p> <p>Measure diagnostic spectral signature (380-900@10nm) of biotic and abiotic components of the aquatic environment with high precision and accuracy (i.e. coral bleaching, storm damage).</p> <p>Selected wavelengths in the short wavelength infrared (1250, 1650, 2250) to enable atmospheric correction for aquatic observations.</p> <p>Measure globally at spatial resolution patch scale relevant for ecosystem 10⁴ to 10⁶ m².</p> <p>Measure seasonally (90 day revisit) through several (3) years to observe the seasonal regional occurrence and trends.</p> <p>Measure with a revisit time of at most 20 days.</p>	<p>Surface reflectance in the solar reflected spectrum for elevation angles >20; Rigorous cal/val program; Monthly lunar cals; Daily solar cals; 6 per year vcal; >3X zero loss compression; ~10:30 AM sun sync LEO orbit; Radiometric calibration; Atmospheric Correction; AC validation; Geolocation; Pointing strategy to minimize sun glint; Avoid terrestrial hot spot; Ground processing; Seasonal latency; 30m (3s) Pointing knowledge;</p>
What are the interactions between invasive species and other types of disturbance?	<p>Measure the distribution and cover of key invasive species that introduce novel life histories or functional types, in concert with disturbance measurements.</p> <p>Measure (disturbance related) changes in vegetation canopy cover, pigments, and water content in ecosystems globally at the seasonal and multiyear time scale.</p> <p>(Measure PV, NPV and Soil using full VSWIR and SWIR algorithms.)</p>	<p>Measure surface reflectance in the VSWIR region (400-2500@10nm) at high precision and accuracy (for spectral mixture algorithms to give insight to subpixel events).</p> <p>Selected wavelengths (760+/-20 - oxygen for surface pressure and atm aerosols; 940 +/- 50 and 1150+/-50 - for water vapor; 1380 +/-20 for cirrus clouds) to allow for atmospheric correction for terrestrial and aquatic observations.</p> <p>Measure diagnostic spectral signature (380-900@10nm) of biotic and abiotic components of the aquatic environment with high precision and accuracy (i.e. coral bleaching, storm damage).</p> <p>Selected wavelengths in the short wavelength infrared (1250, 1650, 2250) to enable atmospheric correction for aquatic observations.</p> <p>Measure globally at spatial resolution patch scale relevant for ecosystem 10⁴ to 10⁶ m².</p> <p>Measure seasonally (90 day revisit) through several (3) years to observe the seasonal regional occurrence and trends.</p> <p>Measure with a revisit time of at most 20 days.</p>	<p>Surface reflectance in the solar reflected spectrum for elevation angles >20; Rigorous cal/val program; Monthly lunar cals; Daily solar cals; 6 per year vcal; >3X zero loss compression; ~10:30 AM sun sync LEO orbit; Radiometric calibration; Atmospheric Correction; AC validation; Geolocation; Pointing strategy to minimize sun glint; Avoid terrestrial hot spot; Ground processing; Seasonal latency; 30m (3s) Pointing knowledge;</p>
How are human-caused and natural disturbances changing the biodiversity composition of ecosystems, e.g.: through changes in the distribution and abundance of organisms, communities, and ecosystems?	<p>Measure the composition of ecosystems and ecological diversity indicators globally and at the seasonal and multiyear time scale.</p> <p>(Measure PV, NPV and Soil using full VSWIR and SWIR algorithms.)</p>	<p>Measure surface reflectance in the VSWIR region (400-2500@10nm) at high precision and accuracy (for spectral mixture algorithms to give insight to subpixel events).</p> <p>Selected wavelengths (760+/-20 - oxygen for surface pressure and atm aerosols; 940 +/- 50 and 1150+/-50 - for water vapor; 1380 +/-20 for cirrus clouds) to allow for atmospheric correction for terrestrial and aquatic observations.</p> <p>Measure diagnostic spectral signature (380-900@10nm) of biotic and abiotic components of the aquatic environment with high precision and accuracy (i.e. coral bleaching, storm damage).</p> <p>Selected wavelengths in the short wavelength infrared (1250, 1650, 2250) to enable atmospheric correction for aquatic observations.</p> <p>Measure globally at spatial resolution patch scale relevant for ecosystem 10⁴ to 10⁶ m².</p> <p>Measure seasonally (90 day revisit) through several (3) years to observe the seasonal regional occurrence and trends.</p> <p>Measure with a revisit time of at most 20 days.</p>	<p>Surface reflectance in the solar reflected spectrum for elevation angles >20; Rigorous cal/val program; Monthly lunar cals; Daily solar cals; 6 per year vcal; >3X zero loss compression; ~10:30 AM sun sync LEO orbit; Radiometric calibration; Atmospheric Correction; AC validation; Geolocation; Pointing strategy to minimize sun glint; Avoid terrestrial hot spot; Ground processing; Seasonal latency; 30m (3s) Pointing knowledge;</p>

Science Question	Scientific (Measurement) Objective	Scientific Measurement Requirement	Mission Functional Requirement
Changes in Disturbance Activity : How are disturbance regimes changing and how do these changes affect the ecosystem processes that support life on Earth?			
How do climate change, pollution and disturbance augment the vulnerability of ecosystems to invasive species? [DS 114,196]	Measure disturbances and ecosystem status. Measure invasive trends. Measure at the seasonal to multiyear time scale. (Measure PV, NPV and Soil using full VSWIR and SWIR algorithms.)	Measure surface reflectance in the VSWIR region (400-2500@10nm) at high precision and accuracy (for spectral mixture algorithms to give insight to subpixel events). Selected wavelengths (760+/-20 - oxygen for surface pressure and atm aerosols; 940 +/- 50 and 1150+/-50 - for water vapor; 1380 +/-20 for cirrus clouds) to allow for atmospheric correction for terrestrial and aquatic observations. Measure diagnostic spectral signature (380-900@10nm) of biotic and abiotic components of the aquatic environment with high precision and accuracy (i.e. coral bleaching, storm damage). Selected wavelengths in the short wavelength infrared (1250, 1650, 2250) to enable atmospheric correction for aquatic observations. Measure globally at spatial resolution patch scale relevant for ecosystem 10 ⁴ to 10 ⁶ m ² . Measure seasonally (90 day revisit) through several (3) years to observe the seasonal regional occurrence and trends. Measure with a revisit time of at most 20 days.	Surface reflectance in the solar reflected spectrum for elevation angles >20; Rigorous cal/val program; Monthly lunar cals; Daily solar cals; 6 per year vcal; >3X zero-loss compression; ~10:30 AM sun sync LEO orbit; Radiometric calibration; Atmospheric Correction; AC validation; Geolocation; Pointing strategy to minimize sun glint; Avoid terrestrial hot spot; Ground processing; Seasonal latency; 30m (3s) Pointing knowledge;
What are the effects of disturbances on productivity, water resources, and other ecosystem functions and services? [DS 196]	Measure disturbances and productivity indicators including ecosystem function and services on the seasonal to multiyear time scale. (Measure PV, NPV and Soil using full VSWIR and SWIR algorithms.)	Measure surface reflectance in the VSWIR region (400-2500@10nm) at high precision and accuracy (for spectral mixture algorithms to give insight to subpixel events). Selected wavelengths (760+/-20 - oxygen for surface pressure and atm aerosols; 940 +/- 50 and 1150+/-50 - for water vapor; 1380 +/-20 for cirrus clouds) to allow for atmospheric correction for terrestrial and aquatic observations. Measure globally at spatial resolution patch scale relevant for ecosystem 10 ⁴ to 10 ⁶ m ² . Measure seasonally (90 day revisit) through several (3) years to observe the seasonal regional occurrence and trends. Measure with a revisit time of at most 20 days.	Surface reflectance in the solar reflected spectrum for elevation angles >20; Rigorous cal/val program; Monthly lunar cals; Daily solar cals; 6 per year vcal; >3X zero-loss compression; ~10:30 AM sun sync LEO orbit; Radiometric calibration; Atmospheric Correction; AC validation; Geolocation; Pointing strategy to minimize sun glint; Avoid terrestrial hot spot; Ground processing; Seasonal latency; 30m (3s) Pointing knowledge;
How do changes in human uses of ecosystems affect their vulnerability to disturbance and extreme events? [DS 196]	Measure status of ecosystems globally and relation to disturbances and major events at the seasonal to multiyear time scale. (Measure PV, NPV and Soil using full VSWIR and SWIR algorithms.)	Measure surface reflectance in the VSWIR region (400-2500@10nm) at high precision and accuracy (for spectral mixture algorithms to give insight to subpixel events). Selected wavelengths (760+/-20 - oxygen for surface pressure and atm aerosols; 940 +/- 50 and 1150+/-50 - for water vapor; 1380 +/-20 for cirrus clouds) to allow for atmospheric correction for terrestrial and aquatic observations. Measure globally at spatial resolution patch scale relevant for ecosystem 10 ⁴ to 10 ⁶ m ² . Measure seasonally (90 day revisit) through several (3) years to observe the seasonal regional occurrence and trends. Measure with a revisit time of at most 20 days.	Surface reflectance in the solar reflected spectrum for elevation angles >20; Rigorous cal/val program; Monthly lunar cals; Daily solar cals; 6 per year vcal; >3X zero-loss compression; ~10:30 AM sun sync LEO orbit; Radiometric calibration; Atmospheric Correction; AC validation; Geolocation; Pointing strategy to minimize sun glint; Avoid terrestrial hot spot; Ground processing; Seasonal latency; 30m (3s) Pointing knowledge;
How do active and post-fire disturbances impact ecosystem processes and related human decisions.	Measure the fuel and intensity properties of actively burning fires and post fire recovery.	Measure surface reflectance in the VSWIR region (400-2500@10nm) at high precision and accuracy (for spectral mixture algorithms to give insight to subpixel events). Selected wavelengths (760+/-20 - oxygen for surface pressure and atm aerosols; 940 +/- 50 and 1150+/-50 - for water vapor; 1380 +/-20 for cirrus clouds) to allow for atmospheric correction for terrestrial and aquatic observations. Measure globally at spatial resolution patch scale relevant for ecosystem 10 ⁴ to 10 ⁶ m ² . Measure seasonally (90 day revisit) through several (3) years to observe the seasonal regional occurrence and trends. Measure with a revisit time of at most 20 days.	Surface reflectance in the solar reflected spectrum for elevation angles >20; Rigorous cal/val program; Monthly lunar cals; Daily solar cals; 6 per year vcal; >3X zero-loss compression; ~10:30 AM sun sync LEO orbit; Radiometric calibration; Atmospheric Correction; AC validation; Geolocation; Pointing strategy to minimize sun glint; Avoid terrestrial hot spot; Ground processing; 6 hr latency; 30m (3s) Pointing knowledge;

VQ4

Science Question	Scientific (Measurement) Objective	Scientific Measurement Requirement	Mission Functional Requirement
Ecosystem and Human Health: How do changes in ecosystem composition and function affect human health, resource use, and resource management?			
<p>How do changes in ecosystem composition and function affect the spread of infectious diseases and the organisms that transmit them[DS155, 160, 161]? For Example, tracking malaria by water fraction, Hantavirus</p>	<p>Measure the ecosystem composition and function globally at the seasonal and multiyear timescale.</p> <p>Relate these to measures of infectious diseases and organisms that transmit them.</p> <p>Understand the impact of climate change on the disease vectors environments and interaction with human settlement changes</p>	<p>Measure surface reflectance of terrestrial ecosystems in the VSWIR region (400-2500@10nm) at high precision and accuracy.</p>	<p>Surface reflectance in the solar reflected spectrum for elevation angles >20; Rigorous cal/val program; Monthly lunar cals; Daily solar cals; 6 per year vcal; >3X zero-loss compression; ~10:30 AM sun sync LEO orbit; Radiometric calibration; Atmospheric Correction; AC validation; Geolocation; Pointing strategy to minimize sun glint; Avoid terrestrial hot spot; Ground processing; Seasonal latency; 30m (3s) Pointing knowledge;</p>
		<p>Selected wavelengths (760+/-20 - oxygen for surface pressure and atm aerosols; 940 +/- 50 and 1150+/-50 - for water vapor; 1380 +/-20 for cirrus clouds) to allow for atmospheric correction for terrestrial and aquatic observations.</p>	
		<p>Measure diagnostic spectral signature (380-900@10nm) of biotic and abiotic components of the aquatic environment with high precision and accuracy</p>	
		<p>Selected wavelengths in the short wavelength infrared (1250, 1650, 2250) to enable atmospheric correction for aquatic observations.</p>	
<p>How will changes in pollution and biogeochemical cycling alter water quality? Water quality monitoring, algal blooms, eutrophication</p>	<p>Measure biogeochemical, pollution, and water quality indicators globally at the seasonal and multiyear time scale.</p>	<p>Measure terrestrial vegetation biogeochemical signatures in the VSWIR spectral signature (400-2500@10nm) acquired at high precision and accuracy.</p>	<p>Surface reflectance in the solar reflected spectrum for elevation angles >20; Rigorous cal/val program; Monthly lunar cals; Daily solar cals; 6 per year vcal; >3X zero-loss compression; ~10:30 AM sun sync LEO orbit; Radiometric calibration; F340Atmospheric Correction; AC validation; Geolocation; Pointing strategy to minimize sun glint; Avoid terrestrial hot spot; Ground processing; Seasonal latency; 30m (3s) Pointing knowledge;</p>
		<p>Selected wavelengths (760+/-20 - oxygen for surface pressure and atm aerosols; 940 +/- 50 and 1150+/-50 - for water vapor; 1380 +/-20 for cirrus clouds) to allow for atmospheric correction for terrestrial and aquatic observations.</p>	
		<p>Measure coastal aquatic vegetation biogeochemical signatures in the VSWIR spectral signature (380-900@10nm) acquired at high precision and accuracy to capture turbidity and water clarity, algal and cyanobacterial growth as well as the size and health (biodiversity) of wetlands.</p>	
		<p>Selected wavelengths in the short wavelength infrared (1250, 1650, 2250) to enable atmospheric correction for aquatic observations.</p>	
<p>How are changes in ecosystem distribution and productivity linked to resource use, and resource management? For forestry management, fire effects, biofuels, agricultural management</p>	<p>Measure ecosystem composition, productivity and distribution globally at the seasonal and multiyear time scale.</p> <p>Relate these to measures of resource use and management.</p> <p>Map the function types (communities) of the forestry resources, biofuel (corn, sugar cane, etc.) Also regionally and locally.</p> <p>Measure seasonal changes in productivity</p>	<p>Measure terrestrial vegetation composition, function and production in the VSWIR spectral signature (400-2500@10nm) acquired at high precision and accuracy.</p>	<p>Surface reflectance in the solar reflected spectrum for elevation angles >20; Rigorous cal/val program; Monthly lunar cals; Daily solar cals; 6 per year vcal; >3X zero-loss compression; ~10:30 AM sun sync LEO orbit; Radiometric calibration; F340Atmospheric Correction; AC validation; Geolocation; Pointing strategy to minimize sun glint; Avoid terrestrial hot spot; Ground processing; Seasonal latency; 30m (3s) Pointing knowledge;</p>
		<p>Selected wavelengths (760+/-20 - oxygen for surface pressure and atm aerosols; 940 +/- 50 and 1150+/-50 - for water vapor; 1380 +/-20 for cirrus clouds) to allow for atmospheric correction for terrestrial and aquatic observations.</p>	
		<p>Measure coastal aquatic vegetation composition, function and production in the VSWIR spectral signature (380-900@10nm) acquired at high precision and accuracy.</p>	
		<p>Selected wavelengths in the short wavelength infrared (1250, 1650, 2250) to enable atmospheric correction for aquatic observations.</p>	
<p>How will changes in climate and pollution affect the health and productivity of aquatic and agricultural resources? Agriculture and Aquaculture.</p>	<p>Measure aquatic and agricultural resource systems globally and through the seasonal and multiyear time frame.</p> <p>Relate these to measures of climate and pollution to detect trends and make predictions.</p> <p>Baseline and monitor changes in the environs on the "culture" area</p>	<p>Measure the composition and productivity of agricultural resource ecosystems using the VSWIR spectral signature (400-2500@10nm) acquired at high precision and accuracy.</p>	<p>Surface reflectance in the solar reflected spectrum for elevation angles >20; Rigorous cal/val program; Monthly lunar cals; Daily solar cals; 6 per year vcal; >3X zero-loss compression; ~10:30 AM sun sync LEO orbit; Radiometric calibration; F340Atmospheric Correction; AC validation; Geolocation; Pointing strategy to minimize sun glint; Avoid terrestrial hot spot; Ground processing; Seasonal latency; 30m (3s) Pointing knowledge;</p>
		<p>Selected wavelengths (760+/-20 - oxygen for surface pressure and atm aerosols; 940 +/- 50 and 1150+/-50 - for water vapor; 1380 +/-20 for cirrus clouds) to allow for atmospheric correction for terrestrial and aquatic observations.</p>	
		<p>Measure the composition and productivity of aquatic resource ecosystems using the VSWIR spectral signature (380-900@10nm) acquired at high precision and accuracy and capture turbidity and water clarity, algal and cyanobacterial growth as well as the size and health (biodiversity) of associated wetlands.</p>	
		<p>Selected wavelengths in the short wavelength infrared (1250, 1650, 2250) to enable atmospheric correction for aquatic observations.</p>	

Science Question	Scientific (Measurement) Objective	Scientific Measurement Requirement	Mission Functional Requirement
Ecosystem and Human Health: How do changes in ecosystem composition and function affect human health, resource use, and resource management?			
<p>What are the economic and human health consequences associated with the spread of invasive species? Mapping invasive species.</p>	<p>Measure the global distribution and seasonal variation of invasive terrestrial and costal aquatic species from one to several years.</p> <p>Relate this to economic and human health factors to support both direct assessment and future trend prediction.</p> <p>Distinguish the invasive species from the natural species</p>	<p>Measure the distribution of invasive terrestrial species using the VSWIR spectral signature (400-2500@10nm) acquired at high precision and accuracy.</p> <p>Selected wavelengths (760+/-20 - oxygen for surface pressure and atm aerosols; 940 +/- 50 and 1150+/-50 - for water vapor; 1380 +/-20 for cirrus clouds) to allow for atmospheric correction for terrestrial and aquatic observations.</p> <p>Measure the distribution of invasive aquatic species using the VSWIR spectral signature (380-900@10nm) acquired at high precision and accuracy.</p> <p>Selected wavelengths in the short wavelength infrared (1250, 1650, 2250) to enable atmospheric correction for aquatic observations.</p> <p>Measure globally at spatial resolution patch scale relevant for ecosystem 10⁴ to 10⁶ m².</p> <p>Measure seasonally (90 day revisit) through several (3) years to observe the seasonal regional occurrence and trends in the coastal regions.</p> <p>Measure regionally-important Plant Functional Type with a revisit time of at most 20 days.</p>	<p>Surface reflectance in the solar reflected spectrum for elevation angles >20; Rigorous cal/val program; Monthly lunar calcs; Daily solar calcs; 6 per year vcalcs; >3X zero-loss compression; ~10:30 AM sun sync LEO orbit; Radiometric calibration; F340Atmospheric Correction; AC validation; Geolocation; Pointing strategy to minimize sun glint; Avoid terrestrial hot spot; Ground processing; Seasonal latency; 30m (3s) Pointing knowledge;</p> <p>Knowledge of local situation vis-à-vis active invasive species of import. Local spectral databases of natural and invasive species.</p>
<p>How does the spatial pattern of policy, environmental management, and economic conditions correlate with the state and changes in ecosystem function and composition? (DS 155 [5-5]?, 230 [8-7]) Cross border examples of biodiversity (us-mexico, haiti-dominican republic).</p>	<p>Measure ecosystem composition, function, and distribution globally and seasonal and multiyear time scale.</p> <p>Relate this to the spatial pattern of environmental management and economic conditions for direct assessment and future prognostication.</p>	<p>Measure terrestrial ecosystem vegetation composition, function and distribution using the VSWIR spectral signature (400-2500@10nm) acquired at high precision and accuracy.</p> <p>Selected wavelengths (760+/-20 - oxygen for surface pressure and atm aerosols; 940 +/- 50 and 1150+/-50 - for water vapor; 1380 +/-20 for cirrus clouds) to allow for atmospheric correction for terrestrial and aquatic observations.</p> <p>Measure aquatic ecosystem vegetation composition, function and distribution using the VSWIR spectral signature (380-900@10nm) acquired at high precision and accuracy.</p> <p>Selected wavelengths in the short wavelength infrared (1250, 1650, 2250) to enable atmospheric correction for aquatic observations.</p> <p>Measure globally at spatial resolution patch scale relevant for ecosystem 10⁴ to 10⁶ m².</p> <p>Measure seasonally (90 day revisit) through several (3) years to observe the seasonal regional occurrence and trends in the coastal regions.</p> <p>Measure regionally-important Plant Functional Type with a revisit time of at most 20 days.</p>	<p>Surface reflectance in the solar reflected spectrum for elevation angles >20; Rigorous cal/val program; Monthly lunar calcs; Daily solar calcs; 6 per year vcalcs; >3X zero-loss compression; ~10:30 AM sun sync LEO orbit; Radiometric calibration; F340Atmospheric Correction; AC validation; Geolocation; Pointing strategy to minimize sun glint; Avoid terrestrial hot spot; Ground processing; Seasonal latency; 30m (3s) Pointing knowledge;</p>
<p>What are the impacts of flooding and sea-level rise on ecosystems, human health, and security? [DS 195, 224, 227, 348, 357] Coastal zone use mapping.</p>	<p>Measure ecosystem composition, function and distribution in the coastal regions globally at the seasonal and multiyear timescale.</p> <p>Relate these measurements to the status of coastal ecosystem and the human health and security implications.</p> <p>Measure of the global, regional and local scales</p>	<p>Measure coastal ecosystem vegetation composition, function and distribution in the terrestrial domain using the VSWIR spectral signature (400-2500@10nm) acquired at high precision and accuracy.</p> <p>Selected wavelengths (760+/-20 - oxygen for surface pressure and atm aerosols; 940 +/- 50 and 1150+/-50 - for water vapor; 1380 +/-20 for cirrus clouds) to allow for atmospheric correction for terrestrial and aquatic observations.</p> <p>Measure coastal ecosystem vegetation composition, function and distribution in the aquatic domain using the VSWIR spectral signature (380-900@10nm) acquired at high precision and accuracy.</p> <p>Selected wavelengths in the short wavelength infrared (1250, 1650, 2250) to enable atmospheric correction for aquatic observations.</p> <p>Measure globally at spatial resolution patch scale relevant for ecosystem 10⁴ to 10⁶ m².</p> <p>Measure seasonally (90 day revisit) through several (3) years to observe the seasonal regional occurrence and trends in the coastal regions.</p> <p>Measure regionally-important Plant Functional Type with a revisit time of at most 20 days.</p>	<p>Surface reflectance in the solar reflected spectrum for elevation angles >20; Rigorous cal/val program; Monthly lunar calcs; Daily solar calcs; 6 per year vcalcs; >3X zero-loss compression; ~10:30 AM sun sync LEO orbit; Radiometric calibration; F340Atmospheric Correction; AC validation; Geolocation; Pointing strategy to minimize sun glint; Avoid terrestrial hot spot; Ground processing; Seasonal latency; 30m (3s) Pointing knowledge;</p>

VQ5

Science Question	Scientific (Measurement) Objective	Scientific Measurement Requirement	Mission Functional Requirement
Earth Surface and Coastal Benthic Composition: What is the land surface soil/rock and shallow coastal benthic compositions?			
What is the distribution of the primary minerals and mineral groups on the exposed terrestrial surface? [DS 218]	<p>Measure the exposed surface rock and soil compositions globally.</p> <p>Measure the available rock forming and alteration minerals and subtle changes in composition via spectral absorption position and shape.</p> <p>Derive fractional abundance through spectral mixture analysis and related approaches.</p>	<p>Measure surface reflectance in the VSWIR region (400-2500@10nm) with high precision and accuracy to capture the diagnostic absorptions features of clay, iron, carbonate and other rock/soil forming minerals.</p> <p>Selected wavelengths (760+/-20 - oxygen for surface pressure and atm aerosols; 940 +/- 50 and 1150+/-50 - for water vapor; 1380 +/-20 for cirrus clouds) to allow for atmospheric correction for terrestrial and aquatic observations.</p> <p>Measurements at a spatial scale to resolve material patches at <100m.</p> <p>Measure yearly (365 day revisit) through several (3) years to observe the seasonal regional occurrence and trends in the coastal regions.</p> <p>Measure regionally-important Plant Functional Type with a revisit time of at most 80 days.</p>	<p>Surface reflectance in the solar reflected spectrum for elevation angles >20; Rigorous cal/val program; Monthly lunar calcs; Daily solar calcs; 6 per year vcalcs; >3X zero loss compression; ~10:30 AM sun sync LEO orbit; Atmospheric Correction; Atmospheric Correction validation; Geolocation; Ground processing; latency: yearly; 30m (3s) Pointing knowledge;</p>
What is the bottom composition (sand, rock, mud, coral, algae, SAV, etc) of the shallow water regions of the Earth?	<p>Measure globally the shallow water regions and inland waters.</p> <p>Derive the composition of the optically available (e.g. non-turbulent) shallow water bottom regions of the coastal oceans and inland waters.</p>	<p>High precision and accuracy spectral signatures in the visible to near infrared (380-900 @10nm sampling) to capture the bottom composition interaction with light.</p> <p>Selected wavelengths in the short wavelength infrared (1250, 1650, 2250) to enable atmospheric correction for aquatic observations.</p> <p>Measurements at a spatial scale to resolve material patches at <100m.</p> <p>Measure yearly (365 day revisit) through several (3) years to observe the seasonal regional occurrence and trends in the coastal regions.</p> <p>Measure regionally-important Plant Functional Type with a revisit time of at most 80 days.</p>	<p>Surface reflectance in the solar reflected spectrum for elevation angles >20; Rigorous cal/val program; Monthly lunar calcs; Daily solar calcs; 6 per year vcalcs; >3X zero loss compression; ~10:30 AM sun sync LEO orbit; Atmospheric Correction; Atmospheric Correction validation; Geolocation; Ground processing; latency: yearly; 30m (3s) Pointing knowledge;</p>
What fundamentally new concepts for mineral and hydrocarbon research will arise from uniform and detailed global geochemistry of the exposed rock/soil surface [DS227]	<p>Measure the exposed surface rock and soil compositions globally.</p> <p>Derive geochemical information (i.e. Ion substitution expressed as spectral signature shifts.)</p>	<p>Measure surface reflectance in the VSWIR region (400-2500@10nm) with high precision and accuracy to capture the diagnostic absorptions features shifts of clay, iron, carbonate and other rock/soil forming minerals due to variations in geochemistry.</p> <p>Selected wavelengths (760+/-20 - oxygen for surface pressure and atm aerosols; 940 +/- 50 and 1150+/-50 - for water vapor; 1380 +/-20 for cirrus clouds) to allow for atmospheric correction for terrestrial and aquatic observations.</p> <p>Measurements at a spatial scale to resolve material patches at <100m.</p> <p>Measure yearly (365 day revisit) through several (3) years to observe the seasonal regional occurrence and trends in the coastal regions.</p> <p>Measure regionally-important Plant Functional Type with a revisit time of at most 80 days.</p>	<p>Surface reflectance in the solar reflected spectrum for elevation angles >20; Rigorous cal/val program; Monthly lunar calcs; Daily solar calcs; 6 per year vcalcs; >3X zero loss compression; ~10:30 AM sun sync LEO orbit; Radiometric calibration; Atmospheric Correction; AC validation; Geolocation; Ground processing; latency: yearly; 30m (3s) Pointing knowledge;</p>
What changes in bottom substrate occur in shallow coastal and inland aquatic environments? [DS 25]	<p>Measure the composition of the optically available shallow water bottom regions of the coastal oceans and inland waters.</p> <p>Bottom substrate composition of sand, coral, mud, SAV, etc. More detailed specificity as possible with the available signal.</p>	<p>Measure surface reflectance in the visible to near infrared (380-900 @10nm) at high precision and accuracy to capture the bottom composition interaction with light.</p> <p>Selected wavelengths in the short wavelength infrared (1250, 1650, 2250) to enable atmospheric correction for aquatic observations.</p> <p>Measurements at a spatial scale to resolve material patches at <100m.</p> <p>Measure seasonally (90 day revisit) through several (3) years to observe the seasonal regional occurrence and trends in the coastal regions.</p> <p>Measure regionally-important Plant Functional Type with a revisit time of at most 20 days.</p>	<p>Surface reflectance in the solar reflected spectrum for elevation angles >20; Rigorous cal/val program; Monthly lunar calcs; Daily solar calcs; 6 per year vcalcs; >3X zero loss compression; ~10:30 AM sun sync LEO orbit; Atmospheric Correction; Atmospheric Correction validation; Geolocation; Ground processing; latency: seasonal; 30m (3s) Pointing knowledge;</p>
How can measurements of rock and soil composition be used to understand and mitigate hazards? [DS 114,227]	<p>Measure the exposed surface rock and soil compositions globally to determine the occurrence of hazard associated minerals (For example, Acid generating minerals, Asbestos, etc.).</p> <p>Derive fractional abundance of hazardous minerals through spectral mixture analysis and related approaches.</p>	<p>Measure surface reflectance in the VSWIR region (400-2500@10nm) with high precision and accuracy to capture the diagnostic absorptions features of acid generating (sulfates), asbestos, minerals.</p> <p>Selected wavelengths (760+/-20 - oxygen for surface pressure and atm aerosols; 940 +/- 50 and 1150+/-50 - for water vapor; 1380 +/-20 for cirrus clouds) to allow for atmospheric correction for terrestrial and aquatic observations.</p> <p>Measurements at a spatial scale to resolve material patches at <100m.</p> <p>Measure yearly (365 day revisit) through several (3) years to observe the seasonal regional occurrence and trends in the coastal regions.</p> <p>Measure regionally-important Plant Functional Type with a revisit time of at most 80 days.</p>	<p>Surface reflectance in the solar reflected spectrum for elevation angles >20; Rigorous cal/val program; Monthly lunar calcs; Daily solar calcs; 6 per year vcalcs; >3X zero loss compression; ~10:30 AM sun sync LEO orbit; Atmospheric Correction; Atmospheric Correction validation; Geolocation; Ground processing; latency: yearly; 30m (3s) Pointing knowledge;</p>

Science Objectives	Measurement Objectives	Measurement Requirements	Instrument Requirements	Other Mission and Measurement Requirements
TQ1. Volcanoes and Earthquakes: How can we help predict and mitigate earthquake and volcanic hazards through detection of transient thermal phenomena?				
Do volcanoes signal impending eruptions through changes in surface temperature or gas emission rates and are such changes unique to specific types of eruptions? [DS 227]	Detect, quantify and monitor subtle variations in: 1) surface temperatures 2) surface emissivity 3) sulfur dioxide concentrations at low, non-eruptive flux background levels. Compilation of long-term baseline data sets.	1) Temperature measurements in the range 243- 573 K. Requires atmospheric correction band and at least three thermal IR bands. 2) Atmospheric correction band and at least five thermal IR bands. 3) Atmospheric correction band, SO ₂ band with one band on either side. 7 day repeat.	Spatial resolution: < 100m Number Spectral channels: 4 Spectral range: 7-12 um. Channel centers: 7.3, 8.5, 11, 12 Channel width: undefined NEAT @ 300K 4 um: undefined NEAT @ 300K 8-12 um: < 0.2K Radiometric accuracy: < 5% Geolocation accuracy: < 30 m Saturation temperature (4 um): undef. Saturation temperature (7-12 um): undef. Bright target recovery: undefined	Temporal resolution: < 7 days Nighttime data acquisitions.
What do changes in the rate of lava effusion tell us about the maximum lengths that lava flows can attain, and the likely duration of lava flow-forming eruptions? [DS 226]	Area covered by active lava flows; Lava flow surface temperatures; Radiant flux from lava flow surfaces.	Temperature measurements in the range 273 to 1473K (active lava), and 273-323K (ambient background). 5 day repeat.	Spatial resolution: < 60m Number spectral channels: 4 Spectral range 4-12 um Channel centers: 4, and 3 between 8-12 Channel width: undef. NEAT @ 300K 4 um:< 1-2 K NEAT @ 300K 8-12 um: < 0.2K Radiometric accuracy: undef. Saturation temperature (4 um): 1200 K Saturation temperature (7-12 um): 373 K Bright target recovery: <2 pixels at 4 um	Temporal resolution: undefined Nighttime data acquisitions. NIR/SWIR hyperspectral data is beneficial. Rapid response off nadir pointing capability. Rapid re-tasking for acquisition of targets of opportunity.
What are the characteristic dispersal patterns and residence times for volcanic ash clouds and how long do such clouds remain a threat to aviation? [DS 224]	Discrimination of volcanic ash clouds from meteorological clouds (both water and ice), in both wet and dry air masses. Day and night measurements	Four spectral channels at 8.5, 10, 11, and 12 µm; Nect of 0.2 K @ 300K Max. repeat cycle of 5 days. Temperature measurements in the range 253.15 to 473.15K.	Spatial resolution: undef Number spectral channels: 4 Spectral range 8-12 um Channel centers: 8.5, 10, 11, 12 Channel width: 50nm at 8.5, 100 nm others NEAT @ 300K 4um: undefined NEAT @ 300K 8-12um: < 0.5K Radiometric accuracy: < 5% Saturation temperature (4 um): undef Saturation temperature (7-12 um): undef Bright target recovery: undef	Temporal resolution: < 5 days NIR/SWIR hyperspectral data valuable to assist in recognition of meteorological clouds and estimation of plume height. Night-time data acquisitions to increase the frequency of observation.
What do the transient thermal anomalies that may precede earthquakes tell us about changes in the geophysical properties of the crust? [DS 227, 229]	Detect and monitor increases in TIR surface radiance surface temperatures along potentially active faults.	Temperature measurements in range 248.15-320.15K 5 day repeat (or better); nighttime data	Spatial resolution: <100 m Number spectral channels: 3 Spectral range 7-12 Channel centers: 8-8.5; 7.3-8,10 Channel width: undef NEAT @ 300K 4um: undef NEAT @ 300K 8-12um: < 0.2K Radiometric accuracy: undef Saturation temperature (4 um): undef Saturation temperature (7-12 um): undef Bright target recovery: undef	Temporal resolution: 5 days Nighttime acquisitions
Can the energy released by the periodic recharge of magma chambers be used to predict future eruptions? [DS 227]How can the release of energy at the surface of volcanic edifices be used to understand magma processes at depth and over time?	Detect and monitor temperature changes of volcanic edifices	Temperature measurements in range of 248.15-1200K; 5 day repeat	Spatial resolution: < 90 m Number spectral channels: 3 Spectral range: 4-12 Channel centers: 4, 10.5, 11.5 Channel width: undef NEAT @ 300K 4um: <1-2K NEAT @ 300K 8-12um: undef Radiometric accuracy: undef Saturation temperature (4 um): undef Saturation temperature (7-12 um): undef Bright target recovery: undef	Temporal resolution: 5 day Nighttime acquisitions

TQ1

Science Objectives	Measurement Objectives	Measurement Requirements	Instrument Requirements	Other Mission and Measurement Requirements
Wildfires: What is the impact of global biomass burning on the terrestrial biosphere and atmosphere, and how is this impact changing over time?				
How are global fire regimes changing in response to, and driven by, changing climate, vegetation, and land use practices? [DS 198]	Fire monitoring, fire intensity, fire extent, spatio-temporal variations in location, fire duration	Monitor smoldering fires as small as ~10 sq. m in size, monitor fire boundary, fire radiative power, fire temperature and area, 4-10 day repeat cycle	Spatial resolution: 50-100m Number spectral channels: 2 Spectral range: 4-12 Channel centers: 4, 11 Channel width: undef NEAT @ 300K 4um: <2-3K NEAT @ 300K 8-12um: <0.2K Radiometric accuracy: undef Saturation temperature (4 um): 1200K Saturation temperature (7-12 um): undef Bright target recovery: undef Interband registration acc: < 0.25/pixel	Temporal resolution: 4-10 days Daytime and nighttime data acquisition, direct broadcast capability, onboard processing, pre and post burn thematic maps. Opportunistic validation.
Is regional and local scale fire frequency changing? [DS 196]	Fire detection	Detect flaming and smoldering fires as small as ~10 sq. m in size, 4-10 day repeat cycle	Spatial resolution: 50-100m Number spectral channels: undef Spectral range: 8-12 Channel centers: undef Channel width: undef NEAT @ 300K 4um: undef NEAT @ 300K 8-12um: undef Radiometric accuracy: < 0.2K Saturation temperature (4 um): undef Saturation temperature (7-12 um): undef Bright target recovery: undef Interband registration acc: undef	Temporal resolution: undef Daytime and nighttime data acquisition (thermal inertia), LEO orbit. Requires historical context from other sensors. Pre and post fire thematic maps. Requires measurement intercalibration (e.g. MODIS vs HyspIRI). HyspIRI establishes a baseline.
What is the role of fire in global biogeochemical cycling, particularly trace gas emissions? [DS 195]	Fire monitoring, fire intensity, fire extent, spatio-temporal variations in location, fire duration.	Detect flaming and smoldering fires as small as ~10 sq. m in size, fire radiative power, 4-10 day repeat cycle	Spatial resolution: 50-100m Number spectral channels: 2 Spectral range: 4-12 Channel centers: 4,11 Channel width: undef NEAT @ 300K 4um: <2-3K NEAT @ 300K 8-12um: <0.2K Radiometric accuracy: undef Saturation temperature (4 um): 1200K Saturation temperature (7-12 um): undef Bright target recovery: undef Interband registration acc: < 0.25/pixel	Temporal resolution: undef Daytime and nighttime data acquisition, sun synchronous orbit. Ancillary global geochemical model to evaluate importance of fire input. Requires fire fuel modeling element.
Are there regional feedbacks between fire and climate change?	Measurement location and extent of fire front. Confirmation of burn scars and their extent.	Detect flaming and smoldering fires as small as ~10 sq. m in size, fire radiative power, 4-10 day repeat cycle	Spatial resolution: 50-100m Number spectral channels: 2 Spectral range: 4-12 Channel centers: 4,11 Channel width: undef NEAT @ 300K 4um: <2-3K NEAT @ 300K 8-12um: <0.2K Radiometric accuracy: undef Saturation temperature (4 um): undef Saturation temperature (7-12 um): undef Bright target recovery: undef Interband registration acc: undef	Temporal resolution: undef Daytime and nighttime data acquisition, sun synchronous orbit

Science Objectives	Measurement Objectives	Measurement Requirements	Instrument Requirements	Other Mission and Measurement Requirements
Water Use and Availability: How is consumptive use of global freshwater supplies responding to changes in climate and demand, and what are the implications for sustaining water resources?				
How is climate variability (and ENSO) impacting the evaporative component of the global water cycle over natural and managed landscapes? [DS 166, 196, 203, 257, 368]	Evapotranspiration (surface energy balance) at scales resolving the typical lengthscales of landsurface moisture heterogeneity	Global coverage of surface radiometric temperature; ~weekly to monthly; resolving land-use components; Surf. Rad. Temp. accurate to <1K; ~10-11 AM local overpass	Spatial resolution: < 100m Number spectral channels: 3 Spectral range: undef Channel centers: undef Channel width: undef NEΔT @ 300K 4um: undef NEΔT @ 300K 8-12um: undef Radiometric accuracy: < 5% Saturation temperature (4 um): undef Saturation temperature (7-12 um): 360K Bright target recovery: undef Interband registration acc: undef	Temporal resolution: 7 days Maps of vegetation index; broadband albedo retrievals (from integrated VSWIR or 3 or more wide bands in green, red, nearIR); landuse; insolation data; Landsat-like mid-morning sun-synchronous overpass. Cloud detection mechanism, (including cirrus); Ancillary meteorological data (varies with process)
What are relationships between spatial and temporal variation in evapotranspiration and land-use/land-cover and freshwater resource management? [DS 196, 203, 368]	Evapotranspiration at scales resolving the typical length scales of land surface moisture and vegetation heterogeneity	Global coverage; resolving e.g., field, riparian patches, reservoirs, water rights (ag. field sized) polygons; LST accurate to <1K; ~10:30AM overpass	Spatial resolution: < 100 m Number spectral channels: 3 Spectral range: 8.5, 11, 12 Channel centers: undef Channel width: undef NEΔT @ 300K 4um: undef NEΔT @ 300K 8-12um: undef Radiometric accuracy: undef Saturation temperature (4 um): undef Saturation temperature (7-12 um): 360K Bright target recovery: undef Interband registration acc: undef	Temporal resolution: 7 days Maps of vegetation index; landuse; insolation data; Landsat-like mid-morning sun-synchronous overpass
Can we improve early detection, mitigation, and impact assessment of droughts at local to regional scales anywhere on the globe? [DS 166, 196, 203, 368]; How does the partitioning of Precipitation into ET, surface runoff and ground-water recharge change during drought?	Stress index at field scales	Global coverage; resolving field-scale (1 ha) patches; LST accurate to <1K; ~10:30AM overpass	Spatial resolution: < 100m Number spectral channels: 3 Spectral range: 8-12 Channel centers: 8.5,11,12 Channel width: undef NEΔT @ 300K 4um: undef NEΔT @ 300K 8-12um: undef Radiometric accuracy: undef Saturation temperature (4 um): undef Saturation temperature (7-12 um): 360 Bright target recovery: undef Interband registration acc: undef	Temporal resolution: 7 days As above; some methods require potential evapotranspiration (based on meteorological data and/or satellite-based insolation); hyperspectral stress signatures will provide supplemental stress info
What areas of Earth have water consumption by irrigated agriculture that is out of balance with sustainable water availability? [DS 196, 368]	Robust detection of pixels with water consumption in excess of rainfall and regional fresh water availability (surface and ground water)	Global coverage; resolving irrigation patches; ~10:30 AM overpass	Spatial resolution: < 100 m Number spectral channels: 3 Spectral range: 8-12 um Channel centers: 8.5, 11, 12 Channel width: undef NEΔT @ 300 4um: undef NEΔT @ 300 8-12um: undef Radiometric accuracy: undef Saturation temperature (4 um): undef Saturation temperature (7-12 um):360K Bright target recovery: undef Interband registration acc: undef	Temporal resolution: weekly to monthly detailed land cover classification (can be improved using hyperspectral); vegetation indices; regional hydrologic water balances and stores; ET quantification

TQ3-1

<p>Can we increase food production in water-scarce agricultural regions while improving or sustaining quality and quantity of water for ecosystem function and other human uses? [DS 196, 368]</p>	<p>Accurate evapotranspiration at sub-field scales</p>	<p>irrigation patches well resolved; LST accurate to 0.5K; ~10:30AM overpass</p>	<p>Spatial resolution: < 50m Number spectral channels: 8,5,11,12 Spectral range: 8-12 um Channel centers: undef Channel width: undef NEΔT @ 300K 4um: undef NEΔT @ 300K 8-12um: undef Radiometric accuracy: undef Saturation temperature (4 um): undef Saturation temperature (7-12 um): 360K Bright target recovery: undef Interband registration acc: undef</p>	<p>Temporal resolution: weekly Vegetation index; accurate local meteorological forcing conditions; means to partition ET into E and T would be valuable</p>
<p>What is the ecological impact of thermal plumes and elevated water temperature stemming from water uses, including desalinization, in inland and coastal water bodies?</p>	<p>thermal plumes and elevated water surface temperature</p>	<p>Multiple TIR channels to detect plumes</p>	<p>Spatial resolution: < 60m Number spectral channels: undef Spectral range: undef Channel centers: undef Channel width: undef NEΔT @ 300K 4um: undef NEΔT @ 300K 8-12um: <0.1K Radiometric accuracy: < 0.5K Saturation temperature (4 um): undef Saturation temperature (7-12 um): undef Bright target recovery: undef Interband registration acc: undef</p>	<p>Temporal resolution: 5 days Atmospheric correction</p>

TQ3-2

Science Objectives	Measurement Objectives	Measurement Requirements	Instrument Requirements	Other Mission and Measurement Requirements
Urbanization and Human Health: How does urbanization affect the local, regional and global environment? Can we characterize this effect to help mitigate its impact on human health and welfare?				
How do changes in local and regional land cover and land use, in particular urbanization affect surface energy balance characteristics that impact human welfare [DS: 160-161, 166-167, 196, 198]	Surface temperature Surface energy fluxes Surface emissivity terrestrial coverage		Spatial resolution: < 60 m Number spectral channels: 4 Spectral range: 8-12 Channel centers: undef Channel width: undef NEAT @ 300K 4um: undef NEAT @ 300K 8-12um: undef Radiometric accuracy: < 1 K Saturation temperature (4 um): undef Saturation temperature (7-12 um): undef Bright target recovery: undef Interband registration acc: undef	Temporal resolution: 7 days Long term validation sites (incl. emissivity targets) and periodic urban campaigns
What are the dynamics, magnitude, and spatial form of the urban heat island effect (UHI), how does it change from city to city, what are its temporal, diurnal, and nocturnal characteristics, and what are the regional impacts of the UHI on biophysical, climatic, and environmental processes? [DS: 158, 166-168]	Day and night surface temperature Urban coverage Intra-seasonal measurements	Min T/Max T 260-360K	Spatial resolution: < 60 m Number spectral channels: 4 Spectral range: undef Channel centers: undef Channel width: undef NEAT @ 300K 4um: undef NEAT @ 300K 8-12um: 0.2-0.3 K Radiometric accuracy: < 1K Saturation temperature (4 um): undef Saturation temperature (7-12 um): undef Bright target recovery: undef Interband registration acc: 0.2/pixel	Temporal resolution: 7 days Cloud masking at night Day and night imaging
How can the factors influencing heat stress on humans be better resolved and measured. [DS: 156, 158, 160, 183-184]	Surface temperature Urban coverage	Vegetated/non-vegetated surfaces	Spatial resolution: < 60 m Number spectral channels: >4 Spectral range: undef Channel centers: undef Channel width: undef NEAT @ 300K 4um: undef NEAT @ 300K 8-12um: 0.2-0.3K Radiometric accuracy: < 1K Saturation temperature (4 um): undef Saturation temperature (7-12 um): undef Bright target recovery: undef Interband registration acc: undef	Temporal resolution: 7 days Air temperature Day and night imaging
How can the characteristics associated with environmentally related health effects, that affect vector-borne and animal-borne diseases, be better resolved and measured? [DS: 156, 158, 160, 183-184]	Surface temperature Terrestrial coverage	Detection of wet/dry surfaces Vegetated/non-vegetated surfaces	Spatial resolution: < 60 m Number spectral channels: 3 Spectral range: undef Channel centers: undef Channel width: undef NEAT @ 300K 4um: undef NEAT @ 300K 8-12um: 0.2-0.3K Radiometric accuracy: 1K Saturation temperature (4 um): undef Saturation temperature (7-12 um): undef Bright target recovery: undef Interband registration acc: undef	Temporal resolution: 7 days Soil moisture or precipitation Air temperature water inundation Day and night imaging
How do horizontal and temporal scales of variation in heat flux and mixing relate to human health, human ecosystems, and urbanization? [DS: 156, 160-161, 166-167, 179,184]	Surface temperature Surface energy fluxes Global coverage		Spatial resolution: < 60 m Number spectral channels: 3 Spectral range: undef Channel centers: undef Channel width: undef NEAT @ 300K 4um: undef NEAT @ 300K 8-12um:0.2-0.3K Radiometric accuracy: 1K Saturation temperature (4 um): undef Saturation temperature (7-12 um): undef Bright target recovery: undef Interband registration acc: undef	Temporal resolution: 7 days Day and night imaging

Science Objectives	Measurement Objectives	Measurement Requirements	Instrument Requirements	Other Mission and Measurement Requirements
Earth Surface Composition and Change: What is the composition and thermal properties of the exposed surface of the Earth? How do these factors change over time and affect land use and habitability?				
What is the spectrally observable mineralogy of the Earth's surface and how does this relate to geochemical and surficial processes? [DS 114]	<i>Mapping spectral emissivity variations associated with mineralogy and rock type in exposed terranes</i>	Variation in silica content and non-silicate <i>minerals</i> based on 8-12 um band shape. (Spectral emissivities to within 0.5%)	Spatial resolution: 60 m Number spectral channels: 7 Spectral range: 8-12 um Channel centers: undef Channel width: undef NEAT @ 300K 4um: undef NEAT @ 300K 8-12um: 0.2K Radiometric accuracy: undef Saturation temperature (4 um): undef Saturation temperature (7-12 um): undef Bright target recovery: undef Interband registration acc: undef	Temporal resolution: Quarterly Geolocation to subpixel accuracy Band to band calibration must be validated, in-flight and radiometric calibration
What is the nature and extent of man-made disturbance of the Earth's surface associated with exploitation of renewable and non-renewable resources? How do these vary over time? [DS 227]	<i>Surface temperature and emissivity variations associated with hydrocarbon and mineral extraction (dumps and pits)</i>	Variation in mineral content based on 8-12 um band shape including detection of sulfate spectral features. <i>At scale of mining activities.</i>	Spatial resolution: 60 m Number spectral channels: 5 Spectral range: 8-12 Channel centers: undef Channel width: undef NEAT @ 300K 4um: undef NEAT @ 300K 8-12um: < 0.2K Radiometric accuracy: undef Saturation temperature (4 um): undef Saturation temperature (7-12 um): undef Bright target recovery: undef Interband registration acc: undef	Temporal resolution: Monthly Geolocation to subpixel accuracy Band to band calibration must be validated, preferably in-flight and radiometric calibration
How do surface temperature anomalies relate to deeper thermal sources, such as <i>hydrothermal systems</i> , buried lava tubes, underground coal fires and engineering structures? How do changes in the surface temperatures relate to changing nature of the deep seated hot source? [DS 243]	Surface temperatures corrected for emissivity variations <i>for temperature anomalies</i>	<i>Measure variations in temperature with high accuracy and precision and spatial resolution</i>	Spatial resolution: 60m Number spectral channels: 3 Spectral range: 8-12 um Channel centers: undef Channel width: undef NEAT @ 300K 4um: undef NEAT @ 300K 8-12um: 0.2K Radiometric accuracy: undef Saturation temperature (4 um): undef Saturation temperature (7-12 um): undef Bright target recovery: undef Interband registration acc: undef	Temporal resolution: 7 days Nighttime data necessary to minimize radiant interference due to solar heating
What is the spatial distribution pattern of surface temperatures and emissivities and how do these influence the Earth's heat budget?	Surface emissivity variations and temperatures of all surficial cover materials	Complex surface emissivity properties based on 8-12 um band shape	Spatial resolution: 60-500m Number spectral channels: 8 Spectral range: 3-12 Channel centers: 3.98 and 7 in 8-12 Channel width: undef NEAT @ 300K 4um: undef NEAT @ 300K 8-12um: 0.2K Radiometric accuracy: undef Saturation temperature (4 um): undef Saturation temperature (7-12 um): undef Bright target recovery: undef Interband registration acc: undef	Temporal resolution: 7 days Accurate methods of temperature emissivity separation applicable to wide range of materials needed.
What are the water surface temperature <i>distributions</i> in coastal, ocean, and inland water bodies, how do they change, and how do they influence aquatic ecosystems? [DS 378]	Spatial and temporal variation in surface temperatures	<i>Measure variations in temperature with high accuracy (<0.5 K) and precision and good to moderate spatial resolution</i>	Spatial resolution: 50-100 m Number spectral channels: 4 Spectral range: 3-12 Channel centers: 3.98 and 3 in 8-12 um Channel width: undef NEAT @ 300K 4um: undef NEAT @ 300K 8-12um: 0.2K Radiometric accuracy: undef Saturation temperature (4 um): undef Saturation temperature (7-12 um): undef Bright target recovery: undef Interband registration acc: undef	Temporal resolution: 7 days Day and night measurements preferable

JPL Publication 09-19



NASA 2008 HypIRI Whitepaper and Workshop Report

HypIRI Group

Prepared for
**National Aeronautics and
Space Administration**

by

**Jet Propulsion Laboratory
California Institute of Technology
Pasadena, California**

May 2009

JPL Publication 09-19

NASA 2008 HypsIRI Whitepaper and Workshop Report

HypsIRI Group



Prepared for
**National Aeronautics and
Space Administration**

by

**Jet Propulsion Laboratory
California Institute of Technology
Pasadena, California**

May 2009

The work described in this publication was performed at a number of organizations, including the Jet Propulsion Laboratory, California Institute of Technology, under a contract with the National Aeronautics and Space Administration (NASA). Compiling and publication support was provided by the Jet Propulsion Laboratory, California Institute of Technology under a contract with NASA.

Reference herein to any specific commercial product, process, or service by trade name, trademark, manufacturer, or otherwise, does not constitute or imply its endorsement by the United States Government, or the Jet Propulsion Laboratory, California Institute of Technology.

Copyright 2009. All rights reserved.

Abstract

From October 21-23, 2008, NASA held a three-day workshop to consider the Hyperspectral Infrared Imager (HyspIRI) mission recommended for implementation by the 2007 report from the U.S. National Research Council Earth Science and Applications from Space: National Imperatives for the Next Decade and Beyond, also known as the Earth Science Decadal Survey. The open workshop provided a forum to present the initial observational requirements for the mission and assess its anticipated impact on scientific and operational applications as well as obtain feedback from the broader scientific community on the mission concept.

The workshop participants concluded the HyspIRI mission would provide a significant new capability to study ecosystems and natural hazards at spatial scales relevant to human resource use. In addition, participants confirmed that the proposed instrument designs could meet the measurement requirements and be implemented through the use of current technology.

The workshop participants, like the Decadal Survey itself, strongly endorsed the need for the HyspIRI mission and felt the mission, as defined, would accomplish the intended science.

Document Contacts

Many researchers provided Inputs for this workshop report. Readers seeking more information about particular details and contacting researchers in certain areas may access that information through the following two individuals.

- Simon J. Hook
MS 183-503
Jet Propulsion Laboratory
4800 Oak Grove Dr.
Pasadena, CA 91109
Email: Simon.J.Hook@jpl.nasa.gov
Office: (818) 354-0974
Fax: (818) 354-5148
- Bogdan V. Oaida
MS 301-165
Jet Propulsion Laboratory
4800 Oak Grove Dr.
Pasadena, CA 91109
Email: Bogdan.Oaida@jpl.nasa.gov
Office: (818) 354-5517
Mobile: (626) 375-5398
Fax: (818) 393-9815

Preface

In 2004, the National Aeronautics and Space Administration (NASA), the National Oceanic and Atmospheric Administration (NOAA), and the U.S. Geological Survey (USGS) requested the National Research Council (NRC) identify and prioritize the satellite platforms and associated observational capabilities that should be launched and operated over the next decade for Earth observation. In addition to providing information for the purpose of addressing scientific questions, the committee identified the need to ensure that the measurements helped benefit society and provide policymakers with the necessary information to make informed decisions on future policies affecting the Earth.

The resulting NRC study *Earth Science and Applications from Space: National Imperatives for the Next Decade and Beyond*, also known as the Earth Science Decadal Survey, (NRC, 2007) recommended launching 15 missions in three time phases. These three time phases are referred to as Tier 1, Tier 2, and Tier 3, respectively. The Hyperspectral Infrared Imager (HypIRI) mission is one of the Tier 2 missions recommended for launch in the 2013–2016 timeframe. This global survey mission provides an unprecedented capability to assess how ecosystems respond to natural and human-induced changes. It will help us assess the status of biodiversity around the world and the role of different biological communities on land and within inland water bodies, as well as coastal zones and at reduced resolution in the ocean. Furthermore, it will help identify natural hazards; in particular volcanic eruptions and any associated precursor activity, and it will map the mineralogical composition of the land surface. The mission will advance our scientific understanding of how the Earth is changing as well as provide valuable societal benefit, in particular, in understanding and tracking dynamic events such as volcanoes and wildfires.

The HypIRI mission includes two instruments: a visible shortwave infrared (VSWIR) imaging spectrometer operating between 0.38 and 2.5 μm at a spatial scale of 60 m with a swath width of 145 km and a boresighted thermal infrared (TIR) multispectral scanner operating between 4 and 12 μm at a spatial scale of 60 m with a swath width of 600 km. The VSWIR and TIR instruments have revisit times of 19 and 5 days, respectively. Several of the other Tier 1 and Tier 2 missions provide complementary measurements for use with HypIRI data, in particular, the DESDynI, ACE, ICESat-II, and GEO-CAPE Decadal Survey missions each of which addresses very different spatial scales compared to the local and landscape scales observable with HypIRI. While the synergy between HypIRI and other sensors, including those on operational satellites, benefits all missions and would support relevant scientific endeavors, the ability of HypIRI to achieve its primary mission goals is not dependent on data from these other instruments.

This report documents a NASA-sponsored three-day workshop held in Monrovia, California, in October 2008 to refine the scientific questions, objectives, and requirements of the HypIRI mission and to identify priority near-term investments to mature the HypIRI concept towards a possible Mission Concept Review (MCR) at the end of 2009. Initially, some background on the NRC Decadal Survey is provided, and this is followed by a discussion of the science, measurement requirements, instrument requirements, and associated mission activities as presented and discussed at the workshop, along with recommendations for future activities.

Executive Summary

NASA held a three-day workshop on October 21–23, 2008 to consider the Hyperspectral Infrared Imager (HyspIRI) mission recommended for implementation by the 2007 NRC Earth Science Decadal Survey (DS, 2007). The workshop was open to the research community as well as members of other communities with an interest in the HyspIRI mission. It provided a forum for the HyspIRI Science Study Group (SSG) to present their initial observational requirements and assess the anticipated impact of HyspIRI on their scientific and operational applications and obtain feedback from the broader scientific community.

As part of the ongoing preparatory studies for the HyspIRI mission, the SSG has developed sets of measurement requirements tied to addressing a particular set of science questions. These requirements together with those already provided by the Decadal Survey formed the basis for the overall instrument and mission requirements presented at the workshop. Workshop participants evaluated the instrument and mission requirements in the context of the science questions, and they identified ancillary measurements that might be required to address these questions. Breakout sessions provided a forum for participants to review the science questions, as well as measurement requirements, and to suggest additional opportunities for enhanced science or applications that might be achieved through synergies with other planned missions and/or with augmentations to the current mission.

Several key conclusions resulted from the workshop:

- HyspIRI provides a unique capability to address a set of specific scientific questions about local and global ecosystems, habitats, biodiversity, and hazards and their response to anthropogenic or natural changes.
- HyspIRI will help integrate terrestrial and aquatic (inland, coastal, and oceanic) ecosystem studies, and allow assessments at spatial scales relevant to resource use by humans.
- The instrument design is capable of meeting the scientific measurement requirements.
- There is a stable set of instrument measurement requirements for HyspIRI, and these requirements are traceable to the science questions for the mission.
- Significant heritage exists from both a design and risk-reduction standpoint for both instruments. This heritage includes missions such as the Moon Mineralogy Mapper and the Advanced Spaceborne Thermal Emission and Reflection Radiometer as well as the associated algorithms to deliver the Level 0 through Level 2 data products.
- There do not appear to be any significant technology “show stoppers,” and the mission is ready for implementation at the earliest opportunity.
- HyspIRI complements measurements from the DESDynI, ACE, and GEO-CAPE missions, each of which addresses very different spatial scales compared to the local and landscape scales observable with HyspIRI.

The research community, like the Decadal Survey, strongly endorsed the need for the HyspIRI mission. There was a strong consensus that the HyspIRI mission, as defined, would accomplish the intended science.

Contents

Abstract		iii
Document Contacts		iii
1 Introduction		1-1
1.1 The Decadal Survey		1-1
1.2 The HyspIRI Workshop.....		1-1
2 Science and Societal Benefits		2-1
2.1 Overarching Thematic Topics.....		2-1
2.1.1 VQ1 - Pattern and Spatial Distribution of Ecosystems		2-1
2.1.2 VQ2 - Ecosystem Function, Physiology and Seasonal Activity		2-4
2.1.3 VQ3 - Biogeochemical Cycles		2-5
2.1.4 VQ4 - Ecosystem Response to Disturbance.....		2-6
2.1.5 VQ5 - Ecosystems and Human Well-being		2-7
2.1.6 VQ6 - Surface and Shallow-Water Bottom Composition		2-10
2.1.7 TQ1 - Volcanoes and Earthquakes.....		2-10
2.1.8 TQ2 - Wildfires		2-12
2.1.9 TQ3 - Water Use and Availability		2-13
2.1.10 TQ4 - Human Health and Urbanization		2-14
2.1.11 TQ5 - Earth Surface Composition and Change.....		2-15
2.1.12 CQ1 - Coastal, Ocean, and Inland-Aquatic Environments		2-16
2.1.13 CQ2 - Wildfires		2-18
2.1.14 CQ3 - Volcanoes		2-18
2.1.15 CQ4 - Ecosystem Function and Diversity		2-20
2.1.16 CQ5 - Land Surface Composition and Change		2-21
2.1.17 CQ6 - Human Health and Urbanization		2-22
2.2 Science Traceability Matrices.....		2-23
3 Measurement Requirements		3-1
3.1 VSWIR Instrument		3-1
3.2 TIR Instrument.....		3-1
4 Mission Concept		4-1
5 Data Products and Algorithms		5-1
6 Synergies		6-1
6.1 VSWIR/TIR Instruments		6-1
6.2 Other Missions and Programs		6-1
7 Conclusions and Recommendations		7-1
8 References		8-1
9 Appendices		9-1
Appendix A – Acronyms		9-1
Appendix B - Workshop Agenda.....		9-4
Appendix C – List of Participants.....		9-6
Appendix D – Science-Traceability Matrices.....		9-9

Figures

- Figure 1: Species-level map of the Santa Ynez Front Range mapped using 20-m AVIRIS data. (Adapted from Dennison and Roberts, 2003a) 2-4
- Figure 2: Presence of *Microcystis* bloom in the Sacramento-San Joaquin delta captured in hyperspectral imagery June 2007. 2-4
- Figure 3: Canopy Nitrogen, Carbon Assimilation, and Albedo in Temperate and Boreal Forests (Ollinger et al. 2008) 2-6
- Figure 4: Maps of canopy cover, nitrogen and water (panels to the left) derived from imaging spectroscopy were used to map highly invasive trees (upper right; red) in a Hawaiian rainforest. A biogeochemical model then showed increased nitrogen gas fluxes from the soils beneath the invader (Asner and Vitousek 2005). 2-7
- Figure 5: Watershed-scale ecosystem responses to disturbance. Disturbance is measured using MODIS imagery (X-axis) and Landsat (panel C), illustrating an inverse response stream nitrogen (A) and foliar nitrogen (B), as derived from Hyperion. (McNeil et al. (2007). 2-8
- Figure 6: Map of surface rock and soil mineralogy at Cuprite, NV using solar reflected imaging spectroscopy measurements from 380 to 2500 nm. (Left: AVIRIS image cube, Center: 1 micron region minerals, Right: 2 micron region minerals) (Swayze et al. 2003)..... 2-10
- Figure 7: (a) ASTER night-time multispectral TIR image of Augustine Volcano showing hot pyroclastic flow deposits (bright in TIR) and eruption plume. Colors indicate spectral variations between materials entrained in plume. Magenta indicates mixtures of water droplets (steam) and silicate ash; red, yellow, and orange indicate mixtures of ash and SO₂. (b) SO₂ map derived from ASTER TIR data. (c) Thermal infrared anomaly associated with the M6.4 Zarand, Iran earthquake of Feb. 22, 2005, as derived from night-time Advanced Very High Resolution Radiometer (AVHRR) images recorded prior to this event (after Saraf et al. 2008). The excess IR intensity emitted from the epicentral region (presented in yellow-orange colors), and 10K temperature increase, are proposed to be indicators of the build-up of stress at the hypocenter. Lower right: Location of the epicenter (star) relative to the region of maximum uplift (red: 25 cm) and subsidence (blue: 17 cm) from Interferometric Synthetic Aperture Radar (InSAR) data. 2-11
- Figure 8: False-color ASTER image of a large fire in southern Africa, acquired on 17 August 2001, with the 2.4, 1.6, and 0.5 μm bands shown as red, green, and blue, respectively. With this color scheme the actively burning fire front appears yellow to red, previously-burned areas appear black, and unburned vegetation appears green. The specialized 4-micron channel of the HypSPiRI thermal sensor will not exhibit the saturation-induced blooming apparent along the more intense portions of the flaming front in this scene. 2-12
- Figure 9: Multi-scale ET maps for 1 July 2002 produced with the ALEXI/DisALEXI surface energy balance models (Anderson, et al. 2007) using surface temperature data from aircraft (30-m resolution), Landsat-7 ETM+ (60m), Terra MODIS (1-km), GOES Imager (5-km) and GOES Sounder (10-km) instruments. The continental-scale ET map is a 14-day composite of clear-sky model estimates. 2-13
- Figure 10: Landsat TM data of the Atlanta, GA metropolitan area showing urban extent in gray (bottom) and corresponding surface thermal responses (top) (Quattrochi et al. 2009) 2-15
- Figure 11: HypSPiRI-like image for the area around Lake Mead, Nevada. Three TIR bands are processed with a decorrelation stretch algorithm and displayed in red, green and blue, respectively (from Hook et al. 2005). .. 2-16
- Figure 12: Weight-specific absorption coefficients ($\text{m}^2 \text{mg}^{-1}$) derived for the major pigment types found in marine phytoplankton (from Bidigare et al. 1989). 2-17
- Figure 13: Top panel: Retrieved fire temperature (in kelvins) from an AVIRIS scene spanning a portion of the large Southern California Fire Complex from October 2003. Bottom panel: False color SWIR-NIR-red composite of the original AVIRIS scene. (Dennison et al. 2006). 2-18
- Figure 14: Hyperion SWIR image of Erta Ale volcano, Ethiopia, showing the active lava lake. Hyperspectral VSWIR and TIR data will allow the cooling rate and gas flux from the lake to be determined. Right: model of cooling and degassing-driven magma convection within an open system volcano. The heat and gas flux data are important boundary conditions for determining magma ascent dynamics and circulation within the conduit (adapted from Frances et al. 1993). 2-19
- Figure 15: Map of *Bromus tectorum* (Cheatgrass) generated using imaging spectrometry. Cheatgrass spreads through a combination of disturbance and strategic use of soil moisture. It alters fire regimes, promoting its spread while early germination of Cheatgrass enables it to produce seed in advance of native plants while reducing available water for competitors. (Noujdina and Ustin 2008). 2-20

Figure 16: False color composite HypsIRI simulated image of Grand Canyon, Arizona derived from TIR (red band - quartz-rich rocks), SWIR (green band - clay and muscovite-rich rocks; blue band - carbonate-rich rocks), and VNIR (dark green - green vegetation) data.....2-21

Figure 17: Temperature and albedo measurements for the Atlanta, GA central business district as derived from multispectral aircraft data (Quattrochi et al. 2009).....2-23

Figure 18: Process for developing the Science-Traceability Matrixes.2-23

Figure 19: HypsIRI-VSWIR Key Signal-to-Noise and Uniformity Requirements.3-1

Figure 20: Number of image acquisitions in 19 days.4-1

Figure 21: Illustration of the Sun illumination at the winter solstice.....4-1

Tables

Table 1: Overarching Thematic Science Questions.....2-2

Table 2: VQ1 Thematic Subquestions2-3

Table 3: VQ2 Thematic Subquestions2-5

Table 4: VQ3 Thematic Sub Questions2-5

Table 5: VQ4 Thematic Subquestions2-6

Table 6: VQ5 Thematic Sub Questions2-8

Table 7: VQ6 Thematic Sub Questions2-10

Table 8: TQ1 Thematic Subquestions2-11

Table 9: TQ2 Thematic Subquestions2-13

Table 10: TQ3 Thematic Subquestions2-14

Table 11: TQ4 Thematic Subquestions2-15

Table 12: TQ5 Thematic Subquestions2-15

Table 13: CQ1 Thematic Subquestions2-17

Table 14: CQ2 Thematic Subquestions2-18

Table 15: CQ3 Thematic Subquestions2-19

Table 16: CQ4 Thematic Subquestions2-21

Table 17: CQ5 Thematic Subquestions2-22

Table 18: CQ6 Thematic Subquestions2-22

Table 19: VSWIR Measurement Characteristics3-2

Table 20: TIR Measurement Characteristics3-3

Table 21: HypsIRI Data Volume, includes illumination constraints for VSWIR, compression and overhead.4-2

1 Introduction

1.1 The Decadal Survey

In 2004, NASA, NOAA, and the USGS commissioned the National Research Council to conduct a Decadal Survey (DS) for Earth science and applications from Space. The 2007 report from that survey is titled: *Earth Science and Applications from Space: National Imperatives for the Next Decade and Beyond*. The objective of the survey was to generate consensus recommendations from the Earth and environmental science and applications communities regarding an integrated approach to future space-based and ancillary observations.

The NRC appointed a committee to undertake the Decadal Survey. The committee participated in—and synthesized work from—seven thematically organized study panels:

- 1) Earth-science applications and societal benefits;
- 2) Land-use change, ecosystem dynamics, and biodiversity;
- 3) Weather;
- 4) Climate variability and change;
- 5) Water resources and the global hydrologic cycle;
- 6) Human health and security and
- 7) Solid-Earth hazards, resources, and dynamics.

Each of these thematic areas identified key science measurements, justified these measurements, and recommended a small number of missions. The Decadal Survey committee consolidated the recommendations from each theme into a short list of prioritized missions. Included in this list as a high priority was the Hyperspectral Infrared Imager (HyspIRI) mission, which would provide global observations of multiple key surface attributes at local and landscape spatial scales

(tens of meters to hundreds of kilometers) for a wide array of Earth-system studies, including integrating assessments of local and landscape changes key to understanding biodiversity in both terrestrial and aquatic (inland, coastal, and oceanic) ecosystems, measuring the condition and types of vegetation on the Earth's surface, and changes in the mineralogical composition of the surface in order to understand the distribution of geologic materials. The mission would help map volcanic gases and surface temperatures, which were identified as indicators of impending volcanic hazards, as well as plume ejecta which pose risks to aircraft and people and property downwind.

The committee recommended that HyspIRI be launched in the 2013–2016 timeframe and include a hyperspectral visible-shortwave infrared (VSWIR) imaging spectrometer and a multispectral thermal infrared (TIR) scanner. The mission would provide global coverage from low Earth orbit with a high temporal frequency, especially in the case of the TIR instrument, which would have a revisit time of 6 days or less.

The NRC Decadal Survey participants recognized that both instruments had strong spaceborne heritage through the Hyperion Instrument on the Earth Observing-1 (EO-1) platform, the Moon Mineralogy Mapper (M3) instrument on the Chandrayaan-1 platform and the Advanced Spaceborne Thermal Emission and Reflection Radiometer (ASTER) instrument on the Terra platform.

1.2 The HyspIRI Workshop

The HyspIRI workshop was held on October 21–23, 2008 in Monrovia, California and was open to all interested parties (US and international). The goals of the workshop were to confirm and clarify the science requirements for the HyspIRI mission and to

provide an open forum for community participation in early planning activities. The agenda sought to introduce participants to the Decadal Survey and associated activities at NASA Headquarters and then provide the measurement requirements for HypsIRI. Next, a series of science presentations and breakout groups on the HypsIRI science questions and associated science traceability matrices led to the refinement of the science traceability matrices, which directly link the science questions to instrument and mission requirements. There were also presentations on technology needs and partnership opportunities and discussions of next steps (see Appendix B for the workshop Agenda). Approximately 150 people participated in the workshop from academia and industry including several international participants from Australia, Canada, Japan, and Europe. Presentations given by NASA and academia addressed key aspects of the mission with additional time for open discussion when appropriate. All the oral presentations can be found on the HypsIRI website at: <http://hyspiri.jpl.nasa.gov>. All workshop participants were encouraged to discuss and refine the mission science goals and methods to maximize the scientific return from the data.

The morning of the first day, the workshop focused on providing background information on the Decadal Survey and NASA's approach to the HypsIRI mission, followed by descriptions of the measurement requirements provided by the Decadal Survey and subsequently reviewed by the HypsIRI Science Study Group (SSG). The SSG is a group of scientists assembled in advance of the workshop by NASA to represent the scientific community and domestic agencies interested in HypsIRI data including the NASA centers. Terrestrial and marine ecologists, geologists, and atmospheric scientists participated in this group. They refined the measurement requirements laid out

in the Decadal Survey to ensure they represented the needs of the scientific community. Doing so involved developing a set of science questions for the two instruments (VSWIR and TIR) and an associated set of science traceability matrices (STMs). The STMs trace each measurement requirement back to a science question(s).

In the late morning and afternoon of the first day, presentations and breakouts focused on the VSWIR instrument. The breakouts worked through both the science questions and the STMs to make sure they were clearly articulated.

The second day began with a discussion of potential airborne precursor activities for HypsIRI. The goal of these discussions was to identify how best to put together simulated HypsIRI data from airborne instrument data, which could subsequently be used for algorithm development. Later that day, participants reviewed the science questions and STMs for the TIR instrument. Again, work focused on ensuring the TIR science questions were clearly articulated and the measurement requirements understood. The end of the second day saw a series of presentations on the potential for advanced technologies to optimize the HypsIRI mission. Of particular interest was inclusion of a direct broadcast system on HypsIRI together with an Intelligent Payload Module, which would allow the download of selected bands and band combinations in near realtime.

The third day of the workshop included a review of the science questions and traceability matrixes for the combined science questions. The combined science questions are questions requiring the use of data from both instruments (VSWIR and TIR). The participants felt these questions were particularly interesting and offered a clear demonstration of synergies arising from,

acquiring data from both instruments simultaneously.

In the afternoon of the last day, participants revisited the measurement requirements for both VSWIR and TIR instruments in light of discussions on previous days and highlighted those areas requiring further study. They noted that both sets of instrument requirements were mature and well matched to the science the instruments would address. Potential opportunities for domestic and international partnerships were the subject of another talk that afternoon. Several agencies expressed interest in the mission, ranging from roles in the distribution of the data products to upgrading foreign ground stations for additional downlink capability. The workshop's final presentation focused on next steps and is described in the subsequent section on conclusions and recommendations.

The remainder of this report is organized as follows. Section 2 presents the science behind the mission and provides top-level questions followed by overarching thematic questions and thematic sub-questions (Table 1 through Table 18 contain these questions).

The subsections address the science underlying these questions. The Science section includes the STMs, which focus on the more detailed sub-level questions. (Appendix D contains the STMs.) Section 3 discusses the measurement requirements that grow from the STMs and the framework provided by the Decadal Survey. Section 4 outlines the Mission Concept, in particular the baseline operations concept. Section 5 provides a preliminary discussion of the expected data products and algorithms. Section 6 explores synergies with other instruments and partnerships. This section is expected to expand as the HypsIRI mission and other Decadal Survey missions mature. Finally, Section 7 provides a set of conclusions and recommendations based on the workshop. A series of appendices offer a list of acronyms, the workshop agenda, a list of workshop participants, and the STMs.

2 Science and Societal Benefits

The HypsIRI mission is science driven. In other words, one can trace back the measurement requirements for the mission to a particular science question. HypsIRI has three top-level science questions related to 1) Ecosystem function and composition, 2) Volcanoes and natural hazards, and 3) Surface composition and the sustainable management of natural resources. The NRC Decadal Survey called out these three areas. The top-level science questions for the HypsIRI mission are:

Ecosystem function and composition

What is the global distribution and status of terrestrial and coastal-aquatic ecosystems and how are they changing?

Volcanoes and natural hazards

How do volcanoes, fires, and other natural hazards behave; and do they provide precursor signals that can be used to predict future activity?

Surface composition and sustainable management of natural resources

What is the composition of the land surface and coastal shallow water regions, and how can they be managed to support natural and human-induced change?

These questions provide a scientific framework for the HypsIRI mission. NASA appointed the HypsIRI Science Study Group (SSG) to refine and expand these questions to a level of detail that was sufficient to define the measurement requirements for the HypsIRI mission. In 2007, the first SSGs were formed, and there was a separate SSG for each instrument (VSWIR and TIR). These groups were then merged in 2008, their overall membership re-assessed, and the HypsIRI SSG formed.

The SSG developed a more detailed set of overarching thematic questions that

were separated into three groups. The first two groups deal with overarching questions that may be addressed by only one of the two instruments. The third group requires data from both instruments. All three groups may require supporting measurements from other instruments, whether spaceborne, airborne, or ground. The three question groups are referred to as the 1) VSWIR questions (VQ), 2) TIR questions (TQ) and 3) Combined questions (CQ), respectively (Table 1). Within each of these overarching thematic questions, there are a set of thematic subquestions, and it is these subquestions that provide the necessary detail to understand the measurement requirements (Table 2 through Table 18). Section 2.1 below provides a summary of the science behind each of the overarching thematic questions.

2.1 Overarching Thematic Topics

2.1.1 VQ1 - Pattern and Spatial Distribution of Ecosystems

Terrestrial and aquatic ecosystems represent an assemblage of biological and non-biological components and the complex interactions among them, including cycles and/or exchanges of energy, nutrients, and other resources. The biological components span multiple trophic levels and range from single-celled microbial organisms to higher order organisms, including vegetation in forests and grasslands, and in coastal and other aquatic environments, as well as animals. In many ecosystems, a dominant or keystone species is critical in how that system functions. Because of their abundance and geographic extent, plant or phytoplankton communities provide distinct characteristics to habitats and ecosystems, and these are visible from great distances, including from space.

Table 1: Overarching Thematic Science Questions

Question #	Area	Question	Lead and Co-Lead
VQ1	Pattern and Spatial Distribution of Ecosystems and their Components	What is the global spatial pattern of ecosystem and diversity distributions, and how do ecosystems differ in their composition or biodiversity?	Roberts, Middleton
VQ2	Ecosystem Function, Physiology, and Seasonal Activity	What are the seasonal expressions and cycles for terrestrial and aquatic ecosystems, functional groups, and diagnostic species? How are these being altered by changes in climate, land use, and disturbance?	Gamon
VQ3	Biogeochemical Cycles	How are the biogeochemical cycles that sustain life on Earth being altered/disrupted by natural and human-induced environmental change? How do these changes affect the composition and health of ecosystems, and what are the feedbacks with other components of the Earth system?	Ollinger
VQ4	Changes in and Responses to Disturbance	How are disturbance regimes changing, and how do these changes affect the ecosystem processes that support life on Earth?	Asner, Knox
VQ5	Ecosystem and Human Health	How do changes in ecosystem composition and function affect human health, resource use, and resource management?	Townsend, Glass
VQ6	Earth Surface and Shallow-Water Substrate Composition	What is the land surface soil/rock and shallow-water substrate composition?	Green, Dierssen
TQ1	Volcanoes and Earthquakes	How can we help predict and mitigate earthquake and volcanic hazards through detection of transient thermal phenomena?	Abrams, Freund
TQ2	Wildfires	What is the impact of global biomass burning on the terrestrial biosphere and atmosphere, and how is this impact changing over time?	Giglio
TQ3	Water Use and Availability	How is consumptive use of global freshwater supplies responding to changes in climate and demand, and what are the implications for sustainable management of water resources?	Anderson, Allen
TQ4	Urbanization and Human Health	How does urbanization affect the local, regional, and global environment? Can we characterize this effect to help mitigate its impact on human health and welfare?	Quattrochi, Glass
TQ5	Surface Composition and Change	What is the composition and temperature of the exposed surface of the Earth? How do these factors change over time and affect land use and habitability?	Prakash, Mars
CQ1	Coastal, ocean, and inland aquatic environments	How do inland, coastal, and open-ocean aquatic ecosystems change due to local and regional thermal climate, land-use change, and other factors?	Muller-Karger,
CQ2	Wildfires	How are fires and vegetation composition coupled?	Giglio,
CQ3	Volcanoes	Do volcanoes signal impending eruptions through changes in the temperature of the ground, rates of gas and aerosol emission, temperature and composition of crater lakes, or health and extent of vegetation cover?	Wright, Realmuto
CQ4	Ecosystem Function and Diversity	How do species, functional type, and biodiversity composition within ecosystems influence the energy, water, and biogeochemical cycles under varying climatic conditions?	Roberts, Anderson
CQ5	Land surface composition and change	What is the composition of the exposed terrestrial surface of the Earth, and how does it respond to anthropogenic and non anthropogenic drivers?	Mars, Prakash
CQ6	Human Health and Urbanization	How do patterns of human environmental and infectious diseases respond to leading environmental changes, particularly to urban growth and change and the associated impacts of urbanization?	Quattrochi, Glass

In diverse ecosystems, often suites of plant or phytoplankton species can be organized into assemblages of organisms with similar form and function, defined as plant functional types (PFTs) or functional groups (FGs). Dominant vegetation types or PFTs that capture the major features of an ecosystem are often amenable to detection via remote sensing.

The distribution of terrestrial and aquatic ecosystems across the Earth is largely controlled by climate, modified by surface elevation, substrate, oceanic and atmospheric circulation, and a number of other factors. Anthropogenic disturbance, primarily in the form of land-cover conversion and, at larger scales, climate change has imposed increasing pressures on Earth's ecosystems. Remote sensing represents perhaps the only viable approach for mapping the current distribution of these ecosystems globally, monitoring their status and improving our understanding of feedbacks among modern ecosystems, climate and disturbance.

At the finest scales, spectral reflectance is largely governed by the concentration of pigments (primarily chlorophylls and carotenoids), important biochemicals (such as cellulose, lignin, starch and water), and the arrangement of internal structures (Gates et al., 1965; Curran 1989) and surface features (waxes and hairs). Scaling up to plant canopies on land or assemblages of marine organisms, spectral reflectance is governed by the arrangement of components (branches, leaves, and trunks on land, and depth and density in a marine environment) and the manner in which multiple scattering and shadowing modify reflectance (Asner, 1998; Hochberg and Atkinson, 2003; Roberts et al., 2004). To the extent that fine-scale chemistry and anatomy and coarser scale structure uniquely define a species or PFT/FG, remote sensing can map the distribution of these organisms and be

used to monitor their response to disturbance and environmental change.

Unique seasonal changes in biochemistry and structure offer additional leverage for discriminating individual species.

Table 2: VQ1 Thematic Subquestions

ID	Question
VQ1a	How are ecosystems organized within different biomes associated with temperate, tropical, and boreal zones; and how are these changing?
VQ1b	How do similar ecosystems differ in size, species composition, fractional cover and biodiversity across terrestrial and aquatic biomes and on different continents?
VQ1c	What is the current spatial distribution of ecosystems, functional groups, or key species within major biomes including agriculture, and how are these being altered by climate variability, human uses, and other factors?
VQ1d	What are the extent and impact of invasive species in terrestrial and aquatic ecosystems?
VQ1e	What is the spatial structure and species distribution in a phytoplankton blooms?
VQ1f	How do changes in coastal morphology and surface composition impact coastal ecosystem composition, diversity and function?

Within a region, the unique spectral signatures of plants have been used to discriminate and map dominant plant species and PFTs. Dennison and Roberts (2003a), used the Airborne Visible Infrared Imaging Spectrometer (AVIRIS) to map dominant plant species in the fire prone Front range of the Santa Ynez Mountains (Figure 1). The ability to discriminate plant species was also found to depend significantly on season of acquisition, defined in this area by a change in soil water balance (Dennison and Roberts, 2003b).

Comparisons between broadband sensors, Hyperion and high fidelity AVIRIS data, demonstrated significant improvements in species-level discrimination using imaging spectrometry. The link between spectroscopy, biochemistry, and biodiversity may also be expressed in the spectral diversity within an ecosystem. For example, Carlson et al. (2007) demonstrated a strong link between field-

measured species diversity in Hawaii and spectral diversity mapped using AVIRIS.

HypSIRI, as a high-fidelity imaging spectrometer with a 19-day repeat pass, has the potential for dramatically improving our ability to identify PFTs/FGs, quantify species diversity, discriminate plant and phytoplankton species, and map their distribution in terrestrial and coastal environments.

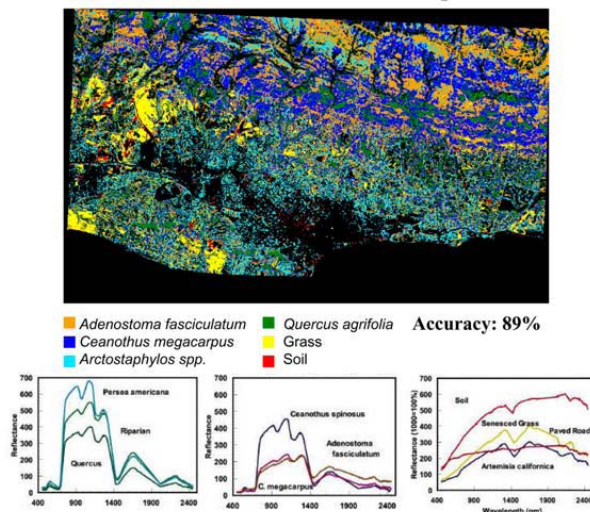


Figure 1: Species-level map of the Santa Ynez Front Range mapped using 20-m AVIRIS data. (Adapted from Dennison and Roberts, 2003a)

2.1.2 VQ2 - Ecosystem Function, Physiology and Seasonal Activity

Vegetation dynamics express themselves across a wide range of time scales from diurnal to inter-annual. Although we well understand broad phenological patterns such as leaf emergence, more subtle patterns of vegetation activity reflecting underlying physiological dynamics are less well known and require the unique hyperspectral capabilities and frequent repeat cycles provided by HypSIRI. Improved assessment of vegetation pigment levels can improve models of carbon exchange and identify periods of stress and reduced photosynthetic activity. For example, xanthophyll cycle

pigments, chlorophyll/carotenoid ratios, or anthocyanin levels—all indicators of physiological state—can only be characterized by the fine spectral resolution provided by hyperspectral sensors (Ustin et al. 2004). Similarly, narrow water-absorption features provide subtle indicators of water content and evapotranspiration (Serrano et al. 2002, Fuentes et al. 2006, Claudio et al. 2006), key physiological variables critical to surface energy balance and climate regulation. Furthermore, expressions of physiological dynamics and biochemistry vary across species and functional types, and provide novel ways to characterize biological diversity from remote sensing (Gamon et al. 2005, Carlson et al. 2007), particularly when combined with frequent repeat cycles that capture key phenological events (such as leaf out, flowering, and senescence). This combination of numerous cycles with narrow spectral bands will also be useful in capturing certain short-lived or rapidly changing phenomena including algal blooms (Figure 2), outbreaks of pathogens or insect infestations (Pontius et al. 2005), or invasive weedy species (Noujdina and Ustin 2008), which can have significant economic or public health consequences (e.g., Kallio et al. (2001) used hyperspectral data to track seasonal changes in water quality in Finnish lakes).

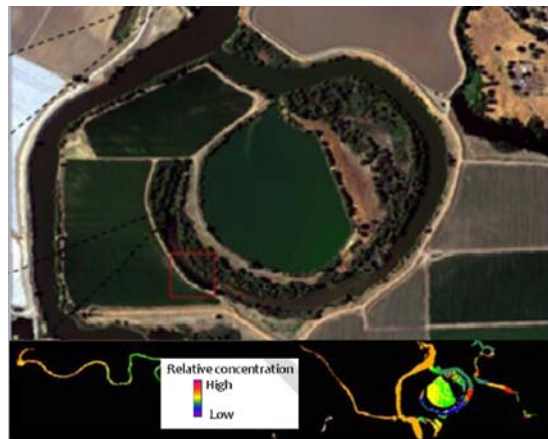


Figure 2: Presence of Microcystis bloom in the Sacramento-San Joaquin delta captured in hyperspectral imagery June 2007.

With the spatial and temporal resolution provided by HypsIRI, subtle differences in phenology and physiology associated with dynamic environmental conditions or microsites can be captured (Gamon et al. 1993, Garcia and Ustin 2001, Zarco-Tejada et al. 2005a, b) providing clear benefits to resource managers in many disciplines including forestry, agriculture, and water-quality management.

Table 3: VQ2 Thematic Subquestions

ID	Question
VQ2a	How are these being altered by changes in climate, land use, and disturbance?
VQ2b	How are seasonal patterns of ecosystem function being affected by climate change?
VQ2c	How do changes in phenology affect productivity, carbon sequestration, and hydrological processes across ecosystems and agriculture?
VQ2d	How do environmental stresses affect the seasonality of the physiological function of water and carbon exchanges within ecosystems?
VQ2e	What is the seasonality and environmental impact of algal blooms in shallow water environments?

2.1.3 VQ3 - Biogeochemical Cycles

The biogeochemical cycles of C, H, O, N, P, S, and dozens of other elements sustain life on Earth, are central to human well-being and are at the core of some of our most pressing environmental concerns. As these elements travel between the atmosphere, biosphere, hydrosphere, and lithosphere, they shape the composition and productivity of ecosystems, they influence the climate regulating properties of the atmosphere, and they affect the quantity and quality of water supplies. Because human livelihood has long been tied to the production of food, fiber, and energy, our activities have had particularly profound effects on cycles of carbon, nitrogen, and water. Issues such as climate change, nitrogen deposition, coastal eutrophication, groundwater contamination, and erosion represent human alterations of these basic biogeochemical cycles (Vitousek et al. 1997).

The HypsIRI instrument stands to advance our understanding of biogeochemical cycling in a number of important ways. Nutrient cycling patterns in both terrestrial and aquatic ecosystems can influence the growth and distribution of species as well as the morphology and chemistry of their tissues (e.g., LeBauer and Treseder 2008, Wright et al. 2004, Reich et al. 2006). Several decades of work with laboratory and aircraft instruments have demonstrated repeatedly that many of these vegetation features can be detected through analysis of high-quality imaging spectrometer data. Examples include the detection of leaf pigments in both terrestrial and aquatic plants (e.g., Asner 1998, Gitelson et al. 2007, Thomas et al. 2008), vegetation chemical constituents such as nitrogen, lignin, and cellulose (Wessman et al. 1988, Roberts et al. 1997, Serrano et al. 2002, Ollinger and Smith 2005) and invasive plants that cause distinct changes in the biogeochemistry of their surroundings (Asner and Vitousek 2005).

Table 4: VQ3 Thematic Sub Questions

ID	Question
VQ3a	How do changes in climate and atmospheric processes affect the physiology and biogeochemistry of ecosystems?
VQ3b	What are the consequences of uses of land and coastal systems, such as urbanization and resource extraction, for the carbon cycle, nutrient fluxes, and biodiversity?
VQ3c	What are the consequences of increasing nitrogen deposition for carbon cycling and biodiversity in terrestrial and coastal ecosystems?
VQ3d	How do changes in hydrology, pollutant inputs, and sediment transport affect freshwater and coastal marine ecosystems?
VQ3e	How do changing water balances affect carbon storage by terrestrial ecosystems?
VQ3f	What are the key interactions between biogeochemical cycles and the composition and diversity of ecosystems?
VQ3e	How do changes in biogeochemical processes feed back to climate and other components of the Earth system?

Because the plant traits being detected play key roles in processes such as carbon assimilation, biomass production, litterfall,

and decomposition, these capabilities have led to substantial improvements in our understanding of biogeochemical properties such as soil nitrogen cycling (Ollinger et al. 2002), algal production and exchanges of carbon and water between the land and atmosphere (e.g., Ustin et al. 2004, Fuentes et al. 2006). The principal limitation of these methods to date has been the spatial extent, frequency, and reliability of data acquisition.

Overcoming the limitations of current sensors will be critical for our ability to integrate field-based knowledge of biogeochemistry with climate research and Earth-system modeling. As an example, recent research with AVIRIS and eddy-covariance tower data revealed a coupling of carbon assimilation and vegetation shortwave albedo that is mediated by nitrogen concentrations in vegetation canopies (Figure 3).

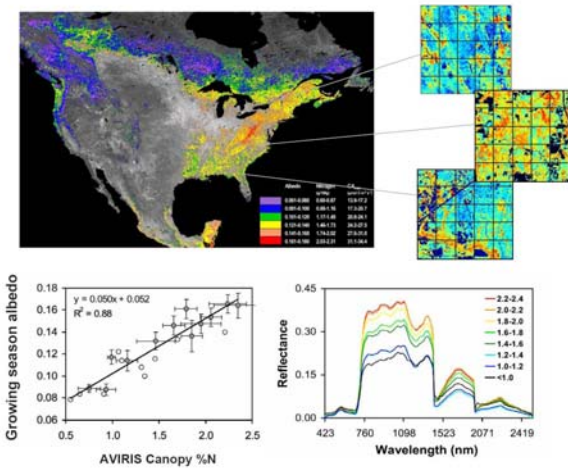


Figure 3: Canopy Nitrogen, Carbon Assimilation, and Albedo in Temperate and Boreal Forests (Ollinger et al. 2008)

This suggests a feedback in the climate system that models do not presently capture, in part because the relevant global data sets are not available from available sensors. Data from HypsIRI would solve this problem by providing the ideal spectral data for mapping both canopy nitrogen and, given its full

spectral coverage, total shortwave surface albedo.

The advent of HypsIRI as an orbital sensor will mark a substantial leap forward for the biogeochemical sciences. It is for this reason that organizations such as the Scientific Organization on Problems of the Environment (SCOPE) have identified hyperspectral technologies as being a key part of future studies of element cycling (Ollinger et al. 2003, Mellilo et al. 2003).

2.1.4 VQ4 - Ecosystem Response to Disturbance

Ecological disturbance plays a central role in shaping the Earth system. Disturbances (such as extreme weather events, fire, forest thinning or dieback, rangeland degradation, insect and pathogen outbreaks, and invasive species) affect vegetation biochemical and physiological processes with cascading effects on whole ecosystems. Similar effects take place based on disturbances to aquatic ecosystems, such as sediment re-suspension, nutrient input, or storm events, among many others. These and other disturbances often occur incrementally at spatial scales that fall well within the pixel size of current global satellite sensors.

Table 5: VQ4 Thematic Subquestions

ID	Question
VQ4a	How do patterns of disturbance vary and change over time within and across ecosystems?
VQ4b	What are the trends in disturbance regimes, compared with previous regional and global observations?
VQ4c	How do climate changes affect disturbances such as fire and insect damage?
VQ4d	How do climate change, pollution, and disturbance alter the vulnerability of ecosystems to invasive species?
VQ4e	What are the effects of disturbances on productivity, water resources, and other ecosystem functions and services?
VQ4f	How do changes in human uses of ecosystems affect their vulnerability to disturbance and extreme events?

Since disturbance often involves changes in vegetation function (physiology and biochemistry) and composition (e.g., the spread of introduced species) that may not be detectable with conventional satellite approaches, detection and quantification often requires the full spectral signatures available from imaging spectroscopy.

HyspIRI's high-fidelity imaging spectrometer will facilitate the study of ecological processes in disturbed areas at a level not possible with current satellite sensors.

HyspIRI will directly address a range of ecological disturbance-response questions central to predictions of future global change. For example, invasive species are considered a major driver of ecological change worldwide. Biological invasions can go unnoticed due to their often subtle impacts on vegetation structure. However, the chemical and physiological effects of invasion can be measured with imaging spectroscopy, as shown using the updated AVIRIS sensor (Figure 4)

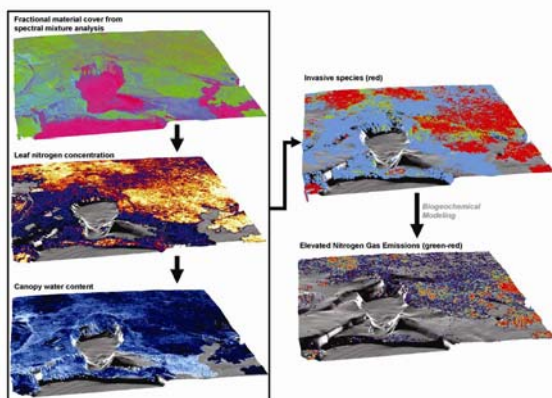


Figure 4: Maps of canopy cover, nitrogen and water (panels to the left) derived from imaging spectroscopy were used to map highly invasive trees (upper right; red) in a Hawaiian rainforest. A biogeochemical model then showed increased nitrogen gas fluxes from the soils beneath the invader (Asner and Vitousek 2005).

Combining multiple plant properties derived from reflectance spectra provided a

means to map invasives in a Hawaiian rainforest. The primary invader was a nitrogen-fixing tree species that raised nutrient flow throughout the ecosystem, as shown in the modeling results using AVIRIS-derived data products. HyspIRI provides an unprecedented capability to examine the effect of similar disturbances in aquatic habitats.

2.1.5 VQ5 - Ecosystems and Human Well-being

Ecosystem condition affects the humans dependent on those ecosystems for life and livelihood. For example, measurements of ecosystem condition derived from hyperspectral imagery can provide important insights into how ecosystem health is related to water quality, and by extension to human health. Similarly, hyperspectral data have been demonstrated to be effective for mapping the presence of invasive or undesirable plant species, which in turn affect the production of natural resources for human use by displacing desirable species with species of comparably lower value. Additional linkages from ecosystem to human condition include the monitoring of changes to ecosystems that may influence disease spread, resource availability, and resource quality. In border areas and areas with high human population densities, such information may provide insights into underlying causes of social, economic, or political conflict. Therefore, measurements of ecosystem condition from HyspIRI provide the potential to better characterize relationships between ecosystem health and human well-being.

The Group on Earth Observations (GEO) Remote Sensing of Water Quality Workshop in Geneva, Switzerland in 2007 stated that an ideal hyperspectral water quality sensor would have a range of 0.35 to 2.4 μm and a spectral resolution of 5–10 nm, which fits well with the HyspIRI VSWIR capability. At these wavelengths and spectral resolutions, key water quality characteristics can be

observed, such as chlorophyll concentration to monitor eutrophication of in-land and coastal water and to determine plankton species type—or possibly the presence of harmful algal blooms (HABs) (Ritchie et al. 2003) as demonstrated by Kutser (2004). Hyperspectral data can also be used to measure directly water quality parameters that relate to nitrogen and phosphorus concentration, chlorophyll-a, colored dissolved organic matter (CDOM), particulate matter and tripton (Giardino et al. 2007, Brando and Dekker 2003, Thiemann and Kaufmann 2002, Fraser 1998), all of which have a bearing on the provision of clean water, water treatment, and hazards to human and animal health. Thus, the hyperspectral imaging capability of HyspIRI can be used to monitor seasonal changes in coastal and in-land waters for human health risks and potential threats to aquatic resources that could have economic impacts (e.g., reduced fish stocks safe for human consumption) and adversely affect the availability of potable water and food.

Table 6: VQ5 Thematic Sub Questions

ID	Question
VQ5a	How do changes in ecosystem composition and function affect the spread of infectious diseases and the organisms that transmit them?
VQ5b	How will changes in pollution and biogeochemical cycling alter water quality?
VQ5c	How are changes in ecosystem distribution and productivity linked to resource use, and resource management?
VQ5d	How will changes in climate and pollution affect the health and productivity of aquatic and agricultural resources?
VQ5d	What are the economic and human health consequences associated with the spread of invasive species?
VQ5e	How does the spatial pattern of policy, environmental management, and economic conditions correlate with the state and changes in ecosystem function and composition?
VQ5f	What are the impacts of flooding and sea level rise on ecosystems, human health, and security?

Furthermore, changes in watershed ecosystems can be tied to changes in water quality. The ability of hyperspectral data to

detect foliar nutrient concentrations has been well documented (Martin et al. 2008). Recently McNeil et al. (2007) showed that disturbance to forests leads to concurrent declines in foliar nutrient quality (measured using Hyperion) and nutrient export to watersheds (measured in situ) that was manifested in declines in downstream water quality disturbed relative to undisturbed watersheds (Figure 5).

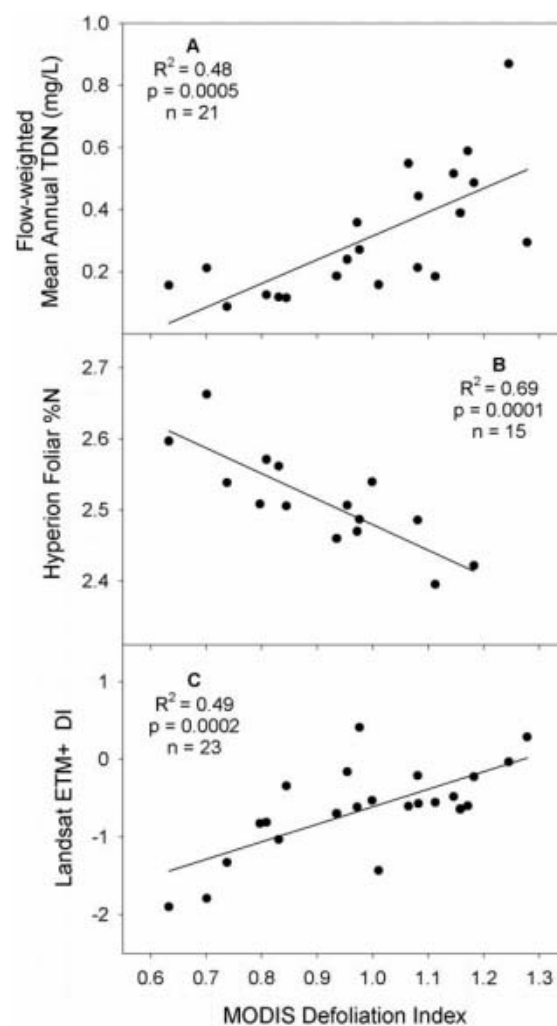


Figure 5: Watershed-scale ecosystem responses to disturbance. Disturbance is measured using MODIS imagery (X-axis) and Landsat (panel C), illustrating an inverse response stream nitrogen (A) and foliar nitrogen (B), as derived from Hyperion. (McNeil et al. (2007).

This points to functional relationships between ecosystem processes and water quality that affect both the availability of clean water for human use, and decisions that resource managers must make with respect to landscape management and water treatment. Hyperspectral imagery is also effective for the detection of other ecosystem changes resulting from flooding (Ip et al. 2006) and saltwater intrusion.

The detection of stress to vegetation from pests and pathogens also represents an important application of hyperspectral imagery with implications for human well-being. In forested ecosystems, Pontius et al. (2005) recently demonstrated the use of AVIRIS imagery to detect early signs of decline in hemlocks as a consequence of infestation by the hemlock woolly adelgid. Hemlock is a valuable species ecologically, economically, and for recreation, meaning that detection of hemlock decline can provide resource managers with opportunities for mitigation response prior to high levels of mortality. Additional studies have also demonstrated the capacity of hyperspectral data to detect plant decline from pathogens affecting economically important species like eucalypts (Stone et al. 2001), pines (Coops et al. 2003), ash (Pontius et al. 2008) and California oaks (Pu et al. 2008), as well forests in general (Treitz and Howarth 1999). Applications to agricultural systems are also widespread, as hyperspectral imagery can provide measures of growth/yield status (Datt et al. 2003), nutrient status (Haboudane et al. 2002, Strachan et al. 2002), and stress (Zarco-Tejada et al. 2005b), and has potential applications for food safety (Kim et al. 2001). Other work has demonstrated the ability of EO-1 Hyperion to detect sugarcane “orange rust” (Apan et al. 2004) as well as fungal diseases in wheat.

Non-native plant species pose a significant threat to ecosystems worldwide. In many areas, invasive plants displace native

species that are depended upon for food, fiber, or ecosystem services such as nutrient retention. Replacement by non-native species may have effects not just on the function, composition, and structure of the native ecosystems (e.g., fauna), but also on the human societies that use these ecosystems. Hyperspectral imagery has been demonstrated to be effective at discriminating invasive species (often resulting from differing nutrient assimilation strategies) in US western coastal habitats (Underwood et al. 2003 and 2006, and Rosso et al. 2005, Judd et al. 2007, Sadro et al. 2007), US eastern coastal habitats (Bachmann et al. 2002), and other wetlands (Hirano et al. 2003, Jollineau and Howarth 2008), as well as specific invasives such as common reed, *Phragmites communis*, formerly *P. australis* (Pengra et al. 2007), leafy splurge in central and western North America (Glenn et al. 2005), Chinese tallow (Ramsey et al. 2005a, Ramsey et al. 2005b), tamarix (Anderson et al. 2005, Pu et al. 2008), and the invasive nitrogen-fixer *Myrica faya* in Hawaii (Asner et al. 2006, Asner and Vitousek 2005). Detection of invasives may be critical to assessing significant changes in ecosystem level nutrient and water availability (Asner and Vitousek 2005). Hyperspectral imagery has also proven effective for discriminating increases in liana dominance of tropical and subtropical forests (Foster et al. 2008, Kalacska et al. 2007, Sanchez-Azofeifa and Castro-Esau, 2004), as liana abundance has been demonstrated to be increasing as a consequence of global change (Phillips et al. 2002). Loss of habitat, as well as of free-standing forests could lead to significant economic strains on societies dependent on these forests. Furthermore, invasives can possibly pose an increased threat to human safety and property. In wetlands, the invasive *Phragmites communis* has been identified as producing more fuel for wildfires around human habitations than native species and

could hamper mosquito control (Marks et al. 1994).

Because of the importance of ecosystem resources to human society, it is expected that information that can be derived from HypsIRI on vegetation stress, invasive species, and other factors relevant to water and food quality and human health will prove valuable for detecting seasonal trends in ecosystems and natural resources that might result in significant declines in human well-being. Data from HypsIRI may provide the opportunity to develop management options to reduce impacts on human societies.

2.1.6 VQ6 - Surface and Shallow-Water Bottom Composition

The surface composition within exposed rock and soils of a wide range of materials is revealed in the solar reflected light spectroscopic signature from 400 to 2500 nm. Figure 6 shows the mapping of iron oxide, clay, carbonate, and other minerals in the desert region of Cuprite, Nevada. HypsIRI will be able to measure the surface composition of those areas with 75% or less vegetation cover, which occur seasonally over 30% of the land surface of the Earth. These HypsIRI measurements will enable new research opportunities for mineral and hydrocarbon resource investigation and emplacement understanding as called for in the Decadal Survey.

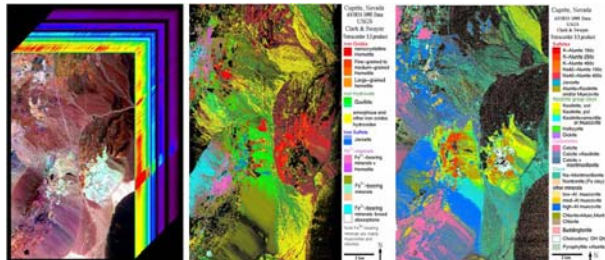


Figure 6: Map of surface rock and soil mineralogy at Cuprite, NV using solar reflected imaging spectroscopy measurements from 380 to 2500 nm. (Left: AVIRIS image cube, Center: 1 micron region minerals, Right: 2 micron region minerals) (Swayze et al. 2003)

With reasonable water clarity in the shallow-coastal and inland water regions, the bottom composition may be derived with imaging spectroscopy measurements in the region from 380 to 800 nm. A high fraction of the world's population lives in close proximity to these shallow water regions. Measurement by HypsIRI globally and seasonally of the composition and change of these environments will support understanding of their condition and associated resources and hazards. HypsIRI will be an important tool with which to assess coastal bathymetry as well as water quality, and the distribution of different benthic habitats such as coral reefs, algae, sand, and other geological components. The mission will help assess their relationship to land processes or disturbance, and how they change seasonally or over longer time scales.

Table 7: VQ6 Thematic Sub Questions

ID	Question
VQ6a	What is the distribution of the primary minerals and mineral groups on the exposed terrestrial surface?
VQ6b	What is the surface composition (sand, rock, mud, coral, algae, etc.) of the shallow-water regions of the Earth?
VQ6c	How can measurements of rock and soil composition be used to understand and mitigate hazards?

Understanding of the detailed surface mineralogy of rocks and soils allows improved understanding and potential mitigation of a range of natural and anthropogenic hazards. The HypsIRI VSWIR, like AVIRIS measurements, should help discover unmapped earthquake faults, natural and anthropogenic asbestos, acid mine drainage, expanding clay soils, and other surface hazard zones.

2.1.7 TQ1 - Volcanoes and Earthquakes

Volcanic eruptions and earthquakes yearly affect millions of lives, causing thousands of deaths, and billions of dollars in property damage. The restless earth provides

premonitory clues of impending disasters; thermal infrared images acquired by HypsIRI will allow us to monitor these transient thermal phenomena. Together with modeling, we will advance our capability to one day predict some natural disasters.

TIR data will allow us to measure changes in SO₂ emissions. Frequent coverage by HypsIRI will allow us to better monitor changes in tropospheric emissions, a capability not offered by existing moderate (~1 km) resolution instruments. Measuring SO₂ gives us information about a volcano’s plumbing system, and state of pressurization of sub-surface magma reservoirs. Multispectral TIR data will allow the identification of the mixture of ash, SO₂, and water vapor in eruptive plumes, providing improved hazards warnings for aviation safety. These capabilities are illustrated in Figure 7 (a and b).

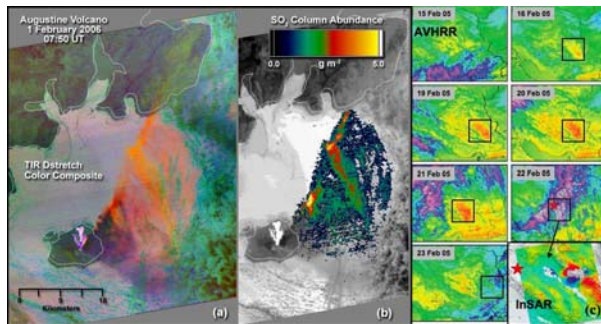


Figure 7: (a) ASTER night-time multispectral TIR image of Augustine Volcano showing hot pyroclastic flow deposits (bright in TIR) and eruption plume. Colors indicate spectral variations between materials entrained in plume. Magenta indicates mixtures of water droplets (steam) and silicate ash; red, yellow, and orange indicate mixtures of ash and SO₂. (b) SO₂ map derived from ASTER TIR data. (c) Thermal infrared anomaly associated with the M6.4 Zarand, Iran earthquake of Feb. 22, 2005, as derived from night-time Advanced Very High Resolution Radiometer (AVHRR) images recorded prior to this event (after Saraf et al. 2008). The excess IR intensity emitted from the epicentral region (presented in yellow-orange colors), and 10K temperature increase, are proposed to be indicators of the build-up of stress at the hypocenter. Lower right: Location of the epicenter (star) relative to the region of maximum uplift (red: 25 cm) and

subsidence (blue: 17 cm) from Interferometric Synthetic Aperture Radar (InSAR) data.

Changing high temperature phenomena include crater lakes, fumaroles, lava lakes, and dome growth. All of these volcanic phenomena are surface manifestations of dynamic sub-surface events occurring within a volcano’s plumbing system. Thermal observations of active lava flows allow effusion rates to be estimated, and these can be used to drive numerical models that forecast lava flow hazards. Thermal observations of dome growth provide clues to upward movement of magma within a volcano, and can also signal blockages of the main conduit. Together, these are possible precursors signaling potential eruptions. Adequate monitoring of these features requires HypsIRI’s high spatial resolution, frequent observational re-visits, and proper spectral resolution.

Table 8: TQ1 Thematic Subquestions

ID	Question
TQ1a	Do volcanoes signal impending eruptions through changes in surface temperature or gas emission rates, and are such changes unique to specific types of eruptions?
TQ1b	What do changes in the rate of lava effusion tell us about the maximum lengths that lava flows can attain, and the likely duration of lava flow-forming eruptions?
TQ1c	What do the transient thermal infrared anomalies that may precede earthquakes tell us about changes in the geophysical properties of the crust?
TQ1d	What are the characteristic dispersal patterns and residence times for volcanic ash clouds, and how long do such clouds remain a threat to aviation?

Research has suggested that some earthquakes may be preceded by thermal infrared anomalies observable from satellites (Ouzounov and Freund, 2004). The anomalies have been noted to precede earthquakes by days to weeks and were associated with earthquakes M>5 and focal depths generally no deeper than 35 km, occasionally down to 50 km in earthquakes related to subduction zones (Figure 7). There may be a relationship between the observed increased IR flux and

tectonic stress and/or processes in the atmosphere. Possible causes may be warming by greenhouse gas release over the epicentral region, changes in latent heat due to an increase of soil moisture and evaporation rate, or a quantum-mechanically driven process arising from the radiative decay of vibrationally excited states of atoms at the Earth surface that result from the recombination of electronic charge carriers stress-activated deep below, at hypocentral depth.

2.1.8 TQ2 - Wildfires

Both naturally occurring wildfire and biomass burning associated with human land-use activities have come to be recognized as having an important role in regional and global climate change. There consequently exists a substantial need for timely, global fire information acquired with satellite-based sensors. While some existing (e.g., MODIS) and planned (e.g., VIIRS) instruments currently provide (or will provide) such information at coarse spatial resolution (~ 1 km), the availability of robust, high-resolution fire information is extremely limited. While ASTER, for example, has yielded high resolution fire imagery (Figure 8), the sensor lacks the radiometric capabilities necessary to reliably map or characterize many flaming fires and most smoldering fires (Giglio et al. 2008).

In conjunction with its long-wave infrared channels, the specialized 4- μm channel of the HypsIRI thermal sensor will fill this void and permit reliable detection of fires at much higher spatial resolution than other current or planned sensors. The unprecedented sensitivity will enable the detection and characterization of small, often land-use-related fires that remain undetected by lower resolution sensors. The 4- μm channel will also permit direct retrieval of the instantaneous rate of energy released by the fire (i.e., fire radiative power - FRP), a

quantity of interest because it is proportional to the rate of fuel combustion and thus supplies useful (and otherwise inaccessible) information about both fire intensity and the rate of emission of trace gases and aerosols (Kaufman et al., 1998; Ichoku and Kaufman, 2005).

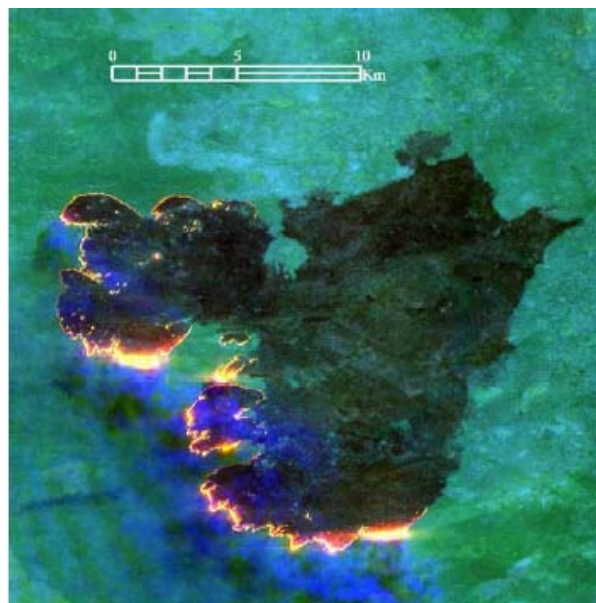


Figure 8: False-color ASTER image of a large fire in southern Africa, acquired on 17 August 2001, with the 2.4, 1.6, and 0.5 μm bands shown as red, green, and blue, respectively. With this color scheme the actively burning fire front appears yellow to red, previously-burned areas appear black, and unburned vegetation appears green. The specialized 4-micron channel of the HypsIRI thermal sensor will not exhibit the saturation-induced blooming apparent along the more intense portions of the flaming front in this scene.

While at present only the Terra and Aqua MODIS sensors, and more recently the Spinning Enhanced Visible and Infrared Imager (SEVIRI) on-board the Meteosat-8 geostationary satellite, can provide radiative power observations over very large spatial scales, they do so at comparatively coarse spatial resolution (1 km and 4.8 km, respectively). The larger fractional area of active burning within the higher resolution HypsIRI pixels will allow for more accurate FRP retrievals. In addition, HypsIRI will provide improved spatial and temporal

coverage than ASTER, needed for more detailed studies of fire regimes.

Table 9: TQ2 Thematic Subquestions

ID	Question
TQ2a	How are global fire regimes (fire location, type, frequency, and intensity) changing in response to changing climate and land use practices?
TQ2b	Is regional and local fire frequency changing?
TQ2c	What is the role of fire in global biogeochemical cycling, particularly trace gas emissions?
TQ2d	Are there regional feedbacks between fire and climate change?

2.1.9 TQ3 - Water Use and Availability

Given current trends in population growth and climate change, accurate monitoring of the Earth’s freshwater resources at field to global scales will become increasingly critical (DS 2007, WGA 2006, 2008). Land surface temperature (LST) is a valuable metric for estimating evapotranspiration (ET) and available water because varying soil moisture conditions yield distinctive thermal signatures: moisture deficiencies in the root zone lead to vegetation stress and elevated canopy temperatures, while depleted water in the soil surface layer causes the soil component of the scene to heat rapidly.

Several techniques have been developed to use TIR remote sensing data to generate accurate estimates of ET at multiple spatial scales (Figure 9; see also review by Kalma et al., 2008). Of particular utility are TIR data at “high” spatial resolution (100 m or finer), resolving natural and anthropogenic land-cover features important to local and regional water management: individual fields and irrigation pivots, riparian zones, canals and riverbeds, reservoirs, and other man-made hydrologic structures. With frequent revisit (< 7 days), high-resolution TIR imaging can provide accurate estimates of consumptive water use at the spatial scale of human management and time scale of vegetation growth, needed to monitor irrigation

withdrawals, estimate aquifer depletion, evaluate performance of irrigation systems, plan stream diversions for protection of endangered species, and estimate historical water use for negotiating water rights transfers (Allen et al. 2007).

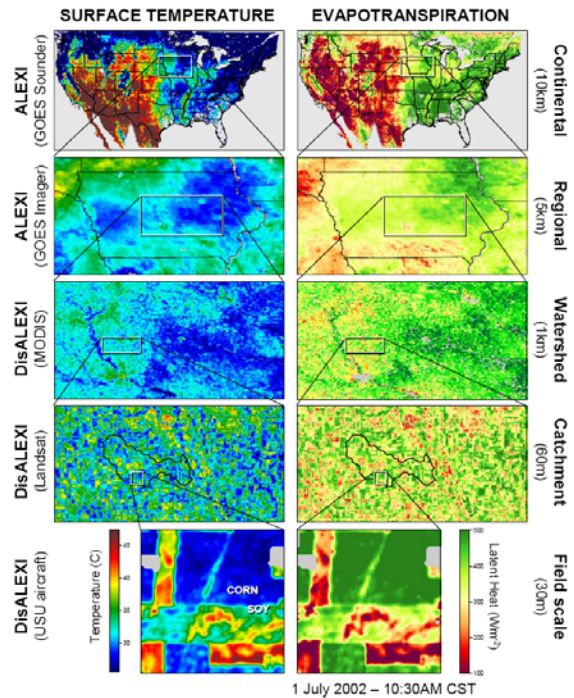


Figure 9: Multi-scale ET maps for 1 July 2002 produced with the ALEXI/DisALEXI surface energy balance models (Anderson, et al. 2007) using surface temperature data from aircraft (30-m resolution), Landsat-7 ETM+ (60m), Terra MODIS (1-km), GOES Imager (5-km) and GOES Sounder (10-km) instruments. The continental-scale ET map is a 14-day composite of clear-sky model estimates.

Climate change may lead to increased frequency of drought and flooding events, and accurate monitoring of extreme moisture conditions at high spatiotemporal resolution will be essential for effective targeted mitigation efforts. Comparisons between satellite-derived maps of actual evapotranspiration (ET) and potential evapotranspiration (PET) provide useful information about anomalously wet and dry conditions at the scale of imaging, without requiring any rainfall data (Anderson et al. 2007). While regional drought can be

reasonably assessed at low spatial resolution with data from ground-based precipitation networks, local information at sub-county and field scales is currently unavailable with uniform quality across the U.S., and can be very sparse in other parts of the world. Furthermore, satellite rainfall estimates are notoriously unreliable over many types of land surfaces. Thermal-based ET/PET maps provide a robust and high-resolution alternative to precipitation-based indices for global drought monitoring. For flood prediction, information about moisture conditions in narrow floodplain zones is critical. In many cases, these floodplains are not resolved at the MODIS TIR 1-km scale.

High-resolution maps of ET/PET, resolving individual fields, can also be used to remotely detect and quantify irrigated land area, an important input field required by land-surface models driving weather, water use, and climate models.

Table 10: TQ3 Thematic Subquestions

ID	Question
TQ3a	How is climate variability impacting the evaporative component of the global water cycle over natural and managed landscapes?
TQ3b	How can information about evapotranspiration and its relationship to land use/land-cover be used to facilitate better management of freshwater resources?
TQ3c	How can we improve early detection, mitigation, and impact assessment of droughts at local to global scales?
TQ3d	What is the current global irrigated acreage, how is it changing with time, and are these changes in a sustainable balance with regional water availability?
TQ3e	Can we increase food production in water-scarce agricultural regions while improving or sustaining water available for ecosystem function and other human uses?
TQ3f	How can improved accuracy in evapotranspiration imaging drive advances in science and understanding of the water cycle and hydrologic processes?

Local depressions in ET over irrigated land area, along with hyperspectral indicators of vegetation stress from HypspIRI, provide early signatures of increasing soil salinity that

can be used to map salinization onset at the global scale.

2.1.10 TQ4 - Human Health and Urbanization

Excess deaths occur during heat waves on days with higher-than-average temperatures and in places where summer temperatures vary more or where extreme heat is rare (e.g., Europe, northeastern U.S.). Exposure to excessive natural heat caused a reported 4,780 deaths during the period 1979-2002, and an additional 1,203 deaths had hyperthermia reported as a contributing factor (CDC, 2005). Urban heat islands (UHI) may increase heat-related impacts by raising air temperatures in cities approximately 1–6 °C over the surrounding suburban and rural areas due to absorption of heat by dark paved surfaces and buildings; lack of vegetation and trees; heat emitted from buildings, vehicles, and air conditioners; and reduced air flow around buildings (EPA, 2006). An example of the extent of the UHI in response to urban land covers is given in Figure 10. The figure shows Atlanta’s urban extent in gray (bottom) and corresponding thermal responses (top) as derived from Landsat TM data. Critical to understanding the extent, diurnal and energy balance characteristics of the UHI is having remote sensing data collected on a consistent basis at high spatial resolutions to enable modeling of the overall responses of the UHI to the spatial form of the city landscape for different urban environments around the world. Unfortunately, current satellite systems do not have adequate revisit times or multiple thermal spectral bands to provide the information needed to model UHI dynamics and its impact on humans and the adjacent environment. HypspIRI will have a return time, spectral characteristics, and nighttime viewing capabilities that will greatly enhance our knowledge of UHI’s form, spatial extent, and temporal characteristics for urban areas across the globe.

Additionally, HypsIRI will provide multispectral thermal IR at a high spatial resolution that is currently not available from other Earth-observation satellites for assessing how urbanization affects adjacent ecosystems.

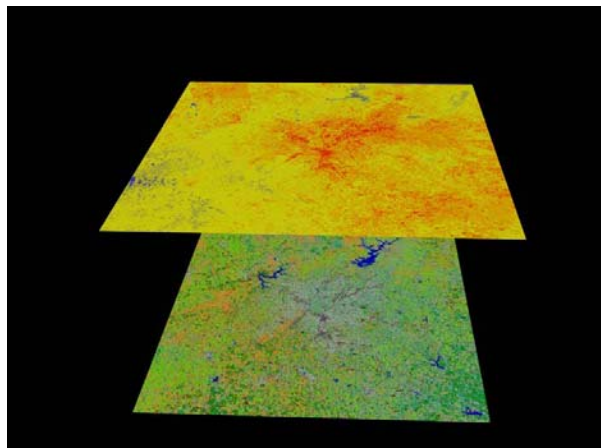


Figure 10: Landsat TM data of the Atlanta, GA metropolitan area showing urban extent in gray (bottom) and corresponding surface thermal responses (top) (Quattrochi et al. 2009)

Table 11: TQ4 Thematic Subquestions

ID	Question
TQ4a	How do changes in land cover and land use affect surface energy balance and the sustainability and productivity of natural and human ecosystems?
TQ4b	What are the dynamics, magnitude, and spatial form of the urban heat island (UHI) effect; how does it change from city to city; what are its temporal, diurnal, and nocturnal characteristics; and what are the regional impacts of the UHI on biophysical, climatic, and environmental processes?
TQ4c	How can the characteristics associated with environmentally related health effects, such as factors influencing heat stress on humans and surface temperatures that affect vector-borne and animal-borne diseases, be better resolved and measured?
TQ4d	How do horizontal and temporal scales of variation in heat flux and mixing relate to human health, human ecosystems, and urbanization?

For example, while urban and suburban landscapes covered about 45 million acres in the lower 48 states (about 2% of the land area) (John Heinz III Center for Science, Economics and the Environment, 2007), the amount of land area that is affected by urbanization continues to grow in the U.S. and around the world. The known affects of the

UHI on natural ecosystems concomitant with urban growth is extremely limited in the developed and developing world. HypsIRI will be able to provide data to assist in measuring and modeling thermal energy balance characteristics of biophysical systems that are, or will be, impacted by urban growth and the subsequent land cover/land use changes that accompany urbanization. HypsIRI will provide high spatial resolution TIR data with excellent revisit times to help us better model the affects of global urbanization on natural ecosystems on a continuous basis.

2.1.11 TQ5 - Earth Surface Composition and Change

The emitted energy from the exposed terrestrial surface of the Earth can be uniquely helpful in identifying rocks, minerals, and soils (Figure 11). Spaceborne measurements from HypsIRI will enable us to derive surface temperatures and emissivities for a variety of Earth's surfaces.

Table 12: TQ5 Thematic Subquestions

ID	Question
TQ5a	What is the spectrally observable mineralogy of the Earth's surface and how does this relate to geochemical and surficial processes?
TQ5b	What is the nature and extent of man-made disturbance of the Earth's surface associated with exploitation of renewable and non-renewable resources? How do these vary over time?
TQ5c	How do surface temperature anomalies relate to deeper thermal sources, such as hydrothermal systems, buried lava tubes, underground coal fires and engineering structures? How do changes in the surface temperatures relate to changing nature of the deep-seated heat source?
TQ5d	What is the spatial distribution pattern of Earth surface temperatures and emissivities, and how do these influence the Earth's heat budget?
TQ5e	What are the water surface-temperature distributions in coastal, ocean, and inland water bodies; how do they change; and how do they influence aquatic ecosystems?

Emissivity variations are particularly useful for mapping structures and areas of mineralization. For example different Si-O bonded structures vary in their interaction

with energy in the thermal infrared region (8-12 μm). Framework silicates, such as quartz and feldspar, show minimum emissivity at shorter wavelengths (8.5 μm). Silicates having sheet, chain, and isolated-tetrahedral structure show minimum emissivity at progressively longer wavelengths (Hunt 1980). This important property helps to discriminate the felsic and mafic rock composition remotely.

Between day and night, Earth surface composition remains the same, but temperature changes. Daytime and nighttime HypsIRI images will be used to map temperatures and extract further information about properties of the surface such as thermal inertia.

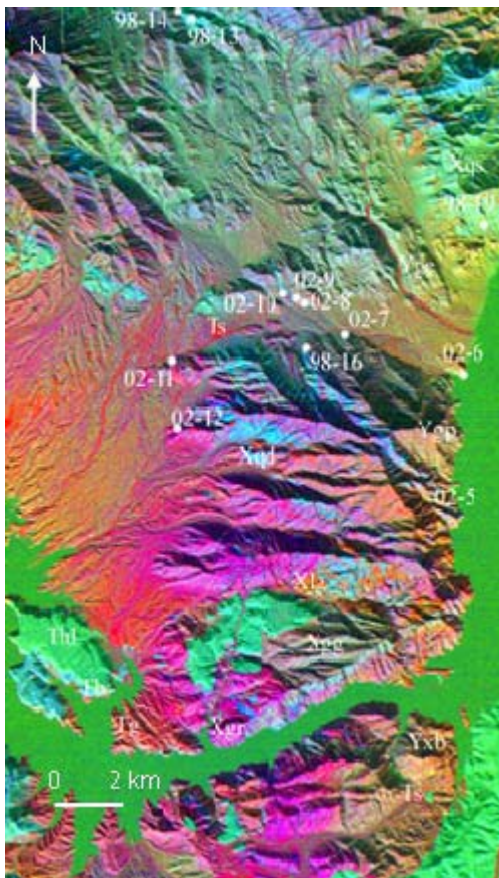


Figure 11: HypsIRI-like image for the area around Lake Mead, Nevada. Three TIR bands are processed with a decorrelation stretch algorithm and displayed in red, green and blue, respectively (from Hook et al. 2005).

Buried sources of high temperatures, (such as lava tubes, underground fires in coal seams and high temperature rocks) cause hot spots on the Earth's surface. The temperature profile across these hot spots holds clues to the depth of the heat source. Assuming that heat is conducting linearly in a semi-infinite medium, numerical modeling reveals that the shallower sources cause distinct thermal profiles, while deeper sources cause broad and more diffuse thermal profiles (Berthelote et al. 2008). HypsIRI data will be used to map temperature anomalies, extract thermal profiles, and numerically derive the depth of the hot sources.

2.1.12 CQ1 - Coastal, Ocean, and Inland-Aquatic Environments

The oceans and inland-aquatic environments, including ice, play a critical role in Earth's climate through the hydrological cycle, and in supporting life and sustaining biodiversity on Earth. The oceans cover more than 70% of the Earth's surface, and about half of the globe's primary productivity occurs within them. More than \$1 trillion of the U.S.'s annual gross domestic product (GDP) is generated within the relatively narrow strip of land immediately adjacent to the coast (USCOP, 2004). Services provided by coastal ecosystems include purification of water through nutrient recycling, sediment storage, shoreline protection, and supplying habitat and food for migratory and resident animals, as well as humans. Aquatic habitats provide important biological and mineral resources for the pharmaceutical, oil, gas, and sand and gravel industries; and they support key tourism, fisheries, and maritime operations, including housing our ports. Yet we know little about the variety of coastal habitats and resources in them. Climate change, land subsidence, aerosol production, and sea-level rise complicate our understanding of the processes

of pollution, development, and structures that alter sediment flow.

Hyperspectral and high spatial resolution data from HypSPIRI will allow for better separation of phytoplankton pigments and phytoplankton FGs such as carbon exporters (diatoms), nitrogen fixers (*Trichodesmium* sp.), calcium carbonate producers (coccolithophores), and the microbial loop organisms (*Prochlorococcus* sp.). More spectral information helps improve the accuracy and diversity in retrievals of absorption and backscattering coefficients as well as other environmental properties through inversion algorithms, including effective discrimination of biogeochemical constituents of the water and seafloor (e.g., colored dissolved organic matter [CDOM], phytoplankton concentration and composition, suspended sediments, bottom type) and physical properties (e.g., temperature, bathymetry, light attenuation) (GEO 2007). HypSPIRI will enable better derivation of chlorophyll retrievals where other materials also change the color of water, such as inland and coastal and estuarine areas (Figure 12, Bidigare et al. 1989; Goodin et al. 1993; Kutser et al. 2006; Craig et al. 2006; Hu et al. 2005).

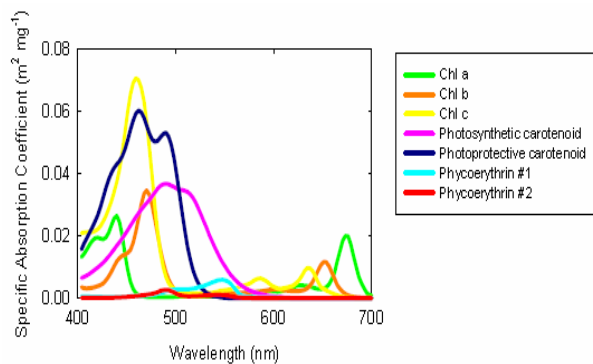


Figure 12: Weight-specific absorption coefficients ($m^2\ mg^{-1}$) derived for the major pigment types found in marine phytoplankton (from Bidigare et al. 1989).

HypSPIRI also will help identify coral reef habitat with assessments of other bottom types (Hochberg and Atkinson, 2006, 2008), floating macroalgae (e.g., *Sargassum*; Gower

et al., 2006), the water column proper (Lee et al., 2007), and aquatic ice communities. HypSPIRI will be a critical tool to study habitats for marine life such as fish, turtles, and other marine organisms (GEO 2007), and to develop better coastal bathymetric charts. The infrared channels will help characterize physical conditions by measuring sea-surface temperature changes over small scales. And the potential for lower resolution global ocean images will allow accurate characterization of key ocean conditions away from land and coastal zones.

The data will augment our capabilities for atmospheric correction over turbid waters with bands between 670 nm and the short-wave infrared (SWIR) (Hu et al. 2000; Wang and Shi 2005), and allow the study of radiative properties of clouds, aerosols, snow, and ice over aquatic systems.

Table 13: CQ1 Thematic Subquestions

ID	Question
CQ1a	What are the feedbacks between climate and change in habitat structure, biogeochemical cycling, biodiversity, and ecosystem productivity of aquatic habitats, including ice-covered habitats? What are the ecological linkages of landscape-scale ocean-atmosphere interactions including the hydrologic cycle, aerosol production and transport, and cloud radiative forcing?
CQ1b	How are small-scale processes in water column, shallow benthic, and ice-covered habitats related to changes in functional community types (including harmful algal blooms and vector-borne diseases), productivity, and biogeochemical cycling (including material fluxes and water quality) at local scales?
CQ1c	How can these observations be used to guide the wise management of living marine and other aquatic resources?

The mission will contribute significantly to, and benefit from, efforts conducted through the National Science Foundation's ORION program, the coastal components of the Integrated Ocean Observing System (IOOS), the Climate Change Science Program (CCSP), and the Global Earth Observation System of Systems (GEOSS). The higher spatial and spectral

resolution will be of particular utility in coastal resource management applications.

2.1.13 CQ2 - Wildfires

While the HypsIRI thermal sensor will provide a greatly improved capability for detecting fires and characterizing their intensity (see TQ2), coupling the multispectral thermal data with hyperspectral VSWIR observations will significantly improve our understanding of the coupling between fires and vegetation and the associated trace-gas emissions. For example, HypsIRI's hyperspectral observations will allow precise mapping of vegetation at the level of individual species (e.g., Roberts et al. 1998). Furthermore, HypsIRI will permit reliable retrieval of fuel moisture (e.g., Serrano et al. 2002), a critically important factor that dictates a host of fire-related variables including fire danger, fire spread rate, and combustion completeness.

Table 14: CQ2 Thematic Subquestions

ID	Question
CQ2a	How do the timing, temperature, and frequency of fires affect long-term ecosystem health?
CQ2b	How do vegetation composition and fire temperature impact trace-gas emissions?
CQ2c	How do fires in coastal biomes affect terrestrial biogeochemical fluxes into estuarine and coastal waters and what is the subsequent biological response?
CQ2d	What are the feedbacks between fire temperature and frequency and vegetation composition and recovery?
CQ2e	How does vegetation composition influence wildfire severity?
CQ2f	On a watershed scale, what is the relationship of vegetation cover, clay-rich soils, and slope to frequency of debris flows?

In addition to improved fuel characterization, HypsIRI's hyperspectral observations will also provide detailed snapshots of the combustion process itself. Green (1996), for example, used ~150 channels of the hyperspectral AVIRIS to observe active fires in Brazil, and applied a two-temperature fire model to estimate average fire temperature

and sub-pixel fire area at 20-m spatial resolution. An improved endmember-library approach was subsequently developed by Dennison et al. (2006), allowing the retrieval of fire temperature and sub-pixel area, and background land cover (Figure 13).

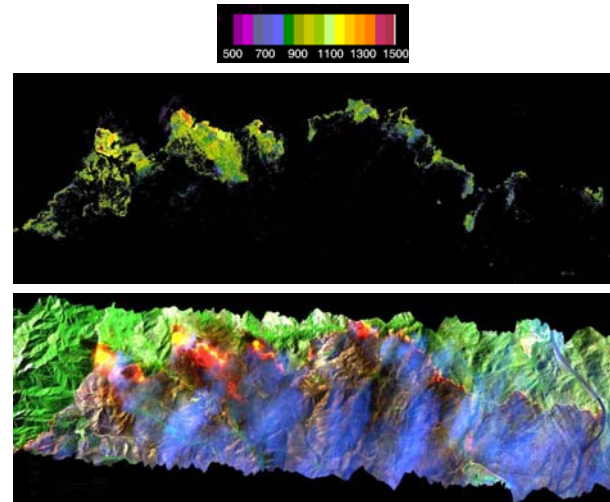


Figure 13: Top panel: Retrieved fire temperature (in kelvins) from an AVIRIS scene spanning a portion of the large Southern California Fire Complex from October 2003. Bottom panel: False color SWIR-NIR-red composite of the original AVIRIS scene. (Dennison et al. 2006).

Such information is necessary for producing accurate estimates of trace-gas fire emissions since the emission factor for a given species depends on the relative proportion of the flaming and smoldering stages.

2.1.14 CQ3 - Volcanoes

The replenishment of shallow magma reservoirs can herald a) the onset of an eruption at a previously inactive volcanic system or, b) significant changes in eruptive behavior at already active volcanoes. This magma brings with it volatiles (such as SO₂) and thermal energy, both of which are ultimately released into the atmosphere. Satellite measurements of the heat and gas emitted by a volcano allow the mass of magma required to sustain the observed fluxes to be quantified (Francis et al., 1993). Determining magma budgets in this way provides information about how ascending

magma is partitioned between the surface (i.e., erupted) and the subsurface (i.e., intruded) as it circulates within the conduit (Figure 14).

Combined observations of cooling and degassing also provide insights into shallow-conduit processes that generate cyclic overpressures at silicic dome-forming volcanoes. Such cyclicity is increasingly recognized as characteristic of these dangerous volcanoes. In short, a permeable shallow conduit allows gas to escape freely, resulting in an elevated gas flux from the dome and an abundance of high temperature cracks on its surface.

Degassing-induced changes in permeability cause the upper conduit to seal, reducing gas flow (and, as a result, the abundance of hot fumaroles), and generating overpressures that result in an explosive eruption, after which the cycle begins anew (Oppenheimer *et al.*, 1993; Matthews *et al.*, 1997).



Figure 14: Hyperion SWIR image of Erta Ale volcano, Ethiopia, showing the active lava lake. Hyperspectral VSWIR and TIR data will allow the cooling rate and gas flux from the lake to be determined. Right: model of cooling and degassing-driven magma convection within an open system volcano. The heat and gas flux data are important boundary conditions for determining magma ascent dynamics and circulation within the conduit (adapted from Frances *et al.* 1993).

Space-based monitoring of dome-surface temperatures and degassing rates using VSWIR and TIR data will allow this cycle, and the transition between effusive and explosive phases, to be monitored, and may constitute a robust eruption precursor.

The surface temperature of an active lava flow controls the rate at which it cools and solidifies, and hence the distance from the vent at which it comes to a halt and the hazard it represents.

Table 15: CQ3 Thematic Subquestions

ID	Question
CQ3a	What do comparisons of thermal flux and SO ₂ emission rates tell us about the volcanic mass fluxes and the dynamics of magma ascent?
CQ3b	Does pressurization of the shallow conduit produce periodic variations in SO ₂ flux and lava-dome surface temperature patterns that may act as precursors to explosive eruptions?
CQ3c	Can measurements of the rate at which lava flows cool allow us to improve forecasts of lava flow hazards?
CQ3d	Do the temperature and composition of volcanic crater lakes change prior to eruptions?
CQ3e	Do changes in the health and extent of vegetation cover indicate changes in the release of heat, gas, and ash from crater regions?

Realistic parameterization of numerical lava-flow models relies on surface temperature data as a boundary condition for determining the rheology of the lava and its ability to flow. Remotely sensed data covering both the SWIR and TIR are necessary to constrain the non-linear mixture models required for the accurate determination of flow surface temperature (which is heterogeneous at the subpixel scale) and lava cooling rates from orbit (Wright and Flynn, 2003).

Precursory earthquakes and changes in temperature and element fluxes into volcanic crater lakes can increase lake turbidity, biological productivity, and the scattering properties of the water (Delmelle and Bernard, 2000). All have been known to result in changes in lake color. A combination of VSWIR and TIR data will allow us to monitor all aspects of volcanic crater lake variability (color and temperature) for signs of eruption.

2.1.15 CQ4 - Ecosystem Function and Diversity

Climate has a strong influence on the distribution of plant and animal species and associated biodiversity (MacDonald 2002). Numerous physiological and biochemical feedbacks exist between climate and ecosystems, where changing climate impacts the presence and functioning of organisms, which in turn modifies regional climate, either enhancing or buffering such changes. A good example of such a feedback is the impact of increased temperatures at higher latitudes, leading to northward expansion of boreal forest into tundra, or the migration of marine species from lower to higher latitudes. The migration of boreal forests enhanced surface temperatures due to lower conifer albedo (Hansen 2008), alterations in surface carbon and water fluxes (Smith et al. 2004), and changes in the incidence of fire (Kasischke and Stocks, 2000). One of the most pronounced indications of these high latitude changes has been an increase in the length of the growing season, readily observed from long-term satellite observations (Myneni et al., 1997). Similarly increased winter temperatures at higher elevations and latitudes facilitate the spread of forest pests, including bark beetles, leading to large-scale increases in forest mortality (Berg et al. 2006). Expansion of invasive plant species throughout the American southwest, such as cheat grass, illustrates numerous feedbacks between an organism and surface composition, modifying wildfire fuels, soil biogeochemistry, surface albedo and soil water balance, promoting further expansion of the invader (Noujdina and Ustin 2008: Figure 15).

Numerous research questions remain difficult to resolve due to limitations in current remote sensing capabilities. For example, changes in the amplitude of the normalized difference vegetation index (NDVI) at high latitudes attributed to enhanced growth could

also be explained by a change in ecosystems from conifer dominated to early successional aspen. No current sensor can simultaneously retrieve canopy temperature and quantify physiological or compositional changes in response to stress.

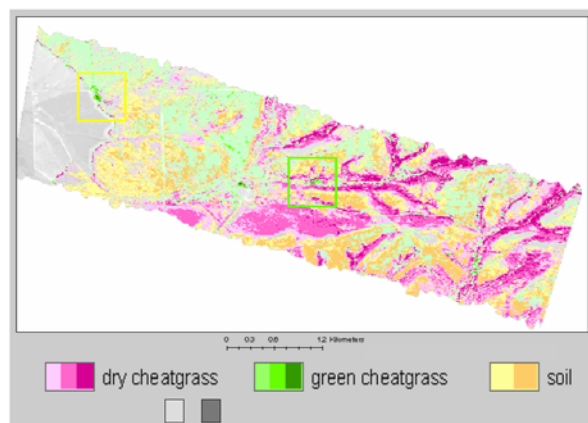


Figure 15: Map of *Bromus tectorum* (Cheatgrass) generated using imaging spectrometry. Cheatgrass spreads through a combination of disturbance and strategic use of soil moisture. It alters fire regimes, promoting its spread while early germination of Cheatgrass enables it to produce seed in advance of native plants while reducing available water for competitors. (Noujdina and Ustin 2008).

Together, the suite of instruments on HypsIRI should significantly improve our ability to partition the surface energy budget between latent and sensible heat and between soil and canopy contributions, combining hyperspectral characterizations of plant type, canopy structure, and surface residue cover with high spatiotemporal resolution measurements of surface temperature. Because access to water is a critical driver of plant species competition, HypsIRI will provide a unique opportunity to study in detail the response of plant populations to changes in moisture availability deduced from the TIR bands. HypsIRI will also provide improved measures of plant physiological function through simultaneous estimates of surface temperature and plant biochemistry, improved estimates of surface biophysical properties (e.g., albedo, crown mortality) and energy

balance, and improved discrimination of plant species and functional types.

The mission represents an important research tool to examine the changes in coastal and inland ecosystems as snow- and glacier-melting patterns change, affecting aquatic communities that receive the discharge.

Table 16: CQ4 Thematic Subquestions

ID	Question
CQ4a	How can we enhance phenological & stress characterization through synergy between reflective and emitted radiation with higher frequency temporal sampling?
CQ4b	How is energy partitioned between latent and sensible heat fluxes as a function of different plant types and fractional cover, and how does this impact hydrology?
CQ4c	How is physiological function affecting water and carbon exchange expressed at the ecosystem scale, especially seasonal down-regulation due to environmental stress factors?
CQ4d	What is the vegetation phenological response to seasonal and interannual changes in temperature and moisture due to climate change and how does this response vary at the community/species level?
CQ4e	What are the feedbacks between changes in canopy composition, mortality, and retrieved canopy temperatures resulting from disturbances (e.g., disease, moisture deficiency, insect attack, fire, land degradation, fragmentation) in natural and managed ecosystems?
CQ4f	How do climate-induced temperature and moisture changes impact the distribution and spread of invasive and native species?

2.1.16 CQ5 - Land Surface Composition and Change

Rocks, soils, and minerals exposed on the terrestrial surface of the Earth reflect and emit energy that can be measured from space. Spaceborne measurements from HypsIRI will obtain the surface reflectance and surface emissivity of the Earth's surface. The reflectance and emissivity information from rocks, soils, and vegetation exhibits diagnostic features at various wavelengths that provide a means for their remote discrimination and

identification. These features are caused by the interaction of electromagnetic energy with the atoms and molecules that make up the material. For example different Si-O bonded structures vary in their interaction with thermal infrared light (8–12 μm). Collectively, the Si-O spectral features in the thermal infrared are referred to as the reststrahlen band. Reststrahlen bands are diagnostic of silicate minerals such as quartz and can be used to map quartz and silica-rich rocks (Figure 16).

Molecular vibrational processes of Al-O-H, CO_3 , MgO-H, and H-O-H produce absorption features in the 2.0 to 2.5 μm region that can be used to map clay, carbonate, amphiboles, and evaporite minerals. (Hunt, 1977). Ferrous and ferric iron, typical in many rocks and soils, has electronic optical absorption features in the 0.5 to 1.85 μm region. Thus, HypsIRI VNIR, SWIR, and TIR data will be used to map the composition of the surface of the Earth.

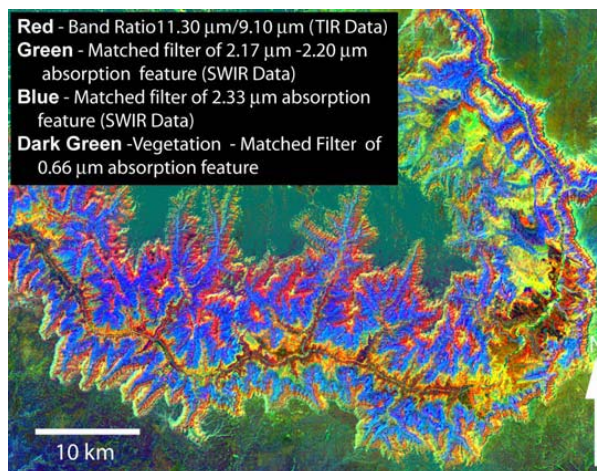


Figure 16: False color composite HypsIRI simulated image of Grand Canyon, Arizona derived from TIR (red band - quartz-rich rocks), SWIR (green band - clay and muscovite-rich rocks; blue band - carbonate-rich rocks), and VNIR (dark green - green vegetation) data.

Hydrothermal systems have produced many of the world's economic deposits of metallic ores. Different types of hydrothermal systems

produce different types of minerals and mineral distributions. For example, porphyry copper hydrothermal systems produce elliptical to circular halos of altered minerals such as kaolinite, alunite, sericite, and quartz (Lowell and Guilbert, 1970).

Table 17: CQ5 Thematic Subquestions

ID	Question
CQ5a	How does the surface mineralogy and soil composition relate to the plant physiology and function on the terrestrial surface of the Earth?
CQ5b	How is the composition of exposed terrestrial surface responding to anthropogenic and non anthropogenic drivers (desertification, weathering, and disturbance [e.g., logging, mining])?
CQ5c	How do types and distributions of altered rocks define regional trends in hydrothermal fluid flow for magmatic arcs and tectonic basins, better define hydrothermal deposit models, and assist in the discovery of new economic deposits?
CQ5d	How do regional trends of minerals and shale thermal maturity within basins better define depositional models and assist in the discovery of new hydrocarbon reserves?
CQ5e	How do changes in land composition affect coastal and inland aquatic ecosystems?

In addition, minerals such as alunite and minerals produced from the weathering of pyritic waste such as jarosite produce acid runoff (Crowley et al. 2001).

Thus, HypsIRI data will have important implications for the mapping and study of hydrothermal systems, and looking for changes related to anthropogenic and non-anthropogenic drivers such as the environmental monitoring of acid runoff from undisturbed hydrothermal deposits and from active and abandoned mines.

2.1.17 CQ6 - Human Health and Urbanization

Over the last 50 years, the world has witnessed a dramatic increase in its urban population. The expansion of cities, both in population and aerial extent, appears to be a relentless process whereby the world's urban population will rise more than 61% by 2030 (UNIS, 2004). Associated with this rapid rise

in worldwide urbanization is a concomitant impact on the local, regional, and even global environment, along with an exacerbation in health problems. HypsIRI measurements will be used to detect, observe, and measure changes in urban growth patterns and provide data that can elucidate how urbanization impacts the environment and human health.

Table 18: CQ6 Thematic Subquestions

ID	Question
CQ6a	How do land-surface characteristics (such as vegetation state, temperature, and land cover composition) affect, and how are they affected by, heat stress and drought, vector-borne diseases, and zoonotic diseases?
CQ6b	What changes can be observed and measured in emissivities of urban surfaces, and how do emissivities change for different cities around the world as they impact the urban heat island and associated land-atmosphere energy-balance characteristics?
CQ6c	How does the distribution of urban and peri-urban impervious surfaces affect regional energy-balance fluxes, hydrologic processes, and biogeochemical fluxes; and what is the response of ecosystems to these changes?

HypsIRI data can be used to evaluate multiple factors affecting human health, such as those contributing to environmental health hazards and contagious and infectious diseases. Moreover, HypsIRI data in combination with other data sources can provide spatial information on environmental conditions for understanding distributions of water-borne disease, air quality, soil, and vegetation as they influence community health and livestock.

Because of its enhanced hyperspectral capabilities in the VSWIR bandwidths and its multiple channels in the TIR, HypsIRI will provide much better data to improve modeling of urban characteristics around the world. One of the issues that has been problematic in the past is retrieving accurate measurements of temperature, albedo, and emissivity for specific surfaces across the complex and heterogeneous urban landscape. Because of its bandwidth design, HypsIRI will facilitate

the derivation of temperature, albedo, and emissivities for surfaces that are the “building blocks” of the urban environment. Figure 17 provides an example of detailed temperature and albedo measurements of the urban surface for Atlanta, Georgia. These data were derived from a multispectral VSWIR and TIR (9–12 μm) aircraft sensor.

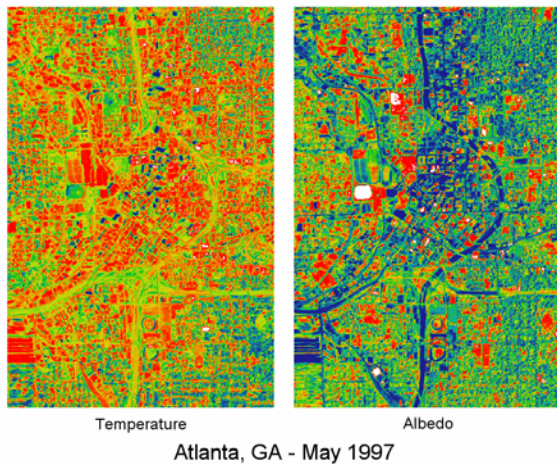


Figure 17: Temperature and albedo measurements for the Atlanta, GA central business district as derived from multispectral aircraft data (Quattrochi et al. 2009)

HyspIRI will expand this kind of information by providing hyperspectral data at regular intervals to better characterize the visible, near-IR, and thermal attributes of urban-specific surfaces with more precision to enable better modeling of urban energy balance characteristics, including emissivities.

HyspIRI will also fill the role of the low Earth orbit (LEO) "Special Event Imager" promoted by the NRC Panel on Human Health and Security, providing multispectral thermal infrared image data with a spatial resolution of 60 m and a revisit cycle of 5 days at the Equator. For mid- to high-latitude regions, such as the United States, the revisit times will be shorter than 5 days.

2.2 Science Traceability Matrixes

The STMs were developed by determining the initial measurement requirements for each of the science subquestions and overarching questions (see Table 2 – Table 18). All of the individual measurement requirements were grouped together to produce a set of science traceability matrixes that were subsequently used to determine the system-level measurement requirements. This was done in an iterative manner as outlined in Figure 18. At the workshop, breakout sessions reviewed each science-traceability matrix for an associated overarching question. Any updates made are reflected in the science-traceability matrixes presented in Appendix D.

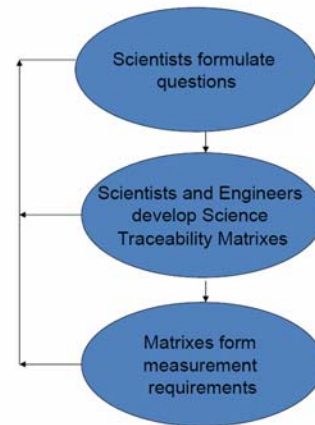


Figure 18: Process for developing the Science-Traceability Matrixes.

3 Measurement Requirements

The STMs helped determine the system-level requirements for the HypSIRI instruments. The system-level requirements for the VSWIR and TIR instruments are presented in Table 19 and Table 20, respectively.

3.1 VSWIR Instrument

The VSWIR instrument will acquire data between 380 and 2500 nm in 10-nm contiguous bands. The position of these bands will be known to 0.5 nm. The instrument performance was modeled for several different input radiances, and these are shown in Figure 19 for several different benchmark radiances. The instrument will have low polarization sensitivity and low scattered light. One of the most challenging measurement conditions is open water where the signal from the water is very small. In addition, open water can produce sunglint under certain viewing geometries, and this can cause instrument saturation. The effect of sunglint is minimized by pointing the instrument 4 degrees in the backscatter direction. The nominal data collection scenario involves observing the land and coastal zone to a depth of < 50 m at full spatial and spectral resolution and transmitting these data to the ground.

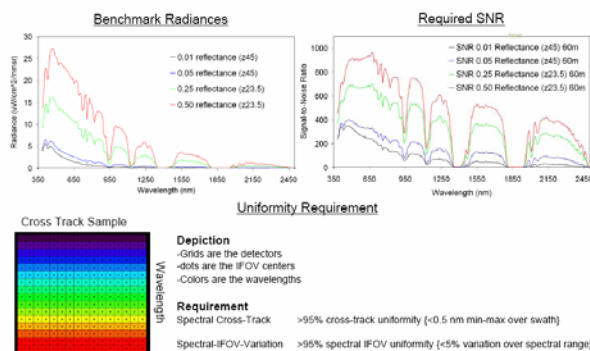


Figure 19: HypSIRI-VSWIR Key Signal-to-Noise and Uniformity Requirements.

Over the open ocean, data will be averaged to a spatial resolution of 1 km and be

transmitted to the ground. All data will be quantized at 14 bits. The instrument will have swath width of 145 km with a pixel spatial resolution of 60 m resulting in a temporal revisit of 19 days at the Equator. The nominal overpass time is 11 a.m., but this may be adjusted by as much as ± 30 minutes to minimize the effects of sunglint.

The absolute radiometric accuracy requirement is greater than 95%, and this will be maintained by using an onboard calibrator as well as monthly lunar views and periodic surface calibration experiments.

3.2 TIR Instrument

The TIR instrument will acquire data in eight spectral bands, seven of these are located in the thermal infrared part of the spectrum between 7 and 13 μm , and the remaining band is located in the mid infrared part of the electromagnetic spectrum around 4 μm . The center position and width of each band is given in Table 20. The exact spectral location of each band was based on the measurement requirements identified in the science-traceability matrices, which included recognition that other sensors were acquiring related data such as ASTER and MODIS. HypSIRI will contribute to maintaining a long time series of these measurements. For example the positions of three of the TIR bands closely match the first three thermal bands of ASTER, and the positions of two of the TIR bands of MODIS typically used for split-window type applications (ASTER bands 12–14 and MODIS bands 31 and 32).

A key science objective for the TIR instrument is the study of hot targets (volcanoes and wildfires), so the saturation temperature for the 4- μm channel is set high (1400 K) whereas the saturation temperatures for the thermal infrared channels are set at 400 K.

Table 19: VSWIR Measurement Characteristics

Visible Shortwave Infrared Measurement Characteristics	
Spectral	
Range	380 to 2500 nm in the solar reflected spectrum
Sampling	10 nm {uniform over range}
Response	<10 nm (full-width-at-half-maximum) {uniform over range}
Accuracy	<0.5 nm
Radiometric	
Range & Sampling	0 to $1.5 \times$ max benchmark radiance, 14 bits measured
Accuracy and stability	>95% absolute radiometric, 98% on-orbit reflectance, 99.5%
Precision (SNR)	See spectral plots at benchmark radiances
Linearity	>99% characterized to 0.1 %
Polarization	<2% sensitivity, characterized to 0.5 %
Scattered Light	<1:200 characterized to 0.1%
Spatial	
Range	>145 km (12 degrees at ~700 km altitude)
Cross-Track Samples	>2400
Sampling	60 m
Response	60 m sampling (FWHM)
Uniformity	
Spectral Cross-Track	>95% cross-track uniformity {<0.5 nm min-max over swath}
Spectral-IFOV-Variation	>95% spectral IFOV uniformity {<5% variation over spectral range}
Temporal	
Orbit Crossing	11 am sun synchronous descending
Global Land Coast Repeat	19 days at equator
Rapid Response Revisit	3 days (cross-track pointing)
Sunlint Avoidance	
Cross Track Pointing	4 degrees in backscatter direction
On Orbit Calibration	
Lunar View	1 per month {radiometric}
Solar Cover Views	1 per week {radiometric}
Surface Cal Experiments	3 per year {spectral & radiometric}
Data Collection	
Land Coverage	Land surface above sea level excluding ice sheets
Water Coverage	Coastal zone –50 m and shallower
Solar Elevation	20 degrees or greater
Open Ocean	Averaged to 1-km spatial sampling
Compression	3:1 lossless

Table 20: TIR Measurement Characteristics

Thermal Infrared Measurement Characteristics	
Spectral	
Bands (8) μm	3.98 μm , 7.35 μm , 8.28 μm , 8.63 μm , 9.07 μm , 10.53 μm , 11.33 μm , 12.05 μm
Bandwidth	0.084 μm , 0.32 μm , 0.34 μm , 0.35 μm , 0.36 μm , 0.54 μm , 0.54 μm , 0.52 μm
Accuracy	<0.01 μm
Radiometric	
Range	Bands 2–8 = 200 K – 400 K; Band 1= 1400 K
Resolution	< 0.05 K, linear quantization to 14 bits
Accuracy	< 0.5 K 3-sigma at 250 K
Precision (NEdT)	< 0.2 K
Linearity	>99% characterized to 0.1 %
Spatial	
IFOV	60 m
MTF	>0.65 at FNy
Scan Type	Push-Whisk
Swath Width	600 km ($\pm 25.5^\circ$ at 623 km altitude)
Cross Track Samples	10,000
Swath Length	15.4 km (± 0.7 degrees at 623 km altitude)
Down Track Samples	256
Band to Band Co-Registration	0.2 pixels (12 m)
Pointing Knowledge	1.5 arcsec (0.1 pixels)
Temporal	
Orbit Crossing	11 a.m. Sun synchronous descending
Global Land Repeat	5 days at Equator
On Orbit Calibration	
Lunar views	1 per month {radiometric}
Blackbody views	1 per scan {radiometric}
Deep Space views	1 per scan {radiometric}
Surface Cal Experiments	2 (day/night) every 5 days {radiometric}
Spectral Surface Cal Experiments	1 per year
Data Collection	
Time Coverage	Day and Night
Land Coverage	Land surface above sea level
Water Coverage	Coastal zone minus 50 m and shallower
Open Ocean	Averaged to 1-km spatial sampling
Compression	2:1 lossless

The temperature resolution of the thermal channels is much finer than the mid-infrared channel, which (due to its high saturation temperature) will not detect a strong signal until the target is above typical terrestrial temperatures. All the TIR channels are quantized at 14 bits.

The TIR instrument will have a swath width of 600 km with a pixel spatial resolution of 60 m resulting in a temporal revisit of 5 days at the equator. The instrument will be on both day and night, and it will acquire data over the entire surface of the Earth. Like the VSWIR, the TIR instrument will acquire full spatial resolution data over the land and coastal oceans (to a depth of < 50 m), but over the open oceans the data will be averaged to a

spatial resolution of 1 km. The large swath width of the TIR will enable multiple revisits of any spot on the Earth every week (at least 1 day view and 1 night view). This is necessary to enable monitoring of dynamic or cyclical events such as volcanic hotspots or crop stress associated with water availability.

The radiometric accuracy and precision of the instrument are 0.5 K and 0.2 K, respectively. This radiometric accuracy will be ensured by using an on-board blackbody and view to space included as part of every row of pixels (60 m \times 600 km) observed on the ground. There will also be periodic surface validation experiments and monthly lunar views.

4 Mission Concept

The HypsIRI satellite will be put in a Sun synchronous, low Earth orbit. The overpass time is expected to be 11:00 a.m. \pm 30 minutes. As noted in Table 19 and Table 20, the VSWIR has a 19-day revisit at the Equator, and the TIR has a 5-day revisit at the Equator. Since the TIR is on both day and night, it acquires 1 daytime image every 5 days and 1 nighttime image every 5 days. The current altitude for the spacecraft is 626 km at the Equator.

The number of acquisitions for different parts of the Earth in a 19-day cycle is shown in Figure 20. The figure is color-coded such that areas that are green meet the requirement and areas that are light blue, dark blue, and black exceed the requirement. Examination of the TIR map indicates that as one moves poleward the number of acquisitions exceeds the requirements with daily coverage at the poles. No data will be acquired poleward of 83° N and 83° S in the VSWIR since this is an inclined orbit. Similarly no data are acquired poleward of 85° N and 85° S in the TIR. The slightly more poleward extension of the TIR instrument is due to its larger swath width.

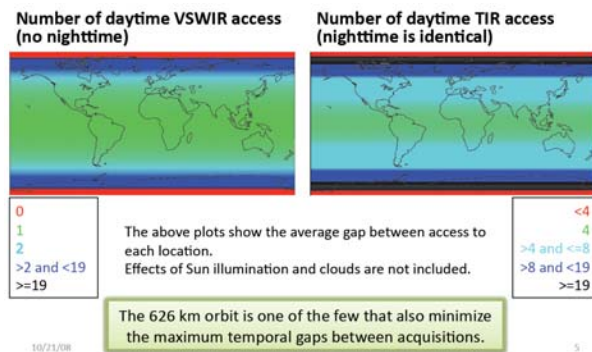


Figure 20: Number of image acquisitions in 19 days.

VSWIR data acquisitions are also limited by the maximum Sun elevation angle with no data being acquired when the Sun elevation angle is less than 20 degrees (Figure 21).

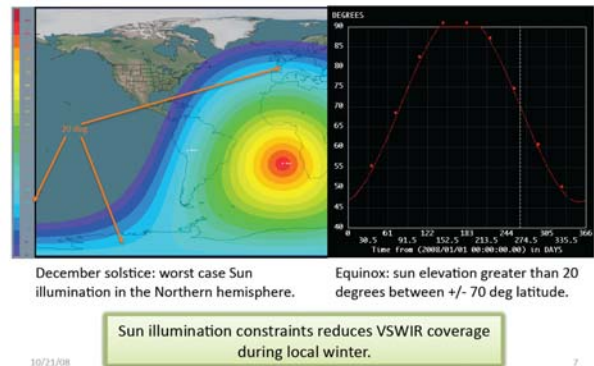


Figure 21: Illustration of the Sun illumination at the winter solstice.

The acquisition scenario for the HypsIRI mission is driven by target maps, with pre-defined maps controlling the acquisition. As noted earlier, the instruments are always on; however, they store data at either high-resolution mode (maximum spatial and spectral) or low-resolution mode. High-resolution mode data are acquired over the land and coastal waters shallower than 50 m. Low-resolution mode data are acquired over the rest of the oceans. The low resolution mode returns data are averaged or sub-sampled to 1 km. This target-map-driven strategy combined with high- and low-resolution modes minimizes the cost of mission operations allowing the instruments to acquire data in a near-autonomous fashion.

The satellite also includes an Intelligent Data Payload (IDP) with a direct broadcast capability that taps into the data feed from the instruments and allows a small subset of the data to be downloaded in real time. The IDP is independent of the onboard data recording and storage system, and it connects to the data stream to pull out the desired wavelengths for direct broadcast. The IDP has no storage capacity. The onboard data recording and storage system takes the data acquired in either low- or high-resolution mode and downlinks them to Earth. These data are then

sent to the appropriate Distributed Active Archive Center (DAAC) for further processing into the different data products.

Table 21 shows the HypsIRI data volume including the rate reduction associated with the VSWIR illumination requirement, compression, and overhead. The continuous averaged data rate is 65 Mbps, which results in a data volume of 372 Gb/orbit and 5.5 Tb/day. Compared to the current Earth Observing System (EOS) missions, the HypsIRI data rates are higher, but they are comparable to other, more recently launched, satellite missions such as WorldView-1 with a data volume of 331 Gb/orbit. The HypsIRI satellite will have an onboard storage capacity of 3 Tb (WorldView-1 has 2.2 Tb of onboard storage).

Table 21: HypsIRI Data Volume, includes illumination constraints for VSWIR, compression and overhead.

	VSWIR	TIR
Rate (Mbps)	288.5	59.2
Duty cycle ratio	0.148	0.400
Effective rate	42.700	23.672
Overhead	10%	10%
Average rate with overhead	46.970	26.039
Obstruction ratio	0.2	0
After screening	37.576	26.039

In the current configuration HypsIRI data will be downloaded using Dual X band, which will be capable of download rates of 600 Mbps. Other options, such as Ka band, are also being considered.

5 Data Products and Algorithms

The product-level definitions for the HypsIRI mission are identical to those in use by EOS today. These data product levels are briefly summarized below:

- * Level 0--Reconstructed unprocessed instrument/payload data at full resolution; any and all communications artifacts (e.g., synchronization frames, communications headers) removed.

- * Level 1A--Reconstructed unprocessed instrument data at full resolution, time-referenced, and annotated with ancillary information, including radiometric and geometric calibration coefficients and georeferencing parameters (i.e., platform ephemeris) computed and appended, but not applied, to the Level 0 data.

- * Level 1B--Level 1A data that have been processed to sensor units.

- * Level 2--Derived geophysical variables at the same resolution and location as the Level 1 source data.

- * Level 3--Variables mapped on uniform space-time grid scales, usually with some completeness and consistency.

- * Level 4--Model output or results from analyses of lower-level data (i.e., variables derived from multiple measurements).

For the HypsIRI mission, it is anticipated that the project will provide the Level 0 through Level 2 data, whereas the Level 3 and above data will be provided by the scientific community. The Level 1B data for HypsIRI will be geolocated radiance at sensor. Note, the data will not be orthorectified. In other words we will know the latitude and longitude for any given pixel, but the image pixels will not be resampled to be on a defined grid and of equal size. The level 2 data will include surface radiance, surface reflectance, surface

temperature, and surface emissivity. There will also be two cloud masks, one for the VSWIR and the other for the TIR. Two masks are necessary due to the difference in the swath width of the VSWIR and TIR sensors. The size of data granules has not been determined yet, but they will be selected to make it straightforward to work with both the VSWIR and TIR products. The Level 0 though Level 2 products will be treated as standard products (i.e., produced for all scenes), whereas the Level 3 and above products will be considered as special products, i.e., produced for a limited time or region.

It is expected that the Level 0 through Level 2 data will be developed at the Science Data System and will be stored at a Distributed Active Archive Center (DAAC). The Science Data System will be developed later in the project.

The current HypsIRI mission includes a direct broadcast capability, which will allow any user with the appropriate antenna to download a subset of the HypsIRI data stream to a local ground station. It is expected that distributed software will be developed to mimic the software that produces the standard products. This will enable direct broadcast users access to HypsIRI products in near real time. The data latency for the standard products has not been determined, but it is anticipated that it will be on the order of a few days to one week.

6 Synergies

6.1 VSWIR/TIR Instruments

The combination of a VSWIR imaging spectrometer and a TIR scanner on the same platform offers the opportunity to acquire some unique data sets that will be used to answer the combined science questions. Although the baseline mission concept includes routine acquisition of nighttime data using the TIR scanner, some of the combined science questions will also require the simultaneous acquisition of nighttime VSWIR data (for selected targets and therefore a limited data volume). High-temperature subjects such as vegetation fires and active lavas emit prodigious amounts of spectral radiance at VSWIR wavelengths. Importantly, at night, this self emissive radiance signal is uncontaminated by reflected sunlight. By acquiring nighttime VSWIR and TIR data, HypsIRI will provide thermal radiance spectra for these targets covering the entire wavelength region of 0.4 to 14 μm . This is important for determining, for example, wildfire combustion temperatures, lava flow temperatures, and lava cooling rates. A mission operations concept that allows for the targeted acquisition of VSWIR data at night will also allow HypsIRI to study urban night lights.

The combination of VSWIR imaging spectrometer and TIR scanner data also provides a promising technique to detect and monitor urban heat islands, which have arisen as a serious issue due to urban expansion and rural land conversion. The combined VSWIR and TIR data will be crucial to obtain regional estimates of evapotranspiration (ET) for climate studies, weather forecasts, hydrological surveys, ecological monitoring, and water resource management.

Synergistic applications of optical spectroscopy and thermal emissivity satellite

data are of a key importance among user communities for the development of improved and more effective operational monitoring system of natural resources, including vegetation, soil, water and natural disaster assessments. HypsIRI will provide the critical information for two of the six interdisciplinary NASA Science Focus Areas: Carbon Cycle and Ecosystems, and Water and Energy Cycle. Information regarding these two Science Focus Areas would enable critical understanding and forecasting of a third Science Focus Area, Climate Variability and Change.

6.2 Other Missions and Programs

Much of the science that serves as the foundation for the NRC Decadal Survey recommendation for HypsIRI is a result of the use of antecedent data from both aircraft-based and spacecraft-based instruments. In particular, the VSWIR sensor science has benefited significantly by the airborne AVIRIS instrument and the spaceborne Hyperion instrument on the Earth Observing-One (EO-1) platform. Similarly, the TIR instrument benefited from the development of the airborne MODIS/ASTER Airborne Simulator (MASTER) instrument and the spaceborne ASTER instrument on the Terra platform (previously called EOS AM-1).

The AVIRIS program contributed two decades of instrument refinements, image collections over research sites, and development of appropriate imaging spectroscopy processing algorithms. Similarly, the airborne MASTER instrument examined a variety of surfaces, and led to development of techniques for thermal image processing. Both of these aircraft sensors have acquired data over a range of spatial resolutions (2–50 m), depending on the flight altitude. However, the satellite instruments have obtained observations at specified spatial

and temporal scales: for Hyperion, 30 m and potentially ≤ 16 day repeats; for ASTER, 90 m collected <weekly. With eight years of Hyperion VSWIR (since 2000) imagery collected at sites around the world, a wide range of science applications have been demonstrated. Likewise, the spaceborne ASTER instrument has provided a number of years of selected late-morning thermal observations at 90-m spatial resolution in conjunction with 8 VSWIR bands at 15–30m spatial resolutions, and also paired with its platform companion, the Moderate Resolution Imaging Spectrometer (MODIS), collecting multispectral VNIR and thermal data at 250–1000 m depending on the bands.

Existing data from all four instruments (ASTER, AVIRIS, Hyperion, and MASTER) are being made freely available for researchers interested in generating precursor datasets for HypsIRI. Also, they can be used for algorithm development. We are also looking forward to the completion of new airborne instruments such as the Hyperspectral thermal emission spectrometer (HyTES) instrument, which is being developed to help prepare for HypsIRI data. Representatives of the Airborne Science Program Airborne Sensor Facility informally presented an analysis of past coincident data collects using AVIRIS and MASTER on the same aircraft at the workshop, and the attendees agreed on the high value of these data and the importance of continued coincident airborne data collects using these instruments over a variety of cover types in order to better assess basic instrument requirements and to provide datasets for development and validation of algorithms for developing the various data products.

The 2009 NASA Research Opportunities in Space and Earth Sciences (ROSES) solicitation calls for proposals using existing spaceborne and airborne imagery for HypsIRI preparatory science.

In addition in 2009, the mission will benefit greatly by already planned AVIRIS and MASTER flights on the NASA ER-2 and Twin Otter aircraft. A much more extensive science campaign encompassing a ridge-to-reef scenario was suggested for 2010, some component of which could be competed through a ROSES solicitation. In the future, synergies with other satellite missions should also be examined, such as NPOESS/VIIRS (launch in 2011), Landsat-8 (the Landsat Data Continuity Mission, LDCM) to be launched in late 2012, and three imaging spectrometers planned for launch in 2011–2013 by Germany, Italy, and India.

7 Conclusions and Recommendations

The HypsIRI workshop re-affirmed the importance and desirability of the HypsIRI mission concept to conduct new and unprecedented science targeted at terrestrial and aquatic ecosystems and the interactions between these ecosystems and anthropogenic and natural forcing functions.

The concept would provide high spatial, spectral, and temporal resolution visible through thermal infrared data of the land surface of the Earth and coastal regions (defined by a water depth of < 50m). Data with the same spectral and temporal resolution but lower spatial resolution would be provided for the open ocean with a depth of > 50m. The measurements would be used to extract the surface spectral reflectance, emissivity and temperature that would be used to address a core set of scientific questions related to research, operations, and their associated societal benefits. The study found the mission proposed by the Decadal Survey could be readily implemented with some small modifications, which further enhanced the science return from the mission.

Several key conclusions resulted from the workshop:

- HypsIRI provides a unique capability to address a set of specific scientific questions about global ecosystems, habitats, biodiversity, and hazards, and their response to anthropogenic or natural changes.
- HypsIRI will help integrate terrestrial and aquatic (inland, coastal, and oceanic) ecosystem studies, and allow assessments at spatial scales relevant to resource use by humans.
- The instrument design is capable of meeting the initial science measurement requirements.
- There is an initial set of instrument measurement requirements for

HypsIRI, which are traceable to the early scientific requirements for the mission.

- Significant heritage exists from both a design and risk-reduction standpoint for both instruments. This heritage includes missions such as the Moon Mineralogy Mapper, Hyperion, and the Advanced Spaceborne Thermal Emission and Reflection Radiometer (ASTER), as well as the associated algorithms to deliver the Level 0 through Level 2 data products.
- There are no technology “show stoppers,” and the mission is ready for implementation at the earliest opportunity.
- HypsIRI complements measurements from the DESDynI, ACE, and GEO-CAPE missions, each of which addresses very different spatial scales compared to the local and landscape scales observable with HypsIRI.

Next steps identified by the Science Study Group and affirmed at the workshop include:

- Defining the requirements for *in situ*, tower, and aircraft instrumentation to support HypsIRI
- Developing spectral libraries to support the reduction and analysis of HypsIRI data
- Developing simulated HypsIRI data sets for algorithm development and testing
- Evaluating how data from HypsIRI can be used synergistically with data from other instruments

There was a strong consensus that the HypsIRI mission as recommended by the Decadal Survey would enable the intended science. The mission was seen as being clearly

defined and ready for implementation at the first available opportunity.

8 References

- Allen, R. G., M. Tasumi, A. Morse, R. Trezza, J. L. Wright, W. G. M. Bastiaanssen, W. J. Kramber, I. Lorite, and C. W. Robison (2007). Satellite-based energy balance for mapping evapotranspiration with internalized calibration (METRIC). *Applications, J. Irrig. Drainage Eng.*, doi:10.1061/(ASCE) 0733-9437(2007)133:4(395).
- Anderson, G. L., R. I. Carruthers, S. K. Ge, and P. Gong (2005). Monitoring of invasive Tamarix distribution and effects of biological control with airborne hyperspectral remote sensing. *International Journal of Remote Sensing* 26:2487-2489.
- Anderson, M. C., J. M. Norman, J. R. Mecikalski, J. P. Otkin, and W. P. Kustas (2007). A climatological study of evapotranspiration and moisture stress across the continental U.S. based on thermal remote sensing: II. Surface moisture climatology. *J. Geophys. Res.*, 112, D11112, doi:11110.11029/12006JD007507.
- Apan, A., A. Held, S. Phinn, and J. Markley (2004). Detecting sugarcane 'orange rust' disease using EO-1 Hyperion hyperspectral imagery. *International Journal of Remote Sensing* 25:489-498.
- Asner, G.P.,(1998). Biophysical and biochemical sources of variability in canopy reflectance. *Remote Sensing of Environment* 64(3): 234-253.
- Asner, G.P. and P.M. Vitousek (2005). Remote analysis of biological invasion and biogeochemical change. *Proceedings of the National Academy of Sciences* 102(12):4,383-4,386.
- Asner, G. P., R. E. Martin, K. M. Carlson, U. Rascher, and P. M. Vitousek (2006). Vegetation-climate interactions among native and invasive species in Hawaiian rainforest. *Ecosystems* 9:1106-1117.
- Bachmann, C.M., T.F. Donato, G.M. Lamela, W.J. Rhea, M.H. Bettenhausen, R.A. Fusina, K.R. Du Bois, J.H. Porter, B.R. Truitt (2002). Automatic classification of land cover on Smith Island, VA, using HyMAP imagery. *IEEE Interactions on Geoscience and Remote Sensing* 40(10):2313-2330.
- Berg, E.E., J.D. Henry, C.L. Fastie, A.D. De Volder, S.M. Matsuoka, (2006). Spruce beetle outbreaks on the Kenai Peninsula, Alaska, and Kluane National Park and Reserve, Yukon Territory: relationship to summer temperatures and regional differences in disturbance regimes. *For. Ecol. Manage.* 227: 219-232.
- Berthelote, A.R., Prakash, A., and J. Dehn (2008). An empirical function to estimate the depths of linear hot sources: Applied to the Kuhio Lava tube. *Hawaii. Bulletin of Volcanology* 70 (7): 813-824.
- Bidigare, R. R., J. H. Morrow, and D. A. Kiefer (1989). Derivative analysis of spectral absorption by photosynthetic pigments in the western sargasso sea. *Journal of Marine Research* 47(2): 323-341.
- Brando, V. E., and A. G. Dekker (2003). Satellite hyperspectral remote sensing for estimating estuarine and coastal water quality. *IEEE Transactions on*

- Geoscience and Remote Sensing* 41: 1378–1387.
- Carlson, K.M., G.P. Asner, R. Flint Hughes, R., Ostertag, and R.E. Martin, (2007). Hyperspectral Remote Sensing of Canopy Biodiversity in Hawaiian Lowland Rainforests. *Ecosystems* 10: 536–549.
- Castro-Esau, K. L., G. A. Sanchez-Azofeifa, and T. Caelli (2004). Discrimination of lianas and trees with leaf-level hyperspectral data. *Remote Sensing of Environment* 90: 353–372.
- CDC, 2005. Heat-related mortality – Arizona, 1993-2002 and United States, 1979-2002. *MMWR – Morbidity and Mortality Weekly Report*. 54(25): 628–630.
- Claudio H.C., J.A. Gamon, Y. Cheng, D. Fuentes, A.F. Rahman, H.-L. Qiu, D.A. Sims, H. Luo, W.C. Oechel (2006). Monitoring drought effects on vegetation water content and fluxes in chaparral with the 970nm water band index. *Remote Sensing of Environment*. 103:304–311.
- Coops, N., M. Stanford, K. Old, M. Dudzinski, D. Culvenor, and C. Stone (2003). Assessment of dothistroma needle blight of *Pinus radiata* using airborne hyperspectral imagery. *Phytopathology* 93: 1524–1532.
- Craig, S. E., S. E. Lohrenz, Z. P. Lee, K. L. Mahoney, G. J. Kirkpatrick, O. M. Schofield, and R. G. Steward (2006). Use of hyperspectral remote sensing reflectance for detection and assessment of the harmful alga, *Karenia brevis*. *Appl. Opt.* 45:5 414–5425.
- Crowley, J.K., J.C. Mars, and J.M. Hammarstrom (2001). *Airborne Imaging Spectrometer and Field Spectroscopic Studies of Mine Wastes at the Elizabeth Mine, Vermont*. Society of Economic Geologists, Guidebook Series, 35, 249–253.
- Curran, P.J. (1989). Remote sensing of foliar chemistry. *Remote Sens. Environ.* 30(3): 271–278.
- Datt, B., T. R. McVicar, T. G. Van Niel, D. L. B. Jupp, and J. S. Pearlman (2003). Preprocessing EO-1 Hyperion hyperspectral data to support the application of agricultural indexes. *IEEE Transactions on Geoscience and Remote Sensing* 41: 1246–1259.
- Delmelle, P., and Bernard, A. (2000). Volcanic lakes. In: Sigurdsson, Houghton, McNutt, Rymer, Stix (Eds.), *The Encyclopedia of Volcanoes*, Academic Press, London, pp. 877–895.
- Dennison, P.E., and Roberts, D.A. (2003a). Endmember Selection for Multiple Endmember Spectral Mixture Analysis using Endmember Average RMSE. *Remote Sensing of Environment*, 87(2-3): 123–135.
- Dennison, P.E., and Roberts, D.A. (2003b). The Effects of Vegetation Phenology on Endmember Selection and Species Mapping in Southern California Chaparral. *Remote Sens. Environ.*, 87(2-3): 123–135.
- Dennison, P. E., K. Charoensiri, D. A. Roberts, S. H. Peterson, and R. O. Green, (2006). Wildfire temperature and land cover modeling using hyperspectral

- data. *Remote Sensing of Environment* 100: 212–222.
- [DS, *Decadal Survey; titles used informally*] *Earth Science and Applications from Space: National Imperatives for the Next Decade and Beyond, 2007. Committee on Earth Science and Applications from Space: A Community Assessment and Strategy for the Future* (2007). National Research Council, National Academies Press. Referred to as the Decadal Survey or NRC 2007.
- EPA (2006). *Excessive Heat Events Guidebook*. Report from the U.S. EPA, EPA 430-B-06-005, 52 pp.
- Foster, J. R., P. A. Townsend, and C. E. Zganjar (2008). Spatial and temporal patterns of gap dominance by low-canopy lianas detected using EO-1 Hyperion and Landsat Thematic Mapper. *Remote Sensing of Environment* 112: 2104–2117.
- Francis, P.W., C. Oppenheimer, and D.S. Stevenson (1993). Endogenous growth of persistently active volcanoes. *Nature*, 366: 554–557.
- Fraser, R. N. (1998). Hyperspectral remote sensing of turbidity and chlorophyll a among Nebraska sand hills lakes. *International Journal of Remote Sensing* 19: 1579–1589.
- Fuentes, D.A., J.A. Gamon, Y. Cheng, H.C. Claudio, H-L Qiub, Z. Mao, D.A. Sims, A.F. Rahman, W. O Luo, and H. Luo (2006). Mapping carbon and water vapor fluxes in a chaparral ecosystem using vegetation indices derived from AVIRIS. *Remote Sensing of the Environment*, 103:312–323.
- Gamon, J.A., C.B. Field, D.A. Roberts, S.L. Ustin, and V. Riccardo (1993). Functional patterns in an annual grassland during an AVIRIS overflight. *Remote Sensing of Environment* 44: 239—253.
- Gamon J.A., K. Kitajima, S.S. Mulkey, L. Serrano, S.J. Wright (2005). Diverse optical and photosynthetic properties in a neotropical forest during the dry season: implications for remote estimation of photosynthesis. *BioTropica* 37(4): 547–560.
- Garcia, M. and Ustin, S.L. (2001). Detection of inter-annual vegetation responses to climatic variability using AVIRIS data in a coastal savanna in California. *IEEE Transactions on GeoScience and Remote Sensing* 39: 1480–1490.
- Gates, D. M., H. J. Keegan, , J. C. Schleter, , and V. R. Weidner,(1965). Spectral properties of plants. *Applied Optics*, 4(1): 11–20.
- GEO (2007). *GEO Inland and Nearshore Coastal Water Quality Remote Sensing Workshop*. Switzerland. http://www.earthobservations.org/meetings/20070327_29_water_quality_workshop_report.pdf
- Giardino, C., V. E. Brando, A. G. Dekker, N. Strombeck, and G. Candiani (2007). Assessment of water quality in Lake Garda (Italy) using Hyperion. *Remote Sensing of Environment* 109:183–195.
- Giglio, L., I. Csiszar, Á. Restás, , J.T. Morisette, , W. Schroeder, D. Morton, and C.O. Justice, (2008). Active Fire Detection and Characterization with the Advanced Spaceborne Thermal

- Emission and Reflection Radiometer (ASTER). *Remote Sensing of Environment*, doi:10.1016/j.rse.2008.03.003.
- Gitelson, A.A., J. Schalles, C.M. Hladik (2007). Remote chlorophyll-a retrieval in turbid productive estuarine: Chesapeake Bay case study. *Remote Sensing of Environment*, 109: 464–472.
- Glenn, N. F., J. T. Mundt, K. T. Weber, T. S. Prather, L. W. Lass, and J. Pettingill (2005). Hyperspectral data processing for repeat detection of small infestations of leafy spurge. *Remote Sensing of Environment* 95: 399–412.
- Goodin D. G., L. Han, R. N. Fraser, et al. (1993). Analysis of Suspended Solids in Water Using Remotely Sensed High Resolution Derivative Spectra. *Photogrammetric Engineering & Remote Sensing* 59 (4): 505–510.
- Gower, J., C. Hu, G. Borstad, and S. King (2006). Ocean color satellites show extensive lines of floating Sargassum in the Gulf of Mexico. *IEEE Trans. Geosci. Remote Sens.* 44: 3619–3625.
- Green, R. O. (1996). Estimation of biomass fire temperature and areal extent from calibrated AVIRIS spectra. *Summaries of the Sixth Annual JPL Airborne Earth Science Workshop*. JPL Publication 96-4, 1, Jet Propulsion Laboratory, Pasadena, California, 105–113.
- Haboudane, D., J. R. Miller, N. Tremblay, P. J. Zarco-Tejada, and L. Dextraze (2002). Integrated narrow-band vegetation indices for prediction of crop chlorophyll content for application to precision agriculture. *Remote Sensing of Environment* 81: 416–426.
- Hansen, J. (2008). Tipping point: Perspective of a climatologist. In *State of the Wild 2008-2009: A Global Portrait of Wildlife, Wildlands, and Oceans*. W. Woods, Ed. Wildlife Conservation Society/Island Press, Washington, DC, pp. 6–15.
- Hirano, A., M. Madden, and R. Welch (2003). Hyperspectral image data for mapping wetland vegetation. *Wetlands* 23: 436–448.
- Hochberg, E. J., and Atkinson, M. J. (2003). Capabilities of remote sensors to classify coral, algae, and sand as pure and mixed spectra. *Remote Sens. Environ.* 85: 174–189.
- Hochberg E.J, A.M. Apprill, M.J. Atkinson, R.R. Bidigare (2006). Bio-optical modeling of photosynthetic pigments in corals. *Coral Reefs* 25: 99–109.
- Hochberg E.J., and Atkinson, M.J. (2008). Coral reef benthic productivity based on optical absorptance and light-use efficiency. *Coral Reefs* 27: 49–59
- Hook, S. J., J. E. Dmochowski, K. A. Howard, L. C. Rowan, K. E. Karlstrom, and J. M. Stock (2005). Mapping variations in weight percent silica measured from multispectral thermal infrared imagery - Examples from the Hiller Mountains, Nevada, USA and Tres Virgenes-La Reforma, Baja California Sur, Mexico. *Remote Sensing of Environment*, 95: 273–289.
- Hu, C., K. L. Carder, and F. E. Muller-Karger, (2000). Atmospheric correction of SeaWiFS imagery: assessment of the use

- of alternative bands. *Appl. Opt.* 39: 3573-3581.
- Hu, C., F. E. Muller-Karger, C. Taylor, K. L. Carder, C. Kelble, E. Johns, and C. Heil (2005). Red tide detection and tracing using MODIS fluorescence data: A regional example in SW Florida coastal waters. *Remote Sens. Environ.* 97: 311–321.
- Hunt, G.R.,= (1977). Spectral signatures of particulate minerals in the visible and near infrared. *Geophysics* 42(3): 501–513.
- Hunt, G. R. (1980). Electromagnetic radiation: The communication link in remote sensing, in *Remote Sensing in Geology*, edited by B. S. Siegal and A. R. Gillespie, John Wiley, New York, pp. 5–45.
- Ichoku, C., and Kaufman, Y. J. (2005). A method to derive smoke emission rates from MODIS fire radiative energy measurements. I 43: 2636–2649.
- Ip, F., J. M. Dohm, V. R. Baker, T. Doggett, A. G. Davies, R. Castano, S. Chien, B. Cichy, R. Greeley, R. Sherwood, D. Tran, and G. Rabideau (2006). Flood detection and monitoring with the autonomous sciencecraft experiment onboard EO-1. *Remote Sensing of Environment* 101: 463–481.
- John Heinz Center (2007). *The State of the Nation's Ecosystems 2007: Measuring the Land, Waters, and Living Resources of the United States*. John Heinz III Center for Science, Economics and the Environment, Washington, DC.
- Jollineau, M. Y., and Howarth, P.J. (2008). Mapping an inland wetland complex using hyperspectral imagery, *International Journal of Remote Sensing*. 29(12):3609–3631.
- Judd, C., S. Steinberg, F. Shaughnessy, and G. Crawford (2007). Mapping salt marsh vegetation using aerial and hyperspectral imagery and linear unmixing in Humboldt Bay, California. *Wetlands* 27(4): 1144–1152.
- Kalacska, M., S. Bohman, G. A. Sanchez-Azofeifa, K. Castro-Esau, and T. Caelli. (2007). Hyperspectral discrimination of tropical dry forest lianas and trees: Comparative data reduction approaches at the leaf and canopy levels. *Remote Sensing of Environment* 109: 406–415.
- Kallio, K., T. Kutser, T. Hannonen, S. Koponen, J. Pulliainen, J. Vepsalainen, T. Pyhalahti (2001). Retrieval of water quality from airborne imaging spectrometry of various lake types in different seasons. *Science of the Total Environment* 268: 59–77.
- Kalma, J. D., T. R. McVicar, and M. F. McCabe (2008). Estimating land surface evaporation: A review of methods using remotely sensing surface temperature data. *Survey Geophys.*, DOI 10.1007/s10712-008-9037-z.
- Kasischke, E.S., and Stocks, B.J. (2000).. *Fire, Climate Change, and Carbon Cycling in the Boreal Forest. Ecological Studies*, Vol. 138, Springer, New York.
- Kaufman, Y. J., C. O. Justice, L. P. Flynn, J. D. Kendall, E. M. Prins, L. Giglio, D. E. Ward, W. P. Menzel, and A. W. Setzer, (1998). Potential global fire monitoring from EOS-MODIS. *Journal*

- of Geophysical Research* 103: 32215–32238.
- Kim, M. S., Y. R. Chen, and P. M. Mehl (2001). Hyperspectral reflectance and fluorescence imaging system for food quality and safety. *Transactions of the ASAE* 44: 721–729.
- Kutser, T. (2004). Quantitative detection of chlorophyll in cyanobacterial blooms by satellite remote sensing. *Limnology and Oceanography* 49: 2179–2189.
- Kutser, T., L. Metsamaa, N. Strombeck, and E. Vahtmae (2006). Monitoring cyanobacterial blooms by satellite remote sensing. *Estuarine Coastal and Shelf Science* 67: 303–312.
- LeBauer D.S., K.K. Treseder (2008). Nitrogen limitation of net primary productivity in terrestrial ecosystems is globally distributed. *Ecology* 89: 371–379.
- Lee, Z.P., B. Casey, R. Arnone, A. Weidemann, R. Parsons, M.J. Montes, B.C. Gao, W. Goode, C.O. Davis, and J. Dye (2007). Water and bottom properties of a coastal environment derived from Hyperion data measured from the EO-1 spacecraft platform. *Journal of Applied Remote Sensing* 1: DOI: 10.1117/1111.2822610
- Lowell, J.D., and Guilbert, J.M. (1970). Lateral and vertical alteration-mineralization zoning in porphyry ore deposits. *Economic Geology and the Bulletin of the Society of Economic Geologists* 65(4): 373–408.
- MacDonald, G.M. (2002). *Biogeography: Space, Time and Life*. John Wiley and Sons, New York. 518 p.
- McNeil, B. E., K. M. de Beurs, K. N. Eshleman, J. R. Foster, and P. A. Townsend. 2007. Maintenance of ecosystem nitrogen limitation by ephemeral forest disturbance: An assessment using MODIS, Hyperion, and Landsat ETM. *Geophysical Research Letters* 34, Art no. L19406, 5 pp.
- Marks, M., B. Lapin, and J. Randall (1994). *Phragmites australis* (P. communis): Threats, management, and monitoring. *Natural Areas Journal* 14: 285–294.
- Martin, M. E., L. C. Plourde, S. V. Ollinge, M. L. Smith, and B. E. McNeil (2008). A generalizable method for remote sensing of canopy nitrogen across a wide range of forest ecosystems. *Remote Sensing of Environment* 112: 3511–3519.
- Matthews, S. J., M. C. Gardeweg, and R.S.J. Sparks (1997). The 1984 to 1996 cyclic activity of Lascar volcano, northern Chile: Cycles of dome growth, dome subsidence, degassing, and explosive eruptions. *Bulletin of Volcanology* 59: 72–82.
- Melillo, J.M., C.B. Field, and B. Moldan (2003). *Interactions of the Major Biogeochemical Cycles: Global Change and Human Impacts*. *Scientific Committee on Problems of the Environment (SCOPE)*. Island Press Publishers, Washington, DC.
- Myneni, R.B., C.D. Keeling, C.J. Tucker, G. Asrar, and R.R. Nemani, (1997), Increased plant growth in the northern high latitudes from 1981 to 1991. *Nature* 386: 698–702.

- Noujdina, N., and Ustin, S.L. (2008). Mapping downy brome (*Bromus tectorum*) using multi-date AVIRIS data. *Weed Science* 56: 173-179.
- NRC 2007 (see DS or *Decadal Survey*)
- Ollinger, S.V., M.L. Smith, M.E. Martin, R.A. Hallett, C.L. Goodale, and J.D. Aber (2002). Regional variation in foliar chemistry and soil nitrogen status among forests of diverse history and composition. *Ecology*, 83, 339–355.
- Ollinger, S.V., O. Sala, G. Ågren, B. Berg, E. Davidson, C. Field, M. Lerdau, J. Neff, M. Scholes, R. Sterner (2003). New Frontiers in the Study of Element Interactions. In: Melillo and Field (Eds.), *Interactions of the Major Biogeochemical Cycles*, Scientific Committee on Problems of the Environment (SCOPE), Island Press Publishers, Washington, DC.
- Ollinger, S.V., and Smith, M-L. (2005). Net primary production and canopy nitrogen in a temperate forest landscape: An analysis using imaging spectroscopy, modeling and field data. *Ecosystems* 8: 760–778.
- Ollinger, S.V., A.D. Richardson, M.E. Martin, D.Y. Hollinger, S.E. Frolking, P.B. Reich, L.C. Plourde, G.G. Katul, J.W. Munger, R. Oren, M-L. Smith, K.T. Paw U, P.V. Bolstad, B.D. Cook, M.C. Day, T.A. Martin, R.K. Monson, H.P. Schmid. 2008. Canopy nitrogen, carbon assimilation and albedo in temperate and boreal forests: Functional relations and potential climate feedbacks. Proceedings of the National Academy of Sciences. 105(49): 19335–19340.
- Oppenheimer, C., P.W. Francis, D.A. Rothery, R.W.T. Carlton, and L.S. Glaze (1993). Infrared image analysis of volcanic thermal features: Lascar Volcano, Chile, 1984–1992. *Journal of Geophysical Research* 98: 4269–4286.
- Ouzounov, D., and Freund, F. (2004). Mid-infrared emission prior to strong earthquakes analyzed by remote sensing, *Adv. Space. Res.* 33: 268–273.
- Pengra, B. W., C. A. Johnston, and T. R. Loveland (2007). Mapping an invasive plant, *Phragmites australis*, in coastal wetlands using the EO-1 Hyperion hyperspectral sensor. *Remote Sensing of Environment* 108: 74–81.
- Phillips, O.L., R.V. Martinez, L. Arroyo, T.R. Baker, T. Killeen, S.L. Lewis, Y. Malhi, A.M. Mendoza, D. Neill, P.N. Vargas M. Alexiades, C. Ceron, A. Di Fiore, T. Erwin, A. Jardim, W. Palacios, M. Saldias, and B. Vinceti (2002). Increasing dominance of large lianas in Amazonian forests. *Nature* 418(6899): 770–774.
- Pontius, J., R. Hallett, and M. Martin (2005). Using AVIRIS to assess hemlock abundance and early decline in the Catskills, New York. *Remote Sensing of Environment* 97: 163–173.
- Pontius, J., M. Martin, L. Plourde, and R. Hallett (2008). Ash decline assessment in emerald ash borer-infested regions: A test of tree-level, hyperspectral technologies. *Remote Sensing of Environment* 112: 2665–2676.

- Pu, R., P. Gong, Y. Tian, X. Miao, R. I. Carruthers, and G. L. Anderson (2008). Invasive species change detection using artificial neural networks and CASI hyperspectral imagery. *Environmental Monitoring and Assessment* 140: 15–32.
- Quattrochi, D.A., Anupma Prakash, Mariana Eneva, Robert Wright, Dorothy K. Hall, Martha Anderson, William P. Kustas, Richard G. Allen, Thomas Pagano, and Mark F. Coolbaugh, 2009. Thermal Remote Sensing: Theory, Sensors, and Applications (Chapter 3). In *Manual of Remote Sensing, American Society for Photogrammetry and Remote Sensing*, (Jackson, Mark W., ed.), Falls Church, VA, (In Press).
- Ramsey, E., A. Rangoonwala, G. Nelson, R. Ehrlich, and K. Martella (2005a). Generation and validation of characteristic spectra from EO1 Hyperion image data for detecting the occurrence of the invasive species, Chinese tallow, *International Journal of Remote Sensing*, 26(8): 1611–1636.
- Ramsey, E., A. Rangoonwala, G. Nelson, and R. Ehrlich (2005b). Mapping the invasive species, Chinese tallow, with EO1 satellite Hyperion hyperspectral image data and relating tallow occurrences to a classified Landsat Thematic Mapper land cover map, *International Journal of Remote Sensing* 26(8): 1637–1657.
- Reich, P.B., B.A. Hungate, and Y. Luo (2006). Carbon-nitrogen interactions in terrestrial ecosystems in response to rising atmospheric carbon dioxide. *Ann. Rev. Ecol. Evol. System.* 37: 611–636.
- Ritchie, J.C., P.V. Zimba, and J.H. Everitt (2003). Remote Sensing Techniques to Assess Water Quality. *Photogrammetric Engineering and Remote Sensing* 69(6): 695–704.
- Roberts, D. A., R.O. Green, and J.B. Adams (1997). Temporal and spatial patterns in vegetation and atmospheric properties from AVIRIS. *Remote Sensing of Environment* 62: 223–240.
- Roberts, D. A., M. Gardner, R. Church, S. Ustin, G. Scheer, and R.O. Green (1998). Mapping chaparral in the Santa Monica mountains using multiple endmember spectral mixture models. *Remote Sensing of Environment* 65: 267–279.
- Roberts, D.A., S.L. Ustin, S. Ogunjemiyo, J. Greenberg, S.Z. Dobrowski, J. Chen, and T.M. Hinckley, (2004). Spectral and structural measures of Northwest forest vegetation at leaf to landscape scales, *Ecosystems* 7: 545–562.
- Rosso, P.H., S.L. Ustin, and A. Hastings, 2005. Mapping marshland vegetation of San Francisco Bay, California, using hyperspectral data. *International Journal of Remote Sensing* 26(23): 5169–5191.
- Sadro, S., M. Gastil-Buhl, J. Melack (2007). Characterizing patterns of plant distribution in a southern Californian salt marsh using remotely sensed topographic and hyperspectral data and local tidal fluctuations. *Remote Sensing of Environment* 110: 226–239.

- Sanchez-Azofeifa, G. A., and Castro-Esau, K. (2006). Canopy observations on the hyperspectral properties of a community of tropical dry forest lianas and their host trees. *International Journal of Remote Sensing* 27: 2101–2109.
- Saraf, Arun K., Vineeta Rawat, Priyanka Banerjee, Swapnamita Choudhury, Santosh K. Panda, Sudipta Dasgupta, and J. D. Das (2008), Satellite detection of earthquake thermal precursors in Iran, *Natural Hazards*, DOI DOI 10.1007/s11069-007-9201-7.
- Serrano, L., S. L. Ustin, D. A. Roberts, J. A. Gamon, , and J. Penuelas (2002). Deriving water content of chaparral vegetation from AVIRIS data. *Remote Sensing of Environment* 74(3): 570–581.
- Smith, L.C., G.M. MacDonald, A.A. Velichko, , D.W. Beilman, O.K. Borisova, , K.E. Frey, K.V. Kremenetski, and Y. Sheng (2004). Siberian peatlands, a net carbon sink and global methane source since the early Holocene. *I* 303: 353–356.
- Stone, C., L. Chisholm, and N. Coops (2001). Spectral reflectance characteristics of eucalypt foliage damaged by insects. *Australian Journal of Botany* 49: 687–698.
- Strachan, I. B., E. Pattey, and J. B. Boisvert (2002). Impact of nitrogen and environmental conditions on corn as detected by hyperspectral reflectance. *Remote Sensing of Environment* 80:213–224.
- Swayze, G. A., R. N. Clark, A. F. Goetz, T. G. Chrien, and N. S. Gorelick (2003). Effects of spectrometer band pass, sampling, and signal-to-noise ratio on spectral identification using the Tetracorder algorithm. *Journal of Geophysical Research-Planets* 108(E9), 5105. doi:10.1029/2002JE001975
- Thiemann, S., and Kaufmann, H. (2002). Lake water quality monitoring using hyperspectral airborne data - a semi-empirical multisensor and multitemporal approach for the Mecklenburg Lake District, Germany. *Remote Sensing of Environment* 81: 228–237.
- Thomas, V.; J. H. Treitz,;T. McCaughey, T. Noland, and L. Rich (2008). Canopy chlorophyll concentration estimation using hyperspectral and lidar data for a boreal mixed wood forest in northern Ontario, Canada. *International Journal of Remote Sensing* 29(4): 1029–1052.
- Treitz, P.M., and P. J. Howarth, P.J. (1999). Hyperspectral remote sensing for estimating biophysical parameters of forest ecosystems. *Progress in Physical Geography* 23: 359–390.
- Underwood, E., S. Ustin, and D. DiPietro (2003). Mapping nonnative plants using hyperspectral imagery. *Remote Sensing of Environment* 86: 150–161.
- Underwood, E.C., M.J. Mulitsch, J.A. Greenberg, M.L. Whiting, S.L. Ustin, S.C. Kefauver (2006). Mapping invasive aquatic vegetation in the Sacramento-San Joaquin Delta using hyperspectral imagery. *Environmental*

- Monitoring and Assessment* 121: 47–64. <http://www.westgov.org/wga/publicat/Water06.pdf>
- UNIS (2004). UN report says world urban population of 3 billion today expected to reach 5 billion by 2030, URL: <http://www.unis.unvienna.org/unis/pre/ssrels/2004/pop899.html>, United Nations Information Service, Vienna, Austria.
- USCOP (2004). U.S. Commission on Ocean Policy. 2004. An Ocean Blueprint for the 21st Century. Final Report of the U.S. Commission on Ocean Policy. Washington, DC, pp. 345, 404.
- Ustin S.L., D.A. Roberts, J.A. Gamon, G.P. Asner, and R.O. Green (2004). Using imaging spectroscopy to study ecosystem processes and properties. *Bioscience*, 54: 523–534.
- Vitousek, P.M., H.A. Mooney, J. Lubchenco, and J.M. Melillo (1997). Human Domination of Earth's Ecosystems. *Science* 277(5325): 494–499.
- Wang, M., and Shi, W. (2005). Estimation of ocean contribution at the MODIS near-infrared wavelengths along the east coast of the U.S.: Two case studies. *Geophys. Res. Lett.* 32: L13606, doi:10.1029/2005GL022917, 2005
- Wessman C. A., J.D. Aber, D.L. Peterson, and J.M. Melillo (1988). Remote sensing of canopy chemistry and nitrogen cycling in temperate forest ecosystems. *Nature* 333: 154–156.
- WGA (2006). Water Needs and Strategies for a Sustainable Future, 2006 report of the Western Governors Association (WGA). Available from <http://www.westgov.org/wga/publicat/Water08.pdf>
- WGA (2008). Water Needs and Strategies for a Sustainable Future: Next Steps, 2008 report of the Western Governors Association. Available from <http://www.westgov.org/wga/publicat/Water08.pdf>
- Wright I.J., P. K. Groom, B. B. Lamont, P. Poot, L. D. Prior, P. B. Reich, E.D. Schulze, E. J. Veneklaas and M. Westoby 2004. The worldwide leaf economics spectrum. *Nature* 428: 821–827.
- Wright, R., and Flynn, L.P. (2003). On the retrieval of lava flow surface temperatures from infrared satellite data. *Geology* 31: 893–896.
- Zarco-Tejada, P.J., S.L. Ustin, and M.L. Whiting, (2005a). Temporal and spatial relationships between within-field yield variability in cotton and high-spatial hyperspectral remote sensing imagery. *Agronomy Journal* 97: 641–653.
- Zarco-Tejada, P. J., A. Berjon, R. Lopez-Lozano, J. R. Miller, P. Martin, V. Cachorro, M. R. Gonzalez, and A. de Frutos (2005b). Assessing vineyard condition with hyperspectral indices: Leaf and canopy reflectance simulation in a row-structured discontinuous canopy. *Remote Sensing of Environment* 99: 271–287.

9 Appendices

Appendix A – Acronyms

abs cal: Absolute Calibration

AC: Coastal Aquatic

ACE: Aerosol-Cloud-Ecosystems (Mission)

ALEXI/DisALEXI: Atmosphere-Land Exchange Inverse / Disaggregated Atmosphere-Land Exchange Inverse

ASTER: Advanced Spaceborne Thermal Emission and Reflection Radiometer

AVHRR: Advanced Very High Resolution Radiometer

AVIRIS: Airborne Visible Infrared Imaging Spectrometer

cal/val: Calibration/Validation

CCSP: Climate Change Science Program

CDOM: Colored Dissolved Organic Matter

CQ: Combined Question(s)

DAAC: Distributed Active Archive Center

DesDynI: Deformation, Ecosystems Structure, and Dynamics of Ice

DS: Decadal Survey

EO-1 Earth Observing-1

EOS : Earth Observing System

ET: Evapotranspiration

FG: Functional Group

FRP: Fire Radiative Power

FWHM: Full Width at Half Maximum

GDP: Gross Domestic Product

GEO: Group on Earth Observations

GEO-CAPE: Geostationary Coastal and Air Pollution Events

GEOSS: Global Earth Observation System of Systems

GOES: Geostationary Operational Environmental Satellite

HAB: Harmful Algal Bloom

HyspIRI: Hyperspectral Infrared Imager

HyTES: Hyperspectral thermal emission spectrometer

ICESat-II: Ice, Cloud, and Land Elevation Satellite II

IDP : Intelligent Data Payload

IFOV: Instantaneous Field of View

InSAR: Interferometric Synthetic Aperture Radar

IOOS : Integrated Ocean Observing System
IR: Infrared
IOOS: Integrated Ocean Observing System
LDCM: Landsat Data Continuity Mission
LEO: Low Earth Orbit
LST: Land Surface Temperature
M3: Moon Mineralogy Mapper
MASTER: MODIS/ASTER Airborne Simulator
MCR: Mission Concept Review
MODIS: Moderate Resolution Imaging Spectroradiometer
NAS: National Academy of Sciences
NASA: National Aeronautics and Space Administration
NDVI: Normalized Difference Vegetation Index
NE: Noise-Equivalent
NEAT: Noise-Equivalent Delta Temperature
NPOESS/VIIRS: National Polar-orbiting Operational Environmental Satellite System / Visible Infrared Imaging Radiometer Suite
NOAA: National Oceanographic and Atmospheric Administration
NPV: Non-Photosynthetic Vegetation
NRC: National Research Council
PET: Potential Evapotranspiration
PFT: Plant Functional Type
PV: Photosynthetic Vegetation
NPV: Non photosynthetic vegetation
ROSES: Research Opportunities in Space and Earth Sciences
SAV: Submerged Aquatic Vegetation
SCOPE: Scientific Organization on Problems of the Environment
SEVIRI: Spinning Enhanced Visible and InfraRed Imager
SNR: Signal-to-Noise Ratio
SSG: (HyspIRI) Science Study Group
STM: Science Traceability Matrix
SWIR: Short-Wave Infrared
T-E Separation: Temperature-Emissivity Separation
TIR: Thermal Infrared
TM: (Landsat) Thematic Mapper
TQ: Thermal Infrared Question(s)
UHI: Urban Heat Island
UNIS: United Nations Information Service

USCOP: U.S. Commission on Ocean Policy

VIIRS: Visible Infrared Imager Radiometer Suite

VNIR : Visible and Near Infrared

VQ : Visible Shortwave Infrared Question(s)

VSWIR: Visible Shortwave Infrared

WGA: Western Governors Association

Appendix B - Workshop Agenda

HyspIRI Workshop Agenda

Oct 21st-23rd, Courtyard Marriott (Monrovia)

Oct 21st

Start Time	Length	Title	Speaker
7:30:00 AM	00:30:00	Registration	
		Welcome and Overview of HyspIRI Science	
8:00:00 AM	00:15:00	Workshop	Woody Turner
		Overview of Decadal Survey Mission and	
8:15:00 AM	00:30:00	HyspIRI Plans and Status	Steve Neeck
8:45:00 AM	00:00:00	Review of Current Baseline HyspIRI Science Measurements Characteristics	
8:45:00 AM	00:30:00	VSWIR Science Measurement Specifications	Rob Green
9:15:00 AM	00:30:00	TIR Science Measurement Specifications	Simon Hook
9:45:00 AM	00:30:00	Review of HyspIRI Mission Characteristics	Francois Rogez
10:15:00 AM	00:30:00	BREAK	
		VQ1 – Pattern and Spatial Distribution of	
10:45:00 AM	00:15:00	Ecosystems and their Components	Dar Roberts
		VQ2 – Ecosystem Function, Physiology and	
11:00:00 AM	00:15:00	Seasonal Activity	Susan Ustin
11:15:00 AM	00:15:00	VQ3 - Biogeochemical Cycles	John Gamon
11:30:00 AM	00:15:00	VQ4 - Ecosystem Response to Disturbance	Greg Asner
11:45:00 AM	00:15:00	VQ5 – Ecosystems and Human Well-being	Betsy Middleton
		VQ6. Earth Surface and Shallow Water Bottom	
12:00:00 PM	00:15:00	Composition	Rob Green
12:15:00 PM	01:00:00	LUNCH	
1:15:00 PM	00:15:00	Science Traceability Matrices 101	Simon Hook
1:30:00 PM	01:15:00	VSWIR Breakout Session 1 (see tab)	Breakout leads
2:45:00 PM	00:30:00	BREAK	
3:15:00 PM	01:15:00	VSWIR Breakout Session 2 (see tab)	Breakout leads
		BREAK (lead and rapporteur prepare for	
4:30:00 PM	00:15:00	plenary)	
4:45:00 PM	01:00:00	Breakout reports in Plenary	Breakout leads
5:45:00 PM		Close	

Oct 22nd

		Potential HyspIRI Mission precursor Airborne	
8:00:00 AM	01:00:00	Campaign	Woody Turner
9:00:00 AM	00:15:00	TQ1 – Volcanoes	Mike Abrams
9:15:00 AM	00:15:00	TQ2 – Wildfires	Rob Wright
9:30:00 AM	00:15:00	TQ3 – Water Use and Availability	Martha Anderson
9:45:00 AM	00:15:00	TQ4 – Human Health and Urbanization	Dale Quattrochi
10:00:00 AM	00:30:00	BREAK	
10:30:00 AM	00:15:00	TQ5 – Earth surface composition and Change	Anupma Prakash
10:45:00 AM	01:15:00	TIR Breakout Session 1 (see tab)	Breakout leads
12:00:00 PM	01:00:00	LUNCH	
1:00:00 PM	01:15:00	TIR Breakout Session 2 (see tab)	Breakout leads
		BREAK (lead and rapporteur prepare for	
2:15:00 PM	00:15:00	plenary)	
2:30:00 PM	00:50:00	Breakout reports in Plenary	Breakout leads
3:20:00 PM	00:30:00	BREAK	

2008 HYSPIRI WHITEPAPER AND SCIENCE WORKSHOP REPORT

3:50:00 PM	01:30:00	Using advanced technologies to optimize the HyspIRI Mission	Steve Ungar
5:20:00 PM	01:00:00	Open Discussion	All
6:20:00 PM		Close	

Oct 23rd

8:00:00 AM	00:15:00	CQ1 – Coastal, ocean, and inland aquatic environments	Dave Siegel
8:15:00 AM	00:15:00	CQ2 – Wildfires	Simon Hook
8:30:00 AM	00:15:00	CQ3 – Volcanoes	Rob Wright
8:45:00 AM	00:15:00	CQ4 – Ecosystem Function and Diversity	Dar Roberts
9:00:00 AM	00:15:00	CQ5 – Land surface composition and change	Lyle Mars
9:15:00 AM	00:15:00	CQ6 – Human Health and Urbanization	Greg Glass
9:30:00 AM	00:30:00	BREAK	
10:00:00 AM	01:15:00	Combined Breakout Session 1 (see tab)	Breakout leads
11:15:00 AM	01:00:00	LUNCH	
12:15:00 PM	01:15:00	Combined Breakout Session 2 (see tab)	Breakout leads
1:30:00 PM	00:15:00	BREAK (lead and rapporteur prepare for plenary)	
1:45:00 PM	01:00:00	Breakout reports in Plenary	Breakout leads
2:45:00 PM	00:30:00	Discussion of VSWIR Measurement Baseline with respect to. Science Questions	Rob Green
3:15:00 PM	00:30:00	BREAK	
3:45:00 PM	00:30:00	Discussion of TIR Measurement Baseline w.r.t. Science Questions	Simon Hook
4:15:00 PM	00:30:00	International and Domestic Partnerships	Rob Green
4:45:00 PM	00:45:00	Review of Workshop and Next Steps	Woody Turner et al.
5:30:00 PM		Close	

Appendix C – List of Participants

Last	First	Last	First
Abrams	Michael	Luvall	Jeffrey
Abuelgasim	Abdel	Mace	Tom
Allen	Richard	Mamo	Tadesse
Anderson	Martha	Mandl	Dan
Armstrong	Ed	MARION	Rodolphe
Asner	Greg	Mars	John
Baldauf	Brian	Mars	John
Baranoski	Gladimir	Matsunago	Tsuneo
Baxter	Jan	McCarthy	John
Berthiaume	Gregory	Mcubbin	Ian
Biradar	Chandrashekhar	Mehall	Greg
Bissett	Paul	Meyer	David
Block	Gary	Middletone	Elizabeth
Boardman	Joseph	Miller	Charles
Brown	Linda	Minnett	Peter
Buckner	Janice	Moersch	Jeffrey
Buermann	Wolfgang	Mouroulis	Pantazis
Campbell	Petya	Muller-Karger	Frank
Cecere	Thomas	Myers	Jeffrey
Chao	Yi	Myneni	Ranga
Chekalyuk	Alexander	Neeck	Steven
Cheng	Yen-Ben	Nemani	Ramakrishna
Chrien	Thomas	Newman	Timothy
Corlett	Gary	Nightingale	Joanne
Corp	Lawrence	Norton	Charles
Crawford	Melba	Oaida	Bogdan
Cwik	Tom	Ogawa	Kenta
Daughtry	Craig	Okin	Gregory
Dennison	Philip	Ong	Lawrence
DiMiceli	Charlene	Pagano	Tom
Driese	Ken	Paine	Christopher
Dobson	Craig	Painter	Thomas

Last	First	Last	First
Dungan	Jennifer	pereira	john
Dwyer	John	Petheram	John
Eastwood	Michael	Petroy	Shelley
Eng	Bjorn	Pieri	David
Enright	Richard	Powell	Dylan
Fladeland	Matthew	Prakash	Anupma
Foote	Marc	Prasad	Saurabh
Francois	Rogez	Procino	Wes
Freeman	Tony	Quattrochi	Dale
French	Andy	Quetin	Gregory
Freund	Friedemann	Quirk	Bruce
Gamon	John	Radelhoff	Volker
Gao	Bo-Cai	Rahman	Abdullah
Giglio	Louis	Ramsey	Michael
Glass	Gregory	Realmuto	Vince
Gould	Richard	Reuter	Dennis
Greb	Steve	Roberts	Dar
Green	Robert	Rodolphe	Marion
Guanter	Luis	Rogez	Francois
Gubbels	Timothy	Russ	Mary
Guess	Abigail	Sarture	Charles
Hall	Jeffrey	Schoenung	Susan
Halligan	Kerry	Shakir	Safwat
Held	Alex	Sheffner	Ed
Helmlinger	Mark	Shu	Peter
Henebry	Geoffrey	Siegel	Dave
Hepner	George	Sikorski	Richard
Hill	Michael	Small	Christopher
Hollinger	Allan	Smith	Robert
Holt	Ben	Spiers	Gary
Hook	Simon	Staehele	Robert
Hosford	Steven	Staenz	Karl
Hu	Steven	Thome	Kurt
Huemmrlich	Karl	Thompson	Patrick

Last	First	Last	First
Hulley	Glynn	Townsend	Phil
Hyon	Jason	Tratt	David
Irons	James	Turmon	Michael
Jacob	Joseph	Turner	Woody
Johnson	Brian	Ungar	Steve
Johnson	William	Ustin	Susan
Kalkhan	Mohammed	Ustin	Susan
Kampe	Thomas	Valle	Tim
Kaufmann	Hermann	van Aardt	Jan
Kavanau	Maria	Vande Castle	John
Knox	Robert	Vannan	Suresh
Knyazikhin	Yuri	Vasudevan	Gopal
Koch	Timothy	Walton	Amy
Kokaly	Raymond	Wang	Le
Kruse	Fred	Wang	Weile
LaBrecque	John	Westberg	Karl
Lau	Gary	Wright	Robert
Lipschultz	Fred	Wright	Conrad
Lodhi	Mahtab	Xiao	Xiangming
		Zhang	Ying

Appendix D – Science-Traceability Matrices

The DS cross-references in the Science Objectives column (first column refer to page numbers in the 2007 Decadal

Science Objectives	Measurement Objectives	Measurement Requirements	Instrument Requirements	Other Mission and Measurement Requirements
VQ1. Pattern and Spatial	Distribution of Ecosystems and their Components: What is the pattern of ecosystem distribution and how do ecosystems differ in their composition or biodiversity? [DS 195]			
How are ecosystems organized within different biomes associated with temperate, tropical, and boreal zones, and how are these changing? [DS 191, 203]	Fractional Cover of Plant Functional Types and Species where possible (terrestrial): e.g. tree, shrub, herbaceous, cryptogam; thick/thin leaves; broad/needle leaves; deciduous/evergreen; nitrogen-fixer/non-fixer; C3/C4 physiology.	Measure diagnostic spectral signature to derive plant functional type and species: Measure seasonally through several years: Measure patch scales of <100 m: Measure regionally important PFT. Requires frequent (at least 20 per day) sampling.	Spectral measurement from 400 to 2500 nm at 10 nm (terrestrial): 380 to 900 nm at 10 nm with additional SWIR for AC (coastal aquatic): > 95% Spectral cal uniformity: SNR 600 VNIR, 300 SWIR (23.5ZA 0.25R); 14 bit precision: >95% abs cal: > 98% on-orbit stability; no saturation of ecosystem targets: <2% polarization sensitivity 380 to 700 nm: >99% linearity 2 to 98% saturation: ≤60 m spatial sampling: >95% Spectral IFOV uniformity: <20 day revisit to minimize cloud obscuration:	Surface reflectance in the solar reflected spectrum for elevation angles >20: Rigorous calibration/validation program: Monthly lunar calcs: Daily solar calcs: 6 per year vicarious calibrations ~700 mbs downlink: >3X zero loss compression: ~11 a.m. Sun sync LEO orbit: Radiometric calibration: Atmospheric Correction: AC validation: Geolocation: Pointing strategy to minimize Sun glint: Avoid terrestrial hot spot: Ground processing: Seasonal latency.
How do similar ecosystems differ in size, species composition, fractional cover, and biodiversity across terrestrial and aquatic biomes? [DS 195]	Measure fraction of dominant Plant Functional Types and Species where possible (terrestrial): e.g. tree, shrub, herbaceous, cryptogam; thick/thin leaves; broad/needle leaves; deciduous/evergreen; nitrogen-fixer/non-fixer; C3/C4 physiology. Dominant aquatic phytoplankton functional types; e.g., phytoplankton (diatoms, dinoflagellates, coccolithophores, N-fixers) Dominant submerged aquatic communities (i.e., coral, sea grass, kelp). Aquatic biogeochemical constituent: (phytoplankton, sediment, CDOM, benthos)	Measure diagnostic spectral signature to derive functional groups, species (terrestrial and aquatic), and critical measurable abiotic components. <ul style="list-style-type: none"> Measure seasonally through several years to capture baseline: Measure patch scales of <100 m. Measure regionally important PFT. Requires frequent (at least every 20 days) sampling. 	Spectral measurement from 400 to 2500 nm at 10 nm (terrestrial): 380 to 900 nm at 10 nm with additional SWIR for AC (coastal aquatic): > 95% Spectral cal uniformity: Terrestrial: SNR 600 VNIR, 300 SWIR (23.5ZA 0.25R); Aquatic: ~SNR 300 (45ZA 0.01R) 14-bit precision: >95% abs cal: > 98% on-orbit stability; no saturation of ecosystem targets: <2% polarization sensitivity 380 to 700 nm: >99% linearity 2 to 98% saturation: ≥ 60 sampling: >95% Spectral IFOV uniformity: <20 day revisit to minimize cloud obscuration:	Surface reflectance in the solar reflected spectrum for elevation angles >20: Rigorous cal/val program: Monthly lunar calcs: Daily solar calcs: 6 per year vcalcs: ~700-mbs downlink: >3X zero loss compression: ~11 a.m. Sun sync LEO: Radiometric calibration: Atmospheric Correction: AC validation: Geolocation: Pointing strategy to minimize Sun glint: Avoid terrestrial hot spot: Ground processing: Seasonal latency:
What is the current spatial distribution of ecosystems, functional groups, or key species within major biomes including agriculture, and how are these being altered by climate variability, human uses, and other factors? [DS 191, 203]	Fractional Cover of Plant Functional Types and Species where possible (terrestrial): e.g. tree, shrub, herbaceous, cryptogam; thick/thin leaves; broad/needle leaves; deciduous/evergreen; nitrogen-fixer/non-fixer; C3/C4 physiology.	Measure diagnostic spectral signature to derive plant functional type and species: Measure seasonally through several years: Measure patch scales of <100 m: Measure regionally important PFT. Requires frequent (at least every 20 days) sampling.	Spectral measurement from 400 to 2500 nm at 10 nm (terrestrial): 380 to 900 nm at 10 nm with additional SWIR for AC (coastal aquatic): > 95% Spectral cal uniformity: SNR 600 VNIR, 300 SWIR (23.5ZA 0.25R); 14 bit precision: >95% abs cal: > 98% on-orbit stability; no saturation of ecosystem targets: <2% polarization sensitivity 380 to 700 nm: >99% linearity 2 to 98% saturation: ≤ 60 sampling: >95% Spectral IFOV uniformity: <20 day revisit to minimize cloud obscuration:	Surface reflectance in the solar reflected spectrum for elevation angles >20: Rigorous cal/val program: Monthly lunar calcs: Daily solar calcs: 6 per year vcalcs: ~700-mbs downlink: >3X zero loss compression: ~11 am sun sync LEO: Radiometric calibration: Atmospheric Correction: AC validation: Geolocation: Pointing strategy to minimize Sun glint: Avoid terrestrial hot spot: Ground processing: Seasonal latency:
What are the extent and impact of invasive species in terrestrial and aquatic ecosystems? [DS 192, 194, 196, 203, 204, 214]	Species-type measurements in terrestrial and coastal aquatic regions.	Measure diagnostic spectral signature to derive plant species: Measure seasonally through several years: Measure patch scales of <100 m: Measure regionally important PFT. Requires frequent (at least 20 per day) sampling. Measure diagnostic spectral signature of aquatic vegetation in coastal regions with < 100 m spatial resolution and temporal repeat to observe the seasonal regional occurrence and trends in the coastal regions. Requires frequent (at least 20 per day) repeat.	Spectral measurement from 400 to 2500 nm at 10 nm (terrestrial): 380 to 900 nm at 10 nm with additional SWIR for AC (coastal aquatic): > 95% Spectral cal uniformity: SNR 600 VNIR, 300 SWIR (23.5ZA 0.25R); 14-bit precision: >95% abs cal: > 98% on-orbit stability; no saturation of ecosystem targets: <2% polarization sensitivity 380 to 700 nm (aquatic): >99% linearity 2 to 98% saturation: ≥ 60 sampling: >95% Spectral IFOV uniformity: <20 day revisit to minimize cloud obscuration:	Surface reflectance in the solar reflected spectrum for elevation angles >20: Rigorous cal/val program: Monthly lunar calcs: Daily solar calcs: 6 per year vcalcs: ~700 mbs downlink: >3X zero loss compression: ~11 a.m. Sun sync LEO: Radiometric calibration: Atmospheric Correction: AC validation: Geolocation: Pointing strategy to minimize Sun glint: Avoid terrestrial hot spot: Ground processing: Seasonal latency:
What is the spatial structure and species distribution in a phytoplankton bloom? [DS 201, 208]	Characterize algal bloom (including harmful) species and spatial structure	Measure diagnostic spectral signature of aquatic vegetation in coastal regions with < 100 m spatial resolution and temporal repeat to observe the seasonal regional occurrence and trends in the coastal regions.	Spectral measurement from 380 to 900 nm at 10 nm with additional SWIR for AC (coastal aquatic): > 95% Spectral cal uniformity: SNR 600 VNIR, 300 SWIR (23.5ZA 0.25R); 14-bit digitization: >95% abs cal: > 98% on-orbit stability; no saturation of ecosystem targets: <2% polarization sensitivity 380 to 700 nm (aquatic): >99% linearity 2 to 98% saturation: ≤ 60 sampling: >95% Spectral IFOV uniformity: <20 day revisit to minimize cloud obscuration:	Surface reflectance in the solar reflected spectrum for elevation angles >20: Rigorous cal/val program: Monthly lunar calcs: Daily solar calcs: 6 per year vcalcs: ~700 mbs downlink: >3X zero loss compression: ~11 a.m. Sun sync LEO: Radiometric calibration: Atmospheric Correction: AC validation: Geolocation: Pointing strategy to minimize sun glint: Avoid terrestrial hot spot: Ground processing: Seasonal latency:
How do changes in coastal morphology and surface composition impact coastal ecosystem composition, diversity and function [DS 41]?	Measure coastal ecosystem functional characteristics and diversity at the seasonal and multiyear time scale.	Measure diagnostic spectral signature of aquatic vegetation in coastal regions with < 100 m spatial resolution and temporal repeat to observe the seasonal regional occurrence and trends in the coastal regions. Requires frequent (at least 20 per day) sampling.	Spectral measurement from 400 to 2500 nm at 10 nm (terrestrial): 380 to 900 nm at 10 nm with additional SWIR for AC (coastal aquatic): > 95% Spectral cal uniformity: SNR 600 VNIR, 300 SWIR (23.5ZA 0.25R); 14-bit precision: >95% abs cal: > 98% on-orbit stability; no saturation of ecosystem targets: <2% polarization sensitivity 380 to 700 nm: >99% linearity 2 to 98% saturation: ≤60 sampling: >95% Spectral IFOV uniformity: <20 day revisit to minimize cloud obscuration:	Surface reflectance in the solar reflected spectrum for elevation angles >20: Rigorous cal/val program: Monthly lunar calcs: Daily solar calcs: 6 per year vcalcs: ~700 mbs downlink: >3X zero loss compression: ~11 a.m. Sun sync LEO: Radiometric calibration: Atmospheric Correction: AC validation: Geolocation: Pointing strategy to minimize Sun glint: Avoid terrestrial hot spot: Ground processing: Seasonal latency:

VQ1

Science Objectives	Measurement Objectives	Measurement Requirements	Instrument Requirements	Other Mission and Measurement Requirements
VQ2. Ecosystem Function, Physiology, and Seasonal Activity: What are the seasonal expressions and cycles for terrestrial and aquatic ecosystems, functional groups and diagnostic species? How are these being altered by changes in climate, land use, and disturbances? [DS 191, 195, 203]				
How does the seasonal activity of ecosystems and functional types vary across biomes, geographic zones, or environmental gradients between the Equator and the poles? How are seasonal patterns of ecosystem function being affected by climate change? [DS 205, 206, 210] (include agriculture?)	Measure the functional type composition of ecosystems globally. Measure these at the spatial scale and temporal scale to address regional to global distributions. Measure these at temporal scale to answer seasonal and several-year trends.	Measure surface reflectance in the VSWIR region at high precision and accuracy. Measure globally at spatial resolution patch scale relevant for ecosystem 10 ⁴ to 10 ⁶ m ² . Measure temporally to have high probability to achieve seasonal measurements. (consider replace measure to retrieve)	Spectral measurement from 400 to 2500 nm at 10 nm (terrestrial): 380 to 900 nm at 10 nm with additional SWIR for AC (coastal aquatic): > 95% Spectral cal uniformity (include spectral and spatial stray light?): SNR 600 VNIR, 300 SWIR (23.5ZA 0.25R): 14-bit precision: >95% abs cal: > 98% on-orbit stability: no saturation of ecosystem targets: <2% polarization sensitivity 380 to 700 nm: >99% linearity 2 to 98% saturation: ≤60 sampling: >95% Spectral IFOV uniformity: <20 day revisit to minimize cloud obscuration: (possibly provide Noise Equivalent delta radiance?) (be specific about wavelength)	Surface reflectance in the solar reflected spectrum for elevation angles >20: Rigorous cal/val program: Monthly lunar cals: Daily solar cals: 6 per year vcals: ~700-mbs downlink: >3X zero loss compression: ~11 am sun sync LEO: Radiometric calibration: Atmospheric Correction: AC validation: Geolocation: Pointing strategy to minimize Sun glint: Avoid terrestrial hot spot: Ground processing: Seasonal latency:
How do seasonal changes affect productivity, carbon sequestration, and hydrological processes across ecosystems and agriculture? [DS 195, 205, 210]	Measure seasonal changes and status of natural ecosystem and agricultural lands over the seasonal and multiyear scale.	Measure surface reflectance spectral reflectance in the VSWIR region at high repeatable accuracy. Measure globally at spatial resolution patch scale relevant for ecosystem 10 ⁴ to 10 ⁶ m ² . Measure temporally to have high probability to achieve seasonal measurements.	Spectral measurement from 400 to 2500 nm at 10 nm (terrestrial): 380 to 900 nm at 10 nm with additional SWIR for AC (coastal aquatic): >95% Spectral cal uniformity: SNR 600 VNIR, 300 SWIR (23.5ZA 0.25R): 14-bit precision: >95% abs cal: > 98% on-orbit stability: no saturation of ecosystem targets: <2% polarization sensitivity 380 to 700 nm: >99% linearity 2 to 98% saturation: ≤60 sampling: >95% Spectral IFOV uniformity: <20 day revisit to minimize cloud obscuration:	Surface reflectance in the solar reflected spectrum for elevation angles >20: Rigorous cal/val program: Monthly lunar cals: Daily solar cals: 6 per year vcals: ~700-mbs downlink: >3X zero loss compression: ~11 a.m. Sun sync LEO: Radiometric calibration: Atmospheric Correction: AC validation: Geolocation: Pointing strategy to minimize Sun glint: Avoid terrestrial hot spot: Ground processing: Seasonal latency:
How do environmental stresses affect the physiological function of water and carbon exchanges at the seasonal time scale within ecosystems (including agriculture)? [DS 203, 206, 210]	Measure the physiological function indicators of ecosystems related to water and carbon exchange over the seasonal and multiyear time frame.	Measure spectral signature in the VSWIR region at high precision and accuracy. Special focus on precision and accuracy in the pigment region of vegetation in the visible portion of the spectrum. Water: 980±50 nm, 1180±50 nm, and broad SWIR water signatures to 2500 nm. Measure globally at spatial resolution patch scale relevant for ecosystem 10 ⁴ to 10 ⁶ m ² . Measure temporally to have high probability to achieve seasonal measurements.	Spectral measurement from 400 to 2500 nm at 10 nm (terrestrial): 380 to 900 nm at 10 nm with additional SWIR for AC (coastal aquatic): >95% Spectral cal uniformity: SNR 600 VNIR, 300 SWIR (23.5ZA 0.25R): 14-bit precision: >95% abs cal: >98% on-orbit stability: no saturation of ecosystem targets: <2% polarization sensitivity 380 to 700 nm: >99% linearity 2 to 98% saturation: ≤60 sampling: >95% Spectral IFOV uniformity: <20 day revisit to minimize cloud obscuration:	Surface reflectance in the solar reflected spectrum for elevation angles >20: Rigorous cal/val program: Monthly lunar cals: Daily solar cals: 6 per year vcals: ~700-mbs downlink: >3X zero loss compression: ~11 a.m. Sun sync LEO: Radiometric calibration: Atmospheric Correction: AC validation: Geolocation: Pointing strategy to minimize sun glint: Avoid terrestrial hot spot: Ground processing: Seasonal latency:
What is the environmental impact of aquatic plants and coral on inland and coastal water environments at the seasonal time scale? [DS 201, 208]	Measure the distribution and type of algal bloom in a sampling sense globally over the seasonal and multiyear timescale.	Measure diagnostic spectral signature of in coastal regions with <100 m spatial resolution and temporal repeat to observe the seasonal regional occurrence and trends in the coastal regions. Measure globally at spatial resolution patch scale relevant for ecosystem 10 ⁴ to 10 ⁶ m ² . Measure temporally to have high probability to achieve seasonal measurements.	Spectral measurement from 380 to 900 nm at 10 nm with additional SWIR for AC (coastal aquatic): > 95% Spectral cal uniformity: SNR 600 VNIR, 300 SWIR (23.5ZA 0.25R): 14-bit digitization: >95% abs cal: > 98% on-orbit stability: no saturation of ecosystem targets: <2% polarization sensitivity 380 to 700 nm: >99% linearity 2 to 98% saturation: ≤60 sampling: >95% Spectral IFOV uniformity: <20 day revisit to minimize cloud obscuration:	Surface reflectance in the solar reflected spectrum for elevation angles >20: Rigorous cal/val program: Monthly lunar cals: Daily solar cals: 6 per year vcals: ~700-mbs downlink: >3X zero loss compression: ~11 a.m. Sun sync LEO: Radiometric calibration: Atmospheric Correction: AC validation: Geolocation: Pointing strategy to minimize Sun glint: Avoid terrestrial hot spot: Ground processing: Seasonal latency:

VQ2

Science Objectives	Measurement Objectives	Measurement Requirements	Instrument Requirements	Other Mission and Measurement Requirements
VQ3. Biogeochemical Cycles: How are the biogeochemical cycles that sustain life on Earth being altered/disrupted by natural and human-induced environmental change? How do these changes affect the composition and health of ecosystems, and what are the feedbacks with other components of the Earth system?				
How do changes in climate and atmospheric processes affect the physiology and biogeochemistry of ecosystems? [DS 194, 201]	Measure the biogeochemistry of both photosynthetic vegetation and non-photosynthetic vegetation.	Measure at high accuracy and precision the spectral signature that is shown to be sensitive to vegetation canopy chemistry. -Pigments: Visible spectral region. - Water: 980 ±50 nm, 1180±50 nm, and broad SWIR water signatures to 2500 nm. - Nitrogen and other components: Spectral region 1300 to 2500 nm at 10 nm. Measure globally at spatial resolution patch scale relevant for ecosystem 10 ⁴ to 10 ⁶ m ² . Measure temporally to have high probability to achieve seasonal measurements.	Spectral measurement from 400 to 2500 nm at 10 nm (terrestrial): 380 to 900 nm at 10 nm with additional SWIR for AC (coastal aquatic): > 95% Spectral cal uniformity: SNR 600 VNIR, 300 SWIR (23.5ZA 0.25R): 14-bit precision: >95% abs cal: > 98% on-orbit stability; no saturation of ecosystem targets: <2% polarization sensitivity 380 to 700 nm: >99% linearity 2 to 98% saturation: ≥60 sampling: >95% Spectral IFOV uniformity: <20 day revisit to minimize cloud obscuration:	Surface reflectance in the solar reflected spectrum for elevation angles >20: Rigorous cal/val program: Monthly lunar calcs: Daily solar calcs: 6 per year vcalcs: ~700-mbs downlink: >3X zero loss compression: ~11 a.m. Sun sync LEO orbit: Radiometric calibration: Atmospheric Correction: AC validation: Geolocation: Pointing strategy to minimize Sun glint: Avoid terrestrial hot spot: Ground processing: Seasonal latency:
What are the consequences of uses of land and coastal systems, such as urbanization, agriculture, and resource extraction, for the carbon cycle, hydrological cycle, nutrient fluxes, and functional composition [DS 196, 197]	Measure biological component and state of land and coastal ecosystems globally at the seasonal to several-year time scales. Relate these to sources, conduits and sinks of relevant elements.	Measure at high accuracy and precision the spectral signature that allows mapping of coastal and land ecosystem elements. Measure globally at spatial resolution patch scale relevant for ecosystem 10 ⁴ to 10 ⁶ m ² . Measure temporally to have high probability to achieve seasonal measurements.	Spectral measurement from 400 to 2500 nm at 10 nm (terrestrial): 380 to 900 nm at 10 nm with additional SWIR for AC (coastal aquatic): > 95% Spectral cal uniformity: SNR 600 VNIR, 300 SWIR (23.5ZA 0.25R): 14-bit precision: >95% abs cal: > 98% on-orbit stability; no saturation of ecosystem targets: <2% polarization sensitivity 380 to 700 nm: >99% linearity 2 to 98% saturation: ≥60 sampling: >95% Spectral IFOV uniformity: <20 day revisit to minimize cloud obscuration:	Surface reflectance in the solar reflected spectrum for elevation angles >20: Rigorous cal/val program: Monthly lunar calcs: Daily solar calcs: 6 per year vcalcs: ~700 mbs downlink: >3X zero loss compression: ~11 a.m. Sun sync LEO: Radiometric calibration: Atmospheric Correction: AC validation: Geolocation: Pointing strategy to minimize Sun glint: Avoid terrestrial hot spot: Ground processing: Seasonal latency:
What are the consequences of increasing nitrogen deposition for carbon cycling and biodiversity in terrestrial and coastal ecosystems? [DS 195, 196]	Measure ecological components of terrestrial and coastal ecosystem including elements of biodiversity. Measure ecological signatures closely tied to nitrogen deposition.	Measure at high accuracy and precision the spectral signatures that allow mapping of aquatic, coastal, and land ecosystem elements. Measure globally at spatial resolution patch scale relevant for ecosystem 10 ⁴ to 10 ⁶ m ² . Measure temporally to have high probability to achieve seasonal measurements	Spectral measurement from 400 to 2500 nm at 10 nm (terrestrial): 380 to 900 nm at 10 nm with additional SWIR for AC (coastal aquatic): > 95% Spectral cal uniformity: SNR 600 VNIR, 300 SWIR (23.5ZA 0.25R): 14-bit precision: >95% abs cal: > 98% on-orbit stability; no saturation of ecosystem targets: <2% polarization sensitivity 380 to 700 nm: >99% linearity 2 to 98% saturation: ≥60 sampling: >95% Spectral IFOV uniformity: <20 day revisit to minimize cloud obscuration:	Surface reflectance in the solar reflected spectrum for elevation angles >20: Rigorous cal/val program: Monthly lunar calcs: Daily solar calcs: 6 per year vcalcs: ~700 mbs downlink: >3X zero loss compression: ~11 a.m. Sun sync LEO: Radiometric calibration: Atmospheric Correction: AC validation: Geolocation: Pointing strategy to minimize Sun glint: Avoid terrestrial hot spot: Ground processing: Seasonal latency:
How do changes in hydrology, pollutant inputs, and sediment transport affect freshwater and coastal marine ecosystems? [DS 196]	Measure diagnostic elements of freshwater and coastal marine ecosystem including sediments, chlorophyll, algal communities, and CDOM.	Measure at high accuracy and precision the spectral signatures that allow derivation of key elements of freshwater and coastal marine ecosystems. Measure spectral region where sediments, chlorophyll, algae, CDOM, etc. provide a usable signal. Measure globally at spatial resolution patch scale relevant for ecosystem 10 ⁴ to 10 ⁶ m ² . Measure temporally to have high probability to achieve seasonal measurements.	Spectral measurement from 400 to 2500 nm at 10 nm (terrestrial): 380 to 900 nm at 10 nm with additional SWIR for AC (coastal aquatic): > 95% Spectral cal uniformity: SNR 600 VNIR, 300 SWIR (23.5ZA 0.25R): 14-bit precision: >95% abs cal: > 98% on-orbit stability; no saturation of ecosystem targets: <2% polarization sensitivity 380 to 700 nm: >99% linearity 2 to 98% saturation: ≥60 sampling: >95% Spectral IFOV uniformity: <20 day revisit to minimize cloud obscuration:	Surface reflectance in the solar reflected spectrum for elevation angles >20: Rigorous cal/val program: Monthly lunar calcs: Daily solar calcs: 6 per year vcalcs: ~700 mbs downlink: >3X zero loss compression: ~11 a.m. Sun sync LEO: Radiometric calibration: Atmospheric Correction: AC validation: Geolocation: Pointing strategy to minimize Sun glint: Avoid terrestrial hot spot: Ground processing: Seasonal latency:
How do changing water balances affect carbon storage by terrestrial ecosystems? [DS 196]	Measure water content of canopies. Measure signals of evapotranspiration.	Measure at high accuracy and precision the spectral signatures that allow derivation of canopy liquid water. Also measure canopy associated water vapor. Measure spectral region where liquid water and water vapor are expressed. Water: 980 ±50 nm, 1180±50 nm, and broad SWIR water signatures to 2500 nm. Measure globally at spatial resolution patch scale relevant for ecosystem 10 ⁴ to 10 ⁶ m ² . Measure temporally to have high probability to achieve seasonal measurements.	Spectral measurement from 900 to 2500 nm at 10 nm (terrestrial): >95% Spectral cal uniformity: SNR 600 VNIR, 300 SWIR (23.5ZA 0.25R): 14-bit precision: >95% abs cal: > 98% on-orbit stability; no saturation of ecosystem targets: <2% polarization sensitivity 380 to 700 nm: >99% linearity 2 to 98% saturation: ≥60 sampling: >95% Spectral IFOV uniformity: <20 day revisit to minimize cloud obscuration:	Surface reflectance in the solar reflected spectrum for elevation angles >20: Rigorous cal/val program: Monthly lunar calcs: Daily solar calcs: 6 per year vcalcs: ~700-mbs downlink: >3X zero loss compression: ~11 a.m. Sun sync LEO: Radiometric calibration: Atmospheric Correction: AC validation: Geolocation: Pointing strategy to minimize Sun glint: Avoid terrestrial hot spot: Ground processing: Seasonal latency:
What are the key interactions between biogeochemical cycles and the composition and diversity of ecosystems? [195, 196]	Measure biogeochemistry elements as well as composition and diversity of ecosystems.	Measure at high accuracy and precision the spectral signature that is shown to be sensitive to vegetation canopy chemistry. -Pigments: Visible spectral region. - Water: 980 ±50 nm, 1180±50 nm, and broad SWIR water signatures to 2500 nm. - Nitrogen and other components: Spectral region 1300 to 2500 nm at 10 nm. Measure spectral signatures across the VSWIR region at high precision and accuracy to derive ecosystem composition and diversity. Measure globally at spatial resolution patch scale relevant for ecosystem 10 ⁴ to 10 ⁶ m ² . Measure temporally to have high probability to achieve seasonal measurements.	Spectral measurement from 400 to 2500 nm at 10 nm (terrestrial): 380 to 900 nm at 10 nm with additional SWIR for AC (coastal aquatic): > 95% Spectral cal uniformity: SNR 600 VNIR, 300 SWIR (23.5ZA 0.25R): 14-bit precision: >95% abs cal: > 98% on-orbit stability; no saturation of ecosystem targets: <2% polarization sensitivity 380 to 700 nm: >99% linearity 2 to 98% saturation: ≥60 sampling: >95% Spectral IFOV uniformity: <20 day revisit to minimize cloud obscuration:	Surface reflectance in the solar reflected spectrum for elevation angles >20: Rigorous cal/val program: Monthly lunar calcs: Daily solar calcs: 6 per year vcalcs: ~700-mbs downlink: >3X zero loss compression: ~11 a.m. Sun sync LEO: Radiometric calibration: Atmospheric Correction: AC validation: Geolocation: Pointing strategy to minimize Sun glint: Avoid terrestrial hot spot: Ground processing: Seasonal latency:
How do changes in biogeochemical processes feed back to climate and other components of the Earth system? [DS 190, 192, 195]	Measure global biogeochemical constituents related to processes involved in feedback to climate and other environmental factors.	Measure at high accuracy and precision the spectral signature that is shown to be sensitive to vegetation canopy chemistry. -Pigments: Visible spectral region. - Water: 980 ±50 nm, 1180±50 nm, and broad SWIR water signatures to 2500 nm. - Nitrogen and other components: Spectral region 1300 to 2500 nm at 10 nm. Measure globally at spatial resolution patch scale relevant for ecosystem 10 ⁴ to 10 ⁶ m ² . Measure temporally to have high probability to achieve seasonal measurements.	Spectral measurement from 400 to 2500 nm at 10 nm (terrestrial): 380 to 900 nm at 10 nm with additional SWIR for AC (coastal aquatic): >95% Spectral cal uniformity: SNR 600 VNIR, 300 SWIR (23.5ZA 0.25R): 14-bit precision: >95% abs cal: > 98% on-orbit stability; no saturation of ecosystem targets: <2% polarization sensitivity 380 to 700 nm: >99% linearity 2 to 98% saturation: ≥60 sampling: >95% Spectral IFOV uniformity: <20 day revisit to minimize cloud obscuration:	Surface reflectance in the solar reflected spectrum for elevation angles >20: Rigorous cal/val program: Monthly lunar calcs: Daily solar calcs: 6 per year vcalcs: ~700-mbs downlink: >3X zero loss compression: ~11 a.m. Sun sync LEO: Radiometric calibration: Atmospheric Correction: AC validation: Geolocation: Pointing strategy to minimize Sun glint: Avoid terrestrial hot spot: Ground processing: Seasonal latency:

VQ3

Science Objectives	Measurement Objectives	Measurement Requirements	Instrument Requirements	Other Mission and Measurement Requirements
VQ4. Changes in Disturbance Activity: How are disturbance regimes changing and how do these changes affect the ecosystem processes that support life on Earth?				
How do patterns of abrupt (pulse) disturbance vary and change over time within and across ecosystems?	Measure changes in fractional cover (from clearing, logging, wetland drainage, fire, weather related, etc.) at the seasonal and multiyear time scales, to characterize disturbance regimes in global ecosystems (e.g., conditional frequencies and/or return intervals for VQ1 ecosystem classes).	Measure spectral signature in the VSWIR region at high precision and accuracy. - Detect fractional surface cover changes > 10%. - Sufficient precision and accuracy for spectral mixture algorithms to give insight to subpixel events. Measure globally at spatial resolution patch scale relevant for ecosystem 10 ⁴ to 10 ⁶ m ² . Cloud-free measurement at least once per season.	Spectral measurement from 400 to 2500 nm at 10 nm (terrestrial): 380 to 900 nm at 10 nm with additional SWIR for AC (coastal aquatic): > 95% Spectral cal uniformity: SNR 600 VNIR, 300 SWIR (23.52A 0.25R): 14-bit precision: >95% abs cal: > 98% on-orbit stability; no saturation of ecosystem targets: <2% polarization sensitivity 380 to 700 nm: >99% linearity 2 to 98% saturation: <60 m spatial sampling: >95% Spectral IFOV uniformity: <20 day revisit to minimize cloud obscuration:	Surface reflectance in the solar reflected spectrum for elevation angles >20: Rigorous cal/val program: Monthly lunar calis: Daily solar calis: 6 per year vcalis: ~700-mbs downlink: >3X zero loss compression: ~11 a.m. Sun sync LEO: Radiometric calibration: accurate enough to simulate historical satellite data through band synthesis. Atmospheric Correction: AC validation: Geolocation: 10 m (1 sigma). Ground processing: Seasonal latency:
How do climate changes affect disturbances such as fire and insect damage? [DS 196]	Measure changes in vegetation canopy cover, pigments, and water content in ecosystems globally at the seasonal and multiyear time scale. Make measurements in such a way that they are backward compatible with pre-existing estimates and algorithms (e.g., band synthesis for historical vegetation indexes), as well as allowing more advanced algorithmic approaches.	Measure characteristic changes or differences in plant pigments (10% changes in total chlorophyll, carotenoids, anthocyanins) and water content. Measure PV, NPV and Soil (+/- 5%) using full VSWIR and SWIR algorithms. Measure globally at spatial resolution patch scale relevant for ecosystem 10 ⁴ to 10 ⁶ m ² . Cloud-free measurement at least once per season. VNIR-SWIR spectra suitable for band synthesis consistent with historical data.	Spectral measurement from 400 to 2500 nm at 10 nm (terrestrial): > 95% Spectral cal uniformity: SNR 600 VNIR, 300 SWIR (23.52A 0.25R): 14-bit precision: >95% abs cal: > 98% on-orbit stability; no saturation of ecosystem targets: <2% polarization sensitivity 380 to 700 nm: >99% linearity 2 to 98% saturation: <60 m spatial sampling: >95% Spectral IFOV uniformity: <20 day revisit to minimize cloud obscuration:	Surface reflectance in the solar reflected spectrum for elevation angles >20: Rigorous cal/val program: Monthly lunar calis: Daily solar calis: 6 per year vcalis: ~700-mbs downlink: >3X zero loss compression: ~11 a.m. Sun sync LEO: Radiometric calibration: Atmospheric Correction: AC validation: Geolocation: Pointing strategy to minimize Sun glint: Avoid terrestrial hot spot: Ground processing: Seasonal latency:
What are the interactions between invasive species and other types of disturbance?	Measure the distribution and cover of key invasive species that introduce novel life histories or functional types, in concert with disturbance measurements. Measure (disturbance related) changes in vegetation canopy cover, pigments, and water content in ecosystems globally at the seasonal and multiyear time scale.	Measure spectral signature in the VSWIR region at high precision and accuracy. -Sufficient precision and accuracy for spectral mixture algorithms to give insight to subpixel events. -Measure species-type and functional type using full spectrum. -Measure PV, NPV, and Soil using full VSWIR and SWIR algorithms. Measure globally at spatial resolution patch scale relevant for ecosystem 10 ⁴ to 10 ⁶ m ² . Cloud-free measurement at least once per season.	Spectral measurement from 400 to 2500 nm at 10 nm (terrestrial): > 95% Spectral cal uniformity: SNR 600 VNIR, 300 SWIR (23.52A 0.25R): 14-bit precision: >95% abs cal: > 98% on-orbit stability; no saturation of ecosystem targets: <2% polarization sensitivity 380 to 700 nm: >99% linearity 2 to 98% saturation: <60 m spatial sampling: >95% Spectral IFOV uniformity: <20 day revisit to minimize cloud obscuration:	Surface reflectance in the solar reflected spectrum for elevation angles >20: Rigorous cal/val program: Monthly lunar calis: Daily solar calis: 6 per year vcalis: ~700-mbs downlink: >3X zero loss compression: ~11 a.m. Sun sync LEO: Radiometric calibration: Atmospheric Correction: AC validation: Geolocation: Pointing strategy to minimize sun glint: Avoid terrestrial hot spot: Ground processing: Seasonal latency:
How are human-caused and natural disturbances changing the biodiversity composition of ecosystems, e.g.: through changes in the distribution and abundance of organisms, communities, and ecosystems?	Measure the composition of ecosystems and ecological diversity indicators globally and at the seasonal and multiyear time scale.	Measure spectral signature in the VSWIR region at high precision and accuracy. -Sufficient precision and accuracy for spectral mixture algorithms to give insight to subpixel events. -Measure species-type and functional type using full spectrum. -Measure PV, NPV, and Soil using full VSWIR and SWIR algorithms. Measure globally at spatial resolution patch scale relevant for ecosystem 10 ⁴ to 10 ⁶ m ² . Measure temporally to have high probability to achieve seasonal measurements.	Spectral measurement from 400 to 2500 nm at 10 nm (terrestrial): > 95% Spectral cal uniformity: SNR 600 VNIR, 300 SWIR (23.52A 0.25R): 14-bit precision: >95% abs cal: > 98% on-orbit stability; no saturation of ecosystem targets: <2% polarization sensitivity 380 to 700 nm: >99% linearity 2 to 98% saturation: <60 m spatial sampling: >95% Spectral IFOV uniformity: <20 day revisit to minimize cloud obscuration:	Surface reflectance in the solar reflected spectrum for elevation angles >20: Rigorous cal/val program: Monthly lunar calis: Daily solar calis: 6 per year vcalis: ~700-mbs downlink: >3X zero loss compression: ~11 a.m. Sun sync LEO: Radiometric calibration: Atmospheric Correction: AC validation: Geolocation: Pointing strategy to minimize sun glint: Avoid terrestrial hot spot: Ground processing: Seasonal latency:
How do climate change, pollution and disturbance augment the vulnerability of ecosystems to invasive species? [DS 114,196]	Measure disturbances and ecosystem status. Measure invasive trends. Measure at the seasonal to multiyear time scale.	Measure spectral signature in the VSWIR region at high precision and accuracy. -Sufficient precision and accuracy for spectral mixture algorithms to give insight to subpixel events. -Measure species-type and functional type using full spectrum. -Measure PV, NPV, and Soil using full VSWIR and SWIR algorithms. Measure globally at spatial resolution patch scale relevant for ecosystem 10 ⁴ to 10 ⁶ m ² . Measure temporally to have high probability to achieve seasonal measurements.	Spectral measurement from 400 to 2500 nm at 10 nm (terrestrial): > 95% Spectral cal uniformity: SNR 600 VNIR, 300 SWIR (23.52A 0.25R): 14-bit precision: >95% abs cal: > 98% on-orbit stability; no saturation of ecosystem targets: <2% polarization sensitivity 380 to 700 nm: >99% linearity 2 to 98% saturation: <60 m spatial sampling: >95% Spectral IFOV uniformity: <20 day revisit to minimize cloud obscuration:	Surface reflectance in the solar reflected spectrum for elevation angles >20: Rigorous cal/val program: Monthly lunar calis: Daily solar calis: 6 per year vcalis: ~700-mbs downlink: >3X zero loss compression: ~11 a.m. Sun sync LEO: Radiometric calibration: Atmospheric Correction: AC validation: Geolocation: Pointing strategy to minimize sun glint: Avoid terrestrial hot spot: Ground processing: Seasonal latency:
What are the effects of disturbances on productivity, water resources, and other ecosystem functions and services? [DS 196]	Measure disturbances and productivity indicators including ecosystem function and services on the seasonal to multiyear time scale	Measure spectral signature in the VSWIR region at high precision and accuracy. -Sufficient precision and accuracy for spectral mixture algorithms to give insight to subpixel events. -Measure species-type and functional type using full spectrum. -Measure PV, NPV, and Soil using full VSWIR and SWIR algorithms. Measure globally at spatial resolution patch scale relevant for ecosystem 10 ⁴ to 10 ⁶ m ² . Measure temporally to have high probability to achieve seasonal measurements.	Spectral measurement from 400 to 2500 nm at 10 nm (terrestrial): > 95% Spectral cal uniformity: SNR 600 VNIR, 300 SWIR (23.52A 0.25R): 14-bit precision: >95% abs cal: > 98% on-orbit stability; no saturation of ecosystem targets: <2% polarization sensitivity 380 to 700 nm: >99% linearity 2 to 98% saturation: <60 m spatial sampling: >95% Spectral IFOV uniformity: <20 day revisit to minimize cloud obscuration:	Surface reflectance in the solar reflected spectrum for elevation angles >20: Rigorous cal/val program: Monthly lunar calis: Daily solar calis: 6 per year vcalis: ~700-mbs downlink: >3X zero loss compression: ~11 a.m. Sun sync LEO: Radiometric calibration: Atmospheric Correction: AC validation: Geolocation: Pointing strategy to minimize sun glint: Avoid terrestrial hot spot: Ground processing: Seasonal latency:
How do changes in human uses of ecosystems affect their vulnerability to disturbance and extreme events? [DS 196]	Measure status of ecosystems globally and relation to disturbances and major events at the seasonal to multiyear time scale.	Measure spectral signature in the VSWIR region at high precision and accuracy. -Sufficient precision and accuracy for spectral mixture algorithms to give insight to subpixel events. -Measure species-type and functional type using full spectrum. -Measure PV, NPV, and Soil using full VSWIR and SWIR algorithms. Measure globally at spatial resolution patch scale relevant for ecosystem 10 ⁴ to 10 ⁶ m ² . Measure temporally to have high probability to achieve seasonal measurements.	Spectral measurement from 400 to 2500 nm at 10 nm (terrestrial): > 95% Spectral cal uniformity: SNR 600 VNIR, 300 SWIR (23.52A 0.25R): 1-bit precision: >95% abs cal: > 98% on-orbit stability; no saturation of ecosystem targets: <2% polarization sensitivity 380 to 700 nm: >99% linearity 2 to 98% saturation: <60 m spatial sampling: >95% Spectral IFOV uniformity: <20 day revisit to minimize cloud obscuration:	Surface reflectance in the solar reflected spectrum for elevation angles >20: Rigorous cal/val program: Monthly lunar calis: Daily solar calis: 6 per year vcalis: ~700-mbs downlink: >3X zero loss compression: ~11 a.m. Sun sync LEO: Radiometric calibration: Atmospheric Correction: AC validation: Geolocation: Pointing strategy to minimize sun glint: Avoid terrestrial hot spot: Ground processing: Seasonal latency:

VQ4

2008 HYSPIRI WHITEPAPER AND SCIENCE WORKSHOP REPORT

Science Objectives	Measurement Objectives	Measurement Requirements	Instrument Requirements	Other Mission and Measurement Requirements
VQ5. Ecosystem and Human Health: How do changes in ecosystem composition and function affect human health, resource use, and resource management?				
How do changes in ecosystem composition and function affect the spread of infectious diseases and the organisms that transmit them [DS155, 160, 161] for example, tracking malaria by water fraction, Hantavirus?	Measure the ecosystem composition and function globally at the seasonal and multiyear timescale. Relate these to measures of infectious diseases and organisms that transmit them. Understand the impact of climate change on the disease vectors environments and interaction with human settlement changes	Measures species/functional type and function through the VSWIR spectral signature acquired at high precision and accuracy. Measure globally at spatial resolution patch scale relevant for ecosystem 10 ⁴ to 10 ⁶ m ² . Measure temporally to have high probability to achieve seasonal measurements.	Spectral measurement from 400 to 2500 nm at 10 nm (terrestrial): 380 to 900 nm at 10 nm with additional SWIR for AC (coastal aquatic): > 95% Spectral cal uniformity: SNR 600 VNIR, 300 SWIR (23.5ZA 0.25R): 14 bit precision: >95% abs cal: > 98% on-orbit stability: no saturation of ecosystem targets: <2% polarization sensitivity 380 to 700 nm: >99% linearity 2 to 98% saturation: <= 60 sampling: >95% Spectral IFOV uniformity: <20 day revisit to minimize cloud obscuration:	Surface reflectance in the solar reflected spectrum for elevation angles >20: Rigorous cal/val program: Monthly lunar cal: Daily solar cal: 6 per year vcal: ~700-mbs downlink: >3X zero loss compression: ~11 a.m. Sun sync LEO orbit: Radiometric calibration: Atmospheric Correction: AC validation: Geolocation: Pointing strategy to minimize sun glint: Avoid terrestrial hot spot: Ground processing: Seasonal latency:
How will changes in pollution and biogeochemical cycling alter water quality?	Measure biogeochemical, pollution, and water quality indicators globally at the seasonal and multiyear time scale.	Measure vegetation biogeochemical signatures in the VSWIR spectral signature acquired at high precision and accuracy. Measure water quality and pollution indicators in the visible portion of the spectrum. Measure globally at spatial resolution patch scale relevant for ecosystem 10 ⁴ to 10 ⁶ m ² . Measure temporally to have high probability to achieve seasonal measurements. Measure turbidity and water clarity, algal and cyanobacterial growth. Measure size and health (biodiversity) of wetlands	Spectral measurement from 400 to 2500 nm at 10 nm (terrestrial): 380 to 900 nm at 10 nm with additional SWIR for AC (coastal aquatic): > 95% Spectral cal uniformity: SNR 600 VNIR, 300 SWIR (23.5ZA 0.25R): 14 bit precision: >95% abs cal: > 98% on-orbit stability: no saturation of ecosystem targets: <2% polarization sensitivity 380 to 700 nm: >99% linearity 2 to 98% saturation: <= 60 sampling: >95% Spectral IFOV uniformity: <20 day revisit to minimize cloud obscuration:	Surface reflectance in the solar reflected spectrum for elevation angles >20: Rigorous cal/val program: Monthly lunar cal: Daily solar cal: 6 per year vcal: ~700-mbs downlink: >3X zero loss compression: ~11 a.m. Sun sync LEO orbit: Radiometric calibration: Atmospheric Correction: AC validation: Geolocation: Pointing strategy to minimize sun glint: Avoid terrestrial hot spot: Ground processing: Seasonal latency:
How are changes in ecosystem distribution and productivity linked to resource use, and resource management such as forestry management, fire effects, biofuels, and agricultural management?	Measure ecosystem composition, productivity and distribution globally at the seasonal and multiyear time scale. Relate these to measures of resource use and management. Map the function types (communities) of the forestry resources, biofuel (corn, sugar cane, etc.) regionally and locally.	Measure vegetation composition, function and production in the VSWIR spectral signature acquired at high precision and accuracy. Measure globally at spatial resolution patch scale relevant for ecosystem 10 ⁴ to 10 ⁶ m ² . Measure temporally to have high probability to achieve seasonal measurements. Measure seasonal changes in productivity	Spectral measurement from 400 to 2500 nm at 10 nm (terrestrial): 380 to 900 nm at 10 nm with additional SWIR for AC (coastal aquatic): > 95% Spectral cal uniformity: SNR 600 VNIR, 300 SWIR (23.5ZA 0.25R): 14 bit precision: >95% abs cal: > 98% on-orbit stability: no saturation of ecosystem targets: <2% polarization sensitivity 380 to 700 nm: >99% linearity 2 to 98% saturation: <= 60 sampling: >95% Spectral IFOV uniformity: <20 day revisit to minimize cloud obscuration: vnir -swir spectra required, polarization requirement may be looser for this application.	Surface reflectance in the solar reflected spectrum for elevation angles >20: Rigorous cal/val program: Monthly lunar cal: Daily solar cal: 6 per year vcal: ~700-mbs downlink: >3X zero loss compression: ~11 a.m. Sun sync LEO orbit: Radiometric calibration: Atmospheric Correction: AC validation: Geolocation: Pointing strategy to minimize sun glint: Avoid terrestrial hot spot: Ground processing: Seasonal latency: validation ground test sites related to the resources to be managed
How will changes in climate and pollution affect the health and productivity of aquatic and agricultural resources?	Measure aquatic and agricultural resource systems globally and through the seasonal and multiyear time frame. Relate these to measures of climate and pollution to detect trends and make predictions.	Measure the composition and productivity of agricultural and aquatic resource ecosystems using the VSWIR spectral signature acquired at high precision and accuracy. Measure globally at spatial resolution patch scale relevant for ecosystem 10 ⁴ to 10 ⁶ m ² . Measure temporally to have high probability to achieve seasonal measurements. Measure surface spectral reflectivity and water spectral absorption sufficient to get at water turbidity for example	Spectral measurement from 400 to 2500 nm at 10 nm (terrestrial): 380 to 900 nm at 10 nm with additional SWIR for AC (coastal aquatic): > 95% Spectral cal uniformity: SNR 600 VNIR, 300 SWIR (23.5ZA 0.25R): 14 bit precision: >95% abs cal: > 98% on-orbit stability: no saturation of ecosystem targets: <2% polarization sensitivity 380 to 700 nm: >99% linearity 2 to 98% saturation: <= 60 sampling: >95% Spectral IFOV uniformity: <20 day revisit to minimize cloud obscuration:	Surface reflectance in the solar reflected spectrum for elevation angles >20: Rigorous cal/val program: Monthly lunar cal: Daily solar cal: 6 per year vcal: ~700-mbs downlink: >3X zero loss compression: ~11 a.m. Sun sync LEO orbit: Radiometric calibration: Atmospheric Correction: AC validation: Geolocation: Pointing strategy to minimize sun glint: Avoid terrestrial hot spot: Ground processing: Seasonal latency:
What are the economic and human health consequences associated with the spread of invasive species?	Measure the global distribution and seasonal variation of invasive species from one to several years. Relate this to economic and human health factors to support both direct assessment and future trend prediction. Distinguish the invasive species from the natural species	Measure the distribution of invasive species using the VSWIR spectral signature acquired at high precision and accuracy. Measure globally at spatial resolution patch scale relevant for ecosystem 10 ⁴ to 10 ⁶ m ² . Measure temporally to have high probability to achieve seasonal measurements. Observe over the growing season with enough temporal resolution to catch the growth cycle points where the likelihood of distinction is maximized.	Spectral measurement from 400 to 2500 nm at 10 nm (terrestrial): 380 to 900 nm at 10 nm with additional SWIR for AC (coastal aquatic): > 95% Spectral cal uniformity: SNR 600 VNIR, 300 SWIR (23.5ZA 0.25R): 14 bit precision: >95% abs cal: > 98% on-orbit stability: no saturation of ecosystem targets: <2% polarization sensitivity 380 to 700 nm: >99% linearity 2 to 98% saturation: <= 60 sampling: >95% Spectral IFOV uniformity: <20 day revisit to minimize cloud obscuration:	Surface reflectance in the solar reflected spectrum for elevation angles >20: Rigorous cal/val program: Monthly lunar cal: Daily solar cal: 6 per year vcal: ~700-mbs downlink: >3X zero loss compression: ~11 a.m. Sun sync LEO orbit: Radiometric calibration: Atmospheric Correction: AC validation: Geolocation: Pointing strategy to minimize sun glint: Avoid terrestrial hot spot: Ground processing: Seasonal latency. Knowledge of local situation vis-à-vis active invasive species of import. Local spectral databases of natural and invasive species.
How does the spatial pattern of policy, environmental management, and economic conditions correlate with the state and changes in ecosystem function and composition? (DS 155 [5-5?], 230 [8-7])	Measure ecosystem composition, function, and distribution globally and seasonal and multiyear time scale. Relate this to the spatial pattern of environmental management and economic conditions for direct assessment and future prognostication.	Measure ecosystem vegetation composition, function and distribution using the VSWIR spectral signature acquired at high precision and accuracy. Measure globally at spatial resolution patch scale relevant for ecosystem 10 ⁴ to 10 ⁶ m ² . Measure temporally to have high probability to achieve seasonal measurements.	Spectral measurement from 400 to 2500 nm at 10 nm (terrestrial): 380 to 900 nm at 10 nm with additional SWIR for AC (coastal aquatic): > 95% Spectral cal uniformity: SNR 600 VNIR, 300 SWIR (23.5ZA 0.25R): 14 bit precision: >95% abs cal: > 98% on-orbit stability: no saturation of ecosystem targets: <2% polarization sensitivity 380 to 700 nm: >99% linearity 2 to 98% saturation: <= 60 sampling: >95% Spectral IFOV uniformity: <20 day revisit to minimize cloud obscuration:	Surface reflectance in the solar reflected spectrum for elevation angles >20: Rigorous cal/val program: Monthly lunar cal: Daily solar cal: 6 per year vcal: ~700-mbs downlink: >3X zero loss compression: ~11 a.m. Sun sync LEO orbit: Radiometric calibration: Atmospheric Correction: AC validation: Geolocation: Pointing strategy to minimize sun glint: Avoid terrestrial hot spot: Ground processing: Seasonal latency:
What are the impacts of flooding and sea-level rise on ecosystems, human health, and security? [DS 195, 224, 227, 348, 357]	Measure ecosystem composition, function and distribution in the coastal regions globally at the seasonal and multiyear timescale. Relate these measurements to the status of coastal ecosystem and the human health and security implications.	Measure coastal ecosystem vegetation composition, function and distribution in both the terrestrial and aquatic domains using the VSWIR spectral signature acquired at high precision and accuracy. Measure globally at spatial resolution patch scale relevant for ecosystem 10 ⁴ to 10 ⁶ m ² . Measure temporally to have high probability to achieve seasonal measurements. Surface reflectance over the vis-swir, and water spectral absorption over the visible spectrum	Spectral measurement from 400 to 2500 nm at 10 nm (terrestrial): 380 to 900 nm at 10 nm with additional SWIR for AC (coastal aquatic): > 95% Spectral cal uniformity: SNR 600 VNIR, 300 SWIR (23.5ZA 0.25R): 14 bit precision: >95% abs cal: > 98% on-orbit stability: no saturation of ecosystem targets: <2% polarization sensitivity 380 to 700 nm: >99% linearity 2 to 98% saturation: <= 60 sampling: >95% Spectral IFOV uniformity: <20 day revisit to minimize cloud obscuration:	Surface reflectance in the solar reflected spectrum for elevation angles >20: Rigorous cal/val program: Monthly lunar cal: Daily solar cal: 6 per year vcal: ~700-mbs downlink: >3X zero loss compression: ~11 a.m. Sun sync LEO orbit: Radiometric calibration: Atmospheric Correction: AC validation: Geolocation: Pointing strategy to minimize sun glint: Avoid terrestrial hot spot: Ground processing: Seasonal latency:

VQ5

Science Objectives	Measurement Objectives	Measurement Requirements	Instrument Requirements	Other Mission and Measurement Requirements
VQ6. Earth Surface and Coastal Benthic Composition: What is the land surface soil/rock and shallow coastal benthic compositions?				
What is the distribution of the primary minerals and mineral groups on the exposed terrestrial surface? [DS 218]	Measure the exposed surface rock and soil compositions globally. Measure the available rock forming and alteration minerals and subtle changes in composition via spectral absorption position and shape. Derive fractional abundance through spectral mixture analysis and related approaches.	Spectral signature in the visible to short wavelength infrared to capture the diagnostic absorptions features of clay, iron, carbonate, and other rock/soil forming minerals.	Spectral measurement from 400 to 2500 nm at 10 nm (terrestrial): > 95% Spectral cal uniformity: SNR >600 VNIR, SNR >300 SWIR (23.5ZA 0.25R): 12-bit precision: >95% abs cal: > 98% on-orbit stability: no saturation of ecosystem targets: >99% linearity 2 to 98% saturation: ≤60 sampling: >95% Spectral IFOV uniformity: <90 day revisit to minimize cloud obscuration globally.	Surface reflectance in the solar reflected spectrum for elevation angles >20: Rigorous cal/val program: Monthly lunar calcs: Daily solar calcs: 6 per year vcalcs: ~700-mbs downlink: >3X zero loss compression: ~11 a.m. Sun sync LEO: Radiometric calibration: Atmospheric Correction: AC validation: Geolocation: Ground processing: Seasonal latency:
What is the bottom composition (sand, rock, mud, coral, algae, SAV, etc.) of the shallow-water regions of the Earth?	Measure the composition of the optically available shallow-water bottom regions of the coastal oceans and inland waters.	High precision and accurate spectral signatures in the visible to near infrared to capture the bottom composition interaction with light. Selected wavelengths in the short wavelength infrared to allow atmospheric correction. Measurements at a spatial scale to resolve material patches at <100 m. Temporal measurements high probability of several tides optimized and clear observations.	Spectral measurement from 380 to 900 nm at 10 nm with additional SWIR for AC (coastal aquatic): >95% Spectral cal uniformity: SNR—violet/blue/green: 400:1, yellow/orange/red: 300:1, wavelength >900 nm: ≥100:1; 14-bit digitization: >95% abs cal: > 98% on-orbit stability: no saturation of ecosystem targets: <2% polarization sensitivity 380 to 700 nm: >99% linearity 2 to 98% saturation: ≤60 sampling: >95% Spectral IFOV uniformity: <20 day revisit to minimize cloud obscuration:	Surface reflectance in the solar reflected spectrum for elevation angles >20: Rigorous cal/val program: Monthly lunar calcs: Daily solar calcs: 6 per year vcalcs: ~700-mbs downlink: >3X zero loss compression: ~11 a.m. Sun sync LEO: Radiometric calibration: Atmospheric Correction: AC validation: Geolocation: Pointing strategy to minimize Sun glint: Avoid terrestrial hot spot: Ground processing: Seasonal latency:
What fundamentally new concepts for mineral and hydrocarbon research will arise from uniform and detailed global geochemistry of the exposed rock/soil surface? [DS227]	Measure the exposed surface rock and soil compositions globally. Derive geochemical information. Ion substitution expressed as spectral signature shifts.	Spectral signature in the visible to short wavelength infrared to capture the diagnostic absorptions features of clay, iron, carbonate, and other rock/soil forming minerals. Spectral regions of absorption features that are sensitive to subtle geochemical changes in composition.	Spectral measurement from 400 to 2500 nm at 10 nm (terrestrial): > 95% Spectral cal uniformity: SNR >600 VNIR, SNR >300 SWIR (23.5ZA 0.25R): 12-bit precision: >95% abs cal: > 98% on-orbit stability: no saturation of ecosystem targets: >99% linearity 2 to 98% saturation: ≤60 sampling: >95% Spectral IFOV uniformity: <90 day revisit to minimize cloud obscuration globally.	Surface reflectance in the solar reflected spectrum for elevation angles >20: Rigorous cal/val program: Monthly lunar calcs: Daily solar calcs: 6 per year vcalcs: ~700-mbs downlink: >3X zero loss compression: ~11 a.m. Sun sync LEO: Radiometric calibration: Atmospheric Correction: AC validation: Geolocation: Ground processing: Seasonal latency:
What changes in bottom substrate occur in shallow coastal and inland aquatic environments? [DS 25]	Measure the composition of the optically available shallow-water bottom regions of the coastal oceans and inland waters. Bottom substrate composition of sand, coral, mud, SAV, etc. More detailed specificity as possible with the available signal.	High precision and accurate spectral signatures in the visible to near infrared to capture the bottom composition interaction with light. Selected wavelengths in the short wavelength infrared to allow atmospheric correction. Measurements at a spatial scale to resolve material patches at <100m. Temporal measurements high probability of several tides optimized and clear observations.	Spectral measurement from 380 to 900 nm at 10 nm with additional SWIR for AC (coastal aquatic): >95% Spectral cal uniformity: SNR—violet/blue/green: 400:1, yellow/orange/red: 300:1, wavelength >900 nm: ≥100:1; 14-bit digitization: >95% abs cal: > 98% on-orbit stability: no saturation of ecosystem targets: <2% polarization sensitivity 380 to 700 nm: >99% linearity 2 to 98% saturation: ≤60 sampling: >95% Spectral IFOV uniformity: <20 day revisit to minimize cloud obscuration:	Surface reflectance in the solar reflected spectrum for elevation angles >20: Rigorous cal/val program: Monthly lunar calcs: Daily solar calcs: 6 per year vcalcs: ~700-mbs downlink: >3X zero loss compression: ~11 a.m. Sun sync LEO: Radiometric calibration: Atmospheric Correction: AC validation: Geolocation: Pointing strategy to minimize sun glint: Avoid terrestrial hot spot: Ground processing: Seasonal latency:
Can measurements of rock and soil composition be used to understand and mitigate hazards? [DS 114,227]	Measure the exposed surface rock and soil compositions globally to determine the occurrence of hazard-associated minerals. For example, Acid-generating minerals, Asbestos, etc.	Spectral signature in the visible to short wavelength infrared to capture the diagnostic absorptions features of acid-generating (sulfates), asbestos, minerals.	Spectral measurement from 400 to 2500 nm at 10 nm (terrestrial): > 95% Spectral cal uniformity: SNR >600 VNIR, SNR >300 SWIR (23.5ZA 0.25R): 12-bit precision: >95% abs cal: > 98% on-orbit stability: no saturation of ecosystem targets: >99% linearity 2 to 98% saturation: ≤60 sampling: >95% Spectral IFOV uniformity: <90 day revisit to minimize cloud obscuration globally.	Surface reflectance in the solar reflected spectrum for elevation angles >20: Rigorous cal/val program: Monthly lunar calcs: Daily solar calcs: 6 per year vcalcs: ~700-mbs downlink: >3X zero loss compression: ~11 a.m. Sun sync LEO: Radiometric calibration: Atmospheric Correction: AC validation: Geolocation: Ground processing: Seasonal latency:

VQ6

Science Objectives	Measurement Objectives	Measurement Requirements	Instrument Requirements	Other Mission and Measurement Requirements
TQ1. Volcanoes and Earthquakes: How can we help predict and mitigate earthquake and volcanic hazards through detection of transient thermal phenomena?				
Do volcanoes signal impending eruptions through changes in surface temperature or gas emission rates and are such changes unique to specific types of eruptions? [DS 227]	Detect, quantify, and monitor subtle variations in: 1) surface temperatures; 2) surface emissivity; and 3) sulfur dioxide concentrations at low, non-eruptive, flux background levels. Compilation of long-term baseline data sets.	Temperature measurements in the range -30 to 200°C. TIR radiance measurements at ~8 µm; 5 sufficient other TIR bands for use in SO ₂ retrieval algorithm; 7-day repeat.	4 TIR channels, 7.3 µm, 8.5 µm, 2 bands between 9-12 µm Pixel size ≤60 m NEΔT ~0.02 K. 0.2 >95% abs. radiometric calibration	Nighttime data acquisitions.
What do changes in the rate of lava effusion tell us about the maximum lengths that lava flows can attain, and the likely duration of lava flow-forming eruptions? [DS 226]	Area covered by active lava flows; Lava flow surface temperatures; Radiant flux from lava flow surfaces.	Temperature measurements in the range 0 to 1200°C (active lava), and 0-50°C (ambient background). 5 day repeat.	1 low gain channel at ~4 µm (NEΔT ~ 1-2 K). 2 nominal gain channels at 10-12 µm Pixel size ≤90 Rapid bright-target recovery at 4 µm (<2 pixels), bands saturate at 1200°C	Nighttime data acquisitions. NIR/SWIR hyperspectral data is beneficial. Rapid response off-nadir pointing capability. Rapid re-tasking for acquisition of targets of opportunity.
What are the characteristic dispersal patterns and residence times for volcanic ash clouds, and how long do such clouds remain a threat to aviation? [DS 224]	Discrimination of volcanic ash clouds from meteorological clouds (both water and ice), in both wet and dry air masses. Day and night measurements	Four spectral channels at 8.5, 10, 11, and 12 µm; NEΔT of 0.2 K, Max. repeat cycle of 5 days. Temperature measurements in the range -20 to 200°C. Multispectral radiance measurements between 8.5 and 12 µm. NEDT>0.5 K. 5-day repeat	4 channels, 8-14 µm. 50 nm at 8.5, 100 nm other bands Pixel size ≤90 m >95% abs. radiometric calibration	NIR/SWIR hyperspectral data valuable to assist in recognition of meteorological clouds and estimation of plume height. Nighttime data acquisitions to increase the frequency of observation.
What do the transient thermal anomalies that may precede earthquakes tell us about changes in the geophysical properties of the crust? [DS 227, 229]	Detect and monitor increases in TIR surface radiance surface temperatures along potentially active faults.	Temperature measurements in range -25C to 50°C. 5-day repeat (or better); nighttime data	1 band at 8-8.5 µm; 1 band 7.3-8 µm ,1 band >10 µm; pixel size 100 m; NEDT = 0.2 K; nighttime data	
Can the energy released by the periodic recharge of magma chambers be used to predict future eruptions? [DS 227] How can the release of energy at the surface of volcanic edifices be used to understand magma processes at depth and over time?	Detect and monitor temperature changes of volcanic edifices	Temperature measurements in range of -25°C to 1200°C; 5-day repeat	1 low-gain channel at ~4 µm (NEΔT ~ 1-2 K) 2 nominal gain channels at 10-12 µm Pixel size ≤90 m	Nighttime data acquisitions.

TQ1

TQ2. Wildfires: What is the impact of global biomass burning on the terrestrial biosphere and atmosphere, and how is this impact changing over time?				
Science Objectives	Measurement Objectives	Measurement Requirements	Instrument Requirements	Other Mission and Measurement Requirements
How are global fire regimes (fire location, type, frequency, and intensity) changing in response to changing climate and land use practices? [DS 198] (feedbacks?)	Fire monitoring, fire intensity	Detect flaming and smoldering fires as small as ~10 sq. m in size, fire radiative power, fire temperature and area, 4–10 day repeat cycle	Low and normal gain channels at 4 and 11 μm (possible dual gain for 11 μm). Low-gain saturation at 1400 K and 1100 K, respectively, with 2–3 K NE Δ T; normal-gain NE Δ T < 0.2 K. Stable behavior in the event of saturation. 50–100 m spatial resolution. Accurate inter-band coregistration (< 0.25 pixel). Opportunistic use of additional bands in 8–14 μm region.	Daytime and nighttime data acquisition, direct broadcast, and onboard processing, pre-fire and post-fire thematic maps, opportunistic validation. Low Earth Orbit.
Is regional and local fire frequency changing? [DS 196]	Fire detection	Detect smoldering fires as small as ~10 sq. m in size, 4–10 day repeat cycle over the duration of the mission	8–12 μm normal gain. normal-gain NE Δ T < 0.2 K. Stable behavior in the event of saturation. 50–100 m spatial resolution. Accurate inter-band coregistration (< 0.25 pixel)	Daytime and nighttime data acquisition. Requires an historical context from other sensors with measurement intercalibration, establishes a baseline. Low Earth Orbit. Daytime and nighttime data acquisition (Thermal inertia)
What is the role of fire in global biogeochemical cycling, particularly trace gas emissions? [DS 195]	Fire detection, fire intensity, fire monitoring, burn severity, delineate burned area	Detect flaming and smoldering fires as small as ~10 sq. m in size, fire radiative power, 4–10 day repeat cycle; fire temperature and area.	Low and normal gain channels at 4 and 11 μm (possible dual gain for 11 μm). Low-gain saturation at 1400 K and 1100 K, respectively, with 2–3 K NE Δ T; normal-gain NE Δ T < 0.2 K. Stable behavior in the event of saturation. 50–100 m spatial resolution. Accurate inter-band coregistration (< 0.25 pixel). Opportunistic use of additional bands in 8–14 μm region.	Daytime and nighttime data acquisition, pre-fire vegetation cover, condition and loads for fuel potential. Requires fuel fire modeling element.
Are there regional feedbacks between fire and climate change?	Extent of fire front and confirmation of burn scars	Detect flaming and smoldering fires as small as ~10 sq. m in size, fire radiative power, 4–10 day repeat cycle; fire temperature and area.	Low and normal gain channels at 4 and 11 μm . Low-gain saturation at 1400 K, 1100 K, respectively, with 2–3 K NE Δ T; normal-gain NE Δ T < 0.2 K. Stable behavior in the event of saturation. 50–100 m spatial resolution. Accurate inter-band coregistration (< 0.25 pixel).	Daytime and nighttime data acquisition, pre-fire vegetation cover, condition and loads for fuel potential. Requires fuel-fire modeling element.

TQ2

Science Objectives	Measurement Objectives	Measurement Requirements	Instrument Requirements	Other Mission and Measurement Requirements
TQ3. Water Use and Availability: How is consumptive use of global freshwater supplies responding to changes in climate and demand, and what are the implications for sustaining water resources?				
How is climate variability impacting the evaporative component of the global water cycle over natural and managed landscapes? (DS 166, 196, 203, 257, 368; WGA)	Evapotranspiration (surface energy balance) at scales resolving the typical length scales of land-surface moisture heterogeneity	Global coverage of surface radiometric temperature; ~weekly to monthly revisit; resolving land-use components; LST accurate to 1 K; ~10–11 A.M. local overpass	<100-m resolution; 3+ bands in the 8–12 micron region (for atmospheric and emissivity correction); Min/Max T 250/360 K; ~weekly revisit; Maximum view angle 20–30 deg from nadir	Maps of vegetation index; coincident broadband albedo retrievals (from integrated VSWIR or 3 or more wide bands in green, red, nearIR); landuse; insolation data; Landsat-like mid-morning Sun-synchronous overpass. Cloud detection mechanism, (including cirrus); Ancillary meteorological data (varies with process)
How can information about evapotranspiration and its relationship to land-use/land-cover be used to facilitate better management of freshwater resources? (DS 196, 203, 368; WGA)	Evapotranspiration at scales resolving the typical length scales of land surface moisture and vegetation heterogeneity	Global coverage; ~weekly revisit; resolving e.g., field, riparian patches, reservoirs, water rights (agricultural field-sized) polygons; LST accurate to 1 K; ~10-11 A.M. overpass	<100-m resolution; 3+ bands as above; Min/Max T 270/360 K	Maps of vegetation index; land use; insolation data; coincident broadband albedo retrievals; Landsat-like mid-morning sun-synchronous overpass
How can we improve early detection, mitigation, and impact assessment of droughts at local to global scales? (DS 166, 196, 203, 368; WGA)	Moisture stress index at field scales	Global coverage; ~weekly revisit; resolving field-scale (1 ha) patches; LST accurate to 1 K; ~10–11 A.M. overpass	<100-m resolution; 3+ bands as above; Min/Max T 270/360 K	As above; some methods require potential evapotranspiration (based on meteorological data and/or satellite-based insolation); hyperspectral stress signatures will provide supplemental stress info
What is the current global irrigated acreage, how is it changing with time, and are these changes in a sustainable balance with regional water availability? (DS 196, 368)	Robust detection of pixels with water consumption in excess of rainfall	Global coverage; ~weekly to monthly revisit; resolving irrigation patches; ~10–11 A.M. overpass	<100-m resolution; 3+ bands as above; Min/Max T 270/360 K	Detailed land cover classification (can be improved using hyperspectral); vegetation indices; coincident broadband albedo retrievals; regional hydrologic water balances and stores
Can we increase food production in water-scarce agricultural regions while improving or sustaining water available for ecosystem function and other human uses? (DS 196, 368; WGA)	Accurate evapotranspiration at sub-field scales	Global coverage, < weekly revisit, irrigation patches well resolved; LST accurate to 1 K; ~10–11 A.M. overpass	<100-m resolution; 3+ bands as above; Min/Max T 270/360 K	Vegetation indices; accurate local meteorological forcing conditions; coincident broadband albedo retrievals; hyperspectral data may improve partitioning of ET into E & T.
How can improved accuracy in evapotranspiration imaging drive advances in science and understanding of the water cycle and hydrologic processes?	Evapotranspiration at scales resolving the typical length scales of land surface moisture and vegetation heterogeneity and across all climate regimes	Global coverage; ~weekly revisit; resolving e.g., fields, riparian patches, reservoirs; LST accurate to 1 K; ~10-11 A.M. overpass	<100-m resolution; 3+ bands as above; Min/Max T 270/360 K	Vegetation indices; coincident broadband albedo retrievals; hyperspectral data may improve partitioning of ET into E and T. Soil moisture retrievals via microwave will improve description of water flow in soils

TQ3

Science Objectives	Measurement Objectives	Measurement Requirements	Instrument Requirements	Other Mission and Measurement Requirements
TQ4. Urbanization and Human Health: How does urbanization affect the local, regional and global environment? Can we characterize this effect to help mitigate its impact on human health and welfare?				
How do changes in local and regional land cover and land use, in particular urbanization, affect surface energy balance characteristics that impact human welfare? [DS: 160-161, 166-167, 196, 198]	Surface temperature, Surface energy fluxes, Surface emissivity, terrestrial coverage	NE Δ T 0.2–0.3 greater than 4 bands distributed between 8 and 12 μ m High spatial resolution (\leq 60 m) Accuracy 1.0 K	260–360 K NE Δ T 0.1 K Acc 0.5 K	High temporal resolution (weekly) Long term validation sites (incl. emissivity targets) and periodic urban campaigns
What are the dynamics, magnitude, and spatial form of the urban heat island effect (UHI); how does it change from city to city; what are its temporal, diurnal, and nocturnal characteristics; and what are the regional impacts of the UHI on biophysical, climatic, and environmental processes? [DS: 158, 166-168]	Day and night surface temperature Urban coverage Intra-seasonal measurements	High spatial resolution (\leq 60 m) Day/night observations Acc 1 K Coregistration 0.2 pix NE Δ T 0.2–0.3	>4 bands for accurate t-e separation Do we need more bands for cloud masking at night? High spatial resolution (\leq 60 m) NE Δ T 0.1 Min T/Max T 260-360K for diurnal observations	High temporal resolution (weekly) Accuracy of 1 deg.K/NE Δ T 0.2–0.3
How can the factors influencing heat stress on humans be better resolved and measured. [DS: 156, 158, 160, 183–184]	Surface temperature Urban coverage	Acc. 1K NedT 0.2-0.3K Daytime/nighttime observations Vegetated/non-vegetated surfaces	>4 bands for T-E separation Diurnal and nocturnal observations Low temperature and high temperature targets (NE Δ T 0.2-0.3 K) Acc 0.5 K	High temporal resolution (weekly) High spatial resolution (\leq 60 m) Accuracy of 1 deg.K/NE Δ T 0.2-0.3 Air temperature
How can the characteristics associated with environmentally related health effects, that affect vector-borne and animal-borne diseases, be better resolved and measured? [DS: 156, 158, 160, 183–184]	Surface temperature Terrestrial coverage	Detection of wet/dry surfaces Daytime/nighttime observations Vegetated/non-vegetated surfaces	Multispectral thermal bands for surface temperature measurements (3–6 bands) Diurnal and nocturnal observations Low temperature and high temperature targets (NE Δ T 0.2–0.3 K)	High temporal resolution (weekly) High spatial resolution (\leq 60 m) Accuracy of 1 deg.K/NE Δ T 0.2–0.3 Soil moisture or precipitation Air temperature water inundation
How do horizontal and temporal scales of variation in heat flux and mixing relate to human health, human ecosystems, and urbanization? [DS: 156, 160-161, 166-167, 179,184]	Surface temperature Surface energy balance Surface energy fluxes Global coverage	Daytime/nighttime observations Multispectral thermal measurements (3–6 bands) High spatial resolution High temporal resolution	Multiple spectral bands (3–6) for surface temperature and energy balance flux measurements Diurnal and nocturnal observations Low-temperature and high-temperature target discrimination	High-temporal resolution (weekly) High spatial resolution (\leq 60 m) Accuracy of 1 deg.K/NE Δ T 0.2–0.3

TQ4

Science Objectives	Measurement Objectives	Measurement Requirements	Instrument Requirements	Other Mission and Measurement Requirements
Earth Surface Composition and Change: What are the composition and thermal properties of the exposed surface of the Earth? How do these factors change over time and affect land use and habitability?				
What is the spectrally observable mineralogy of the Earth's surface, and how does this relate to geochemical and surficial processes? [DS 114]	<i>Mapping spectral emissivity variations associated with mineralogy and rock type in exposed terrains</i>	Variation in silica content and non-silicate <i>minerals</i> based on 8–12 μm band shape. (Spectral emissivities to within 0.5%)	7 bands in 8–12 μm range with NE Δ T < 0.2 K; spatial resolution < 60 m; temporal repeat quarterly	<i>Geolocation to subpixel accuracy</i> Band to band calibration must be validated, in-flight <i>and radiometric calibration</i>
What is the nature and extent of man-made disturbance of the Earth's surface associated with exploitation of <i>renewable</i> and non-renewable resources? How do these vary over time? [DS 227]	<i>Surface temperature and emissivity variations associated with hydrocarbon and mineral extraction (dumps and pits)</i>	Variation in mineral content based on 8–12 μm band shape including detection of sulfate spectral features. <i>At scale of mining activities.</i>	<i>At least 5 bands</i> in 8–12 μm range with NE Δ T < 0.2 K; spatial resolution < 60 m; temporal repeat monthly	<i>Geolocation to subpixel accuracy</i> Band to band calibration must be validated, preferably in-flight <i>and radiometric calibration</i>
How do surface temperature anomalies relate to deeper thermal sources, such as <i>hydrothermal systems</i> , buried lava tubes, underground coal fires and engineering structures? How do changes in the surface temperatures relate to changing nature of the deep seated hot source? [DS 243]	Surface temperatures corrected for emissivity variations <i>for temperature anomalies</i>	<i>Measure</i> variations in temperature with high <i>accuracy and</i> precision and spatial resolution	3+ bands in 8-12 μm range with NE Δ T < 0.2 K; Spatial resolution < 60 m; temporal repeat weekly	Nighttime data necessary to minimize radiant interference due to solar heating
What is the spatial distribution pattern of surface temperatures and emissivities, and how do these influence the Earth's heat budget?	Surface emissivity variations and temperatures of all surficial cover materials	Complex surface emissivity properties based on 8–12 μm band shape	<i>1 band at 3.98 μm and 7 bands</i> in 8–12 μm range with NE Δ T < 0.2 K; spatial resolution 60–500 m; temporal repeat weekly	Accurate methods of temperature emissivity separation applicable to wide range of materials needed.
What are the water-surface temperature <i>distributions</i> in coastal, ocean, and <i>inland water bodies</i> how do they change; and how do they influence <i>aquatic ecosystems</i> ? [DS 378]	Spatial and temporal variation in <i>surface</i> temperatures	<i>Measure</i> variations in temperature with high <i>accuracy (<0.5 K)</i> and precision and good to moderate spatial resolution	<i>1 band at 3.98 μm and 3+ bands</i> in 8-12 μm range with NE Δ T < 0.2 K; Spatial resolution 50 to 100 m; temporal repeat <i>weekly</i>	Day and night measurements preferable

TQ5